CORA Cork Open Research Archive
Cartlann Taighde Oscailte Chorcaí

Title	Hydrodynamic optimisation of an array of wave-power devices
Authors	McGuinness, Justin P. L.
Publication date	2018
Original Citation	McGuinness, J. P. L. 2018. Hydrodynamic optimisation of an array of wave-power devices. PhD Thesis, University College Cork.
Type of publication	Doctoral thesis
Rights	© 2018, Justin P.L. McGuinness. - http://creativecommons.org/licenses/by-nc-nd/3.0/
Download date	2026-09-18 12:56:17
Item downloaded from	https://hdl.handle.net/10468/6259

UCC
University College Cork, Ireland
Coláiste na hOllscoile Corcaigh

Hydrodynamic Optimisation of an Array of Wave-Power Devices

Justin P.L. McGuinness
B.Sc.
109437576

NATIONAL UNIVERSITY OF IRELAND, CORK

Department of Applied Mathematics

Thesis submitted for the degree of Doctor of Philosophy

May 2018

Head of Department: Prof. Sebastian Wieczorek

Supervisor: Dr. Gareth Thomas

Research supported by The Irish Research Council

Contents

List of Figures iv
List of Tables xi
Abstract xv
Acknowledgements xvii
Nomenclature xix

1 Background & Literature review **1**
1.1 Introduction 1
1.1.1 Wave Energy Background: Why Wave Energy? 1
1.1.2 Categories of WEC 4
1.2 Single WEC Analysis & Performance 11
1.2.1 Hydrodynamic Coefficients 11
1.2.2 Shape of WEC 12
1.3 WEC Array Analysis & Performance 16
1.3.1 Investigation of Basic Interaction Effects: Small Arrays of Less Than Four Devices 17
1.3.2 Investigations of Arrays of Four or More Devices 19
1.3.3 Optimisation of Arrays 28
1.4 Physical Testing of Arrays 39
1.5 Research Shortcomings 44

2 Mathematical Formulation **47**
2.1 Introduction 47
2.2 Wave Theory 48
2.2.1 Mathematical Model of Water Waves 48
2.2.2 Linear Wave Theory 52
2.3 Interaction of Waves with a Structure 57
2.3.1 Velocity Potential due to Interaction with a Structure . . 57
2.3.2 The Radiation Problem 59
2.3.3 The Scattering Problem – Multiple Scattering Method . 60
2.3.4 Hydrodynamic Forces on the Devices 63
2.4 Wave-Power Array Theory 67
2.4.1 Wave Energy 67
2.4.2 Wave-Power Absorption 71
2.4.3 Array Coordinates 72
2.4.4 WEC Array Power Absorption Theory 74
2.4.5 Array Quality Measures 76
2.4.6 Point Absorber Theory 79
2.5 Irregular Sea Theory 82
2.5.1 Introduction 82
2.5.2 Description of Irregular Waves 83
2.5.3 Power in Irregular Seas 83

3 Preliminary Optimisation of Linear Arrays in Regular Waves **87**
3.1 Introduction 87

3.1.1 Previous Research on Linear Arrays 88
3.2 Optimisation Method 91
3.3 Optimal Linear Arrays of One Variable 93
3.3.1 Linear Symmetric Array 1 (LS1) 95
3.3.2 Linear Symmetric Array 2 (LS2) 111
3.3.3 Linear Asymmetric Array 3 (LS3) 119
3.4 Discussion of Results 127

4 Optimisation of General Five-Device Linear Arrays in Regular Waves 133
4.1 Introduction 133
4.2 Optimisation Method 134
4.2.1 Implementation 135
4.3 Unconstrained Optimisation Results 137
4.3.1 Head Seas: $\beta_0 = 0$ 137
4.3.2 $\beta_0 = \frac{\pi}{8}$ 140
4.3.3 The Intermediate Angle: $\beta_0 = \frac{\pi}{4}$ 143
4.3.4 $\beta_0 = \frac{3\pi}{8}$ 144
4.3.5 Beam Seas: $\beta_0 = \frac{\pi}{2}$ 146
4.4 Discussion of Results 149

5 Optimisation of General Circular Arrays in Regular Waves 152
5.1 Introduction 152
5.2 Optimisation Method 154
5.3 Behaviour of Uniform Circular Arrays 155
5.4 Optimisation Results 157
5.4.1 Circular Arrays without a Central Device 159
5.4.2 Circular Arrays including Central Device 173
5.5 Discussion of Results 189

6 Constrained Optimisations of Linear Arrays in Regular Waves 194
6.1 Introduction 194
6.2 Optimisation Methodology 195
6.3 Constrained Optimisation Results 199
6.3.1 Comparison of Unconstrained Optimal Layout 199
6.3.2 Undetermined Layout 201
6.4 Discussion of Results 211

7 Optimisation of Linear Arrays over Incident Wave Angle in Regular Waves 215
7.1 Introduction 215
7.2 Optimisation Methodology 216
7.3 Uniform Array Performance 218
7.4 Layout Optimisation Results 223
7.4.1 Unconstrained Optimisation 224
7.4.2 Constrained Optimisation 225
7.5 Analysis of Optimal Arrays 227

7.5.1 Head Seas $\beta \in [-\frac{\pi}{8}, \frac{\pi}{8}]$ 227
7.5.2 Intermediate Seas $\beta \in [\frac{\pi}{8}, \frac{3\pi}{8}]$ 231
7.5.3 Beam Seas $\beta \in [\frac{3\pi}{8}, \frac{5\pi}{8}]$ 234
7.6 Discussion of results 238

8 Optimisation of General 2D Arrays over Incident Wave Angle 243
8.1 Optimisation Methodology 244
8.2 Optimisation Results 247
8.2.1 Unconstrained Motions 247
8.2.2 Constrained Motions 250
8.3 Analysis of Optimal Arrays 252
8.3.1 Narrow-Banded $\beta \in [\frac{7\pi}{16}, \frac{9\pi}{16}]$ 252
8.3.2 Intermediate-Banded $\beta \in [\frac{3\pi}{8}, \frac{5\pi}{8}]$ 255
8.3.3 Broad-Banded $\beta \in [\frac{\pi}{4}, \frac{3\pi}{4}]$ 259
8.4 Discussion of Results 262

9 Optimisation of Linear Arrays in Irregular Waves 266
9.1 Introduction 266
9.2 Optimisation Method 267
9.3 Optimisation of Three-WEC Linear Arrays with Fixed Length . 271
9.3.1 Uniform Layout 273
9.3.2 Optimised Layout 279
9.4 Discussion of Results 284

10 Discussion & Conclusion 288
10.1 Summary & Discussion 288
10.2 Conclusion & Recommendations 294
10.3 Future Work 296

A Supplementary Results to Chapter 3 301

B Supplementary Results to Chapter 4 311

C Supplementary Results to Chapter 5 313

D Supplementary Results to Chapter 6 324

List of Figures

1.1 Diagram of the operating principle of an overtopping device. Source: www.wavedragon.net 5
1.2 Diagram of the operating principle of a floating OWC WEC . . 6
1.3 Operation of a flap type device, e.g. Aquamarine Oyster 8
1.4 Operation of a hinge type device, e.g. Pelamis 9
1.5 Diagram of a heaving point absorber WEC 10
1.6 Example of optimal array layout found by McGuinness (2013) . 38
1.7 Example of "satellite" array configuration suggested by McGuinness (2013) 39

2.1 General configuration of WECs 2 and 3 in an array, showing the corresponding array coordinates. 73

3.1 Diagram of uniform linear array with spacing d between consecutive devices. 89
3.2 Variation of q-factor with non-dimensional uniform spacing kd for beam, head and intermediate (dashed curve) seas. Taken from Thomas & Evans (1981). 90
3.3 Diagram of array LS1, with mirror symmetry about the middle WEC. 94
3.4 $I(n_1)$ against n_1 for for array LS1 with $\beta_0 = 0$. 95
3.5 Diagram of optimised array LS1 for $\beta_0 = 0$, with $ks_1 = 4.9$ and $ks_2 = 0.1$. 96
3.6 Interaction factor q against kL for array LS1 for different values of n_1, with $\beta = \beta_0 = 0$ and $kL \in [5, 15]$. $q = 1$ is shown by dashed line. 97
3.7 Interaction factor q against non-dimensional length kL and array layout parameter n_1 for array LS1 with $\beta = \beta_0 = 0$. 97
3.8 Predicted non-dimensional optimal WEC displacements in optimised array LS1 (as in Figure 3.5) with $n_1 = 49$ for $\beta = \beta_0 = 0$. 99
3.9 Suggested possible optimal "satellite" array for array LS1, corresponding to figure 3.5, with larger device in place of groups of devices. 100
3.10 Interaction factor q against angle of wave incidence β for optimal LS1 array for $kL = 10$ (with $n_1 = 49$). 100
3.11 Interaction factor q against non-dimensional length kL and incident wave angle β for optimal array LS1 ($n_1 = 49$). 101
3.12 Sensitivity analysis for optimised array LS1 for $\beta_0 = 0$, with $n_1 = 49$. 103
3.13 $I(n_1)$ against n_1 for linear array LS1 for several values of β_0. . . 105
3.14 Interaction factor q against kL for optimal LS1 array for several values of β_0. 107
3.15 Interaction factor q vs β for array LS1 for several values of β_0, with $kL = 10$. 108

3.16 Diagram of array LS2, with translational symmetry about the middle WEC. 111
3.17 $I(n_1)$ against n_1 for $n_1 \in [1, 49]$ for array LS2 with $\beta_0 = 0$. . . . 112
3.18 Diagram of optimised array LS2 for $\beta_0 = 0$, with $ks_1 = 0.1$ and $ks_2 = 4.9$. 112
3.19 Interaction factor q against kL for array LS2 for different values of n_1, with $kL \in [5, 15]$ and $\beta_0 = 0$. $q = 1$ is shown by dashed line. 113
3.20 Predicted non-dimensional optimal WEC displacements in optimised array LS2 (as in Figure 3.18) with $n_1 = 49$ for $\beta = \beta_0 = 0$. 115
3.21 Suggested possible optimal satellite array for array LS2, corresponding to figure 3.18, with larger device in place of groups of devices. 116
3.22 $I(n_1)$ against n_1 for array LS2 for several values of β_0. 116
3.23 Interaction factor q against kL for all optimal LS2 arrays for several values of β_0. 117
3.24 Interaction factor q against β for array LS2 optimised for for several values of β_0, with $kL = 10$. 118
3.25 Diagram of array LS3, with asymmetry about WEC 3. 120
3.26 $I(n_1)$ against n_1 for $n_1 \in [1, 49]$ for array LS3 with $\beta_0 = 0$. . . . 120
3.27 Diagram of optimised array LS3 for $\beta_0 = 0$, with $ks_1 = 0.3$ and $ks_2 = 4.7$. 121
3.28 Interaction factor q against kL for array LS3 for different values of n_1, with $kL \in [5, 15]$ and $\beta = 0$. $q = 1$ is shown by dashed line. . 121
3.29 Predicted non-dimensional optimal WEC displacements in optimised array LS3 (as in Figure 3.27) with $n_1 = 3$ for $\beta = \beta_0 = 0$. 122
3.30 Suggested possible optimal "satellite" array for array LS3, corresponding to figure 3.27, with larger device in place of groups of devices. 123
3.31 Plot of $I(n_1)$ against n_1 for array LS3 for several values of β_0. . 124
3.32 Plot of q against kL for optimised LS3 array for several values of β_0. 125
3.33 Plot of q against β for optimised LS3 array for several values of β_0, with $kL = 10$. 126

4.1 General five-device linear array (without imposed symmetry) . . 135
4.2 Optimal interaction factor q against non-dimensional length kL for the best linear arrays found for each value of β_0 examined. The horizontal dotted line represents $q = 1$ 138
4.3 Optimal interaction factor q against incident wave angle β for the best linear arrays found for each value of β_0 examined. The horizontal dotted line represents $q = 1$ 139
4.4 Optimal linear array found for $\beta_0 = 0$ 139
4.5 Optimal displacement amplitudes for best optimised linear array with $\beta_0 = 0$. The displacements of WECs 3 and 4 are very similar to WECs 2 and 1 respectively and are thus omitted for clarity. . 141
4.6 Optimal linear array found for $\beta_0 = \frac{\pi}{8}, \frac{\pi}{4}$ 142

4.7 Optimal displacements of WECs for best linear array optimised for $\beta_0 = \frac{\pi}{8}$ 142
4.8 Optimal displacements of WECs for best linear array optimised for $\beta_0 = \frac{\pi}{4}$ 144
4.9 Optimal linear array found for $\beta_0 = \frac{3\pi}{8}$ 145
4.10 Optimal displacements of WECs for best linear array optimised for $\beta_0 = \frac{3\pi}{8}$ 146
4.11 Optimal linear array found for $\beta_0 = \frac{\pi}{2}$ 147
4.12 Optimal displacements of WECs for best linear array optimised for $\beta_0 = \frac{\pi}{2}$ 148

5.1 General six-device circular array, without middle device 155
5.2 Interaction factor q against non-dimensional radius kr for uniform six and seven WEC arrays, with $\beta = 0$ 156
5.3 Interaction factor q against incident wave angle β for uniform six and seven WEC arrays, with $kr = 10$ 156
5.4 Interaction factor q against non-dimensional length kr for the optimal six-WEC circular arrays for $\beta_0 \in [0, \frac{7\pi}{8}]$ 160
5.5 Variation of interaction factor q for different angles of incidence β for the optimal six-WEC circular arrays, with $kr = 10$ fixed. The data is presented in two figures for clarity. 161
5.6 Optimal six-device circular arrays for $\beta_0 = 0$ 162
5.7 Predicted displacement amplitudes for optimal six-WEC circular array with $\beta_0 = 0$ 163
5.8 Optimal six-device circular arrays for $\beta_0 = \frac{\pi}{8}$. The third best layout is very similar to the second and is omitted for clarity 165
5.9 Predicted displacement amplitudes for optimal six-WEC circular array with $\beta_0 = \frac{\pi}{8}$ 166
5.10 Optimal six-device circular arrays for $\beta_0 = \frac{\pi}{4}$ 167
5.11 Predicted displacement amplitudes for optimal six-WEC circular array with $\beta_0 = \frac{\pi}{4}$ 168
5.12 Optimal six-device circular arrays for $\beta_0 = \frac{3\pi}{8}$ 169
5.13 Predicted displacement amplitudes for optimal six-WEC circular array with $\beta_0 = \frac{3\pi}{8}$ 170
5.14 Optimal six-device circular arrays for $\beta_0 = \frac{\pi}{2}$ 171
5.15 Predicted displacement amplitudes for optimal six-WEC circular array with $\beta_0 = \frac{\pi}{2}$ 172
5.16 Interaction factor q against non-dimensional length kr for the optimal seven-WEC circular array for $\beta_0 = 0, \frac{\pi}{8}, \frac{\pi}{4}, \frac{3\pi}{8}, \frac{\pi}{2}, \frac{5\pi}{8}, \frac{3\pi}{4}, \frac{7\pi}{8}$. 175
5.17 Variation of interaction factor q against angle of incidence β for the optimal seven-device arrays, with $kr = 10$ fixed. The data is presented in two figures for clarity. 176
5.18 Optimal seven-device circular arrays for $\beta_0 = 0$ 177
5.19 Predicted displacement amplitudes for optimal seven-WEC circular array with $\beta_0 = 0$ 178
5.20 Optimal seven-device circular arrays for $\beta_0 = \frac{\pi}{8}$ 179

5.21 Predicted displacement amplitudes for optimal seven-WEC circular array for $\beta_0 = \frac{\pi}{8}$ 180
5.22 Optimal seven-device circular arrays for $\beta_0 = \frac{\pi}{4}$ 181
5.23 Predicted displacement amplitudes for optimal seven-WEC circular array for $\beta_0 = \frac{\pi}{4}$ 183
5.24 Optimal seven-device circular arrays for $\beta_0 = \frac{3\pi}{8}$ 184
5.25 Predicted displacement amplitudes for optimal seven-WEC circular array for $\beta_0 = \frac{3\pi}{8}$ 185
5.26 Optimal seven-device circular arrays for $\beta_0 = \frac{\pi}{2}$ 186
5.27 Predicted displacement amplitudes for optimal seven-WEC circular array for $\beta_0 = \frac{\pi}{2}$ 188

6.1 Constrained and unconstrained optimal linear arrays for $\beta_0 = 0$. The optimal layout for the $\delta \leq 3$ case is very similar to the $\delta \leq 2$ case and is omitted for clarity 204
6.2 Performance of constrained and unconstrained linear arrays for variation in kL with $\beta = \beta_0 = 0$ 204
6.3 Performance of constrained and unconstrained linear arrays for variation in β with $\beta_0 = 0$ and $kL = 10$ 205
6.4 Constrained and unconstrained optimal linear arrays for $\beta_0 = \frac{\pi}{4}$. 206
6.5 Performance of constrained and unconstrained linear arrays for variation in kL with $\beta = \beta_0 = \frac{\pi}{4}$ 207
6.6 Performance of constrained and unconstrained linear arrays for variation in β with $\beta_0 = \frac{\pi}{4}$ and $kL = 10$ 208
6.7 Constrained and unconstrained optimal linear arrays for $\beta_0 = \frac{\pi}{2}$. The optimal layout for $\delta \leq 3$ is identical to the $\delta \leq 2$ case and is omitted for clarity 209
6.8 Performance of constrained and unconstrained linear arrays for variation in kL with $\beta = \beta_0 = \frac{\pi}{2}$ 210
6.9 Performance of constrained and unconstrained linear arrays for variation in β with $\beta_0 = \frac{\pi}{2}$ and $kL = 10$ 211

7.1 Performance of uniform array against incident wave angle for target range $\beta \in [-\frac{\pi}{8}, \frac{\pi}{8}]$ (shown by horizontal dashed lines) 220
7.2 Performance of uniform array against incident wave angle for target range $\beta \in [\frac{\pi}{8}, \frac{3\pi}{8}]$ (shown by horizontal dashed lines) 221
7.3 Performance of uniform array against incident wave angle for target range $\beta \in [\frac{3\pi}{8}, \frac{5\pi}{8}]$ (shown by horizontal dashed lines) 221
7.4 Performance of constrained uniform arrays against relative incident wavenumber. The target β ranges are given in the legend. For each curve, β is fixed at the midpoint of the appropriate target range. Solid curves represent a constraint of $\delta_{max} = 3$ while dashed curves correspond to $\delta_{max} = 2$ 222
7.5 Constrained and unconstrained optimal linear arrays for head seas ($\beta \in [-\frac{\pi}{8}, \frac{\pi}{8}]$). The optimal layout for the $\delta \leq 3$ case is very similar to the $\delta \leq 2$ case and is omitted for clarity 228

7.6 Interaction factor against incident wave angle β for optimal constrained and unconstrained linear five-WEC array, optimised for $\beta \in [-\frac{\pi}{8}, \frac{\pi}{8}]$. The target range of wave angles is indicated by the vertical dashed lines. 229
7.7 Interaction factor against wavenumber k for optimal constrained and unconstrained linear five-WEC array, optimised for $\beta \in [-\frac{\pi}{8}, \frac{\pi}{8}]$. 229
7.8 Optimal displacement amplitudes against incident wave angle for optimal unconstrained linear five-WEC array, optimised for $\beta \in [-\frac{\pi}{8}, \frac{\pi}{8}]$ (shown by horizontal dashed lines) 230
7.9 Constrained and unconstrained optimal linear arrays for intermediate seas ($\beta \in [\frac{\pi}{8}, \frac{3\pi}{8}]$). 232
7.10 Interaction factor against incident wave angle β for optimal constrained and unconstrained linear five-WEC array, optimised for $\beta \in [\frac{\pi}{8}, \frac{3\pi}{8}]$. The target range of wave angles is indicated by the vertical dashed lines. 232
7.11 Interaction factor against wavenumber k for optimal constrained and unconstrained linear five-WEC array, optimised for $\beta \in [\frac{\pi}{8}, \frac{3\pi}{8}]$. 233
7.12 Optimal displacement amplitudes against incident wave angle for optimal unconstrained linear five-WEC array, optimised for $\beta \in [\frac{\pi}{8}, \frac{3\pi}{8}]$ (shown by horizontal dashed lines) 234
7.13 Constrained and unconstrained optimal linear arrays for beam seas ($\beta \in [\frac{3\pi}{8}, \frac{5\pi}{8}]$). 235
7.14 Interaction factor against incident wave angle β for optimal constrained and unconstrained linear five-WEC array, optimised for $\beta \in [\frac{3\pi}{8}, \frac{5\pi}{8}]$. The target range of wave angles is indicated by the vertical dashed lines. 235
7.15 Interaction factor against wavenumber k for optimal constrained and unconstrained linear five-WEC array, optimised for $\beta \in [\frac{3\pi}{8}, \frac{5\pi}{8}]$. 236
7.16 Optimal displacement amplitudes against incident wave angle for optimal unconstrained linear five-WEC array, optimised for $\beta \in [\frac{3\pi}{8}, \frac{5\pi}{8}]$ (shown by horizontal dashed lines) 237

8.1 Diagram of optimal unconstrained arrays for each range of incident wave angle 249
8.2 Diagram of optimal arrays for narrow-banded range of incident wave angle $\beta \in [\frac{7\pi}{16}, \frac{9\pi}{16}]$ 253
8.3 Interaction factor against incident wave angle β for optimal constrained and unconstrained five-WEC arrays, optimised for $\beta \in [\frac{7\pi}{16}, \frac{9\pi}{16}]$. The target range of wave angles is indicated by the vertical dashed lines. 253
8.4 Interaction factor against wavenumber $\frac{k}{k_{opt}}$ for optimal narrow-banded constrained and unconstrained five-WEC arrays, with $\beta = \frac{\pi}{2}$. 254
8.5 Optimal displacement amplitudes against incident wave angle for optimal unconstrained five-WEC array, optimised for $\beta \in [\frac{7\pi}{16}, \frac{9\pi}{16}]$ (shown by horizontal dashed lines) 255

8.6 Diagram of optimal arrays for intermediate-banded range of incident wave angle $\beta \in [\frac{3\pi}{8}, \frac{5\pi}{8}]$ 256
8.7 Interaction factor against incident wave angle β for optimal constrained and unconstrained five-WEC arrays, optimised for $\beta \in [\frac{3\pi}{8}, \frac{5\pi}{8}]$. The target range of wave angles is indicated by the vertical dashed lines. 257
8.8 Interaction factor against wavenumber $\frac{k}{k_{opt}}$ for optimal constrained and unconstrained five-WEC arrays, optimised for $\beta \in [\frac{3\pi}{8}, \frac{5\pi}{8}]$, with $\beta = \frac{\pi}{2}$. 257
8.9 Optimal displacement amplitudes against incident wave angle for optimal unconstrained five-WEC array, optimised for $\beta \in [\frac{3\pi}{8}, \frac{5\pi}{8}]$ (shown by horizontal dashed lines) 258
8.10 Diagram of optimal arrays for broad-banded range of incident wave angle $\beta \in [\frac{\pi}{4}, \frac{3\pi}{4}]$ 259
8.11 Interaction factor against incident wave angle β for optimal constrained and unconstrained five-WEC arrays, optimised for $\beta \in [\frac{\pi}{4}, \frac{3\pi}{4}]$. The target range of wave angles is indicated by the vertical dashed lines. 260
8.12 Interaction factor against wavenumber $\frac{k}{k_{opt}}$ for optimal constrained and unconstrained five-WEC arrays, optimised for $\beta \in [\frac{\pi}{4}, \frac{3\pi}{4}]$, with $\beta = \frac{\pi}{2}$. 261
8.13 Optimal displacement amplitudes against incident wave angle for optimal unconstrained five-WEC array, optimised for $\beta \in [\frac{\pi}{4}, \frac{3\pi}{4}]$ (shown by horizontal dashed lines) 261

9.1 Normalised Power spectrum $\frac{S_P(\omega)}{P_T}$ against frequency ω for several values of γ_p. 268
9.2 Diagram of three-WEC uniform linear array. 272
9.3 Power absorbed $P_{abs}^{(N)}(\omega, \beta_0)$ in kilowatts against frequency ω for optimised uniform arrays with $\beta_0 = 0$ (head seas). 275
9.4 Power absorbed $P_{abs}^{(N)}(\omega, \beta_0)$ in kilowatts against frequency ω for optimised uniform arrays with $\beta_0 = \frac{\pi}{4}$ (intermediate seas). . . . 275
9.5 Power absorbed $P_{abs}^{(N)}(\omega, \beta_0)$ in kilowatts against frequency ω for optimised uniform arrays with $\beta_0 = \frac{\pi}{2}$ (beam seas). 276
9.6 Power absorbed $P_{abs}^{(N)}(\omega_p, \beta)$ in kilowatts at peak frequency $\omega = \omega_p = 0.5$ against incident wave angle β for uniform arrays optimised in head seas with $\beta_0 = 0$ (shown by y-axis). 277
9.7 Power absorbed $P_{abs}^{(N)}(\omega_p, \beta)$ in kilowatts at peak frequency $\omega = \omega_p = 0.5$ against incident wave angle β for uniform arrays optimised with $\beta_0 = \frac{\pi}{4}$ (shown by the vertical dashed line). 277
9.8 Power absorbed $P_{abs}^{(N)}(\omega_p, \beta)$ in kilowatts at peak frequency $\omega = \omega_p = 0.5$ against incident wave angle β for uniform arrays optimised in beam seas with $\beta_0 = \frac{\pi}{2}$ (shown by y-axis). 278
9.9 Power absorbed $P_{abs}^{(N)}(\omega, \beta_0)$ in kilowatts against frequency ω for optimised non-uniform arrays with $\beta_0 = 0$ (head seas). 281

9.10 Power absorbed $P_{abs}^{(N)}(\omega, \beta_0)$ in kilowatts against frequency ω for optimised non-uniform arrays with $\beta_0 = \frac{\pi}{4}$ (intermediate seas). . 281
9.11 Power absorbed $P_{abs}^{(N)}(\omega, \beta_0)$ in kilowatts against frequency ω for optimised non-uniform arrays with $\beta_0 = \frac{\pi}{2}$ (beam seas). 282
9.12 Power absorbed $P_{abs}^{(N)}(\omega_p, \beta)$ in kilowatts at peak frequency $\omega = \omega_p = 0.5$ against incident wave angle β for non-uniform arrays optimised in head seas with $\beta_0 = 0$ (shown by y-axis). 282
9.13 Power absorbed $P_{abs}^{(N)}(\omega_p, \beta)$ in kilowatts at peak frequency $\omega = \omega_p = 0.5$ against incident wave angle β for non-uniform arrays optimised with $\beta_0 = \frac{\pi}{4}$ (shown by the vertical dashed line). . . . 283
9.14 Power absorbed $P_{abs}^{(N)}(\omega_p, \beta)$ in kilowatts at peak frequency $\omega = \omega_p = 0.5$ against incident wave angle β for non-uniform arrays optimised in beam seas with $\beta_0 = \frac{\pi}{2}$ (shown by y-axis). 283

A.1 Interaction factor q vs kL vs β for array LS1 optimised for several values of β_0. 302
A.2 Interaction factor q vs kL vs n_1 for array LS1 for several values of β_0. 303
A.3 Predicted optimal displacement amplitudes for array LS1 for several values of β_0. 304
A.4 Interaction factor q vs kL vs β for array LS2 optimised for several values of β_0. 305
A.5 Interaction factor q vs kL vs n_1 for array LS2 for several values of β_0. 306
A.6 Predicted optimal displacement amplitudes for array LS2 for several values of β_0. 307
A.7 Interaction factor q vs kL vs β for array LS3 optimised for several values of β_0. 308
A.8 Interaction factor q vs kL vs n_1 for array LS3 for several values of β_0. 309
A.9 Predicted optimal displacement amplitudes for array LS3 for several values of β_0. 310

C.1 Optimal six-device circular arrays for $\beta_0 = \frac{5\pi}{8}$ 316
C.2 Optimal six-device circular arrays for $\beta_0 = \frac{3\pi}{4}$ 317
C.3 Optimal six-device circular arrays for $\beta_0 = \frac{7\pi}{8}$. The third array is very similar to the second and is omitted for clarity 318
C.4 Optimal seven-device circular arrays for $\beta_0 = \frac{5\pi}{8}$ 321
C.5 Optimal seven-device circular arrays for $\beta_0 = \frac{3\pi}{4}$ 322
C.6 Optimal seven-device circular arrays for $\beta_0 = \frac{7\pi}{8}$ 323

List of Tables

3.1 Optimisation results for array LS1 with different incident wave angles. 110
3.2 Optimisation results for array LS2 with different incident wave angles. 119
3.3 Optimisation results for array LS3 with different incident wave angles. 127

4.1 Optimal linear array parameters for each value of β_0 considered 137

5.1 Average interaction factors I for uniformly spaced circular arrays 157
5.2 Optimal array parameters for the six-device circular arrays (without middle device) for eight values of β_0 159
5.3 Optimal array parameters for the seven-device circular arrays (including a middle device) for eight values of β_0 174

6.1 Optimum isolated WEC displacement parameters 197
6.2 Performance of optimal layouts from Chapter 4 subject to motion constraints 199
6.3 Optimal WEC displacement parameters for optimal layouts from Chapter 4 subject to constraints 200
6.4 Optimal linear array layout parameters subject to motion constraints 201
6.5 Optimal WEC displacement parameters for constrained optimal layouts in table 6.4 202

7.1 Performance of unconstrained uniform linear array with $ks_1 = ks_2 = ks_3 = ks_4 = 2.5$ 218
7.2 Performance of constrained uniform linear array with $ks_1 = ks_2 = ks_3 = ks_4 = 2.5$ 219
7.3 Optimal array parameters for the unconstrained five-device linear array 224
7.4 Optimal array layout parameters for the constrained five-device linear array 226
7.5 Optimal displacement parameters for the corresponding optimal constrained five-device linear arrays identified in table 7.4 226

8.1 Optimal position variables for the general 2D unconstrained five-device array 248
8.2 Optimal position variables for the general 2D constrained five-device array 250
8.3 Optimal displacement variables for the corresponding general 2-D constrained five-device arrays in table 8.2 250

9.1 Optimisation results for uniform three-WEC linear array 274
9.2 Optimisation results for non-uniform three-WEC linear array . . 280

B.1 Optimal linear array parameters for $\beta_0 = 0$ 312
B.2 Optimal linear array parameters for $\beta_0 = \frac{\pi}{8}$ 312
B.3 Optimal linear array parameters for $\beta_0 = \frac{\pi}{4}$ 312
B.4 Optimal linear array parameters for $\beta_0 = \frac{3\pi}{8}$ 312
B.5 Optimal linear array parameters for $\beta_0 = \frac{\pi}{2}$ 312

C.1 Optimal array parameters for the six-device circular array (without middle device) with $\beta_0 = 0$. The best result found by McGuinness & Thomas (2016) is marked "M" 313
C.2 Optimal array parameters for the six-device circular array (without middle device) with $\beta_0 = \frac{\pi}{8}$ 313
C.3 Optimal array parameters for the six-device circular array (without middle device) with $\beta_0 = \frac{\pi}{4}$. The best result found by McGuinness & Thomas (2016) is marked "M" 314
C.4 Optimal array parameters for the six-device circular array (without middle device) with $\beta_0 = \frac{3\pi}{8}$ 314
C.5 Optimal array parameters for the six-device circular array (without middle device) with $\beta_0 = \frac{\pi}{2}$. The best result found by McGuinness & Thomas (2016) is marked "M" 314
C.6 Optimal array parameters for the six-device circular array (without middle device) with $\beta_0 = \frac{5\pi}{8}$ 315
C.7 Optimal array parameters for the six-device circular array (without middle device) with $\beta_0 = \frac{3\pi}{4}$ 315
C.8 Optimal array parameters for the six-device circular array (without middle device) with $\beta_0 = \frac{7\pi}{8}$ 315
C.9 Optimal array parameters for the seven-device circular array (including a middle device) with $\beta_0 = 0$. The best result found by McGuinness & Thomas (2016) is marked "M" 316
C.10 Optimal array parameters for the seven-device circular array (including a middle device) with $\beta_0 = \frac{\pi}{8}$ 317
C.11 Optimal array parameters for the seven-device circular array (including a middle device) with $\beta_0 = \frac{\pi}{4}$. The best result found by McGuinness & Thomas (2016) is marked "M" 318
C.12 Optimal array parameters for the seven-device circular array (including a middle device) with $\beta_0 = \frac{3\pi}{8}$ 319
C.13 Optimal array parameters for the seven-device circular array (including a middle device) with $\beta_0 = \frac{\pi}{2}$. The best result found by McGuinness & Thomas (2016) is marked "M" 319
C.14 Optimal array parameters for the seven-device circular array (including a middle device) with $\beta_0 = \frac{5\pi}{8}$ 319
C.15 Optimal array parameters for the seven-device circular array (including a middle device) with $\beta_0 = \frac{3\pi}{4}$ 320
C.16 Optimal array parameters for the seven-device circular array (including a middle device) with $\beta_0 = \frac{7\pi}{8}$ 320

D.1 Optimal linear array layout parameters subject to $\delta \leq 2$ for $\beta_0 = 0$ 325
D.2 Optimal linear array layout parameters subject to $\delta \leq 3$ for $\beta_0 = 0$ 325

D.3 Optimal linear array layout parameters subject to $\delta \leq 2$ for $\beta_0 = \frac{\pi}{4}$ 325
D.4 Optimal linear array layout parameters subject to $\delta \leq 3$ for $\beta_0 = \frac{\pi}{4}$ 325
D.5 Optimal linear array layout parameters subject to $\delta \leq 2$ for $\beta_0 = \frac{\pi}{2}$ 325
D.6 Optimal linear array layout parameters subject to $\delta \leq 3$ for $\beta_0 = \frac{\pi}{2}$ 325

This is to certify that the work I am submitting is my own and has not been submitted for another degree, either at University College Cork or elsewhere. All external references and sources are clearly acknowledged and identified within the contents. I have read and understood the regulations of University College Cork concerning plagiarism.

Justin P.L. McGuinness

Abstract

Third generation wave-power devices are usually envisaged as being either a single large device or an array of smaller devices. The benefit of an array, compared to a single device, is that the individual components are relatively inexpensive to repair and replace; however issues arise due to interaction between the array members, which can lead to constructive or destructive interference of the wave-field, thus increasing or decreasing the power that can be absorbed. This thesis is concerned with the optimal formation and design of these arrays of wave-power devices from a hydrodynamic perspective. Previous literature has indicated that a deterministic optimisation of the array layout, which directly maximises the array performance, results in high sensitivity of the optimal performance to incoming wave parameters. This work considers a more robust optimisation, where the mean performance of the array is maximised.

Determining the optimal array configuration is associated with numerical optimisation. Previous studies have shown that a balance must be struck between accurately modelling the devices of the array (including their interactions) and the requirement of establishing a reliable optimisation process. Thus, linear wave theory and the point absorber approximation are utilised within this work. Several array geometries are investigated, including linear and circular arrays, along with a general 2D optimisation without any imposed symmetry. Both constrained and unconstrained WEC motions are considered. Regular waves are assumed for the majority of this work, with a preliminary extension to irregular waves also investigated for elementary linear arrays.

In general, it is shown that optimal unconstrained arrays tend to contain closely spaced groups of WECs, while constrained arrays are more spread out. A trade-off between peak performance and performance stability is identified for general WEC arrays, while linear arrays also exhibit a trade-off between stability to wavenumber variations and incident wave angle variations. Overall, it is shown that linear arrays perform poorly for some orientations, regardless of the array layout. Better constructive interaction can be achieved in beam seas for unconstrained motions, while head seas allow for the best interaction when WEC motions constraints are applied. As expected, better interaction can be achieved for more general array layouts, without a prescribed geometry.

If it was easy, someone smarter would have already done it.

Acknowledgements

First and foremost, I would like to extend my sincere gratitude to my supervisor Dr. Gareth Thomas. Over the last few years, I have grown to consider him more of a mentor and a friend than a supervisor. He was always very approachable for any issues and was always happy to talk about anything, work related or otherwise. His assistance was always prompt, insightful and often went beyond what was required of him. He has selflessly given much of his time to assist me in this endeavour, particularly given that this previous year coincided with the first year of his retirement. He showed considerable confidence in my abilities (even when I did not) and has imparted many words of wisdom which have improved both this thesis and my life greatly.

I would also like to thank my advisor Dr. David Henry for the assistance and support he has provided through my years as a student, both undergrad and postgrad. I must also thank him for his assistance in acquiring the appropriate numerical software packages used in this project; without them, this work would have been considerably more difficult.

My family have been a constant pillar of support throughout my academic career. In particular, my parents are owed considerable credit for enabling me to achieve what I have. They have always provided counseling, advice, a reassuring word and some home comforts whenever required. This was all alongside their considerable financial contribution to my early education and my BSc., for which I am unspeakably grateful. I could not have achieved this without them.

My colleagues and fellow PhD students also deserve a mention, including among others Adrian, Andy, Azzam, Catherine, Chris, Dave, James, Pat, Paul, Tony and Vahid. There were many constructive (and pointless) conversations had in our office and elsewhere, which made the whole PhD process more enjoyable. Admittedly some of those listed were more of a distraction than an aid to my work! However distractions were not only welcome but required at times. A particular mention is given to Dave Hawe, who passed on some insightful advice and selflessly gave much of his time to help review and improve this thesis. I also am grateful to my friends back in my home town of Wexford, namely Anto, Daithí, Dean, Kav and Liam, for keeping me grounded in reality throughout my time as a PhD student.

I would also like to thank my host institution, UCC, and all the staff that have aided me throughout my years in Cork. Whether the help I received was academic, administrative or social, it is greatly appreciated and made my time at UCC some of the most enjoyable of my life.

I should also thank the staff at CIT for welcoming me into the fold during a trying and unexpected forth year of this project. In particular, Dr. Áine Ní Shé deserves considerable thanks for offering me employment in my time of need and for her understanding and assistance while I was finishing this thesis.

Finally, I would like to gratefully acknowledge the financial support of the Irish Research Council. I was honoured to receive a Government of Ireland Postgraduate Scholarship which enabled me to devote my full time and attention to this project, for three of the four years at least. This thesis would not have been possible without the support of the IRC.

Nomenclature

α_m	Angular position of the mth device
α_p	Phillips constant of JONSWAP spectrum
β	Incident wave angle
β_0	Prescribed value of β
δ_{jl}	Kronecker delta
ϵ	Small error
η	Free surface elevation
Γ	Legendre Gamma function
γ	Coefficient of kinematic viscosity
γ_p	Peak enhancement factor of JONSWAP spectrum
λ	Wavelength
$\mathbb{A}, a_{lj}$	Added mass matrix and lj^{th} component
$\mathbb{B}, b_{lj}$	Radiation damping matrix and lj^{th} component
$\mathbb{C}, \frac{c_{lj}}{\omega^2}$	Hydrostatic force matrix and lj^{th} component
$\mathbb{J}$	Matrix of Bessel functions $\{\mathbb{J}\}_{mn} = J_0(kd_{mn})$
$\mathbf{D}$	Complex WEC displacement vector
$\mathbf{D}_{opt}$	Optimal complex WEC displacement vector
$\mathbf{F}, F_j$	Hydrodynamic force and j^{th} component
$\mathbf{f}, f_j$	Complex amplitude of the hydrodynamic force and j^{th} component
$\mathbf{F}_e$	Excitation force
$\mathbf{F}_r, \boldsymbol{\mathcal{F}}_r$	Generalised radiation force and complex amplitude
$\mathbf{F}_{hs}$	Hydrostatic force
$\mathbf{M}, M_j$	Hydrodynamic moment vector and j^{th} component
$\mathbf{n}$	Unit normal vector out of the fluid
$\mathbf{u}$	Fluid velocity vector $\mathbf{u} = (u, v, w)$

$\mathbf{U}, U_j$	Body velocity vector and j^{th} component
$\mathbf{V}$	Total velocity of a point on a floating body
$\mathbf{X}, X_j$	Complex amplitude of excitation force and j^{th} component
$\mathbf{X}_{FK}$	Froude-Krylov force (Complex amplitude)
$\mathcal{C}, \mathcal{D}$	Havelock coefficients
$\mathcal{J}$	Power per unit width of the incident wave for arbitrary water depths
$\mathcal{L}_{abs}$	Absorption length
$\mathcal{L}_{opt}$	Maximum absorption length
$\mathcal{O}$	Order of symbol
$\mathcal{P}, \mathcal{P}_j$	Instantaneous power absorbed by the array and j^{th} device
$\mathcal{V}, \mathcal{S}$	Integration volume and boundary surface
ν_n	Arbitrary velocity of fluid volume
ω	Angular wave frequency
ω_p	Peak angular wave frequency
$\overline{}$	Time average over one wave period
$\overline{I_\beta}$	Mean of the averaged interaction factor $\overline{q}$ over β
$\overline{I}$	Mean of the averaged interaction factor $\overline{q}$ over kL
$\overline{q}$	Averaged interaction factor
Φ, ϕ	Total wave potential and complex amplitude
ϕ_0, ϕ_r, ϕ_d	Complex amplitude of incident, radiated and diffracted wave potentials
ϕ_s	Complex amplitude of scattered wave potential $\phi_s = \phi_0 + \phi_d$
$\boldsymbol{\chi}$	Total time-dependent body displacements
$\boldsymbol{\ell}$	WEC phase factor vector
$\boldsymbol{\mathcal{F}}$	Complex amplitude of generalised hydrodynamic force
$\boldsymbol{\mathcal{N}}$	Generalised unit normal vector
$\boldsymbol{\mathcal{U}}, \mathcal{U}_j$	Complex amplitude of body velocity and j^{th} component

$\boldsymbol{\mathcal{U}}_{opt}$ Optimal WEC velocity vector

$\boldsymbol{\mu} = (\mu_1, \mu_2, \mu_3)$ Complex amplitude of the hydrodynamic moment

$\boldsymbol{\Omega} = (\Omega_1, \Omega_2, \Omega_3)$ Rotational body velocity vector

$\boldsymbol{\xi}$ Complex amplitude of body displacement vector

ρ Fluid density

σ_p Peak width parameter of JONSWAP spectrum

Im[ ] Imaginary part of expression

Re[ ] Real part of expression

θ_j Relative angular position of jth WEC in a circular array $\theta_j = \alpha_j - \alpha_{j+1}$

ε Perturbation parameter

$\varkappa_j$ Roots of $\omega^2 + g\varkappa_j \tan(\varkappa_j h) = 0$

φ_j Complex amplitudes of the radiated velocity potentials due to device oscillation in mode j with unit velocity amplitude

Ξ Phase function

ζ Complex amplitude of free surface elevation

* Complex conjugate

† Complex conjugate transpose

^{T} Matrix transpose

A Wave amplitude

a WEC radius

c Phase velocity

c_g Group velocity

d Uniform linear array spacing

d_m Radial position of mth device

d_{mn} Distance between the mth and n^{th} devices

E Total wave energy

E_{ke} Kinetic wave energy

E_{pot}	Potential wave energy
$f_j(\theta)$	Far-field amplitude of the radiated wave-field from device j
g	Acceleration due to gravity $g = 9.81\text{ms}^{-2}$
h	Fluid depth
I	Mean of the interaction factor q over kL
i	$\sqrt{-1}$
I_β	Mean of the interaction factor q over β
I_{gen}	Mean of the generalised interaction factor q_{gen} over kL
J_m	m^{th} order Bessel function of the first kind
k	Wavenumber
K_m	m^{th} order Bessel function of the second kind
L	Linear array total length
N	Number of WECs in array
P	Average power absorbed by array over one wave period
p	Pressure
P_∞	Total power contained in the incident wave spectrum
p_a	Atmospheric pressure
p_d	Hydrodynamic pressure $p_d = -\rho\frac{\partial\Phi}{\partial t}$
p_g	Gauge pressure $p_g = p - p_a$
P_T	Targeted power contained in the incident wave spectrum
P_w	Power per unit width of the incident wave in deep water
P_{abs}	Average Power absorbed (non-optimal) by array
P_{opt}	Maximum average power absorbed by array
Q	Irregular wave objective function
q	Interaction factor
q_{gen}	Generalised interaction factor
r	Circular array radius

R, θ, z Cylindrical Coordinates

$S(\omega)$ Wave energy (frequency) spectrum

$S_\beta(\beta)$ Incident wave angle spectrum

s_j Consecutive WEC spacing between j^{th} and $(j+1)^{\text{th}}$ WECs

$S_P(\omega)$ Wave power spectrum

S_{B_j} Wetted surface of the jth body

t Time

x, y, z Cartesian Coordinates

Chapter 1

Background & Literature review

The literature on the modelling of wave-power devices is vast: ranging from the modelling of single devices, including investigations of their optimal shapes and control, to the interaction of arrays of different geometries. Varying levels of approximations are employed, each with their associated advantages, disadvantages and accuracies. The review presented herein is not intended to be an exhaustive summary of the total field but is instead a summary of information most relevant to this Ph.D. topic. Gaps that exist in the literature are highlighted and include those addressed in this thesis. A brief description of the concept of wave energy is given first, in Section 1.1. The types of wave energy converter (WEC) that have been invented, studied, developed and successfully deployed are summarised. The relevant literature concerning single WEC analysis and performance is summarised in Section 1.2, while WEC arrays are discussed in Section 1.3. Physical (wave tank) testing is discussed in Section 1.4 and the associated difficulties salient to WEC arrays are described. Finally, shortcomings identified by this literature review are outlined in Section 1.5 and some of those shortcomings that are to be addressed within this thesis are highlighted.

1.1 Introduction

1.1.1 Wave Energy Background: Why Wave Energy?

Energy and power generation have become a vital requirement of modern society, with demand increasing every year. As fossil fuels are becoming less

abundant and more costly in the long term, alternative sources of energy will be required. Furthermore, an energy source which has low environmental impact is more desirable. For society to rely on renewable energy, a diversity of resources are required for redundancy and to meet demand. Thus, a combination of wind, solar, tidal and wave energy would be ideal, though this is dependent on the resources available to a given location. Given Ireland's position near the Atlantic Ocean and the considerable wave resource available off the West coast, wave power is potentially one of the most promising and lucrative areas of renewable "green" energy.

Wave energy development is in its infancy compared to some other forms of renewable energy. It is an area that requires participation from several varied fields, including oceanography, mathematics and engineering, to solve the many problems associated with wave energy conversion. These problems include the design and construction of a viable device, capable of wave energy extraction and survival in a cost effective manner; the design of methods of either storing this energy or efficiently feeding it into the grid; the assessment of the wave energy resource available at particular sites; and the modelling and optimisation of device design, deployment and operation.

A distinction must be made between the resources of wave energy, hydro-energy and tidal energy. Hydro-energy is power extraction from a water flow, typically a river or a dammed lake. Tidal energy is that extracted from the tidal flow of the sea, usually near-shore or onshore, often in an estuary. Wave energy is where power is extracted from the undulation in the water surface due to the propagation of waves across the body of water. In this sense, the flow of water does not typically result in wave-power extraction, though some wave energy devices do utilise both water flow and wave undulation for power extraction.

Ireland's total wave energy resource is estimated at 525TWh per year by the Sustainable Energy Authority of Ireland (SEAI), although it is further estimated that only 21TWh of this could be feasibly accessed[1]. In 2015, Ireland's electricity consumption was estimated at 29TWh[2], so wave energy has the potential to provide a significant proportion of this requirement. Although electricity consumption has almost certainly increased since 2015, wave-power still has the potential to provide a large fraction of the Irish electricity

[1] Accessible Wave Energy Resource Atlas: Ireland: 2005. www.marine.ie (accessed July 2017)

[2] Energy in Ireland 1990–2015, SEAI report, 2015. www.seai.ie/resources/publications/ (accessed June 2017)

requirements. Similar arguments in favour of wave energy can be applied to many coastal countries and world-wide.

In 2009, the EU published its renewables directive (2009/28/EC), which sets the target that 20% of all energy consumed by the EU must be provided by renewable sources by the year 2020. This target was divided among member states, with Ireland committing to a 2020 target of 16% renewable energy. To attain this target, considerable investment has been made into renewable energy research of all forms, though primarily into wind. Ireland is one of the best positioned countries in the EU to harness wave energy, due to its direct access to the Atlantic ocean and the accompanying wave resource.

All energy sources originate from the sun, primarily in a form of solar power. The sun causes atmospheric pressure changes due to differential heating of the Earth's surface, creating weather systems, which give rise to wind. Wind action is the primary mechanism of the waves on the oceans. Therefore, it can be considered that solar power causes wind power, which in turn causes wave-power, as described by Lewis (2014). The important consideration is that as power is transferred down this path it becomes more concentrated, so that wave energy contains the greatest energy per meter of these renewable energy sources, typically $\mathcal{O}(10 - 100\ \mathrm{kW/m})$. This makes the harvesting of wave energy an attractive, albeit challenging, prospect.

The majority of this wave resource is located in the deep ocean, where waves are in a water depth greater than half the wavelength. Accessing this resource is a intimidating task, due to the difficulty of operation and maintenance of devices in the open ocean, far from shore. Survivability of the devices is also a concern; a WEC must be capable of absorbing power efficiently during average conditions while also being able to survive infrequent storm conditions. The cost of constructing a WEC is partly associated with the survivability of the device in peak storm conditions, while the income from a WEC is only from the mean conditions when the device is absorbing power. In this sense, the survivability of a WEC is a substantial barrier to achieving financial viability of wave energy, though this is only one of the many considerations. For example, cabling of the WECs to the shore also carries a considerable cost.

It has been accepted more recently that WECs need to be large in size or deployed in arrays of many small devices for wave energy sites to provide enough power to be economically viable. The latter requires consideration of the performance of the array as a whole, which is a much more intricate

problem than the performance of a single device. The interactions between array members can increase or decrease the power absorbed. The problem of array interactions is present in most forms of renewable energy; for example the park effect of reduced resource available behind a wind or tidal turbine. However, the interaction effect is much more complicated for WECs, as the wave field is affected in all directions around a single device and not just behind it, due to radiated and scattered waves.

1.1.2 Categories of WEC

The primary focus of wave energy research is the design of a device capable of extracting power from the waves and either storing this power or feeding it into the grid. Wind power has been studied extensively; the best method for extracting energy from wind has converged within the literature to the wind turbine. The design of wind turbines has also been optimised, though it is acknowledged that there are many varying types of optimisation and corresponding wind turbines. Conversely, there is a large variation in the design of wave energy devices under consideration and these vary in power extraction (interface) method, mooring, power take-off (PTO) and specific device designs. Although some current prototypes show considerable promise, a standard WEC has not yet been agreed.

Most of the WECs under development can be divided into two main categories: floating or submerged. These devices can be fixed or freely floating and are further categorised by the interface elements, i.e. how the devices interact with the waves, and by the PTO. Some other devices are also built fixed into the shoreline or a breakwater. The principal classes of devices are listed below corresponding to the interface elements employed; the corresponding PTO is also discussed. Examples and diagrams of some current devices are also provided.

1.1.2.1 Overtopping Devices

An overtopping device is one which uses the elevation of wave motion to fill a reservoir, from where the water is released to sea level through a low head hydro-turbine PTO to generate electricity. In this way, these devices essentially absorb the potential energy within the waves. Many such devices employ ramps

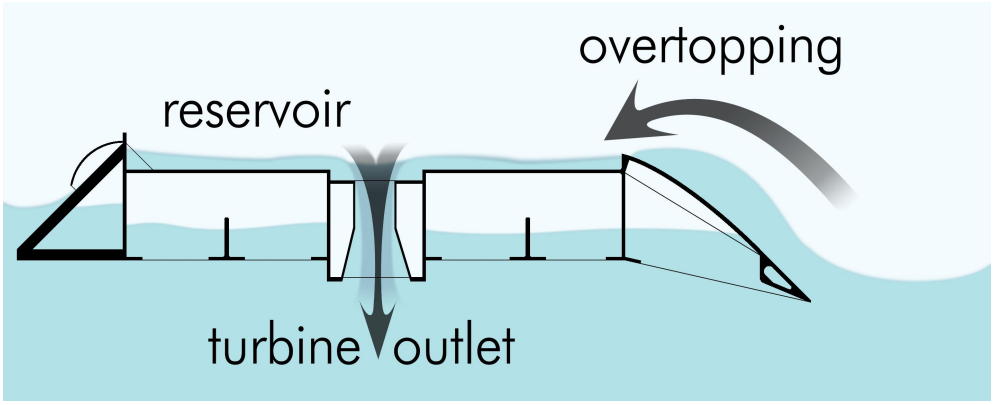

Figure 1.1: Diagram of the operating principle of an overtopping device. Source: www.wavedragon.net

which help to direct the water into the reservoir and thus can capture extra water and hence extra energy. Therefore some of the kinetic energy of the waves is also absorbed. This method of wave-power absorption is shown in figure 1.1. Ramps make use of a phenomenon in waves called wave shoaling. As the waves hit the ramp, they enter shallower water which causes an increase in wave height, thus allowing more water to be captured in the reservoir. These are atypical wave energy devices in the sense that they extract power from a water flow rather than oscillations in the PTO. Overtopping devices are either fixed or floating on the water surface.

A current example of such a floating device is the Wave Dragon[3]. This device is built with directing arms, which direct the waves towards the ramp and into the reservoir using wave reflection. This device has been tested from small- to large-scale, including 1:50 scale tests at the Hydraulics and Maritime Research Centre (HMRC) in University College Cork (UCC). It was involved in several full scale test deployments, including a 7MW demonstrator device in Wales and a 50MW farm near Portugal, though the prototype was scrapped in 2011. An example of a fixed overtopping WEC is the Tapchan[4] (short for "Tapered Channel"), which is built onshore into the coastline and operates on the same principles as described above. The Tapchan WEC has the advantage of being entirely onshore, thus reducing the cost associated with operation and maintenance.

[3]www.wavedragon.net (accessed June 2015)
[4]https://taperedchannelwaveenergy.weebly.com/ (accessed September 2017)

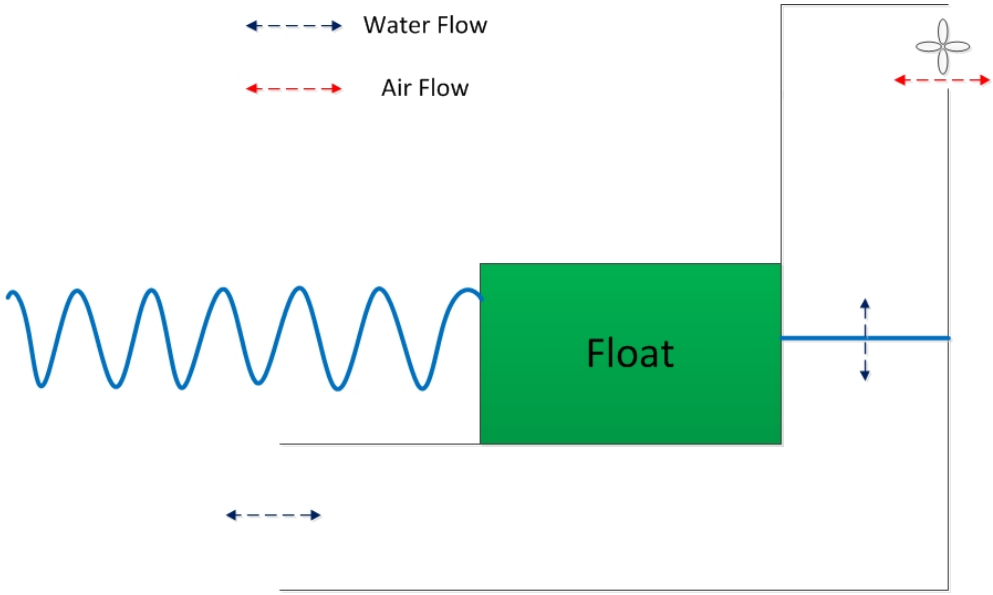

Figure 1.2: Diagram of the operating principle of a floating OWC WEC

1.1.2.2 Oscillating Water Column (OWC)

An oscillating water column WEC contains an internal chamber, within which is a volume of water beneath a volume of air. When waves are incident onto the device, the wave motion causes the internal water surface to oscillate vertically, which in turn compresses and decompresses the air above it. An opening in the air chamber, which contains the PTO in the form of a self rectifying air turbine, allows the air to escape and enter through this turbine, thus generating electricity. A self-rectifying turbine is one that rotates in the same direction regardless of the direction of air flow, so that energy is generated both when air is escaping and being sucked back into the chamber. These WECs can be built as fixed devices as part of a breakwater or into the coast; however, recent research has concentrated on floating OWC devices. A basic diagram of the operation of such a floating OWC WEC is shown in Figure 1.2. The mathematical modelling of such WECs is relatively complicated due to the combination of hydrodynamic and aerodynamic domains, as well as the compressibility of the air which results in thermodynamic effects.

The OWC concept was first used to power self-sufficient navigation buoys by Masuda in the late 1940s, which are still in place today. This was later studied and optimised as a means of power extraction for onshore consumption. One of the first OWC prototypes designed specifically for wave power extraction with a view to general consumption was built in Islay, Scotland in 1980. In 2000, a second OWC prototype built into the Islay coastline, named the LIMPET

(Land Installed Marine Power Energy Transmitter) device. This device successfully extracted power from the waves and fed this into the grid, though the parent company WaveGen was closed down in 2013 and this device has ceased operation. One of the largest prototype OWCs was the OSPREY which was built in 1995 and intended to be sunk into place at a site off the Scottish coast. However, it was destroyed by the waves shortly after being towed to the desired site. Another example of a fixed OWC WEC is the Pico plant built in the Azores in Portugal in 1999 which is still in operation today. One problem with fixed OWCs is the relatively few locations they can be built and the high cost of construction. Currently, it is only financially viable to build such a device if a breakwater is already being constructed, primarily due to the high cost of concrete construction.

More recently, there has been a renewed focus on floating OWC devices as one possible means of wave energy extraction. These devices operate in a similar manner to their fixed counterparts, with the advantage of cheaper construction costs (less concrete) and the ability to be placed in more locations. In some cases, they can be controlled to absorb more power than their fixed counterparts. There are many prototypes of floating OWC WECs, one such example is the Ocean Energy Buoy (OEBuoy)[5]. This device was tested at model scale (1:50) in UCC at the HMRC and also at 1:4 scale in Cork Harbour. This device is still in development with the current phase concentrating on the testing of near commercial scale prototypes.

1.1.2.3 Floats, Flaps and Hinges

Another class of WEC is one that uses the motion of the waves to move some or all of the device; this movement is then used by the PTO to generate power. As suggested by the subsection title, this type of device can be split into three categories, namely float, flap and hinge devices. These devices can be free-floating or submerged.

Flap devices operate such that the wave action forces the movement of a flap, which in turn generates electricity. One of the most well known WEC concepts of this type is the Salter Duck, designed by Stephen Salter in the 1970s. This device is a pear shaped floater, which is rotated by the action of the waves. Power is taken off through this rotational motion and converted to electricity by

[5] oceanenergy.ie (accessed July 2016)

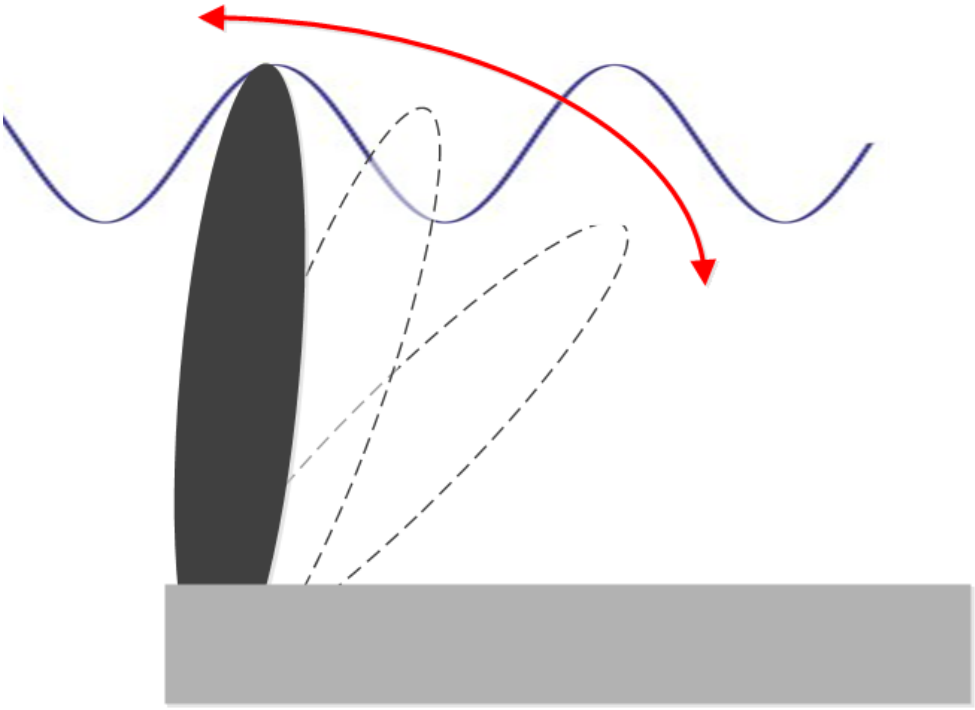

Figure 1.3: Operation of a flap type device, e.g. Aquamarine Oyster

a generator. Construction and testing of the device was very costly and funding for the study of the device was subsequently cut in the 1980s. Thus, no large scale devices of this type have be produced on a commercial scale.

A well known commercial device in this category is the Aquamarine Oyster[6]. This device uses the action of the waves to drive the flap, which in turn drives a pump to drive water to an onshore power generation plant. One disadvantage of this device is that it is almost completely underwater, making deployment, repairs and maintenance difficult and expensive. However, one major advantage of this WEC is that it operates in shallow water near shore, which reduces the costs involved.

A hinge type device is one which uses the wave-induced motion of one part of the device relative to another section of the device, to extract power via the joint. This joint contains the PTO, which is usually a hydraulic pump generator. The principle of operation of these class of devices is illustrated in Figure 1.4.

The most successful and advanced device of this type is the Pelamis device, particularly the P2 prototype[7]. It should be noted that this device is considered to be a second generation device, intended for near shore deployment. This

[6]http://www.aquamarinepower.com/ (accessed July 2015)
[7]www.pelamiswave.com/ (accessed June 2015

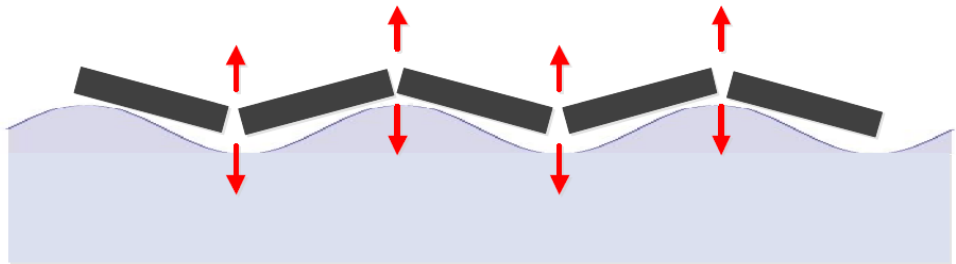

Figure 1.4: Operation of a hinge type device, e.g. Pelamis

prototype was tested at a site in Orkney, Scotland and gave promising results. The next step would be to test arrays of these devices; it was hoped that this would be accomplished at the WestWave project site off the west coast of Ireland in the coming years. However, Pelamis wave-power went into administration in November 2014.

The class of device that is employed in this thesis is the float type device, which is moved by the action of the waves and extracts power either using an internal reference power generation system or via the mooring using a sea-bed mounted linear electric (electromagnetic) generator. In principle, floats can operate and withdraw energy in any of the six degrees of freedom, although most devices are constrained to move in only one mode and extract power from this one mode. Some devices can extract in multiple modes but usually at most two. Complications arise with construction, modelling and testing of WECs that can extract power in multiple modes. The majority of float WECs under development are axisymmetric, as this simplifies their construction, modelling and operation. This also allows a single WEC to perform analogously for all incident wave directions, though it should be noted that this is not true for arrays of such devices. Most float WECs operate in either heave, surge or both. Only float type devices that operate in heave are considered herein, such as shown in Figure 1.5.

One example of real devices of this type is the WaveBob[8] WEC, which operates in heave. This device underwent considerable scale tests, including 1:50 scale tests at the HMRC in UCC and 1:4 scale tests in Galway Bay. However, due to financial difficulties, WaveBob was closed down in 2013.

[8]https://en.wikipedia.org/wiki/Wavebob (accessed August 2017)

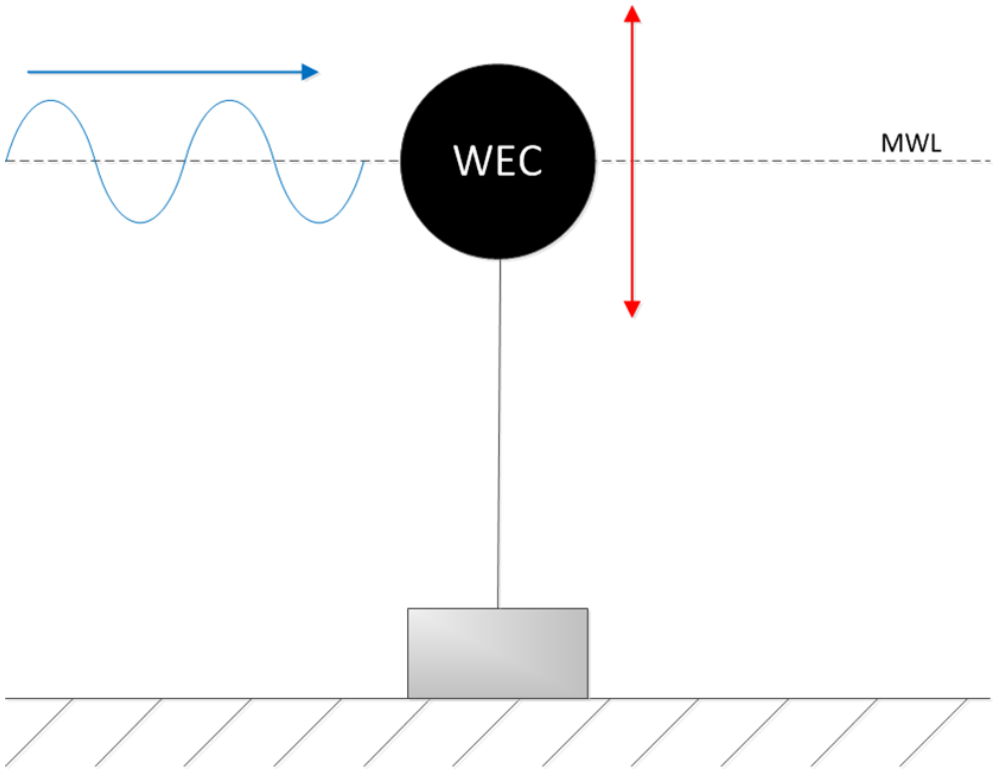

Figure 1.5: Diagram of a heaving point absorber WEC

1.1.2.4 Other Methods of Wave-Energy Extraction

There are a myriad of different types of WEC under development, each with different types of PTO and a discussion of all designs is not attempted. Some of the methods of wave energy extraction are atypical and so this section discusses a selection of some of the more well known WECs that are not covered by the preceding sections.

One such device is the Lancaster Flexible Bag WEC. This attenuating device operates by allowing a variable width along its length. The wave motion acts upon the device and forces a fluid contained inside the WEC (air or water) through a turbine to generate electricity. There are many variations on this concept, with different designs, internal content and forms of PTO.

The same broad concept is utilised by a similar device currently under development by Checkmate SeaEnergy, named the Anaconda. This is a long snake like device consisting of a water-filled rubber tube. It is faced into the oncoming wave and the differential wave forces across the WEC causes localised squeezing and enlarging effects, which drives the internal water from one end of the device to the other. A combination of valves and turbines are then utilised as the PTO from this water flow. This device has undergone physical testing at

the 1:30 scale at the Danish Hydraulic Institute (DHI). The development of a sub-scale sea trial prototype is currently underway.

1.2 Single WEC Analysis & Performance

This section presents the relevant literature on the modelling of single WECs and their performance. The extension to arrays of devices is considered in Section 1.3. An understanding of a single device performance is vital before an attempt to understand array behaviour is made. A number of aspects of the analysis of a single WEC are discussed, beginning with the hydrodynamic parameters of the given device in Section 1.2.1. A discussion on the shape of a WEC is given in Section 1.2.2.

1.2.1 Hydrodynamic Coefficients

Some of the earliest work on oscillating devices in a fluid, and their application to energy extraction, is by Masuda in the late 1940s. The earliest work concerning heaving point absorber spherical WECs is that of Havelock (1955). This is the earliest work related to the present strand of wave-energy research, as it considers the motion of the fluid due to heaving oscillations of a semi-submerged sphere in deep water. A representation of the velocity potential due to the small heaving motions of the sphere is obtained. This is comprised of an infinite series of wave free potentials, a cylindrical radiating wave term and a source term, where the coefficients of the series are given as solutions of an infinite system of equations. This series representation, and the corresponding system of equations for the coefficients, can be truncated so that a solution can be attained numerically. The order of truncation chosen does not appear to greatly affect the result. It is shown by Hulme (1982) that the series representation of the velocity potential and the system of equations for the coefficients are well behaved, so that increasing the order of the system increases the accuracy of the solution very slowly.

There are two primary coefficients from the cylindrical wave term in this description, denoted as $\mathcal{C}$ and $\mathcal{D}$, which are the Havelock coefficients. The values of $\mathcal{C}$ and $\mathcal{D}$ are dependent on the radius of the sphere non-dimensionalised with respect to the wavelength. The added mass and damping of an oscillating sphere can be determined using the Havelock coefficients. These are the components of

the radiation force that are in phase with the body acceleration and velocity respectively, which are important for power absorption and array analysis.

The radiation and scattering of water waves by a heaving submerged sphere is also considered by Linton (1991). The corresponding sway problem is also considered but this is not relevant to the present work. Havelock's approach was extended by Linton (1991) to finite depth. The potential was expressed as a multipole expansion with unknown coefficients. This gives an infinite system of equations, which can be solved numerically following truncation. It was found that truncation from an infinite system to an $N \times N$ system, with $N = 4$ was sufficient to provide results accurate to three significant figures. Expressions for the added mass and damping, including dependence on the depth, were obtained and studied for variations in sphere radius and water depth. The immersion depth to radius ratio was kept fixed such that the WEC was fully submerged. It was found that the nearer the sphere was to the sea bed the greater the added mass for the heave radiation problem. It was noted that the added mass results obtained by Linton (1991) can be viewed as deviations of the infinite depth case. The scattering problem for the submerged sphere was also solved by Linton (1991) via multipole expansion. The effect of reducing water depth was to decrease the vertical force and to increase the horizontal force. A far-field approximation to the scattering problem is also presented and compared to the exact solution, with good agreement found for large enough distances away from the device.

1.2.2 Shape of WEC

Following Section 1.1.2, there are many types of WEC and within each broad class of device there will be variation in design. Therefore, the shape of the device can vary from developer to developer. This poses the question: what is the best shape of WEC? The hydrodynamic effect of the shape of the device is certainly significant but there are other factors which may affect the shape of a good device, such as design and construction difficulties, financial constraints, stability of the performance of the device, lifetime and survivability of the device.

An early study into WEC performance due to its shape and design is by Thomas & Gallachóir (1993). A single Bristol Cylinder WEC is considered and a numerical optimisation is performed over the design parameters of the device,

namely the device radius, submergence and specific gravity. The aim was to match the efficiency curve of the device to a given wave spectrum. This was achieved and the optimised device attained a power absorption level of 85.2% of the available resource, with the device performing well across the entire frequency spectrum considered. However, the optimal design parameters resulted in a large radius, which increases the construction costs, and a low submergence, which increases the exposure to large waves thus affecting survivability. It was noted that the specific gravity did not have a large influence on the WEC performance, which may be important as lighter devices would result in larger mooring forces. The results are highly dependent on the spectrum considered and also the targeted portion of this spectrum. This optimisation method is not restricted to the Bristol Cylinder and can be applied to other WECs; further details are given by Thomas (2008).

Another preliminary study into WEC performance due to hydrodynamic effects of the shape of a device is that of Alves, Traylor, & Sarmento (2007). In this work, a buoy which absorbs power in heave with its PTO attached to the sea bed is considered. An attempt to optimise the shape with respect to the power absorbed is made using a boundary element method (BEM) numerical code. The buoy is initially considered to be a vertical circular cylinder, which is then transformed into two components: an upper component called the "surface buoy", which crosses the free surface; and a submerged component, called the "submerged mass", placed deeper in the fluid.

The aim of Alves *et al.* was to design a surface buoy with high hydrodynamic damping (and thus high power absorption) and a submerged body with correct mass to tune the system resonance to a desired frequency, while avoiding damping of the surface buoy by placing it at a sufficient depth. Several shapes are considered for both upper and lower buoys, including cylindrical, conical and spherical. It was found that a large increase in the mean power can be achieved by significantly reducing the cylinder volume and submerging the remaining volume. This has the effect of increasing the hydrodynamic damping and added mass, which thus increases the power absorbed. It is recognized by Alves *et al.* that having a large submerged volume at a significant depth will create engineering difficulties and financial costs.

It should be noted that the design of the WEC was quite specialised and the optimisation considered was only partial, as only five different shapes for the submerged mass were considered. Thus this can be considered as more of a case

comparison rather than a full optimisation. Furthermore, some of these shapes considered may result in significant viscous effects in a real fluid, which would negatively affect performance.

A more detailed investigation into the optimal shape of the interface element of a WEC is contained in McCabe, Aggidis, & Widden (2009), McCabe, Aggidis, & Widden (2010) and McCabe (2013). The first two papers describe the optimisation of a surge and pitch wave energy device, while the third considers just a surging device. In all three cases, the optimisation is performed via a genetic algorithm (GA); this is a metahuristic optimisation procedure, where the search space of possible solutions is investigated in a random manner in an attempt to find a close to optimal solution. A parametric description of the WEC geometry is employed, based upon bi-cubic B-spline surfaces generated from several vertices, whose coordinates are the variables of the GA optimisation. A detailed description and application of GAs can be found in Mitchell (1998).

Two types of WEC symmetry are enforced in McCabe *et al.* (2009) and McCabe *et al.* (2010) to reduce the variable space of the problem. The most general of these is a unisymmetric WEC, with symmetry about a horizontal axis, while a stricter case also considered symmetry about both a horizontal axis and a vertical axis. A simple objective function was first devised, which was proportional to the power absorbed by the WEC (P) and inversely proportional to the amplitude of the wave (A), the surge velocity amplitude (U) and the submerged volume of the device ($\mathcal{V}$), so that the objective function was of the form $\frac{P}{AU\mathcal{V}}$. In this way, small power absorption, large velocities/amplitudes (which violate linear theory and present engineering difficulties) and large device volumes (which increase production costs) are all penalized. The WECs considered were investigated in a regular wave regime.

Using the GA strategy, over half a million shapes were investigated by McCabe *et al.* (2009, 2010), with only eleven performing better than the benchmark cuboid shape. This suggests that the search space is largely populated with poorly performing solutions. The best shape discovered was unisymmetric, with a bulbous body and wings that slope backwards from the bottom up. It was recognized that this is merely a preliminary optimisation and that the shapes discovered need to be analysed with regard to a more detailed hydrodynamic critique identifying the actual power absorbed, thus assessing the validity of the cost function employed. For example, the benchmark cuboid shape and any

optimal shape with sharp edges would perform poorly in viscous flows, which is not accounted for.

A more specific device is considered by McCabe (2013), which is unisymmetric and operates in surge only. The WEC is optimised using three different cost functions within the GA, which are distinguished by the severity of penalty placed on displaced volume. The optimum shapes obtained were compared to benchmark "box" shapes of the same volume.

For the first cost function, which imposed no penalty on device size, it was found that the best shapes returned were largely hemispherical and relatively large (approximately 3100 m^3 to 3500 m^3). In most cases, these shapes performed poorer than the benchmark box shape of same volume. For the cost function which imposed the greatest penalty on device volume, devices which exhibited pronounced asymmetry in direction of wave propagation, with pointed prows and sterns, were obtained. These devices were considerably smaller than those obtained for the first cost function, with volumes between 250 m^3 and 350 m^3. They also performed considerably better than the benchmark shapes. The results obtained for the second cost function represented an intermediate case between the other two. Overall, McCabe (2013) found that the different cost functions have a far greater impact on the optimum shape obtained than either displacement or power constraint. It was also discovered that the optimum device shapes performed increasingly better than the benchmark box shapes as the volume decreases.

One of the major weaknesses of this shape optimisation is that the model does not account for viscosity, yet some of the optimal shapes obtained involve sharp edges or points. It has not been established that these shapes would perform well in real viscous fluids, where vortex shedding and other viscous effects would play a significant role. Furthermore, even in the inviscid regime, it may be that the optimal shapes only perform well for a very specific set of wave conditions and may be sensitive to changes in wave parameters.

An example of the optimisation of a heaving WEC is the work of Goggins & Finnegan (2014). This work considers the optimisation of the shape of a heaving WEC, in terms of average annual power absorption, for a given wave energy spectrum. The shape is optimised by considering five shapes, namely a truncated vertical cylinder, a half immersed sphere, a truncated cylinder with a hemispherical bottom, and two other shapes comprised of a truncated cylinder with different shapes attached to the base. The optimisation of device shape is

then performed by maximising the significant velocity of the device with respect to the device shape and the device radius. This objective function is related to the response amplitude operator (RAO) of the device. Thus it matches the device motions with the incident wave spectrum, while avoiding slamming by limiting the maximum value of the RAO. One weakness of this objective function is that it does not directly optimise the power absorbed of the device, but rather a quantity upon which the power absorbed is dependent. A further calculation is then needed to assess the power absorbed relative to the PTO damping coefficient.

It was found that the best shape overall was a cylinder with hemispherical base, with a draft to radius ratio of 2.5 and with a radius of between 8m to 10m. This device shape is also used in the numerical and physical tank tests of Stratigaki (2014). Another good reason for this choice of shape, compared to say a truncated cylinder, is that the hemispherical base has the effect of reducing vortex shedding and other viscous effects at the corners of the cylinder. It would also be a closer approximation to the shape of real devices, as opposed to a sphere or cylinder which are modelling idealities. However, analytical hydrodynamic modelling of a cylinder with hemispherical base is relatively complex.

Unfortunately, the literature contains little research into the optimum shape of a heaving wave energy device. This is perhaps because there is a general acceptance within the literature as to the best shape of a heaving WEC, that being symmetric about the vertical axis, and having a spherical waterplane area. As a result, most heaving WEC research considered devices which are either spherical or vertical circular cylindrical in shape, or a combination of the two. The former is examined within the work of this thesis.

1.3 WEC Array Analysis & Performance

Having reviewed the relevant literature regarding a single WEC, the extension to farms or arrays of devices can now be made. Modern wave-power devices are usually envisaged as being either a single large device or an array of smaller devices. The benefit of an array, in comparison to a single device, is that the individual components are relatively inexpensive to repair and replace. The hydrodynamics of an array of WECs is more complicated than that of a single device, due to interactions between the devices, which can lead to constructive

or destructive interference of the wave-field and thus increasing or decreasing the power that can be absorbed.

The interaction between devices intended to extract other forms of renewable energy is conceptually simpler than for wave energy. For example, tidal and wind energy devices leave a decreased resource available in their wake which is to be avoided, though turbulence and viscous effects also result in considerable challenges for wind and tidal arrays. However, the wave-field caused by the motion of wave energy devices is omnidirectional, not just in its lee. Therefore, the modelling of this interaction and specifically the optimisation of the layout of an array is much more challenging. A control and arrangement strategy which makes use of the constructive effect and minimises the destructive effect is desirable, thereby increasing the efficiency of an array and the power generated to obtain maximum benefit. It should be noted that although the destructive effect of the array can be minimised, it cannot be removed entirely. Early studies of these types of control strategies attempted to maximise the constructive effect. However, the importance of minimising the destructive effect is recognised in more modern studies.

1.3.1 Investigation of Basic Interaction Effects: Small Arrays of Less Than Four Devices

Before arrays of many devices are investigated, smaller arrays of only two or three devices should be considered to gain an understanding of the basic interaction between the devices. The simplest case of two devices will give a clear picture of the effect that device 1 has on device 2, and *visa-versa*, without the complications of interactions to and from other devices. This practice of investigating the interaction between two devices is not common in the literature on theoretical modelling of WECs, though it is often performed in physical modelling tests, in wave tanks and flumes.

To assess the influence of interaction between array members, the array performance is often compared the performance of an isolated WEC. The interaction factor is introduced and defined as a measure of the ratio of the performance of the array to the performance of the same number of isolated devices. Thus, an interaction factor of unity indicates no net interaction, while values above and below this correspond to constructive and destructive interference respectively. This quantity is often employed within the literature

as an objective function or as a means of assessing array performance.

The work of Folley & Whittaker (2009), which employs the point absorber approximation, considers an array of two hemispherical devices of 10m diameter in both attenuator (parallel to incident wave direction) and terminator (perpendicular to incident wave direction) arrangements, before looking at arrays of more devices. For optimal two-WEC arrays, it is shown that mis-tuning of greater than 8% in terminator arrays and 3% in attenuator arrays is sufficient to cause destructive interference in the array. This is important since most tuning of WECs is expected to be real tuning, where the reactive force applied is sub-optimal. It should be emphasised that these results are obtained using the point absorber approximation and it was acknowledged that the calculated motions of the WECs using WAMIT differ slightly to the point absorber calculations. Thus the point absorber approximation may not have sufficient accuracy in some situations, particularly for the attenuator array mistuning result.

In the absence of reactive energy control, it is shown that the two-device array interaction factors remain close to unity for a large variation in incident wave period. It is also shown that the imposition of WEC motion amplitude constraints will affect attenuator arrays more than terminator arrays, due to the relatively large motion amplitudes attained by devices in the attenuator layouts.

A detailed investigation into the effect of distance on the interaction between two devices was conducted by Babarit (2010). Arrays of two semi-submerged cylindrical devices, with a diameter and draught of 10m, which operate in heave with an idealised PTO are considered. The interaction between the devices is assessed by a modified interaction factor, defined for one device in an array as the difference between the power absorbed by that device and that absorbed by an isolated device, divided by the maximum power absorbed by an isolated device. This was used because it gives better assessment of the power absorbed, in comparison to the standard definition of the interaction factor which only assesses the interaction and hides the real amount of power absorbed. The effect of separation on array performance was investigated for distance ranges up to 20km, for both regular and irregular waves.

For regular waves, it was found that the effect of the interaction decreased in proportion to the square root of the distance between the devices. It was shown, for arrays in regular waves, that interaction effects remain at approximately 5-15% even at distances of 2km. For the majority of cases, it was also shown

that the angle of incidence does not greatly effect the performance for large separation distances of over 1km.

For irregular waves, Babarit found that interaction effects had less of an impact on array performance, although this effect was still significant. Over a yearly average, it was seen that constructive and destructive effects tended to compensate. The interaction effects for irregular waves were found to decrease faster with separation when compared to regular waves and were reduced to less than 10% for separations of more than 400m. Therefore, it was suggested that it is reasonable to neglect interaction effects, within irregular analysis, for device separations of greater than 500m. Strong interaction effects were present in all cases investigated for separations under 100m and thus should be carefully considered for these separation distances. For intermediate separations of between 100m to 500m, no recommendation as to the neglection of interaction effects can be made, as it depends strongly on the device type, array configuration and incident angle.

The optimisation of small arrays of three and five devices is performed by Fitzgerald (2006). An interesting result of this work is that the optimal five-device arrays found often contain the same arrangement of one or more of the optimised three-device arrays (or combinations of them). Fitzgerald goes on to suggest that there may exist certain "base" optimal 3 device arrays from which all optimum arrays would be constructed. The work of Fitzgerald (2006) is discussed in more detail in Section 1.3.3.

1.3.2 Investigations of Arrays of Four or More Devices

The earliest work to consider the modelling of groups of devices intended to absorb wave-power was by Budal (1977). Using linear wave theory, it was shown that all incident power on a linear array can be absorbed if either:

1. the devices operate in two modes of oscillation, or
2. two linear parallel rows are used.

This holds in spite of considerable gaps that may exist between the devices. Although these results were presented for a linear array (or linear rows), the theory is also valid for a general array geometry. It should be noted that the array is essentially modelled as an infinite array, where all WECs behave the same and any edge effects are neglected. A measure of the effectiveness of

placing devices in an array, compared to placing them in isolation, was also introduced in this paper. This was the first use of the interaction factor (or q-factor) and gives the ratio of the maximum power absorbed by the N-device array to that absorbed by the N devices in isolation. A small body/point absorber approximation was employed such that the devices were assumed to be small compared to the distance separating them; this required that the far-field waves generated by the devices were not affected by the presence of other devices. Thus it assumed that the devices do not create a diffracted wave-field and the interaction is described by the incident and radiated wave-fields only.

In deriving an expression for the q-factor, Budal made the assumption that all devices in the array oscillated with the same amplitude and then maximised the power absorbed. It is a very restrictive assumption which, in general, is not true (c.f. equations (2.163) and (2.162)). This was shown by Evans (1979) who presented a corrected version of the interaction factor without the assumption of equal motion amplitudes. It was also shown that the amplitude of oscillation of each WEC depended on the exciting force and damping coefficient of the device, which in general are not equal for all array members. Evans also considered devices possessing an elongated "thin ship" geometry, with the intuitive idea that heaving motion of these devices would create a beaming of waves along a line perpendicular to the incident wave.

The radiation of plane waves from an finite number of infinitely long rows, for arbitrary angle of incidence, was considered by Falnes & Budal (1982). The bodies in each row are assumed to be identical. Each of the bodies can oscillate in all six modes of motion. It is shown that plane waves emit in certain directions due to constructive interference between the devices and are quantitatively related to the circular waves radiated from each individual body; these plane waves emitted from the array are referred to as plane wave "rays". A relation between the amplitude of the radiated plane wave and the far-field coefficients of the individual bodies is derived. The maximum absorbed power was shown to occur when the optimum phase of the oscillating velocity is approximately equal to the phase of the excitation force.

The maximisation of the absorbed power with no constraints was also investigated and it was shown that, for four parallel rows of heaving point absorbers, 100% power absorption is possible with the interspacing between rows is larger than the wavelength. Cancellation of the radiated plane wave rays is necessary to obtain 100% absorption, as the power emitted in these rays is

lost to the far-field and not absorbed. It is also shown that if the interspacing between the bodies in each row is greater than one wavelength that at least four rows are required to absorb 100% of the incident power, and that greater spacings between bodies require greater number of point absorbers in each group to maintain 100% absorption.

This paper shows that 100% wave-power absorption is possible, in principle, for arrays of heaving point absorbers and that this can be achieved despite large gaps that may exist between the WECs. However, optimal unconstrained motions are assumed which may not be physically implementable in practice. Furthermore, the arrays considered are essentially infinite arrays where the WECs all behave the same and any edge effects are ignored.

The above work by Falnes & Budal (1982) was extended by Falnes (1984), where it was shown that all incident power may be absorbed by an infinite array provided that the total number of oscillation modes in each group is greater than or equal to the number of plane wave rays that would be radiated from the array. The number of oscillating modes in a group is the number of devices in the group multiplied by the number of modes in which they operate. It was also explicitly shown that a condition for maximum power absorption is that the intensity of all the radiated rays tend to zero. The number of oscillators in each group must increase with the interspacing of these groups if 100% absorption is to be maintained. It should be noted that this analysis was for unconstrained oscillator amplitudes.

A study of the interaction of waves with submerged spheres was undertaken by Wu (1995), where a multipole expansion was used to analyse wave diffraction and radiation by an arbitrary group of spheres. Four cases are considered:

- a single sphere of radius a
- two such spheres separated centre-to-centre by $4a$
- a square array of four such devices, of length $4a$
- arrays with the spheres spaced uniformly on a circle of radius $4a$, thus creating a triangle for three spheres, a square for four, a pentagon for five *etc.*

In each configuration, the spheres were completely submerged with a sphere centre to surface distance of between $1.5a$ and $2a$. Truncation of infinite sums to finite sums within the multipole expansion was required to provide numerical

results.

The added mass, damping coefficient, exciting force and drift force were calculated for each array layout and for each mode of motion (surge, sway, heave). Note that the drift force first appears at second order, at which point it depends only on first order terms. These quantities are presented for one sphere in each array only but are due to the entire configuration. The drift forces are calculated with the spheres held stationary. A comparison of the results obtained with those derived from far-field equations showed excellent agreement, giving a verification of the results. An important finding was that the effect of interaction on added mass and damping is greater than that on the excitation force. The drift force was also seen to be influenced by interactions, but the force itself was quite small. The total heave drift force on the array was found to be approximately equal to the force on an isolated sphere multiplied by the number of spheres; this suggested that there is little effect on the heave drift force due to interaction.

A preliminary comparison of the point absorber approximation, the wide-spacing (plane-wave) approximation and an exact interaction theory was presented by McIver, Mavrakos, & Singh (1996), which was then extended by Mavrakos & McIver (1997). These studies consider uniform and unequal linear arrays of five truncated vertical circular cylinder WECs in a finite depth regime, where the depth was taken to be eight times the cylinder radius. It was found that, for most non-dimensional wave-numbers of interest ($0.1 \leq ka \leq 0.8$, where a is a device radius), the point absorber approximation was in agreement with the exact theory for the geometries considered. However for $ka > 1$, the point absorber method proved to be less accurate; this is to be expected, since the point absorber approximation essentially assumes a small body with $ka \ll 1$ and $ka > 1$ clearly violates this. It is perhaps surprising that the range of validity of $ka \ll 1$ extends as high as $ka = 0.8$.

The plane wave method is a large spacing approximation and assumes that the device spacing in regular waves is much greater than the wavelength. This allows evanescent modes to be neglected and non-planar outgoing (radiated) waves to be approximated as plane waves. The method is advantageous as it may be used to calculate all relevant hydrodynamic quantities (such as exciting forces and added mass) not just the power absorbed, as is the case with the point absorber theory. The plane wave method produced values for the excitation forces and added mass that were in excellent agreement with the

exact theory. However calculation of the interaction factor using this method led to difficulties for long wavelengths, since the required damping matrix becomes singular in this range. This is expected: the plane wave method assumes large non-dimensional spacing, while long wavelengths result in small non-dimensional spacing, thus violating the assumption. Therefore, the plane wave method performs best for short wavelengths.

Justino & Clement (2003) studied three types of arrays, each containing five submerged spherical devices which can oscillate and absorb power via heave, surge and/or sway modes. The three array configurations were terminator (uniform linear array in beam seas), attenuator (uniform linear array in head seas) and cross (four devices at the vertices of a square with one in the middle). The influence of spacing upon performance was also investigated. The BEM program AQUADYN was used to calculate the hydrodynamic coefficients for the arrays and thus assess the power absorbed (relative to isolated devices) and the interference effects. It was found that the power absorbed was highest for the terminator array for separation-to-wavelength ratio of 0.8. However, large device velocity amplitudes were obtained for the optimal cases, thus violating the underlying linear wave theory and the numerical method.

A square array of four circular cylinders was investigated by Cruz *et al.* (2009) for both regular and irregular waves. Devices that absorbed energy in surge or heave were considered within a regular wave regime but only heaving devices are considered in irregular waves. Linear wave theory was used and the hydrodynamic coefficients and exciting forces found using the BEM software WAMIT. The BEM results were compared with semi-analytical models to ensure validity, with good correlation except at large wavelengths. An analysis of a more complicated geometry and multi-body WECs is much more difficult using semi-analytical methods, showing the advantage of BEM solutions. The interaction factor for an array of surging and an array heaving WECs was investigated and optimal parameter values were identified. Peaks along intermediate incident wave angles were noted and attributed to near trapping, as the array configuration is changed from square to diamond.

The performance of a single WEC in irregular waves was initially considered and then extended to the study of an array. The isolated device was taken to have sub-optimal damping settings, so that large motions were avoided and a realistic estimate of performance was obtained. It was found that the heaving cylinder was very sensitive to changes in peak frequency of the sea state, with a narrow

range of noticeable response. Since the WEC is axisymmetric, the wave angle variation had no effect on the single device but did affect array performance. The interaction factor is calculated for irregular waves by comparing the power absorbed by the array in the given sea state to the analogous power absorbed by a single cylinder in the same sea state. It was found that the values of the interaction factors of the array ranged from 0.92 to 0.98 for different sea states. Finally, an assessment of the values of the damping coefficient on each WEC was made and good performing values were identified. Although the configuration investigated was relatively simple, the results obtained were substantial and demonstrated the value of a well-planned preliminary investigation.

Garnaud & Mei (2009b) compared an array of smaller buoys to a single larger device, with the array analysis including both radiation and scattering effects. The device investigated is a heaving truncated vertical circular cylinder. It is confirmed numerically that the maximum capture width[9] for a single heaving buoy of any size is $\frac{1}{k} = \frac{\lambda}{2\pi}$, where k is the wavenumber and λ is the wavelength, agreeing with previous literature. This occurs at resonance, when the wavelength is of the same order as device radius. However, a buoy with a radius of the order of 100m-200m may not be feasible from an engineering or financial perspective. The resonance bandwidth increases as device size decreases, which suggests possible advantage of smaller buoys. However, it is not possible to have both low resonant frequency and large bandwidth, without adding a sophisticated control system to the PTO.

Arrays of many small buoys are then considered and modelled using the perturbation method of multiple scales to reduce computational effort. The number of buoys is not explicity included in the model, which considers the area fraction covered by the buoys relative to the array area; the specific examples investigated consider circular arrays of three buoys. Using this analysis, the kinematic and dynamic boundary conditions on the buoy bottom are combined to give an averaged boundary condition for the array. The averaged condition is a weighted sum of the condition on the bottom of a buoy moving in harmonic motion plus that on an unoccupied free surface, weighted by the fraction of solid matter within the array. It is shown that gathering many point absorbers close together in a compact array increases the number of degrees of freedom of the system, which can be advantageous to power absorption. By comparing arrays of this type to large buoys containing same volume, it was discovered

[9]The *capture width* is defined as ratio of mean power absorbed to the mean power per unit crest wave width of the incident wave

that greater energy was absorbed over a greater frequency band by the array. This suggests that large numbers of arrays of smaller bodies (arrays of arrays) may be advantageous, although further difficulties arise with the operation and maintenance of the array, its construction and the control of the individual WECs.

One major shortcoming of this method is the omission of any interaction effects between the array members. This preliminary work makes the simplifying assumption that the compact array behaves analogously to a large device with the hydrodynamic forces and bottom boundary conditions weighted by the area fraction of the array covered by the buoys. While this may give a good approximation of the forces on the WECs, interaction effects would play a significant role. In particular, shadowing would have a considerable effect in a closely spaced array and would probably result in reduced performance of the WECs at the back of the array. Furthermore, no consideration is given to the individual control systems of each buoy, which may play a significant role in a physical device. Other studies, many of which are related the a Manchester Bobber type device, also suggest that a single large cylinder is equivalent to many small ones, such as Garnaud & Mei (2009a). However, these are not discussed in detail as arrays of WECs are the main concern of this thesis.

The concept of comparing the performance of a single large device to that of more than one smaller devices was also considered by McGuinness (2013), where arrays containing both large and small devices are proposed. This followed the increase in constructive interaction that was achieved with arrays of small devices bunched close together to achieve optimal performance; it was then suggested that these bunches could be replaced by fewer larger devices. Investigation of mixed arrays of this type, containing both large and small devices arranged intelligently to harness constructive interference, is lacking. It was, however, admitted by McGuinness (2013) that these mixed arrays are merely tentative suggestions for further research based on preliminary work. This work is discussed further in Section 1.3.3.

Larger arrays were considered by Borgarino, Babarit, & Ferrant (2012), where triangular and square arrays of 9, 16 and 25 devices are examined. An irregular wave regime with a JONSWAP spectrum was used. The BEM software Aquaplus was used and the underlying numerical theory was outlined in Babarit (2010). Although arrays of generic point absorbers were investigated, the effects of diffracted waves were included in the analysis. The average yearly energy

production was considered, and it was found that the interaction effects (constructive and destructive) generally negated each other and device positioning played little (but not insignificant) role in yearly power absorption. This agreed with the results of Babarit (2010).

The performance of individual devices and rows of devices was also assessed by Borgarino *et al.* (2012). It was found that rows further back in the array (3rd, 4th, etc.) performed poorer due to shielding effects of the front rows, whereas the front rows were relatively unshielded and benefited from radiation effects of the other rows. The first row benefited the most and outperformed the second row by approximately 20%. A linear relationship between the two array spacing variables was identified that determined if constructive interference resulted. It was stated that heaving cylinders are less efficient than surging ones and thus lead to less of a shielding effect. It was suggested that positive interactions are more probable for arrays of heaving cylinders due to the axisymmetry.

The damping values of the devices were obtained and it was suggested that the values which optimised the yearly output of isolated devices were desirable. This is in contrast to much of the previous literature which optimised the hydrodynamic performance (via resonance) of a single device at a very specific frequency. The work suggests that wide-banded devices that are optimised to yearly output should be used and that the yearly average power output varies slowly with device separating distances. It is also suggested that if very efficient devices are used (e.g. surging barges) then square arrays are to be avoided and triangular arrays should be employed. It should also be noted that surge modes are associated with greater viscous effects, which would adversely affect performance. Conversely, if axisymmetric devices (e.g. heaving cylinders) are utilised, then square arrays give good results due to constructive side-to-side interactions. It should be emphasised that an appropriate spacing and control strategy is required for this to be the case.

A literature review on the interaction effect within WEC arrays was given by Babarit (2013), where tentative guidelines on WEC array design are also proposed. It is suggested for large arrays of more than ten typical devices (10m to 20m in diameter) that the number of rows should be limited as much as possible, to avoid significant destructive interaction. This negative interaction increases with the number of rows for larger arrays with a fixed layout. This finding is confirmed by the work of Stratigaki (2014), who similarly recommends limiting the number of rows in an array as much as possible. Babarit (2013)

also suggests for small arrays of less that ten devices that regular or staggered grids with device separations of 100m to 200m are ideal, as the park effect is quite small for these arrays. Stratigaki (2014) recommended that the device separation be as large as possible in small arrays to avoid destructive interference. However, this may be counterproductive if the separation is so wide that the site area becomes excessively large and each array member essentially behaves as an isolated device.

Investigation into arrays was the main aim of the thesis of Stratigaki (2014). This work was separated into three parts. The first was the design and construction of a suitable scale experimental WEC model device, which would be used to conduct experiments. The chosen WEC design was that of a vertical semi-submerged circular cylinder with a hemispherical base.

The second part concerned the accurate modelling of both the intra-array interactions and the extra-array effects of a WEC farm. A shortcoming with most modelling methods is that they are successful in performing one of these tasks but are inefficient or unable to perform the other simultaneously. For example, BEM codes (e.g. WAMIT) give good results for the wave-field within an array but become computationally prohibitive when the field behind the array is also examined. Computational fluid dynamics (CFD) codes similarly require high computation time and/or processing power when considering both array interactions and the effects of the wave-field in the lee of the array. On the other hand, wave propagation models are good at accessing the wave-field in the lee of an array. However, these models approximate the WECs as wave sources/sinks with coefficients determined empirically; this does not give an accurate model of the WEC and its surrounding wave-field within the array. To overcome this, a coupling of the two different modelling softwares was achieved using a similar method previously used by Beels (2009). The BEM code WAMIT was used to model the wave-field around the WECs. This data was then used as input for a wave generating circle which surrounds the device in the wave propagation model, MILDwave. In this manner, both the intra-array interactions and extra-array effects are accurately modelled in a numerically efficient manner.

The third and main aim was the conduction of array model experiments and the creation of a WEC array database which includes information on the performance of several types of array layouts. This work was also presented in a joint paper by Stratigaki *et al.* (2014). Many different array geometries were

investigated, including a single device, rows and columns of two, three & five devices, square arrays of nine, sixteen and twenty-five devices (staggered and rectilinear), with different device spacings. The power absorption, interaction factors and the wave-field surrounding the arrays were measured and analysed. In general, it was found that a wave height increase occurred in front of the first devices meeting the waves, due to diffraction or reflection effects, while a wave height decrease was observed behind the array due to shadowing. These results varied in percentage and location for different wave conditions. Using these results, the WEC array database was created. Finally, by analysing this database, along with the available literature, general guidelines for the layout of an array of WECs is presented. These guidelines are discussed in Section 1.3.3, which concerns array optimisation.

1.3.3 Optimisation of Arrays

The concept of optimal array formulation was introduced by Thomas & Evans (1981), who examined equally spaced linear arrays of five semi-immersed point absorber spheres that operate in heave only. The non-dimensional separation between the devices was altered and the effect on the interaction factor was investigated for linear arrays in head, intermediate and beam seas. This can be considered as a variation in the physical separations for a fixed wavelength or as a variation in wavelength for fixed physical separations. It was shown that the arrays generally performed better in beam seas, agreeing with the intuitive idea that greater frontage to incoming waves allows greater absorption of power. It was also shown that areas of both constructive and destructive interference exist in the ranges of non-dimensional lengths considered and that a relatively small change can result in a move from constructive to destructive interference.

The device displacement amplitudes were also presented and considered for the optimal motion case. It was found that these amplitudes were of the order of two to three times the incident wave amplitude for head seas, with beam sea device amplitudes being considerably larger. In general, larger values of the interaction factor are accompanied by correspondingly large WEC amplitudes. Since the large device amplitudes are a violation of the underlying linear wave theory employed (and would also present significant engineering challenges for real devices), the imposition of amplitude constraints on the device motions was considered. Imposing a constraint of three times the wave amplitude reduced the maximum of the peaks of the power absorption, but still allowed areas of

constructive interference, while areas of poor performance were relatively unaffected. However, a constraint of two times the wave amplitude was severely restrictive and reduced the power absorbed considerably.

Two parallel rows of five devices were also considered and compared to the single row array. It was found that the double row array performed marginally better than the single row array, though the interaction factor contained more variability in the double row case. Arrays of thin ship devices were also considered, which suffered even more greatly from the imposition of amplitude constraints. Finally, it was found that array interaction was affected more by device separation than device shape, with the latter affecting the actual power absorbed.

It was shown by McIver (1993, 1994) that linear arrays are sensitive to changes in the incident wave direction, more so for devices that operate in heave compared to surge. This was the first investigation of unequally spaced linear arrays; only equal spacing had been previously considered. For a specific case of unequal spacing, it was shown that the array performed better than uniform spacing for certain non-dimensional array lengths. Similar to Thomas & Evans (1981), device amplitude constraints were also shown to have a severe effect on the peak power absorption. Finally, due to the high sensitivity of peaks in power absorption to the non-dimensional spacing, the incident wave direction and the imposition of constraints, it was suggested that the best strategy might be to seek to reduce the destructive effects, rather than to increase the array power absorption using the constructive effects.

McIver, Mavrakos, & Singh (1996) attempted to find the best strategy for choosing a WEC array geometry. This was done by considering variations in the inter-WEC separations of a non-uniform symmetric linear array of five point absorbers. In the conclusions of that work, it was proposed that the best strategy is might be to choose an arrangement which minimises net interaction effects. This is primarily due to the high sensitivity of arrays to small changes in the wave-field and constraints. Devices which absorbed power by oscillating in two translational modes of motion were also considered and the point absorber approximation was extended to model devices of this type. Clearly these devices absorb more power but the practical and engineering challenges of designing a device capable of absorbing in two modes are significant. It may be that a simple device which operates in only one mode is better in terms of reducing the difficulty and the cost of modelling, production, operation and/or

maintenance of WECs and arrays.

Irregular seas and sea spectra are applied using the point absorber approximation in the same paper, although the method used is not very realistic as it assumes optimum device performance for each frequency in the spectrum. For both plane and irregular seas, it was found that the array performance is largely independent of the device spacing for low wave frequencies. For plane waves with a wavelength of the order of the WEC spacing, it was shown that equal spacing performs best, while for wavelengths less than the device spacing, unequal spacing is more beneficial. This shows that the incident wave parameters have an effect on the optimal array layout. In irregular seas, shifting the spectrum peak to higher frequencies produces interaction factors that are more oscillatory but there is less evidence that a particular spacing is more advantageous, contrary to the plane wave results.

An approach to optimising the layout of an array of heaving semi-submerged spherical WECs was devised by Fitzgerald (2006) and a summary of the results are presented in the paper by Fitzgerald & Thomas (2007). The small body/point absorber approximation was used and the interaction factor optimised numerically for general 2D arrays of three and five devices, with the positions of the devices being the optimisation variables. Prior to this study, most arrays considered were 1D (linear), or constrained to some prescribed geometry.

An important condition was derived by Fitzgerald (2006) which states that the mean of the interaction factor with respect to the angle of incidence is unity for general configurations (see Section 2.4.6, equation (2.164)). This was identified by Fitzgerald from the optimal configurations and then formally derived using the point absorber approximation for general arrays. It was shown by Child (2011) that this does not strictly hold when non-optimal motions are enforced and the scattered wave-field is accounted for but that the mean tends to be slightly less than unity. This still implies that configurations that attempt to utilise constructive interference to gain large interaction factors must be offset by areas of destructive interference for other angles of incidence. Thus, a large constructive peak in the interaction factor must be accompanied by regions of destructive interference.

In the optimised array study of Fitzgerald (2006), it was usually found that a large narrow central peak in the interaction factor occurred at the target wave angle and this implies that these arrays are not suited to sea-states where the

incident direction has large variability. It was suggested that the wave climate at the array location should be studied prior to optimisation; if a large variability in the incident wave angle is present, then it is best to arrange the array so that it performs reasonably well over a large range, rather than achieving very good performance for small range with poor performance elsewhere.

As in the earlier studies, Fitzgerald (2006) found that optimal array performance was accompanied by unacceptably large WEC displacement amplitudes. Constraints on the amplitudes were investigated and the constrained results of Thomas & Evans (1981) were confirmed in a more general arena. An interesting observation by Fitzgerald (2006) is that optimal 5 device arrays often contain the same arrangement of one or more of the optimised 3 device arrays (or combinations of them). Fitzgerald suggested that there may exist certain "base" optimal 3 device arrays from which all optimum arrays would be constructed.

The condition proved by Fitzgerald (2006), involving the incident wave direction (equation (2.164)), is a special case of a general result derived subsequently by Wolgamot, Taylor, & Eatock Taylor (2012). It was shown that, for general devices of any size and shape, the average of the maximum power absorbed by an N-device array is related to the power per unit width of incident wave front and the wavenumber (see equation (2.168)). The earlier result of Fitzgerald (2006) is obtained if heaving axisymmetric devices are assumed. Another consequence of Wolgamot *et al.* (2012) is that, for a single non-axisymmetric device, the directional averaged maximum power the device can absorb is the same as for an axisymmetric device. This is to be expected since if the device is shaped so that it absorbs well in one particular direction, then it must perform poorer in other directions. This suggests that careful preparation on the proposed site of a wave energy array should be preformed before considering the size and shape of both the individual devices and the array. Wolgamot *et al.* (2012) also verified the relation derived to a reasonable accuracy via numerical simulations of four types of arrays comprised of three types of WECs. These calculations were performed using the BEM program DIFFRACT and included the diffracted wave field. The results of Child (2011) and Wolgamot *et al.* (2012) together suggest that this condition does not hold for non-optimal motions (i.e. non-optimal power absorption).

In addition to the work discussed in Section 1.3.1, Folley & Whittaker (2009) also performed an investigation into the performance of an optimal five-device

array identified by Fitzgerald & Thomas (2007). The performance of this optimal array was analysed for variation in incident wave period and incident wave angle. It was shown that the array achieved considerable constructive interaction at the optimum values but this was surrounded by regions of destructive interference to a significant extent. This further suggested that an ideal strategy may be to seek to minimize destructive interference effects rather than achieve high constructive interference, as first suggested by McIver (1994).

The radiation pattern of this optimal array was also investigated. Using the Haskind relations, it is known that an array's ability to absorb power from a certain direction is directly related to its ability to radiate wave in that direction, as shown in Falnes (2002). It is also known that high interaction factors are only achieved by highly directional array radiation patterns, with a large sharp peak in array performance with respect to the target incident wave angle. This results in large sensitivity of the arrays to changes in wave conditions. This is illustrated by the highly directional pattern of the optimal array of Fitzgerald & Thomas (2007).

The performance of the same optimal array and a two-WEC array in a given annual wave climate was also assessed by Folley & Whittaker (2009). It was found that the performance of the arrays considered in spectral wave climates is not as high as predicted using the regular wave theory. In general, the configuration of the array appeared to have a much smaller effect on performance in the irregular wave case but net constructive/destructive interference was still possible. The optimal interaction factor for a two-WEC array was analysed with respect to the relative WEC positions in the same wave climate. This suggested that the optimal position of the second WEC is at a very close proximity to the first (less than or equal to 25m) with an orientation approximately parallel to the peak direction of the incident spectrum. Similar results were found for an analogous three-WEC array, with preliminary searches for alternative configurations of more than three WECs resulting in a combination of similar terminator or attenuator layouts. This suggested that the general arguments presented for these two-device arrays could be tentatively extended to larger arrays. Although the increase/decrease of power absorption in spectral wave climates is not as significant as predicted in the regular wave case, these effects may still prove significant for an array over a large period of time, thus affecting the financial viability of commercial scale arrays.

A staggered grid array of twelve point absorber buoys was considered by

De Backer, Vantorre, Beels, De Rouck, & Frigaard (2009). The buoys consist of a cone shaped base with a cylindrical upper part of diameter 5m and an equilibrium draft of 3m. The array was contained within a square of length 36m. The influence of slamming and stroke restrictions, as well as constraints within the PTO, are investigated using WAMIT within an invicid regime and compared to the performance of a single buoy. A slamming constraint is imposed such that the buoy is not permitted to leave the free surface. A stroke/amplitude constraint on the device motion is also considered, as the motions of real-life devices will be limited by the PTO. Furthermore, a constraint on the tuning force is considered, since optimal control parameters may result in large control forces.

Optimisations of the array were carried out for an irregular wave climate. Three optimisation strategies were considered, with different optimal control strategies applied to the WECs in each case. It was found that the array performance for each of the control strategies is significantly different, with motion amplitude constraints also limiting power absorption.

An alternative interaction factor was defined to be the ratio of total power absorbed by the array to that absorbed by the same number of isolated devices, with the same constraints and exposed to the same conditions. It may be expected that this would act as a good objective function, as it compares the real constrained performance of the array to the analogous performance of isolated devices, thus giving a reasonable measure of the interaction effect of placing the WECs in an array. However, in some cases this factor was increased due to the poor performance of the single devices rather than good performance of the array, as isolated devices were more negatively effected by constraints. This may lead to deceptive objective function values and knowledge of the absolute power absorbed by both the array and the isolated WEC is required. It was shown that the array performed slightly better as an aligned grid rather than a staggered grid. Finally, the effects of mistuning were investigated by optimising the control parameters for a wave angle that differs from the incident wave by 45° and the power loss was found to be less than 2%.

Bellew, Stallard, & Stansby (2009) considered uniform linear arrays of five devices in head and beam seas. This work attempted to obtain values of device mass and mechanical damping such that the net power output of the array is maximised and the variation of average power output across the array is minimised. For a given frequency the simplest way to modify the power

absorbed is to vary the mechanical damping and/or the device mass. The value of net power absorbed is investigated for four different cases of mechanical damping. For beam sea arrays, the power absorbed by allowing an unlimited mechanical damping gives a 12% increase in the peak power absorption; when constraints are placed on the choice of such damping, the peak performance increase is reduced to 7%. For head seas, the peak mechanical damping values were less than the constraint considered, so imposing the constraint had little effect. The unlimited damping case again performed best within and outside the peak region, with the percentage increase at the peak being 18% compared to the constrained case.

While it may be desirable from an engineering perspective to minimise the variation in power absorption across the array, it may not be advantageous from a hydrodynamic interaction perspective to essentially have all WECs working equally as hard. Forcing all WECs to perform similarly may be an overly restrictive condition and act in direct opposition to the maximisation of array output. Thus it may not be possible to obtain both the array power maximisation and power variation minimisation simultaneously in a reasonable manner.

The same authors also investigated the variation of device mass to determine the maximum net power absorbed. This was achieved by considering a supplementary mass on the WECs. For the case where the mechanical damping is taken to be the diagonal of the radiation damping, it was found that the peak frequency increased as supplementary mass increased, with the peak value decreasing. For low frequencies, changing damping appeared to be more effective for increasing power absorbed, whilst changing the supplementary mass was more beneficial for higher frequencies.

The arrangement of an array of wave-power devices was also investigated by Child (2011) with the results published in four papers: Child & Venugopal (2007, 2008, 2009, 2010). The WEC shape is taken to be a truncated circular cylinder and an exact hydrodynamic solution, including the scattered wave-field, is employed. This was achieved by representing the scattered and radiated wave fields as a linear combination of basis functions and solving the associated hydrodynamic problems in two domains, an interior region underneath the cylindrical device and an exterior region outside of this, with matching of the solutions enforced between these regions. A detailed analysis was initially performed on a single isolated WEC, including various PTO

mechanisms and device control strategies. The ideal tuning strategy was called real tuning or damping tuning, where the PTO damping coefficient was maximised at a given frequency and subject to the PTO spring coefficient being fixed at zero. This tuning resulted in more moderate (and thus physically manageable) device displacement amplitudes but less power was absorbed in comparison to other tuning mechanisms considered.

Arrays of five devices in regular seas were then optimised by two methods. The first was termed the Parabolic Intersection (PI) method. This uses the phase of the total wave-field to place devices on (or near) curves of constructive interference to optimise the array layout. The second method of array layout optimisation was by means of a Genetic Algorithm (GA), with the array layouts as the solution population and the interaction factor as the objective function. Both methods were used to maximise the performance of the arrays that were real tuned. Reactive tuning (also known as spring-damping tuning) of array members was also considered, where both the PTO spring and damping coefficients are optimised. This resulted in higher performance due to the better tuning afforded by optimising both coefficients at a given frequency, though this was often accompanied by large motion amplitudes due to resonance. A third case was also considered where the performance was minimised for reactively tuned arrays in an attempt to find a worst case scenario for array arrangement. The GA optimisation was also applied to an irregular wave regime.

A number of optimised arrays were presented which satisfied each of the three above criteria. The optimised arrays for regular seas found were then analysed in irregular seas, and performed reasonably well under these conditions. The first attempt to optimise arrays in irregular seas was then conducted using genetic algorithms in an exact hydrodynamic situation. These arrays performed slightly better in irregular seas than the analogous arrays optimised for regular seas. Previous literature has suggested that array interactions have a smaller overall impact when irregular waves are considered. The work of Child shows that arrays can be optimised to perform well in irregular waves, however this performance may be sensitive to the specific incident wave climate considered. For both regular and irregular seas, it was found that small changes in array configuration could lead to considerable changes in array performance. This shows that the optimal array layouts were highly sensitive to changes in non-dimensional parameters and this problem of sensitivity of optimal arrays is discussed further in Section 1.5.

In Section 1.3.2, it was stated that Stratigaki (2014) gave general guidelines for layout of an array of WECs, based on the results obtained from numerical and physical modelling. Different guidelines were given for large and small arrays and different recommendations were also given depending upon the requirement, for example, whether maximum power absorption is desired or if minimum wave-field effect (minimum environmental impact) is preferred. A summary of those guidelines for general arrays in terms of improving power absorption alone are discussed here as wave-field impact is not of primary concern in this thesis.

The best power absorption found was for staggered arrays or largely spaced arrays, with the staggered arrays having a greater detrimental impact on the wave height in the lee of the array. It was also found that the number of rows in an array should be limited as much as possible, as row performance decreases along the depth of the array after the 2nd row. However, the columns of WECs, which are aligned parallel to the incident wave direction, perform in a similar manner to each other and thus increasing the number of columns may be a method of efficiently increasing power absorption. This essentially increases the frontage of the array to the incident wave. This may be a better solution than largely spaced arrays, particularly if limited sea area is available. The guidelines detail different recommendations for small arrays (typically ten or less WECs), large arrays (more than ten WECs, typically twenty or more) and all general arrays; those summarised here correspond to general arrays alone.

An analytical solution for the optimisation of the two-WEC point absorber problem is derived by Snyder (2013) and optimisation of arrays of point absorbers was investigated by Snyder & Moarefdoost (2014). The usual point absorber approximation is employed which gives the simplified expression for the interaction factor. No device geometry was specified as the WEC displacements were not considered. Snyder stated that a standard deterministic optimisation which seeks to maximise the interaction factor often results in an array layout which performs very well in only a very specific set of conditions, again highlighting the problem of high sensitivity of optimal arrays. Therefore, two different optimisation models were discussed: 1) a robust optimisation which sought to maximise the minimum bound of the interaction factor; and 2) a stochastic optimisation which sought to maximise the expected value of the interaction factor. An example of each optimisation was performed using a GA and the resulting array performance is compared to that of a deterministic optimal array solution from Fitzgerald & Thomas (2007). It was found that the peak performance is lower, but the solution in each case is more stable than the

deterministic solution.

The paper concluded by proposing a heuristic algorithm to optimise array layouts of a general number of WECs. This algorithm places one WEC at the origin and sequentially adds WECs to the array and then re-optimises the layout locally with respect to the interaction factor. This is repeated until the desired number of WECs are included in the array. This algorithm may result in a computational saving compared to a general optimisation, however, it assumes that the inclusion of extra WECs does not drastically alter the optimal layout and that the local optimisation will converge to the best layout at each iteration.

The work of Snyder & Moarefdoost (2014) is extended in Snyder & Moarefdoost (2015), where explicit analytical formulations for both the robust and stochastic cases were given for the two-WEC problem. It was shown that the robust optimisation attains a maximum interaction factor of unity for an incident wave angle range of π; it was expected that values greater than unity can be obtained if a smaller range of incident wave angle was considered. The average interaction factor for a spectral wave climate is defined as the product of the standard interaction factor with the wave power spectrum, summed over the individual spectral wave components and scaled by the total power contained in the spectrum; a two-WEC and a five-WEC array were investigated using this objective function. The results show that the optimal separation distance in the two-WEC array decreases for larger variation in incident wave angle and concluded by suggesting that the work be extended to arrays of three or more WECs and by considering the effect of a variation in both wave angle and wavenumber.

Preliminary work prior to this Ph.D. thesis has been conducted by McGuinness (2013). The optimal configuration of a five-device array of heaving point absorber WECs in regular waves was investigated, where all the devices are constrained to lie on a straight line, with a fixed non-dimensional length of the array. This was the first optimisation of the individual spacings between the WECs in a linear array of fixed non-dimensional length. The formulation was simplified by enforcing symmetry across the array layout, thereby reducing the problem to a single variable. The interaction factor was then optimised for the given symmetry.

Within the optimal configurations found by McGuinness (2013), the devices tended to bunch very close together in groups of two or three, as in figure 1.6. It is interesting that, within the theory of point absorbers, the optimal

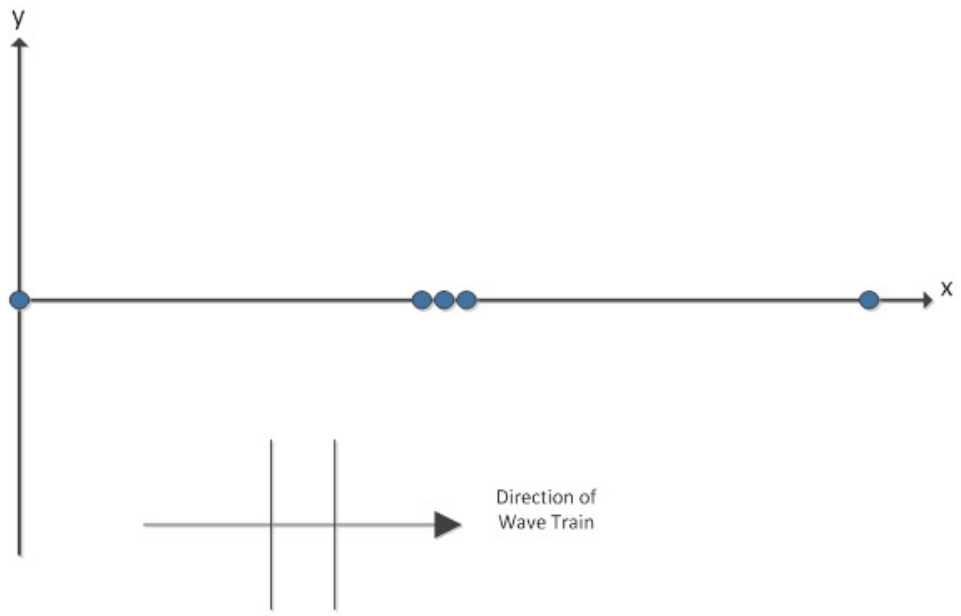

Figure 1.6: Example of optimal array layout found by McGuinness (2013)

configuration is with the devices very close together. This is perhaps due to the assumption of optimal (unconstrained) motions, which implies that the maximum constructive interaction can be achieved by placing the WECs as close as possible.

It was hypothesised by McGuinness (2013) that replacing these groups of devices by larger devices, perhaps two or three times the size of a standard device, may provide good wave-power absorption. This would create a so-called "satellite" array, with both larger and smaller devices in the same array. The term "satellite" was used due to the appearance of the proposed array shown in figure 1.7, with one large device in the centre surrounded by two smaller devices. It is acknowledged that the analysis performed by McGuinness (2013) is associated with point absorbers and does not address device sizes or motions. Therefore, this suggestion is only a tentative preliminary proposal and further investigation is needed to assess the viability of these types of arrays. The preliminary work of McGuinness (2013) is further discussed and extended in Chapter 3.

Extensions of this were considered by Costigan (2014), Fennell (2015) and Lawton (2017), where the WECs were constrained to lie on a circle, triangle and ellipse respectively. The uniform versions of these layouts were investigated to provide a benchmark for optimisation results. In each case, the number of array optimisation variables is reduced to one by defining symmetries in the array

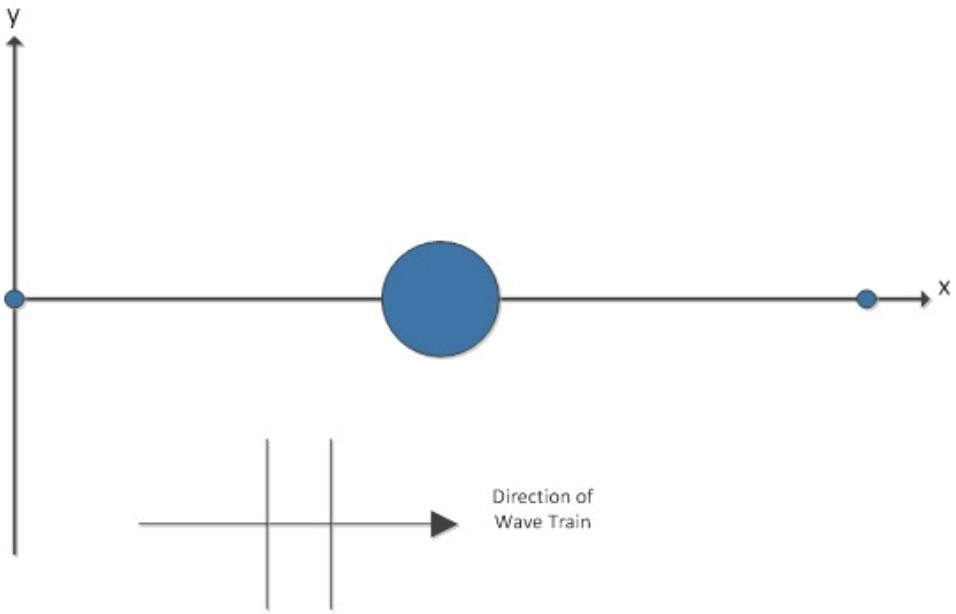

Figure 1.7: Example of "satellite" array configuration suggested by McGuinness (2013)

layouts. For the circular array, it was found that the inclusion a WEC in the centre provided an improved performance, though this was not as clear for the triangular case. Depending upon the incident wave angle, the optimal circular, triangular and elliptical arrays resulted in closely spaced grouped WECs in some cases, as with McGuinness (2013). In other cases, layouts similar or identical to the uniform benchmark cases were found to be optimal. This suggests that the incident wave angle, the array orientation to the incident wave and the array geometry play a crucial role in the array interaction.

1.4 Physical Testing of Arrays

In addition to numerical modelling, physical wave tank tests are the only other viable way to investigate WEC arrays. It is acknowledged that numerical models are deficient in some respects, due to the impositions of assumptions and approximations, but primarily because of their lack of verification. Physical testing provides an alternative to numerical modelling and can also be used to verify and validate a numerical model and its predictions. However, the use of a wave tank is expensive, thus it is prudent to thoroughly investigate the behaviour using numerical models before proceeding to physical testing. Physical testing and its associated models and techniques are described by

Hughes (1993).

There are two main types of testing facility: wave flumes and wave basins. Flumes are also known as channels and are long narrow tanks, typically 20m to 35m in length, 1m to 5m in width and 0.5m to 2m in depth. They usually employ a wave absorbing beach at the opposite end to the wave-makers to reduce wave reflection. Wave flumes are primarily used for the preliminary testing of single devices and can also be used to model the interaction effect of an infinite line of devices due to the side wall reflections. Wave basins, also known as wave tanks, are larger tanks with a width comparable to its length, which is typically 20m to 35m, with a depth of 0.5m to 3m deep. Wave basins are better for array testing, as the waves can be incident onto a model array and the effects measured. Most of these tanks can simulate regular and irregular seas of a desired specification, using programmable wave paddles at one or more sides of the tank.

Wave flumes and tanks do however have shortcomings associated with them. For example, side wall effects are the most common problem in physical tests of arrays; this is especially true in flumes, where the distance from the testing device(s) to the wall is small. If a WEC is placed in the centre of an ideal wave flume, it models a uniform infinite linear array of such WECs due to the reflections off the side walls. If the WEC is placed off-centre in the flume, then the reflections model an infinite linear array layout of the recurring symmetric pattern given by the relative position of the WEC in the flume. Note that a main difference between a single device (or a finite array) and an infinite line of devices is the presence of edge effects.

In other experiments, the side walls can introduce unwanted reflected waves into the system, which can be almost the same order of magnitude as the wave incident onto the walls. Modern tanks attempt to overcome this problem by using wave absorbing walls at the sides and beaches at the wave receiving end of the tank but some reflection effects often still persist. Even with these mitigating factors, reflections can be of the order of 10% of the wave-field incident onto the wall, thought this is dependent on the wavelengths involved. Non-linear effects may also be present in the wave tank, for example due to viscous effects, which may be unwanted. Another shortcoming with tanks and flumes is the relatively small depths which some possess, often in the range 0.5m-1m. This makes modelling large depth cases such as deep seas or oceans difficult due to the appropriate scaling. Obviously the larger the scale, the

closer the situation is to that of the real WEC but the small depths and wave generating capability of a basin could severely limit this scale, depending on the specific tank used. Sarmento & Thomas (2008) give some recommendations on scales for testing of different phenomena. For example, basic offshore device behaviour testing can be performed between 1:50 and 1:100 scale, while the larger scale of 1:5 is suggested for testing of nonlinear and other hydrodynamic effects.

The difficulties with wave tank experiments have been studied by many authors. One example is O'Boyle, Elsaesser, Folley, & Whittaker (2011), who investigated the variation of the wave-field within the wave basin at Queens University Belfast, with regard to the impact on WEC array model testing. In this work, a wave packet containing several wave components of different frequencies and amplitudes was assessed. Using Fast Fourier Transform at each data location, small variations in the measured frequency amplitude spectrum relative to the target were found. These discrepancies were largest for the highest and lowest frequency components, possibly due to noise in the data or errors in measurements due to the small amplitude of these components.

It was also found that the amplitude of each wave component varied in an oscillatory manner across the tank, achieving the target value only at certain locations. A definite geometry of the amplitude variations of the different components was observed, although this changed with frequency, suggesting that the variation in amplitude is frequency dependent. This may be related to Benjamin-Feir instability, where the main progressive wave train is affected by residual wave motions at similar frequencies and results in energy transference to the main wave train. It was suggested that phase locked (standing) waves may be set up across the wave tank by diffraction/reflection effects and that this causes the variation in the amplitudes observed. Poor absorption by the wave absorbing beach at the far end of the wave basin is given as another possible reason.

A Boussinesq numerical model was used to further investigate and attempt to predict this effect. This is an averaged depth model and so is not accurate for deep water waves. As the experiments considered waves mostly in the shallow water regime, this numerical model was considered reasonably accurate except for the highest frequency waves investigated. The numerical results were compared to the corresponding experimental results and good agreement was observed. However, when the entire JONSWAP spectrum was analysed, it

showed little variation in the significant wave height, despite variations in the amplitudes of each component. This probably is due to the relative cancellation of the amplitude differences between the components, which may give the incorrect impression of homogeneity of the wave basin. The effects identified above have a significant impact when testing WECs, especially WEC arrays and array interactions, since it would be unclear if the differences observed for an array are due to array interactions or variations in the wave-field of the basin.

The uncertainties in the wave-field of a wave tank, together with their effects and implications on WEC array experiments, was extended by Lamont-Kane, Folley, & Whittaker (2013). This work considered the effect of uncertainty in physical and numerical modelling of WEC array performance and was also investigated using the wave basin at the Queen's University Belfast Marine Laboratory. The physical WEC model used was that of a truncated vertical circular cylinder with a hemispherical bottom. This shape was chosen primarily to simplify modelling as much as possible, by reducing the vortex shedding that would occur at the sharp edges of the cylinder in the absence of the base. Both single device tests and array tests were performed, with the array being a square comprised of four devices and a device separation of three times the diameter of the device.

Numerical investigations of WECs and WEC arrays often employ simplifying assumptions, e.g. linear wave theory, the point absorber approximation, regular sea states *etc.*. Thus, the predications of numerical studies must be validated; this is usually accomplished by comparing the numerical results to a "benchmark" physical test. However, one difficulty of physical testing is knowing exactly what effects are present in the wave tank and accounting for these effects in the experimental measurements. For example, physical tests often involve scaling issues, such as those associated with viscous effects, which may not accounted for in the model design. Furthermore, there may be errors or uncertainties associated with the instrumentation or physical set up employed. Since the effect of array interaction is often relatively small, of the order of 5% of measured quantities, e.g. power absorbed, body motion *etc.*, uncertainties in these quantities of a similar magnitude would make accurate investigation of array effects difficult. Such uncertainty ranges can overcome and mask the array interaction effects.

To reduce these uncertainties and condense the error ranges of measurements, Lamont-Kane *et al.* (2013) recommended that a statistical analysis of physical

tests is performed. Five possible sources of uncertainty were identified, namely: 1) Spatial variation of the wave-field within the wave basin, 2) Temporal variation of the wave-field from one repeat to another, 3) The repeatability of model response for any single individual WEC, 4) The reproducibility of model response between various nominally identical WECs, and 5) Variation of the time-series of an incident irregular wave train. Each of these sources of errors was analysed and it was found that the wave-field variability (sources 1 and 2) had a contributed most to the errors in the measurements, although sources 3 - 5 were also significant in some cases. However, it was suggested that this could be curtailed by considering normalised results. If physical data results are to be used for numerical model validation, then these uncertainties would have less impact if the wave-field variability can be incorporated in the numerical model. Therefore, in all cases, repeatability of the wave-field is a much more important consideration.

Finally, it was suggested that using different quantities for measuring the interaction, e.g. displacements instead of power capture *etc.*, may be useful as the uncertainty in one quantity may be different to that in another. It was shown, for a specific irregular sea, that the relative uncertainty in the displacement amplitudes of each device in an array is considerably less than the corresponding uncertainty in power capture. This suggests that perhaps device displacement would be a better quantifier of array interactions due to the smaller relative errors, though uncertainty in phase measurements may also have an effect on the quantification of array interaction.

Experimental wave tank testing difficulties were also encountered by Stratigaki (2014), where wave-field variability was noted in some of the results. In some tests, the wave height was noticeably larger or smaller in certain sections of the wave tank; this effect occurred both with and without devices present in the water. As a result, this increased the challenge of distinguishing WEC array effects from wave-field variability effects within the wave tank. Following private communications with Stratigaki, it was learned that temporal variation of the wave-field in the wave tank was also a difficulty. Even with no devices or supporting struts in the wave tank, the wave-field produced within the tank varied from run-to-run; this may have been due to the set-up of the wave paddles in the DHI wave basin. This presented a major problem for physical testing of WEC arrays and questions are raised about the experimental findings.

The physical tank testing of WECs can provide useful information and prove

especially useful when verification/validation of numerical models are desired; this has yet to be fully established for arrays. However, the cost alone for the use of a wave tank facility can be prohibitive, with tank time costing anywhere from €2000 to €20000 per day, depending on the facility and experimental set-up available. Together with the other difficulties identified, this shows that physical tank testing of WECs may not provide definitive verification. It is acknowledged that tank testing is an important step in the process of investigating a WEC device and WEC arrays, but extensive use of numerical modelling prior and during physical modelling is prudent and should not be neglected.

1.5 Research Shortcomings

Conducting this literature review enabled some shortcomings and open questions to be identified. The aim of this thesis is to investigate some of these unanswered questions and attempt to fill the gaps in the literature that are outlined below.

The principal shortcoming identified within the literature was the high sensitivity of optimal array layouts to changes in array parameters. This was shown, in particular, for the optimal arrays of Fitzgerald (2006) and Child (2011). In both of these studies, either a small change in the non-dimensional spacing between the devices or in the incident wave angle typically resulted in a considerable loss in performance from the optimal arrangement. The best and poorest performing array layouts were surprisingly similar, further indicating this sensitivity. This is highly undesirable, as WEC array sites on the open ocean would contain some variability in the incident wave and available deployments.

To overcome this deficiency, it is suggested that the array perfromance be optimised by maximising over a range of parameters, rather than for specific parameter values. This could be achieved by using the mean of array performance as the objective function of an optimisation procedure, rather than array performance itself. In principle, this would return good performance over a broader range of the parameter(s) for which the mean is defined. This is effectively a form of de-tuning and will be the main focus of this thesis.

This strategy is first examined for a mean defined over a prescribed range of

non-dimensional array length in Chapters 3 - 6, where the array length is dependent on the geometry imposed. It is first implemented in very simple arrays, whose layouts have prescribed geometry and symmetry so that they are described by one variable only. The main focus is on linear arrays initially and is then extended to circular arrays and subsequently to more general cases without prescribed symmetry.

It is acknowledged that array performance often appears to be more sensitive to incident wave angle than to wavenumber variation. Therefore, Chapters 7 and 8 consider the situation where the objective function of an optimisation is the mean of the interaction factor over a range of incident wave angle. This formulation does not require any imposed geometry and thus has the advantage of increased freedom within the optimisation but will also increase the intensity of the numerical algorithm. The result of Fitzgerald (2006), regarding the mean of the interaction factor, applies only over an interval of length π and thus optimising the mean over a smaller range is conceptually possible, since the necessary offset of poor performance could be located outside the range of interest.

An analysis in regular waves provides an insight into array interactions without an excessive computational demand. However, the influence of irregular waves on array optimisations of this type must also be considered. Thus, a preliminarily attempt is made in Chapter 9 to optimise arrays in an irregular regime. An array is sought which performs as well as possible over the entire (non-zero) spectrum considered, thus maximising the overall power absorbed by the array. This mirrors similar studies for single devices, such as Thomas & Gallachóir (1993) on the Bristol Cylinder and Weber & Thomas (2000, 2003, 2005) on an OWC device. The relevance of different types of spectrum should be investigated, as the array will probably perform differently in narrow-banded spectra in comparison to broad-banded spectra. The implementation of a spectrum introduces considerable numerical challenges and greatly intensifies the computational demand. Hence, a simple linear array geometry with fewer WECs is considered to ensure that the problem remains tractable within a reasonable time-frame.

The outstanding WEC array shortcoming is the absence of a complete numerical optimisation of the configuration of arrays using a full interaction regime, including the scattered wave-field. The nearest to this goal appears to be that of Fitzgerald (2006) and Child (2011). The former optimised arrays

numerically but a point absorber approximation was employed, so that the scattered field is neglected. The latter optimises the arrays of cylindrical devices in a full interaction regime, but used a GA, which is a semi-random heuristic optimisation procedure and thus it is not known how the optimal solution is converged to or whether a true global optimum (rather than just a local optimum) is found. However, performing a general numerical array layout optimisation in a full interaction regime is computationally prohibitive and not possible in this work.

A less obvious, more specific and perhaps simpler target is the optimisation of WEC arrays constrained to certain geometries. Some work on this topic is undertaken by Thomas & Evans (1981) and McIver (1994), where uniform and certain unequal array spacings were investigated using the point absorber approximation. This was extended by McGuinness (2013) who optimised symmetric linear arrays of fixed non-dimensional length, again using the point absorber theory. This is the first optimisation of an array of fixed length relative to the individual spacings between WECs. This could be extended to more general arrays without imposed symmetry and an investigation of the WEC motions should also be performed. A constrained optimisation, where the WEC motions are limited to a reasonable physical value, would provide further insight. Also of interest would be array geometries other than straight lines. For example Costigan (2014), Fennell (2015) and Lawton (2017) performed preliminary layout optimisations of arrays of point absorbers constrained to lie in a circular, triangular and elliptical arrangements respectively. This could also be extended to investigate the optimum arrangements in a more general arena and to include an analysis of the device sizes, motions and constraints.

Chapter 2

Mathematical Formulation

2.1 Introduction

To assess the hydrodynamic interaction between WEC array members, it is necessary to calculate certain hydrodynamic quantities associated with device behaviour. Array quality measures are derived to quantify array performance and are then used to define appropriate objective functions for the forthcoming optimisations. An appropriate mathematical model is chosen for this task and is outlined in this chapter.

A brief description of hydrodynamics and wave theory is first provided; this is to give the relevant basic mathematical background. Linear wave theory is then derived and the material presented is based on this formulation. The theory of wave energy and wave-power absorption, for both single devices and arrays, is then provided for regular seas. Different array quality measures are defined and their uses outlined and compared. Finally, a basic theory for WEC arrays in irregular seas is presented. Further details and an in-depth description of some of the mathematical principles discussed here can be found in Newman (1977), Linton & McIver (2001) and Falnes (2002).

2.2 Wave Theory

2.2.1 Mathematical Model of Water Waves

A Cartesian coordinate system (x, y, z) is adopted with the z-axis pointing vertically upwards, with $z = 0$ being in the plane of the undisturbed fluid surface and time is denoted by t. The basic equations of fluid dynamics are the continuity (mass conservation) equation and the Navier-Stokes (N-S) equations. Before presenting these equations, it is convenient for notational purposes to introduce the convective derivative

$$\begin{aligned} \frac{D}{Dt} &= \frac{\partial}{\partial t} + (\mathbf{u}.\boldsymbol{\nabla}) \\ &= \frac{\partial}{\partial t} + u\frac{\partial}{\partial x} + v\frac{\partial}{\partial y} + w\frac{\partial}{\partial z}, \end{aligned} \tag{2.1}$$

where $\mathbf{u} = (u, v, w)$ is the fluid velocity vector in an Eulerian frame of reference. The continuity equation, which describes the conservation of mass in a fluid flow, is

$$\frac{D\rho}{Dt} + \rho\nabla.\mathbf{u} = 0, \tag{2.2}$$

where ρ is the fluid density. The N-S equations are written in vector form as

$$\frac{D\mathbf{u}}{Dt} = -\frac{1}{\rho}\boldsymbol{\nabla}p + \mathbf{F} + \gamma\left[\nabla^2\mathbf{u} + \frac{1}{3}\boldsymbol{\nabla}\left(\nabla.\mathbf{u}\right)\right], \tag{2.3}$$

where p is the pressure in the fluid, $\mathbf{F}$ is the total body-force present in the fluid (defined per unit mass) and γ is the coefficient of kinematic viscosity of the fluid, which is assumed to be time-independent. It is assumed that there is no variation in temperature and thus temperature effects are neglected in this model. Within this thesis, it is assumed that the only body force present is due to gravity and so $\mathbf{F} = -g\widehat{\mathbf{z}}$, where g is the acceleration due to gravity and $\widehat{\mathbf{z}}$ is the unit vector in the z-direction. To simplify the above equations, several assumptions and approximations are made.

If the fluid under consideration is considered to be incompressible then $\rho =$ constant and $\frac{D\rho}{Dt} = 0$. Equation (2.2) then becomes the incompressible fluid condition

$$\nabla.\mathbf{u} = 0. \tag{2.4}$$

This also simplifies the N-S equations to

$$\frac{D\mathbf{u}}{Dt} = -\frac{1}{\rho}\boldsymbol{\nabla} p + \mathbf{F} + \gamma \nabla^2 \mathbf{u}. \tag{2.5}$$

The next assumption is that of an inviscid fluid, so that the approximation $\gamma = 0$ applies. Along with (2.5), this gives the Euler equations

$$\frac{D\mathbf{u}}{Dt} = -\frac{1}{\rho}\boldsymbol{\nabla} p + \mathbf{F}. \tag{2.6}$$

A further simplifying assumption is that the fluid motion is irrotational, which is expressed as

$$\nabla \times \mathbf{u} = \mathbf{0}. \tag{2.7}$$

Since the curl of the velocity is zero, the velocity vector can be expressed as the gradient of a scalar function

$$\mathbf{u} = \boldsymbol{\nabla}\Phi, \tag{2.8}$$

where Φ is the velocity (scalar) potential.

Using (2.7)-(2.8), the Euler equation (2.6) can be rewritten as

$$\boldsymbol{\nabla}\left(\frac{\partial \Phi}{\partial t} + \frac{1}{2}|\boldsymbol{\nabla}\Phi|^2 + \frac{p}{\rho} + gz\right) = \mathbf{0} \tag{2.9}$$

$$\Leftrightarrow \quad \frac{\partial \Phi}{\partial t} + \frac{1}{2}|\nabla\Phi|^2 + \frac{p}{\rho} + gz = f(t), \tag{2.10}$$

where $f(t)$ is an arbitrary function of time and $\mathbf{F} = -g\hat{\mathbf{z}}$ has been used. Equation (2.10) is known as the Bernoulli Equation. The function $f(t)$ can be eliminated by absorbing it into the potential Φ to create an alternate potential

$$\widetilde{\Phi} = \Phi + \int^t \left[\frac{p_a}{\rho} - f(t')\right] dt', \tag{2.11}$$

which when substituted into (2.10) gives the more common form of Bernoulli's equation

$$\frac{\partial \widetilde{\Phi}}{\partial t} + \frac{1}{2}\left|\boldsymbol{\nabla}\widetilde{\Phi}\right|^2 + \frac{p - p_a}{\rho} + gz = 0, \tag{2.12}$$

where p_a is the atmospheric pressure, assumed constant. The inclusion of p_a in the above is for both convenience and simplification. The quantity $p_g = p - p_a$ is sometimes termed the gauge pressure, i.e. it is the relative pressure of the fluid to that of the atmosphere. Note that the physical characteristics of the

flow are not altered by the transformation $\Phi \to \widetilde{\Phi}$ since the gradient is unchanged, so $\mathbf{u} = \boldsymbol{\nabla}\widetilde{\Phi} = \boldsymbol{\nabla}\Phi$ and the tilde notation is henceforth dropped. Combining (2.8) with the incompressible form of the continuity equation (2.4) gives the Laplace equation

$$\nabla^2\Phi = 0. \tag{2.13}$$

Thus, the continuity equation (2.2) and N-S equations (2.5), which govern the flow, have been simplified to the Bernoulli equation (2.12) and Laplace equation (2.13), which hold in the entire domain of the fluid, including upon the boundaries. Suitable boundary conditions must be imposed to find a solution to the hydrodynamic problem.

2.2.1.1 Boundary Conditions

The water-wave problem is more complicated than most other wave problems, such as electromagnetism and acoustics, due to the existence of a free surface. Boundary conditions must be imposed upon this free surface as well as other boundaries of the fluid domain, including the sea bed and the surfaces of any bodies present in the fluid.

Let the vertical elevation of a point on the free surface be given by

$$z = \eta(x, y, t). \tag{2.14}$$

Both dynamic and kinematic boundary conditions must be applied on the free surface. The kinematic free surface boundary condition (KFSBC) states that fluid particles must not cross the fluid-surface boundary and this is initially expressed as

$$\frac{D}{Dt}\left[z - \eta(x, y, t)\right] = 0 \qquad \text{on} \quad z = \eta(x, y, t), \tag{2.15}$$

which when expanded becomes

$$\frac{\partial\Phi}{\partial z} = \frac{\partial\eta}{\partial t} + \frac{\partial\Phi}{\partial x}\frac{\partial\eta}{\partial x} + \frac{\partial\Phi}{\partial y}\frac{\partial\eta}{\partial y} \qquad \text{on} \quad z = \eta(x, y, t). \tag{2.16}$$

If surface tension is neglected (which is valid for waves that are longer than a few centimetres), the dynamic free surface boundary condition (DFSBC) for an inviscid fluid states that the pressure must be continuous across the fluid-air interface. Since air has a relatively small density compared to water and atmospheric pressure varies negligibly over the small elevations of the free

surface, the pressure across the free surface is taken to be constant. Using Bernoulli's equation (2.12) and taking $p = p_a$ on the free surface, the DFSBC is expressed as

$$\frac{\partial \Phi}{\partial t} + \frac{1}{2}|\boldsymbol{\nabla}\Phi|^2 + g\eta = 0 \qquad \text{on} \quad z = \eta(x, y, t). \tag{2.17}$$

Let the sea bed be described by $z = -h(x, y)$, where $h\,(x, y) > 0$. The appropriate boundary condition on the sea bed is a no-flow condition, which is

$$\mathbf{u}.\mathbf{n} = 0 \qquad \text{on} \quad z = -h(x, y), \tag{2.18}$$

where $\mathbf{n}$ is the unit normal vector into the sea bed (out of the fluid). This boundary condition can also be written in terms of the velocity potential,

$$(\boldsymbol{\nabla}\Phi)\,.\mathbf{n} = 0 \qquad \text{on} \quad z = -h(x, y). \tag{2.19}$$

This kinematic condition is satisfied by the normal component of the velocity relative to the bottom surface only; no dynamic condition exists because it is a fluid-solid boundary. Care is needed with the fluid-solid boundary conditions; there cannot be a dynamical boundary condition except for equal and opposite action and reaction. The continuity expressed in equation (2.18) is due to the lack of viscosity.

A similar condition to (2.19) applies on the surface of any structures present in the fluid. However, in general, these structures will not be stationary. Therefore, the condition specifies that, on the surface of a body, the normal component of the fluid velocity must equal the velocity of the body in the same direction. Let S_{Bj} be the wetted surface of the jth body. Then the no-flow boundary is

$$(\boldsymbol{\nabla}\Phi)\,.\mathbf{n} = \mathbf{U}^{(j)}.\mathbf{n} \qquad \text{on} \quad S_{B_j}, \tag{2.20}$$

where $\mathbf{U}^{(j)}$ is the translational velocity vector of the jth body and $\mathbf{n}$ is the unit normal into the body surface (out of the fluid). This must hold for all bodies in the fluid. If the body is stationary, then the right hand side of (2.20) becomes zero and a condition analogous to (2.19) is recovered. As the fluid is inviscid, only a normal condition exists.

The full set of boundary conditions has now been obtained, along with the equations describing the flow. For completeness, the full set of equations and

boundary conditions describing the flow are presented:

$$\begin{aligned}
\nabla^2\Phi &= 0 && \text{throughout the fluid} \\
(\boldsymbol{\nabla}\Phi)\,.\mathbf{n} &= 0 && \text{on} \quad z = -h(x,y) \\
(\boldsymbol{\nabla}\Phi)\,.\mathbf{n} &= \mathbf{U}^{(j)}.\mathbf{n} && \text{on} \quad S_{B_j}\ \forall\, j \\
\frac{\partial\Phi}{\partial t} + \frac{1}{2}|\boldsymbol{\nabla}\Phi|^2 + g\eta &= 0 && \text{on} \quad z = \eta(x,y,t) \\
\frac{\partial\Phi}{\partial z} = \frac{\partial\eta}{\partial t} + \frac{\partial\Phi}{\partial x}\frac{\partial\eta}{\partial x} + \frac{\partial\Phi}{\partial y}\frac{\partial\eta}{\partial y} && \text{on} \quad z = \eta(x,y,t).
\end{aligned} \tag{2.21}$$

2.2.2 Linear Wave Theory

The nonlinearity in the boundary conditions (2.16) and (2.17) along with the application of (2.16), (2.17) and (2.20) on a moving surface or boundary, namely $\eta(x,y,t)$ or S_{B_j}, makes the task of acquiring analytical solutions extremely difficult. For sufficiently small motions, it is valid to linearize the governing equations about the undisturbed or equilibrium state. This requires the amplitude of the fluid motion to be small compared to the wavelength and depth of the fluid throughout the domain, including in the vicinity of structures or bodies. Hence, the amplitude of structural motions must also be small relative to the wave motion. From the perspective of wave energy, the individual WEC motion amplitudes must be at most the same order of magnitude as the wave motion in order for this linearisation to remain consistent.

The main idea of linear theory is to assume that the wave motion is a perturbation of the undisturbed state, such that Φ, η and their derivatives are assumed to be $\mathcal{O}(\varepsilon)$ and where ε is a perturbation parameter satisfying $\varepsilon \ll 1$. Only the terms of lowest order in ε are retained in the governing equations and boundary conditions, so that terms such as $\frac{1}{2}|\boldsymbol{\nabla}\Phi|^2$ and $\frac{\partial\Phi}{\partial x}\frac{\partial\eta}{\partial x}$ will be $\mathcal{O}(\varepsilon^2)$ and hence neglected. Linear theory also allows the boundary conditions (2.16) and (2.17) to be applied on the mean free surface $z = 0$ instead of the moving surface $z = \eta(x,y,t)$. This can be seen using Taylor expansions of the relevant quantities and again only keeping the lowest order in ε. For example, let $f(x,z,t)$ be a quantity of $\mathcal{O}(\varepsilon)$ that is to be evaluated on the free surface

$z = \eta(x, y, t)$. The Taylor expansion of f about the mean free surface ($z = 0$) is

$$\begin{aligned} f\left(x, \eta(x,y,t), t\right) &= f(x,0,t) + \eta(x,z,t)\left|\frac{\partial \eta}{\partial z}\right|_{z=0} + \frac{\eta^2(x,z,t)}{2}\left|\frac{\partial^2 \eta}{\partial z^2}\right|_{z=0} + \dots \\ &= f(x,0,t) + \mathcal{O}\left(\varepsilon^2\right). \end{aligned} \tag{2.22}$$

Similarly, the boundary conditions (2.20) on the bodies within the fluid can be applied on the equilibrium position of the body surfaces $\overline{S_{B_j}}$, instead of S_{B_j}.

After linearisation, the free surface boundary conditions (2.16) and (2.17) respectively become

$$\frac{\partial \Phi}{\partial t} + g\eta = 0 \qquad \text{on} \quad z = 0, \tag{2.23}$$

$$\frac{\partial \Phi}{\partial z} = \frac{\partial \eta}{\partial t} \qquad \text{on} \quad z = 0. \tag{2.24}$$

These can be combined into one condition by differentiating (2.23) with respect to t and substituting for $\frac{\partial \eta}{\partial t}$ in (2.24) to give

$$\frac{\partial^2 \Phi}{\partial t^2} + g\frac{\partial \Phi}{\partial z} = 0 \qquad \text{on} \quad z = 0, \tag{2.25}$$

which is sometimes known as the linearized free surface boundary condition (LFSBC).

For completeness and to allow comparison with the original non-linearised governing equations, the linearized wave problem equations are presented:

$$\begin{aligned} \nabla^2 \Phi &= 0 && \text{throughout the fluid} \\ (\boldsymbol{\nabla}\Phi).\mathbf{n} &= 0 && \text{on} \quad z = -h(x,y) \\ (\nabla\Phi).\mathbf{n} &= \mathbf{U}^{(j)}.\mathbf{n} && \text{on} \quad \overline{S_{B_j}}\ \forall\, j \\ \frac{\partial^2 \Phi}{\partial t^2} + g\frac{\partial \Phi}{\partial z} &= 0 && \text{on} \quad z = 0. \end{aligned} \tag{2.26}$$

It is usual to assume harmonic time-dependence of all fluid motions and of the motions of any structures present in the fluid. This time dependence, which is assumed to have frequency ω, can be separated from the spatial dependence of all relevant quantities. The velocity potential is thus written as

$$\Phi(x,y,z,t) = \mathrm{Re}\left[\phi(x,y,z)e^{-i\omega t}\right], \tag{2.27}$$

where $\phi(x, y, z)$ is the complex amplitude of the potential and Re denotes the real part. Similarly, the free surface elevation is written

$$\eta(x, y, t) = \mathrm{Re}\left[\zeta(x, y)e^{-i\omega t}\right], \tag{2.28}$$

for a corresponding complex amplitude $\zeta(x, y)$. Using (2.27), the governing equations of the flow (2.26) simplify to

$$\nabla^2\phi = 0 \qquad \text{throughout the fluid} \tag{2.29}$$

$$(\boldsymbol{\nabla}\phi)\,.\mathbf{n} = 0 \qquad \text{on} \quad z = -h\,(x, y) \tag{2.30}$$

$$(\boldsymbol{\nabla}\phi)\,.\mathbf{n} = \mathbf{U}^{(j)}.\mathbf{n} \qquad \text{on} \quad \overline{S_{B_j}}\ \forall\, j \tag{2.31}$$

$$\frac{\partial\phi}{\partial z} = \frac{\omega^2}{g}\phi \qquad \text{on} \quad z = 0. \tag{2.32}$$

Initially, waves in the absence of any structures are considered. The corresponding solution to the linearised water-wave problem is written as ϕ_0 and will represent a progressive wave in a uniform body of fluid. This will then be utilised as the incident wave onto any structures present in the fluid and the principle of superposition of wave-fields will be employed.

Consider the simpler case where the sea bed is at a constant depth $h\,(x, y) = h$, which enables an analytical solution to be obtained. Using the method of separation of variables enables a non-decaying progressive wave solution to the Laplace equation to be found, which in Cartesian coordinates (x, y, z) is written as

$$\phi_0 = -\frac{igA}{\omega}\frac{\cosh\left[k\,(z+h)\right]}{\cosh kh}e^{ik(x\cos\beta + y\sin\beta)}, \tag{2.33}$$

or alternatively, in cylindrical coordinates (R, θ, z),

$$\phi_0 = -\frac{igA}{\omega}\frac{\cosh\left[k\,(z+h)\right]}{\cosh kh}e^{ikR\cos(\theta-\beta)}. \tag{2.34}$$

This represents a plane progressive wave, travelling in direction β, measured relative to the positive x-axis, with amplitude A and wavenumber k, where k is related to the wavelength λ by

$$k = \frac{2\pi}{\lambda}. \tag{2.35}$$

The potential (2.34) corresponds to a free surface elevation

$$\zeta(R, \theta) = Ae^{ikR\cos(\theta-\beta)} \tag{2.36}$$

via (2.23), (2.27) and (2.28). Requiring ϕ_0 to satisfy the LFSBC (2.32) gives a relationship which ω and k must satisfy

$$\omega^2 = gk \tanh kh \tag{2.37}$$

and is called the dispersion relation.

The wave-power devices considered in this project are those that would be placed off-shore, in relatively deep water; these types of devices are sometimes termed Third Generation wave-power devices. If the depth is large enough, greater simplification can be achieved. In water wave theory, “deep water” or "water of infinite depth" refers to the case where $kh \gg 1$, or equivalently $\frac{\lambda}{h} \ll 1$. The boundary condition on the sea bed is thus replaced by the asymptotic condition

$$|\boldsymbol{\nabla}\phi| \to 0 \qquad \text{as} \quad z \to -\infty \tag{2.38}$$

and the plane wave potential takes the Cartesian form

$$\phi_0 = -\frac{igA}{\omega} e^{kz} e^{ik(x\cos\beta + y\sin\beta)}. \tag{2.39}$$

Equivalently, in cylindrical coordinates

$$\phi_0 = -\frac{igA}{\omega} e^{kz} e^{ikR\cos(\theta-\beta)}. \tag{2.40}$$

The dispersion relationship then simplifies to

$$\omega^2 = gk. \tag{2.41}$$

The notion of deep water is often misunderstood, as the validity of the deep water approximation does not depend directly on the depth of the water, but rather the ratio of depth-to-wavelength. Hence, tsunami type waves are often considered in a shallow water regime, due to the large wavelengths involved, while ripples in a glass of beer would be considered as deep water waves.

The plane wave potentials (2.39) or (2.40) are used to describe the incident wave on the wave-power devices in preliminary studies concerning regular waves. However, even in this simple case, the plane wave then interacts with the structures of the WECs and is scattered by the devices. The devices are also excited into oscillations and thus create radiated waves. The effect of these interactions on the performance of the array of WECs is a primary area of

interest in this project.

Some quantities often used to describe the wave-field are the phase velocity c and the group velocity c_g. The phase velocity is defined as

$$c = \frac{\omega}{k} \tag{2.42}$$

and this is the velocity at which the wave crest propagates. From the dispersion relationship (2.37) for arbitrary finite depth, the phase velocity can be written

$$c = \frac{g}{\omega} \tanh kh = \sqrt{\frac{g}{k} \tanh kh}. \tag{2.43}$$

The group velocity is defined as

$$c_g = \frac{d\omega}{dk} \tag{2.44}$$

and is the velocity at which mean energy is transported in a wave. Note that in general $\frac{c}{2} \leq c_g \leq c$, with equality holding at the lower and upper limits for deep water and shallow water respectively. For arbitrary depths, using (2.37), the ratio of group velocity to phase velocity can be written as

$$\frac{c_g}{c} = \frac{1}{2}\left[1 + \frac{2kh}{\sinh 2kh}\right]. \tag{2.45}$$

Simpler expressions exist for the group velocity and phase velocity in the infinite depth regime. Using the infinite depth dispersion relationship (2.41),

$$c = \frac{g}{\omega} \tag{2.46}$$

and

$$c_g = \frac{g}{2\omega}, \tag{2.47}$$

so that in deep water the group velocity is exactly half the phase velocity.

2.3 Interaction of Waves with a Structure

2.3.1 Velocity Potential due to Interaction with a Structure

Consider a plane wave incident on a single floating body. This incident wave is scattered by the presence of the body to produce a diffracted wave-field. As the body is free floating, it is excited into oscillation by the incident wave and thus also produces a radiated wave-field. Assuming linear wave theory is valid and that all hydrodynamic boundary conditions are applied on the mean wetted surface of the body, there are three separate wave-fields: namely incident, diffracted and radiated. The total wave-field can then be written using linear superposition, as

$$\phi = \underbrace{\phi_0 + \phi_d}_{\phi_s} + \phi_r, \tag{2.48}$$

where again the time-dependence is removed from each potential in the usual manner. In this representation ϕ_0 is the incident wave potential, ϕ_d represents the diffracted wave-field for the device held fixed and ϕ_r is the radiated wave-field generated by the forced oscillations of the device in the absence of an incident wave. The scattered wave-field $\phi_s = \phi_0 + \phi_d$ is the combination of the incident and diffracted wave-fields. Each potential satisfies the Laplace equation (2.29).

If the body under consideration is rigid and three-dimensional, its motion will possess six degrees of freedom. Three of these are translational in the x, y and z directions, named surge, sway and heave respectively. The second three degrees of freedom are due to rotational motion about the x, y and z axes and termed roll, pitch and yaw respectively. Radiation of waves can occur independently for each of these modes of motion. To describe this, the velocity of the body must be defined for each mode of oscillation. Let the translational velocity of the body in global (x, y, z) directions be given by $\mathbf{U} = (U_1, U_2, U_3)$ and let the corresponding rotational velocity be $\mathbf{\Omega} = (\Omega_1, \Omega_2, \Omega_3)$. The velocity of a point on the body due to rotation is $\mathbf{\Omega} \times \mathbf{r}'$, where $\mathbf{r}'$ is the local displacement vector of the point from the centre of rotation of the body. The total velocity of a point on the structure for a general motion of the body is given by

$$\mathbf{V} = \mathbf{U} + \mathbf{\Omega} \times \mathbf{r}'. \tag{2.49}$$

For a freely floating body, the centre of rotation is the centre of floatation, which is on the same z-axis as the centre of gravity and lies in the waterplane area of the device. From this, the normal velocity of the body can be defined as

$$V_n = \mathbf{V}.\mathbf{n} = \mathbf{U}.\mathbf{n} + (\mathbf{\Omega} \times \mathbf{r}')\,.\mathbf{n}. \tag{2.50}$$

For convenience, the second term can be written in an alternate form to give

$$V_n = \mathbf{V}.\mathbf{n} = \mathbf{U}.\mathbf{n} + \mathbf{\Omega}.\,(\mathbf{r}' \times \mathbf{n})\,, \tag{2.51}$$

so that the normal is separated explicitly in each term.

Since the structure is held fixed for the scattering problem, the appropriate boundary condition is

$$\frac{\partial \phi_s}{\partial n} = 0 \qquad \text{on} \quad \overline{S_B} \tag{2.52}$$

$$\Leftrightarrow \quad \frac{\partial \phi_d}{\partial n} = -\frac{\partial \phi_0}{\partial n} \qquad \text{on} \quad \overline{S_B}, \tag{2.53}$$

where $\overline{S_B}$ is the equilibrium surface of the body being considered and the notation $(\boldsymbol{\nabla}\psi)\,.\mathbf{n} = \frac{\partial \psi}{\partial n}$ is used. In the radiation problem, the devices undergo forced oscillations in the absence of an incident wave and thus the boundary condition is

$$\frac{\partial \phi_r}{\partial n} = V_n \qquad \text{on} \quad \overline{S_B}. \tag{2.54}$$

It should be emphasised that the underlying linear wave theory requires that the magnitude of these oscillations should be at most the same order as the wave amplitude.

It should be noted that it is necessary to impose a radiation condition on the wave fields that emanate from a body, namely ϕ_d and ϕ_r. This radiation condition specifies that the waves corresponding to these potentials must propagate away from the bodies and is expressed in three dimensions as

$$\lim_{kR\to\infty} R^{1/2}\left(\frac{\partial \phi_d}{\partial R} - ik\phi_d\right) = 0\ , \tag{2.55}$$

where R is the horizontal polar coordinate, with a similar expression for ϕ_r.

The simplest WEC array interaction to model is where a plane wave is incident on an array of floating devices. Each device then produces a diffracted and a radiated wave-field, although most approximate models neglect the diffracted wave-field. The formulation given in this section can be easily extended to an

array of many devices by including appropriate indexes on the quantities involved. Therefore the total, incident, radiated, diffracted and scattered potentials are denoted as $\phi^{(j)}, \phi_0^{(j)}, \phi_r^{(j)}, \phi_d^{(j)}, \phi_s^{(j)}$ respectively for the jth device, while the boundary conditions are applied on the mean wetted surface $\overline{S_{B_j}}$ with normal velocity $U_n^{(j)}$ of the jth device, for all j.

2.3.2 The Radiation Problem

It is convenient to extend the definition of the translational velocity of the body to that of a six-dimensional generalised velocity, which also includes the rotational motion. The quantity $\mathbf{U}$ is henceforth redefined as the generalised velocity, which contains all the velocities of the body, rotational and translational. The jth component of $\mathbf{U}$ is now defined as the normal (x, y, z) translational velocities for $j = 1, 2, 3$ as above, and the vector dimension is extended to include the rotational velocities so that

$$\begin{aligned} U_j &= U_j \qquad \text{for} \quad j = 1, 2, 3 \\ &= \Omega_{j-3} \qquad \text{for} \quad j = 4, 5, 6 \end{aligned} \tag{2.56}$$

$$\Leftrightarrow \ \mathbf{U} = (U_1, U_2, U_3, \Omega_1, \Omega_2, \Omega_3)\,.$$

Corresponding to this, the generalised normal $\boldsymbol{\mathcal{N}}$ is also defined as

$$\begin{aligned} \mathcal{N}_j &= n_j \qquad \text{for} \quad j = 1, 2, 3 \\ &= (\mathbf{r}' \times \mathbf{n})_{j-3} \qquad \text{for} \quad j = 4, 5, 6. \end{aligned} \tag{2.57}$$

The general normal velocity of the body can now be written concisely as

$$U_n = \mathbf{U}.\,\boldsymbol{\mathcal{N}} = \sum_{j=1}^{6} U_j \mathcal{N}_j. \tag{2.58}$$

Consider the complex amplitude of the radiated wave velocity potential ϕ_r, which is a superposition of the radiated waves due to each of the six modes of oscillation. This can be written

$$\phi_r = \sum_{j=1}^{6} (-i\omega\xi_j)\varphi_j, \tag{2.59}$$

where $\varphi_j(x, y, z)$ is a function of proportionality that corresponds to a unit displacement, and ξ_j is the complex amplitude of the body displacements, where

the total time-dependent body displacements are given by

$$\boldsymbol{\chi} = \mathrm{Re}\left[\boldsymbol{\xi} e^{-i\omega t}\right]. \tag{2.60}$$

The body velocity can be written as the time derivative of the displacements, so that

$$\begin{aligned} \mathbf{U} &= \frac{d\boldsymbol{\chi}}{dt} \\ &= \mathrm{Re}\left[-i\omega\boldsymbol{\xi} e^{-i\omega t}\right]. \end{aligned} \tag{2.61}$$

Therefore, the complex amplitude of the generalised velocity (2.56) is $-i\omega\boldsymbol{\xi}$, where $\boldsymbol{\xi}$ is extended to a six-dimensional vector by including the rotational motion in the appropriate way. Using this form of ϕ_r, the boundary condition (2.54) can be written as

$$\frac{\partial \varphi_i}{\partial n} = \mathcal{N}_i \qquad \text{on} \quad \overline{S_B} \tag{2.62}$$

for $i = 1, \ldots, 6$. The potentials φ_j can be interpreted as the functions related to the radiated velocity potentials due to device oscillation in mode j with unit velocity amplitude (i.e. with $-i\omega\xi_j = 1$). The radiation problem has now been reformulated in terms of the unknowns φ_j, $j = 1, \ldots, 6$, which must satisfy the Laplace equation

$$\nabla^2 \varphi_j = 0, \tag{2.63}$$

the sea bed boundary condition

$$\frac{\partial \varphi_j}{\partial z} = 0 \qquad \text{on} \quad z = -h, \tag{2.64}$$

and the LFSBC

$$\frac{\partial \varphi_j}{\partial z} = \frac{\omega^2}{g}\varphi_j \qquad \text{on} \quad z = 0, \tag{2.65}$$

along with boundary condition (2.62) applied on all bodies present in the fluid.

2.3.3 The Scattering Problem – Multiple Scattering Method

The multiple scattering method and associated theory in this subsection is described in detail in Mavrakos & Koumoutsakos (1987) and Mavrakos (1991) and outlined in Mavrakos & McIver (1997); a brief summary is provided here for comparative purposes. The method of Mavrakos & Koumoutsakos (1987) is

in principle exact, whereas some preliminary work in this area has neglected scattering effects via a point absorber approximation or by considering the Froude-Krylov forces only (see equation (2.88)). The multiple scattering method accurately accounts for the interference effects between N identical axisymmetric devices, of radius a, placed in fluid and relies on single-body hydrodynamic effects of the devices.

Consider the velocity potential of an undisturbed incident plane wave as in (2.34), but rewritten in the alternate form with cylindrical coordinates (R_q, θ_q, z) with origin O_q at body q:

$$\phi_0\left(R_q, \theta_q, z\right) = -i\omega A \frac{\cosh\left[k(z+h)\right]}{k\sinh(kh)} \widetilde{\phi_0}\left(R_q, \theta_q\right), \tag{2.66}$$

where

$$\widetilde{\phi_0}\left(R_q, \theta_q\right) = e^{il_{0_q}\cos\left(\theta_{0_q}-\beta\right)} \sum_{m=-\infty}^{\infty} i^m J_m\left(kR_q\right) e^{im(\theta_q-\beta)}, \tag{2.67}$$

where J_m is the mth order Bessel function of first kind and $\left(l_{0_q}, \theta_{0_q}\right)$ are the coordinates of body q relative to the global origin O. Due to the interaction of ϕ_0 with body q, the body produces a first order scattered field of

$${}^1\phi_d^{(q)} = -i\omega A \sum_{m=-\infty}^{\infty} i^m \sum_{j=0}^{\infty} {}^1F_{mj}^{(q)} \frac{K_m\left(\varkappa_j R_q\right)}{K_m\left(\varkappa_j a\right)} Z_j(z) e^{im\theta_q}, \tag{2.68}$$

where a is the body radius, K_m is the mth order modified Bessel function of second kind and $Z_j(z)$ are orthonormal functions defined in the domain $[-h, 0]$ by

$$Z_j(z) = \left(\frac{1}{2}\left[\frac{1+\sin\left(2\varkappa_j h\right)}{2\varkappa_j h}\right]\right)^{-\frac{1}{2}} \cos\left[\varkappa_j\left(z+h\right)\right], \tag{2.69}$$

and $\varkappa_j$ are the roots of

$$\omega^2 + g\varkappa_j \tan\left(\varkappa_j h\right) = 0, \tag{2.70}$$

with $\varkappa_0 = -ik$. The first order scattering coefficient ${}^1F_{mj}^{(q)}$ can be obtained via the solution of the diffraction problem around body q, using for example the method of matched eigenfunction expansions. More explicitly, the diffraction problem states that the diffraction potential ϕ_d satisfies the Laplace equation (2.29), the LFSBC (2.32), the sea bed condition (2.30) and the body boundary condition (2.54).

The scattered waves of first order emanating from the other bodies ($\neq q$) cause a second order excitation of body q within the multiple scattering method,

which is written

$$ {}^{2}\phi_0^{(q)} = \sum_{p=1}^{N} \left(1 - \delta_{pq}\right) {}^{1}\phi_d^{(p)}, \tag{2.71} $$

where δ_{pq} is the Kronecker delta. In response to this, body q radiates its second order of scattering ${}^{2}\phi_d^{(q)}$, which is written similarly to (2.68) with the appropriate indices altered and corresponding second order scattering coefficients introduced. The total second order potential is then

$$ {}^{2}\phi^{(q)} = {}^{2}\phi_0^{(q)} + {}^{2}\phi_d^{(q)}, \tag{2.72} $$

and this satisfies the appropriate imposed boundary conditions.

To solve the second order scattering problem, ${}^{1}\phi_d^{(p)}$ needs to be expressed in terms of the coordinate system of body q. Completing this and manipulation of algebra gives

$$ {}^{2}\phi_0^{(q)} = -i\omega A \sum_{m=-\infty}^{\infty} i^m \sum_{j=0}^{\infty} {}^{2}Q_{mj}^{(q)} \frac{I_m\left(\varkappa_j R_q\right)}{I_m\left(\varkappa_j a\right)} Z_j(z) e^{im\theta_q}, \tag{2.73} $$

where

$$ {}^{2}Q_{mj}^{(q)} = \sum_{p=1}^{N} \left(1 - \delta_{pq}\right) \sum_{n=-\infty}^{\infty} i^{m+n} \frac{K_{n-m}\left(\varkappa_j l_{pq}\right)}{K_n\left(\varkappa_j a\right)} I_m(\varkappa_j a) {}^{1}F_{nj}^{(p)} e^{i(n-m)\theta_{pq}}, \tag{2.74} $$

with the notation

$$ {}^{1}Q_{mj}^{(q)} = i^m \frac{e^{ikl_{0p}\cos\left(\theta_{0p}-\beta\right)} e^{-im\beta}}{Z_0'(0)} I_m\left(\varkappa_j a\right) \delta_{0j}. \tag{2.75} $$

Proceeding as above, in general the lth order scattering can be obtained and then summing up all orders gives the total wave-field (incident and scattered), which can be used to calculate the hydrodynamic coefficients and forces. The total scattered wave-field ($\phi_s = \phi_0 + \phi_d$) is written as

$$ \phi^{(q)} = -i\omega A \sum_{m=-\infty}^{\infty} i^m \sum_{j=0}^{\infty} \left[Q_{mj}^{(q)} \frac{I_m\left(\varkappa_j R_q\right)}{I_m\left(\varkappa_j a\right)} + F_{mj}^{(q)} \frac{K_m\left(\varkappa_j R_q\right)}{K_m\left(\varkappa_j a\right)} \right] Z_j(z) e^{im\theta_q}, \tag{2.76} $$

where the notation

$$ Q_{mj}^{(q)} = \sum_{l=1}^{\infty} {}^{l}Q_{mj}^{(q)} \qquad \text{and} \qquad F_{mj}^{(q)} = \sum_{l=1}^{\infty} {}^{l}F_{mj}^{(q)} \tag{2.77} $$

has been defined.

Evaluation of this method involves truncation of the infinite series and matching of solutions at the appropriate boundaries. Depending upon the accuracy required, the infinite series above can be truncated to a certain order l, so that the desired accuracy or computation time is achieved. This task is not trivial to complete in a computational sense.

Due to the complicated nature of this method and the large associated computation times, numerical array calculations of this type are often intractable when scattering effects are included. This combined with the relatively small amplitude of diffracted waves in most cases justifies its neglect and a large saving in computation can achieved for only a small accuracy penalty. Accounting for the diffracted wave-field and the method of multiple scattering are computationally prohibitive and are beyond the scope of this thesis.

2.3.4 Hydrodynamic Forces on the Devices

A body submersed or partially submersed in a fluid will be subject to forces due to the pressure of the fluid. From the linearised form of Bernoulli's equation (2.12), and considering the pressure p_g, which is written here as p without the subscript, rearranging gives

$$p = -\rho g z - \rho \frac{\partial \Phi}{\partial t}. \tag{2.78}$$

The first term is the hydrostatic pressure and varies with depth only. The second term is the one of interest and is called the hydrodynamic pressure. This pressure, also known as the wavelike pressure or the excess pressure, is denoted herein as $p_d = -\rho \frac{\partial \Phi}{\partial t}$ and is due to the fluid motion. The total force on the body is a sum of the hydrodynamic and hydrostatic forces due to these pressures and is written as

$$\mathbf{F}_{tot} = \mathbf{F}_d + \mathbf{F}_{hs}. \tag{2.79}$$

The hydrodynamic force can be further decomposed into an exciting force $\mathbf{F}_e$ due to the wave motion and a radiation force $\mathbf{F}_r$ due to the radiation of waves away from the device. Thus, the total force on the structure is

$$\mathbf{F}_{tot} = \mathbf{F}_e + \mathbf{F}_r + \mathbf{F}_{hs}. \tag{2.80}$$

Since WECs absorb power from the hydrodynamic motion of the waves and not from the hydrostatic force, attention is initially limited to the pressure on the structures due to this hydrodynamic pressure only. The hydrodynamic force $\mathbf{F}_d$ on the structure is found by integrating the hydrodynamic pressure over the equilibrium surface of structure, such that

$$\begin{aligned}\mathbf{F}_d(t) &= \iint_{\overline{S_B}} p_d \mathbf{n}\, dS \\ &= -\rho \iint_{\overline{S_B}} \frac{\partial \Phi}{\partial t} \mathbf{n}\, dS,\end{aligned} \tag{2.81}$$

where $\mathbf{n}$ is the unit normal out of the fluid domain. Introducing the harmonic time-dependence in Φ as in (2.27), with $\mathbf{F}_d(t) = \mathrm{Re}\,[\mathbf{f} e^{-i\omega t}]$, this becomes

$$\mathbf{f} = i\omega\rho \iint_{\overline{S_B}} \phi \mathbf{n}\, dS. \tag{2.82}$$

Similarly, the moment $\mathbf{M}_d = \mathrm{Re}\,[\boldsymbol{\mu} e^{-i\omega t}]$ can be written as

$$\boldsymbol{\mu} = i\omega\rho \iint_{\overline{S_B}} \phi\,(\mathbf{r}' \times \mathbf{n})\, dS. \tag{2.83}$$

Using the generalised normal $\boldsymbol{\mathcal{N}}$ and analogously defining the generalised force as $\mathbf{F}_d = \mathrm{Re}\,[\boldsymbol{\mathcal{F}}_d\, e^{-i\omega t}]$, with $\mathbf{F}_d = (F_{d1}, F_{d2}, F_{d3}, M_{d1}, M_{d2}, M_{d3})$ and $\boldsymbol{\mathcal{F}}_d = (f_1, f_2, f_3, \mu_1, \mu_2, \mu_3)$, then $\boldsymbol{\mathcal{F}}_d$ can be written

$$\boldsymbol{\mathcal{F}}_d = i\omega\rho \iint_{\overline{S_B}} \phi \boldsymbol{\mathcal{N}}\, dS. \tag{2.84}$$

As previously stated, the force (2.84) can be separated into the force due to excitation from the scattered wave-field and the force resulting from induced oscillations via the radiated wave-field. This is written as

$$\boldsymbol{\mathcal{F}}_d = \mathbf{X} + \boldsymbol{\mathcal{F}}_r, \tag{2.85}$$

where

$$\mathbf{X} = i\omega\rho \iint_{\overline{S_B}} (\phi_0 + \phi_d) \boldsymbol{\mathcal{N}}\, dS \tag{2.86}$$

is the complex amplitude of the exciting force ($\mathbf{F}_e = \mathrm{Re}\,[\mathbf{X}e^{-i\omega t}]$), and

$$\boldsymbol{\mathcal{F}}_r = i\omega\rho \iint_{\overline{S_B}} \phi_r \boldsymbol{\mathcal{N}}\, dS \tag{2.87}$$

is the complex amplitude of the radiation force ($\mathbf{F}_r = \mathrm{Re}\,[\boldsymbol{\mathcal{F}}_r\, e^{-i\omega t}]$), due to forced oscillations and the radiated wave-field. A common approximation of the exciting force is used if the diffracted field ϕ_d is sufficiently small compared to the incident field ϕ_0 and the corresponding force components also satisfy a similar condition. This allows the contribution of the diffracted field in (2.86) to be neglected and is called the Froude-Krylov approximation; the corresponding force is thus termed the Froude-Krylov force and is given by

$$\mathbf{X}_{FK} = i\omega\rho \iint_{\overline{S_B}} \phi_0 \boldsymbol{\mathcal{N}}\, dS. \tag{2.88}$$

Since diffracted waves are neglected within this work, the Froude-Krylov approximation to the excitation force is used throughout and the $_{FK}$ subscript notation is henceforth dropped.

Using (2.59), $\boldsymbol{\mathcal{F}}_r$ can be rewritten as

$$\boldsymbol{\mathcal{F}}_r = \sum_{j=1}^{6} \mathfrak{f}_j(-i\omega\xi_j), \tag{2.89}$$

where the lth component of $\mathfrak{f}_j$ is

$$\mathfrak{f}_{lj} = i\omega\rho \iint_{\overline{S_B}} \varphi_j \mathcal{N}_l\, dS. \tag{2.90}$$

This is the lth component of force resulting from forced oscillations in mode j. It is usual to decompose $\mathfrak{f}_{lj}$ further into its real and imaginary parts by writing

$$\mathfrak{f}_{lj} = i\omega\left(a_{lj} + i\frac{b_{lj}}{\omega}\right), \tag{2.91}$$

where a_{lj} is termed the added mass coefficient and b_{lj} is the damping coefficient. Since the motions are harmonic, the generalised velocity can be written as $\mathbf{U} = \mathrm{Re}\,[\boldsymbol{\mathcal{U}}\, e^{-i\omega t}]$ from equation (2.56). Thus, the velocity and acceleration of the body are written as $\boldsymbol{\mathcal{U}}$ and $-i\omega\boldsymbol{\mathcal{U}}$ respectively. Therefore, writing the radiation force in terms of a_{lj} and b_{lj} as in equation (2.91) essentially separates

the parts which are in phase with the acceleration and velocity of the device respectively. In this way, the radiation force can be written as

$$\{\boldsymbol{\mathcal{F}}_r\}_l = \sum_{j=1}^{6} \Big(-a_{lj}\dot{\mathcal{U}}_j(t) - b_{lj}\mathcal{U}_j(t)\Big), \tag{2.92}$$

where $\mathcal{U}_j$ is the jth component of the complex amplitude of the generalised velocity.

By considering the body displacements, as defined in equation (2.60), the radiation force can also be expressed as

$$\{\boldsymbol{\mathcal{F}}_r\}_l = \sum_{j=1}^{6} \Big(\omega^2 \xi_j a_{lj} + i\omega \xi_j b_{lj}\Big). \tag{2.93}$$

Explicitly, the added mass and damping coefficients can be written as

$$a_{lj} = \text{Re}\left[\rho \iint_{S_B} \varphi_j \, \mathcal{N}_l \; dS\right], \tag{2.94}$$

$$b_{lj} = \text{Im}\left[\omega\rho \iint_{S_B} \varphi_j \, \mathcal{N}_l \; dS\right], \tag{2.95}$$

where "Im" demotes the imaginary part. These coefficients can be written in matrix form $\mathbb{A}$ and $\mathbb{B}$, where $\{\mathbb{A}\}_{lj} = a_{lj}$ and $\{\mathbb{B}\}_{lj} = b_{lj}$, and these are termed the added mass matrix and damping matrix respectively. Thus, the radiation force is written as

$$\mathbf{F}_r = -\mathbb{A}\,\dot{\mathbf{U}} - \mathbb{B}\,\mathbf{U}. \tag{2.96}$$

Using Green's theorem, it is shown by Linton & McIver (2001) that the matrices $\mathbb{A}$ and $\mathbb{B}$ are both symmetric. It is further shown that Green's theorem can also be used to write b_{lj} in terms of a far-field integral, as

$$b_{lj} = \omega\rho \iint_{S_\infty} \varphi_l \varphi_j^* \; dS, \tag{2.97}$$

where $*$ denotes complex conjugate and S_∞ is the surface at infinity which can be considered to be a cylinder of infinite depth and radius R with $R \to \infty$.

To find the total force on a structure, the hydrostatic force must also be

calculated. This is shown in Newman (1977) to be given by

$$\{\mathbf{F}_{hs}\}_j = \mathrm{Re}\left[-\sum_{l=1}^{6} c_{jl}\xi_l e^{-i\omega t}\right], \tag{2.98}$$

where c_{jl} are elements of the hydrostatic restoring force matrix, which is diagonal so that $c_{jl} = 0$ for $j \neq l$. The hydrostatic restoring force elements are related to the corresponding modes of motion. These elements are each analogous to the restoring force felt by a mass on a spring, only here the restoring force is due to the buoyancy of the body (hydrostatic stiffness), not the stiffness of a spring. The hydrostatic force above can be written in matrix form as

$$\mathbf{F}_{hs} = \mathrm{Re}\left[\mathbb{C}\dot{\boldsymbol{\mathcal{U}}}e^{-i\omega t}\right], \tag{2.99}$$

where $\{\mathbb{C}\}_{lj} = \frac{c_{lj}}{\omega^2}$. Now the total force on a body which responds to an incident wave can be written in matrix form as

$$\mathbf{F}_{tot}(t) = \mathbf{F}_e + \mathbb{C}\,\dot{\mathbf{U}} - \mathbb{A}\,\ddot{\mathbf{U}} - \mathbb{B}\,\mathbf{U}, \tag{2.100}$$

or equivalently in time-independent form, using $\mathbf{F}_{tot} = \mathrm{Re}\left[\boldsymbol{\mathcal{F}}_{tot}e^{-i\omega t}\right]$ and $\mathbf{F}_e = \mathrm{Re}\left[\mathbf{X}e^{-i\omega t}\right]$, as

$$\boldsymbol{\mathcal{F}}_{tot} = \mathbf{X} + \mathbb{C}\dot{\boldsymbol{\mathcal{U}}} - \mathbb{A}\ddot{\boldsymbol{\mathcal{U}}} - \mathbb{B}\boldsymbol{\mathcal{U}}, \tag{2.101}$$

where the first term is due to the exciting force, the second is the hydrostatic force, and the last two terms are due to the radiation of waves away from the body (the radiation force). For notational purposes, $\mathbf{F}_{tot}$ and $\boldsymbol{\mathcal{F}}_{tot}$ will be written as $\mathbf{F}$ and $\boldsymbol{\mathcal{F}}$ respectively hereafter.

2.4 Wave-Power Array Theory

2.4.1 Wave Energy

The energy of waves in a fluid is divided into kinetic energy and potential energy. The total potential energy of the fluid, per unit width of wave crest, can be written as

$$E_{pot} = \iiint_{\mathcal{V}} \rho g z \; d\mathcal{V}, \tag{2.102}$$

where $\mathcal{V}$ is the fluid volume. Similarly, the total kinetic energy is

$$E_{ke} = \iiint_{\mathcal{V}} \frac{1}{2}\rho u^2 \; d\mathcal{V}, \tag{2.103}$$

where $\mathbf{u}$ is the fluid velocity and $u^2 = \mathbf{u}.\mathbf{u} = |\mathbf{u}|^2$. The total instantaneous energy stored in the fluid is thus

$$E = E_{pot} + E_{ke} = \rho \iiint_{\mathcal{V}} \left(\frac{1}{2}u^2 + gz\right) \; d\mathcal{V}. \tag{2.104}$$

Now consider a vertical column of fluid, of upper plane surface area δS, bounded below by the sea bed and above by the free surface. The potential energy, due to the elevation of the water is given by

$$E_{pot} = \rho g \; \delta S \int_{-h}^{\eta} z \; dz = \frac{1}{2}\rho g \; \delta S \; \left(\eta^2 - h^2\right), \tag{2.105}$$

so that the total potential energy in the column, per unit surface, is

$$E_{pot} = \underbrace{\frac{1}{2}\rho g \eta^2}_{\text{hydrodynamic}} - \underbrace{\frac{1}{2}\rho g h^2}_{\text{hydrostatic}} . \tag{2.106}$$

The $-\frac{1}{2}\rho g h^2$ term is the hydrostatic potential energy of the water due to its height above the sea bed. The quantity of interest here is the hydrodynamic energy due to the wave motion (corresponding to the $\frac{1}{2}\rho g \eta^2$ term), so the hydrostatic term is neglected. Thus, the hydrodynamic potential energy in the column due to wave motion, per unit surface area, is

$$E_{pot} = \frac{1}{2}\rho g \eta^2. \tag{2.107}$$

Taking the incident wave to be a plane wave of amplitude A as in equations (2.28) and (2.36) and taking the average over time and space gives

$$\overline{E_{pot}} = \frac{1}{4}\rho g A^2. \tag{2.108}$$

Similarly, the kinetic energy of the column per unit surface area can be written as

$$E_{ke} = \frac{1}{2}\rho \int_{-h}^{\eta} |\mathbf{u}|^2 \; dz = \frac{1}{2}\rho \int_{-h}^{\eta} |\boldsymbol{\nabla}\Phi|^2 \; dz. \tag{2.109}$$

This can be separated into two integrals as

$$E_{ke} = \frac{1}{2}\rho \int_{-h}^{0} |\boldsymbol{\nabla}\Phi|^2 \, dz + \frac{1}{2}\rho \int_{0}^{\eta} |\boldsymbol{\nabla}\Phi|^2 \, dz. \tag{2.110}$$

The integrand in each integral is $\mathcal{O}(A^2)$. However, the range of integration of the second integral is $\mathcal{O}(A)$. Thus, the first term is $\mathcal{O}(A^2)$ and the second is $\mathcal{O}(A^3)$. Since linear wave theory is assumed and $A \ll h$, the second term can be neglected, giving

$$E_{ke} = \frac{1}{2}\rho \int_{-h}^{0} |\boldsymbol{\nabla}\Phi|^2 \, dz. \tag{2.111}$$

Taking the incident wave to be a plane progressive wave with $\beta = 0$ from equation (2.33) and calculating $\boldsymbol{\nabla}\Phi$ gives after simplification

$$\begin{aligned} E_{ke} =& \frac{\rho g^2 k^2 A^2}{2\omega^2 \cosh^2 kh} \\ &\times \int_{-h}^{0} \left[\cosh^2[k(z+h)]\cos^2(kx-\omega t) + \sinh^2[k(z+h)]\sin^2(kx-\omega t)\right] \, dz. \end{aligned} \tag{2.112}$$

Performing the integral gives

$$E_{ke} = \frac{\rho g^2 k A^2}{2\omega^2}\left[\frac{kh\cos 2(kx-\omega t)}{\cosh^2 kh} + \tanh kh\right]. \tag{2.113}$$

Taking the time and spacial average gives

$$\begin{aligned} \overline{E_{ke}} &= \left(\frac{\omega}{2\pi}\right)\left(\frac{k}{2\pi}\right)\int_0^{\frac{2\pi}{\omega}}\int_0^{\frac{2\pi}{k}} E_{ke} \, dx \, dt \\ &= \frac{1}{4}\rho g A^2. \end{aligned} \tag{2.114}$$

Comparing (2.108) and (2.114), it can be seen that the average kinetic energy and average potential energy contribute equal amounts to the average total energy stored in a wave, so that

$$\overline{E} = \overline{E_{pot}} + \overline{E_{ke}} = \frac{1}{2}\rho g A^2 \tag{2.115}$$

for a plane progressive incident wave.

Now consider the rate of change of the total energy E, which is the rate of energy flux. Allowing the fluid volume $\mathcal{V}$, which is contained within a boundary

surface $\mathcal{S}$, to move with velocity ν_n yields

$$\begin{aligned}\frac{dE}{dt} &= \rho\frac{d}{dt}\iiint_{\mathcal{V}}\left(\frac{1}{2}u^2+gz\right)\,d\mathcal{V}\\ &= \rho\iiint_{\mathcal{V}}\frac{\partial}{\partial t}\left(\frac{1}{2}u^2+gz\right)\,d\mathcal{V}+\rho\iint_{\mathcal{S}}\left(\frac{1}{2}u^2+gz\right)\nu_n\,d\mathcal{S},\end{aligned} \tag{2.116}$$

which, using (2.8) and the divergence theorem, simplifies to

$$\frac{dE}{dt} = \rho\iint_{\mathcal{S}}\left[\frac{\partial\Phi}{\partial t}\frac{\partial\Phi}{\partial n}+\left(\frac{1}{2}u^2+gz\right)\nu_n\right]\,d\mathcal{S}. \tag{2.117}$$

Application of Bernoulli's equation (2.12) yields

$$\frac{dE}{dt} = \rho\iint_{\mathcal{S}}\left[\frac{\partial\Phi}{\partial t}\frac{\partial\Phi}{\partial n}-\left(\frac{p-p_a}{\rho}+\frac{\partial\Phi}{\partial t}\right)\nu_n\right]\,d\mathcal{S}. \tag{2.118}$$

Once again, restrict attention to a vertical column of fluid, bounded above by the free surface and below by sea bed. There is no contribution to (2.118) from the top or bottom surfaces of $\mathcal{S}$. Since (2.118) holds for arbitrary ν_n, if $\nu_n = \nu = constant$ in the direction of wave propagation, this implies that the energy enters one side at the same mean rate as it leaves the other side. Therefore, the mean rate of energy flux across any vertical control surface $x = constant$, per unit width in the y-direction, is

$$\overline{\frac{dE}{dt}} = \overline{\rho\int_{-h}^{\eta}\left[\frac{\partial\Phi}{\partial t}\frac{\partial\Phi}{\partial n}+\left(\frac{1}{2}u^2+gz\right)\nu\right]\,dz}. \tag{2.119}$$

Now, if $\overline{\frac{dE}{dt}} = 0$, then ν is the mean velocity of energy flux in the fluid, and can be expressed as

$$\begin{aligned}\nu &= -\rho\overline{\int_{-h}^{\eta}\frac{\partial\Phi}{\partial t}\frac{\partial\Phi}{\partial n}\,dz}\Big/\rho\overline{\int_{-h}^{\eta}\left(\frac{1}{2}u^2+gz\right)\,dz}\\ &= \frac{-\rho\overline{\int_{-h}^{\eta}\frac{\partial\Phi}{\partial t}\frac{\partial\Phi}{\partial n}\,dz}}{\frac{1}{2}\rho g A^2},\end{aligned} \tag{2.120}$$

since the denominator is the energy density $\overline{E}$ from (2.115). It can be shown, for arbitrary depth h, that (2.120) simplifies to

$$\nu = c_g, \tag{2.121}$$

where c_g is the group velocity. Therefore, mean energy in the wave propagates at the group velocity, as stated earlier. This is straightforward to show for the plane progressive wave potential, as given in equation (2.33) and is thus applicable for linear wave theory only. Furthermore, the mean rate of energy flux across a fixed control surface is the product of the group velocity and the energy density,

$$\overline{\frac{dE}{dt}} = c_g \overline{E}. \tag{2.122}$$

2.4.2 Wave-Power Absorption

The power absorption by a single device is now considered. This will be extended to array power absorption in Section 2.4.4. When a wave is incident on a wave-power device, the wave does work on the device and sets it into oscillatory motion. Using conservation of energy, the power absorbed by the device is equal to the rate of work of the fluid on the device. The instantaneous power absorbed by a device operating in mode j is

$$\mathcal{P}_j = F_j U_j, \tag{2.123}$$

where $F_j = \{\mathbf{F}\}_j$ and $U_j = \{\mathbf{U}\}_j$ are the jth components of the total generalised force (2.100) and generalised velocity (2.56) respectively. The total instantaneous power absorbed is the sum of all such contributions from each mode of motion, which for a general body is

$$\mathcal{P} = \sum_{j=1}^{6} F_j U_j. \tag{2.124}$$

However, all quantities related to the wave-field, including the force on the device and the resulting motion of the device, will have a harmonic time-dependence. Thus, the value of (2.124) will oscillate with time. Therefore, a more useful measure of the power absorbed would be the average power absorbed P over one wave period $T = \frac{2\pi}{\omega}$, written as

$$P = \frac{\omega}{2\pi} \int_0^{\frac{2\pi}{\omega}} \mathbf{F}(t).\mathbf{U}(t)\ dt, \tag{2.125}$$

or equivalently, considering $\mathbf{F}$ and $\mathbf{U}$ to be column vectors,

$$P = \overline{\mathbf{F}^T \mathbf{U}}, \tag{2.126}$$

where ^{T} denotes matrix transpose and the over-bar denotes time average over one wave period. Using (2.100) and (2.126), it can be shown that

$$P = \overline{\left(\mathbf{F}_e(t) + \mathbb{C}\dot{\mathbf{U}}(t) - \mathbb{A}\dot{\mathbf{U}}(t) - \mathbb{B}\mathbf{U}(t)\right)^T \mathbf{U}} = \overline{\mathbf{F}_e^T\mathbf{U}} - \overline{\mathbf{U}^T\mathbb{B}\mathbf{U}}. \tag{2.127}$$

since $\overline{\dot{\mathbf{U}}^T\mathbf{U}} = 0$.

2.4.3 Array Coordinates

In general, cylindrical polar coordinates (R, θ, z) are adopted to describe the layout of the arrays within this work. To reduce the non-uniqueness in array formations and to simplify the geometry, one device is usually placed at a fixed location, which is often taken to be the global origin O. Since the devices are all floating structures as in figure 1.5, the z-coordinate is not of interest for the array geometry and the array layout (i.e. the position of the array members) can be considered in a 2D coordinate system.

Let the position of the mth device relative to O be given by $(R, \theta, z) = (d_m, \alpha_m, 0)$. Then, an array of N devices is described by $2(N-1)$ variables (2 coordinate variables for each device except the one with fixed position). Now define the local origins O_j in the centre of each device j and local coordinates (R_j, θ_j) relative to each O_j. Let d_{mn} be the distance between the mth and n^{th} device and the α_{mn} be the corresponding angle between the mth and n^{th} device (measured from the positive x-axis), so that the coordinates of device n relative to the origin at device m (denoted O_m) are $(R_m, \theta_m) = (d_{mn}, \alpha_{mn})$. These can be expressed in terms of the global coordinates as

$$d_{mn} = \left[d_m^2 + d_n^2 - 2d_m d_n \cos\left(\alpha_m - \alpha_n\right)\right]^{1/2} \tag{2.128}$$

and

$$\tan\left(\alpha_{mn}\right) = \frac{d_m \sin\left(\alpha_m\right) - d_n \sin(\alpha_n)}{d_m \cos\left(\alpha_m\right) - d_n \cos\left(\alpha_n\right)}. \tag{2.129}$$

Note also that $d_{mn} = d_{nm}$ and $\alpha_{mn} = \pi + \alpha_{nm}$. A general configuration showing the coordinates of WECs 2 and 3 is presented in figure 2.1

In the case of linear arrays, it is often convenient to fix one device at the origin and express certain quantities in terms of consecutive device separations. Rather than employing a combination of d_m or d_{mn} terms, a shorter notation for

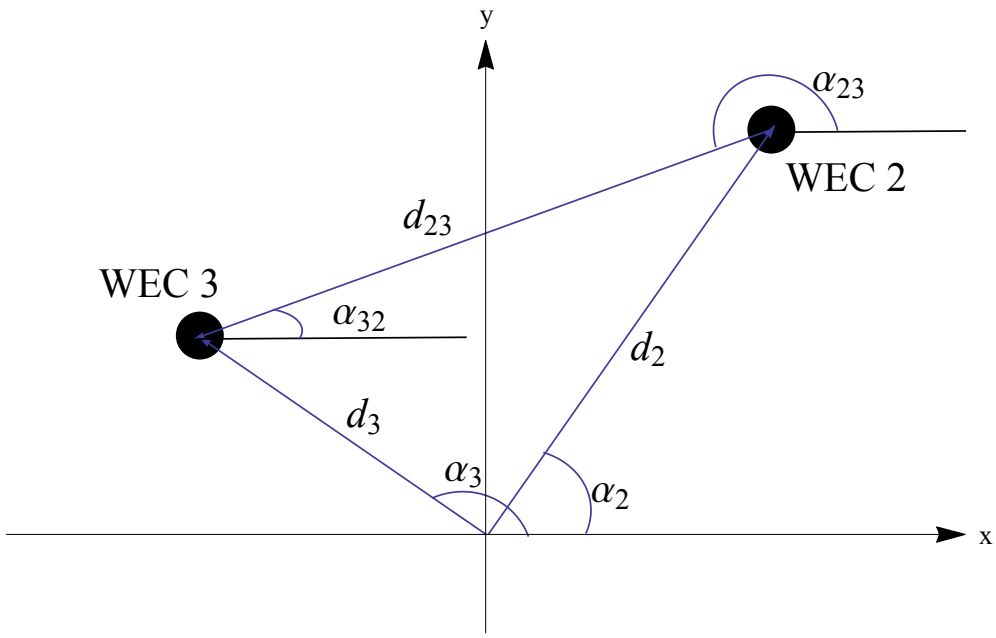

Figure 2.1: General configuration of WECs 2 and 3 in an array, showing the corresponding array coordinates.

consecutive separations is introduced where

$$s_m = d_{m(m+1)}. \tag{2.130}$$

Similarly, if circular arrays are considered, the most convenient coordinate system is to set the origin in the circle centre and define the positions of the WECs by their angular positions on the circle. A convenient notation is introduced to define the relative angles θ_j between each device, so that

$$\theta_j = \alpha_j - \alpha_{j+1}, \tag{2.131}$$

where the angular position of one device will be fixed.

This notation increases clarity in some expressions and enables a recognition of which separation is being considered. In many cases, the evaluation of quantities is in numerical computations where it is convenient to program the variables in this manner. Therefore, expressions that are evaluated numerically in this work are programmed in the same form as they are written in this thesis, wherever possible.

2.4.4 WEC Array Power Absorption Theory

Since arrays of WECs may contain many devices, matrix notation is ideal for a mathematical representation. Previously, there were six dimensions to the single body problem, accounting for the six degrees of freedom - three translational and three rotational. However, the devices considered within this thesis are assumed to absorb power in one mode of oscillation alone, namely heave. The WECs are also restricted to moving only in heave. Therefore, all column vectors are altered such that their j^{th} components represent the corresponding quantities for the heave mode of the jth device. Consider an array of N devices so that the dimension of the vectors and matrices are now N and $N \times N$ respectively. In the formulation, modifications are necessary in the body boundary conditions to remain consistent.

Let S be the wetted surfaces of all devices in equilibrium so that $S = \overline{S_{B_1}} \cup \overline{S_{B_2}} \cup \cdots \cup \overline{S_{B_N}}$, where $\overline{S_{B_j}}$ is the mean wetted surface of the jth body. In this formulation, the radiation body boundary condition only applies to the body which is radiating, so that (2.62) becomes

$$\frac{\partial \varphi_j}{\partial n} = n_l \delta_{jl} \qquad \text{on} \quad \overline{S_{B_l}}, \quad l = 1, 2, \ldots, N, \tag{2.132}$$

where δ_{jl} is the Kronecker delta, φ_j is the radiation potential of the jth body for the heave mode and $n_l = \{\mathbf{n}\}_l$ is the lth component of the unit normal to surface $\overline{S_{B_l}}$. Similarly the scattering boundary condition becomes

$$\frac{\partial \phi_s}{\partial n} = 0 \qquad \text{on} \quad \overline{S_{B_l}}, \quad l = 1, 2, \ldots, N. \tag{2.133}$$

The radiation force matrix must also be modified and the added mass and damping matrices are now

$$a_{jl} = \mathrm{Re}\left[-\rho \iint_S \varphi_j n_l \, dS\right] = \mathrm{Re}\left[-\rho \iint_{\overline{S_{B_l}}} \varphi_j \frac{\partial \varphi_l}{\partial n} \, dS\right], \tag{2.134}$$

$$b_{jl} = \mathrm{Im}\left[-\omega\rho \iint_S \varphi_j n_l \, dS\right] = \mathrm{Im}\left[-\omega\rho \iint_{\overline{S_{B_l}}} \varphi_j \frac{\partial \varphi_l}{\partial n} \, dS\right]. \tag{2.135}$$

The total mean power absorbed is given by equation (2.127), where the quantities are now generalised to correspond to the heave quantity of each body

as before. Thus, taking the mean rate of working of the hydrodynamic forces on one device and then summing over the N devices in the array gives the power absorbed. Thomas & Evans (1981) showed that the mean contribution to power absorption from the added mass and hydrostatic force are zero. Therefore, equation (2.127) now holds for an array of N heaving WECs.

Using $\mathbf{F}_e = \mathrm{Re}\,[\mathbf{X}e^{-i\omega t}]$ and $\mathbf{U} = \mathrm{Re}\,[\boldsymbol{\mathcal{U}}\, e^{-i\omega t}]$, (2.127) can be simplified to

$$P = \frac{1}{2}\mathrm{Re}\left[\mathbf{X}^{\dagger}\boldsymbol{\mathcal{U}}\right] - \frac{1}{2}\boldsymbol{\mathcal{U}}^{\dagger}\,\mathbb{B}\boldsymbol{\mathcal{U}}, \tag{2.136}$$

where † denotes the complex conjugate transpose. Assuming $\mathbb{B}$ is non-singular, it is also shown by Thomas & Evans (1981), after some manipulation, that the power absorbed by an array of WEC's is given by

$$P = \frac{1}{8}\mathbf{X}^{\dagger}\mathbb{B}^{-1}\mathbf{X} - \frac{1}{2}\left(\boldsymbol{\mathcal{U}} - \frac{1}{2}\mathbb{B}^{-1}\mathbf{X}\right)^{\dagger}\mathbb{B}\left(\boldsymbol{\mathcal{U}} - \frac{1}{2}\mathbb{B}^{-1}\mathbf{X}\right). \tag{2.137}$$

This quantity can be maximised by taking the second (negative) term to be zero, which occurs when the velocity is

$$\boldsymbol{\mathcal{U}}_{opt} = \frac{1}{2}\mathbb{B}^{-1}\mathbf{X}, \tag{2.138}$$

so that the maximum power absorbed by the array, as found by Thomas & Evans (1981), is

$$P_{opt} = \frac{1}{8}\mathbf{X}^{\dagger}\mathbb{B}^{-1}\mathbf{X} = \frac{1}{2}\boldsymbol{\mathcal{U}}_{opt}^{\dagger}\mathbb{B}\boldsymbol{\mathcal{U}}_{opt}. \tag{2.139}$$

It should be noted that, via an application of Green's Theorem and the method of stationary phase, the radiation damping matrix $\mathbb{B}$ can be expressed in terms of the exciting forces in deep water as

$$\{\mathbb{B}\}_{jl} = b_{jl} = \frac{1}{8\lambda P_w}\int_0^{2\pi} X_j(\theta)X_l^*(\theta)\; d\theta, \tag{2.140}$$

where

$$P_w = \frac{\rho g^2 A^2}{4\omega} \tag{2.141}$$

is the power per unit frontage of the incident wave. This was shown by Thomas & Evans (1981) for the application of wave energy. In this way, the maximum power absorbed can be expressed in terms of the exciting forces alone.

As previously discussed, the individual device displacement amplitudes are also of interest, since very large displacements are not only physically impractical,

but also invalidate the linear wave theory employed. The displacements are represented by the non-dimensional column vector $\mathbf{D}$, such that the displacement of the jth device is given by $\text{Re}\,[AD_j e^{-i\omega t}]$. This is equivalent to writing $\mathbf{D} = \frac{\boldsymbol{\xi}}{A}$. For maximum power absorption, the optimal displacements can be written as

$$\mathbf{D}_{opt} = \frac{i}{2\omega A}\mathbb{B}^{-1}\mathbf{X}. \tag{2.142}$$

To find the power absorbed, knowledge of the exciting forces $\mathbf{X}$ (on each device) is required. Consider an incident plane wave in the direction β as given in equation (2.40), with dispersion relationship (2.41). Now consider the radiation potentials emitted from the devices in the far-field region, where $kR \to \infty$. These potentials must satisfy the radiation condition and thus, for device j, must be of the asymptotic form

$$\varphi_j \sim \frac{ig}{\omega}\left(\frac{2}{\pi kR}\right)^{\frac{1}{2}} e^{kz+ikR} g_j(\theta), \tag{2.143}$$

where deep water is assumed; $g_j(\theta)$ contains the angular variation of the wave amplitude and a phase factor due to the location of body j. This can be written as

$$g_j(\theta) = f_j(\theta) e^{ikd_j \cos(\beta-\alpha_j)}, \tag{2.144}$$

where $f_j(\theta)$ is the far-field amplitude of the radiated wave-field from device j. The exciting force is related to the far-field amplitude $f_j(\theta)$; for N bodies operating in one mode of motion, Srokosz (1979) shows that

$$X_j(\beta) = \sqrt{2\pi}\frac{\rho g A}{k} f_j(\beta) e^{ikd_j \cos(\beta-\alpha_j) - \frac{3}{4}i\pi}. \tag{2.145}$$

2.4.5 Array Quality Measures

To assess the nature of the arrangement of an array of WECs, quantities of array interaction or array performance need to be defined. An absolute measure of the power absorption is not ideal as this does not give an indication of the power absorption capabilities of one array compared to other arrays or to an isolated device and thus would not be a clear measure of the interaction effects within the array. These absolute measures also lose generality by requiring certain quantities to be specified explicitly, such as the wave amplitude A and

device radius a. Therefore, one relative power measure is the absorption length

$$\mathcal{L}_{abs} = \frac{P}{P_w}, \tag{2.146}$$

which can be considered as the width of a wave train having the same mean energy as that extracted by the array. Using (2.139), the maximum absorption width is given by

$$\mathcal{L}_{opt} = \frac{P_{opt}}{P_w}. \tag{2.147}$$

It can be shown from equations (2.139) and (2.140) that the maximum absorption length of a single WEC restricted to operating in heave alone is

$$\mathcal{L}^{(1)}_{opt,heave} = \frac{\lambda}{2\pi}, \tag{2.148}$$

where the superscript denotes that the quantity is referring to a single WEC. Similarly, if the WEC operates in surge alone, then the maximum absorption length is

$$\mathcal{L}^{(1)}_{opt,surge} = \frac{\lambda}{\pi}, \tag{2.149}$$

though this will be dependent on the incident wave direction relative to the surge direction of the WEC.

The array effectiveness will now be compared to that of N devices operating in isolation, thus giving a measure of the performance of the array arrangement in terms of the interaction effects. The maximum absorption length (2.147) is recast in the alternate form

$$\mathcal{L}_{opt}\left(\beta\right) = \frac{\lambda}{2\pi} N q\left(\beta\right), \tag{2.150}$$

where β is the angle of the incident wave. The $\frac{\lambda}{2\pi}$ factor is the optimal absorption length of a single isolated device absorbing power in heave from equation (2.148), so that $q(\beta)$ measures the optimal performance of an array of N devices, compared to that of N devices operating in isolation. The quantity $q(\beta)$ is called the interaction factor or q-factor; this was first introduced incorrectly by Budal (1977) and then in this correct form by Evans (1979). Using the above formulation, this can be written as

$$q\left(\beta\right) = \frac{2\pi}{\lambda N} \frac{P_{opt}\left(\beta\right)}{P_w}. \tag{2.151}$$

The q-factor can also be represented as

$$\begin{aligned} q(\beta) &= \frac{\text{maximum absorbtion length for the array}}{N \times \text{maximum absorption length for isolated device}} \\ &= \frac{\text{maximum power absorption for array}}{N \times \text{maximum power absorption for isolated device}}. \end{aligned} \tag{2.152}$$

Note that $q(\beta)$ can be expressed in terms of the exciting forces alone, using (2.151), (2.139) and (2.140) to give

$$q(\beta) = \sum_{m,n=1}^{N} X_m^{\dagger}(\beta) \left[\frac{1}{2\pi} \int_0^{2\pi} X_i(\theta) X_j^*(\theta)\, d\theta \right]_{mn}^{-1} X_n(\beta), \tag{2.153}$$

where $[a_{ij}]_{mn}^{-1}$ denotes the $(m,n)^{th}$ term of the inverse of the matrix whose $(i,j)^{th}$ term is given in $[a_{ij}]$. This was shown by Thomas & Evans (1981) for this particular application of WEC array modelling.

It should be noted that the above definition of the interaction factor only compares the *optimal* performance of the array to the *optimal* performance of N isolated devices. However, as previously discussed, if constraints are placed on the WEC motions, then the optimal performance may not be achievable. Therefore, alternative versions of the interaction factor must be considered. One such quantity is termed the averaged interaction factor $\overline{q}(\beta)$ and is defined as

$$\begin{aligned} \overline{q}(\beta) &= \frac{\text{absorption length for array subject to constraints}}{N \times \text{optimal absorption length for isolated device}} \\ &= \frac{\text{power absorbed by array subject to constraints}}{N \times \text{maximum power absorbed by isolated device}}. \end{aligned} \tag{2.154}$$

where the *actual* (not optimal) power absorbed by the array is utilised. Another version of the interaction factor is called the generalised q-factor, q_{gen}, which relates the *constrained* performance of the array to the *constrained* performance of an isolated device, so that

$$\begin{aligned} q_{gen} &= \frac{\text{absorption length for array subject to constraints}}{N \times \text{absorption length for isolated device subject to constraints}} \\ &= \frac{\text{power absorbed by array subject to constraints}}{N \times \text{power absorbed by isolated device subject to constraints}}. \end{aligned} \tag{2.155}$$

Each of these measures of array interaction has its individual strengths and weaknesses. Clearly, it is more desirable to examine constrained performance, as this will more accurately model a real life scenario. However, using the optimal

interaction factor q in the first instance is preferable as it is relatively easy to calculate and provides an upper limit on what can be achieved. When constraints are considered, intuitively it is more appropriate to compare constrained performance of the array to the constrained performance of isolated WECs, since the optimal performance of a single WEC may not be achievable in the constrained regime. However, this requires knowledge of the single WEC optimal displacement amplitudes and phases subject to the given constraints. Thus, the calculation of q_{gen} is more involved and requires greater computational resources. However, as $\overline{q}$ compares the constrained array performance to the maximum isolated WEC performance, no such knowledge of the displacements are required and the calculation of $\overline{q}$ is less intensive.

In general, $q \geq q_{gen} \geq \overline{q}$. Equality will result between q_{gen} and $\overline{q}$ if the optimal isolated WEC displacement amplitude is less than the constraint amplitude. Furthermore, equality will hold for all three interaction factors if the optimal displacements for all WECs in the array are also less than the constraint amplitude.

2.4.6 Point Absorber Theory

The point absorber theory essentially assumes that the devices are small enough that they do not produce a scattered wave-field. The corresponding mathematical assumption is that $ka \ll 1$, for a device radius a. This assumption allows the far-field angular dependence of the mth device $f_m(\theta)$ to be expressed as

$$f_m(\theta) = f(\theta), \tag{2.156}$$

where $f(\theta)$ is the far-field dependence for an isolated device oscillating in heave. Further, since all devices are axisymmetric and heaving, it is assumed that $f(\theta) = f = constant$. For the case of semi-submerged spheres, the far-field amplitude is shown by Havelock (1955) to be

$$f(\theta) = \sqrt{2\pi} k a^2 e^{-\frac{1}{4}i\pi} (\mathcal{C} - i\mathcal{D}), \tag{2.157}$$

where $\mathcal{C}$ and $\mathcal{D}$ are constants often referred to as the Havelock coefficients.

This allows analytical expressions for the excitation forces $\mathbf{X}$ and the radiation

damping $\mathbb{B}$ to be determined. These are written as

$$\mathbf{X} = 2\pi\rho g a^2 A(\mathcal{C} - i\mathcal{D})\,\boldsymbol{\ell} \tag{2.158}$$

$$\mathbb{B} = \frac{2\pi\rho a^4\omega^3(\mathcal{C}^2 + \mathcal{D}^2)}{g}\,\mathbb{J}, \tag{2.159}$$

where $\boldsymbol{\ell}$ is an N component column vector with components

$$\ell_m = e^{ikd_m\cos(\beta-\alpha_m)}, \tag{2.160}$$

and $\mathbb{J}$ is an $N \times N$ matrix with elements

$$\mathbb{J}_{mn} = J_0\left(kd_{mn}\right), \tag{2.161}$$

for devices operating in heave, where $J_0(x)$ is the zeroth order Bessel function of first kind.

Thus, the q-factor of the array can be expressed in terms of the phases due to the device positions and Bessel functions. It is shown by Evans (1979) that the q-factor can be expressed, for an array of N devices, as

$$q\left(\beta\right) = \frac{1}{N}\boldsymbol{\ell}^\dagger\mathbb{J}^{-1}\boldsymbol{\ell}. \tag{2.162}$$

Equation (2.162) holds for a general array, where the amplitudes of each device are in general not equal. This is in contrast to the expression for the q-factor derived by Budal (1977), which only holds for the special case when all device motion amplitudes are equal. Budal's expression for the interaction factor, denoted q_B, can be expressed as

$$q_B\left(\beta\right) = \left[\frac{1}{N}\boldsymbol{\ell}^\dagger\mathbb{J}\boldsymbol{\ell}\right]^{-1}. \tag{2.163}$$

Clearly (2.162) and (2.163) are not the same and the latter is a very special case of the former, since via (2.142), the assumption of equal device amplitudes is not true in general. This is because the motion amplitudes of each device depend on the exciting forces and radiation damping coefficients.

A consistency relation for the q-factor was derived by Fitzgerald (2006). This states, for optimal WEC motions within the limitation of the point absorber approximation, that

$$\frac{1}{2\pi}\int_0^{2\pi} q(\beta)\;d\beta = 1. \tag{2.164}$$

It can also be shown that the q-factor for an array is invariant if the angle of incidence is altered by π, hence

$$q\left(\beta+\pi\right)=q\left(\beta\right). \tag{2.165}$$

Thus, (2.164) can also be written as

$$\frac{1}{\pi}\int_0^{\pi} q(\beta)\ d\beta=\frac{1}{\pi}\int_{\pi}^{2\pi} q(\beta)\ d\beta=1. \tag{2.166}$$

For arrays with symmetry about the x and y-axes, such as linear arrays, the above can be simplified further and written

$$\frac{2}{\pi}\int_0^{\pi/2} q(\beta)\ d\beta=1. \tag{2.167}$$

Note that (2.164) and its extensions only hold for optimal WEC motions and is not expected to be true for non-optimal motions. Results from Child (2011) indicate that $\frac{1}{2\pi}\int_0^{2\pi} q(\beta)\ d\beta$ is slightly less than unity when the scattered wave-field is included and a realistic PTO is applied. This was shown by Child (2011) for optimal arrays determined using both the Parabolic Intersection (PI) and Genetic Algorithm (GA) methods.

As discussed in Section 1.3.3, the result (2.164) obtained by Fitzgerald (2006) is a special case of a more general result derived by Wolgamot, Taylor, & Eatock Taylor (2012). Consider an N-device array with devices of arbitrary size and shape. Now consider the numerator of the q-factor (2.152), which can be written as in (2.139). Wolgamot *et al.* (2012) shows that the average of this numerator with respect to the angle of incidence β is given by

$$\frac{1}{2\pi}\int_0^{2\pi}\frac{1}{8}\mathbf{X}^{\dagger}\mathbb{B}^{-1}\mathbf{X}\ d\beta=N\frac{\mathcal{J}}{k}, \tag{2.168}$$

where $\mathcal{J}=\frac{\rho g^2A^2}{4\omega}\left\{\left[1+\frac{2kh}{\sinh 2kh}\right]\tanh kh\right\}$ is the power per unit width of incident wave front for arbitrary water depths; in deep water, this is simplified to $\mathcal{J}=\frac{\rho g^2A^2}{4\omega}=P_w$. This more fundamental result is valid for general device shape. For heaving axisymmetric devices, (2.168) reduces to the result (2.164) of Fitzgerald (2006).

Another implication of (2.168) is that, for a single non-axisymmetric device, the directional averaged maximum power the device can absorb is the same as for an axisymmetric device. This shows that if a device is shaped so that it absorbs

energy very well in a particular direction β, than it will perform poorly for other values of β, as expected, so that the average is preserved. Therefore, detailed investigation of the wave resource at a proposed array location should be carried out before consideration of the size and shape of both the individual devices and the array. It is also important to note that this only applies to regular waves.

Expressions for the averaged and generalised interaction factors can also be derived. Using $\boldsymbol{\mathcal{U}} = -i\omega A\mathbf{D}$ and simplifying gives

$$\overline{q} = \frac{4\pi(ka)^2}{N}\left(-\mathrm{Re}\left[(\mathcal{D}+i\mathcal{C})\mathbf{D}^\dagger\boldsymbol{\ell}\right] - \pi(ka)^2(\mathcal{C}^2+\mathcal{D}^2)\mathbf{D}^\dagger\mathbb{J}\mathbf{D}\right). \tag{2.169}$$

Similarly, by defining $D_{1,opt}$ as the (complex) optimal displacements of an isolated device (subject to constraints), the generalised interaction factor can be written

$$q_{gen} = \frac{1}{N}\frac{\mathrm{Re}\left[(\mathcal{D}+i\mathcal{C})\mathbf{D}^\dagger\boldsymbol{\ell}\right] + \pi(ka)^2(\mathcal{C}^2+\mathcal{D}^2)\mathbf{D}^\dagger\mathbb{J}\mathbf{D}}{\mathrm{Re}\left[(\mathcal{D}+i\mathcal{C})D_{1,opt}\right] + \pi(ka)^2(\mathcal{C}^2+\mathcal{D}^2)|D_{1,opt}|^2}. \tag{2.170}$$

2.5 Irregular Sea Theory

2.5.1 Introduction

Only theory involving regular waves has been presented thus far. However, in most realistic sea states, regular waves do not occur, as is evident to any observer on a ship or beach. The intricacy of these waves and in particular the notion of modelling such irregular behaviour appears daunting. One reason for this is that the waves in the ocean appear random in nature, due to their complex sources and causes. The ocean's waves are caused by the weather in the Earth's atmosphere, predominately the wind, which is itself difficult to predict. Ocean waves are also affected by travelling great distances and encountering random non-uniformities in the air and water. One can consider a regular plane wave as being created by a singular "storm" event very far from the point of interest, so that the non-linear effects of the storm are no longer present. However, even this case results in waves of several wavenumbers; thus, real waves cannot be thought of so simply as single wavelength regular plane waves. Therefore, real irregular ocean waves must be described in a stochastic manner.

One simplifying idea is that an irregular wave can be thought of as being composed of several regular wave components of different amplitudes,

wavenumbers and angles and thus can be written as a superposition of regular waves.

2.5.2 Description of Irregular Waves

It is assumed that an irregular wave η can be expressed as a superposition of regular waves η_j, which are of the form in (2.28) and (2.36), so that the free surface is written in integral form as

$$\eta = \mathrm{Re}\left[\int_0^\infty A\left(\omega\right)\ e^{i[k(\omega)r\cos(\theta-\beta_0)-\omega t+\Xi(\omega)]}\ d\omega\right], \tag{2.171}$$

for a wave travelling in the direction β_0, where $\Xi(\omega)$ is a phase function and $k\left(\omega\right) > 0$. Extending (2.171) to include waves from all possible directions gives

$$\eta = \mathrm{Re}\left[\int_0^{2\pi}\int_0^\infty A\left(\omega,\beta\right)\ e^{i[k(\omega)r\cos(\theta-\beta)-\omega t+\Xi(\omega)]}\ d\omega\ d\beta\right]. \tag{2.172}$$

Equation (2.171) can represented approximately as linear sum of an infinite number of wave frequency components and is written as

$$\eta = \sum_j \eta_j = \mathrm{Re}\left[\sum_j A_j e^{i[k_j r\cos(\theta-\beta_0)-\omega_j t+\Xi_j]}\right], \tag{2.173}$$

where $k_j = k\left(\omega_j\right)$ is given by the dispersion relationship (2.37) and A_j is the amplitude of the discrete frequency ω_j with a phase difference Ξ_j. Comparing equations (2.171) and (2.173) shows that the discrete and continuous measure of the amplitude are related by $A_j = A(\omega)\ d\omega$. Thus, $A(\omega)$ can be considered as an amplitude density function.

2.5.3 Power in Irregular Seas

The average energy, per unit surface area, is proportional to $\eta^2 = \eta^*\eta$ and is written as

$$\overline{E} = \rho g\int_0^\infty\int_{-\pi}^{\pi} S(\omega,\beta)\ d\beta\ d\omega, \tag{2.174}$$

where $S(\omega,\beta)$ is the energy density of the waves for a frequency ω and wave angle β; this is often referred to as the wave energy spectrum or the wave spectrum. This representation allows for both directional and frequency variation in the sea state. The non-directional frequency spectrum $S_\omega(\omega)$ can be

found by integrating over β, so that

$$S_\omega(\omega) = \int_0^{2\pi} S(\omega, \beta)\, d\beta. \tag{2.175}$$

It should be noted that only $S_\omega(\omega)$ can be obtained from taking data of the free surface elevation at one point (e.g. by use of a single buoy, though some buoys can measure directionality also). If the directional variability of the wave environment is very small, it can be assumed that the waves are long-crested and hence unidirectional; in this case (2.175) is sufficient to describe the sea-state. This is the case when the waves can be considered to be generated by a far off "storm" event.

The directional spectrum $S(\omega, \beta)$ is often assumed to be separable into a frequency dependent part and a directionally dependent part, as

$$S(\omega, \beta) = D(\omega, \beta)\, S_\omega(\omega), \tag{2.176}$$

where, for consistency, $D(\omega, \beta)$ must satisfy

$$\int_0^{2\pi} D(\omega, \beta)\, d\beta = 1. \tag{2.177}$$

It is often assumed that the frequency dependence is independently separable from $S(\omega, \beta)$, so that $D(\omega, \beta) = D(\beta)$ is independent of frequency. If desired $S_\omega(\omega), S(\omega, \beta)$ and $D(\omega, \beta)$ can be written in terms of the wavenumber k instead of frequency ω by employing the appropriate dispersion relation (2.37), or (2.41) for deep water. Further details of the mathematical description of power in irregular seas can be found in Falnes (2002).

For the purposes of this thesis, a JONSWAP spectrum is chosen similar to that used in Child (2011). The wave frequency spectrum, written in terms of angular frequency ω is

$$S_\omega(\omega) = \frac{\alpha_p g^2}{\omega^5} \exp\left[-\frac{5}{4}\left(\frac{\omega_p}{\omega}\right)^4\right] \gamma_p^Y \tag{2.178}$$

$$Y = \exp\left[-\frac{1}{2}\left(\frac{\frac{\omega}{\omega_p} - 1}{\sigma_p}\right)^2\right], \tag{2.179}$$

where α_p is the Phillips constant, γ_p is the peak enhancement factor, σ_p is the peak width parameter and ω_p is the value of the frequency ω at the spectrum peak. Typical values of the above constants, such as those used in Child (2011),

are

$$\alpha_p = 0.0081, \tag{2.180}$$

$$\gamma_p = 3.3, \tag{2.181}$$

$$\sigma_p = \begin{cases} 0.07 & \text{for} \quad \omega \leq \omega_p \\ 0.09 & \text{for} \quad \omega > \omega_p \end{cases} . \tag{2.182}$$

The total wave spectrum is assumed to be separable into a product of an ω-dependent and a β-dependent component (a special case of (2.176)). This is written as

$$S(\omega, \beta) = S_\omega(\omega) S_\beta(\beta), \tag{2.183}$$

where $S_\beta(\beta)$ is the incident wave angle spectrum. One possible form of the angle spectrum is

$$S_\beta(\beta) = \frac{2^{2s_p-1}}{\pi} \frac{\Gamma^2(s_p+1)}{\Gamma(2s_p+1)} \cos^{2s_p}\left[\frac{1}{2}(\beta - \beta_p)\right], \tag{2.184}$$

where s_p is the spreading parameter, β_p is the dominant incident wave direction and Γ is the Gamma function.

Typical values of the spreading parameter for S_β can be chosen between $s_p = 5, 10, 15$, in line with Child (2011), depending on how wide an angle spectrum is desired. The peak angle direction β_p can be chosen as desired, namely $\beta_p = 0, \frac{\pi}{4}, \frac{\pi}{2}$, *etc.*. A standard value for peak frequency could be taken as $\omega_p = 0.5$, as this roughly corresponds to ocean wavelengths of between 200m - 250m ($\omega = 0.5 \Rightarrow \lambda = 246$m) and is intended to represent a typical case.

To analyse the implications of the wave spectrum on power absorption, the power spectrum needs to be formulated. This is formed as

$$S_P(\omega, \beta) = 2\pi\rho g S(\omega, \beta) c_g(\omega), \tag{2.185}$$

where $c_g(\omega)$ is the group velocity, defined by equation (2.44) (or equation (2.47) for deep water), and an analytical expression can be obtained from the dispersion relationship. The factor of 2π is introduced in (2.185) since $\frac{d\omega}{df} = 2\pi$ and this is needed to remain consistent with the total power contained in the spectrum.

Using a unidirectional version of (2.185), where it is assumed that there is no

β-dependency, the total power contained in the incident spectrum is

$$P_\infty = \int_0^\infty S_P(\omega)\ d\omega.$$

However, numerical calculations of this can be simplified by taking a smaller range of ω that is of primary interest. Most often, the spectrum will only be non-zero for a relatively small finite range of ω. Limiting the numerical integration to this range will significantly reduce the computation time required, without an appreciable loss of accuracy. It may also be desirable to avoid certain highly oscillatory (bad-behaved) parts of the range of ω. Therefore, the targeted power is introduced as

$$P_T = \int_{\omega_l}^{\omega_u} S_P(\omega)\ d\omega, \tag{2.186}$$

for appropriate values of ω_l and ω_u.

Chapter 3

Preliminary Optimisation of Linear Arrays in Regular Waves

3.1 Introduction

The principal objective of this chapter is the numerical optimisation of the layout of elementary arrays of spherical point absorber WECs, that are constrained to a linear geometry. Different array geometries, such as circular arrays, are investigated in subsequent chapters together with arrays without a prescribed geometry. Before a general optimisation is attempted, the case of a simpler single-variable problem is considered, which involves symmetric linear arrays of five point absorber WECs. This one variable set-up approximates the more general problem and allows for greater visualisation of the results. Another advantage is that the single-variable optimisation involves considerably less computational effort. However, meaningful results are still obtained. The results detailed herein also provide a benchmark for comparison in later chapters, which consider more general problems and constrained motions.

The majority of existing work has considered the optimisation of WEC arrays through maximisation of the interaction factor q, with respect to the array geometry and device spacing, see for example Thomas & Evans (1981) and McIver (1994). However, recent studies has shown that large values or peaks of the q-factor are usually surrounded by troughs of significantly lower performance. This can result in a move from constructive to destructive interference for just small changes in non-dimensional spacing and incident wave direction, as shown by Fitzgerald (2006), Child (2011), McGuinness (2013),

Costigan (2014), Fennell (2015) and Lawton (2017). This is severely restrictive, as the q-factor measures the optimum performance of an array and assumes optimal WEC motions and maximum power absorption. The q-factor does not account for device efficiency or losses in performance, such as those due to mooring. Therefore, if $q < 1$, this may represent poor performance in the case of real devices.

As the values of q can be sensitive to changes in some parameters, it is desirable to design the array such that the interaction factor is either approximately unity, or preferably that $q > 1$ for a large range of parameter values. In order to achieve this, an array layout is sought such that the integral of q over a range of non-dimensional spacing is maximised; this effectively maximises the mean value of q in the specified range of interest. A detailed description of this optimisation method is given in Section 3.2.

The work presented in this chapter is summarised by McGuinness & Thomas (2015). This is an extension of the preliminary study by McGuinness (2013), which subsequently led to the work of Costigan (2014) on circular array geometries, Fennell (2015) on triangular arrays and Lawton (2017) on elliptical arrays. The results presented by McGuinness & Thomas (2015) are extended here to an in-depth analysis of the array performance, device displacements and a sensitivity analysis of the optimal performance.

It is important to be aware that the device motions can have a large impact on the interaction factor. Large motion amplitudes are undesirable for several reasons, including associated engineering difficulties in terms of the PTO and the fact that large device motions will violate the assumptions of the underlying linear wave theory. For example, if a large value of q is accompanied by large device displacements, the imposition of a realistic PTO will tend to dampen the motion of the devices and this will have a detrimental effect on the array performance. Furthermore, large device displacements may cause the device to leave the water surface, which will lead to slamming forces on re-entry and affect the device survivability.

3.1.1 Previous Research on Linear Arrays

The simplest and most investigated array geometry is that of a straight line of WECs. This removes all the angular device coordinates and a one dimensional coordinate system can be used. Linear arrays have been extensively studied, for

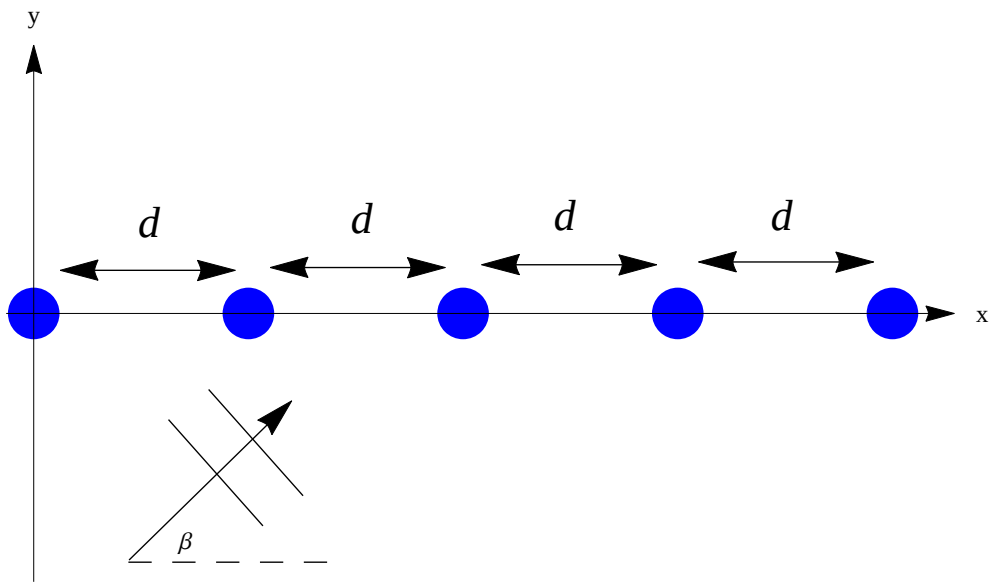

Figure 3.1: Diagram of uniform linear array with spacing d between consecutive devices.

example by Budal (1977), Evans (1979), Thomas & Evans (1981) and McIver (1994). The most considered class is the uniform array, where the spacing between each of the devices is identical. This was first studied by Thomas & Evans (1981), where uniform linear arrays of five devices were investigated for several angles of wave incidence. A diagram of this array is shown in figure 3.1. The value of q was investigated with respect to the uniform non-dimensional distance between devices kd.

Figure 3.2 from Thomas & Evans (1981) shows that relatively small changes in kd can result in large changes in q. Considering the peak in beam seas near $kd = 5$, a unitary change to $kd = 6$ results in much poorer performance. In particular, these changes can result in a move from $q > 1$ to $q < 1$, i.e. from constructive to destructive interference. This is undesirable as the wave conditions are not constant in real seas and may vary, which in turn will alter the non-dimensional separation kd. The same problem generally occurs for variation of the incident wave angle.

It can be seen that the array performs better overall in beam seas compared to head seas, which is consistent with the intuitive idea that greater frontage to the waves allows greater power absorption. For beam seas, $q > 1$ for the majority of the domain $kd \in [1, 10]$ considered; while the converse is true for head seas. This effect is related to the condition (2.164) derived by Fitzgerald (2006), as this states that the average interaction factor over all wave angles

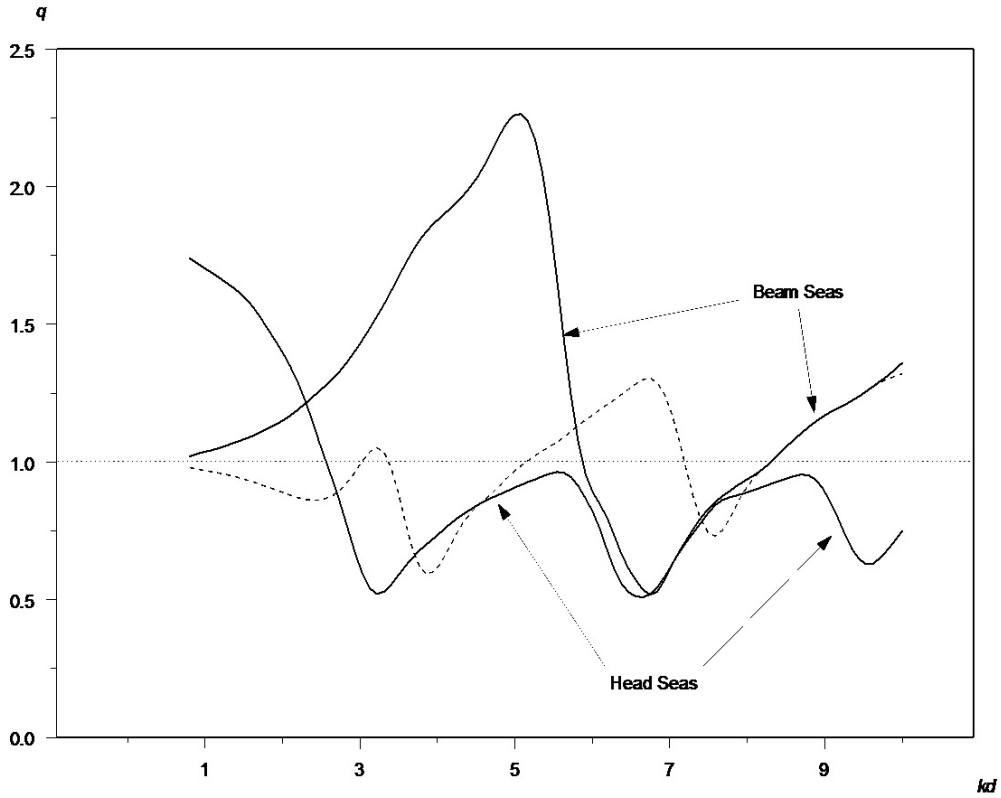

Figure 3.2: Variation of q-factor with non-dimensional uniform spacing kd for beam, head and intermediate (dashed curve) seas. Taken from Thomas & Evans (1981).

must be unity. Thus good performance at one wave angle must be accompanied by analogously poor performance at other wave angles. Note that the total length of this array is $L = 4d$. In order to allow comparison between Thomas & Evans (1981) and the notation of this chapter, the relationship between kd in figure 3.2 and kL used here is $kL = 4kd$.

One aspect that has been neglected in the literature on linear arrays concerns the optimal separations between devices within an array, for a given array length. The objective is to optimise the layout of linear arrays of five WECs, so that improved performance was achieved which was also stable (in some sense) to changes in non-dimensional spacing. This was achieved by maximising the mean of the interaction factor over a range of non-dimensional array length. The procedure for general linear arrays is outlined below, while a detailed presentation of the simplified optimisation procedure for the arrays investigated by McGuinness & Thomas (2015) is given in Section 3.3.

3.2 Optimisation Method

Consider an array of N devices with the coordinates of each device given as described in Section 2.4.3. One device is fixed at the origin to avoid unnecessary replication of results. This means that the array is described by $2(N-1)$ variables, which represent the positions of all the other WECs. If the array geometry is prescribed as linear, then all the α_ms are zero (or can be set to zero by an appropriate coordinate rotation) and the number of array variables is reduced to $N-1$.

The objective is to maximise the mean value of q. For a linear array of total length L between the first and N^{th} devices, this is defined as

$$I_{line}(ks_1, \ldots, ks_{N-1}; \beta_0) = \frac{1}{kL_u - kL_l} \int_{kL_l}^{kL_u} q\left(ks_1, \ldots, ks_{N-1}, \beta_0\right) \; d[kL], \tag{3.1}$$

where kL_u and kL_l are the upper and lower limits of the range of non-dimensional length of the linear array. The fixed prescribed incident wave angle is β_0 and the convenient notation $s_j = d_{j(j+1)}$ for consecutive device separations has also been used. As the objective function is an integral, maximising (3.1) is not trivial and numerical maximisation will need to be employed.

The values of $[kL_l, kL_u]$ define the range of interest over which q is to be optimised, with the expected or target value of kL at the centre of this range. The value of kL_l is usually chosen to not only define the lower bound of the optimisation range, but also high enough to avoid rapid large oscillations in both the q-factor and the displacements $\mathbf{D}$ for arrays with very small non-dimensional spacings. The oscillatory manor of the expressions for q and $\mathbf{D}$ for low values of non-dimensional spacing is computationally prohibitive. Low values of kL_l may also result in touching or coincident WECs, which is to be avoided.

The integration variable kL does not appear explicitly in the integrand of (3.1) and is dependent on the sum of all the ks_j's. One way of circumventing this is to reparameterise these variables and investigate a discrete set of values of these variables to locate the maximum. This is done by writing

$$ks_j = \frac{n_j \; kL}{M}, \tag{3.2}$$

where n_j is taken to be an integer value which defines the consecutive spacing

between the jth and $(j+1)^{\text{th}}$ devices relative to the array length and M is a chosen discretisation integer parameter such that $M = \sum_{j=1}^{N-1} n_j$. In this way, the n_j's are integer variables that become the parameters of the optimisation. Equation (3.1) can now be written as

$$I_{line}(n_1, \ldots, n_{N-1}; \beta_0) = \frac{1}{kL_u - kL_l} \int_{kL_l}^{kL_u} q\left(n_1, \ldots, n_{N-1}, kL; \beta_0\right) \; d[kL]. \tag{3.3}$$

The integration variable kL appears explicitly in the integrand and numerical integration can be performed. Since the sum of all consecutive device separations is the total array length, then

$$\sum_{j=1}^{N-1} ks_j = kL, \tag{3.4}$$

which in terms of the n_js implies

$$\sum_{j=1}^{N-1} n_j = M. \tag{3.5}$$

Therefore, one separation variable can be written in terms of all others, for example

$$n_{N-1} = M - \sum_{j=1}^{N-2} n_j, \tag{3.6}$$

thus reducing the number of position variables within the optimisation to $N-2$, since kL is the variable of integration in the objective function. In general, for a linear array of N WECs, the objective function is thus written as

$$I_{line}(n_1, \ldots, n_{N-2}; \beta_0) = \frac{1}{kL_u - kL_l} \int_{kL_l}^{kL_u} q\left(n_1, \ldots, n_{N-2}, kL; \beta_0\right) \; d[kL]. \tag{3.7}$$

In this chapter, integer values of the n_j's are investigated for arrays of $N = 5$ WECs with $M = 100$. This was due to the computational limitations of Mathematica 9.0, in which all calculations of this chapter were performed. In general, however, the n_j's do not need to be integer and in later chapters involving more general optimisations, real (non-integer) values of n_j are allowed.

To perform a preliminary optimisation of this type of array efficiently, it is desirable to have as few variables describing the array as possible. In theory, this optimisation can be performed for any number of variables but a larger

number of variables increases the numerical intensity of the procedure and the computational resources required for the optimisation considerably.

3.3 Optimal Linear Arrays of One Variable

This section considers linear arrays of $N = 5$ devices. Within this optimisation regime, this results in arrays that are described by three variables. Two symmetries (or asymmetries) are enforced, so that each array investigated can be described by one variable, namely kd_1 or n_1. In each case, these symmetries are defined such that $ks_n = ks_m$, for two values of n and m between 1 and 4 ($n \neq m$). This allows two of the unknowns to be dropped, reducing the number of optimisation variables to one. For example, mirror symmetry across the middle of the array forces that $ks_1 = ks_4$ and $ks_2 = ks_3$, which in turn gives

$$\begin{aligned} kL &= ks_1 + ks_2 + ks_3 + ks_4 \\ &= 2\left(ks_1 + ks_2\right) \end{aligned} \tag{3.8}$$

$$\Rightarrow ks_2 = \frac{kL}{2} - ks_1. \tag{3.9}$$

Using (3.2), (3.4) and (3.5), this can be written in terms of the parameters n_1 and n_2 as

$$n_2 = \frac{M}{2} - n_1. \tag{3.10}$$

Equation (3.7) can then be simplified to

$$I_{line}(n_1; \beta_0) = \frac{1}{kL_u - kL_l} \int_{kL_l}^{kL_u} q(n_1, kL; \beta_0)\ d[kL] \tag{3.11}$$

and the optimisation can now be performed in terms of one variable (n_1) only. For notational convenience, the line subscript is dropped hereafter.

Certain conditions must be imposed on the value of n_1 for this formulation to remain consistent. One requirement is that n_1 must be positive, as $n_1 \leq 0$ gives a non-dimensional separation of $ks_1 \leq 0$ which is not physically possible. Similarly, $n_2 > 0$ must be enforced. Using equation (3.10), this requires that $n_1 \in \left(0, \frac{M}{2}\right)$. Setting $M = 100$, this corresponds to $n_1 \in [1, 49]$ for integer n_1. The accuracy of this (discrete) optimisation method can be increased by taking larger values of M or allowing non-integer values of n_1. However, this requires a

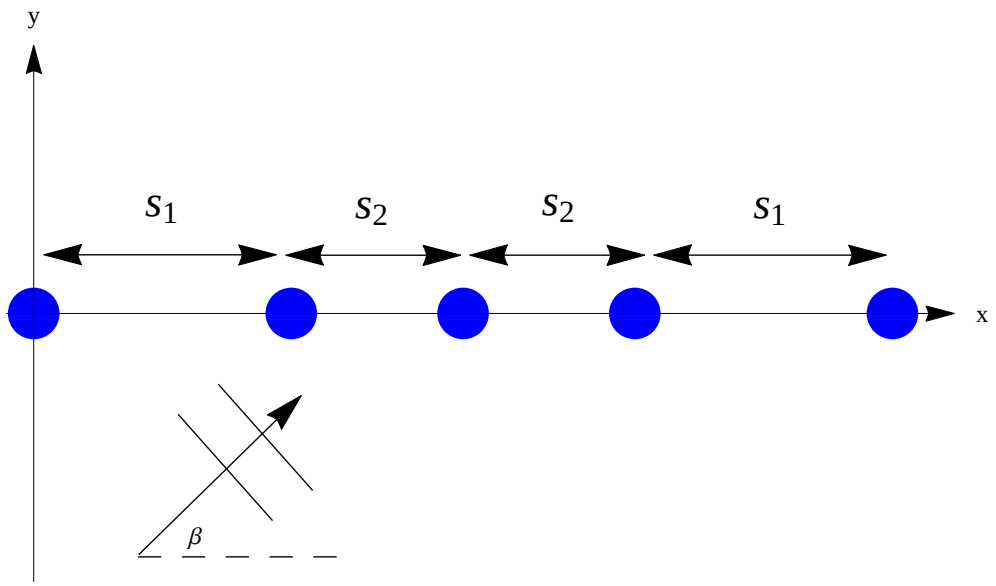

Figure 3.3: Diagram of array LS1, with mirror symmetry about the middle WEC.

larger range of parameter values to be investigated.

The linear arrays shown in the following subsection were optimised for the non-dimensional length range $kL \in [kL_l, kL_u] = [5, 15]$, as this represents a valid range of variation for kL for a target value of $kL = 10$. This is chosen arbitrarily but is intended to represent a typical case. WECs are usually envisaged to have separations of between 50m to 100m between them, giving an array length of between 250m and 500m for a five-WEC linear array. For $kL = 10$, these array lengths correspond approximately to wavelengths of between 150m and 320m, which are reasonable for ocean waves.

The WEC motions can only be recovered if the geometry is known. To enable calculations of the WEC displacements, particularly the displacement amplitudes, the WECs are assumed to be semi-submerged spheres with a fixed non-dimensional radius of $ka = 0.4$. The work of Havelock (1955) can then be used to calculate the WEC motions using equation (2.142).

Three different types of array symmetry are investigated in Sections 3.3.1 - 3.3.3. In each case, the array is optimised using the method described for several fixed values in incident wave angle β_0. The optimal arrays are then analysed for variations in the wave-field and the stability of their performance is assessed.

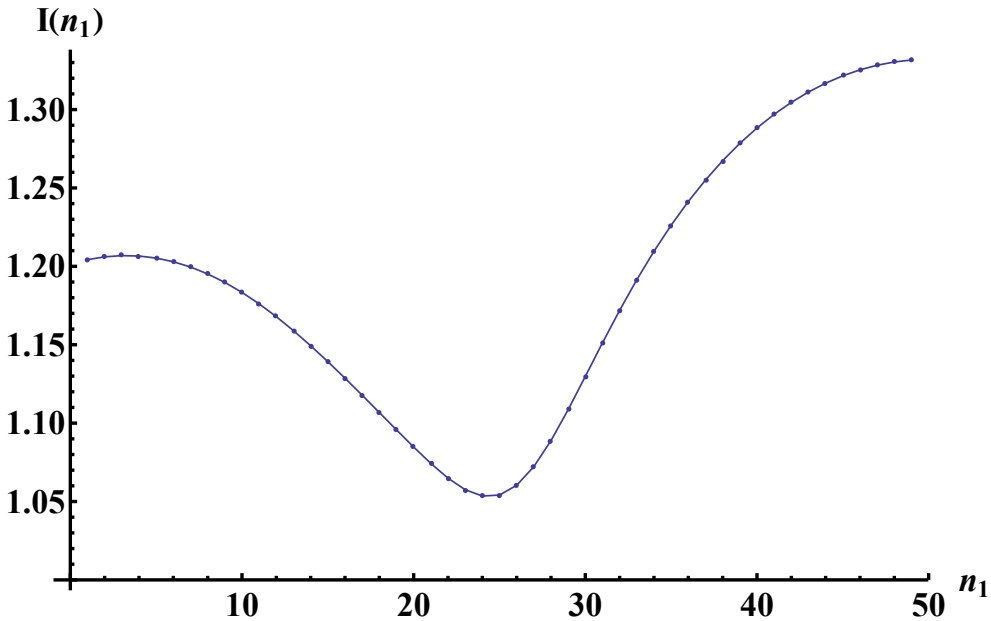

Figure 3.4: $I(n_1)$ against n_1 for for array LS1 with $\beta_0 = 0$.

3.3.1 Linear Symmetric Array 1 (LS1)

Consider a five device linear array such that $s_1 = s_4$ and $s_2 = s_3$, so that the array exhibits mirror symmetry about the middle device. This array is shown in figure 3.3 and is referred to as Linear Symmetric Array 1, which is abbreviated to LS1. This array is described by two variables, ks_1 and ks_2, or equivalently n_1 and n_2. Using (3.10) with $M = 100$ means the array is governed by a single unknown n_1. The array geometry is then optimised with respect to n_1 by maximising the value of $I(n_1)$ (equation (3.11)) for $n_1 \in [1, 49]$. This is done for several values of incident wave angle, namely $\beta_0 = 0, \frac{\pi}{8}, \frac{\pi}{4}, \frac{3\pi}{8}, \frac{\pi}{2}$. A detailed analysis is provided for the head seas ($\beta_0 = 0$) case, including a sensitivity analysis of the optimal array and a comparison of the optimal result to non-optimal layouts. The predicted optimal WEC displacements are also analysed; it should be stressed that linear wave theory requires that the amplitudes of these displacements are at most the same order of the wave amplitude. For the other values of β_0, the results are summarised and only the optimal arrays are considered in detail.

3.3.1.1 Optimisation and Analysis of Array LS1 in Head Seas

The mean performance of array LS1 in head seas is shown for all allowed values of the array layout variable n_1 in figure 3.4. It is clear that the maximum value

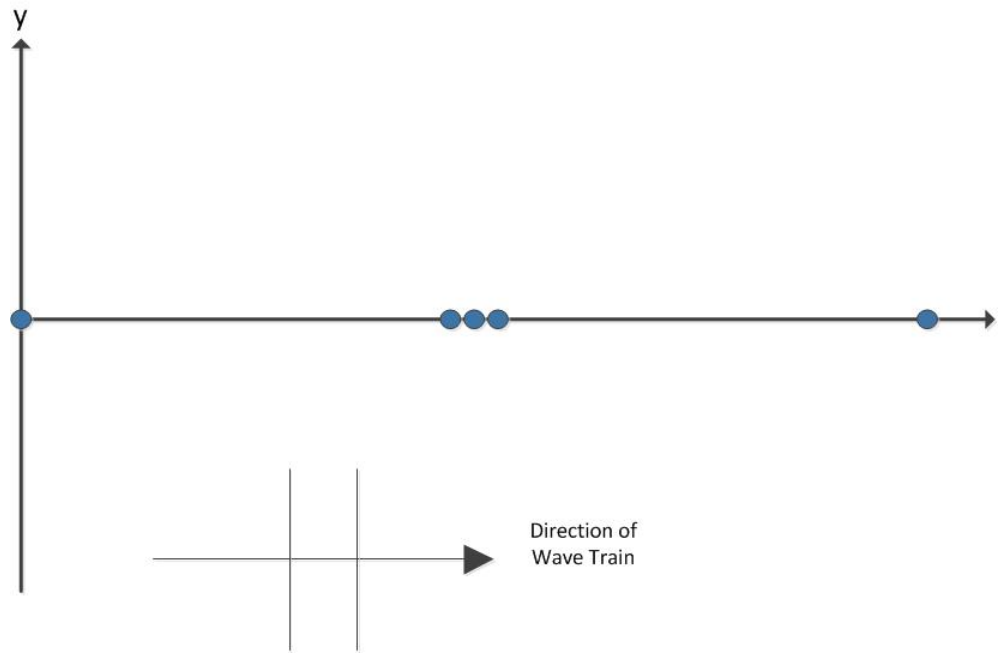

Figure 3.5: Diagram of optimised array LS1 for $\beta_0 = 0$, with $ks_1 = 4.9$ and $ks_2 = 0.1$.

of I is for the largest allowed value of $n_1 = 49$. This gives non-dimensional separations of $ks_1 = 4.9$ and $ks_2 = 0.1$ for the target non-dimensional length $kL = 10$. A diagram of the array with this optimised spacing is illustrated in figure 3.5. This shows that the devices in the centre of the array are bunched very close together, with a non-dimensional separation of $\frac{kL}{100}$ (1% of the total array length). This configuration is very different from the uniform spacing of figure 3.1. It may violate the point absorber approximation used, which requires that $ka << 1$; thus the validity of these results depend strongly on the device radius, or more specifically, on the ratio d/a. It may be unreasonable to neglect the scattered waves if the WECs are in such close proximity, as shadowing may have a significant effect. Also, depending on the physical value of k, the physical separation of the devices may be small enough that collisions of the WECs may become a concern.

Regardless of any difficulties with this result, the q-factor is investigated for this optimal array. Figure 3.6 shows the interaction factor of array LS1 in head seas for $kL \in [5, 15]$ for various values of the parameter n_1, including the optimal value of $n_{1,opt} = 49$. This clearly shows that the q-factor for $n_1 = 49$ is larger on average over the range $kL \in [5, 15]$ for $\beta = 0$. The optimal q-factor is greater than unity over this entire range; the lowest value obtained is $q \approx 1.1$ at $kL \approx 11.7$. Although the plot for $n_1 = 1$ outperforms the optimal case of

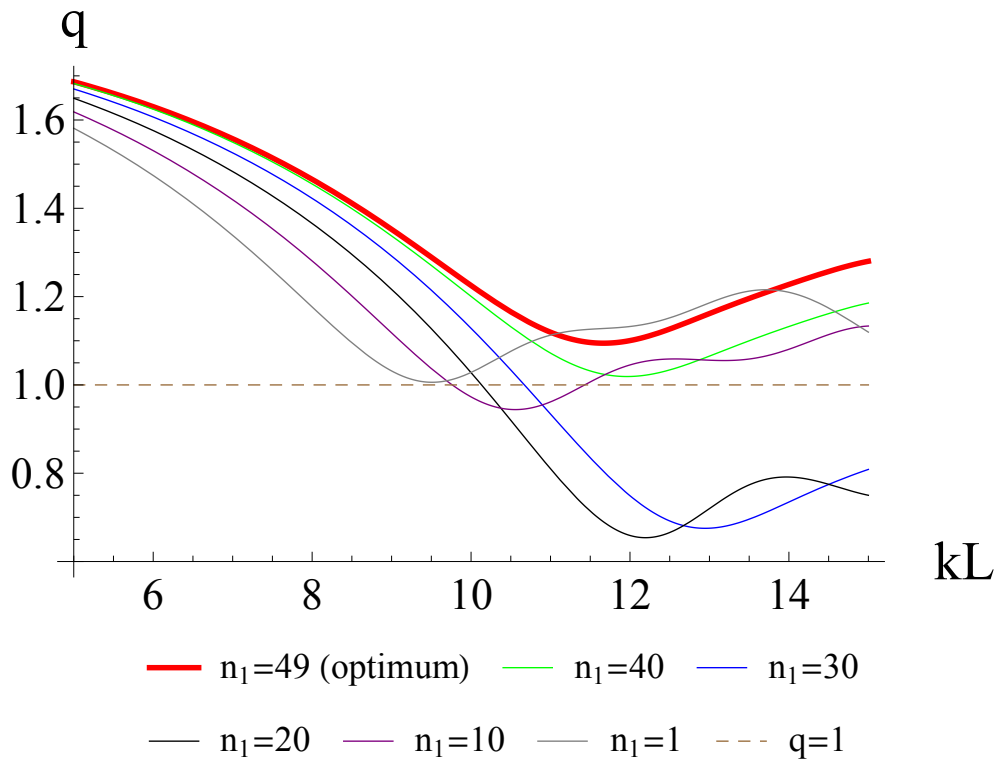

Figure 3.6: Interaction factor q against kL for array LS1 for different values of n_1, with $\beta = \beta_0 = 0$ and $kL \in [5, 15]$. $q = 1$ is shown by dashed line.

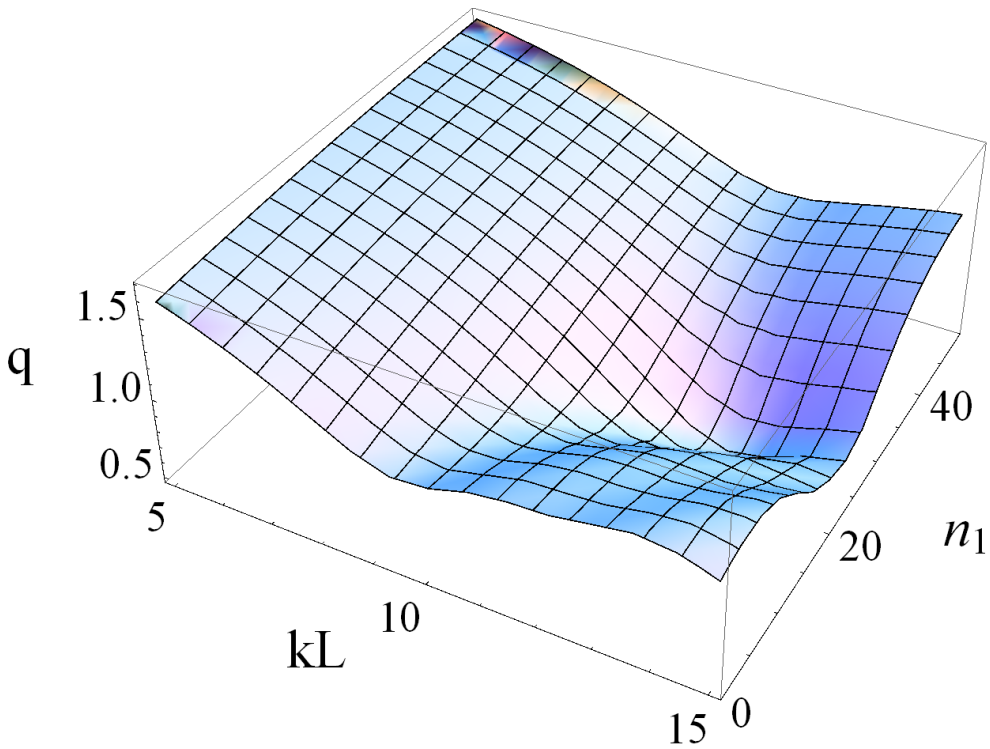

Figure 3.7: Interaction factor q against non-dimensional length kL and array layout parameter n_1 for array LS1 with $\beta = \beta_0 = 0$.

$n_1 = 49$ within $kL \in [11, 14]$, the average performance of $n_1 = 49$ is better over the whole domain and thus more desirable.

A 3D plot of q vs kL and n_1 is shown in figure 3.7, where the effect of varying both the non-dimensional length and the layout of the array (in terms of n_1) can be seen. The array appears to perform best for smaller kL, with the overall optimum occurring for $kL = 5$ and $n_1 = 49$. A large area of poor performance can be seen for $kL \in [10, 15] \cap n_1 \in [15, 35]$. This is due to large destructive interference in this region with the value of q dropping as low as 0.5. This plot serves to show a broader view of the performance of the array for varying n_1 and also confirms the optimal result of $n_{1,opt} = 49$. This suggests that the general performance of an array is poorer for larger kL, particularly for a uniform array ($n_1 = 25$). The increased performance of the smaller arrays is probably due to the better constructive interference possible as a result of the optimal motions and the reduced spacing between the devices. This is an important result which indicates that arrays with larger inter-device spacings perform poorer in terms of WEC interaction for head seas.

Figure 3.8 shows the predicted displacements (non-dimensionalised with respect to the wave amplitude A) of the WECs within this optimal array. These values are computed assuming optimal device motion and performance within the point absorber and linear wave theories using equation (2.142). The devices are assumed to be semi-submerged spheres with a non-dimensional radius of $ka = 0.4$. This shows that high q-factor values correspond to larger WEC motions. Clearly, the devices within the group in the optimal array (WECs 2, 3 and 4) have unacceptably large device motions, while those in relative isolation surrounding this group exhibit more reasonable displacements, though still too large for lower values of kL. The large device motions, particularly of the central devices, are in violation of linear wave theory which assumes that these motions are at most $\mathcal{O}(1)$. Furthermore, the implementation of a realistic PTO would prevent such large motions and this would have an adverse effect on the power absorption of the devices, and hence, the performance of the array.

As a result of these large motions of the grouped devices, it is proposed that replacing these devices with a single larger device may reduce the device amplitudes while retaining the good performance of the array. Figure 3.9 shows the proposed array with the central group of three devices replaced by a single device of three times the radius. These arrays with large devices instead of groups of devices will be referred to as "satellite" arrays, as the isolated devices

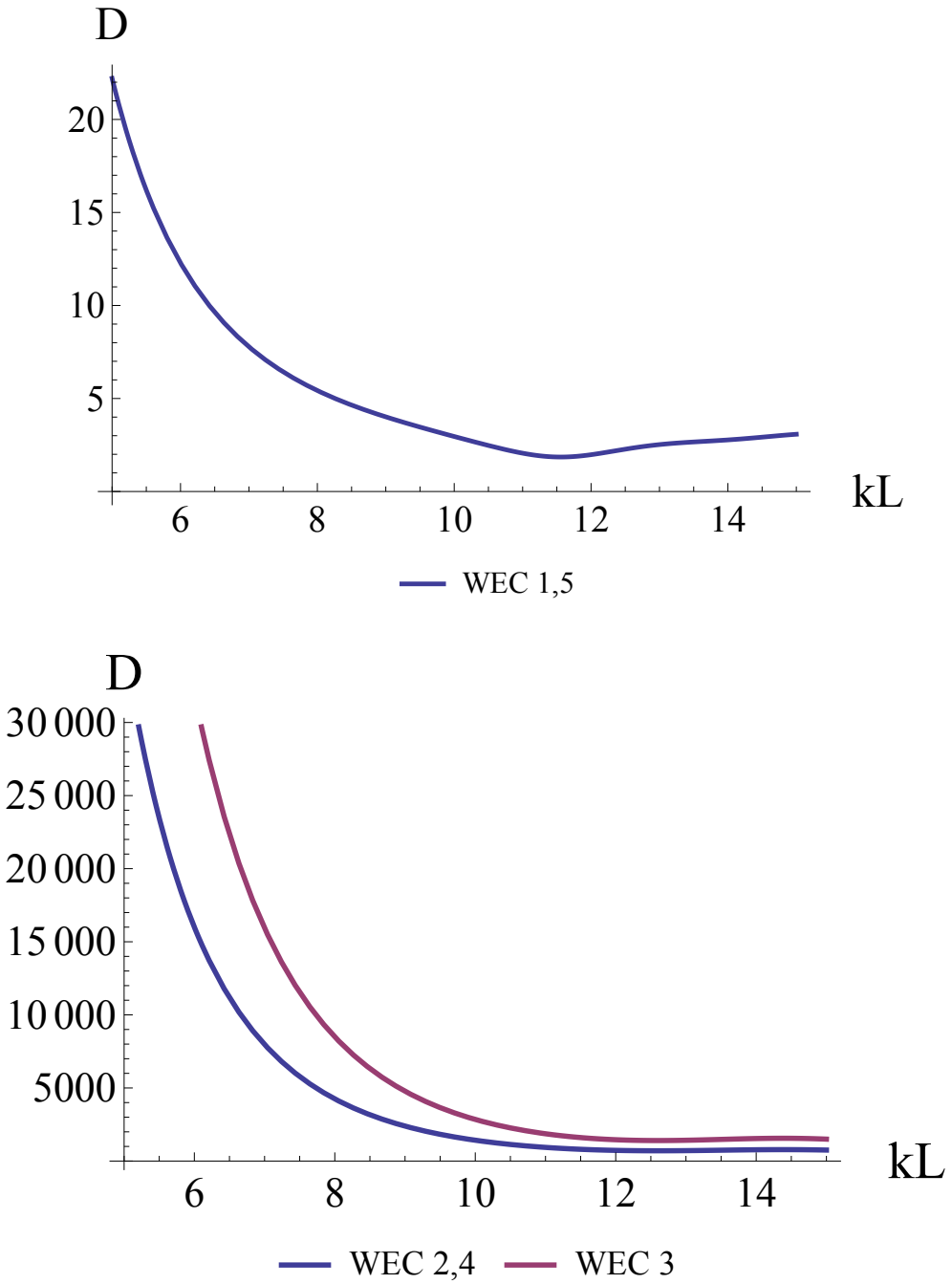

Figure 3.8: Predicted non-dimensional optimal WEC displacements in optimised array LS1 (as in Figure 3.5) with $n_1 = 49$ for $\beta = \beta_0 = 0$.

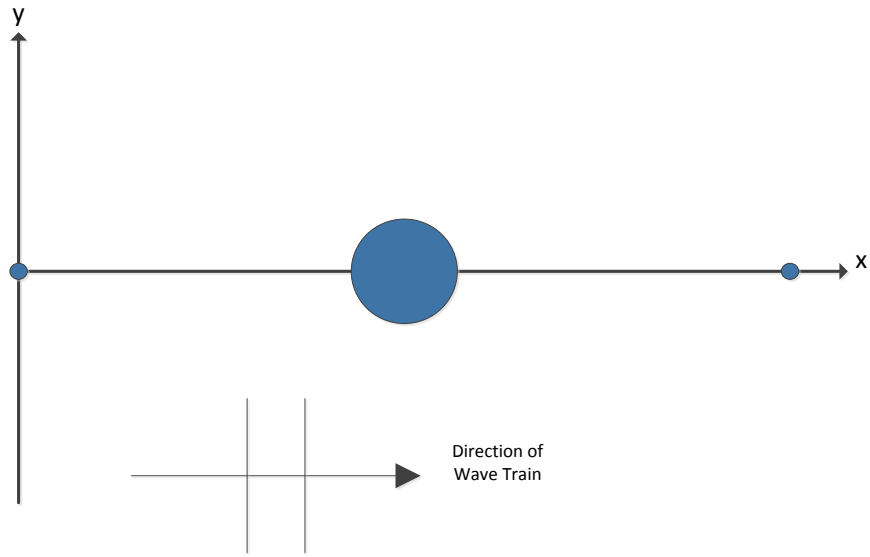

Figure 3.9: Suggested possible optimal "satellite" array for array LS1, corresponding to figure 3.5, with larger device in place of groups of devices.

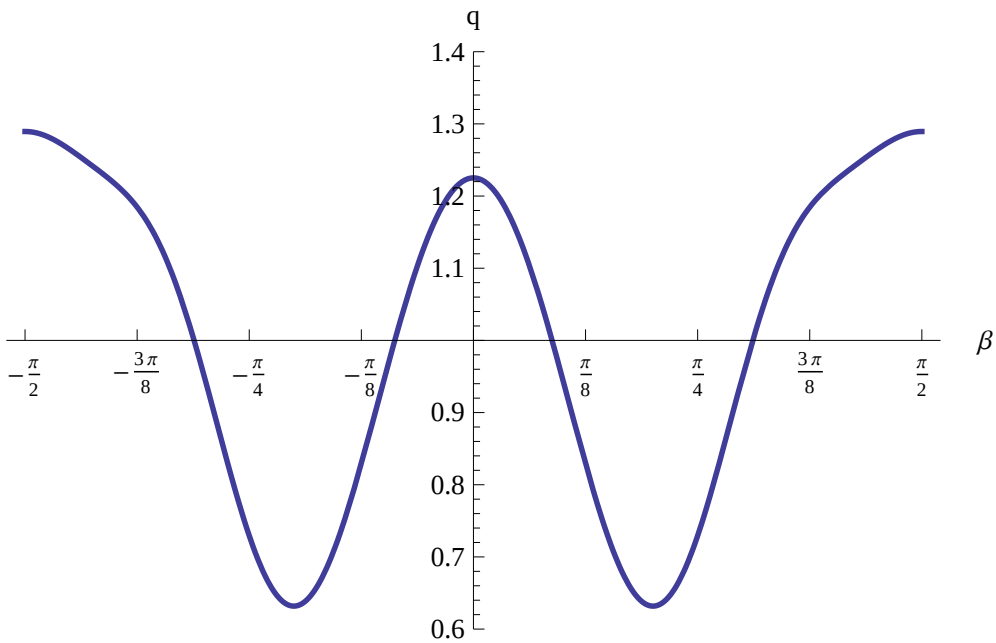

Figure 3.10: Interaction factor q against angle of wave incidence β for optimal LS1 array for $kL = 10$ (with $n_1 = 49$).

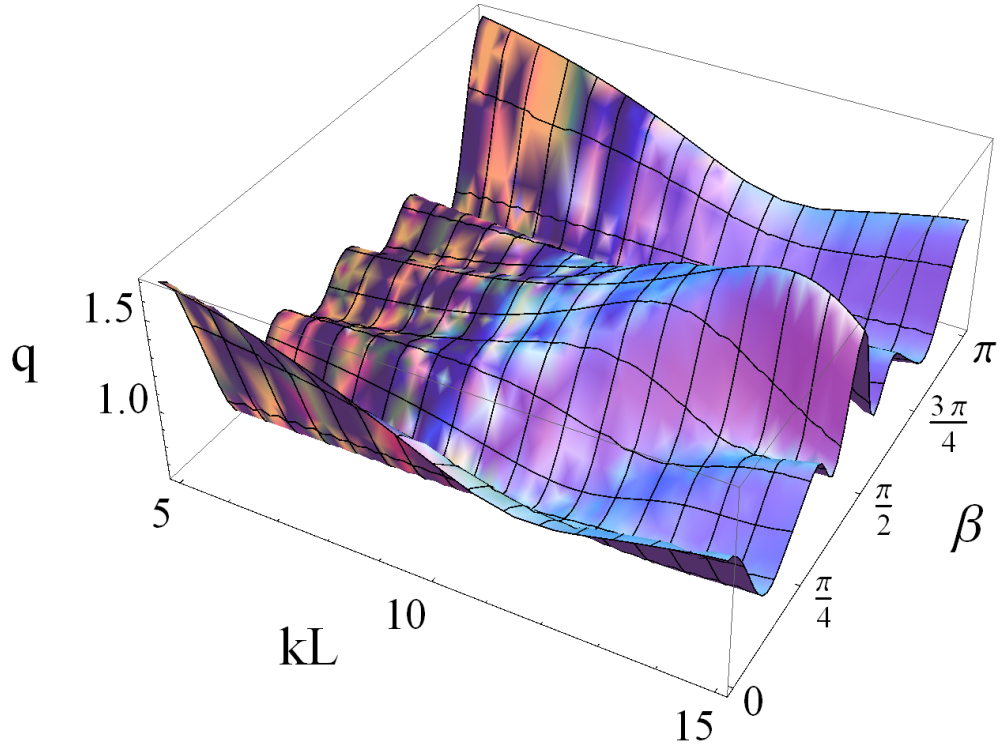

Figure 3.11: Interaction factor q against non-dimensional length kL and incident wave angle β for optimal array LS1 ($n_1 = 49$).

can be considered to be flanking or orbiting the central large device.

Replacing a group of several WECs would only work if the grouped WEC motions were in phase with each other, otherwise the appropriate interaction effects would not be recreated. It was found that the grouped WECs all oscillated with opposite phases to each other, thus this idea of a larger WEC may not be appropriate. However, if the groups were replaced by a WEC that operated in more than one mode of motion, then it is possible that the same interaction effects could be created. However, a multi-modal WEC would complicate the model considerably and introduce some significant engineering challenges.

The effect of varying the incident wave angle on the optimal LS1 array (with $n_1 = 49$) is shown in figure 3.10, for $kL = 10$ fixed. As discussed in the previous chapters, Fitzgerald (2006) showed that the mean of the interaction factor with respect to incident wave angle is unity, as in equation (2.164). This is evident from figure 3.10, where the plot of q against β oscillates about the average of $q = 1$. It can be seen that $\beta = 0$ is not the best performing value, as q is greater for $\beta = \pi/2$. This suggests that better results could be obtained for $\beta_0 = \frac{\pi}{2}$. However, it is noted that this is just for $kL = 10$ fixed.

A more complete picture is shown in figure 3.11, where a 3D plot of q against kL and β is presented. The effect of the wave angle β on q alters as kL is changed, and visa versa. Therefore, results obtained must be critically analysed for stability to changes not only in non-dimensional length kL but also in incident wave angle β. It should be noted that generating this figure requires considerable computational effort within Mathematica 9.0. Analysing each array over both kL and β simultaneously is computationally demanding and reduces the overall clarity of the results. Henceforth, when β-variations are assessed, the non-dimensional length will be fixed at $kL = 10$, as this will give the performance of array at the target value, which is of greatest concern.

3.3.1.2 Sensitivity Analysis for Optimal Symmetric Array LS1 in Head Seas

In order to assess whether or not the optimal array obtained is stable to small errors in non-dimensional separation between the devices, a stability analysis is preformed; this examines the effect of an error in the separations ks_1 and ks_2 on the interaction factor q. A detailed sensitivity analysis is presented in figure 3.12, which shows the effect of different combinations of small errors in the device separations ks_j (and hence in kL). These errors are assumed to follow the symmetry of the array, i.e. the error ϵ_1 appears in the separations of the first-second and fourth-fifth devices, and ϵ_2 appears in the separations of the second-third and third-fourth device. Figure 3.12 shows the effect of these errors on the interaction factor for several fixed values, namely $\epsilon = 0, \pm 0.025kL, \pm 0.05kL$.

For $kL \in [5, 10]$, the effect of any small errors in the device positions is relatively linear, where a negative error slightly increases the interaction factor and a positive error slightly decreases it. This is because these negative/positive errors have the effect of decreasing/increasing the total non-dimensional length respectively; this results in a positive/negative effect on the interference effects within the array. As previously discussed, the array seems to perform better for smaller kL, where greater constructive interference occurs. This result is echoed here, where an error that decreases kL results in an increase of q, while an error that increases kL causes a decrease in q.

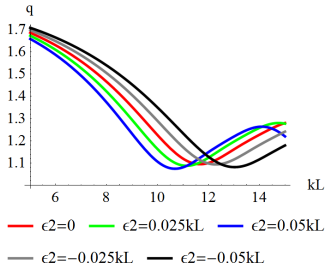

(a) $\epsilon_1 = 0$

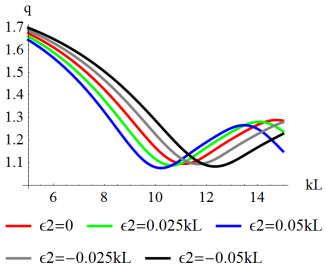

(b) $\epsilon_1 = 0.025kL$

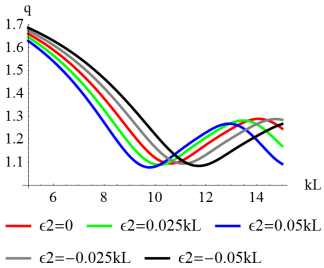

(c) $\epsilon_1 = 0.05kL$

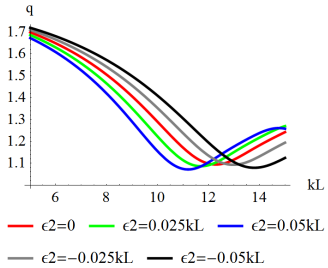

(d) $\epsilon_1 = -0.025kL$

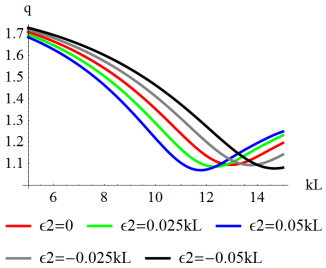

(e) $\epsilon_1 = -0.05kL$

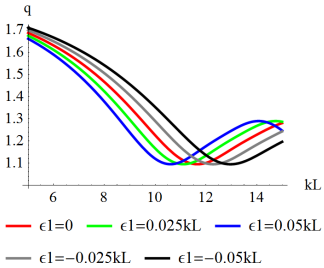

(f) $\epsilon_2 = 0$

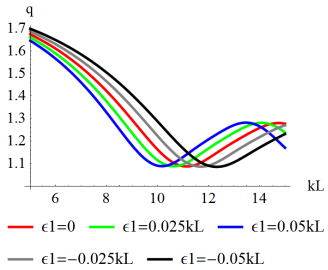

(g) $\epsilon_2 = 0.025kL$

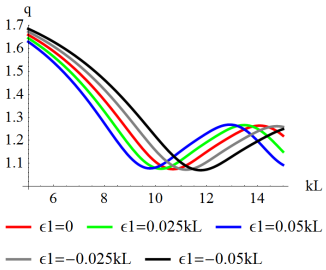

(h) $\epsilon_2 = 0.05kL$

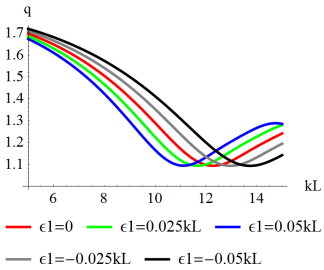

(i) $\epsilon_2 = -0.025kL$

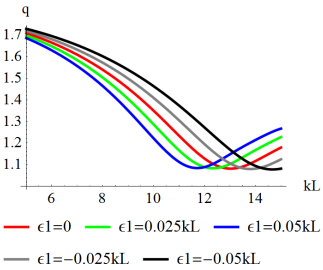

(j) $\epsilon_2 = -0.05kL$

Figure 3.12: Sensitivity analysis for optimised array LS1 for $\beta_0 = 0$, with $n_1 = 49$.

The effect of the errors for $kL \in [10, 15]$ appears more complex. This is again due to the general performance of the optimal q-factor ($n_1 = 49$) shown in figure 3.6. The minimum of this curve occurs at $kL \approx 12$. However, if the total length of the array is altered by an error, then the location of this trough will be shifted left or right if the error is positive or negative respectively.

The errors ϵ_1 and ϵ_2 have slightly different effects on the behaviour of the array, especially for $kL \in [10, 15]$. This is possibly due to the larger relative error of $\frac{\epsilon_2}{ks_2}$ compared to $\frac{\epsilon_1}{ks_1}$. In the optimum LS1 array for head seas,

$$ks_1 = \frac{n_1}{100}kL = \frac{49kL}{100} \tag{3.12}$$

and

$$ks_1 = \frac{n_2}{100}kL = \frac{50 - n_1}{100} = \frac{kL}{100}. \tag{3.13}$$

If it is assumed that the same error is applied to each quantity, so that $\epsilon_1 = \epsilon_2 = \delta kL$, then the relative error of ks_1 is $\frac{\epsilon_1}{ks_1} = \frac{100}{49}\delta$, whereas that of ks_2 is $\frac{\epsilon_2}{ks_2} = 100\delta$, which is 49 times larger. This is perhaps the reason why the array is slightly more sensitive to errors in ks_2. As expected, the errors have the greatest effect when they are combined and are both present simultaneously. However, in spite of this, each of the errors still have a relatively small overall effect on the array performance.

It should be noted that the errors are investigated up to a value of $\pm 0.05kL$. It is expected that the error in the deployment of these arrays will not exceed this, as this would involve a miss-deployment of the appropriate devices of 5% of the total physical length of the array. The physical length of these arrays will be of the order of 200m-400m for an average incident wave length of 150m, so the maximum error of $0.05kL$ corresponds to a physical error of approximately 10m-20m. It is unlikely that a WEC would be miss-deployed by a distance greater than this.

From figure 3.12, it is clear that the plots of q for non-zero ϵ_1 or ϵ_2 are perturbations of the original plot with $\epsilon_1 = \epsilon_2 = 0$. The curves maintain their basic shape and the values of q obtained are relatively similar for all combinations of ϵ_1, ϵ_2 investigated. This shows that the optimal head seas case of array LS1 with $n_1 = 49$ is stable to errors in the device separation up to $\pm 5\%$ of the total length.

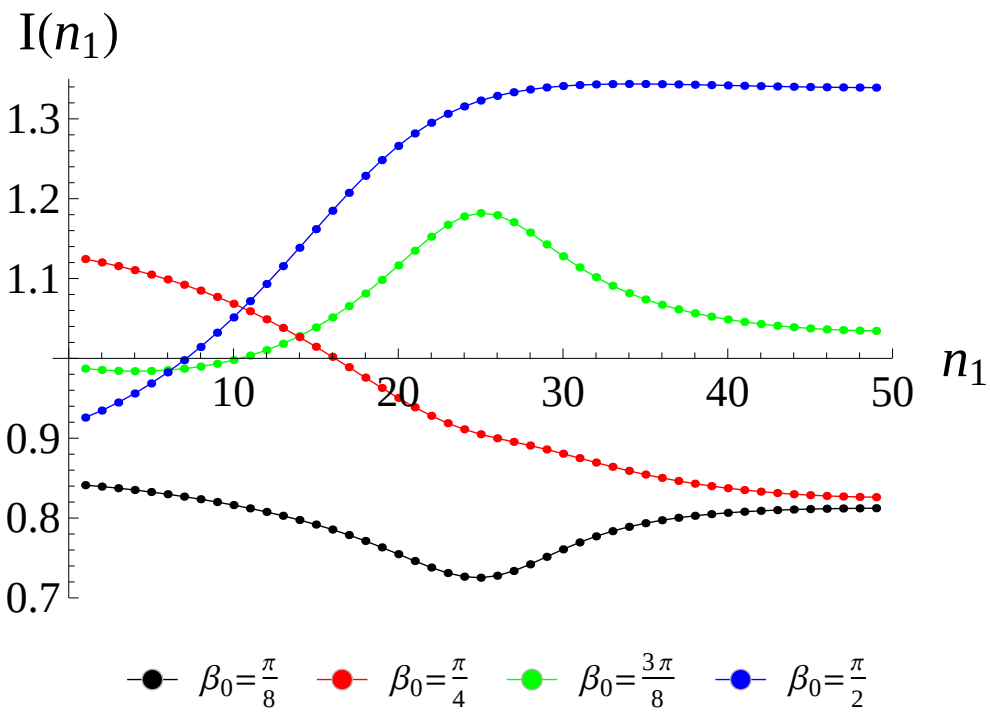

Figure 3.13: $I(n_1)$ against n_1 for linear array LS1 for several values of β_0.

3.3.1.3 Optimisation and Analysis of Array LS1 for Alternate Incident Wave Angles

By examining the behaviour of the array with respect to incident wave angle (see figures 3.10 and 3.11), it is clear that $\beta_0 = 0$ (head seas) may not the best way to arrange a mirror symmetric linear array. This seems to be true in general for linear arrays, as previous research, for example Thomas & Evans (1981), has shown that these arrays tend to preform better in beam seas ($\beta_0 = \frac{\pi}{2}$) in line with the idea that greater frontage to the waves allows greater power extraction. Therefore, the optimisation procedure used for $\beta_0 = 0$ is repeated for different values of wave incidence for the LS1 array, namely $\beta_0 = \frac{\pi}{8}, \frac{\pi}{4}, \frac{3\pi}{8}$ and $\frac{\pi}{2}$.

Firstly, the behaviour of the average interaction factor $I(n_1)$ is assessed and the optimal value of $n_{1,opt}$ is identified, for each case. An analysis of the resulting behaviour of the interaction factor in the optimal cases is then presented. The effect of altering the non-dimensional length and the incident wave angle on the optimal arrays is examined. Finally, a brief summary of all results relating to array LS1 are presented in Section 3.3.1.4.

Figure 3.13 shows plots of the average interaction factor $I(n_1)$ for $\beta_0 = \frac{\pi}{8}, \frac{\pi}{4}, \frac{3\pi}{8}$ and $\frac{\pi}{2}$. Most notable is that the optimum value of n_1 changes for different wave

angles. The optimum values are $n_1 = 1, 1, 25$ and 34 for $\beta_0 = \frac{\pi}{8}, \frac{\pi}{4}, \frac{3\pi}{8}$ and $\frac{\pi}{2}$ respectively, while earlier it was found that the optimum for $\beta_0 = 0$ was $n_1 = 49$. This indicates that even when a certain symmetry is enforced, the layout of a linear array (particularly the spacing between the devices) has a considerable impact on the power absorption. These results also indicate that the incident wave angle has a very large effect on optimal array layout and performance, in keeping with the result of Fitzgerald (2006).

It should be noted that the general performance of the array, even in optimal cases, is severely limited for some values of β_0. Consider, for example, the $\beta_0 = \frac{\pi}{8}$ case. Figure 3.13 shows that the best value of $I(n_1)$ in this regime is approximately 0.84, which is the average interaction factor of the array over $kL \in [5, 15]$. This implies that destructive interference dominates in this regime. On the other hand, for beam seas ($\beta_0 = \frac{\pi}{2}$), the array achieves $I(n_1) \in [0.92, 1.35]$ for all allowed array configurations, with the majority of n_1 values producing $I(n_1) > 1$. This shows that constructive interference can be utilised at this wave angle by intelligent arrangement of the devices, without overwhelming destructive effects. Thus, if a given WEC array site has a low variation in incident wave angle, the directionality of the incident waves can be utilised by arranging the WEC array in this manner.

It is interesting to note the relatively small change in performance of the beam seas array for $n_1 \in [30, 49]$. This range of n_1 corresponds to a significant alteration in the array layout, ranging from a unequally spaced (but relatively separated) array to an array with three grouped WECs in the centre. Despite this considerable layout variation, the mean performance of the array varies only slightly within this range. It should also be noted that the mean performance of the beam seas array is much higher than the others presented and performs slightly better than the head seas array at its optimal values.

The performance of each of the optimal LS1 arrays identified for the different incident wave angles is now analysed. For each value of β_0 considered, the optimal interaction factor q for each optimal array is investigated for kL-variation in figure 3.14 and for β-variation in figure 3.15.

As presented earlier, performance at some wave angles appears to be extremely limited in even the optimal cases. The poorest case occurs for $\beta_0 = \frac{\pi}{8}$, as shown in figure 3.14. It is clear that $q < 1$ for all values of kL considered, even for the optimum case where $n_1 = 1$. The relatively poor performance of the linear array at $\beta_0 = \frac{\pi}{8}$ is also echoed in the I values achieved. This suggests that waves

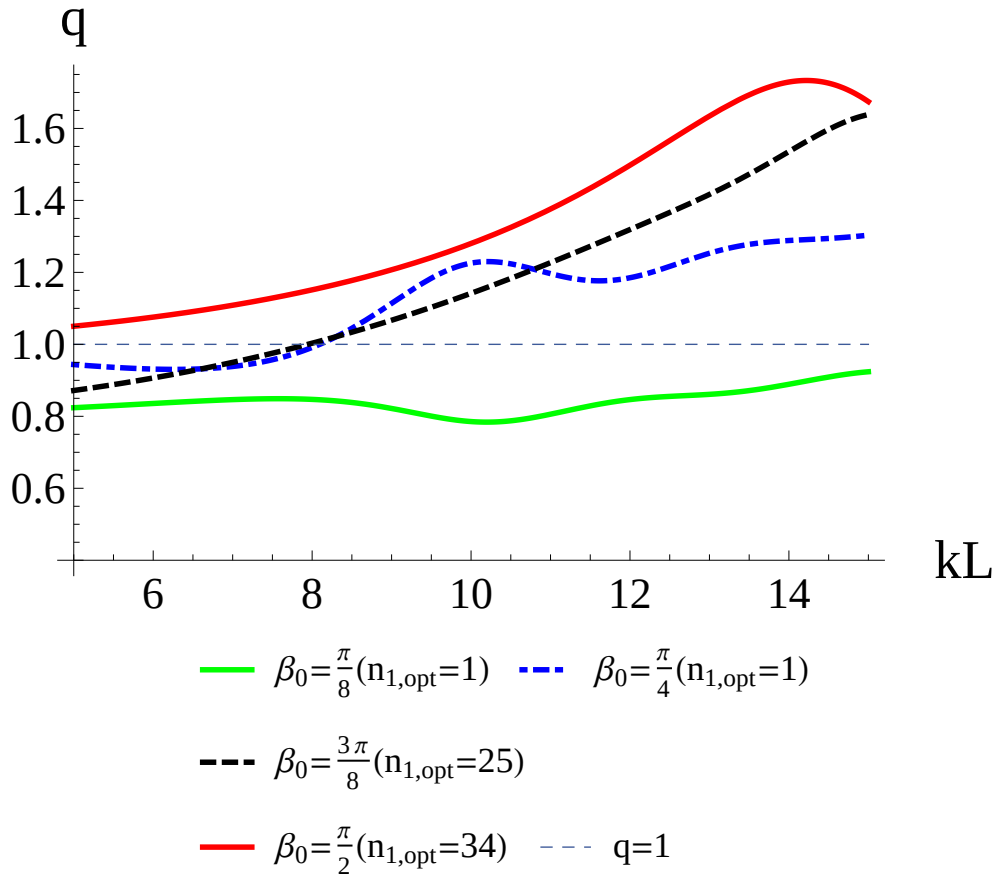

Figure 3.14: Interaction factor q against kL for optimal LS1 array for several values of β_0.

angles near $\beta = \frac{\pi}{8}$ should be avoided.

The highest value of $I(n_1)$ was achieved in the beam seas case ($\beta_0 = \frac{\pi}{2}$). The optimum layout ($n_1 = 34$) produced an average interaction factor of $I(n_{1,opt}) = 1.34$, which is slightly higher than the optimum of $I = 1.33$ achieved for $\beta_0 = 0$. It is intuitive that a linear array in beam seas would perform better, as this layout would provide the greatest frontage to the incident waves. However, the overall effect is not this simple; very good performance can also be achieved for head seas, which corresponds to the minimum frontage to the incident waves.

An interesting comparison can be made between the optimal interaction factor for head and beam seas. As previously shown, the optimal array layout is considerably different for head and beam seas. For head seas, the best case is $n_1 = 49$, which corresponds to a group of three devices at the centre of the array; while for beam seas, the optimal value of $n_1 = 34$ corresponds to an

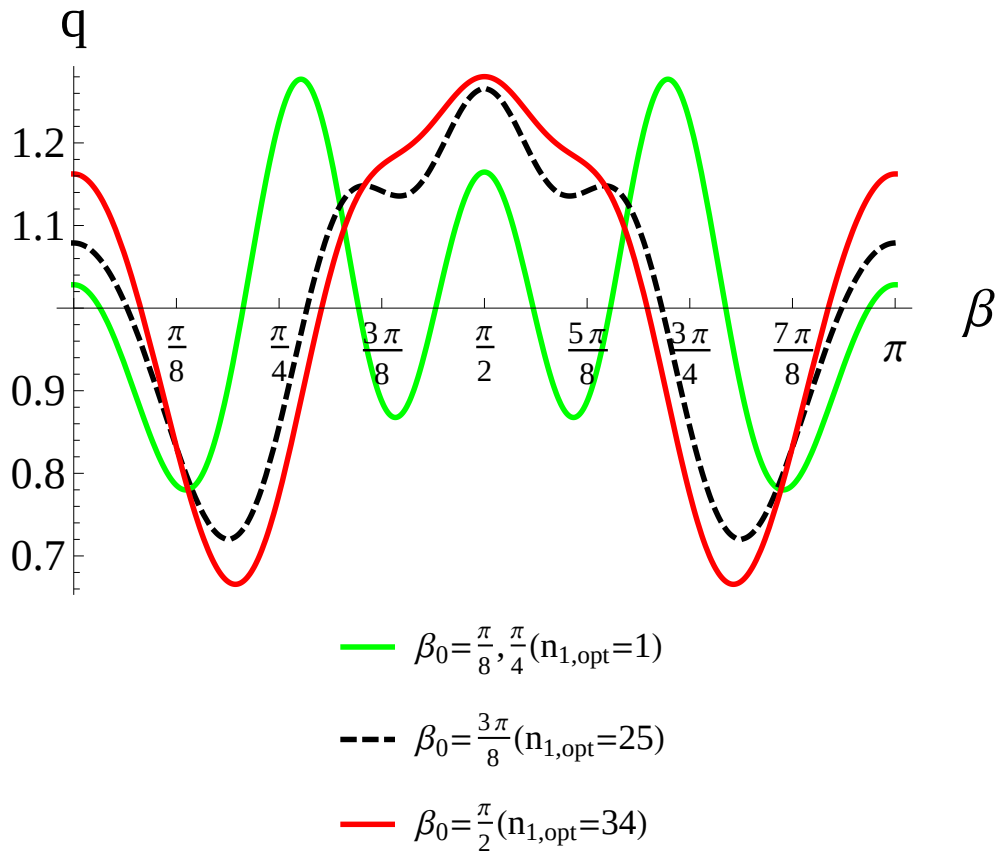

Figure 3.15: Interaction factor q vs β for array LS1 for several values of β_0, with $kL = 10$.

unequally separated array (quite similar to that investigated in McIver (1994)). The optimal average interaction factor is almost identical in both cases, with $I = 1.33$ and $I = 1.34$ for head and beam seas respectively.

However, by examining figures 3.6 and 3.14, it is clear that the $\beta_0 = 0$ optimal array performs better in the first half of the range of kL, namely $kL \in [5, 10]$. Conversely, the $\beta_0 = \frac{\pi}{2}$ optimal array performs better for the second half of the range, $kL \in [10, 15]$. It seems as if the optimal plots of q for head and beam seas are almost mirror images of each other. This would allow for further optimisation if the deployment site of the array contained a tighter range of incident wavelengths. If it was known that kL would stay within a range of $[5, 10]$, then $n_1 = 49$ with $\beta_0 = 0$ would seem an intelligent choice; while if kL was to fall within $[10, 15]$, then $n_1 = 34$ with $\beta_0 = \frac{\pi}{2}$ would appear better.

This would also allow more freedom in the choice of physical length L of the array, which also affects the parameter kL. The range of kL for a given site can be contrived by an intelligent choice of physical length L, depending on the

wavelength variation present at the site. This may also be useful if one array layout was more preferable than the other. For example, placing the WECs so close together (separated by 1% of kL) in the $\beta_0 = 0$ optimal array results in very large WEC motions, particularly for the grouped devices. This close spacing between WECs may cause further complications due to shadowing effects and possible collisions. Therefore, the array spacing that is optimal for beam seas may be more desirable, as it may avoid some problems associated with closely spaced WECs.

An overall observation of the results here indicates that incident wave angles around $\beta = \frac{\pi}{8}$ result in poor performance (even when optimised) and should be avoided. However, head and beam seas appear the most conducive to optimisation, although the large WEC motions would present a problem; this is an artefact of the unconstrained optimisation performed in this chapter.

The behaviour of q for variation in β is an important consideration, since the incident angle of the waves at a given site can change with the sea conditions. Ideally, an optimal array would perform well over a large range of both kL and β, thus being stable to variations in both incident wavenumber and wave angle.

Figure 3.15 shows the β-variation of the q-factor for the optimal LS1 arrays for each value of β_0 investigated. In some cases, the optimal array layouts are identical, thus the β-variation is also the same. Symmetry of all plots can be observed about $\frac{\pi}{2}$, this is due to equation (2.165) and the inherent symmetry of the linear array.

It was previously discussed how the optimal array at $\beta_0 = \frac{\pi}{8}$ is undesirable, due to low optimal performance, and this is echoed by the β-variation of this array shown in figure 3.15. An examination of figure 3.15 shows an oscillatory behaviour for $\beta_0 = \frac{\pi}{8}$ and $\beta_0 = \frac{\pi}{4}$ (which have the same optimal array layout), where performance moves between $q \approx 1.3$ to $q \approx 0.78$ for a change in β of approximately $\frac{\pi}{8}$. The period between peaks and troughs is approximately $\frac{\pi}{8}$, with larger peaks occurring near $\beta = \frac{\pi}{4}$ and $\beta = \frac{3\pi}{4}$.

The beam seas array appears to be relatively stable to changes in β around the target value of $\beta_0 = \frac{\pi}{2}$. The array maintains $q > 1$ for a β-variation of approximately $\pm\frac{5\pi}{24}$. Similar performance is noted for the $\beta_0 = \frac{3\pi}{8}$ case, where the optimal array layout is uniform. A comparison can be made between the $\beta_0 = \frac{3\pi}{8}$ case and the beam seas case in terms of β-variation, as the q vs β curves are rather similar. However, the $\beta_0 = \frac{3\pi}{8}$ case does not exhibit the same stability

Table 3.1: Optimisation results for array LS1 with different incident wave angles.

β_0	$n_{1,opt}$	$I(n_{1,opt})$	Array Layout
0	49	1.33	* *** *
$\frac{\pi}{8}$	1	0.84	** * **
$\frac{\pi}{4}$	1	1.12	** * **
$\frac{3\pi}{8}$	25	1.18	* * * * *
$\frac{\pi}{2}$	34	1.34	* * * * *

as the beam seas case, since the target value occurs to the left of the peak.

3.3.1.4 Summary of Results for Array LS1

Table 3.1 provides a brief summary of the optimisation results of array LS1 for the different wave angles considered. For each value of β_0, the optimal spacing parameter $n_{1,opt}$ and the mean interaction factor $I(n_{1,opt})$ at this value are presented, together with a schematic of the optimal array configuration.

The optimal value of n_1, and hence of the optimal array layout, varies considerably depending on the value of β_0 assumed. The value $n_1 = 49$ (optimal for head seas $\beta_0 = 0$) corresponds to a group of three WECs at the centre and two isolated WECs at the ends of the array; $n_1 = 1$ (optimal for $\beta_0 = \frac{\pi}{8}, \frac{\pi}{4}$) corresponds to two groups of two devices at the ends of the array, with a single device in the centre; $n_1 = 25$ (optimal for $\beta_0 = \frac{3\pi}{8}$) corresponds to a uniformly spaced array; while $n_1 = 34$ (optimal for beam seas $\beta_0 = \frac{\pi}{2}$) almost corresponds to the case of unequal spacing investigated in McIver (1994). It can also be seen that the array performs quite poorly for $\beta_0 = \frac{\pi}{8}$, since the optimal configuration gives a mean interaction factor of $I = 0.84$, indicating that destructive interference dominates at this wave angle. Good performance is seen at $\beta_0 = \frac{\pi}{2}$ (beam seas) and this complies with the intuitive concept that greater frontage to the waves allows for greater power absorption. However, similar performance is also obtained for the optimal head seas case.

The displacement amplitudes of the WECs for each optimal array were analysed, but are not presented for brevity. Overall, the same trends as in figure 3.8 were observed, where larger motions are seen for grouped WECs and for lower values of kL. Large amplitudes in excess of the $\mathcal{O}(1)$ requirement were

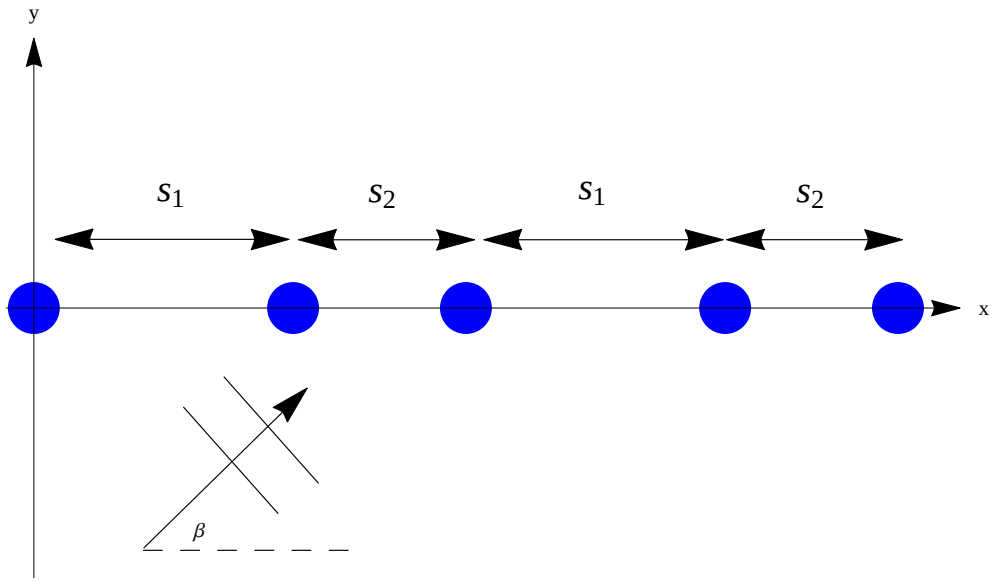

Figure 3.16: Diagram of array LS2, with translational symmetry about the middle WEC.

present in each optimal array.

The advantage of the objective function utilised is highlighted by the sensitivity analysis in figure 3.12. Since the *mean* of the interaction factor is maximised within the optimisation, this precludes the case of a large sharp peak in performance that is surrounded by troughs being considered as optimal. The sensitivity analysis proved that small changes in each WEC separation resulted in only small changes in performance, thus confirming the stability of the optimal performance and the usefulness of this approach.

3.3.2 Linear Symmetric Array 2 (LS2)

A five-device linear array such that $s_1 = s_3$ and $s_2 = s_4$ is now considered, so that the array has translational symmetry about the middle device, as shown in figure 3.16. This array is herein referred to as array LS2.

A detailed description is provided for the optimisation and optimal results of the head seas ($\beta_0 = 0$) case in Section 3.3.2.1, while the results for other wave angles are summarised in Section 3.3.2.2. The results for all wave angles follow a similar pattern as those presented and so a detailed analysis is omitted in Section 3.3.2.2 for brevity. Further supplementary results are provided in Appendix A. All optimisation results for array LS2 are summarised in table 3.2.

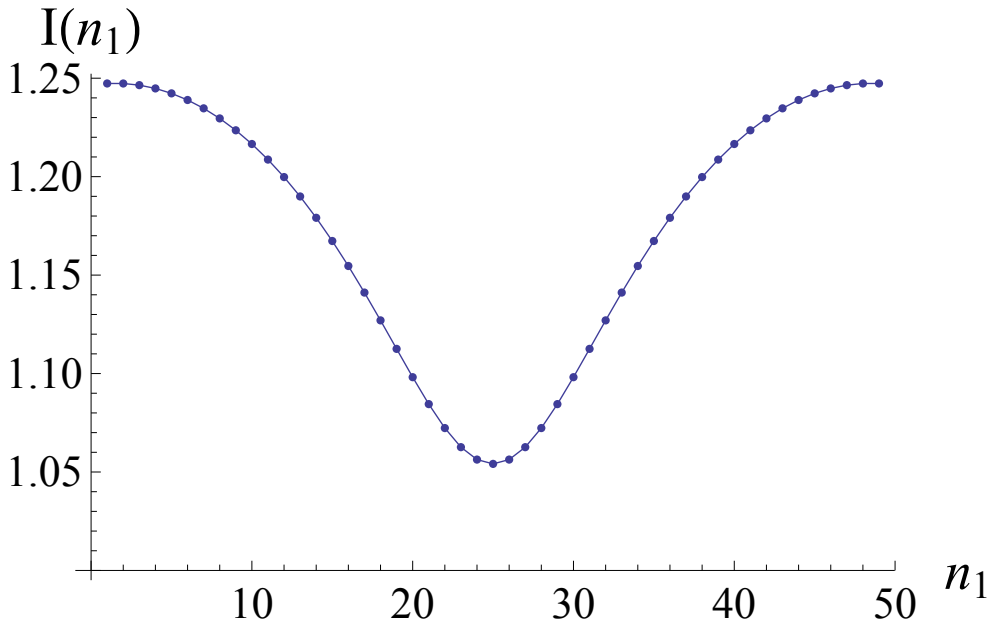

Figure 3.17: $I(n_1)$ against n_1 for $n_1 \in [1, 49]$ for array LS2 with $\beta_0 = 0$.

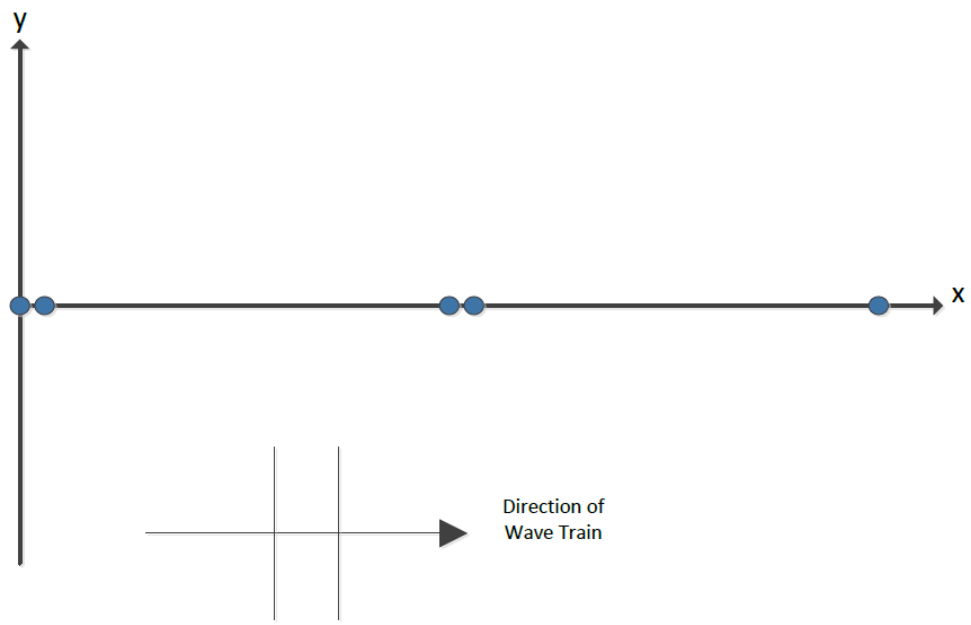

Figure 3.18: Diagram of optimised array LS2 for $\beta_0 = 0$, with $ks_1 = 0.1$ and $ks_2 = 4.9$.

3.3.2.1 Optimisation and Analysis of Array LS2 in Head Seas

The effect of the parameter n_1 on the mean value of q for array LS2 with $\beta_0 = 0$ is shown in figure 3.17, which shows that the optimum case is when either $n_1 = 1$ or $n_1 = 49$. This is to be expected, as the physical layout of array LS2 with $n_1 = 1$ and $n_1 = 49$ are the reverse of each other, so the interaction factors

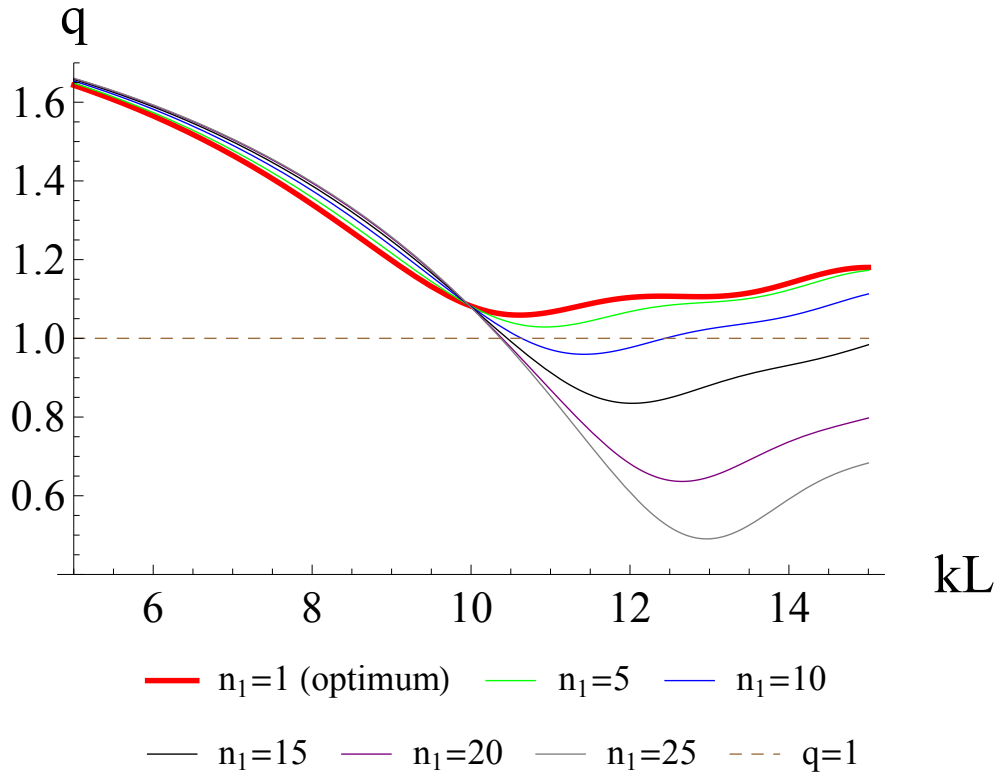

Figure 3.19: Interaction factor q against kL for array LS2 for different values of n_1, with $kL \in [5, 15]$ and $\beta_0 = 0$. $q = 1$ is shown by dashed line.

are the same by (2.165) and the symmetry of the system. In either case, this configuration consists of two groups of two devices and an isolated fifth device, as shown in figure 3.18, where $n_1 = 1$ is the chosen configuration.

The variation of the interaction factor for different values of n_1 with respect to kL is shown in figure 3.19. In this figure only $n_1 \in [1, 25]$ needs to be considered, due to the same symmetry identified above. For example, the interaction factor for $n_1 = 5$ behaves the same as that for $n_1 = 45$.

There is very little difference in the performance of array LS2 for all values of n_1 in the lower half of the domain, i.e. $kL \in [5, 10]$. The optimal array with $n_1 = 1$ performs poorest in this region, but only by a small amount. The main difference is noticed for $kL \in [10, 15]$ where the optimal array outperforms all others by a more considerable margin. For the optimal array with $n_{1,opt} = 1$, the array maintains $q > 1$ for all $kL \in [5, 15]$, with $q \in [1.06, 1.65]$. A 3D plot of the array performance for variation in both kL and n_1 is presented in figure A.5 in Appendix A. Similar behaviour to the LS1 array is observed, where the array generally performs better for smaller kL and a trough exists for

$kL \in [10, 15] \cap n_1 \in [15, 30]$.

The predicted optimal displacements for this optimal array are shown in figure 3.20. Similarly to array LS1, the main concern occurs for the grouped WECs, where excessively large motions are seen. The displacement amplitudes of WECs 1-4 are $\mathcal{O}(100)$ times the wave amplitude. These motions are required to be at most $\mathcal{O}(1)$ by the underlying model. Therefore these motions invalidate the model and would probably be damped by any realistic PTO, thus reducing the array performance. The motion of WEC 5 is within acceptable limits for $kL \in [9, 15]$, but for lower values of kL the amplitude can no longer be considered $\mathcal{O}(1)$ and is thus also unacceptable.

A similar satellite array to that described in Section 3.3.1 can be proposed for this array, where the grouped pairs of devices are replaced by devices that are twice as large. This is shown in figure 3.21. Further analysis is needed to assess the viability of such an array, which is beyond the scope of this thesis.

A sensitivity analysis similar to that in Section 3.3.1 was performed for array LS2. Similar results to array LS1 were found, where the errors in WEC positions merely caused perturbations in the interaction factor and overall performance was maintained. Hence the details of this analysis are omitted for brevity.

3.3.2.2 Optimisation and Analysis of Array LS2 for Alternate Incident Wave Angles

Optimisation of array LS2 was also performed for a number of incident wave angles, namely $\beta_0 = \frac{\pi}{8}, \frac{\pi}{4}, \frac{3\pi}{8}, \frac{\pi}{2}$. Figure 3.22 shows the optimisation results for these values of β_0, while figures 3.23 and 3.24 show the performance of the optimal arrays for variation in kL and β respectively.

Diminished performance is seen for $\beta_0 = \frac{\pi}{8}$, with the maximum value of $I(n_{1,opt}) \approx 0.82$ obtained. This also results in the poorest overall performance for the wave angles considered, as illustrated in figures 3.22-3.24. However, unlike array LS1, the optimal array layout for $\beta_0 = \frac{\pi}{8}$ is identical to the $\beta_0 = 0$ case. Similarly poor performance is seen for $\beta_0 = \frac{\pi}{4}$ with $I < 1$, although better than the $\beta_0 = \frac{\pi}{8}$ case. Again, the optimal array layout is unchanged from $\beta_0 = \frac{\pi}{8}$ with $n_1 = 1$. It is clear that both $\beta_0 = \frac{\pi}{8}$ and $\beta_0 = \frac{\pi}{4}$ should be avoided, since these cases maintained $I < 1$, even in the optimal cases.

It is interesting to note how little the array layout parameter n_1 effects the

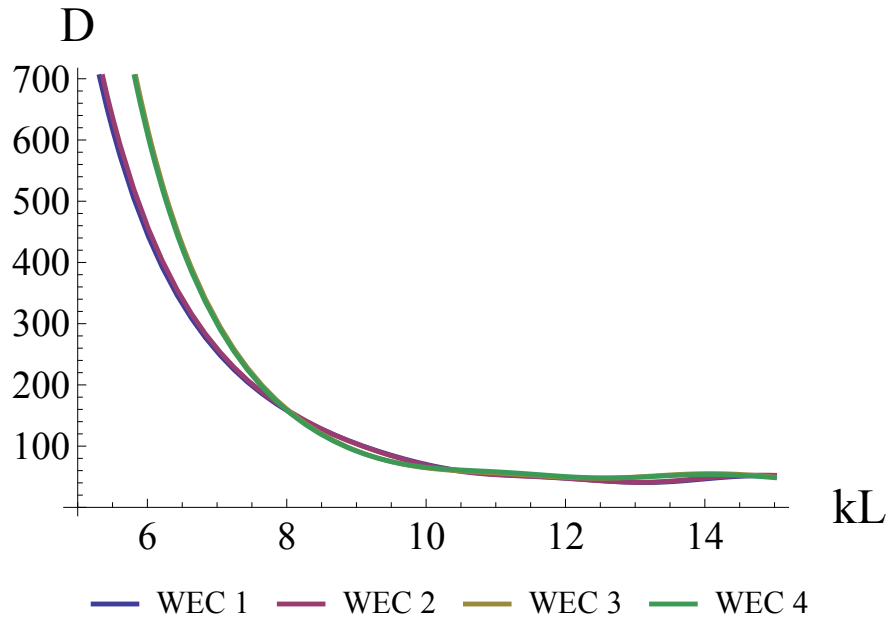

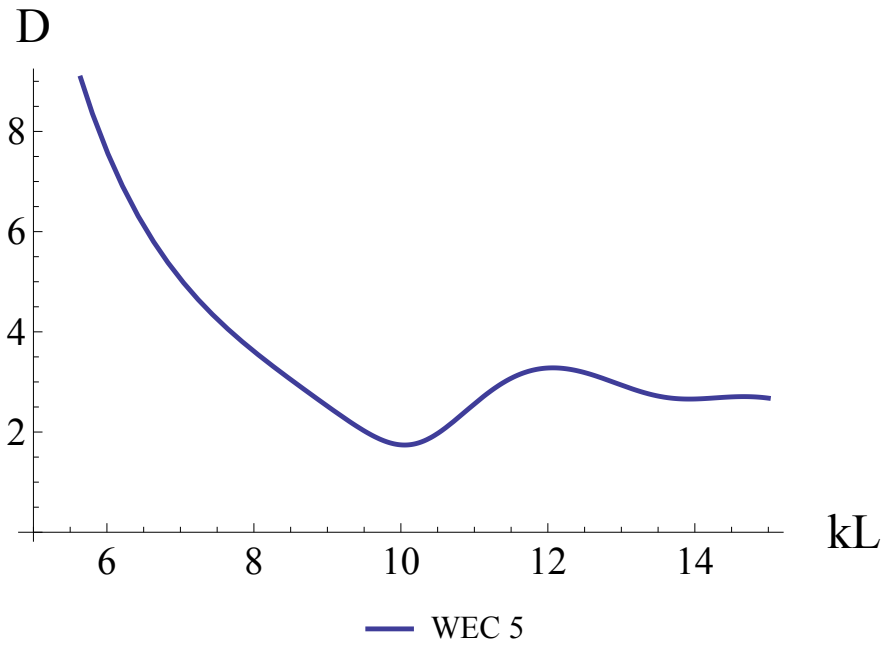

Figure 3.20: Predicted non-dimensional optimal WEC displacements in optimised array LS2 (as in Figure 3.18) with $n_1 = 49$ for $\beta = \beta_0 = 0$.

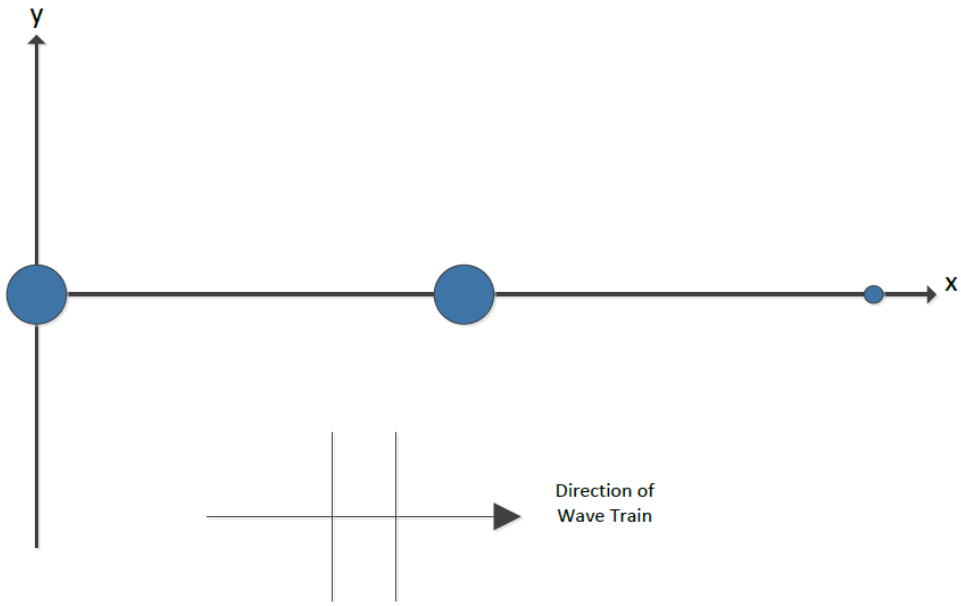

Figure 3.21: Suggested possible optimal satellite array for array LS2, corresponding to figure 3.18, with larger device in place of groups of devices.

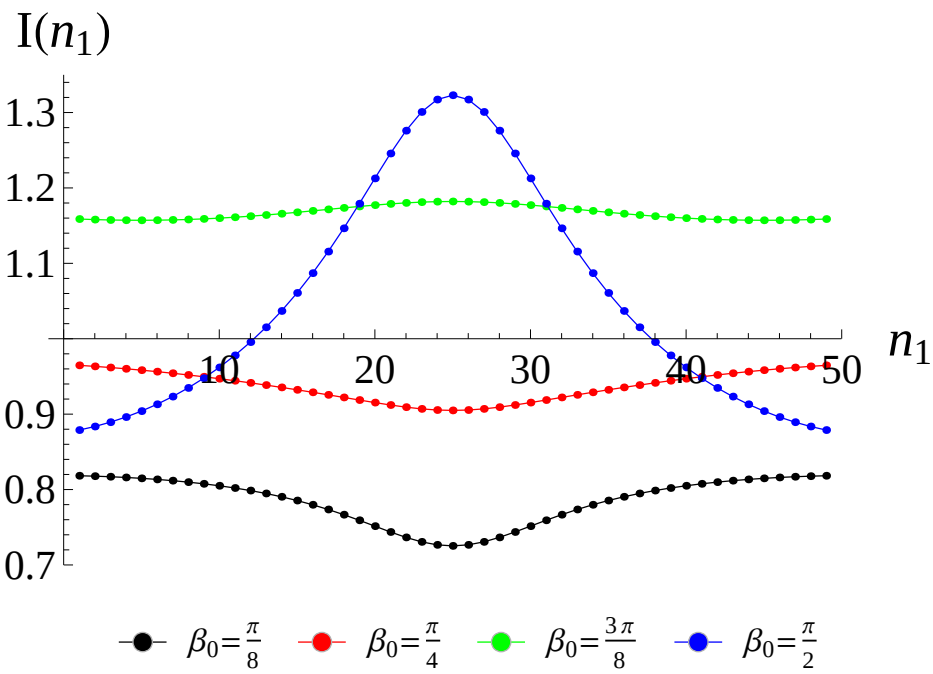

Figure 3.22: $I(n_1)$ against n_1 for array LS2 for several values of β_0.

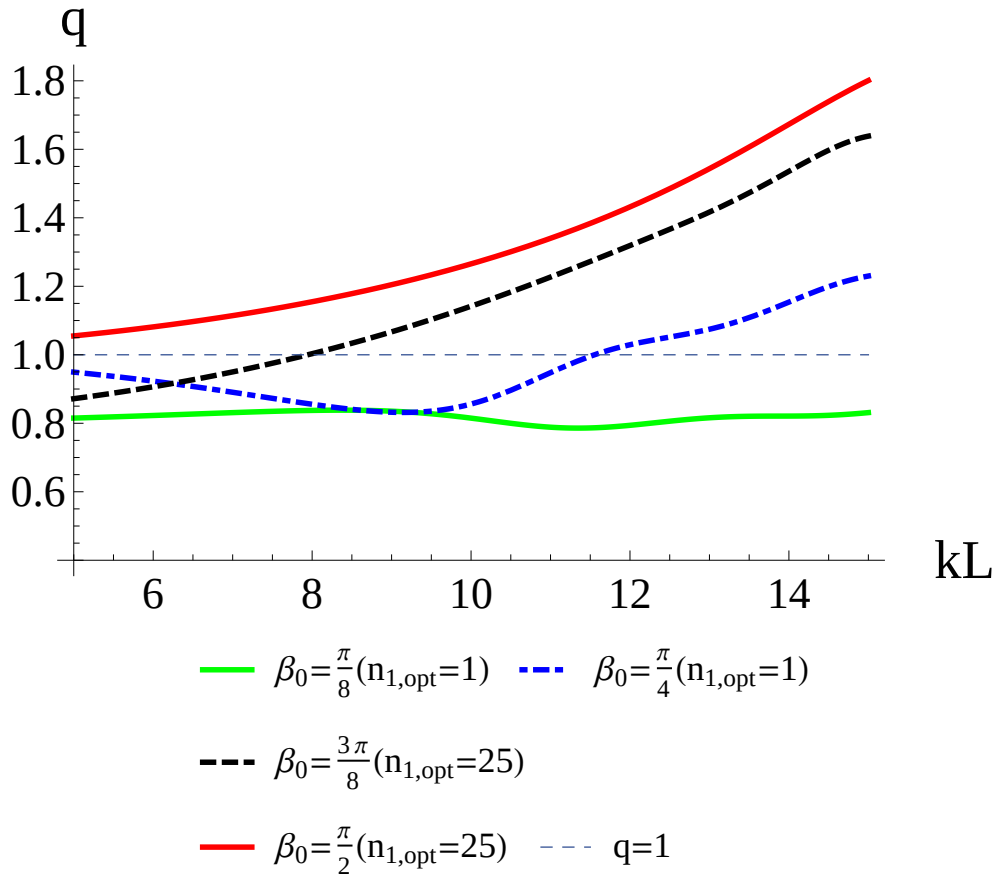

Figure 3.23: Interaction factor q against kL for all optimal LS2 arrays for several values of β_0.

average performance of the $\beta_0 = \frac{3\pi}{8}$ case, where $I \approx 1.16$ for all $n_1 \in [1, 49]$. Thus, decent performance is seen for all possible layouts at $\beta_0 = \frac{3\pi}{8}$, despite large gaps or groups of WECs that exist for some of these configurations.

It is clear from figure 3.23 that the best case is for beam seas, where $q > 1$ for all $kL \in [5, 15]$. Furthermore, q is increasing with kL, indicating that the array performs better for larger kL in beam seas. This agrees with the analogous results for array LS1. It is interesting to note that the poorest performance corresponds to optimal arrays that consist of closely spaced groups of WECs ($n_{1,opt} = 1$ for $\beta_0 = \frac{\pi}{8}$ and $\beta_0 = \frac{\pi}{4}$). Conversely, the best performance is seen for optimal arrays with uniform layouts $n_{1,opt} = 25$ for $\beta_0 = \frac{3\pi}{8}$ and $\beta_0 = \frac{\pi}{2}$.

Rather surprisingly, the β-variation of array LS2 for both $n_1 = 1$ and $n_1 = 25$ are very similar and only deviate near $\beta = \frac{\pi}{2}$, as shown in figure 3.24. This shows that the beam seas optimal array is quite stable to changes in β, as it maintains $q > 1$ for a variation of approximately $\pm\frac{5\pi}{24}$, similarly to array LS1.

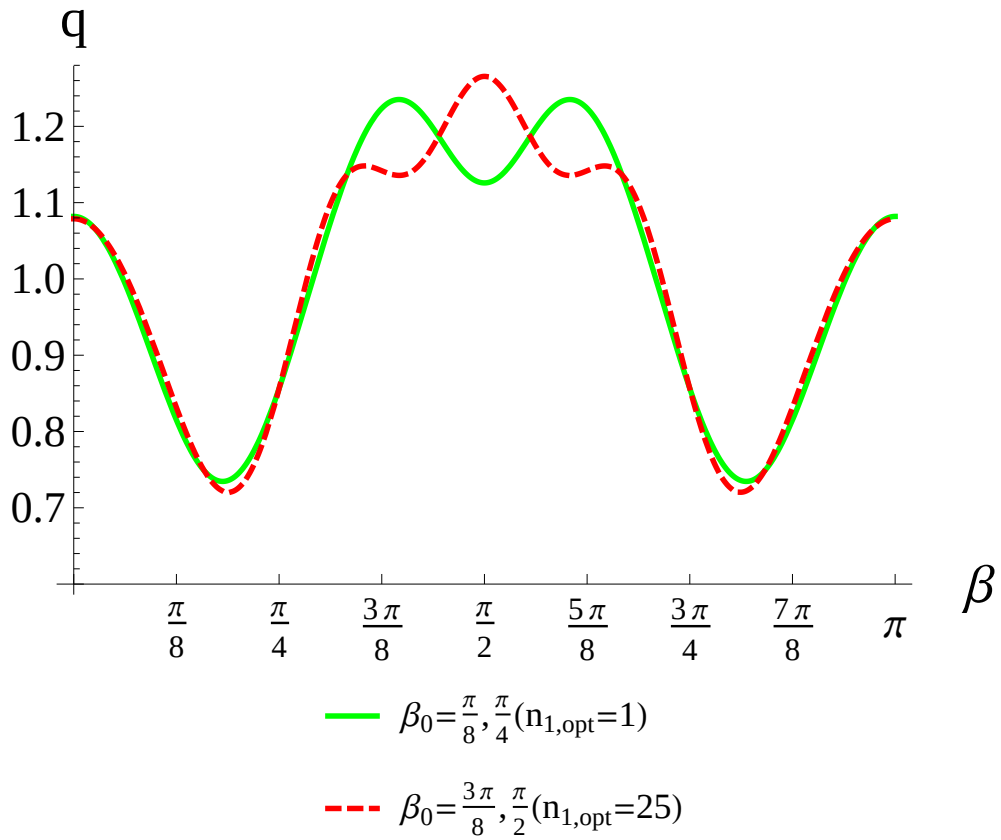

Figure 3.24: Interaction factor q against β for array LS2 optimised for for several values of β_0, with $kL = 10$.

This is not as ideal for the other values of β_0, since the target wave angle occurs away from the central peak at $\beta = \frac{\pi}{2}$.

3.3.2.3 Summary of Results for Array LS2

The results for array LS2 are concisely presented and summarised for each value of β_0 in table 3.2, which lists the optimal value of the spacing parameter n_1 ($n_{1,opt}$), the optimal mean value of q, and also shows a schematic of the optimal array layout. As in Section 3.3.1, the general array performance and the optimal array layouts differ considerably for changing values of β_0.

Once more, the incident wave angle changes the optimal arrangement in some cases. For this prescribed symmetry, the optimal situation jumps from two groups of two devices $n_1 = 1, 49$ to the uniform array $n_1 = 25$ between $\beta_0 = \frac{\pi}{4}$ and $\beta_0 = \frac{3\pi}{8}$. As with array LS1, both the beam and head seas cases perform the best, with the former slightly outperforming the latter. For $\beta_0 = \frac{\pi}{8}$ the

Table 3.2: Optimisation results for array LS2 with different incident wave angles.

β_0	$n_{1,opt}$	$I(n_{1,opt})$	Array Layout				
0	1	1.25	**		**		*
$\frac{\pi}{8}$	1	0.82	**		**		*
$\frac{\pi}{4}$	1	0.97	**		**		*
$\frac{3\pi}{8}$	25	1.18	*	*	*	*	*
$\frac{\pi}{2}$	25	1.32	*	*	*	*	*

optimal array performs quite poorly, with destructive interference dominating, similarly to array LS1.

3.3.3 Linear Asymmetric Array 3 (LS3)

The final linear array considered in this chapter is an asymmetric one such that $s_1 = s_2$ and $s_3 = s_4$, as shown in figure 3.25; this array is referred to as array LS3. The same procedure is followed and the array is analysed for several incident wave angles. The effect of the parameter n_1 is investigated in each case and the optimal array formation is also assessed in terms of performance and stability. A detailed analysis of results is provided for $\beta_0 = 0$ in Section 3.3.3.1, while the results for other wave angles are summarised in Section 3.3.3.2.

3.3.3.1 Optimisation and Analysis of Array LS3 in Head Seas

The optimisation results for array LS3 in head seas are shown in figure 3.26. As with array LS2, symmetry exists about $n_1 = 25$, so only $n_1 \in [1, 25]$ needs to be considered. The optimal case is when $n_1 = 3$ or $n_1 = 47$, which results in the array layout shown in figure 3.27, where $n_1 = 3$ is demonstrated. This results in a closely spaced group of three WECs to the left of the array, with two isolated WECs in the centre and to the right of the array.

The performance of array LS3 in head seas is shown for several values of n_1 in figure 3.28. Similar to array LS2, very little variation is seen in q for different n_1 values for $kL \in [5, 10]$, and the optimal value of $n_1 = 3$ is almost the poorest in this region, with $n_1 = 1$ producing slightly lower performance. However, for $kL \in [10, 15]$, the optimal array outperforms all others and maintains $q > 1$,

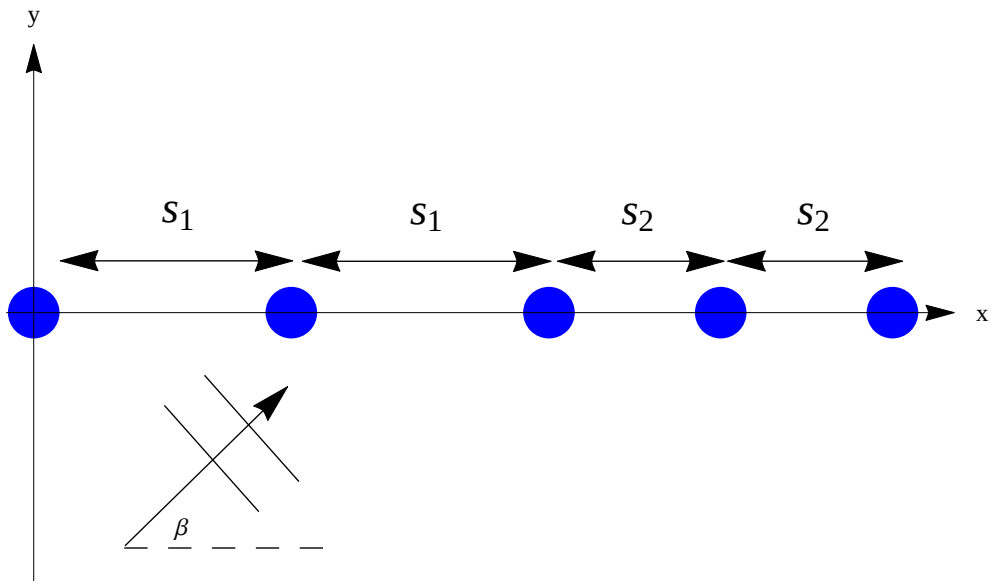

Figure 3.25: Diagram of array LS3, with asymmetry about WEC 3.

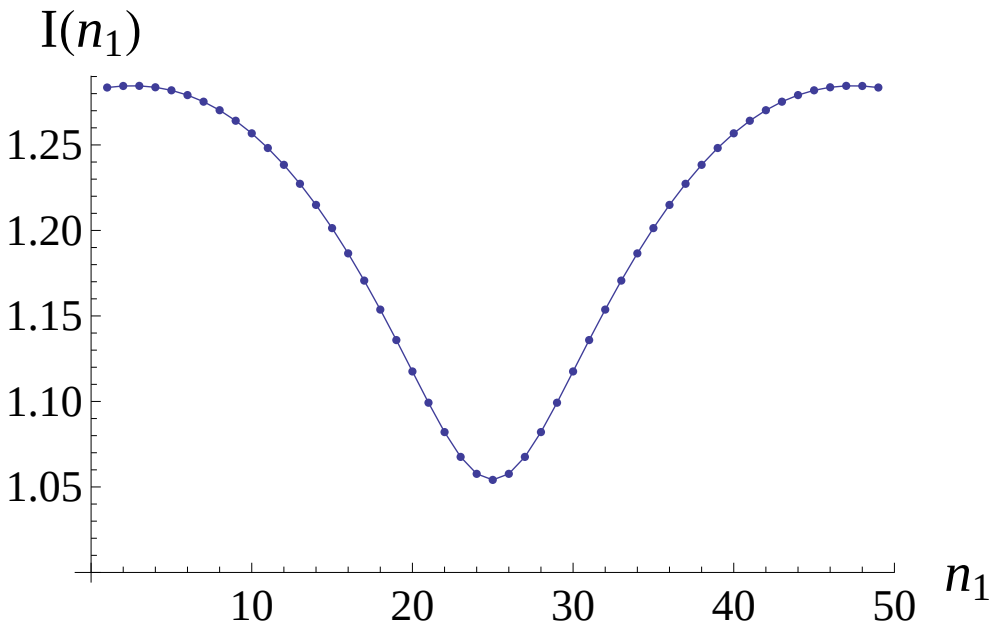

Figure 3.26: $I(n_1)$ against n_1 for $n_1 \in [1, 49]$ for array LS3 with $\beta_0 = 0$.

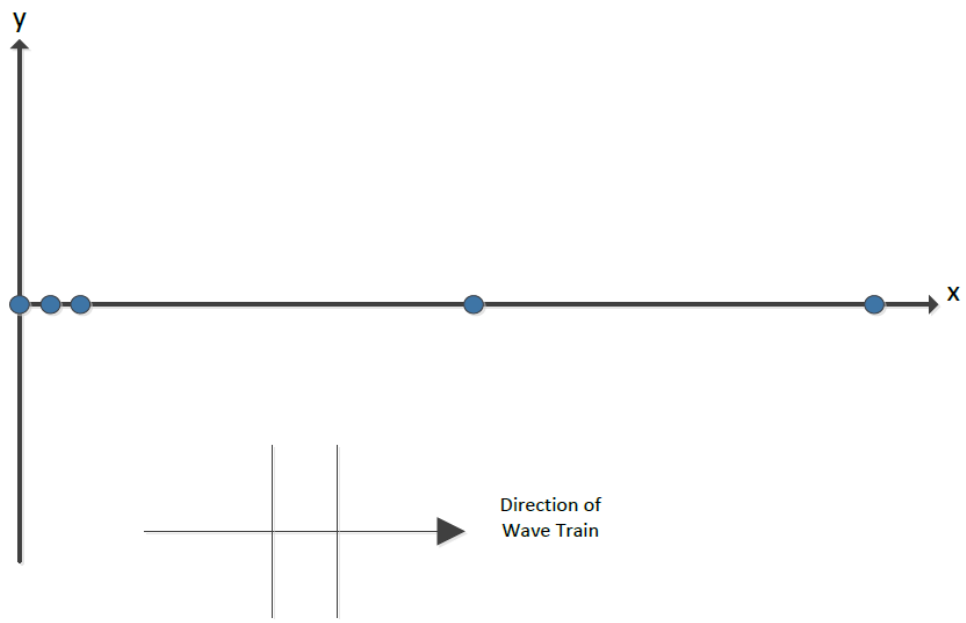

Figure 3.27: Diagram of optimised array LS3 for $\beta_0 = 0$, with $ks_1 = 0.3$ and $ks_2 = 4.7$.

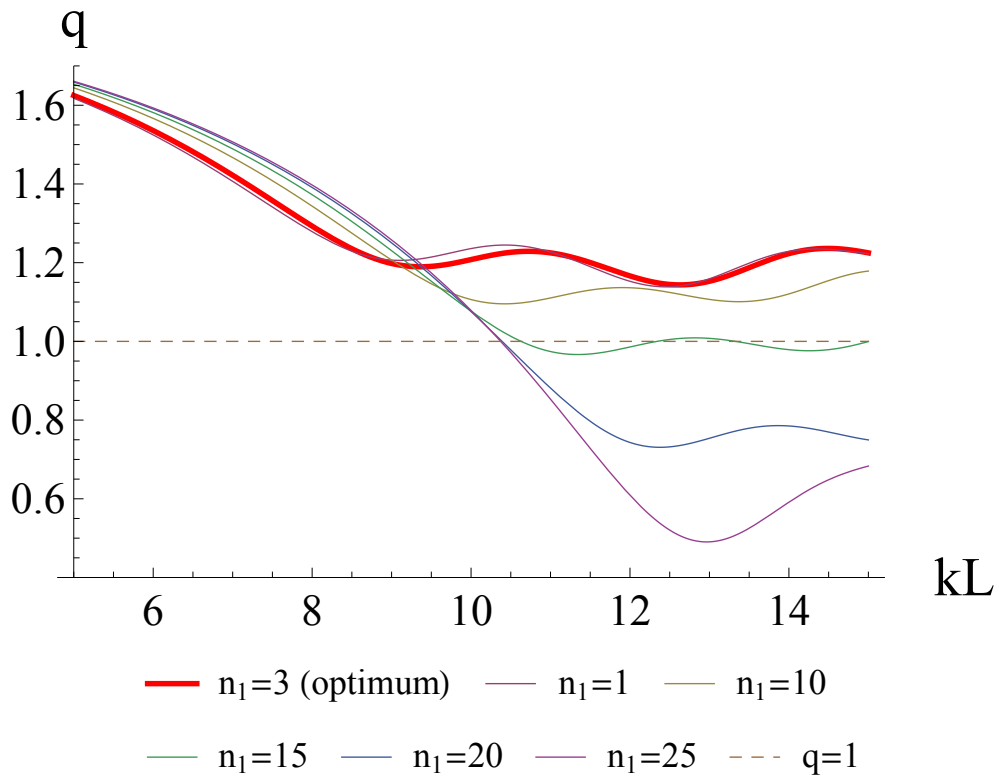

Figure 3.28: Interaction factor q against kL for array LS3 for different values of n_1, with $kL \in [5, 15]$ and $\beta = 0$. $q = 1$ is shown by dashed line.

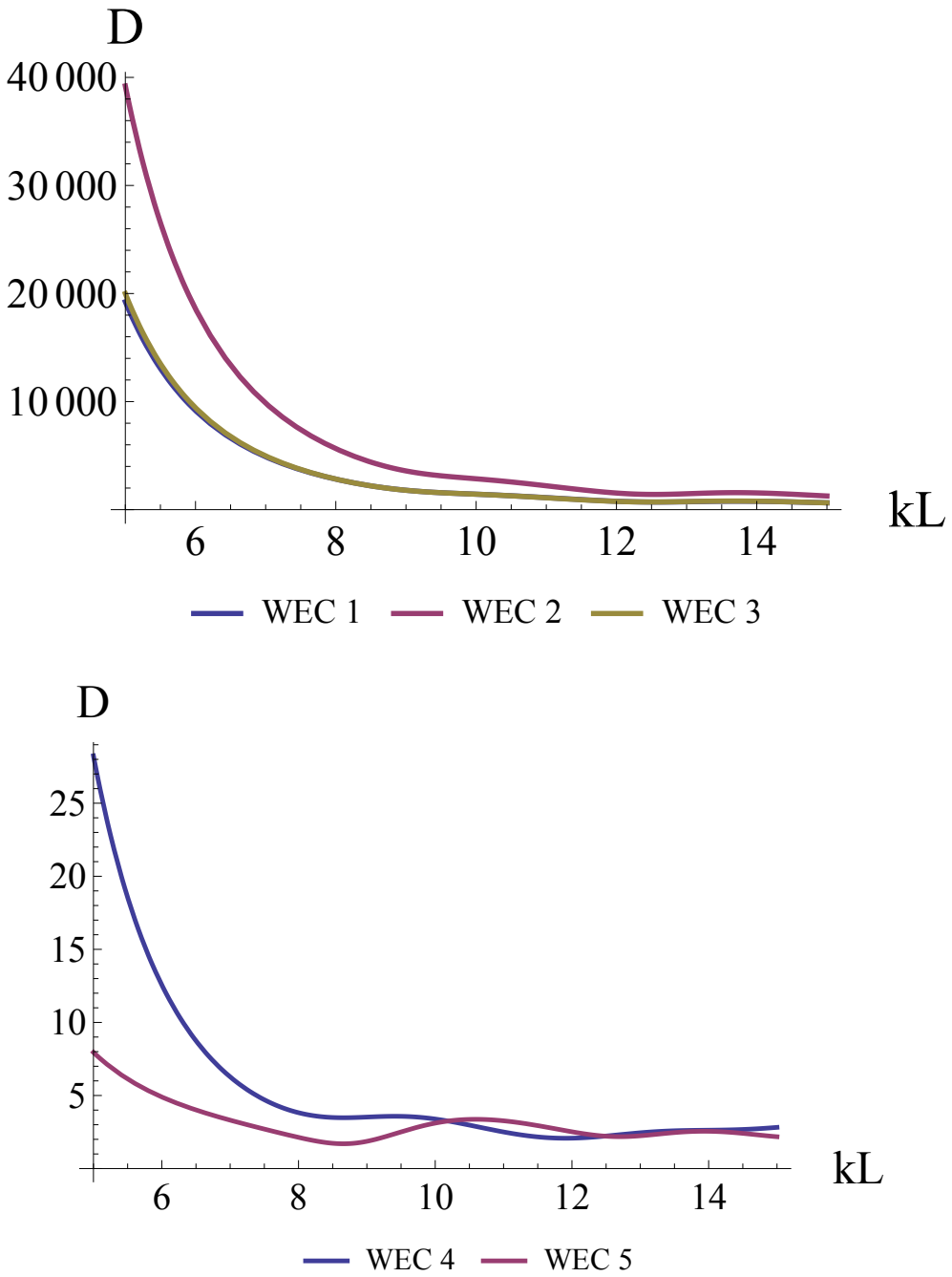

Figure 3.29: Predicted non-dimensional optimal WEC displacements in optimised array LS3 (as in Figure 3.27) with $n_1 = 3$ for $\beta = \beta_0 = 0$.

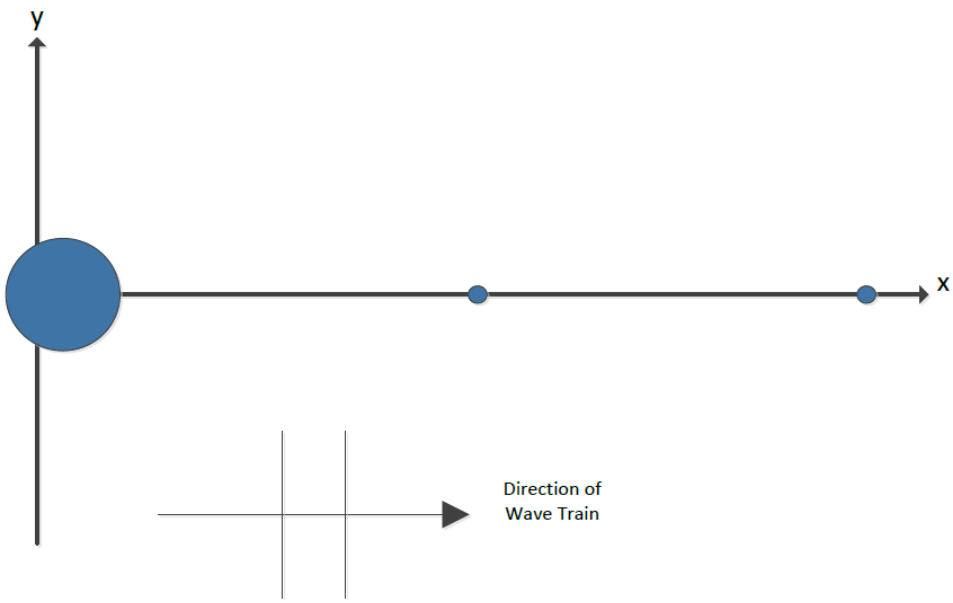

Figure 3.30: Suggested possible optimal "satellite" array for array LS3, corresponding to figure 3.27, with larger device in place of groups of devices.

with $q \in [1.15, 1.63]$ for all $kL \in [5, 15]$.

As with previous optimal arrays, the WEC displacement amplitudes are shown in figure 3.29 to be excessively large. This is particularly true for the group of devices (WECs 1-3), whose motions are $\mathcal{O}(1000)$ to $\mathcal{O}(10000)$ times the incident wave amplitude. The isolated devices (WECs 4 and 5) exhibit reasonable motions for $kL \in [8, 15]$, but for smaller kL these also exceed the $\mathcal{O}(1)$ limit.

Following the previous discussion, one possible solution to this is to replace the group of WECs with an appropriately larger WEC, creating an analogous satellite array, as shown in figure 3.30. Again, this requires further investigation and validation that is beyond the scope of this thesis.

A sensitivity analysis was also performed for array LS3, analogous to that in figure 3.12 for array LS1. Similar performance to arrays LS1 and LS2 is seen, where an error in either separation has little effect on the overall performance and is merely a perturbation of the undisturbed array. As no further insight is provided by the sensitivity analysis in this case, it is omitted for brevity.

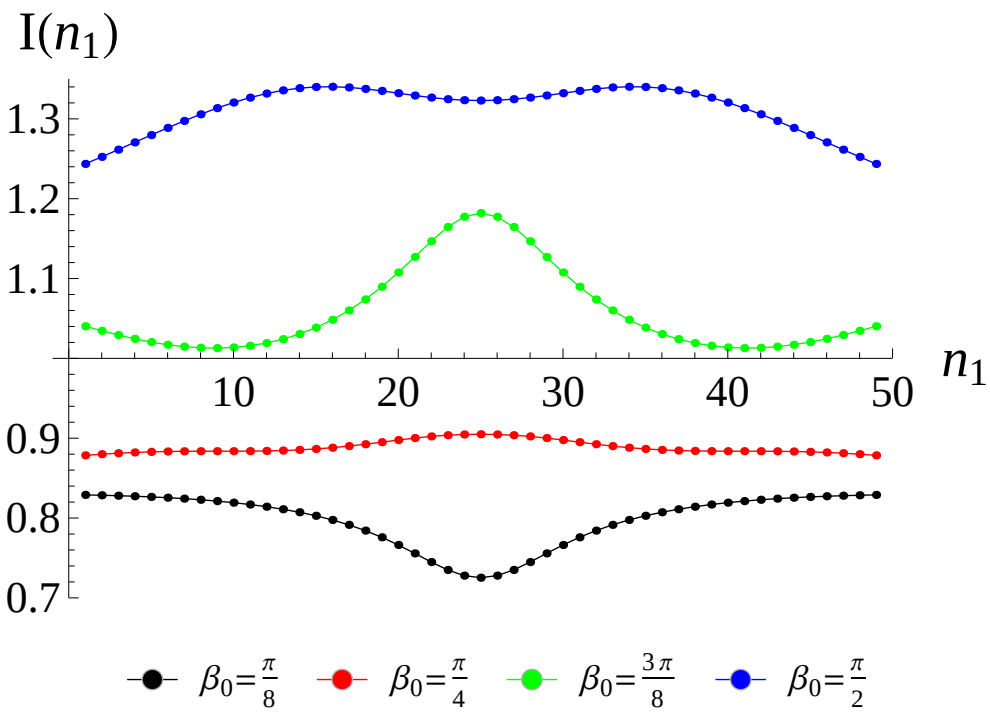

Figure 3.31: Plot of $I(n_1)$ against n_1 for array LS3 for several values of β_0.

3.3.3.2 Optimisation and Analysis of Array LS3 in Alternate Incident Wave Angles

The optimisation results for array LS3 with $\beta_0 = \frac{\pi}{8}, \frac{\pi}{4}, \frac{3\pi}{8}$ and $\frac{\pi}{2}$ are shown in figure 3.31. Similar results to the previous arrays are obtained, with $\beta_0 = \frac{\pi}{8}$ performing poorest and $\beta_0 = \frac{\pi}{2}$ performing best.

The beam seas array shows very little variation in mean performance for all allowed values of n_1. This is rather surprising as the extreme values of n_1 result in large gaps in the array and groups of three devices. A similar argument can be made for the intermediate seas $\beta_0 = \frac{\pi}{4}$ case, though the overall performance of the array is much lower, even in the optimal case.

Figure 3.32 shows that the beam sea optimal array outperforms those at other wave angles and maintains $q > 1$ for all $kL \in [5, 15]$. The array performs better for larger kL values, as with previous beam seas arrays investigated. Similar performance is seen for the $\beta_0 = \frac{3\pi}{8}$ case, where q increases almost linearly with kL. In this case, $q < 1$ for $kL < 8$, however $q > 1$ is maintained for the rest of the domain. Both the $\beta_0 = \frac{\pi}{8}$ and $\beta_0 = \frac{\pi}{4}$ cases perform quite poorly, with $q < 1$ for the majority or all of the domain of kL.

Broadly similar behaviour is seen for all optimal arrays with respect to

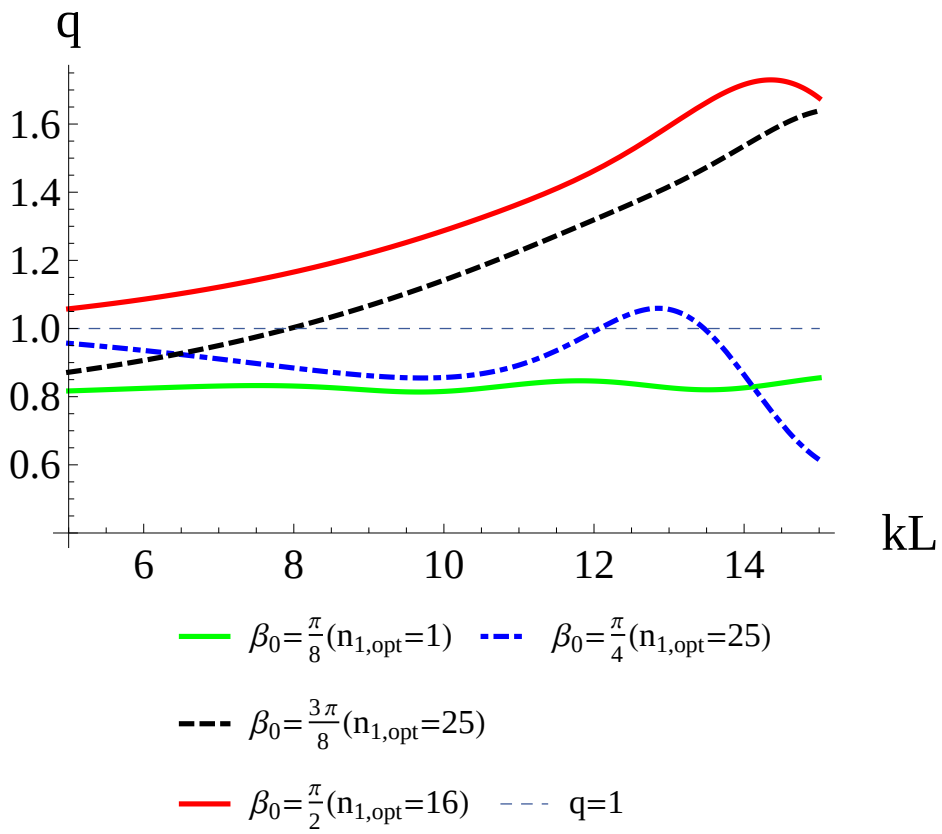

Figure 3.32: Plot of q against kL for optimised LS3 array for several values of β_0.

β-variation in figure 3.33, with a peaked performance at or near $\beta = \frac{\pi}{2}$ and a secondary peak at $\beta = 0$. The beam seas array achieves relatively stable performance around the target value of $\beta = \frac{\pi}{2}$, where $q > 1$ is maintained for a $\pm\frac{5\pi}{24}$ variation around this target. The performance for the other values of β_0 is not as good, since the peak in the q vs β curve appears away from the target values.

3.3.3.3 Summary of Results for Array LS3

Table 3.3 shows a summary of the optimisation results corresponding to array LS3. For each wave angle considered, the optimal spacing parameter $n_{1,opt}$, the mean of the interaction factor at this value $I(n_{1,opt})$ and a rough diagram of the resulting optimal array are presented. Again, this shows the relative importance of the incident wave angle β, since different array layouts are identified as optimal for different values of β_0, with varying optimal performance. Both $\beta_0 = \frac{\pi}{8}$ and $\frac{\pi}{4}$ achieved optimal mean performance of $I < 1$, indicating that destructive interference dominates at these wave angles. The best array is the

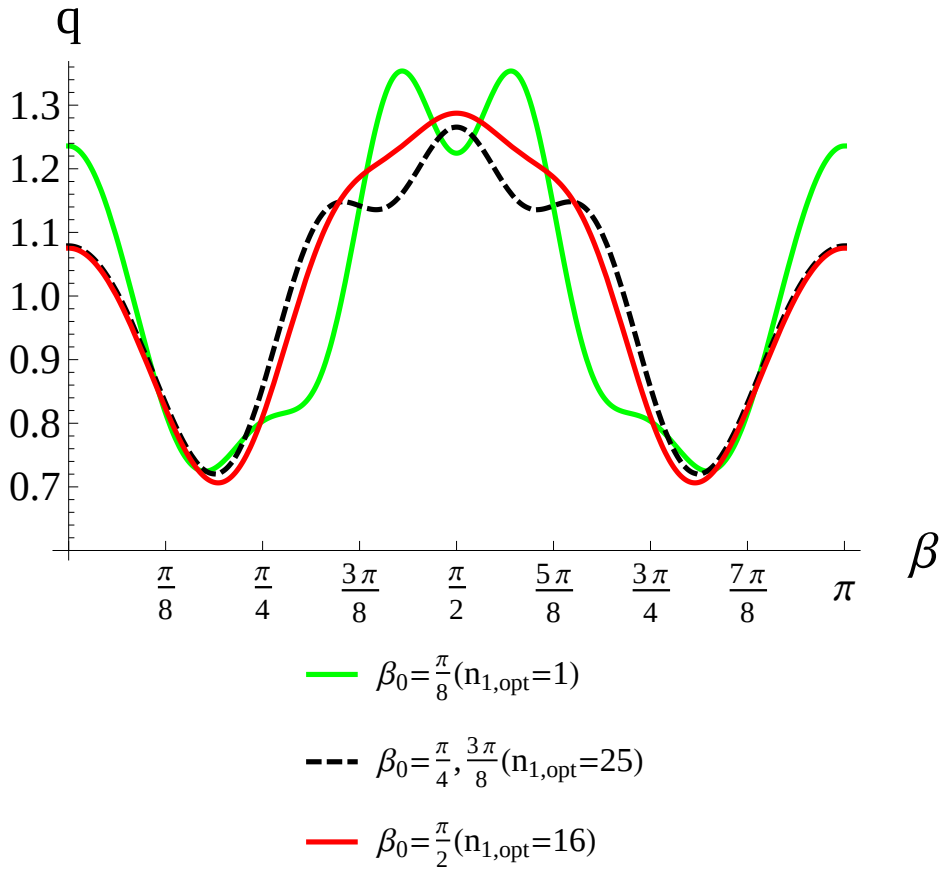

Figure 3.33: Plot of q against β for optimised LS3 array for several values of β_0, with $kL = 10$.

beam seas array, which achieved $I = 1.34$ with an unevenly spaced array layout, although the array contains no closely spaced WECs.

The head sea optimum occurs for $n_1 = 3$, which is quite similar to the $n_1 = 1$ case. It is clear that taking $n_1 = 1$ results in only a very small decrease in $I(n_1)$. Therefore, arrays with uniform ($n_1 = 25$) or extremely grouped ($n_1 = 1, 3$) layouts are found to be optimal (depending on the angle in consideration). However, for this prescribed symmetry, a small improvement on the uniform array can be obtained for beam seas, by taking $n_1 = 16$. This results in an asymmetric array which is unequally spaced.

It is also evident that array LS3, optimised for $\beta_0 = \frac{\pi}{2}$ with $n_1 = 16$, gave the highest value of mean interaction factor $I = 1.34$. Therefore, this may be a good choice for array layout if the wave direction is relatively constant at the site location. However, caution should be exercised in making such a judgement, as a large mean interaction factor may not necessarily correspond to good performance over the entire domain; the exact form of the interaction factor

Table 3.3: Optimisation results for array LS3 with different incident wave angles.

β_0	$n_{1,opt}$	$I(n_{1,opt})$	Array Layout
0	3	1.28	* * * * *
$\frac{\pi}{8}$	1	0.83	* * * * *
$\frac{\pi}{4}$	25	0.90	* * * * *
$\frac{3\pi}{8}$	25	1.18	* * * * *
$\frac{\pi}{2}$	16	1.34	* * * * *

must be investigated. An example of this can be seen by comparing the interaction factor for optimal arrays LS1 and LS3 for $\beta_0 = 0$. Array LS1 had the higher value of $I = 1.33$, however the plot of q varied over a larger range $q \in [1.1, 1.7]$; array LS3 had $I = 1.28$ but less variance in interaction factor, $q \in [1.18, 1.65]$. Depending on the desires of the user, the latter case may be preferred.

3.4 Discussion of Results

The principal objectives of this chapter were to consider the preliminary optimisation procedure, introduce the objective function utilised, consider the concept of maximising the mean of performance and to examine the simplest case of this problem, namely where it is reduced to one variable. By enforcing symmetry and writing the objective function in terms of one variable only, this allows preliminary results to be achieved relatively quickly in Mathematica. This also serves to provide an appreciation of the problem by looking at the simplest case first, before considering more general problems with increased difficulty. The single-variable optimisation also allows the optimisation to be visualised and the behaviour of the optimisation variable explicitly shown, which proved insightful.

Three types of symmetric five device linear arrays were investigated. A certain symmetry or asymmetry was imposed in each case to reduce the number of variables with respect to which the array is optimised. The symmetries chosen are merely examples of three of the simplest cases. Many other types of symmetry and asymmetry exist, such as enforcing one separation to be an integer multiple of another (e.g. $s_1 = 2s_3$ *etc.*). Also, a less stringent geometry

could be enforced by stipulating that only one separation is the same as another, thereby allowing the linear five device arrays to be described by two variables instead of one. However, an increase in variables complicates the optimisation considerably and increases the computational effort for a given algorithm. This also prevents an in-depth analysis of how the array behaves within the optimisation process, since the performance can no longer be visualised as a function of one array parameter. More general cases without imposed symmetry are examined in subsequent chapters.

The most noteworthy result in this chapter is the fact that the optimal array layout changes considerably depending on the incident wave angle β_0 considered. A relatively small change in β_0 of $\pm\frac{\pi}{8}$ can result in a considerable alteration of the array performance and also the optimal array layout. This is illustrated most clearly by the results listed in tables 3.1 - 3.3. For example, table 3.1 shows that moving from $\beta_0 = 0$ to $\beta_0 = \frac{\pi}{8}$ results in a considerable change in $n_{1,opt}$, from one extreme with $n_1 = 49$ to the other with $n_1 = 1$. These values correspond to considerably different layouts; one with a group of three WECs in the centre of the array, the other with two groups of two WECs at the edges of the array. This indicates the influence of the incident wave angle on array performance, particularly for the directionally dependent geometry of a linear array.

Overall, the best performance for all symmetries is achieved in beam seas ($\beta_0 = \frac{\pi}{2}$) with optimal objetive function values of $I = 1.34$, $I = 1.32$ and $I = 1.34$ for arrays LS1, LS2 and LS3 respectively. This resulted in each optimal beam seas array maintaining $q > 1$ for all $kL \in [5, 15]$. These arrays also exhibited a large range of good performance for varying β where, for each symmetry, $q > 1$ is maintained for approximately $\beta = \frac{\pi}{2} \pm \frac{5\pi}{24}$. Furthermore, the optimal layouts for all symmetries at beam seas did not include grouped WECs; these were either uniformly or unequally spaced (with the minimum separation between devices being 16% of the total array length). This avoids the difficulty of having devices so close that they may collide or shadow each other.

Throughout this chapter, there is a notable difference between the optimal array layout/performance between the head and beam seas cases. In general, optimal head seas arrays contain groups of closely spaced WECs. This is to maximise the possible constructive interaction between the WECs. For head seas, the wave travels along the same line as the WEC array. Since the radiated wave-field decays as it propagates, the maximum constructive interference can

be achieved by placing the WECs as close as possible and contriving the WEC motions as necessary.

In contrast, the members of optimal beam seas arrays are more spread out, with uniform or unequal separations. This suggests that when a linear array faces the incoming wave in a terminator type layout, it is better not to have large gaps between the WECs, through which wave energy can escape. Spreading the WECs to give a greater frontage to the incoming wave appears to be best for beam seas.

It is shown here that constructive interaction can be achieved for head seas; the optimal head seas performance was competitive with that of beam seas in terms of the interaction factor. This is counter-intuitive to some extent, since head seas arrays provide the smallest frontage to the incoming waves. However, for each symmetry investigated, this optimal performance in head seas required the devices to be in closely spaced groups of two or three WECs. The head seas optimal performance is also more sensitive to changes in β compared to beam seas. This is shown by the analysis of q with respect to changes in β and also by the optimal performance of the arrays at nearby wave angles such as $\beta_0 = \frac{\pi}{8}$. At this target wave angle, change of $\pm\frac{\pi}{12}$ is enough to result in destructive interference. This indicates that the head seas arrays are considerably less stable to β-variation than beam seas arrays.

It can be seen for all symmetries that arrays optimised for $\beta_0 = \frac{\pi}{8}$ perform very poorly compared to other angles. The best optimal value achieved at this angle was an average interaction factor of $I = 0.84$. This is severely limiting, especially since this work assumes maximum power absorption of the array and does not take the PTO (and any related inefficiencies) into account. This value is an upper bound on what can theoretically be achieved; therefore the performance of a real array in this scenario is liable to be much poorer.

A similar argument can be applied for arrays with $\beta_0 = \frac{\pi}{4}$, though the destructive effect is not as severe at this wave angle. The value $I = 1.12$ is achieved for the optimal array LS1 for $\beta_0 = \frac{\pi}{4}$; though this is the only example where constructive interference dominates at this wave angle.

A broader investigation of the effect of the array parameters kL, β and n_1 is given in Appendix A, where 3D plots involving these parameters are presented. Due to the nature and volume of these plots, these are omitted for clarity from this chapter for all but head seas arrays.

Sensitivity analyses similar to figure 3.12 were performed for each optimal array in this chapter. Broadly similar results were obtained for each symmetry, such that the errors (up to $\pm 0.05kL$) had little effect on the optimal performance, hence showing the stability of the optimal arrays. This is only shown explicitly for the head seas array LS1 and omitted for brevity for other arrays, as no further insight is provided by the analogous plots for the other array symmetries.

The WEC displacement amplitudes are only shown for the head seas array for each symmetry investigated in this chapter. The displacement amplitudes for other values of β_0 are presented in Appendix A. For the other wave angles, similar displacement behaviour was seen where larger motions occurred for grouped WECs and for lower values of kL. Slightly lower motion amplitudes are observed for the more separated arrays, such as uniform layouts with $n_{1,opt} = 25$. It is possible that the imposition of constraints would have less of a detrimental effect on such layouts. However, with optimal unconstrained motions, each array investigated still contained displacement amplitudes above the $\mathcal{O}(1)$ requirement. The effect of motion constraints are considered in subsequent chapters.

The associated optimal device motions is one major source of difficulty with the arrays investigated in this chapter. It is suggested by Thomas & Evans (1981) that a reasonable upper limit of device amplitudes could be three times the incident wave amplitude; this limit is considerably exceeded for all grouped devices in the optimal arrays found. These motions are predicted using linear wave theory which assumes all motions are at most of the same order as the wave motion, which is assumed to be small in some sense. Large device motions violate this approximation and thus invalidate the underlying linear wave theory. Furthermore, the application of a physical PTO will not allow these large motions, which in turn will affect device interaction and hence power performance.

A potential way to reduce the large device motions, while retaining the benefit of the constructive interference caused by the groups of devices, may be to replace these groups with larger devices corresponding to the group size. Following this proposal, the optimised array LS1 for $\beta_0 = 0$ would have the central group of three devices replaced by a device three times the radius of the original devices, giving the array shown in figure 3.9. Similarly, groups of two devices would be replaced by a device of twice the original radius. The idea of

arrays of WECs of different sizes has not been investigated previously and would be a natural extension of this work.

Preliminary calculations have been performed and show the device motions can indeed be reduced to acceptable values. It is also hoped that the larger power absorption of the larger devices (due to the increased mass, momentum, PTO *etc.*) would offset the reduction of array members. A full interaction theory is needed to confirm this hypothesis, as the scattered wave-field from the larger devices may become significant. Also, the original devices are assumed to have a radius $ka = 0.4$, so that the larger devices would have radii of $ka = 0.8$ and $ka = 1.2$, which would violate the point absorber approximation, although the results of Mavrakos & McIver (1997) suggest that the point absorber approximation may be accurate enough for the smaller of these larger devices.

A further optimisation method was investigated, which optimised the array layout with respect to the mean of the interaction factor over non-dimensional length and over a range of incident wave angle simultaneously. The objective function (analogous to equation (3.1)) is written as

$$I^{\beta}(n_1, \ldots, n_{N-1}) = \frac{1}{(\beta_u - \beta_l)(kL_u - kL_l)} \int_{\beta_l}^{\beta_u} \int_{kL_l}^{kL_u} q(n_1, \ldots, n_{N-1}, kL, \beta)\ d[kL]\ d\beta, \tag{3.14}$$

where the average is now taken over both $kL \in [kL_l, kL_u]$ and $\beta \in [\beta_l, \beta_u]$. This methodology therefore accounts for varying incident wave angle as well as non-dimensional length and the method was used to optimise similar arrays for small ranges of angular variation. Preliminary calculations of this nature showed little difference to the results presented within this chapter. It was found again that the angular range considered had a large impact on the optimal array geometry.

It should be noted, however, that this optimisation strategy assumes that each wave angle in the range $[\beta_l, \beta_u]$ is equally important and thus occurs equally often. This is perhaps a good approximation for seas states which have a small wave angle variation. However, for sea states which have considerable angular variation there is often a dominant direction, in which case irregular wave modelling and wave spectra should be used. Optimisations of this nature, where the mean is defined over the incident wave angle, are examined in Chapters 7 and 8.

The algorithms used in this chapter were implemented in Mathematica 9.0 and

involved evaluation of the objective function at discrete (integer) values of the single array variable. This was due to the circumstance that numerical calculations of this type are very slow in Mathematica, compared to implementations in other programs and languages. Consequently, the calculations in subsequent chapters are performed in a FORTRAN implementation, with the aid of Numerical Analysis Group (NAG) routines. This gives a much quicker run-time of optimisations and allows optimisation over an increased number of variables within a reasonable time frame.

An obvious extension of this simple problem is to somehow extend the single-variable optimisation to a two-variable optimisation. However, there is no clear non-arbitrary way of defining symmetry in a five-device array. It would be possible to examine a four-device array in this manner as a two-variable problem. However, this is omitted in favour of more general optimisations of arrays of five or more WECs in subsequent chapters.

Chapter 4

Optimisation of General Five-Device Linear Arrays in Regular Waves

4.1 Introduction

Chapter 3 considered optimisation of arrays with symmetry imposed, so that each array is described by just a single variable. The case of a non-symmetric linear array is investigated here, without any stipulated enforced symmetry. Thus, for an array of N WECs, each layout is described by $N-1$ variables in total, since one WEC will be fixed at the origin. However, the objective function of the optimisation describes the mean performance over the non-dimensional array length. Hence, the number of variables in the optimisation involves $N-2$ device separation variables. For an array of $N=5$ devices, this results in three optimisation variables, rather than one as in the previous chapter. The results of Chapter 3 and McGuinness & Thomas (2015) are extended in a more general formulation.

All calculations in Chapter 3 were performed using Mathematica 9.0, but due to the increased generality of the present problem, the calculations were moved to a FORTRAN implementation with the aid of Numerical Analysis Group (NAG) routines[1]. This was employed due to the increased speed and accuracy of the NAG routines in comparison to Mathematica, which was found to perform extensive numerical calculations very slowly. For the single-variable

[1] http://www.nag.co.uk

optimisations in the previous chapter, using the NAG routines enabled the optimal solutions to be determined approximately 1000 times faster compared to Mathematica. Appropriate NAG routines were employed to calculate and numerically integrate the interaction factor, as well as perform the optimisation.

This chapter details the results published in McGuinness & Thomas (2016) concerning linear arrays, as well as extended results omitted from this publication for brevity. These include results for optimisations with more values of the fixed incident wave angle β_0 and a discussion of the resulting implications. A more extensive list of the optimisation results obtained are provided in Appendix B, while a summery of these results is provided herein.

4.2 Optimisation Method

The overall setup and optimisation method follows that described in Chapter 3. No symmetry is imposed and the array is described by three variables, namely ks_1, ks_2, ks_3. A slightly different parameterisation is also made here, where

$$ks_j = n_j \; kL, \tag{4.1}$$

and the n_j are real quantities. This formulation requires that $n_j \in (0, 1)$, with the only difference between Chapter 3 and here being the absence of the scaling factor $M = \sum_{j=1}^{N-1} n_j$ in the reparameterisation. Since the sum of all separations is the total length, $\sum_{j=1}^{N-1} ks_j = kL$ and consistency requires

$$\sum_{j=1}^{N-1} n_j = 1. \tag{4.2}$$

This formulation is essentially identical to the previous chapter with $M = 1$.

The array is now described by the three real variables $n_1, n_2, n_3 \in (0, 1)$. For a non-dimensional length that remains within $kL \in [kL_l, kL_u]$, the objective function for the unconstrained optimisation is defined as

$$I(n_1, n_2, n_3; \beta_0) = \frac{1}{kL_u - kL_l} \int_{kL_l}^{kL_u} q(n_1, n_2, n_3, kL; \beta_0) \; d[kL], \tag{4.3}$$

for a fixed prescribed incident wave angle β_0. It is assumed, as previously, that the target non-dimensional length of a given array is $kL = 10$ and that the sea state under consideration is such that kL remains within the range

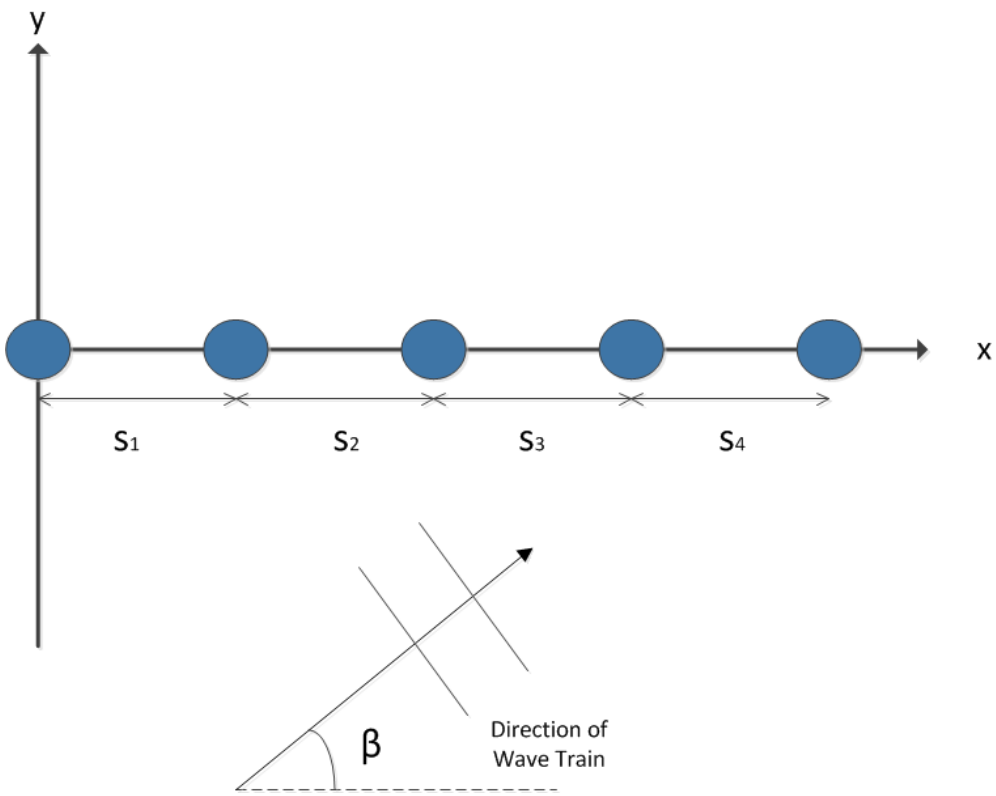

Figure 4.1: General five-device linear array (without imposed symmetry)

$[kL_l, kL_u] = [5, 15]$. The method can be applied to any range of kL as required, as the values used in this work are chosen arbitrarily but are intended to represent a typical case.

A diagram of the array under consideration is shown in figure 4.1. Initially, constraints on the device motions are not considered and the objective is simply to maximise the mean of the interaction factor with respect to the array layout, under the assumption of maximum power absorption.

4.2.1 Implementation

Numerical calculations were performed on a Dell Latitude E6330 running Windows 7 with 8GB of RAM and an Intel Core i3-3130M (2.6GHz) processor. The optimisation routine chosen to find the maximum of (4.3) is NAG routine E04UCF[2], with appropriate algorithms employed for the calculation of Bessel functions, matrix inversion and quadrature. This algorithm searches for the minimum value of the objective function using a sequential quadratic

[2]https://www.nag.co.uk/numeric/fl/manual/pdf/E04/e04ucf.pdf

programming method. In order to find the maximum rather than the minimum, the negative of (4.3) is supplied to the algorithm. A starting point is required as input to the optimisation algorithm. The algorithm initially uses the gradient of the objective function at this point to define a search direction, with the step size chosen such that a sufficient decrease in a Lagrangian type merit function is achieved. This procedure is repeated until an optimum is found. The algorithm E04UCF is essentially identical to the subroutine NPSOL as described by Gill *et al.* (1986).

The interaction factor is acknowledged as being a highly oscillatory function, with many local maxima and minima. However, the results of this and previous work indicate that the mean of the interaction factor is a more well-behaved function, particularly for the case of linear arrays. Despite this, it is prudent to perform an exhaustive search of the variable space for optimal values. This is conducted in a similar manner to Fitzgerald (2006), where the optimisation routine is run for a wide range of initial starting points for each variable. All permissible unique combinations of starting points with $n_j = \{0.1, 0.2, \ldots, 0.7\}$ with $j = 1, \ldots, 4$ were investigated, where some combinations were omitted due to consistency considerations in line with equation (4.2). For each value of β_0 investigated, the resulting optimal variable parameters and optimal mean interaction factor are then tabulated and presented. Diagrams of the best performing array layouts are also presented and analysed in each case.

This exhaustive search of the variable space involves many iterations of the optimisation routine for different starting values of each variable, resulting in many optimisation outputs. The global optima can then be chosen from these, provided it is converged to frequently enough to give confidence in the optimality of the solution. To avoid unnecessary presentation of data, the optimisation results are summarised within this chapter and the more detailed results are provided in Appendix B.

Minimum and maximum values of each separation parameter were enforced within the optimisation procedure so that $0.05 \leq n_j \leq 0.85$ for $j = 1, \ldots, 4$. This ensures that no device will be within 5% of the total array length of another device. The upper bound of 0.85 was chosen to allow the possibility that all but one of the separations coincided with the minimum bound. Linear constraints on the sum of the separations were also included in the algorithm in order to ensure consistency. This minimum bound is more limiting than that used in Chapter 3 and McGuinness & Thomas (2015), where a minimum value

Table 4.1: Optimal linear array parameters for each value of β_0 considered

β_0	n_1	n_2	n_3	n_4	I_{opt}
0	0.0500	0.0500	0.0500	0.8500	1.4802
$\frac{\pi}{8}$	0.0500	0.8500	0.0500	0.0500	0.8794
$\frac{\pi}{4}$	0.0500	0.8500	0.0500	0.0500	1.1431
$\frac{3\pi}{8}$	0.2512	0.2488	0.2488	0.2512	1.1822
$\frac{\pi}{2}$	0.0500	0.2252	0.3859	0.3359	1.3643

of 0.01 was allowed. It may be unrealistic to allow devices to be positioned within 1% of the total array length of each other, as the devices will be touching or intersecting for all but very large array lengths. A 5% constraint was chosen here as it is a more feasible scenario. This value also avoided potential calculation difficulties due to numerical inaccuracies and poor behaviour of the objective function caused by small non-dimensional separation arguments.

4.3 Unconstrained Optimisation Results

The best optimal arrays found for each value of $\beta_0 = 0, \frac{\pi}{8}, \frac{\pi}{4}, \frac{3\pi}{8}, \frac{\pi}{2}$ are presented in table 4.1. More detailed lists of all optimal solutions found by the optimisation are given in Appendix B in tables B.1-B.5. Within these tables, arrays that were found to be similar to those presented, either by symmetry or a negligible change in layout or performance, are omitted for brevity. For the best layout for each value of β_0, the behaviour of the optimal interaction factor is shown with respect to changes in kL and β in figures 4.2 and 4.3 respectively.

4.3.1 Head Seas: $\beta_0 = 0$

A diagram of the best array found for head seas is shown in figure 4.4. The optimal array variables determined by the algorithm are given in detail in table B.1 of the Appendix, in descending order of performance. The best array for head seas is when four of the devices are grouped closely together at one side of the array, with a relatively isolated device at the other end. This array achieves an average interaction factor of $I = 1.48$, which is considerably greater than unity; this is the best average value obtained for all the optimal linear arrays. It is clear from figure 4.2 that good performance is achieved over the entire

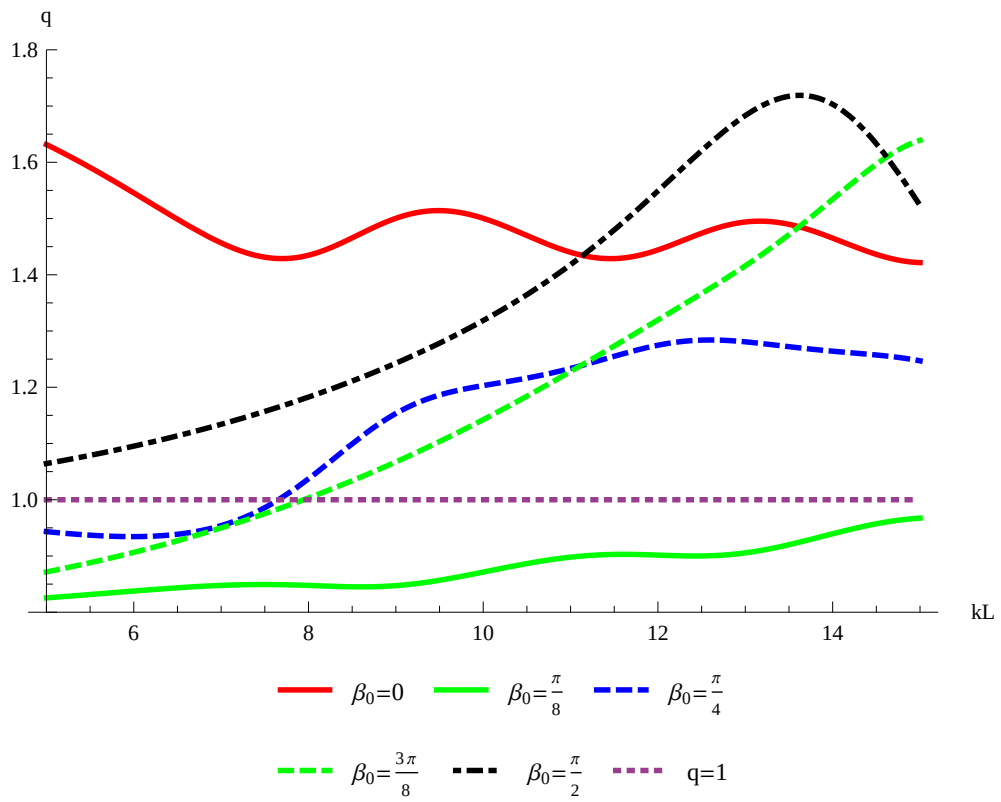

Figure 4.2: Optimal interaction factor q against non-dimensional length kL for the best linear arrays found for each value of β_0 examined. The horizontal dotted line represents $q = 1$

domain considered, with $q \in [1.42, 1.64]$ for $kL \in [5, 15]$. The plot of q against kL can be seen to perform small oscillations about the average value of $q = 1.48$. The range of variability of q is also surprisingly small and this may be desirable so as to provide more certainty for a given WEC array developer over a range of conditions.

Figure 4.3 shows that there is a range of approximately $\pm\frac{\pi}{10}$ around $\beta = 0$ where q remains greater than unity; outside this range, the array moves into areas of destructive interference. This behaviour is quite similar to that observed in Chapter 3 and McGuinness & Thomas (2015), for some of the arrays optimised in head seas. However, a greater peak in q is obtained here, which is also accompanied by larger troughs at non-optimal wave angles; this is probably due to the increased freedom of the array layout within this optimisation.

The optimal displacements of the WECs within the optimal array for $\beta_0 = 0$ are presented in figure 4.5; these are calculated using equation (2.142). As expected, these optimal displacements are unacceptably large ($|D| > 100$) for the grouped devices, agreeing with previous results. This is enhanced for the

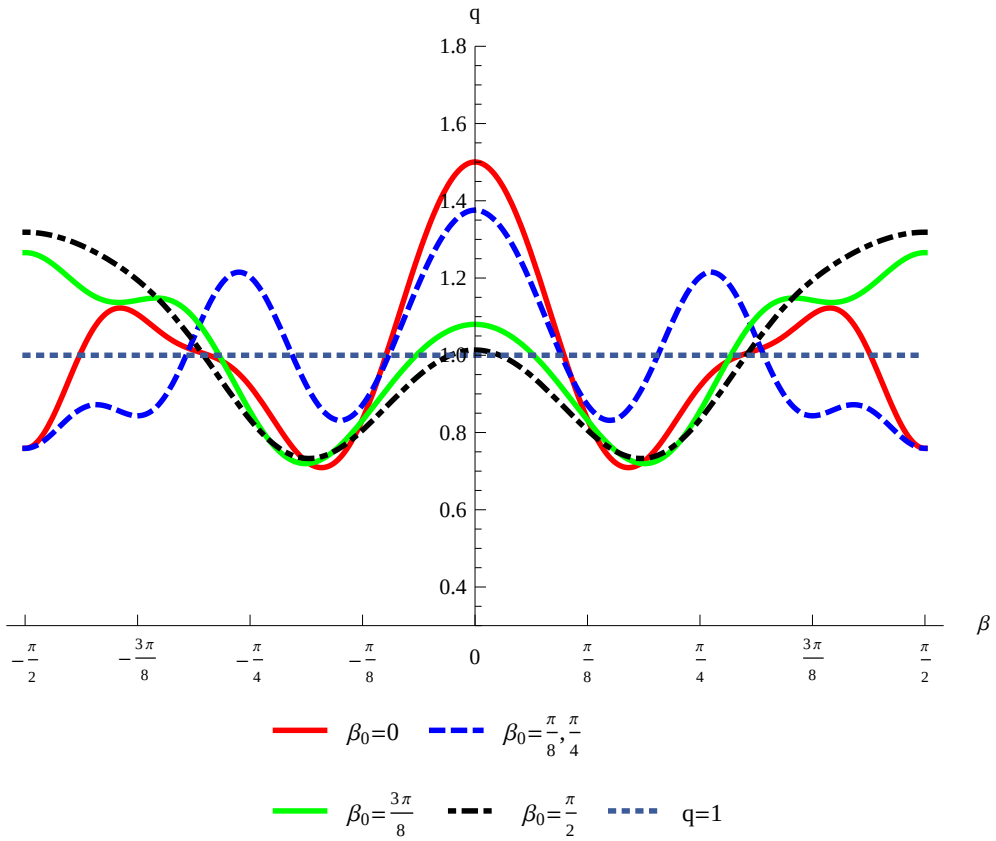

Figure 4.3: Optimal interaction factor q against incident wave angle β for the best linear arrays found for each value of β_0 examined. The horizontal dotted line represents $q = 1$

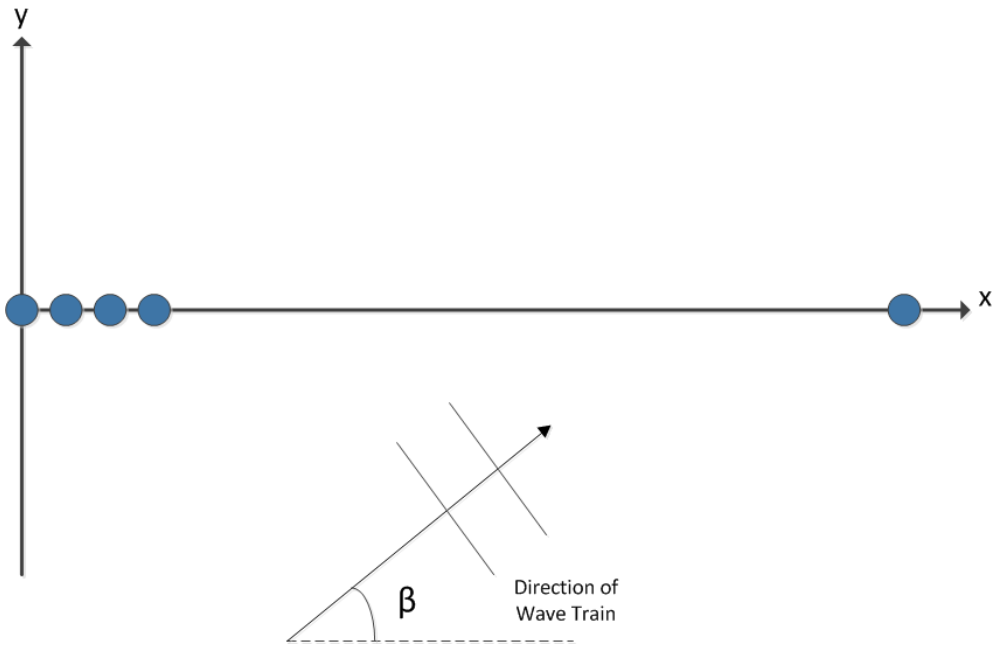

Figure 4.4: Optimal linear array found for $\beta_0 = 0$

smaller non-dimensional array lengths, where the predicted optimal displacements increase with decreasing kL. The isolated device exhibits more reasonable motions of $|D| \approx 3$ for the entire domain.

It should be noted that the array layout obtained here is highly dependent on the constraints and consistency relations imposed within the calculations. Firstly, all of the optimal separation parameters are at their maximum or minimum allowable values. This suggests that if these variable constraints were altered, the resulting optimal array layout and performance would also change. Calculations have been performed with different minimum values of n_j and in each case the optimal array tended to an analogous optimal layout, with n_1, n_2 and n_3 at the minimum allowed values. Secondly, the isolated device in these optimal array layouts is an artefact of the formulation employed, particularly via (4.2). In the optimal case, this consistency forces one of the separations to be considerably larger than the others in order to preserve the total length of the array. It may be the case that allowing the fifth device to be closer to the group may give improved performance, although it is acknowledged that this would cause deployment difficulties and even larger displacements.

In the case of head seas, the incident wave direction is parallel to the line of devices and the optimisation pushes all the devices as close together as possible, with one device preserving the total length of the array. This may be due to the decrease in radiating wave amplitude as it moves away from the originating WEC. Therefore, since optimal unconstrained device motions are assumed, the optimisation wants to place the WECs as close as possible to maximise the constructive interference due to the radiated wave field. This physical interpretation only applies to linear arrays in head seas since the wave direction and the interaction direction are parallel.

4.3.2 $\beta_0 = \frac{\pi}{8}$

The best array for $\beta_0 = \frac{\pi}{8}$ is comprised of two separated groups of two and three devices at either end of the array, shown in figure 4.6. This configuration only obtained an average interaction factor of $I = 0.8794$, which is considerably lower than unity and poorer performing than all other optimal arrays in this section. The detailed optimisation results for $\beta_0 = \frac{\pi}{8}$ are given in table B.2, which show that all the optimal arrays obtained have a considerably reduced performance at this wave angle.

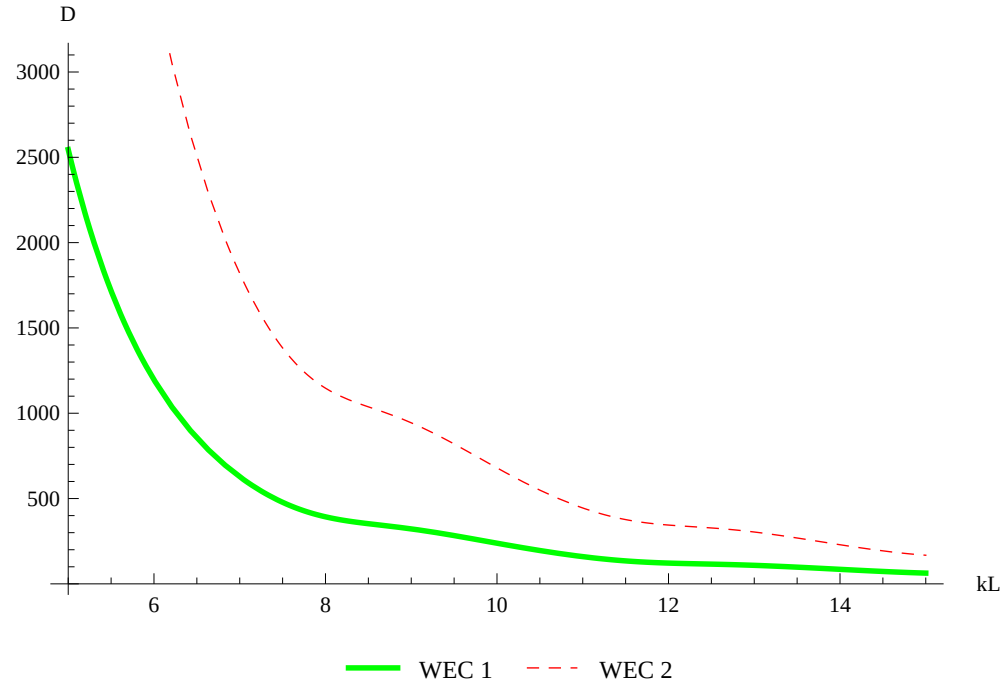

(a) Grouped WECs

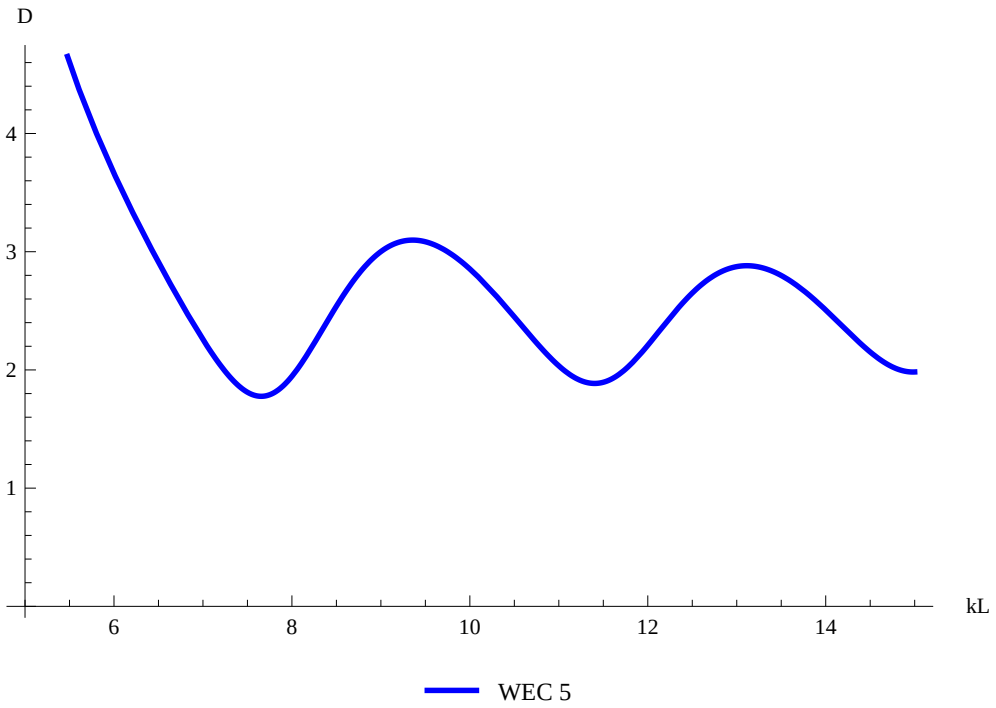

(b) Isolated WEC

Figure 4.5: Optimal displacement amplitudes for best optimised linear array with $\beta_0 = 0$. The displacements of WECs 3 and 4 are very similar to WECs 2 and 1 respectively and are thus omitted for clarity.

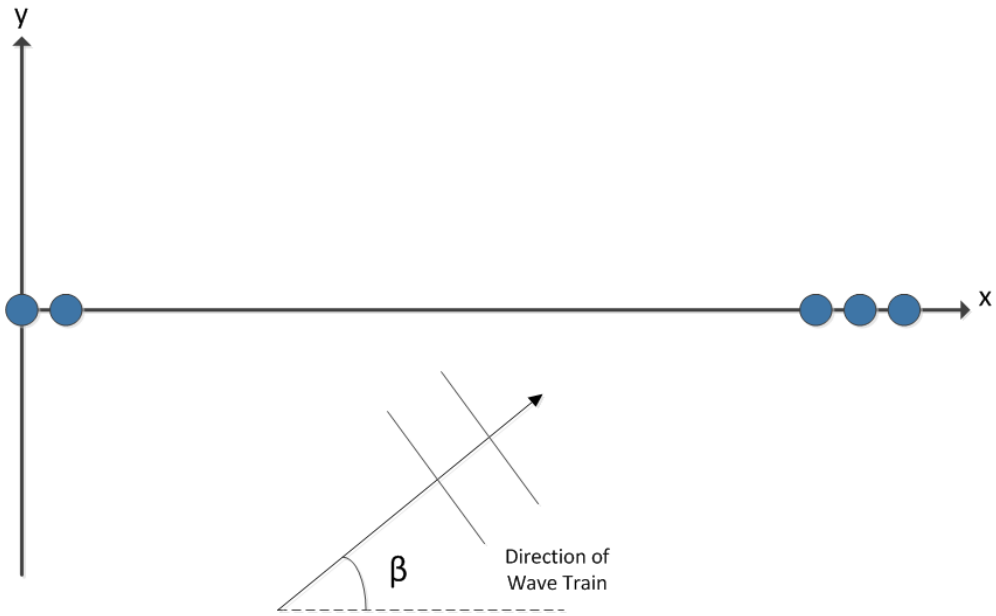

Figure 4.6: Optimal linear array found for $\beta_0 = \frac{\pi}{8}, \frac{\pi}{4}$

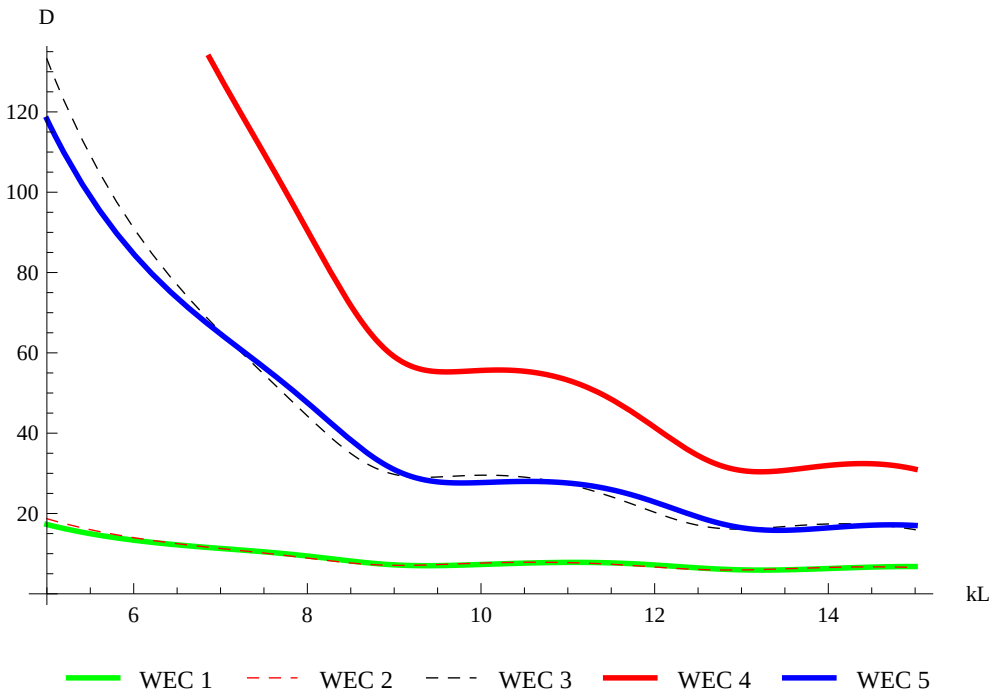

Figure 4.7: Optimal displacements of WECs for best linear array optimised for $\beta_0 = \frac{\pi}{8}$

Clearly, figure 4.2 shows that $q < 1$ for the entire domain of kL, although q is increasing with kL. A similar β-variation is observed in figure 4.3 to the $\beta_0 = 0$ case, with poor performance at $\beta = \frac{\pi}{8}$ (although slightly better than the analogous performance for $\beta_0 = 0$).

The predicted optimal displacements are presented in figure 4.7. This shows that, despite the relatively poor performance of the array, all devices still exhibit unacceptably large motion amplitudes of $|D| \geq 10$. Therefore, when motion constraints are imposed in practice, performance may be much poorer, resulting in an array which has very low power absorption due to array interactions.

A similar physical explanation to that in Section 4.3.1 can be applied to the optimal layout for $\beta_0 = \frac{\pi}{8}$. However, due to the intermediate wave angle, the interaction is not as simple, since the wave direction and interaction direction are no longer collinear. More spacing between devices, albeit in two groups at either end of the array, outperforms the case when all devices are pushed together. This may be because an increased frontage becomes important for non-head seas and both groups interact well while spanning the length of the array.

4.3.3 The Intermediate Angle: $\beta_0 = \frac{\pi}{4}$

The best array layout for $\beta_0 = \frac{\pi}{4}$ is identical to that for $\beta_0 = \frac{\pi}{8}$, as shown in figure 4.6. The detailed optimisation results for this case are shown in Table B.3 of Appendix B.

It can be seen from figure 4.2 that, for $\beta_0 = \frac{\pi}{4}$, this array achieves $q > 1$ for the majority of the domain, with the exception of when $kL < 7.7$. A maximum value of $q \approx 1.29$ is achieved at $kL \approx 12.5$, while the minimum value is $q \approx 0.93$ at $kL \approx 6$. The average performance obtained is $I = 1.1431$, which is considerably less than the corresponding optimal array for head seas. Comparing the β-variation in figure 4.3 with that of the $\beta_0 = 0$ case: there also exists a much smaller range of approximately $\pm\frac{\pi}{16}$ around the optimal value of $\beta = \frac{\pi}{4}$ where q is greater than unity.

The displacements of this optimal array are presented in figure 4.8. Similar to the previous case, large motions of $|D| > 10$ are required for all values of kL, with the general trend that the displacement amplitudes increase for decreasing kL. Although the motions are smaller overall than the optimal $\beta_0 = 0$ case,

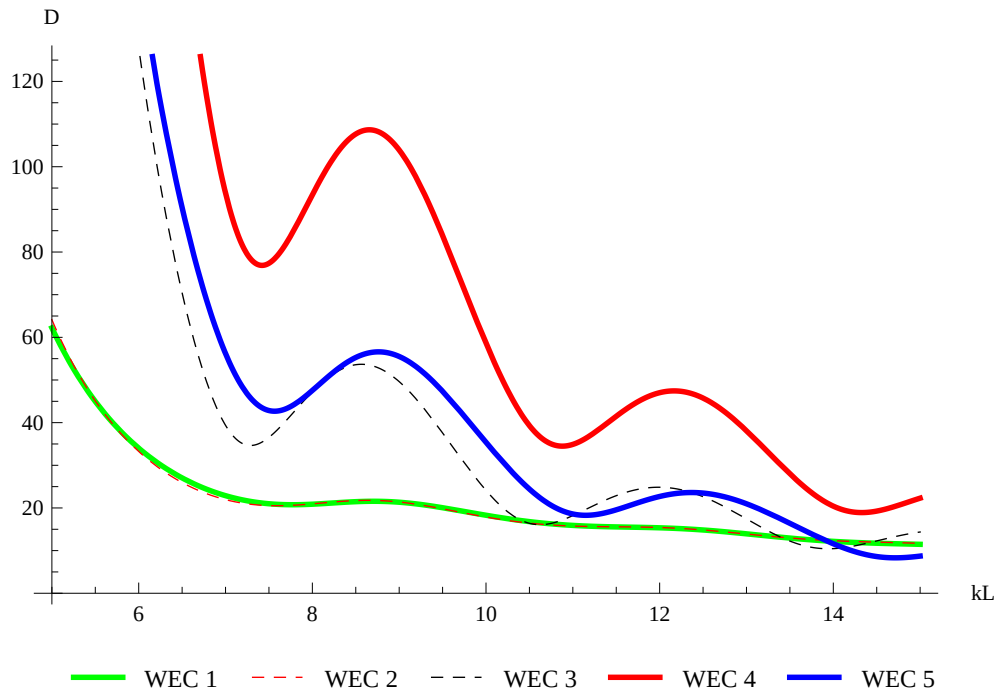

Figure 4.8: Optimal displacements of WECs for best linear array optimised for $\beta_0 = \frac{\pi}{4}$

these displacements are clearly still unacceptably large. This, combined with the more modest performance and the presence of closely spaced groups of WECs within the array, suggests this may not be a good choice of layout.

Similarly to $\beta_0 = \frac{\pi}{8}$, the interaction direction is no longer parallel to the wave direction for this intermediate wave angle. Therefore, the same physical justification for the optimal layout is proposed.

4.3.4 $\beta_0 = \frac{3\pi}{8}$

The best array for $\beta_0 = \frac{3\pi}{8}$ is symmetric about the middle device and is very close to a uniform array layout, with the two separation values differing by only 0.24% of kL, as shown in figure 4.9. This result agrees with those of McGuinness & Thomas (2015), where for each symmetry investigated, a uniform array layout was found to be optimal for $\beta_0 = \frac{3\pi}{8}$. The result presented here is a slight refinement, where WECs 2 & 4 are slightly closer to the middle WEC compared to a uniform layout. The detailed optimisation results for this incident wave angle are given in table B.4 of Appendix B.

It is clear from figure 4.2 that $q > 1$ for the majority of the domain of kL for

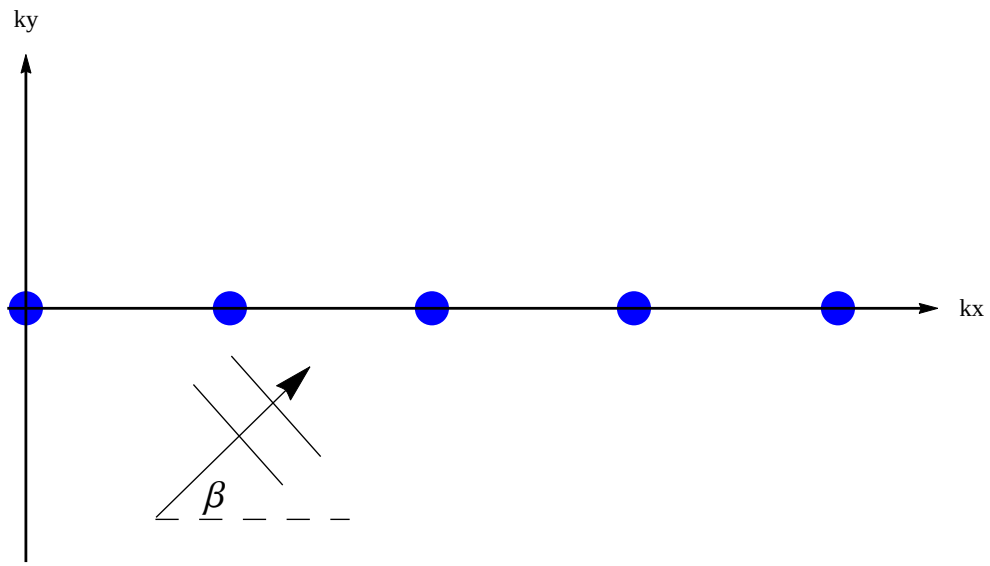

Figure 4.9: Optimal linear array found for $\beta_0 = \frac{3\pi}{8}$

$\beta = \beta_0 = \frac{3\pi}{8}$, except for $kL < 8$. It is also shown that q increases with kL within the range examined. The array also achieves a respectable average interaction factor of $I = 1.1822$. A notable difference in the plot of q against β is observed in figure 4.3 for this array. It is clear the plot has shifted to reduced performance at $\beta = 0$ and increased performance around $\beta = \frac{\pi}{2}$. This has the effect of increasing the performance at the desired wave angle of $\beta = \frac{3\pi}{8}$.

The optimal displacements for this array are shown to be much more reasonable in figure 4.10 compared to previous arrays. The displacement amplitudes are all $|D| < 10$ for $kL \in [5, 15]$, although for the most part $|D| > 4$, which is still too large from a practical perspective. In theory, the displacements must be $\mathcal{O}(1)$ and it can be argued that $D \approx 4$ both does or does not violate this. The imposition of constraints on these motions may be less detrimental to array performance due to their already low optimal values. It is interesting to note that for $kL \approx 8$, WEC 3 (the middle WEC) has a zero motion amplitude, indicating that it does not move in the optimal case at this value of kL. The lower values of displacement amplitude are probably due to the larger spacing between the individual devices, and importantly, the lack of grouping of the devices. Therefore, this may be a more desirable array layout depending on the effect of limiting the device motions on the performance of this and other arrays.

For $\beta_0 = \frac{3\pi}{8}$, the interaction direction differs considerably from the wave direction, although it is not perpendicular. The resulting optimal layout is almost uniform, suggesting that wider spacing is more beneficial approaching

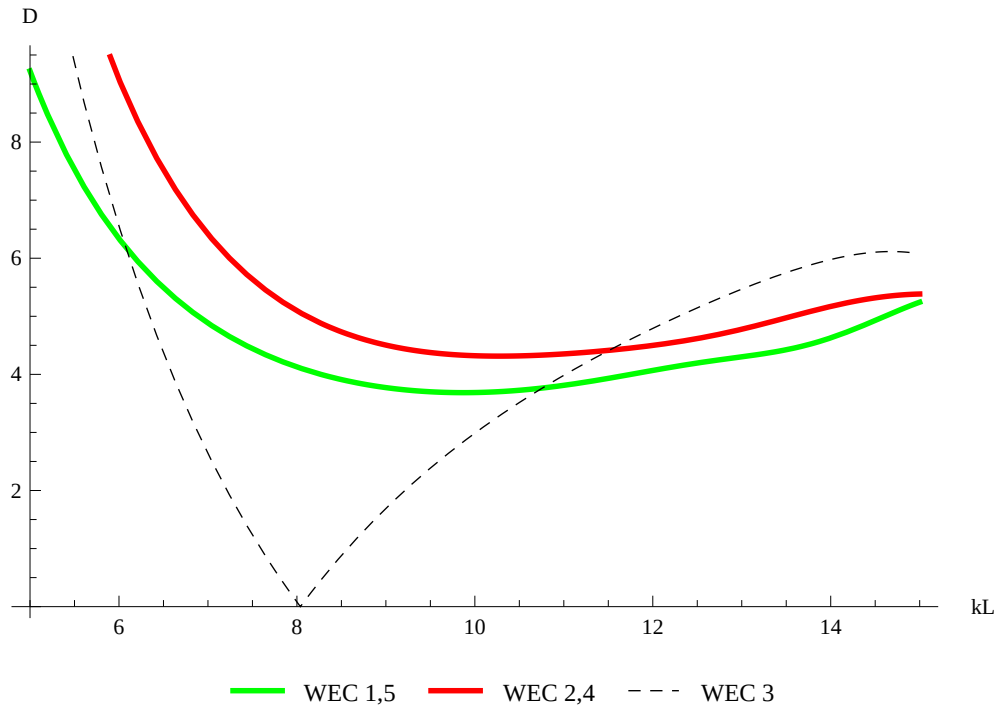

Figure 4.10: Optimal displacements of WECs for best linear array optimised for $\beta_0 = \frac{3\pi}{8}$

normal incidence. This conforms with the idea that a greater frontage to the waves allows a greater power absorption. It may be that groups of devices with large spaces between these groups would not be ideal for this incident wave angle, as much of the power incident on the spaces may escape through the array. This is only a tentative explanation of the more spread-out layout obtained here.

4.3.5 Beam Seas: $\beta_0 = \frac{\pi}{2}$

The premier optimal array for beam seas is shown in figure 4.11, which consists of a group of two devices accompanied by three relatively separated devices. The detailed optimisation results for $\beta_0 = \frac{\pi}{2}$ are shown in table B.5 of Appendix B. Only two unique optimal array layouts were discovered by the exhaustive search and the optimisation algorithm for this wave angle. The implication of this is that the optimisation is very stable, with a dominant global maximum. For all iterations performed, the optimisation converged to the global optimum and one local optimum, with the majority converging to the former.

It is interesting that despite the array orientation to the incoming wave, the

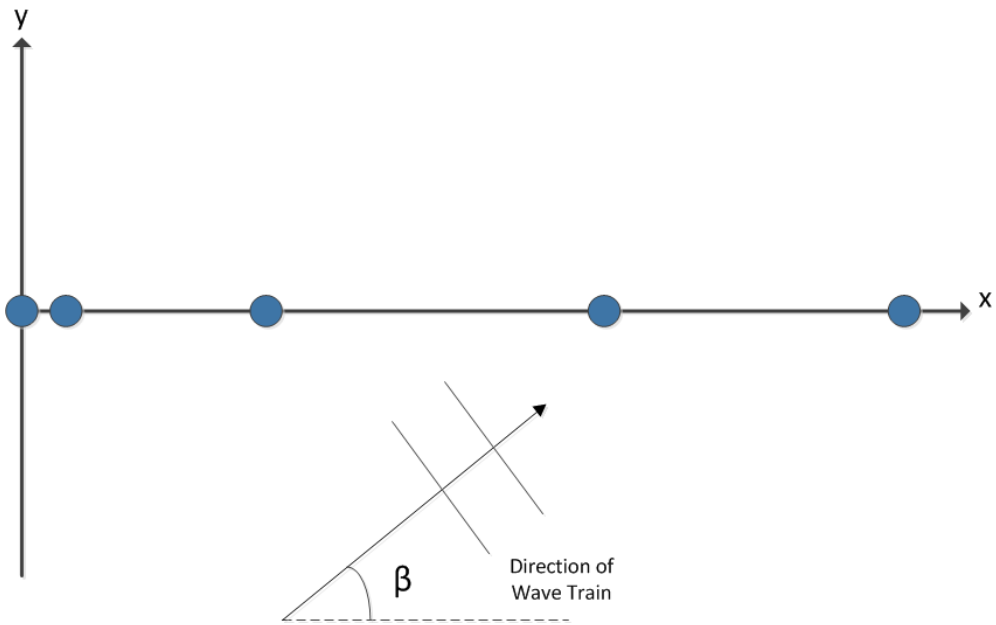

Figure 4.11: Optimal linear array found for $\beta_0 = \frac{\pi}{2}$

optimal layout is not symmetric as may have been expected for beam seas. It may be the case that an increased benefit is obtained from having a greater constructive interaction between the closely spaced pair on the one side, while maintaining a greater separation at the other side to avoid large gaps through which wave energy could escape unabsorbed. The array presented in figure 4.11 achieves an average interaction factor of $I = 1.3643$. The results of Chapter 3 show that a uniform array achieves a value of $I = 1.32$ in beam seas (table 3.2) and the best symmetric array found achieved $I = 1.34$ (table 3.1), both of which are outperformed by the non-symmetric array determined by this more general optimisation.

Figure 4.2 illustrates that this array achieved $q > 1$ for the entire range of $kL \in [5, 15]$ at the optimal wave angle ($\beta = \beta_0 = \frac{\pi}{2}$). An average interaction factor of $I = 1.3643$ is achieved along with an impressive maximum of $q \approx 1.7$ around $kL = 13.7$. The interaction factor increases with kL until it reaches this maximum value, where it begins to decrease with increasing kL. Although this is the highest peak in q achieved by any of the optimal arrays thus far, the average value of $I = 1.3643$ falls below that of the best $\beta_0 = 0$ array in Section 4.3.1.

There is a surprisingly large range of approximately $\pm\frac{3\pi}{16}$ around the optimal value of $\beta = \beta_0 = \frac{\pi}{2}$ where q remains greater than unity, as shown in figure 4.3. Comparing all the curves of q against β for the different optimal arrays, it is

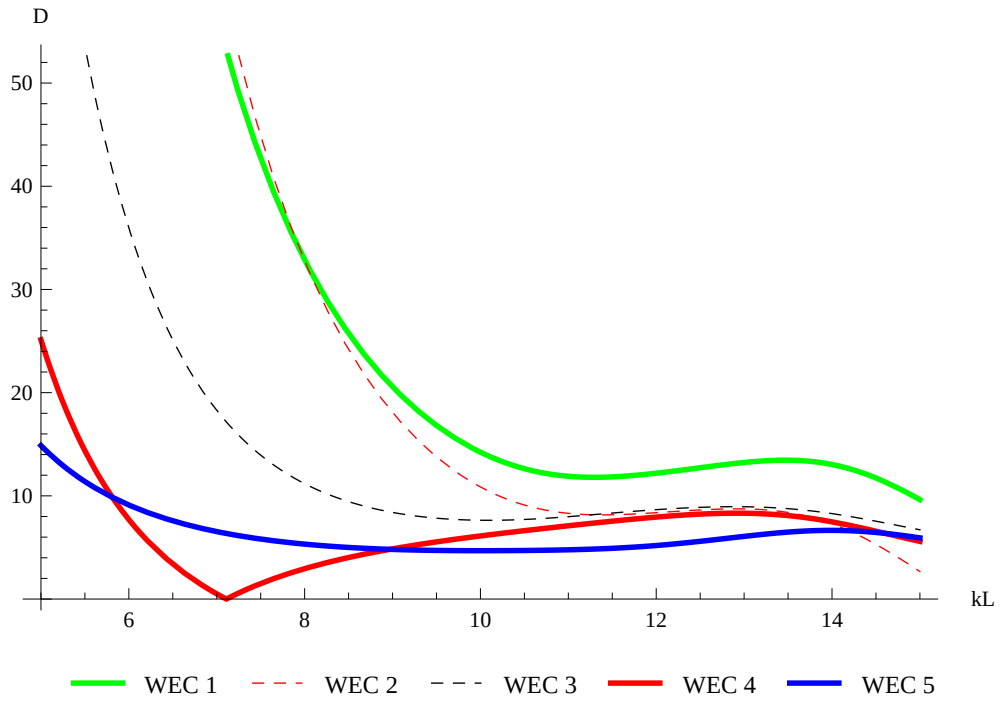

Figure 4.12: Optimal displacements of WECs for best linear array optimised for $\beta_0 = \frac{\pi}{2}$

clear that the shape of the curve is altered so as to achieve good performance at $\beta = \beta_0 = \frac{\pi}{2}$, which results in poorer performance at other wave angles. It is interesting to compare the curves in figure 4.3 and note the change in behaviour as different optimal wave angles are considered. As the incident wave angle changes, the plot of q against β alters to increase at the desired value of $\beta = \beta_0$; this necessarily results in poorer performance at other angles.

The displacements for this optimal array are shown in figure 4.12. These are unacceptably large ($|D| > 5$) for the entire domain of $kL \in [5, 15]$ for all but WEC 4, whose displacements approach zero only in the close vicinity of $kL \approx 7$. In general, larger displacements are predicted for smaller kL. All devices have $|D| < 20$ for $kL \in [10, 15]$, suggesting that this region may not be as much affected by imposition of motion constraints. As expected, the grouped devices exhibit larger motions than the relatively isolated WECs. It is interesting that, in the optimal scenario, WEC 4 has $|D| = 0$ near $kL \approx 7.1$. The combination of high q-factor, large range of β-stability and relatively low displacements in the region $kL \in [10, 15]$ indicate this array may be an ideal candidate for WEC array design. This is discussed further in Chapter 6, where constrained optimisations linear arrays are considered.

Due to the normal wave incidence onto the array (wave direction and interaction direction are perpendicular), it is perhaps that greater frontage would result in better overall performance as opposed to groups of WECs. However, one closely spaced pair is still present at one side, indicating that uniform spacing is not optimal. It should be noted that since $q(\beta + \pi) = q(\beta)$ applies, the mirror image of this optimal array also represents the same optimum and performs equally well. It is unclear why this layout is not symmetric; perhaps this is due to the fact that the optimisation is maximising the *mean* of q over $kL \in [5, 15]$. Another possible explanation is that there exists a optimum which is symmetric about the middle WEC but which is also very unstable, such that a small change in array parameters destroys this optimum and thus the optimisation failed to converge to it.

4.4 Discussion of Results

This chapter describes the optimisation of general linear five-device arrays, such that the optimal array layouts are stable to changes in non-dimensional parameters. The arrays considered have no enforced symmetry and are therefore an extension of the results presented in the previous chapter. It has been shown that it is possible to obtain arrays that perform well over a very large range of non-dimensional length for fixed incident wave angle. It has also been shown that this performance was maintained for large ranges of incident wave angle (up to $\beta_0 \pm \frac{\pi}{5}$), so that a small change in incident wave angle does not result in destructive interference between the array members. However, it is unclear if this will be the case if WEC motion constraints are enforced.

One major difficulty with the optimal arrays obtained is the large magnitude of the associated device motions. In general, better performing arrays are expected to involve larger device motions in an unconstrained optimisation. However, it was noticed that closely grouped devices exhibited much larger motions than more separated ones, in line with the results of Chapter 3. Arrays which contained groupings of two or more devices had larger motions in general; thus the presence of such grouping in optimal layouts is an indication that large optimal motions are probable.

In some of the cases presented here, better performance was achieved relative to other optimal arrays, despite smaller predicted device motions. This may indicate that the imposition of device motion constraints may not be as limiting

and it is possible that good performance can be maintained. It may be beneficial to deploy a sub-optimal array layout, which may not have the best optimal performance but has relatively large separation between devices and low predicted optimal device motions. This is suggested since the imposition of constraints may be less harmful to array performance in such cases. The large device separations would also avoid other physical difficulties associated with closely spaced groups of WECs. These difficulties may include device collisions and the possibility of wave shadowing, which would invalidate the underlying point absorber (small body) approximation.

Many optimal arrays obtained possessed groupings of two, three or four devices; the difficulties associated with this have been discussed. One possible solution to this problem may be to replace these groups of devices with an appropriately-sized larger device, as suggested in Chapter 3. These arrays would then contain devices of different sizes, a possibility the literature has broadly neglected. These arrays could then be considered as satellite arrays, since one could often describe such arrays as involving several smaller devices orbiting a larger device. It is not known what the effect on power absorption and array performance would be. Another possibility would be to replace these groups of devices with a single device that absorbs power (oscillates) in two modes of motion, thereby recreating the dipole effect often exhibited by the pairs of devices in optimal layouts. It is hoped that either a larger device or one that operates in two (or more) modes would recreate the constructive interference pattern without the problems of close deployment and large motions.

The results of this chapter agree well with those of the previous chapter and provide a slight improvement on the resulting performance. This small benefit in performance indicates that the simpler one-variable optimisation gives good results relative to the more general optimisation in this chapter. In particular, the overall performance for different wave angles was quite similar in this more general case. The optimal performance at $\beta_0 = \frac{\pi}{8}$ was quite poor in both the one-variable case of Chapter 3 and the more general case presented here. The increased freedom within the optimisation allowed only a small improvement from an average interaction factor of $I \approx 0.84$ to $I \approx 0.88$. This indicates that array interactions at this wave angle are necessarily destructive for linear arrays, even in the optimal cases. Hence, it is recommended that this incident wave angle should be avoided. It should be noted that array performance relative to isolated device performance is measured, rather than actual power absorption. Therefore, it is possible that a larger amount of power may be absorbed at this

angle compared to others. These results merely relate to the array *interaction*, showing that it is destructive for $\beta_0 = \frac{\pi}{8}$.

Within the unconstrained optimisation, the array which had the best average interaction factor was the $\beta_0 = 0$ case, with $I = 1.4802$. This layout was comprised of four grouped devices at one side of the array, with a relatively isolated device at the other. As postulated earlier, the isolated device position may be an artefact of the problem formulation, as it is necessary to preserve the total length of the array. However, this array may be undesirable from the perspective of a physical implementation, due to its closely spaced devices and associated large motion amplitudes.

A contender for the best overall array discovered within the unconstrained optimisation was the optimal linear array for $\beta_0 = \frac{\pi}{2}$, which had a balance between good performance and relatively small motions, as discussed in Section 4.3.5. Within the region of $kL \in [10, 15]$, this array achieves $q \in [1.3, 1.7]$, while the non-dimensional displacement of all the array members are $|D| \in [5, 15]$. These displacements are considerably lower than WECs within other optimal arrays. Since a motion constraint would have a lesser relative effect on these motions, it is reasonable to suggest that this constraint would also have a less relative impact on array performance. The array also has a large range of approximately $\pm\frac{3\pi}{16}$ around the optimal value of $\beta_0 = \frac{\pi}{2}$ where $q > 1$ is maintained. The effect of constraints on this and other arrays are discussed in future chapters.

The results of this chapter show considerable variations in the optimum configuration of a linear array for different prescribed incident wave angles β_0. Tentative physical explanations are provided as to the reasons for the optimal layout in each case. The overall behaviour suggests that groups of closely spaced WECs are more beneficial for parallel incidence ($\beta_0 = 0$), while a more separated configuration is better for normal incidence ($\beta_0 = \frac{\pi}{2}$). Contrary to expectation, a symmetric (and almost uniform) layout is found to be optimal for $\beta_0 = \frac{3\pi}{8}$, while an asymmetric layout containing a closely spaced pair of WECs is found for $\beta_0 = \frac{\pi}{2}$. Due to the uniform layout, reasonable performance ($I = 1.1822$) and relatively small optimal WEC motions, the $\beta_0 = \frac{3\pi}{8}$ is also a candidate for the best overall linear array.

Chapter 5

Optimisation of General Circular Arrays in Regular Waves

5.1 Introduction

This chapter builds upon Chapter 4, by extending the previous results to arrays of an alternate geometry, namely circular arrangements. Some preliminary work on elementary circular arrays, described by one variable, was performed by Costigan (2014). This was then extended in McGuinness & Thomas (2016) to a more general circumstance. The mean performance of the arrays is defined over a prescribed range of a non-dimensional radius. This provides the objective function when optimising these circular arrays. The results published in McGuinness & Thomas (2016) for circular arrays are outlined and extended herein.

Initially, the investigation of circular arrays was motivated by the idea of an isotropic array, i.e. one that looks and behaves the same from all wave directions. This would then normalise the performance over all wave angles, so that the interaction factor is approximately unity from all directions. This is an ideal concept and not achievable in practice. This was shown by Costigan (2014) for the case of a uniform six-device circular array, where an oscillatory pattern with a period of $\frac{2\pi}{N} = \frac{\pi}{3}$ was seen for $q(\beta)$. Extending this to a larger number of devices will approach the scenario of an isotropic array, namely that of a single large toroidal device.

Although it is impossible to construct an array that is complectly isotropic, an

array could be arranged so that it is approximately isotropic for a small range of incident wave angle of primary interest. Alternatively, if the wave climate at a given site contains relatively low angular variability, an array could be formed so that its performance is good over the entire range of interest. For such cases, the necessary poor performance at other wave angles, due to (2.164), would be inconsequential.

Calculation of the array performance, particularly the mean performance, is more complicated for circular arrays in comparison to the linear array. The WEC position variables for a circular geometry depend on both the distance and angle from the origin, whereas in linear arrays only the distance from the origin was needed as the angular positions of all WECs were zero. This angular dependency of the device positions manifests itself as a trigonometric term within an exponential, of which the average is taken. Greater computation time for each call to the objective function is required and hence longer run times for the optimisation routine.

The previous work presented for linear arrays is extended to consider general non-symmetric circular array geometries, with the WECs constrained to lie on the circumference; the possibility of including a further device in the circle centre is also investigated. The arrays are described by angular variables, which the arrays are optimised with respect to. The most convenient coordinate system is to take the centre of the circle at the origin and fix the angle of WEC 1 (α_1). Thus the N circumferential devices are a fixed distance from the centre (commonly notated as r for radius). There are $N+1$ variables describing the array layout. However, since WEC 1 will have a fixed angular position (without loss of generality) and the objective function is the average over kr, the optimisation involves $N-1$ variables.

For a circular array of radius r, the position variables of the devices can be simplified, since $d_m = r$ for each device on the circle circumference. If the mth device is in the centre of the circle, $d_m = 0$ since it is fixed at the origin. This does not add any extra variables to the problem, thus giving a total of $N-2$ array variables when a central device is included.

5.2 Optimisation Method

For a circular array of radius r, the position variables are the angular positions of each device on the circle. A convenient notation is introduced to define the relative angles θ_j between each device, so that

$$\theta_j = \alpha_j - \alpha_{j+1}. \tag{5.1}$$

As one device will be at a fixed angular separation, this can be used to remove one variable from the optimisation process. There are now $N-1$ variables and consistency requires that

$$\sum_{j=1}^{N} \theta_j = 2\pi. \tag{5.2}$$

In keeping with earlier chapters, the mean of the interaction factor is defined over a range of non-dimensional radius kr. Similarly, the upper and lower bounds of the non-dimensional array radius are denoted as kr_u and kr_l respectively. The objective function for circular arrays is written as

$$I_{circle}(\theta_1, \ldots, \theta_{N-1}; \beta_0) = \frac{1}{kr_u - kr_l} \int_{kr_l}^{kr_u} q(\theta_1, \ldots, \theta_{N-1}, kr; \beta_0)\ d[kr], \tag{5.3}$$

for a fixed prescribed incident wave angle β_0. For convenience, the circle subscript is henceforth dropped.

The optimisation is performed for $\beta_0 \in [0, \frac{7\pi}{8}]$ in multiples of $\frac{\pi}{8}$. In contrast to the linear array, symmetry about $\beta = \frac{\pi}{2}$ cannot be assumed so the range of investigation is $\beta_0 \in [0, \pi)$. As with the linear arrays in Chapter 4, NAG[1] routines implemented in FORTRAN were used to evaluate the objective function and perform the optimisation. This optimisation method involves iterations of a routine for many different starting points, with the best solutions obtained analysed in detail. In order to avoid unnecessary presentation of data, the optimisation results are summarised in this chapter with a more detailed output given in Appendix C.

Two cases of circular arrays are considered and compared in this chapter. The first is an array with $N = 6$ devices constrained to lie on a circle circumference of radius r. The second is an array of $N = 7$ devices, with the extra device fixed in the centre of the circle. Clearly, the optimisation of each array involves the

[1] https://www.nag.co.uk/

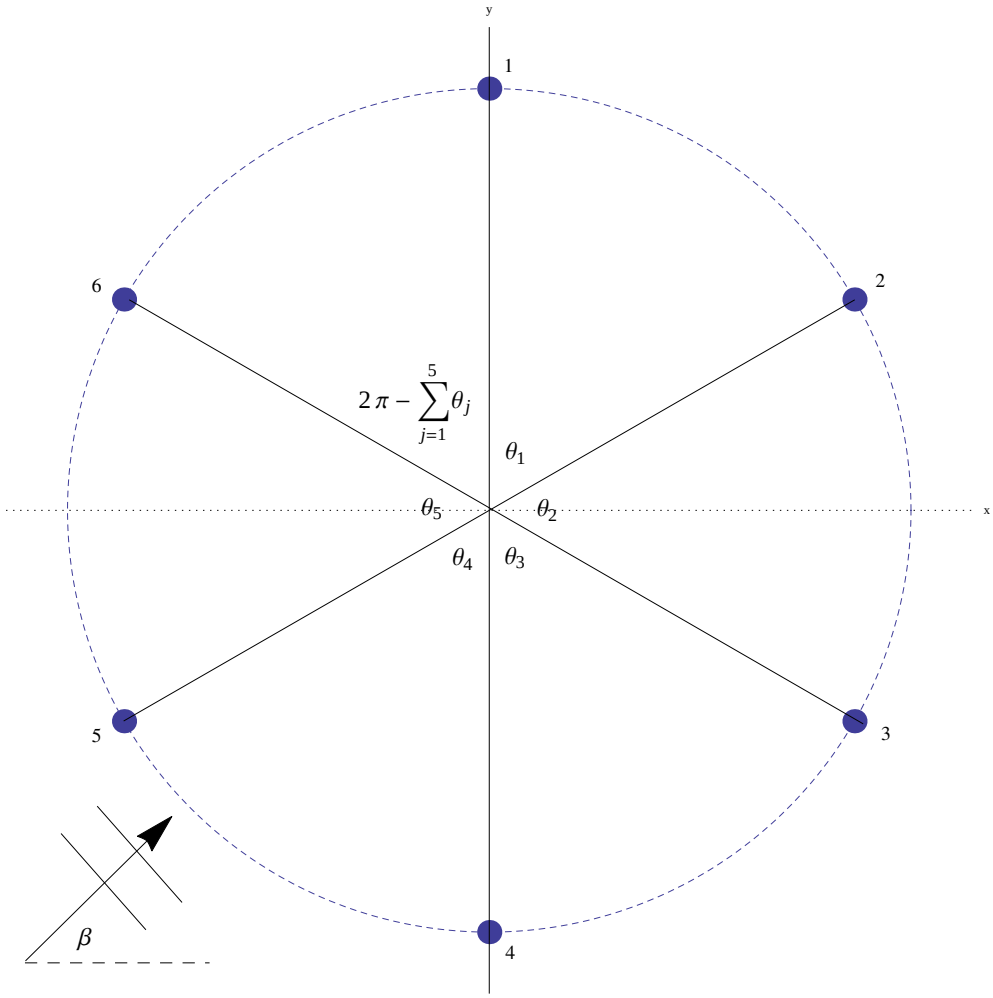

Figure 5.1: General six-device circular array, without middle device

same number of variables (five), although the calculation of the objective function and hence the optimisation is expected to be longer in the second case. A diagram of the array without a central device is shown in figure 5.1.

5.3 Behaviour of Uniform Circular Arrays

The performance of the uniform versions of these arrays ($\theta_1 = \cdots = \theta_5 = \frac{\pi}{3}$), both with and without the central WEC are presented. Figures 5.2 and 5.3 show the variation of the q-factor for the uniform array with changes in kr and β respectively. The average interaction factor for these arrays for two different values of incident wave angle are shown in table 5.1, with $[kr_l, kr_u] = [5, 15]$. Since the performance of the uniform arrays are $\frac{\pi}{3}$ periodic and symmetric about multiples of $\frac{\pi}{3}$, only the mean performance for $\beta_0 = 0$ and $\frac{\pi}{6}$ is shown.

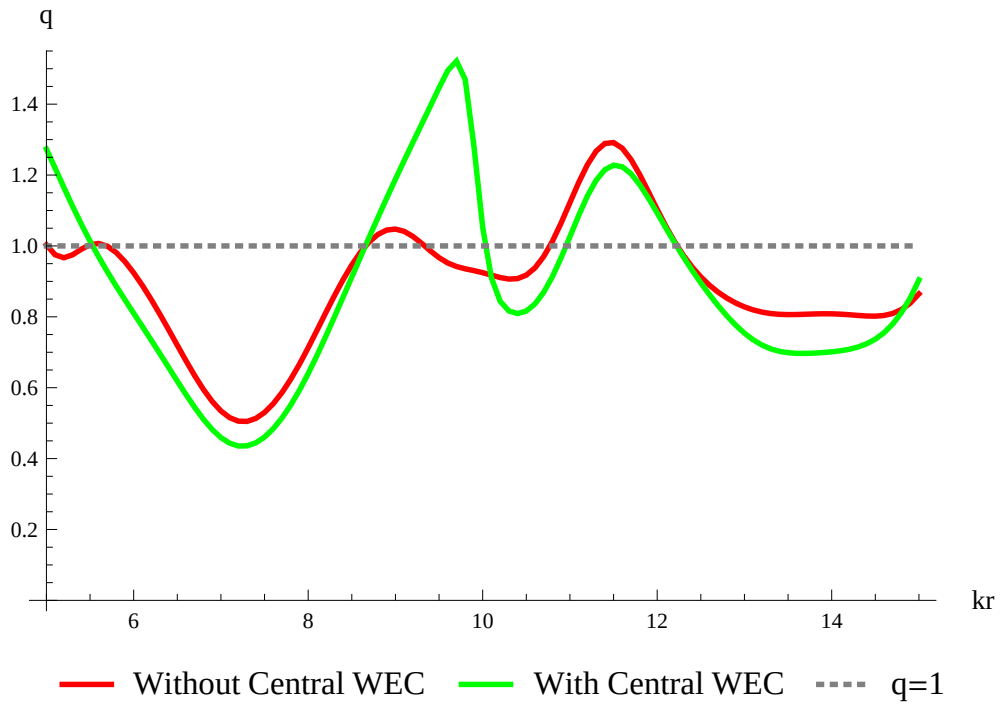

Figure 5.2: Interaction factor q against non-dimensional radius kr for uniform six and seven WEC arrays, with $\beta = 0$

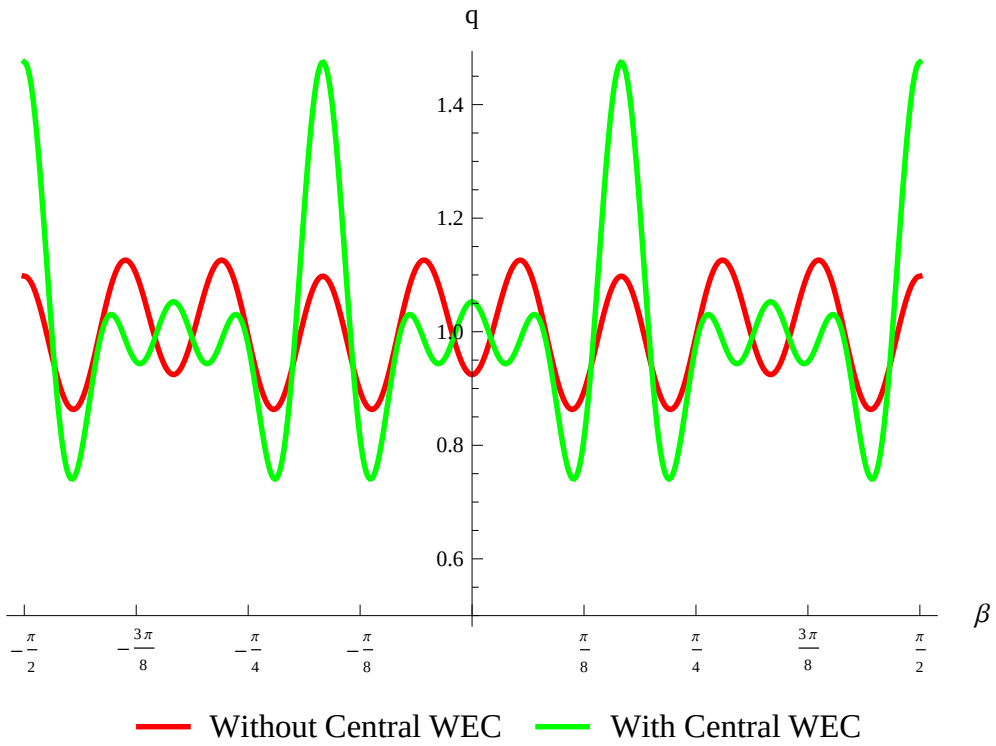

Figure 5.3: Interaction factor q against incident wave angle β for uniform six and seven WEC arrays, with $kr = 10$

Table 5.1: Average interaction factors I for uniformly spaced circular arrays

	β_0	I
Without Central Device	0	0.890253
	$\frac{\pi}{6}$	1.0654
With Central Device	0	0.883032
	$\frac{\pi}{6}$	1.12195

Overall, the uniform layouts do not perform well over the range of $kr \in [5, 15]$ and performance is very oscillatory for changes in β. The inclusion of a central device improves performance only in some regions and decreases performance slightly in others. The interaction factor (and its mean) appear to be highly dependent on the incident wave angle for the uniform cases.

It is also clear from table 5.1 that the mean performance of the uniform arrays is better for $\beta_0 = \frac{\pi}{6}$ in comparison to $\beta_0 = 0$. This suggests that greater constructive interference is achieved if a lone device is facing the incoming waves (WEC 5 in figure 5.1 for $\beta = \frac{\pi}{6}$), rather than two WECs meeting the incident waves at the same time (WECs 5 and 6 in figure 5.1 for $\beta = 0$).

5.4 Optimisation Results

The angular position of one device (WEC 1) is fixed and is arbitrarily forced to lie at the top of the array, so $\alpha_1 = \frac{\pi}{2}$. These arrays have five optimisation variables, namely $\theta_1, \ldots, \theta_5$, which define the positions of the WECs on the circumference, shown in figure 5.1. As in previous chapters, the array is optimised about the target value of $kr = 10$ and it is assumed that the sea state is such that $[kr_l, kr_u] = [5, 15]$. Similarly to the range of kL utilised in Chapters 3 and 4, this range of kr is arbitrarily chosen but is intended to represent a typical case. However, it should be noted that numerical difficulties arise for $kr < 5$, as this corresponds to small spacings between the devices. As before, constraints on the device motions are not imposed.

In order to enforce similar spacing restrictions to the linear arrays in Chapter 4, each angular parameter was limited to remain within $0.1 \leq \theta_j \leq 2\pi - 0.5$ and the consistency constraint equation (5.2) was also enforced. This minimum bound of $\theta_j \geq 0.1$ is slightly more restrictive than that in Chapter 4, as it corresponds to a minimum separation between consecutive devices of approximately $0.1\,kr$. However, this was found to be necessary to avoid

calculation difficulties when calling the objective function, particularly when the array possesses a central device. The upper constraint of $\theta_j \leq 2\pi - 0.5$ is to allow the possibility that all but one of the variables are at their minimum allowed value of 0.1, while retaining consistency.

An exhaustive search routine similar to the linear array case is performed over the search space of possible starting values of the parameters, to insure that the best global optima are found. Within McGuinness & Thomas (2016), all permissable combinations of $\theta_j = \{\frac{\pi}{5}, \frac{2\pi}{5}, \ldots \pi\}$ for $j = 1, \ldots, 6$ were investigated as starting points for the optimisation routine, with some combinations omitted due to consistency considerations. It was noticed for circular array geometries that the objective function was not as well behaved as in the linear array case. This is perhaps due to the increased number of variables or to an increased numerical intensity of the interaction factor (and hence its mean) due to the array geometry. It was thus acknowledged by McGuinness & Thomas (2016) that the above selection of starting points may not result in the optimisation finding all the possible optimal solutions. The optimisation often converged to a "best" array layout for only one run, indicating that the solution is not particularly stable or that it was not a true global optimum. Preliminary results for McGuinness & Thomas (2016) showed that increasing the number of starting points, by subdividing the range further, results in improvements of optimal values of I by the order of 2-5%. This also requires a considerably longer run time for the optimisation, which rendered it unfeasible in the short term. Therefore, the above set of starting points was chosen as the best practical case at the time.

In the present study, more starting points were allowed in the exhaustive search and resulted in longer run times for the optimisation. Here, the starting points were taken to be $\theta_j = \{\frac{\pi}{10}, \frac{2\pi}{10}, \ldots \frac{15\pi}{10}\}$ for $j = 1, \ldots, 6$ with consistency enforced via equation (5.2). This resulted in a slight improvement of the results presented in McGuinness & Thomas (2016) at the penalty of considerably increased computation time. The optimisation tended to repeatedly converge to a given solution, suggesting that it was indeed a global optimum. This gives confidence in the optimisation results as the routine continuously converges to a given solution from many starting variable combinations.

Table 5.2: Optimal array parameters for the six-device circular arrays (without middle device) for eight values of β_0

β_0	θ_1	θ_2	θ_3	θ_4	θ_5	I_{opt}
0	0.1000	1.4868	1.4171	0.1000	0.1000	1.5910
$\frac{\pi}{8}$	1.1547	1.4619	0.1000	0.1000	3.3666	1.5802
$\frac{\pi}{4}$	0.6388	0.3423	1.2086	0.1000	0.1000	1.5563
$\frac{3\pi}{8}$	0.3539	0.3235	1.1056	0.1000	0.1000	1.5883
$\frac{\pi}{2}$	1.4417	0.1000	0.1000	3.1329	0.1000	1.5921
$\frac{5\pi}{8}$	4.3001	0.1000	0.1000	1.1056	0.3235	1.5883
$\frac{3\pi}{4}$	3.8935	0.1000	0.1000	1.2086	0.3423	1.5563
$\frac{7\pi}{8}$	0.1000	3.3666	0.1000	0.1000	1.4619	1.5802

5.4.1 Circular Arrays without a Central Device

The optimal parameter values for six-device arrays without a central WEC are summarised in table 5.2. A detailed list of optimal solutions found by the routine are presented in Appendix C in tables C.1 - C.8. These provide the values of the optimal mean interaction factor I and the optimal layout variables $\theta_1, \ldots, \theta_5$, with the remaining angular separation given by

$$\theta_6 = 2\pi - \sum_{j=1}^{5} \theta_j, \tag{5.4}$$

from equation (5.2). All values within these tables have been provided to five significant figures. The top eight optimal cases discovered by the routine are given for each angle of incidence. The best cases found by McGuinness & Thomas (2016) are also highlighted (marked by "M") in the corresponding tables, namely table C.1, table C.3 and table C.5. This allows comparison with the more detailed results presented in Appendix C and shows the effect of allowing an increased number of starting points within the optimisation.

It can be seen from table 5.2 that symmetry exists in the optimal array layouts and performance about $\beta_0 = \frac{\pi}{2}$. The optimal array for an incident wave angle $\beta_0 \in [0, \pi)$ performs the exact same as that for $\pi - \beta_0$. Further examination of the tabulated results shows that this is due to the symmetry in array layouts: an array optimised at β_0 is essentially the same as that for $\pi - \beta_0$ rotated to face

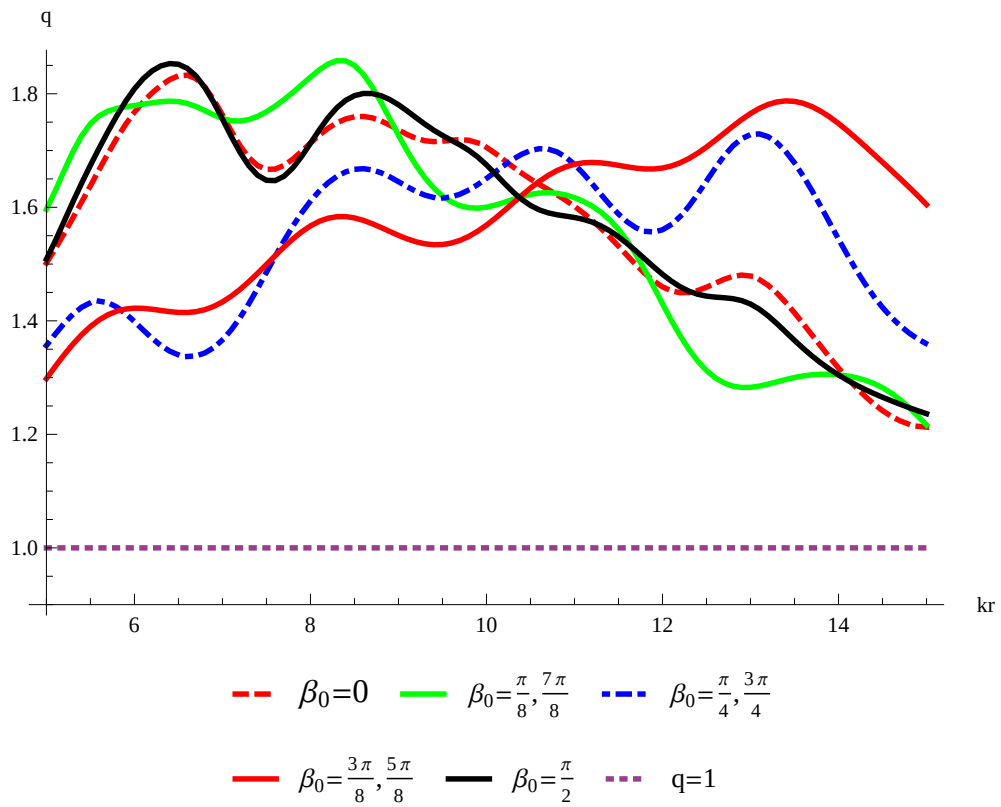

Figure 5.4: Interaction factor q against non-dimensional length kr for the optimal six-WEC circular arrays for $\beta_0 \in [0, \frac{7\pi}{8}]$

the incoming wave in the same way. This was confirmed by behaviour of the optimal q against kr curves, as the behaviours were the same for β_0 and $\pi - \beta_0$.

Due to this symmetry, only the best performing optimal arrays for $\beta_0 \in [0, \frac{\pi}{2}]$ are analysed with respect to the array layout and optimal displacements in the following subsections. A diagram of the top three optimal layouts is presented for all cases and these show the symmetry in the optimisation about $\beta_0 = \frac{\pi}{2}$. The predicted displacements for the optimal arrays are also presented; these again show symmetry about $\beta_0 = \frac{\pi}{2}$ and are omitted for wave angles $\beta_0 > \frac{\pi}{2}$. The variation of the interaction factor of all the optimal arrays with changes in kr and β are shown in figures 5.4 and 5.5 respectively.

5.4.1.1 $\beta_0 = 0$ Case

The best three array layouts discovered by the optimisaiton are shown in figure 5.6 and the optimal layouts presented differ from each other. However, all involve closely spaced groups of two and three devices. These layouts are quite

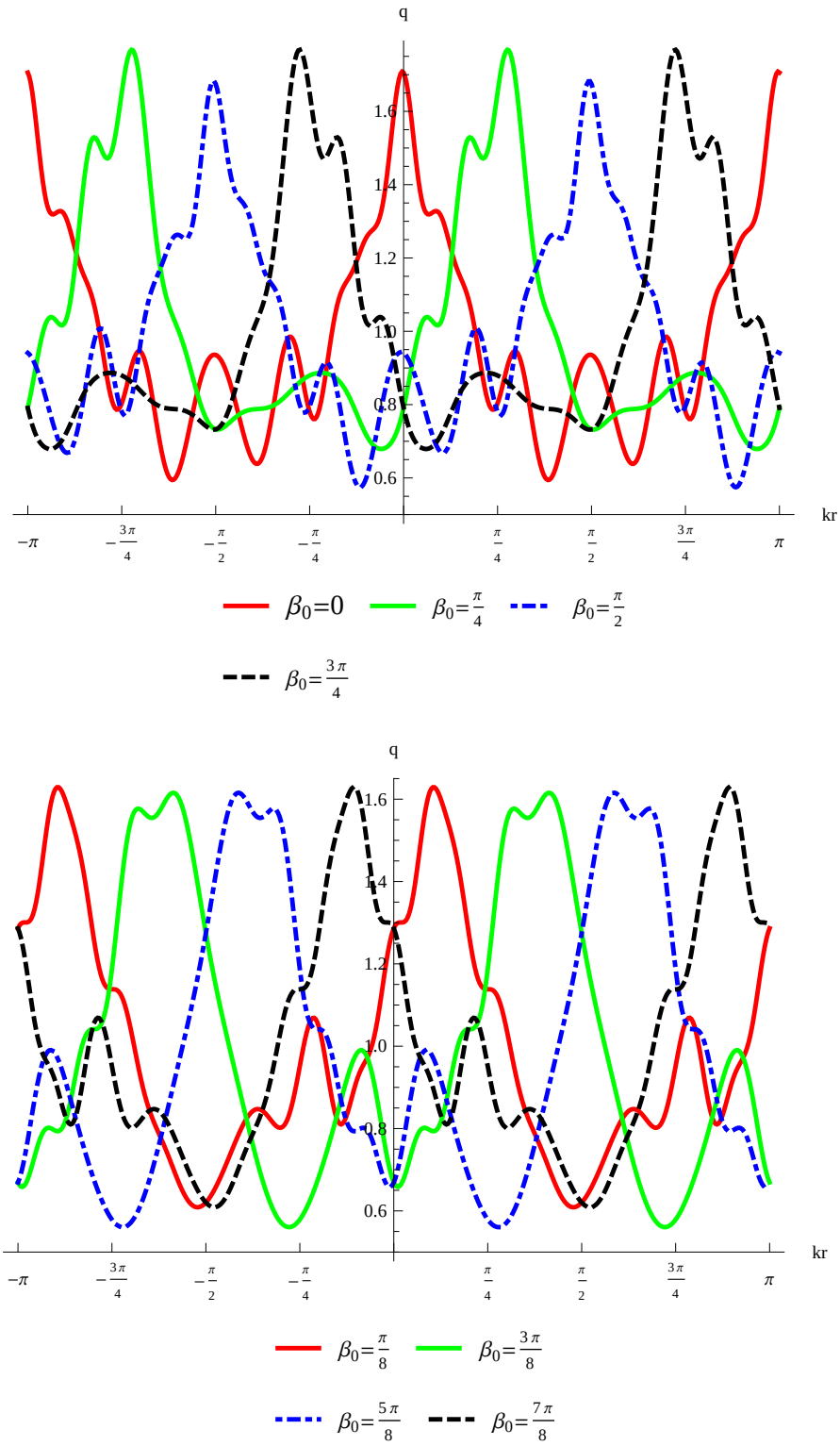

Figure 5.5: Variation of interaction factor q for different angles of incidence β for the optimal six-WEC circular arrays, with $kr = 10$ fixed. The data is presented in two figures for clarity.

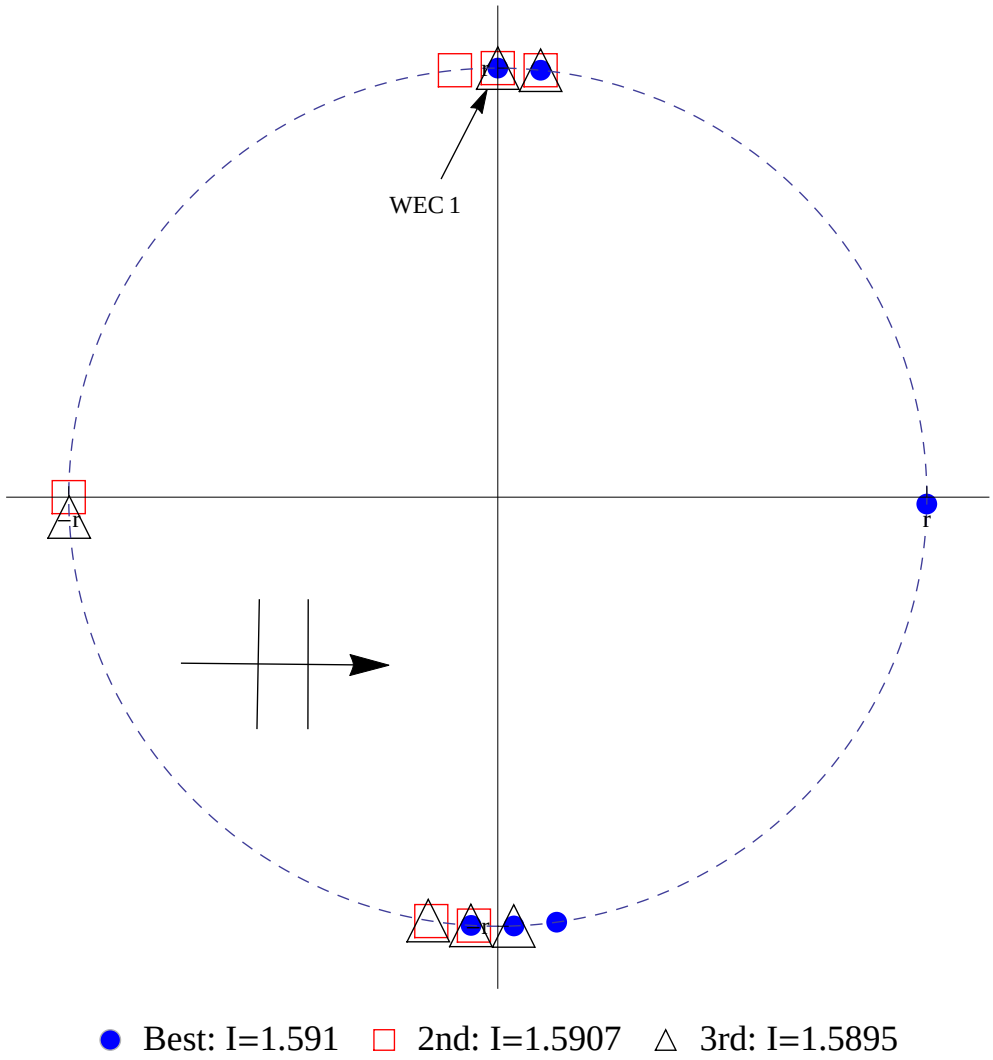

Figure 5.6: Optimal six-device circular arrays for $\beta_0 = 0$

similar to each other and differ by either slight perturbations in WEC positions or through mirror symmetry, or both. It would be anticipated that the optimisation routine would converge to layouts such as these, since they are analogous and perform in the same manner. Convergence to one optimal layout, or its symmetric analog, is dependent on the starting points of the optimisation. A more detailed list of the optimisation results for the six-device circular array with $\beta_0 = 0$ are provided in Appendix C in table C.1.

It was shown via a sensitivity analysis in Chapter 3 that the optimal layouts that maximised the mean of q were relatively stable to changes in array layout parameters. This is also true for the circular array though not explicitly shown for brevity. Thus, a small change in WEC positions from the optimal case would result in only a small change in performance. Hence, the optimisation

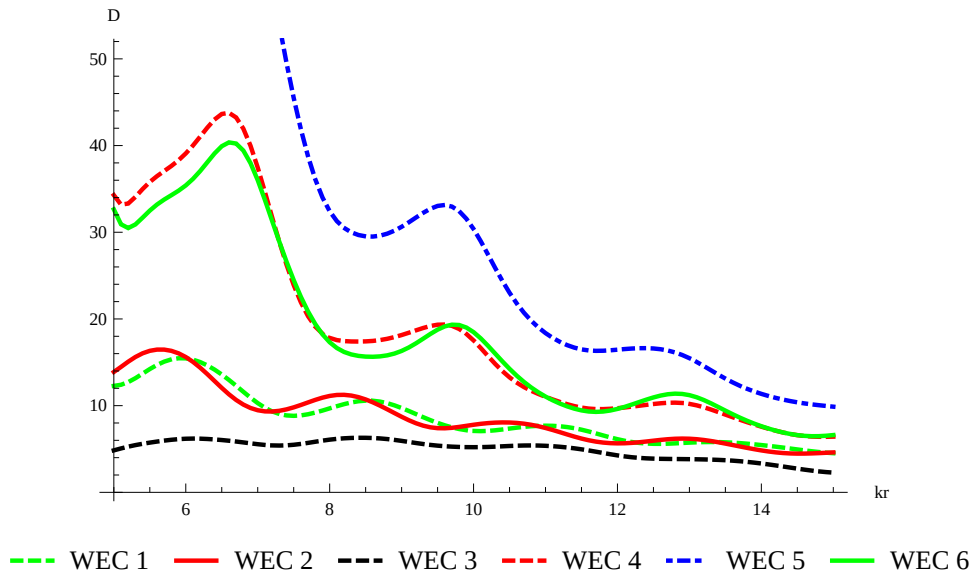

Figure 5.7: Predicted displacement amplitudes for optimal six-WEC circular array with $\beta_0 = 0$

converged to some secondary optimal arrays which were only slightly different and performed only slightly poorer.

The optimal layout occurs with groups of two and three devices at the top and bottom of the array respectively and an isolated device to the right. It is noteworthy that the devices can be considered to be arranged almost within a semicircle orientated opposing to the incident wave direction. This optimal array achieves an average interaction factor of $I = 1.5910$ and figure 5.4 shows that it achieves a peak value of $q \approx 1.82$ around $kr \approx 6.6$. A secondary maximum of $q \approx 1.76$ is seen around $kr = 8.6$. Above this value of kr, q decreases to the minimum value of $q \approx 1.2$ at $kr = 15$.

Figure 5.5 indicates that there is a relatively large range of approximately $\pm\frac{\pi}{5}$ about $\beta = 0$, where q remains greater than unity. Away from this range, it is also evident that quite poor performance occurs at other wave angles, as would be expected.

The non-dimensional displacement amplitudes of each WEC in this optimal array are presented in figure 5.7. In keeping with previous findings, the grouped devices exhibit relatively large motions compared with the isolated device. The displacement of the isolated device (WEC 3) is maintained around $|D| \approx 5$ for the entire domain of kr. All other devices have $|D| > 6$ for all $kr \in [5, 15]$, with the group of three devices at the bottom of the array (WECs 4, 5 and 6) having considerably larger displacements, especially for lower kr. It worth noting that

the displacements of exhibited in figure 5.7 are much lower than those for the optimal linear arrays in Chapters 3 and 4.

A similar physical interpretation to the optimal linear arrays in Chapter 4 (particularly Sections 4.3.3 and 4.3.5) may apply here. The two groups at either end of the array seem to cause constructive interference, with WEC 3 required to capture power incident through the middle of the array, that would otherwise escape. The semicircular arrangement may be due to a need to avoid rows of devices, i.e. devices stacked behind one another, unless these device are within an interacting group.

5.4.1.2 $\beta_0 = \frac{\pi}{8}$ Case

The top three optimal array layouts for $\beta_0 = \frac{\pi}{8}$ are shown in figure 5.8, while a detailed list of optimisation results are provided in table C.2 of Appendix C. The best array is one with a group of two devices at the top, a group of three devices offset to the right of the bottom, and a relatively isolated device between these groups. The next best arrays are rather different; these contain two groups of two devices at similar positions to the groups in the best array, with two relatively separated devices between these groups.

As with the $\beta_0 = 0$ case, in each of the top array layouts, the WECs can be considered to be lying almost within a semicircle opposite the incident wave direction. The best array attains a mean performance of $I = 1.5802$, while figure 5.4 shows that a maximum of $q \approx 1.86$ is achieved around $kr \approx 8.5$. Performance is reduced for larger kr with a minimum of $q \approx 1.2$ at $kr = 15$ (the same as the $\beta_0 = 0$ case). However, good performance is maintained over $kr \in [5, 11]$ with $q \geq 1.6$ within this range.

The variation with β shown in figure 5.5 indicates broadly similar performance to the $\beta_0 = 0$ case, with a range of approximately $\pm\frac{\pi}{5}$ where q remains greater than unity. This range is centred about the target wave angle of $\beta = \beta_0 = \frac{\pi}{8}$. Outside this range, poor performance is observed, dropping as low as $q \approx 0.6$ for some wave angles.

The optimal displacement amplitudes for the best array with $\beta_0 = \frac{\pi}{8}$ are shown in figure 5.9. A similar pattern to the previous case emerges, with the grouped WECs predicted to have larger displacements than isolated WECs. It is also clear that the devices in larger groups exhibit larger motions than those in smaller groups. Here, WEC 2 (which is isolated) maintains $|D| \in [2, 6]$ for all

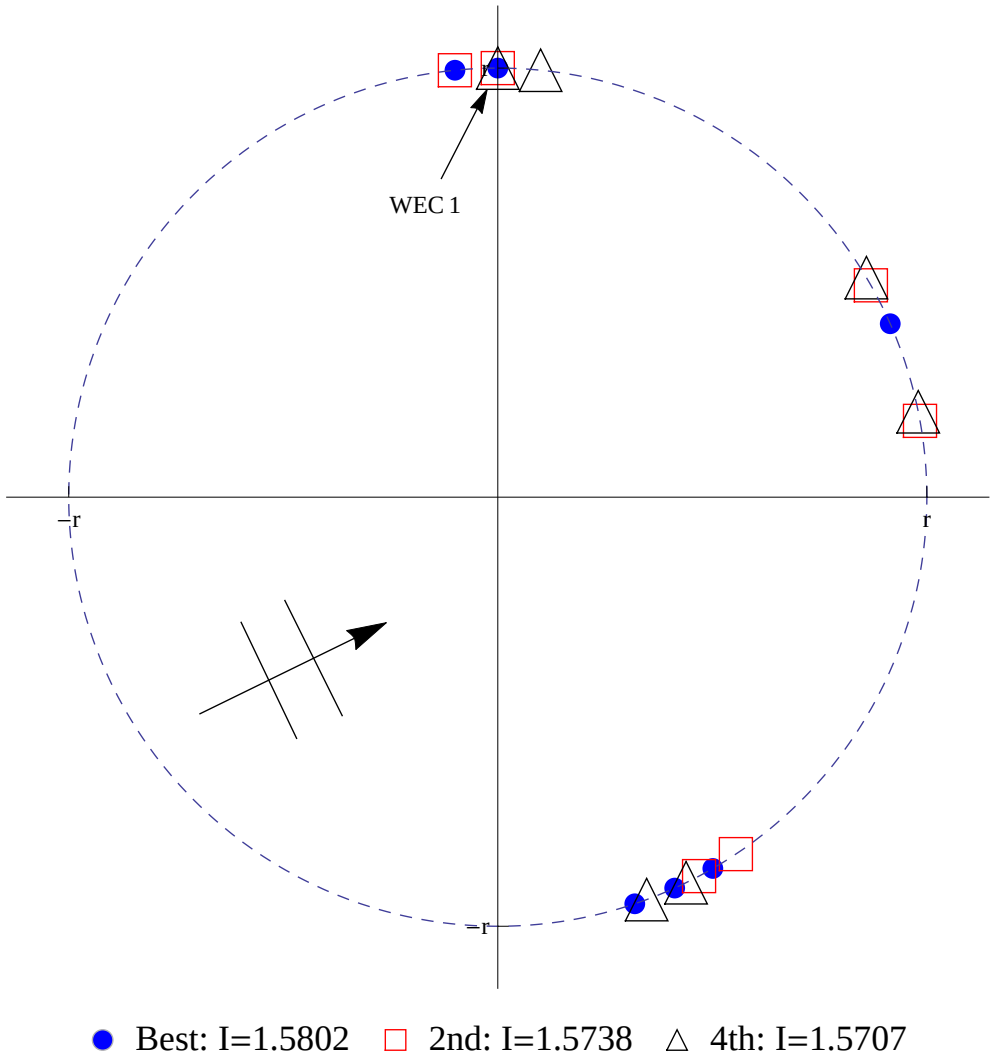

Figure 5.8: Optimal six-device circular arrays for $\beta_0 = \frac{\pi}{8}$. The third best layout is very similar to the second and is omitted for clarity

$kr \in [5, 15]$, while the WECs in the group of two devices (WECs 1 & 6) have $6 \leq |D| \leq 18$ and those in the group of three devices (WECs 3 - 6) have $|D| \geq 8$. Although not explicitly shown, WEC 4 is predicted to have a maximum of $|D| \approx 90$ at $kr \approx 5$. Another trend shown is that for groups of three WECs, the central WEC has larger displacements that the surrounding devices. Finally, it can also be seen that the WECs in general exhibit larger motions for smaller kr, indicating that the closer they are positioned, the larger the predicted optimal motions.

Since the optimal array layout is similar to that of Section 5.4.1.1, an analogous physical interpretation of the array layout applies. The two groups (WECs 1 & 6 and WECs 3 - 5) appear to provide good constructive interaction with the

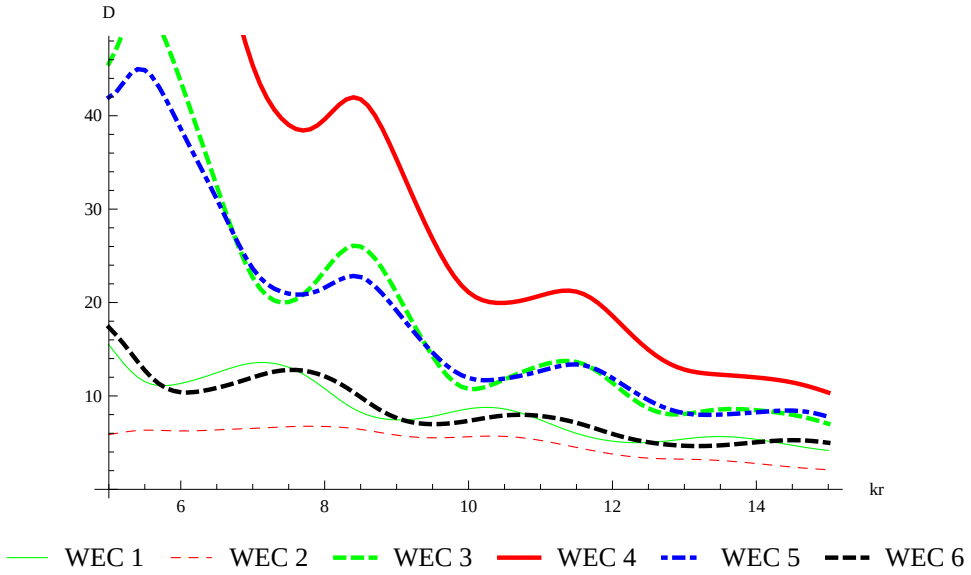

Figure 5.9: Predicted displacement amplitudes for optimal six-WEC circular array with $\beta_0 = \frac{\pi}{8}$

isolated device (WEC 2) capturing power incident on the large gap between these groups, even though WEC 2 operates with a relatively small displacement amplitude.

5.4.1.3 $\beta_0 = \frac{\pi}{4}$ Case

The top three optimal array layouts for $\beta_0 = \frac{\pi}{4}$ are visualised in figure 5.10. A more detailed list of the optimal arrays found by the optimisation is given in Appendix C in table C.3. The best array contains a group of three devices offset to the right of the bottom of the array, with three relatively isolated devices spaced between this group and the top of the array. The next best performing arrays contain either two groups of two devices or a group of two and three devices, with isolated device(s) between them. As before, all these arrays are mostly contained within a semicircle opposite the incident wave angle.

The top array achieves an average performance of $I = 1.5563$, this is only approximately 1-2% better than the next best arrays found for this incident wave angle. Figure 5.4 shows that this optimal array achieves a maximum of $q \approx 1.72$ near $kr \approx 13$ and a minimum of $q \approx 1.34$ when $kr \approx 6.6$. There exists an area of stable good performance for $kr \in [8, 14]$, where $q \approx 1.6$ throughout.

It is shown in figure 5.5 that there is a similar range of $\pm\frac{\pi}{5}$ around $\beta = \beta_0 = \frac{\pi}{4}$ where $q \geq 1$ is maintained. The minimum value achieved outside this range is

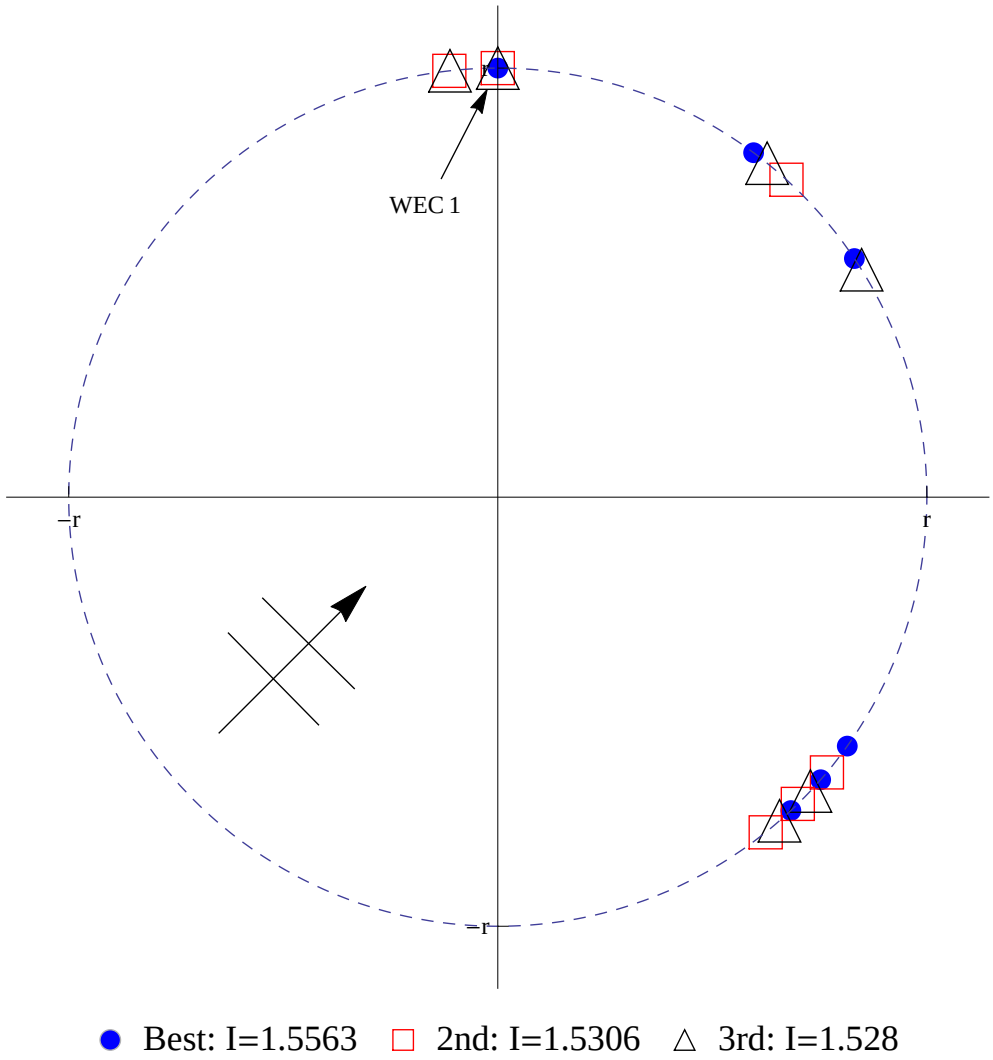

Figure 5.10: Optimal six-device circular arrays for $\beta_0 = \frac{\pi}{4}$

$q \approx 0.7$, which not as poor as other cases. Also, examination of the plot shows that the non-optimal performance (outside this range where $q \geq 1$) is less oscillatory than other cases.

The predicated optimal displacement amplitudes for the best array with $\beta_0 = \frac{\pi}{4}$ are presented in figure 5.11. The three isolated devices (WECs 1 - 3) have relatively low motion amplitudes of $|D| \approx 5$ for all $kr \in [5, 15]$, while the grouped devices (WECs 4 - 6) have considerably larger motions with $|D| > 8$. The motions of these grouped devices increase as kr decreases, while all devices have similar motion amplitudes of $|D| \in [4, 12]$ when $kr = 15$.

A similar physical explanation to the array in Section 5.4.1.1 can be applied to this array layout, with two groups at either end of the array (with respect to the incident wave direction) and a single WEC bridging the gap between these

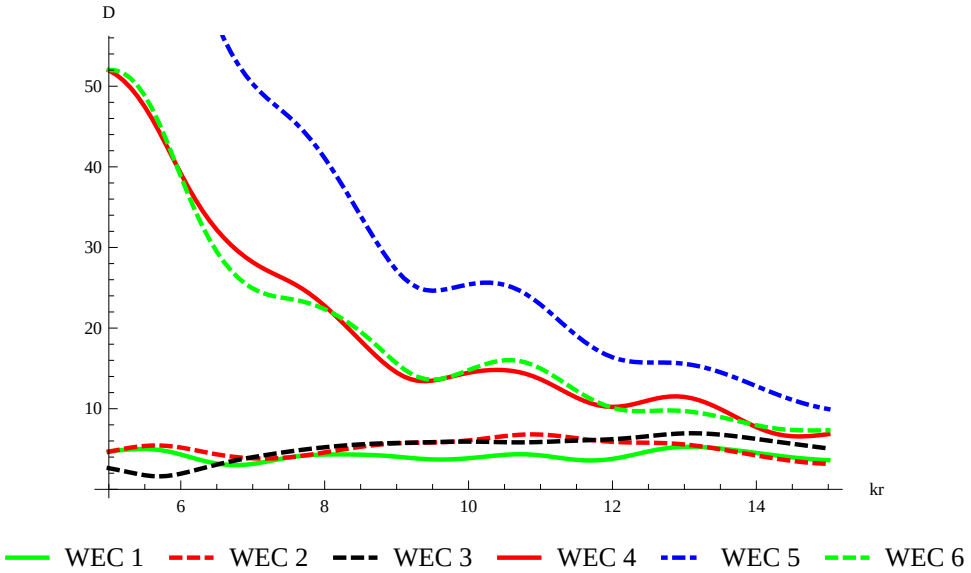

Figure 5.11: Predicted displacement amplitudes for optimal six-WEC circular array with $\beta_0 = \frac{\pi}{4}$

groups. The performance of this array is less that that in Section 5.4.1.1, presumably due to the fixed position of WEC 1 and the associated lack of freedom.

5.4.1.4 $\beta_0 = \frac{3\pi}{8}$ Case

The best three array layouts found for $\beta_0 = \frac{3\pi}{8}$ are presented in figure 5.12. The detailed optimisation results are given in table C.4 of Appendix C. The best array layout is quite similar to that of the $\beta_0 = \frac{\pi}{4}$ case, with a group of three devices offset to the bottom right of the array and three relatively isolated devices between the top of the array and the group of three. This layout is located within approximately one third of the circle and so still follows the pattern of lying within a semicircle opposite the incident wave direction. This holds for all of the top three arrays presented. These layouts are similar to each other, in that they all consist of a group of three devices with three relatively isolated WECs at the top of the array.

The best layout achieved an average performance of $I = 1.5883$, with a maximum of $q \approx 1.8$ at $kr \approx 13.5$ and a minimum of $q = 1.3$ at $kr = 5$, as shown in figure 5.4. The behaviour of q tends to increase with kr up to the maximum value, after which it decreases. Good performance is maintained for $kr \in [10, 15]$, where $q \geq 1.6$ for the majority of this domain.

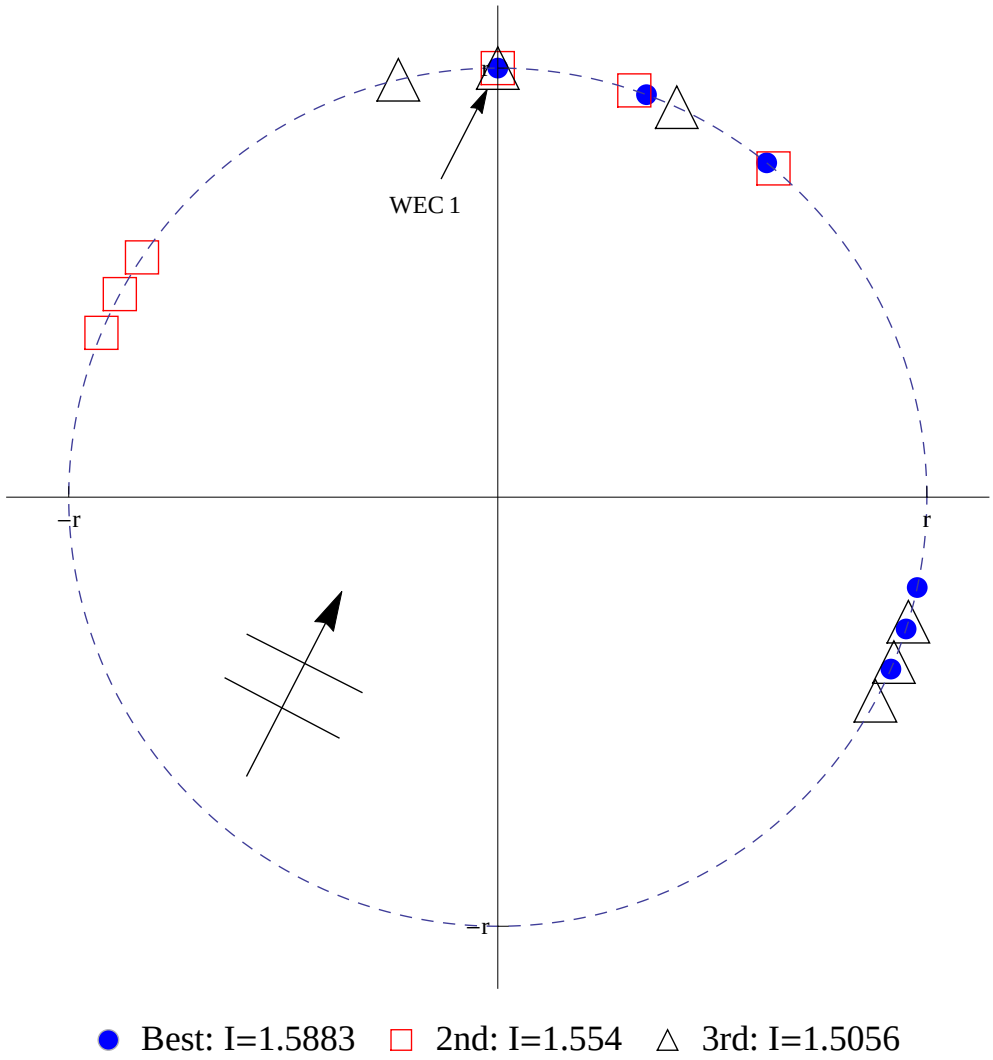

Figure 5.12: Optimal six-device circular arrays for $\beta_0 = \frac{3\pi}{8}$

Similar behaviour to the previous optimal arrays is shown in figure 5.5 for variation in β, where a range of approximately $\pm\frac{\pi}{5}$ exists around the target value of $\beta = \beta_0 = \frac{3\pi}{8}$ such that $q > 1$ is maintained. There also exists a broad peak in β-variation, where $q \geq 1.5$ for a range of $\pm\frac{\pi}{8}$ around $\beta = \beta_0 = \frac{3\pi}{8}$. This is due to a double peak around $\beta = \frac{3\pi}{8}$, which has the effect of widening the near peak performance, so that $q \approx 1.55$ is maintained for small changes around $\beta = \beta_0 = \frac{3\pi}{8}$.

The optimal motion amplitudes for the best array are shown in figure 5.13. As expected, relatively small displacements $|D| \leq 8$ are observed for the more isolated devices, while the grouped devices all have $|D| > 8$ for all $kr \in [5, 15]$. The displacements of the grouped devices (WECs 4 - 6) appear to increase for decreasing kr, while the non-grouped device motions are more stable with

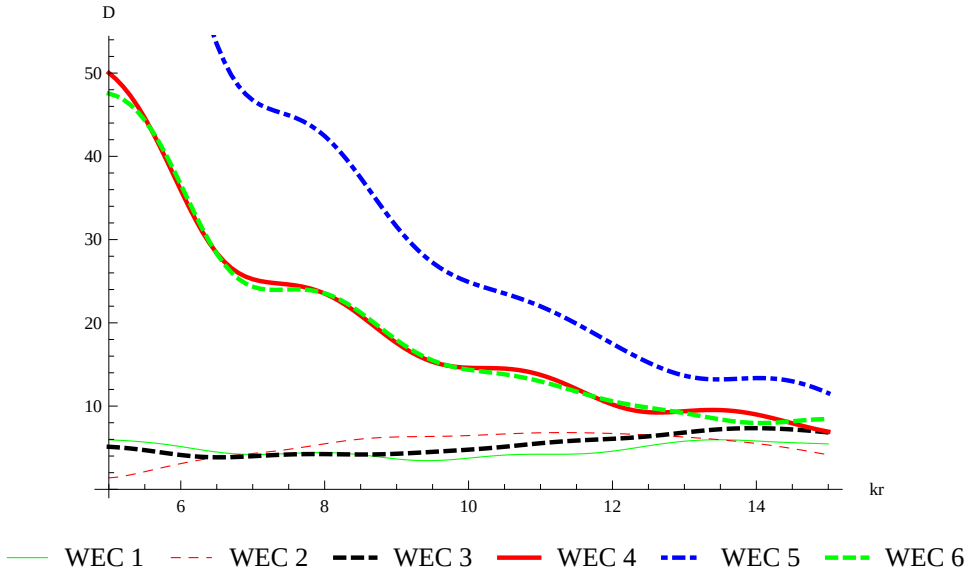

Figure 5.13: Predicted displacement amplitudes for optimal six-WEC circular array with $\beta_0 = \frac{3\pi}{8}$

$|D| \approx 6$. Note that the maximum interaction factor of $q \approx 1.8$ at $kr \approx 13.5$ corresponds to a case where the motions are all within $|D| \in [5, 14]$. These motions are still too large to be considered $\mathcal{O}(1)$, which realistically requires that $|D| \leq 3$. However, it may be inferred that since the motions are smaller for this optimal array, the imposition of displacement constraints would have a less relative impact; thus, this may have a less detrimental impact on array performance. It should further be stressed that the displacement amplitudes of this array are much lower than the linear arrays analysed in previous chapters.

The array presented here is slightly different to previous arrays and thus the physical interpretation of the optimal result is moderately altered. As with previous arrays, a closely spaced group of three devices is present but there is no corresponding pair of devices. Devices 1 - 3 are separated at the top-right of the array. The group (WECs 4 - 6) causes constructive interference as previously outlined while WECs 1 - 3 are more separated to capture power at the top of the array. This indicates that a greater frontage or coverage of area to avoid large gaps is more beneficial in this case. Note that the average performance of this array is less than those for previous wave angles. One would expect that a simple rotation of the optimal array would occur for different β_0. However, this result suggests that the constrained position of WEC 1 prevents a group of two or three devices forming in the optimal case.

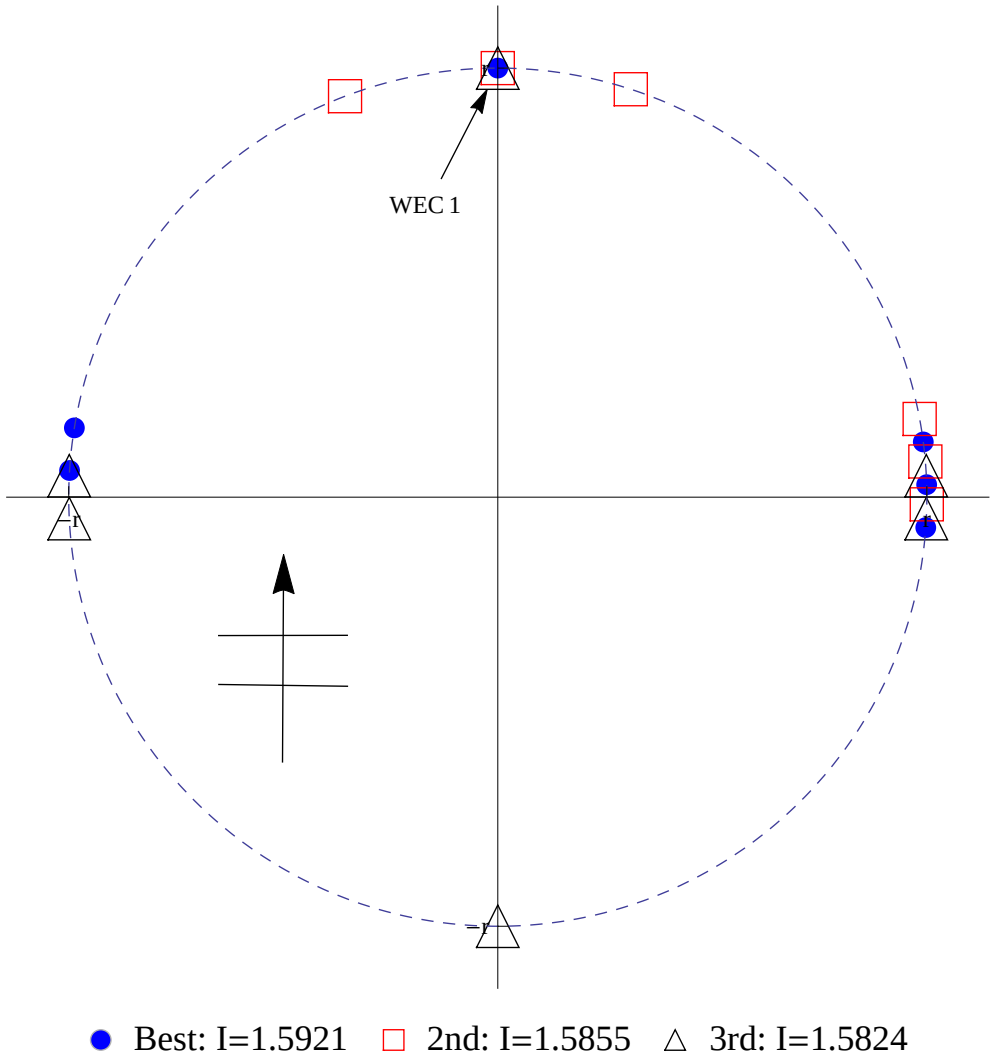

Figure 5.14: Optimal six-device circular arrays for $\beta_0 = \frac{\pi}{2}$

5.4.1.5 $\beta_0 = \frac{\pi}{2}$ Case

The top three optimal arrays for $\beta_0 = \frac{\pi}{2}$ are visualised in figure 5.14, while table C.5 in Appendix C gives a more comprehensive list of the optimisation results. The optimal array consists of groups of two and three WECs at the left and right of the array respectively, with an isolated device between these groups at the top of the array. The second best layout is similar to the optimal arrangements of the previous two cases, with a group of three devices at the right, with three relatively separated WECs at the top. Notably, the third best array has a perfectly symmetric layout, with groups of two devices at the left and right, with isolated WECs at the top and bottom. Apart from the third case, the other arrays again almost lie within a semicircle opposite the incident wave direction.

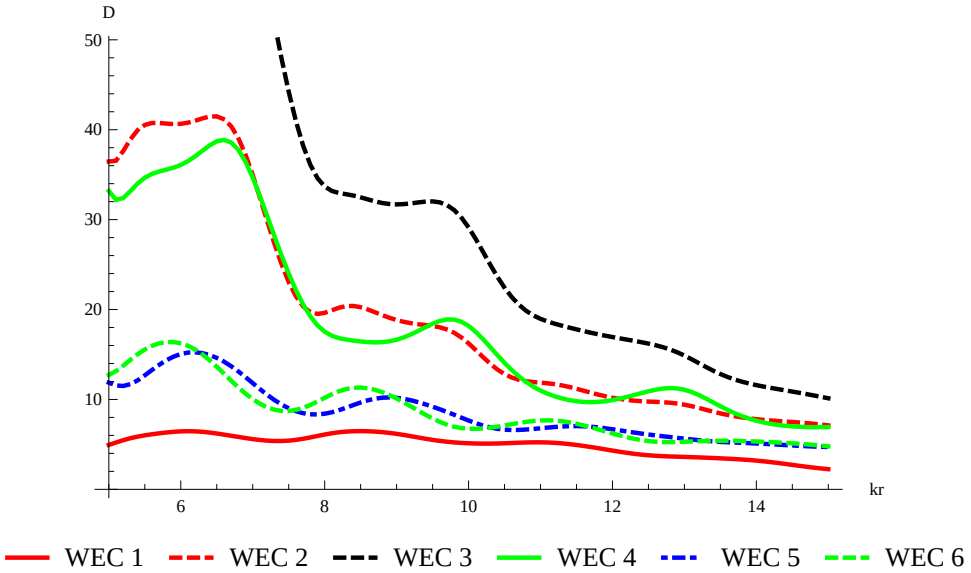

Figure 5.15: Predicted displacement amplitudes for optimal six-WEC circular array with $\beta_0 = \frac{\pi}{2}$

The best array layout achieves an average interaction factor of $I = 1.5921$, while figure 5.4 shows that a maximum of $q \approx 1.85$ at $kr \approx 6.5$ and a minimum of $q \approx 1.25$ at $kr = 15$ is obtained. A secondary maximum of $q \approx 1.8$ is also seen at $kr \approx 8.6$, above which q decreases with increasing kr to the minimum value. The best area of performance is $kr \in [5, 12]$, as $q \geq 1.5$ is maintained within this domain.

The β-variation presented in figure 5.5 shows that there is a similar range to previous optimal arrays of $\pm\frac{\pi}{5}$ around the target of $\beta = \beta_0 = \frac{\pi}{2}$. The plot also shows one of the poorest performances away from the optimal angle, as the interaction factor drops as low as $q \approx 0.56$ near $\beta \approx \frac{3\pi}{4}$.

The optimal motion amplitudes shown in figure 5.15 are in line with expectations, with the WECs in the group of three (WECs 2 - 4) exhibiting the largest motions (particularly for the central device WEC 3). The devices in the group of two also undertake large displacements but less than the group of three, while the isolated device exhibits the smallest motions, although still too large to be considered $\mathcal{O}(1)$ with $3 \leq |D| \leq 7$. The general trend of smaller displacements for larger kr is upheld, with all devices having $|D| \in [3, 11]$ for $kr = 15$. It is noteworthy that the maximum performance in q was for relatively small values of kr and thus would be accompanied by large motions of most devices.

This optimal array layout is a special case, since the fixed device (WEC 1) is in

line with the incoming wave direction. The array is almost identical to that in Section 5.4.1.1, with the incident wave angle and array rotated by $\frac{\pi}{2}$. Hence, a similar physical interpretation of the array applies, with the two groups providing good interaction at the sides and the isolated WEC absorbing power incident on the large gap between these groups.

5.4.1.6 $\beta_0 = \frac{5\pi}{8}, \frac{3\pi}{4}, \frac{7\pi}{8}$ Cases

The optimisation results for $\beta_0 = \frac{5\pi}{8}, \frac{3\pi}{4}$ and $\frac{7\pi}{8}$ are detailed in Appendix C in table C.6, table C.7 and table C.8 respectively. The diagrams of the top three array layouts corresponding to these optimisation results are shown shown in Appendix C in figure C.1, figure C.2 and figure C.3 respectively. Since these arrays for $\beta_0 = \frac{5\pi}{8}, \frac{3\pi}{4}, \frac{7\pi}{8}$ are essentially the same as the previous arrays discussed for $\beta_0 = \frac{3\pi}{8}, \frac{\pi}{4}, \frac{\pi}{8}$ respectively by symmetry, a detailed discussion on their behaviour is omitted and reference can be made to the previous sections. The interaction factor curves for both variation in kr and β, as well as the optimal displacement amplitudes, are identical to the analogous arrays previously discussed.

5.4.2 Circular Arrays including Central Device

The configuration is now extended to a circular array of seven devices, with the additional device in the centre of the circle. In this way, one device is fixed at the origin, which is denoted as WEC 7 with $(d_7, \alpha_7) = (0, 0)$. The angular position of another device (WEC 1) remains fixed at the top of the array with $\alpha_1 = \frac{\pi}{2}$ as before. The number of optimisation variables is therefore the same as the previous case (namely five) and the process follows in a similar manner to Section 5.4.1, with all other optimisation parameters the same.

Optimal parameter values are presented in Appendix C in detailed tabular form for $\beta_0 \in [0, \frac{7\pi}{8}]$ in multiples of $\frac{\pi}{8}$ in tables C.9 - C.15, which list the best eight solutions found by the optimisation routine. The best cases found by McGuinness & Thomas (2016) are also marked. These results are summarised in table 5.3, which gives the best case found at each wave angle. The behaviour of the interaction factor is shown for variation in kr in figure 5.16 and for variation in β in figure 5.17. Diagrams of the optimal array layouts and plots of the predicted optimal displacements are also provided for each case. The top

Table 5.3: Optimal array parameters for the seven-device circular arrays (including a middle device) for eight values of β_0

β_0	θ_1	θ_2	θ_3	θ_4	θ_5	I_{opt}
0	0.1000	2.9420	0.1000	0.1000	2.9420	1.5680
$\frac{\pi}{8}$	1.1503	1.4850	0.1000	0.1000	3.3479	1.5320
$\frac{\pi}{4}$	0.7534	1.4852	0.1000	0.1000	3.7020	1.4957
$\frac{3\pi}{8}$	0.3465	0.3231	1.1262	0.1000	0.1000	1.4785
$\frac{\pi}{2}$	1.3060	0.1000	3.2065	0.1000	0.1000	1.5361
$\frac{5\pi}{8}$	4.2874	0.1000	0.1000	1.1262	0.3231	1.4785
$\frac{3\pi}{4}$	0.1426	3.7020	0.1000	0.1000	1.4852	1.4957
$\frac{7\pi}{8}$	0.1000	3.3479	0.1000	0.1000	1.4850	1.5320

three optimal layouts are visualised for each value of β_0.

5.4.2.1 $\beta_0 = 0$ Case

A diagram showing the best three layouts for $\beta_0 = 0$ is shown in figure 5.18 and the detailed results of the seven-WEC array optimisation for this are presented in Appendix C in table C.9. The premier array layout contains two groups of three devices, one at the top and bottom of the array, with the central device between them. Interestingly, this array is symmetric about the origin (both x and y-axes). The second best array is only a perturbation of the first, with both groups of three WECs moved slightly. The third best layout contains the same group of three at the top of the array, but has a group of two WECs offset to the right of the bottom and an isolated device on the right. It should be noted that there is only a small difference of approximately 2% in performance between these arrays. The best array is quite similar to some optimal linear arrays discovered in previous chapters, where two groups of WECs were positioned at each end of an array with an isolated device between them, though a different incident wave angle β_0 was considered in that case. Most devices in all the optimal arrays presented lie within a semicircle opposite the incident wave direction, as with arrays which were previously investigated.

The best array obtained an average interaction factor of $I = 1.568$, with a maximum of $q \approx 1.88$ at $kr \approx 8.0$ and a minimum of $q \approx 1.38$ near $kr \approx 10.6$, as

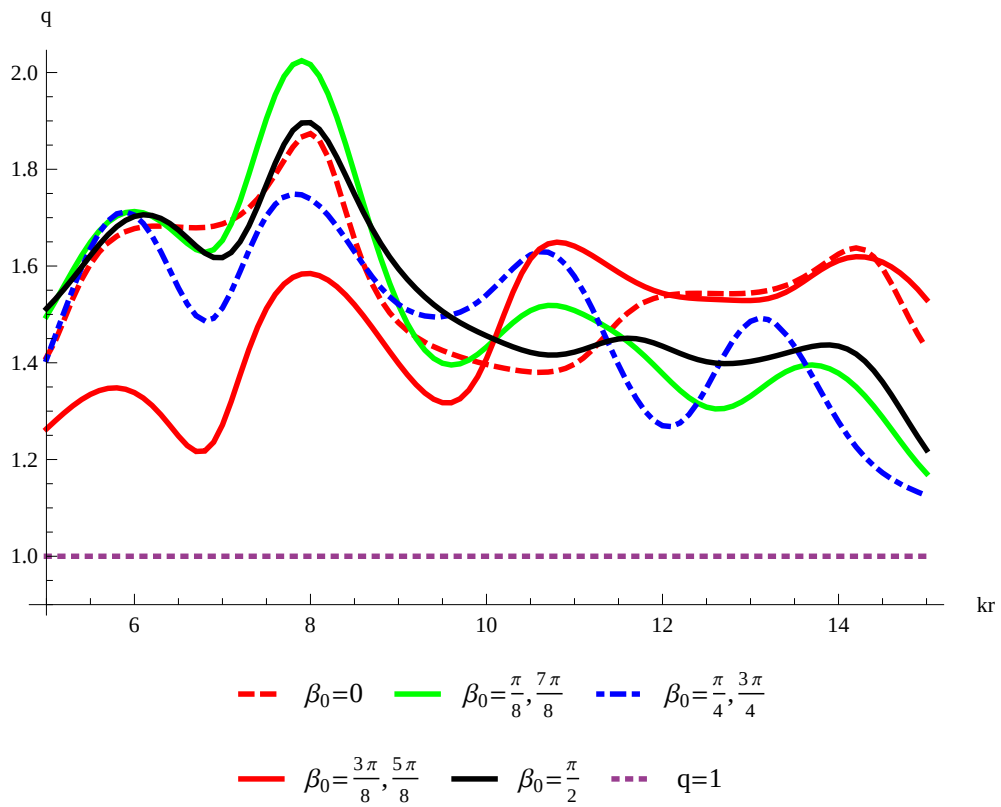

Figure 5.16: Interaction factor q against non-dimensional length kr for the optimal seven-WEC circular array for $\beta_0 = 0, \frac{\pi}{8}, \frac{\pi}{4}, \frac{3\pi}{8}, \frac{\pi}{2}, \frac{5\pi}{8}, \frac{3\pi}{4}, \frac{7\pi}{8}$

shown in figure 5.16. Relatively good and stable performance is obtained over the entire domain considered, as $q > 1.38$ for all $kr \in [5, 15]$. Areas of stable constructive interference are found within $kr \in [5.5, 8.5]$ where $q > 1.6$ and also for $kr \in [12, 14.5]$ where $q \approx 1.55$.

Figure 5.17 shows that there a relatively large range of $\pm\frac{\pi}{5}$ around the target wave angle $\beta = \beta_0 = 0$, where the interaction factor remains greater than unity, similar to previous arrays. If this condition is relaxed slightly, there exists a very large range of approximately $\pm\frac{\pi}{3}$ where $q > 0.9$, which appears to be larger than most other arrays investigated. This effect is due to a small secondary peak near $\beta \approx \pm\frac{\pi}{3}$. As expected, this area of good performance is offset by considerably poor performance away from the optimal wave angle, where the interaction factor drops as low as $q \approx 0.52$.

The optimal displacements corresponding to the best array for $\beta_0 = 0$ are shown in figure 5.19. As with previous arrays involving groups of three devices, the grouped devices exhibited prohibitively large motions, particularly for the WECs in the centre of the groups (WECs 1 and 4). These grouped devices

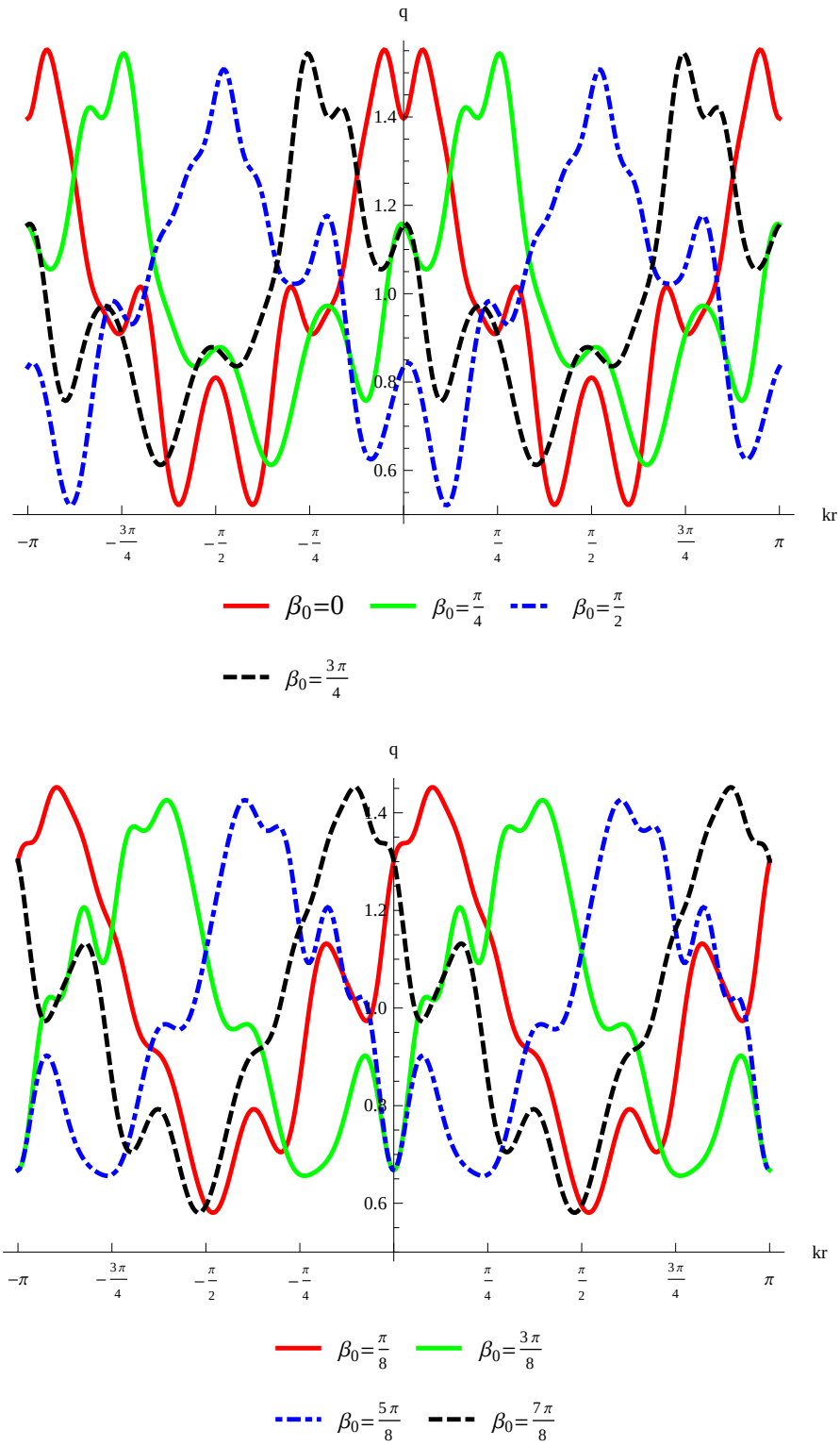

Figure 5.17: Variation of interaction factor q against angle of incidence β for the optimal seven-device arrays, with $kr = 10$ fixed. The data is presented in two figures for clarity.

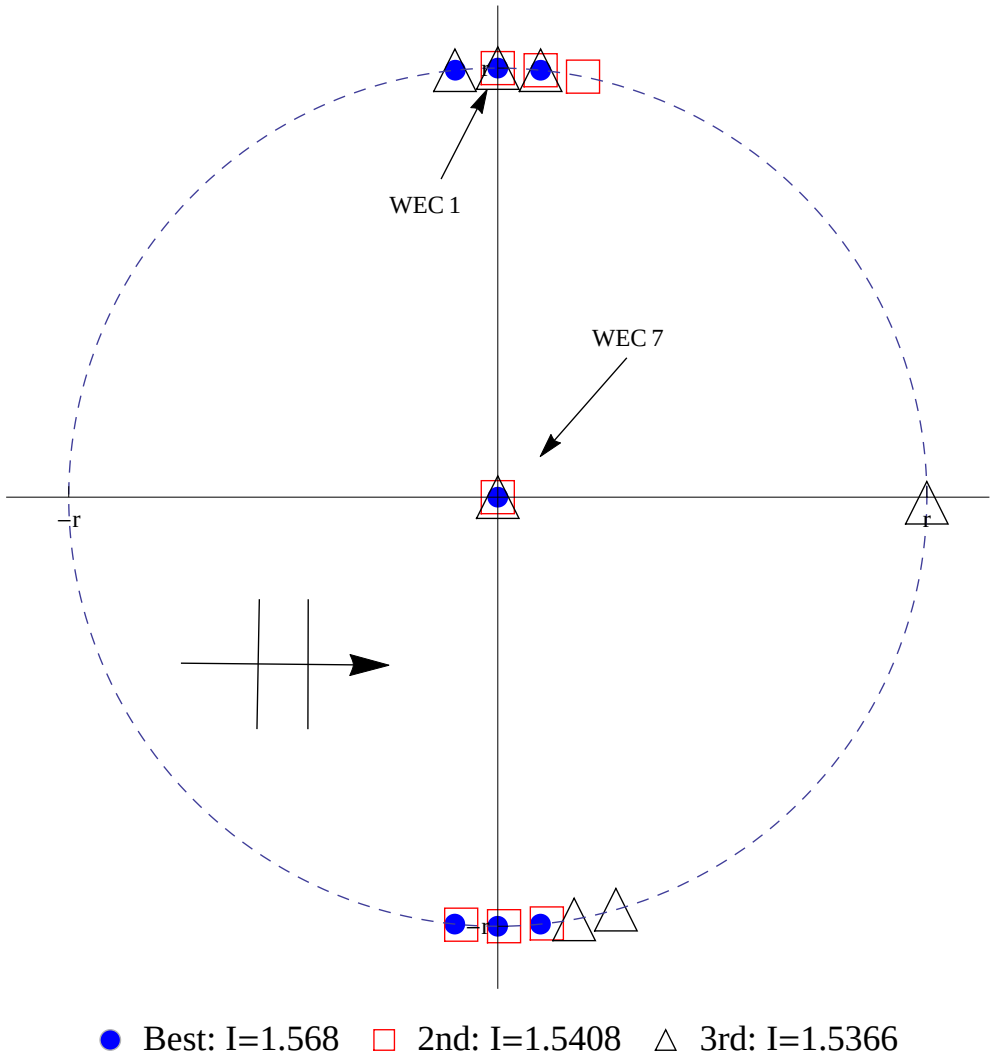

Figure 5.18: Optimal seven-device circular arrays for $\beta_0 = 0$

(WECs 1 - 6) have $|D| > 10$ for all $kr \in [5, 15]$, while the isolated device (WEC 7) has $|D| \approx 5$ for the entire domain. The general trend of larger displacements for smaller kr is mostly upheld. Note that the maximum in q around $kr = 8$ corresponds to a small peak in $|D|$ for all devices. The secondary area of good performance for $kr \in [12, 14.5]$ corresponds to motion amplitudes of $5 \leq |D| \leq 20$, which are lower than the rest of the range. In particular, the displacements in this area are lower than those for the peak performance around $kr = 8$. Therefore, this secondary area of good performance may be preferable, as the imposition of motion constraints may not be as limiting.

A physical interpretation analogous to that in Section 5.4.1.1 can be made to the optimal layout presented here, since these layouts are quite similar. As WEC 7 is forced to be in the centre of the array, another WEC is not needed

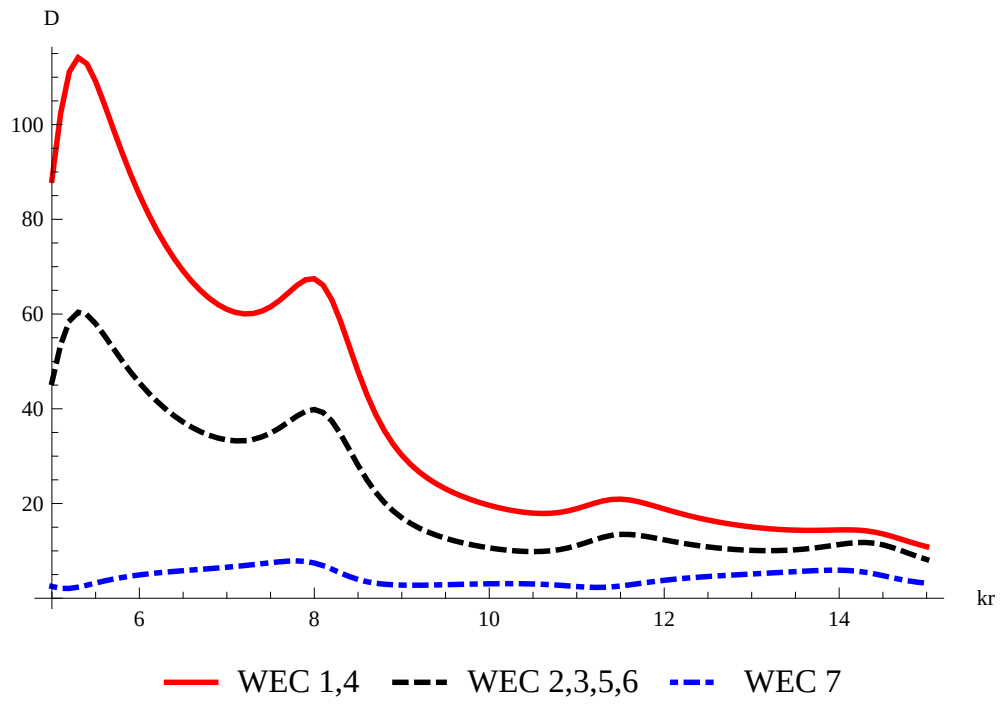

Figure 5.19: Predicted displacement amplitudes for optimal seven-WEC circular array with $\beta_0 = 0$

along the x-axis to absorb power in the gap between the groups. This results in the two groups containing three devices, presumably to maximise the constructive interference. It should be stressed that although the best array presented here has a slightly lower value of I than that in Section 5.4.1.1, more power is absorbed by this array due to the extra device.

5.4.2.2 $\beta_0 = \frac{\pi}{8}$ Case

The best three optimal array layouts for $\beta_0 = \frac{\pi}{8}$ are presented in figure 5.20 and the detailed optimisation results are listed in Appendix C in table C.10. The top performing array consists of groups of two and three WECs at the top of the array and offset to the right of the bottom of the array respectively, along with isolated devices between these groups to the right of the array and in the centre. The second and third best arrays are quite similar to this configuration, as they are either small perturbations or mirror images of the best array or both, hence the small difference of approximately 1% - 3% in mean performance. As with previous optimal arrays, the first and second best arrays are located within a semicircle opposite the incident waves, while the third array is approximately positioned in a semicircle facing the incident waves.

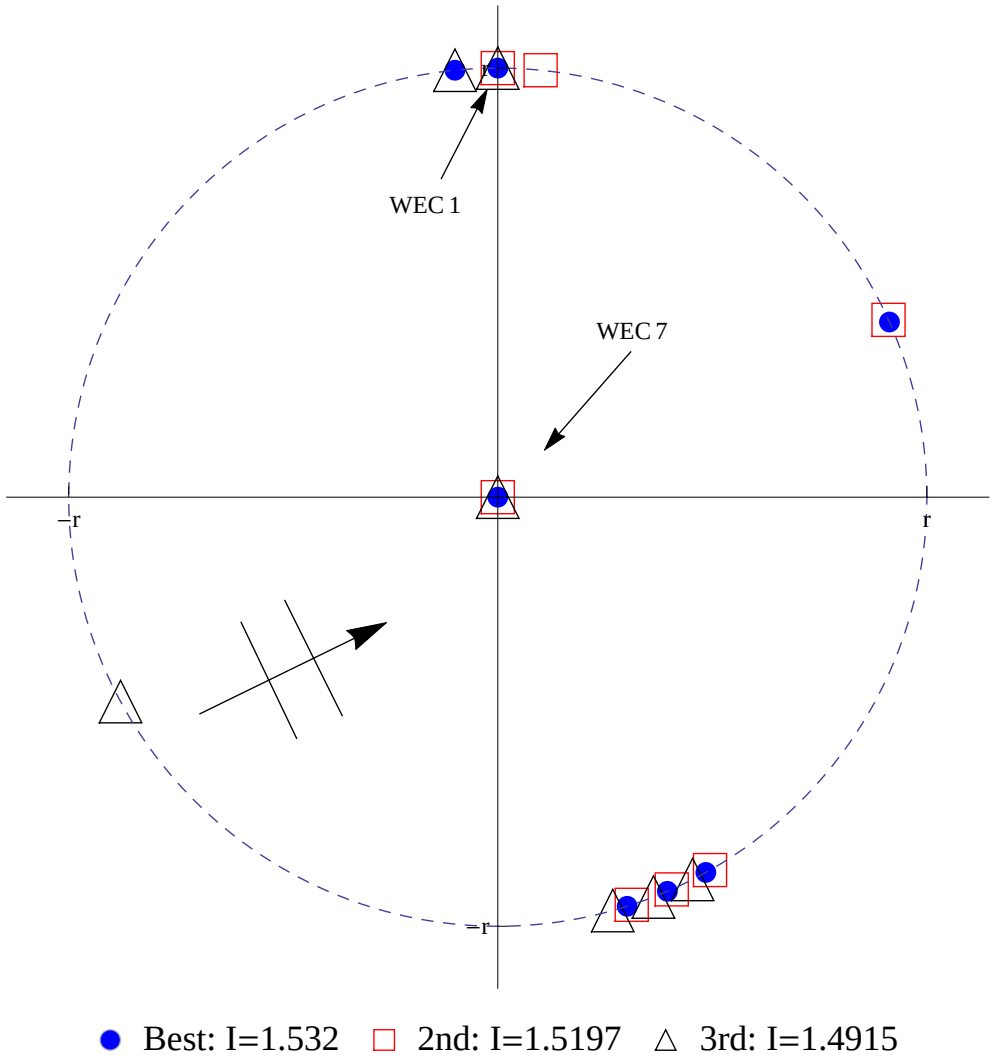

Figure 5.20: Optimal seven-device circular arrays for $\beta_0 = \frac{\pi}{8}$

The optimal array achieves a mean performance of $I = 1.532$ and figure 5.16 shows that this encompasses an impressive maximum of $q \approx 2.2$ near $kr \approx 7.8$ and a minimum of $q \approx 1.19$ at $kr = 15$. A large area of good performance is seen for $kr \in [5, 9]$, where $q \geq 1.5$, which includes the aforementioned maximum.

A slightly smaller range of approximately $\beta_0 \pm \frac{3\pi}{16}$ exists where constructive interference ($q > 1$) is maintained by this array compared to others, as shown in figure 5.17. However, due to a secondary peak at $\beta \approx -\frac{3\pi}{16}$, this range is considerably larger ($-\frac{\pi}{4} \leq \beta \leq \frac{5\pi}{16}$) if the condition is relaxed to $q > 0.9$. Note that this larger domain is extended further to the left of the optimal wave angle than the right, so that the domain length is no longer symmetric about $\beta_0 = \frac{\pi}{8}$. As expected, poor performance is seen away from this range, with $q \approx 0.6$ for $\beta \approx \pm\frac{\pi}{2}$.

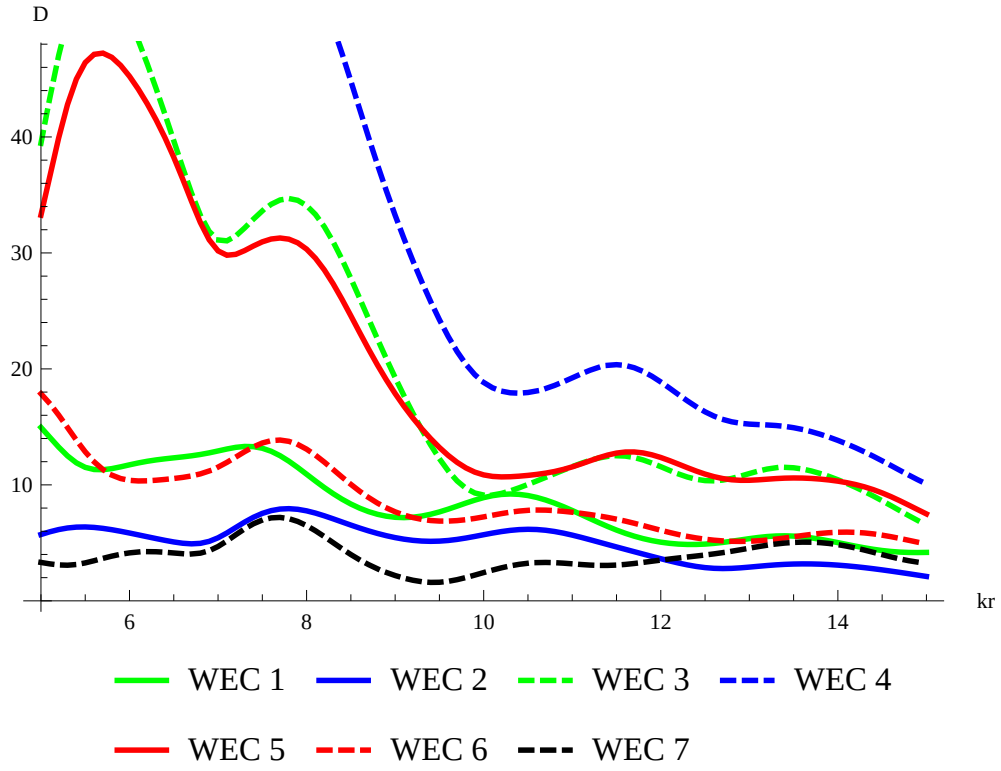

Figure 5.21: Predicted displacement amplitudes for optimal seven-WEC circular array for $\beta_0 = \frac{\pi}{8}$

The optimal WEC displacement amplitudes for this case are shown in figure 5.21. The group of three devices (WECs 3 - 5) exhibit larger motions, especially the central of these (WEC 4). The paired devices (WECs 1 and 6) also exhibit larger motions compared to the more isolated devices (WECs 2 and 7), which have $|D| \approx 5$ for all $kr \in [5, 15]$. In general, smaller values of kr correspond to larger motions. The peak in q at $kr \approx 7.8$ corresponds to a slight peak in the motion amplitudes of all devices. At $kr = 15$, all devices have $|D| \in [2, 12]$.

This array is slightly different to the previous one, as WEC 2 is isolated. It appears that the constraint on the position of WEC 1 prevents a group of three WECs forming at the top of the array in the optimal solution, hence the slightly lowered optimal value of I. As a result, WEC 2 is moved to bridge the gap between the two groups, thus aiding WEC 7 in absorbing the power that would escape through this region.

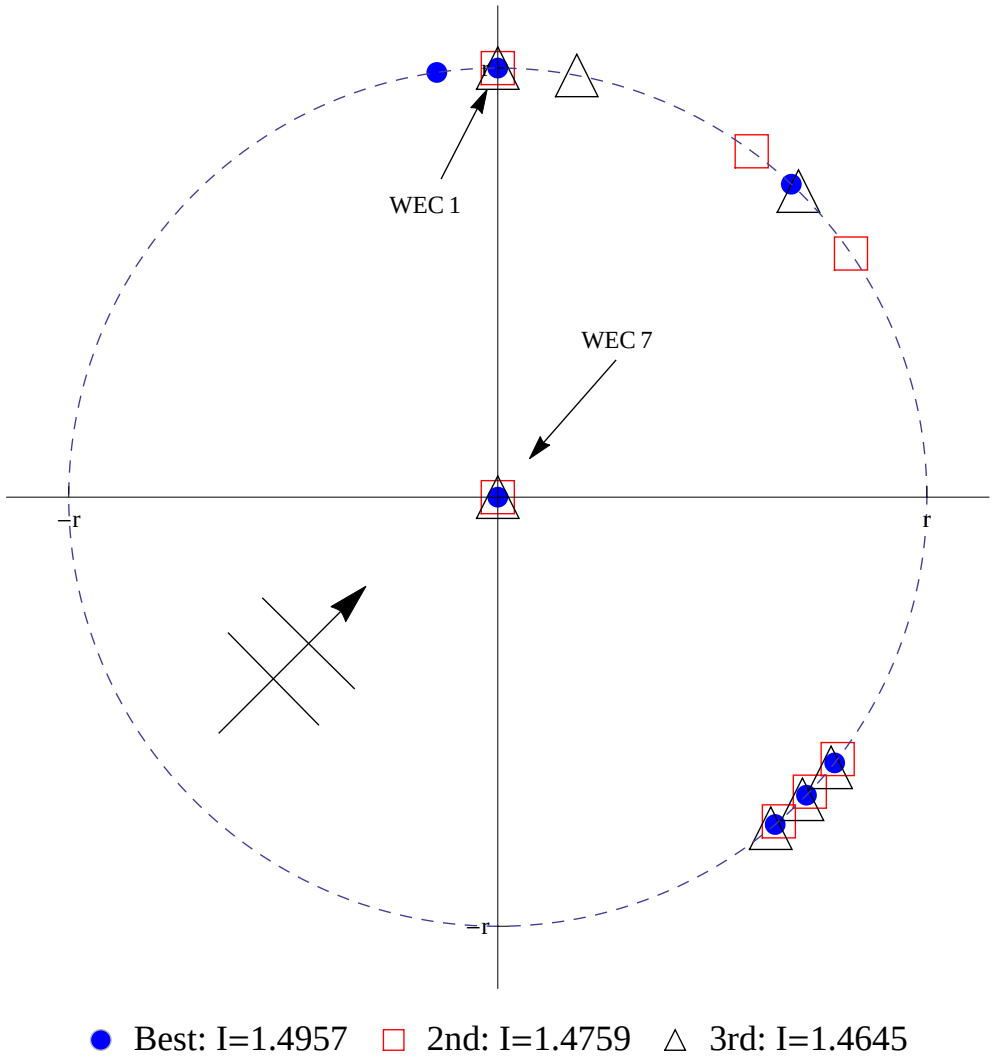

Figure 5.22: Optimal seven-device circular arrays for $\beta_0 = \frac{\pi}{4}$

5.4.2.3 $\beta_0 = \frac{\pi}{4}$ Case

The top three optimal layouts for $\beta_0 = \frac{\pi}{4}$ are illustrated in figure 5.22 and the detailed optimisation results are listed in table C.11 of Appendix C. The best array is comprised of a pair of closely spaced WECs at the top of the array, a group of three WECs offset to the bottom right and two relatively isolated devices between these groups (one on the top right and one in the centre). The group of three devices is present in all the top three layouts and is located in approximately the same position for each. The second best array is slightly different from the first in that WECs 1 - 3 are spaced relatively far apart at the top to top-right of the array, while the third best array is very similar to the first with the pair of WECs at the top mirrored about the y-axis. It is noteworthy that all these arrays are again almost situated within a semicircle

opposite the incident wave direction.

The best array achieved $I = 1.4957$ with a maximum of $q \approx 1.75$ near $kr \approx 7.8$ and a minimum of $q \approx 1.19$ at $kr = 15$, as shown in figure 5.16. It should be noted that the minimum achieved here is the smallest for arrays of this type with seven devices. Overall, the behaviour of this array is quite oscillatory, with the q against kr curve showing a wavy nature, with peaks and troughs for every two or three unit changes in kr. The range of performance of q with changes in kr is slightly smaller than other arrays, with $q \in [1.19, 1.75]$ for $kr \in [5, 15]$. There exists a large domain of good performance for $kr \in [5, 11]$, where $q > 1.4$.

The β-variation for this array shown in figure 5.17 is not the same as with previous arrays. As expected, a peak is achieved near the optimal value of $\beta = \beta_0 = \frac{\pi}{4}$ and there exists a range with an approximate length of $\frac{2\pi}{5}$ where q remains greater than unity. However, this range is not centred about the target wave angle of $\beta = \beta_0 = \frac{\pi}{4}$. Instead, the range runs approximately within $\beta \in [-\frac{\pi}{12}, \frac{3\pi}{8}]$, which is skewed to the left of the optimal wave angle. This behaviour appears to be due to a secondary peak at $\beta = 0$, which stretches the constructive interference area more to the left of the target wave angle.

The optimal displacement amplitudes are shown in figure 5.23 for each WEC in this optimal array. Similar behaviour to previous arrays is observed, with the grouped devices (WECs 3 - 5) exhibiting larger motions than isolated WECs and the overall trend that motions are larger for smaller kr (though this is not true for all devices). It is noteworthy that the paired device motions (WECs 1 and 6) are not excessively large with $|D| \in [3, 10]$. This is perhaps due to this pair being more separated than previous pairs, with $\theta_6 = 0.1426$. Both isolated devices (WECs 2 and 7) have small displacements of $|D| \approx 5$ throughout $kr \in [5, 15]$. The grouped devices exhibit very large motions of $|D| \geq 10$ for the lower half of the domain ($kr \in [5, 10]$) while all other devices have $|D| < 12$. The minimum in q at $kr = 15$ corresponds to displacements of $2 \leq |D| \leq 12$ for all devices.

A similar physical explanation to the previous array with $\beta_0 = \frac{\pi}{8}$ is given for the best layout presented here. The two groups at the top and bottom of the array may maximise constructive interference by the radiated wave field. WECs 2 and 7 may be located in the middle of the array to absorb the power that would otherwise escape through the gap between these groups.

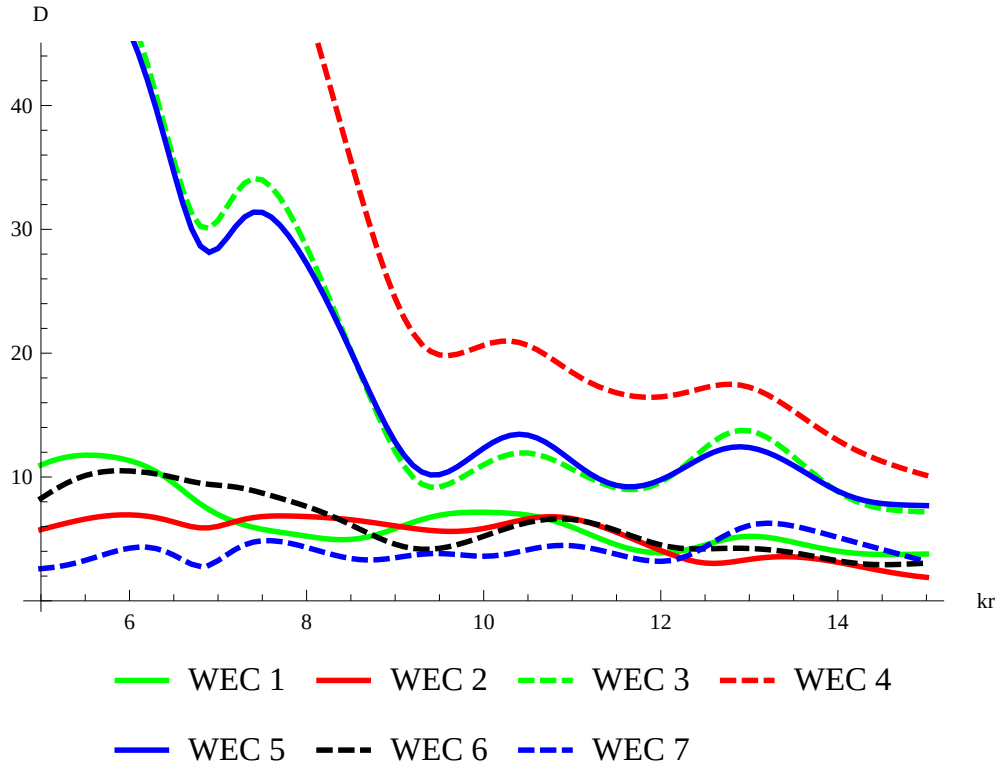

Figure 5.23: Predicted displacement amplitudes for optimal seven-WEC circular array for $\beta_0 = \frac{\pi}{4}$

5.4.2.4 $\beta_0 = \frac{3\pi}{8}$ Case

Figure 5.24 shows the top three optimal layouts for the target wave angle $\beta_0 = \frac{3\pi}{8}$, while the optimisation results are listed in detail in table C.12 of Appendix C. The best array is comprised of three relatively isolated devices at the top right of the array with a closely spaced group of three WECs on the right. The second best array is very similar to the first, with the group of three devices in a mirrored position on the opposite side of the array. The third best array has the grouped devices in roughly the same location as the first, the other three devices are more separated across the top of the array, with one device to the left and one to the right of WEC 1 at the top. Similar to previous results, the pattern of being located within a semicircle opposite β_0 is also upheld for each array.

The best array achieves an average performance of $I = 1.4785$ with a maximum of $q \approx 1.65$ near $kr \approx 10.8$ and a minimum of $q \approx 1.21$ at $kr \approx 6.8$, as shown in figure 5.16. This maximum is the lowest for each of the seven-WEC circular arrays investigated. However, good stable performance of $q \approx 1.6$ is maintained

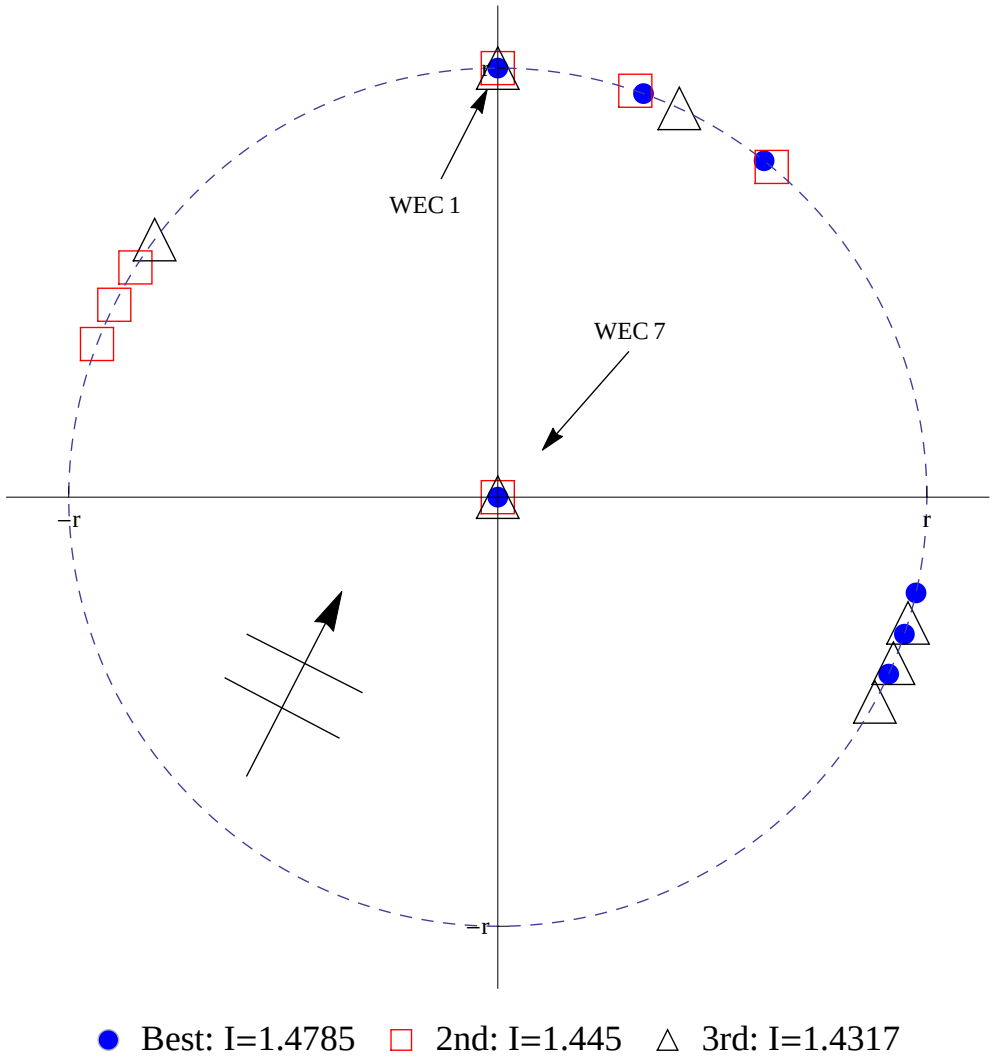

Figure 5.24: Optimal seven-device circular arrays for $\beta_0 = \frac{3\pi}{8}$

within $kr \in [10, 15]$, with very little variability in interaction factor, suggesting this as possible area for viable array deployment.

Figure 5.17 shows a large range of $\beta \in [\frac{\pi}{16}, \frac{9}{16}]$ where constructive interference ($q > 1$) is maintained. Similarly to the $\beta_0 = \frac{\pi}{4}$ case, this range is non-symmetric about the target angle of $\beta_0 = \frac{3\pi}{8}$, with a larger domain to the left of this value than the right. This is due to a secondary peak near $\beta = \frac{5\pi}{16}$ and a tertiary peak near $\beta = \frac{3\pi}{16}$, which improves performance in this region.

The predicted displacement amplitudes required for optimal performance of this array are shown in figure 5.25. Similar trends are seen, with grouped devices having larger motion amplitudes than the more isolated devices, particularly for smaller kr. The most noteworthy behaviour is that of the central device (WEC 7), whose displacement approaches zero for $kr \approx 6.8, 9.6, 13.2$ (though it never

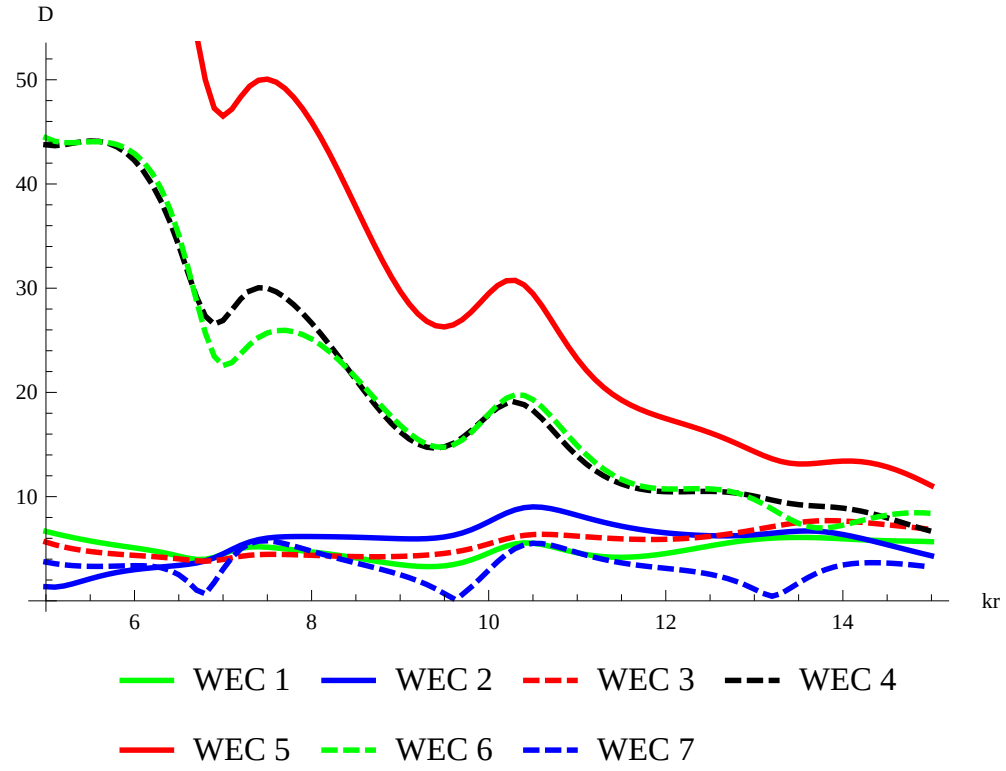

Figure 5.25: Predicted displacement amplitudes for optimal seven-WEC circular array for $\beta_0 = \frac{3\pi}{8}$

reaches zero). All isolated devices (WECs 1, 2, 3 and 7) have $|D| \leq 10$, while the grouped devices have displacement amplitudes of $|D| \geq 9$ which increase to $|D| \geq 22$ for $kr < 8$. Also shown are slight peaks in the displacement amplitudes of some devices at $kr \approx 7.5, 10.3$; these are most prominent for the grouped devices. Comparing figure 5.16 and figure 5.25, it is clear that the stable area of good performance of $q \approx 1.6$ for $kr \in [10, 15]$ identified above corresponds to motions of $|D| \in [0.5, 32]$. This can be improved further by considering the domain $kr \in [12, 15]$, where $q \in [1.52, 1.65]$ and all devices have optimal motions within $|D| \in [0.5, 18]$, with the central of the grouped devices (WEC 5) having the largest motion amplitude.

The array layout here is similar to the analogous array in Section 5.4.1.4, with the inclusion of WEC 7 in the circle centre. A similar physical interpretation of the behaviour of the optimal layout is proposed. The group of three WECs 4 - 6 create constructive interaction while the forced position of WEC 1 prevents a group forming at the top of the array. Consequently, WECs 1 - 3 are spread across the top right of the array. Therefore, WECs 1 - 3 along with WEC 7 absorb power in the gap between the top of the array and the group of three

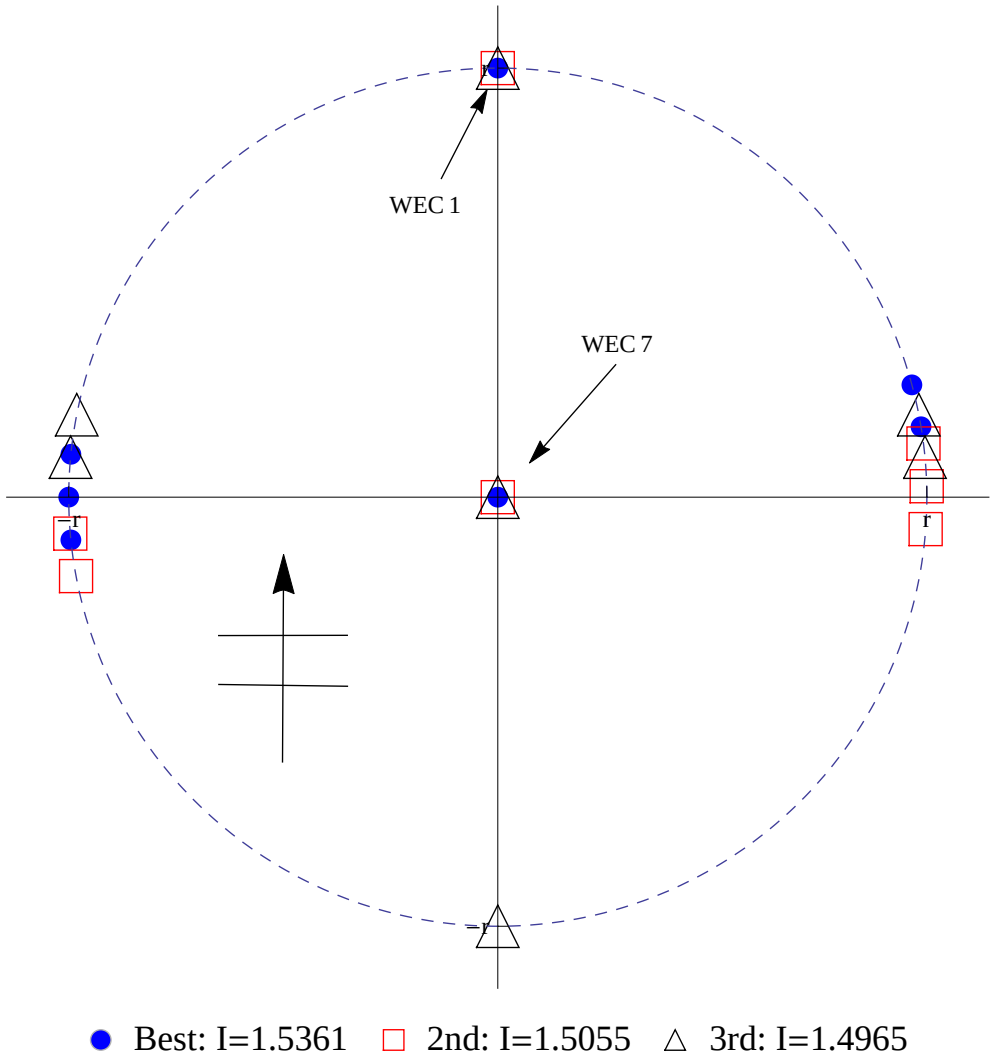

Figure 5.26: Optimal seven-device circular arrays for $\beta_0 = \frac{\pi}{2}$

devices.

5.4.2.5 $\beta_0 = \frac{\pi}{2}$ Case

Figure 5.26 illustrates the optimal array layouts discovered by the optimisation for $\beta_0 = \frac{\pi}{2}$, while the detailed optimisation results are listed in table C.13 of Appendix C. The array layout with the best mean interaction factor consists of groups two and three devices at the right and left of the array respectively, with isolated devices at the top and centre. The group of three is centred on the x-axis and the pair is offset slightly above the x-axis. The second best array is almost a mirror image about the y-axis of the first array, with the groups of two and three devices on opposite sides. The third best array consists of two pairs of

closely spaced devices at the left and right (offset just above the x-axis) and isolated devices at the top, bottom and centre. Apart from the third case, the pattern of these arrays mostly being located within a semicircle opposite β_0 is upheld.

The best array for this incident wave angle attained an average performance of $I = 1.5361$, which encompassed a maximum interaction factor of $q \approx 1.9$ at $kr \approx 8.0$ and a minimum value of $q \approx 1.25$ at $kr = 15$, as shown in figure 5.16. There is an area of very stable performance within $kr \in [10, 14]$ where $q \approx 1.45$, with very little variation in q with kr.

It is shown in figure 5.17 that there exists a large range of approximately $\beta \in [\frac{5\pi}{16}, \frac{5\pi}{6}]$ where $q > 1$ is maintained. As with the previous case, this range is non-symmetric about the target value of $\beta = \beta_0 = \frac{\pi}{2}$, with a larger range to the right of this value than to the left. This is due to a secondary peak near $\beta = \frac{13\pi}{16}$ which extends the domain of $q > 1$ in this region. Unlike the previous cases where there was a nonsymmetric domain of constructive interference about β_0, the larger domain is now to the right of β_0, rather than the left. As expected, poor performance is seen away from this region, where a minimum of $q \approx 0.52$ is reached near $\beta = \frac{\pi}{8}$.

The optimal displacements for this array are shown in figure 5.27. Previously identified patterns are again observed, with the group of three devices (WECs 4 - 6) exhibiting largest motions (largest for central device), followed by the paired devices (WECs 2 and 3), with the lowest amplitudes of $|D| \approx 5$ shown by the relatively isolated devices (WECs 1 and 7). Motions are also generally larger for smaller kr. It can be seen that the peak in interaction factor near $kr = 8$ corresponds to large motions for most devices, with subtle peaks in displacement amplitudes for some devices at this value. The minimum performance at $kr = 15$ corresponds to the lowest motions of $|D| \in [3, 11]$. Interestingly, the area of stable good performance within $kr \in [10, 14]$ corresponds to relatively low and stable displacements, with little change in the motion amplitudes of each device throughout this domain. This area has the smallest displacements for most devices, with $|D| \in [2, 22]$, indicating the possibility that constructive interference may be maintained after the imposition of motion constraints.

The physical justification behind the optimal layout here is similar to the analogous array in Section 5.4.1.5 and to the array in Section 5.4.2.2. There are two groups at either side of the array to maximise constructive interference, while two devices (WECs 1 and 7) are present in the centre of the array (along

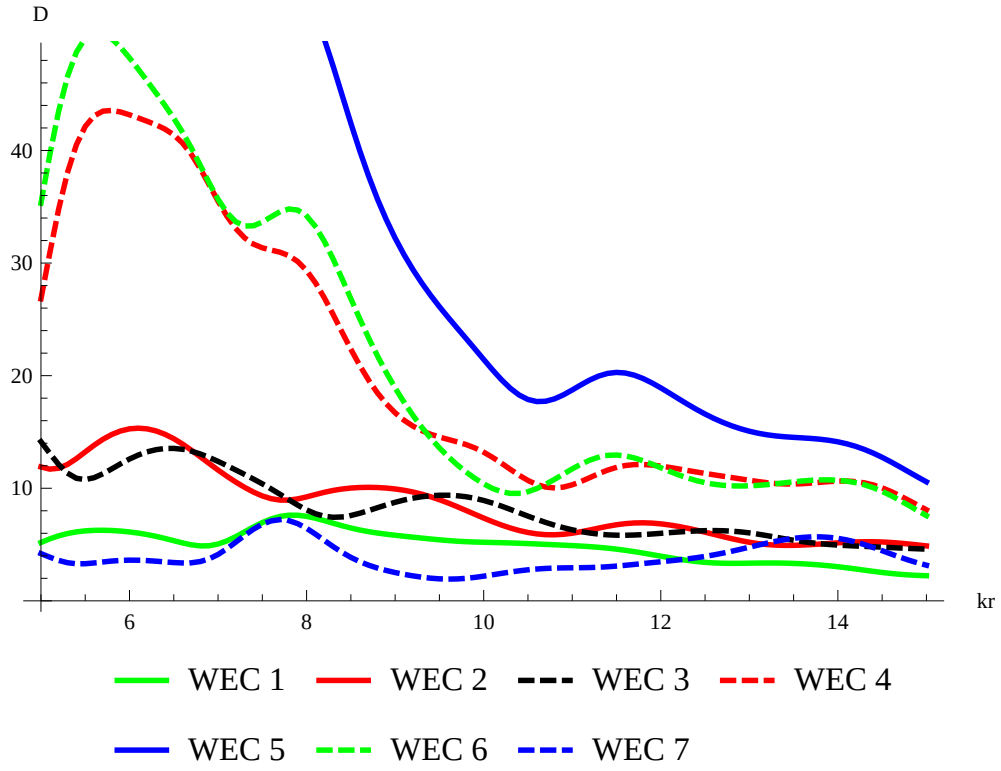

Figure 5.27: Predicted displacement amplitudes for optimal seven-WEC circular array for $\beta_0 = \frac{\pi}{2}$

the y-axis) to bridge the gap between these groups. It may have been expected that the optimal array layout would simply be a rotation of that in Section 5.4.2.1. However, the fixed position of WEC 1 forbids this and so the layout found is optimal given this restriction.

5.4.2.6 $\beta_0 = \frac{5\pi}{8}, \frac{3\pi}{4}, \frac{7\pi}{8}$ Cases

The detailed optimisation results for $\beta_0 = \frac{5\pi}{8}, \frac{3\pi}{4}$ and $\frac{7\pi}{8}$ are listed in Appendix C in tables C.14, C.15 and C.16 respectively. The diagrams of the top three unique array layouts corresponding to these optimisation results are also shown in Appendix C in figures C.4, C.5 and C.6 respectively. As with the six-WEC arrays, the arrays for $\beta_0 = \frac{5\pi}{8}, \frac{3\pi}{4}, \frac{7\pi}{8}$ are essentially the same as those discussed for $\beta_0 = \frac{3\pi}{8}, \frac{\pi}{4}, \frac{\pi}{8}$ due to rotation and symmetry. A detailed discussion on their behaviour and presentation of the the q vs kr and displacement curves are omitted and reference is made to the previous sections and diagrams.

5.5 Discussion of Results

This chapter examines the unconstrained optimisation of arrays of WECs which are constrained to lie in a circular geometry. The arrays contain six WECs that lie on the circumference of a circle; the case where a seventh device is placed at the centre of the circle centre is also investigated. As in Chapter 4, no symmetry is imposed on the layout of the array and only the angular position of WEC 1 is fixed to avoid replication of results. These circular arrays are optimised over the non-dimensional radius of $kr \in [5, 15]$, analogous to the previous optimisations on linear arrays. Each array is thus described by five angular positional variables and the mean optimal performance is maximised with respect to these optimisation variables.

In general, this study shows that optimal six and seven member circular arrays can perform better than optimal five member linear arrays, as shown by the higher values of I obtained in comparison to those of Chapter 4. This may be due to the enforced geometry performing better in the circular case, or it may be due to the increased freedom in the optimisation due to the larger number of variables. It should also be noted that the optimisation calculation took considerably longer to execute for the circular arrays in comparison to that for linear arrays. This was probably due to the combination of an increase in numerical intensity of the objective function (due to the geometry) and to the increased number of variables.

The results pertaining to circular arrays in this thesis are presented as optimal, in contrast to the results of McGuinness & Thomas (2016). Time constraints did not permit the long run-times required by the optimisation algorithm to find a global optimum in that paper. However, for this thesis, a finer scan of the starting variable space was conducted. This resulted in a 20 - 40 fold increase in run-time of the optimisations and allowed these global optima to be recovered within a high certainty. Overall, comparing the results of the more intense optimisation here to those of McGuinness & Thomas (2016), it can be seen that the large increase in run-time resulted in an improvement of at most 5% in the optimal solutions. In some cases (table C.11 and table C.13 in Appendix C), the global optimum was found by the shorter optimisation. The difference between the results of the long and short optimisations are relatively minor, with only small increases in the objective values and slight differences in optimal array layouts.

It should be stressed that in order to reliably find the global optima as described, the optimisation routine required run-times of the order of twenty to forty hours for each case. As anticipated, the calculations were more intense for the seven member arrays and consistently required run-times closer to forty hours.

One major difficulty with the optimal arrays obtained in this study is the magnitude of the associated device motions. Previous studies, such as Thomas & Evans (1981) and Fitzgerald (2006), suggest that an upper limit of device motions should be at most three times the incident wave amplitude. This limit was exceeded by the majority of WECs in all the optimal arrays discovered. These motions are predicted using linear wave theory, which assumes all motions are at most of the same order as the wave motion and are assumed to be small in some sense. Large device motions violate this approximation and thus invalidate the underlying linear wave theory. Furthermore, the application of a realistic PTO would prevent such large motions, which in turn will adversely affect device interaction and hence array performance.

In general, better performing arrays are expected to involve larger device motions. In some cases presented here, better performance was achieved relative to other optimal arrays, despite smaller predicted device motions. This may indicate that the imposition of device motion constraints may not be as limiting and it is possible that good performance can be maintained. The concept of constrained motion amplitudes is examined in Chapter 6 with respect to linear arrays and where the results are compared to the unconstrained optimisations of Chapter 4.

Many of the optimal array layouts presented here include closely spaced groups of two or three devices. These groups of WECs are predicted to exhibit the largest motions, with larger motion amplitudes for larger groups. Placing WECs in such close proximity identifies other possible difficulties, such as collisions between devices. In addition, the point absorber approximation may no longer be valid, as it may be unreasonable to neglect the scattered wave field if the WECs are in such close proximity to each other.

As proposed in previous chapters, one possible solution may be to replace these groups of closely spaced devices with a single appropriately-sized larger device. These arrays would then contain devices of different sizes, a possibility previous literature seems to have largely neglected. These arrays could be considered as satellite arrays, since one could often describe such arrays as involving several

smaller devices orbiting a larger device. This idea was initially suggested by McGuinness & Thomas (2015), where it was observed that larger devices did indeed reduce device motions within the point absorber approximation. However, it is not known what the effect on power absorption and array performance would be. Another possibility would be to replace these groups of devices with a single device that absorbs power in two modes of motion, thereby recreating the dipole effect often exhibited by the pairs of devices in optimal layouts. It is hoped that either a larger device or one that operates in two (or more) modes would recreate the constructive interference pattern without the complications of close deployment and large motions.

Comparing the results of Sections 5.4.1 and 5.4.2, it is clear that the addition of the seventh device in the centre of the circle influences the array performance and optimal array layout, even though this does not add any extra variables to the optimisation. The results shown here, particularly the optimal values of I, suggest that the inclusion of an extra device reduces the average optimum interaction factor. This is contrary to expectation, as preliminary results by Costigan (2014), on similar symmetric arrays of one variable, suggested the opposite. Costigan's work optimised circular arrays with different (a)symmetries imposed, so that each array is described by just one variable. The arrays were optimised by maximising the mean of the interaction factor over the non-dimensional radius. It may be that, due to the strict assumptions of array layouts (symmetry, one variable etc.), the inclusion of a central device improved performance in those special cases and that this does not hold for a more general layout. The work of Costigan (2014) also showed that the optimal arrays tended to contain groups of devices, albeit in a simpler optimisation regime. This agrees with the results presented here and with those of McGuinness & Thomas (2015, 2016). It should be stressed that a decreased average interaction factor I does not necessarily mean that the array absorbers less power. It is probable that the arrays in Section 5.4.2 absorb greater power due to the extra WEC. This result merely states the *interaction* is slightly less constructive.

It was found that the arrays considered here often converged to a layout that was contained approximately in a semicircle facing in the same direction as the incident wave angle. It is interesting that optimal interaction and constructive interference seems to occur when all devices are located in a semicircle, the orientation of which is dependent on the incident wave angle. Future research could examine this effect further and investigate the possibility of limiting an optimisation to a semicircle, which would be computationally more efficient.

It can be seen from figure 5.16 that a peak in q is present for each optimal seven-WEC array near $kr \approx 8$. This peak is the highest performance of q for all optimal seven-WEC arrays except $\beta_0 = \frac{3\pi}{8}, \frac{5\pi}{8}$, where it instead represents a local maximum. Corresponding peaks can be seen in the optimal displacements of the WECs in these arrays in most cases, near the same value of $kr \approx 8$. This is particularly pronounced for the grouped devices which have larger displacements in general. These peaks do not represent the largest values of the displacements for $kr \in [5, 15]$, but a clear pattern of peaks at $kr \approx 8$ is visible for most optimal seven-device circular arrays. It is unclear why this behaviour occurs, but it is of little interest due to the relatively large corresponding optimal motions.

The best performing array in this chapter, which obtained the largest average performance is the optimal six-WEC array for $\beta_0 = \frac{\pi}{2}$. This layout achieved an average interaction factor of $I = 1.5921$, which is a subtle improvement of the corresponding six-WEC array for $\beta_0 = 0$, which achieved $I = 1.5910$. These array layouts and their performance differ by very little, with a very slight improvement in the $\beta_0 = \frac{\pi}{2}$ case, probably due to the fixed position of WEC 1. However, these arrays have their best performance of $q \approx 1.7$ for $kr \in [5, 10]$, which correspond the displacements of $|D| > 5$ for all devices. A more modest performance of $q \approx 1.25$ is achieved at the upper end of the domain and is accompanied by smaller motions of $|D| \in [2, 11]$.

It could be proposed that the best overall array is not the one outlined above, for the restricting reasons of closely spaced devices and large motions. Therefore, the optimal six-WEC and seven-WEC arrays for $\beta_0 = \frac{\pi}{4}$ are suggested as good performing arrays overall. Although these arrays both contain a group of three WECs, the other devices are separated and are accompanied by moderate displacement amplitudes, particularly for larger kr. For the upper bound of $kr = 15$, the device motions are $|D| \in [2, 11]$ for both the six-WEC and seven-WEC layouts, suggesting that the imposition of constraints may not have too large an effect on these arrays. Both arrays also have a relatively large range of β-variation where constructive interference in maintained.

Chapter 6 will consider device motion constraints and assess the effect on array performance and optimal array layout for a linear array geometry. This will be achieved by including the device displacements as variables in the objective function, with upper limits imposed on the amplitudes. Possibilities for further work include examining other array geometries, such as triangular and elliptical

layouts. It should be noted that in order to define the mean of the interaction factor over some non-dimensional length, it is necessary to define an array geometry as the mean interaction factor has no sensible definition for general two-dimensional geometries. Further investigation into semicircular array layouts could be conducted and extended to semi-elliptical arrays, as results in this chapter suggest that this may be the optimal case when devices are constrained to such geometries.

Chapter 6

Constrained Optimisations of Linear Arrays in Regular Waves

6.1 Introduction

In earlier chapters, array formations were optimised while permitting optimal motions of the individual WECs. In many cases, this resulted in an optimal array whose members exhibited unacceptably large motions, sometimes of the order of one hundred to one thousand times the wave amplitude. These large motions would create engineering difficulties, as discussed in Chapters 3 - 5. More importantly, they would violate the underlying linear wave theory, which requires that the device motions are at most of the same order of magnitude as the wave motions, which are assumed small in some sense.

In this chapter, an extension of previous optimisations of linear arrays is investigated, where the WEC motions are limited to a specified value, such that linear wave theory remains consistent. Since the amplitude of the non-dimensional device displacements $\mathbf{D}$ must be $\mathcal{O}(1)$, upper limits of $|D_j| \leq 2$ or $|D_j| \leq 3$ are imposed on all WECs within the array. These limits have been considered by Thomas & Evans (1981) and Fitzgerald (2006), who showed that constructive interference is still possible for a constraint of $|D_j| \leq 3$, while a constraint of $|D_j| \leq 2$ may be severely limiting. Most importantly, these upper limits of device motions can be considered to be within the $\mathcal{O}(1)$ requirement for the validity of the underlying theory. A summary of the results of this chapter is given by McGuinness & Thomas (2017a).

6.2 Optimisation Methodology

The optimal interaction factor q can no longer be used within the optimisation for the constrained motions considered, as this assumes optimal motions $\mathbf{D}_{opt} = \frac{i}{2\omega A}\mathbb{B}^{-1}\mathbf{X}$. Therefore, objective functions analogous to equation (4.3) are employed here using the averaged interaction factor $\overline{q}$ (2.169) and/or the generalised interaction factor q_{gen} (2.170).

The same notation for consecutive device separations (ks_j) and reparameterisations thereof (n_j), from Chapter 4, are retained in this chapter. Two objective functions are defined, one as the mean of $\overline{q}$ and the other as the mean of q_{gen}. Including all the relevant variables, the first objective function can be written

$$\overline{I}(\mathbf{n}, \mathbf{D}; \beta_0) = \frac{1}{kL_u - kL_l} \int_{kL_l}^{kL_u} \overline{q}(\mathbf{n}, \mathbf{D}, kL; \beta_0)\ d[kL], \tag{6.1}$$

where $\mathbf{n}$ is an $N-2$ component vector containing all the n_j parameters, such that $\{\mathbf{n}\}_j = n_j$, and $\mathbf{D}$ is an N component vector containing the complex displacements of the devices. Similarly, the q_{gen} variant of this can be written as

$$I_{gen}(\mathbf{n}, \mathbf{D}; D_{1,opt}, \beta_0) = \frac{1}{kL_u - kL_l} \int_{kL_l}^{kL_u} q_{gen}(\mathbf{n}, \mathbf{D}, kL; D_{1,opt}, \beta_0)\ d[kL], \tag{6.2}$$

where $D_{1,opt}$ is the optimal non-dimensional complex displacement of an isolated device subject to constraints. Note that $\overline{I}$ assesses the average performance of the constrained array relative to the same number of unconstrained isolated WECs, while I_{gen} measures the average performance of the constrained array relative to the constrained performance of isolated WECs. Therefore, $I_{gen} \geq \overline{I}$ in general, with equality holding if the optimal single WEC motions do not exceed the applied constraint over the range of kL considered.

Since the displacements $\mathbf{D}$ are complex quantities that contain both the amplitude and phase of the WEC motions, it is beneficial to separate these quantities explicitly for numerical implementation. Let $\boldsymbol{\delta}$ and $\boldsymbol{\psi}$ be N-component real vectors containing the motion amplitudes and phases of each device respectively, so that the non-dimensional complex displacement of the jth device is given by

$$D_j = \delta_j e^{i\psi_j}. \tag{6.3}$$

Using this notation and explicitly including all real variables, the objective

functions are written as

$$\overline{I}(\mathbf{n}, \boldsymbol{\delta}, \boldsymbol{\psi}; \beta_0) = \frac{1}{kL_u - kL_l} \int_{kL_l}^{kL_u} \overline{q}(\mathbf{n}, \boldsymbol{\delta}, \boldsymbol{\psi}, kL; \beta_0) \; d[kL] \tag{6.4}$$

$$I_{gen}(\mathbf{n}, \boldsymbol{\delta}, \boldsymbol{\psi}; \delta_{1,opt}, \psi_{1,opt}, \beta_0) = \frac{1}{kL_u - kL_l} \int_{kL_l}^{kL_u} q_{gen}(\mathbf{n}, \boldsymbol{\delta}, \boldsymbol{\psi}, kL; \delta_{1,opt}, \psi_{1,opt}, \beta_0) \; d[kL], \tag{6.5}$$

where $D_{1,opt} = \delta_{1,opt} e^{i\psi_{1,opt}}$. In the above expressions, the optimisation variables are listed first and the prescribed fixed constants of the optimisation follow the semi-colon. In each optimisation, there are $2N$ displacement variables (δ_j and ψ_j) and $N-2$ position variables (n_j), giving a total of $3N-2$ variables upon which these objective functions depend. These functions will be maximised using a similar procedure to that in Chapter 4, with appropriate constraints placed on the variables. If δ_{max} denotes the upper limit of displacement constraint applied, then $\delta_{max} = 2$ or 3 is applied.

The displacement amplitude δ_j is required to be positive by definition, so for a maximum displacement constraint of δ_{max}, the range of the displacement variables would be $0 \leq \delta_j \leq \delta_{max}$ and $0 \leq \psi_j \leq 2\pi$. However, this is equivalent to allowing the amplitude to be both positive and negative, and restricting the phase to $0 \leq \psi_j \leq \pi$. Since the ψ_j variables are contained within a complex exponential expression, the variation over this variable within the optimisation would be more computationally intensive than variation over δ_j, albeit only slightly. However, given the large number of calls to the objective function and the large number of iterations of the optimisation necessary, every effort was made to make the calculations as efficient as possible. Therefore, in this implementation, a new variable $\widetilde{\delta}_j$ is introduced and the displacements are written as

$$D_j = \widetilde{\delta}_j e^{i\psi_j}. \tag{6.6}$$

If δ_{max} is a given amplitude constraint, then the limits on the displacement variables are $-\delta_{max} \leq \widetilde{\delta}_j \leq \delta_{max}$ and $0 \leq \psi_j \leq \pi$ for $j = 1, \ldots, N$.

The optimal isolated WEC displacement is found from maximising the absorption length of an isolated device. Therefore, the optimal values $\widetilde{\delta_{1,opt}}$ and

Table 6.1: Optimum isolated WEC displacement parameters

Constraint	$\widetilde{\delta_{1,opt}}$	$\psi_{1,opt}$
$\delta \leq \infty$	-3.30738	1.72658
$\delta \leq 3$	-3	1.72658
$\delta \leq 2$	-2	1.72658

$\psi_{1,opt}$ are found from the following maximisation

$$\max_{\substack{|\widetilde{\delta_1}| \leq \delta_{max} \\ 0 \leq \psi_1 \leq \pi}} \left[-4\pi(ka) \left(\mathrm{Re}[(\mathcal{D} + i\mathcal{C})\widetilde{\delta_1} e^{i\psi_1}] + \pi(ka)(\mathcal{C}^2 + \mathcal{D}^2)\widetilde{\delta_1}^2 \right) \right]. \tag{6.7}$$

The values of $\widetilde{\delta_{1,opt}}$ and $\psi_{1,opt}$ are listed for the unconstrained case and for both constrained cases in table 6.1. Note that the phase in each case is $\psi_{1,opt} = 1.72658$, which corresponds to approximately 0.549587π.

Throughout this procedure, the non-dimensional radius of the WECs is assumed to have a fixed value of $ka = 0.4$ in line with previous chapters. This value is chosen as a typical case that is within the point absorber regime and is applied to the implementation of both objective functions.

To enable comparison with the results of Chapter 4, the optimisations are performed using both objective functions $\overline{I}$ and I_{gen} with respect to the layout of the array. It was found that the optimisations involving I_{gen} produced the same optimal array layouts as those for $\overline{I}$. The optimal performance as described by q_{gen} was found to be a slightly increased version of the optimal $\overline{q}$, with both following the same overall performance patterns. This is to be expected given the definitions of the interaction factors (equations (2.154) and (2.155)) and the results in table 6.1, as the application of constraints reduces the single WEC performance slightly, which affects the denominator of q_{gen}. Thus, there is no significant difference between the results obtained by the use of either objective function.

Both $\overline{q}$ and q_{gen} measure the constrained performance of the array relative to the performance of isolated devices. However, $\overline{q}$ compares the array performance to unconstrained isolated WECs, while the denominator of q_{gen} is the constrained isolated WEC performance. Thus, q_{gen} gives a more realistic measure of array interaction when considered alone. However, $\overline{q}$ (and hence $\overline{I}$) would give a better comparison between the unconstrained and constrained regimes, as both q and $\overline{q}$ contain the same denominator. Since the implementation of the I_{gen}

optimisations require greater computational effort and provide no further insight, attention is restricted to the $\overline{I}$ optimisations which allow a better direct comparison to the unconstrained results of Chapter 4.

Two cases are examined within this chapter. Firstly, the constrained performance of unconstrained optimal array layouts from Chapter 4 is assessed in Section 6.3.1. Writing $\mathbf{n}^*$ as the unconstrained optimal layout, the objective function can be written

$$\overline{I}(\boldsymbol{\delta}, \boldsymbol{\psi}; \mathbf{n}^*, \beta_0) = \frac{1}{kL_u - kL_l} \int_{kL_l}^{kL_u} \overline{q}(\boldsymbol{\delta}, \boldsymbol{\psi}, kL; \mathbf{n}^*, \beta_0) \; d[kL]. \tag{6.8}$$

Since the WEC positions are prescribed, there is a total of $2N$ variables in this optimisation. Secondly, in Section 6.3.2, the array layout is not prescribed and an optimisation is performed over both the WEC motions and positions. Finally, a discussion of the results is given in Section 6.4, together with conclusions.

The optimisation algorithm involves a similar procedure to that in Chapter 4 and is performed using NAG routine E04UCF[1]. An exhaustive search procedure of the set of possible starting points is again used, with all possible combinations of $n_l \in \{0.1, 0.2, \ldots, 0.7\} \cup \psi_j \in \{0, \frac{\pi}{2}, \pi\} \cup \widetilde{\delta}_j \in \{-3, -1, 1, 3\}$ for $l = 1, \ldots, 4$ and $j = 1, \ldots, 5$ examined for the upper constraint $\delta \leq 3$. For the lower constraint $\delta \leq 2$, the set of starting points for WEC motion amplitude was taken to be $\widetilde{\delta}_j \in \{-2, 0, 2\}$. It was found that the optimisation behaved satisfactorily with respect to the starting values of $\widetilde{\delta}_j$ and ψ_j, hence the relatively sparse sampling of starting points of these variables.

As in Chapters 4 and 5, the exhaustive search outlined above involves many iterations of the optimisation routine. The results are summarised in this chapter with the best results chosen for analysis. For brevity, the detailed optimisation results are omitted from this chapter and are provided in Appendix D.

[1]https://www.nag.co.uk/numeric/fl/manual/pdf/E04/e04ucf.pdf

Table 6.2: Performance of optimal layouts from Chapter 4 subject to motion constraints

β_0	n_1^*	n_2^*	n_3^*	n_4^*	$I_{opt}(\delta \leq \infty)$	$\overline{I}_{opt}(\delta \leq 3)$	$\overline{I}_{opt}(\delta \leq 2)$
0	0.0500	0.0500	0.0500	0.8500	1.4802	0.5469	0.4691
$\frac{\pi}{4}$	0.0500	0.8500	0.0500	0.0500	1.1431	0.3070	0.2624
$\frac{\pi}{2}$	0.0500	0.2252	0.3859	0.3359	1.3643	0.9486	0.7693

6.3 Constrained Optimisation Results

6.3.1 Comparison of Unconstrained Optimal Layout

The constrained performance of the optimal formation of an array of five devices in a linear geometry, previously considered in Chapter 4 and McGuinness & Thomas (2016), is now examined. With the optimal spacing denoted by $\mathbf{n}^*$, the array is subject to the direction of the incident waves. Since the layout is prescribed before the optimisation, there are ten optimisation variables for $N = 5$ devices, namely the amplitudes $\widetilde{\delta}_j$ and phases ψ_j of the displacements of each WEC. The objective function is given by (6.8) and is maximised with respect to these variables subject to the limits enforced. The increased number of variables in this optimisation requires a considerable increase in computational effort and only results pertaining to $\beta_0 = 0, \frac{\pi}{4}, \frac{\pi}{2}$ are presented in this chapter.

Table 6.2 lists the optimal layouts $\mathbf{n}^*$ from the unconstrained optimisation in Chapter 4, together with the performance of these arrays in the unconstrained case and a motion constraint of $\delta \leq 2$ or $\delta \leq 3$ is enforced. The optimal values of the displacement variables $\widetilde{\delta}_j$ and ψ_j are also listed in table 6.3. The computation time for each case examined in this section was of the order of one to five minutes. This was due to the exhaustive search and optimisation routines scanning over ten variables.

As expected, performance is considerably poorer when constraints are applied, with the lower constraint having a greater impact. Where $\beta_0 = 0$ or $\frac{\pi}{4}$, the application of the $\delta \leq 3$ constraint causes a reduction in performance of between 63% and 73%, with only a further small difference between $\delta \leq 2$ and $\delta \leq 3$. This is probably due to the presence of grouped devices in these layouts and the associated large optimal WEC motions. Since the optimal motions are

Table 6.3: Optimal WEC displacement parameters for optimal layouts from Chapter 4 subject to constraints

β_0	δ_{max}	$\widetilde{\delta}_1$	$\widetilde{\delta}_2$	$\widetilde{\delta}_3$	$\widetilde{\delta}_4$	$\widetilde{\delta}_5$	ψ_1	ψ_2	ψ_3	ψ_4	ψ_5
0	2	-2.0000	-2.0000	2.0000	2.0000	-0.5326	0.8933	1.7679	0.0542	1.0235	2.5317
	3	-3.0000	-3.0000	-3.0000	3.0000	-0.5174	0.5977	1.8731	3.1236	1.3434	2.6386
$\frac{\pi}{4}$	2	-2.0000	-2.0000	-1.2500	2.0000	-1.4587	1.1384	2.6780	1.5186	0.8910	0.1221
	3	-3.0000	-3.0000	-1.6884	3.0000	-1.9200	0.8875	2.9290	1.3618	0.8832	0.3028
$\frac{\pi}{2}$	2	-2.0000	-1.1760	-2.0000	-2.0000	-2.0000	1.7266	1.7266	1.7266	1.7266	1.7266
	3	-3.0000	-0.1103	-3.0000	-3.0000	-3.0000	1.7266	1.7266	1.7266	1.7266	1.7266

predicted to be $\mathcal{O}(100) - \mathcal{O}(1000)$ from Chapter 4, it is expected that limiting the motions to $\mathcal{O}(1)$ would have a large effect on array performance. This also explains the relatively small difference between the two constraints, as the relative difference between $\delta = 2$ or 3 and $\delta = \mathcal{O}(100) - \mathcal{O}(1000)$ is also small.

The application of constraints has a smaller impact on the $\beta_0 = \frac{\pi}{2}$ array, as was anticipated in Chapter 4. This is due to the larger spacing between most of the devices in this layout and the smaller associated motions. The application of the $\delta \leq 3$ and $\delta \leq 2$ constraints is associated with performance losses of 30.5% and 43.6% respectively. Given these fixed layouts, it does not appear to be possible to maintain average constructive interference ($\overline{I} > 1$) after the application of constraints; although moderate performance of $\overline{I} = 0.94859$, albeit slightly destructive, is achieved for $\beta_0 = \frac{\pi}{2}$ with $\delta \leq 3$.

Table 6.3 shows that the majority of the amplitude variables $\widetilde{\delta}_j$ attained the enforced limit of ± 2 or ± 3. All optimal arrays resulted in one or two of the δ_j values smaller than the limit and requiring some value in the centre of the allowed range. This indicates that within the constrained problem, the best solution does not result from simply setting all device amplitudes to their largest allowed values. The optimal case appears to be when one or two WECs oscillate at a slightly smaller amplitude, which appears to improve interference. This could be an artifact of forcing the WECs to be arranged in a layout which was optimised for unconstrained motions. The displacement phases of each WEC are all different within each optimal solution found, with the obvious exception of the $\beta_0 = \frac{\pi}{2}$ array. For both constraints applied, all the WEC phases were equal in the optimal beam seas array.

Table 6.4: Optimal linear array layout parameters subject to motion constraints

β_0	δ_{max}	$n_{opt,1}$	$n_{opt,2}$	$n_{opt,3}$	$n_{opt,4}$	$\overline{I}_{opt}$
0	2	0.0978	0.0532	0.1139	0.7351	0.49441
	3	0.1057	0.0504	0.1048	0.7391	0.58438
$\frac{\pi}{4}$	2	0.0940	0.1532	0.2259	0.5269	0.42508
	3	0.1310	0.3066	0.1103	0.4521	0.45507
$\frac{\pi}{2}$	2	0.2679	0.2321	0.2321	0.2679	0.87771
	3	0.2679	0.2321	0.2321	0.2679	1.06779

6.3.2 Undetermined Layout

A more detailed analysis of the constrained performance of these arrays is now undertaken, where the array layout is allowed to vary within a constrained optimisation. The performance of the array layouts, identified previously as optimal in the unconstrained optimisation, are then compared to the performance of the arrays where the WEC positions are not fixed and are also fed into the optimisation as variables.

The optimisation is without a prescribed layout, so that the array formation and the device displacements are variables of the optimisation, giving a total of $3N - 2 = 13$ variables for $N = 5$ WECs. This is performed for two different maximum displacement constraints of $\delta \leq 2, 3$ and the three values of prescribed incident wave angle $\beta_0 = 0, \frac{\pi}{4}, \frac{\pi}{2}$. The results of the optimisations are summarised in table 6.4 and the corresponding optimal values of $\widetilde{\delta}_j$ and ψ_j are listed in table 6.5. The detailed results of the optimisations are provided in tables D.1 - D.6 of Appendix D, where all solutions found by the optimisation are listed. These tables are omitted from this chapter for brevity and only the best cases found by the optimisation are presented and examined. The optimal constrained layouts are denoted as $\mathbf{n}_{opt}$. In this section, the computation times for each case examined was of the order of one hour. The increase in computation time was due to the exhaustive search and optimisation routines scanning over 13 variables, three more variables than the optimisation in Section 6.3.1. These three extra WEC position variables also required a finer scan within the exhaustive search routine, further adding to the computational effort.

As in the procedure employed in McGuinness & Thomas (2016), minimum and maximum values of each separation parameter were enforced within the

Table 6.5: Optimal WEC displacement parameters for constrained optimal layouts in table 6.4

β_0	δ_{max}	$\widetilde{\delta}_1$	$\widetilde{\delta}_2$	$\widetilde{\delta}_3$	$\widetilde{\delta}_4$	$\widetilde{\delta}_5$	ψ_1	ψ_2	ψ_3	ψ_4	ψ_5
0	2	-2.0000	-2.0000	2.0000	2.0000	-0.5044	0.9841	2.6244	0.3064	2.0858	2.5309
	3	-3.0000	-3.0000	3.0000	3.0000	-0.4828	0.7737	2.6660	0.3878	2.4455	2.5965
$\frac{\pi}{4}$	2	-2.0000	-2.0000	2.0000	1.5094	0.5083	1.1987	2.6658	0.5846	1.9964	2.0989
	3	-3.0000	3.0000	2.4695	-1.7879	0.5566	1.2333	0.1285	1.0368	0.2747	2.4616
$\frac{\pi}{2}$	2	-2.0000	-2.0000	-2.0000	-2.0000	-2.0000	1.7266	1.7266	1.7266	1.7266	1.7266
	3	-3.0000	-3.0000	-3.0000	-3.0000	-3.0000	1.7266	1.7266	1.7266	1.7266	1.7266

optimisation so that $0.05 \leq n_l \leq 0.85$ for $l = 1, \ldots, 4$. This ensures that no device will be within 5% of the total array length of another device. The upper bound of 0.85 was chosen to allow the possibility that all but one of the separations was exactly the minimum bound. A 5% minimum constraint was chosen as this value also avoided possible difficulties due to numerical inaccuracies and poor behaviour of the objective function caused by small non-dimensional separation arguments. It is also a physically reasonable lower bound on WEC separation distances.

In the following subsections, the unconstrained optimal layout $\mathbf{n}^*$ and the constrained optimal layouts $\mathbf{n}_{opt}$ are presented for each of $\beta_0 = 0, \frac{\pi}{4}$ and $\frac{\pi}{2}$; the performance of the arrays are also analysed for variation in kL and β respectively. There are five curves in each $\overline{q}$ plot for each value of β_0 and these are intended to show the performance of the unconstrained optimal array $q(\mathbf{n}^*)$, the constrained arrays with the unconstrained optimal layout $\overline{q}(\mathbf{n}^*)$ for both $\delta \leq 2$ and $\delta \leq 3$ and the optimal constrained arrays with re-optimised layouts $\overline{q}(\mathbf{n}_{opt})$ for both $\delta \leq 2$ and $\delta \leq 3$.

It is anticipated *a priori* that each constrained array would perform poorer that the unconstrained equivalent and it is also expected that

$$\overline{I}(\mathbf{n}_{opt}, \delta \leq 3) > \overline{I}(\mathbf{n}^*, \delta \leq 3) > \overline{I}(\mathbf{n}_{opt}, \delta \leq 2) > \overline{I}(\mathbf{n}^*, \delta \leq 2). \tag{6.9}$$

However, it is unclear how sharp the inequalities will be, i.e. how close to equality they can become. It is only by consideration of the individual cases that this information can be obtained.

Similar conclusions to the previous section can be drawn from table 6.5, where the majority of δ_j values require the limit of δ_{max} imposed. In head and intermediate seas, one or two δ_j did not converge to the maximum allowed value

and all WECs have different phases ψ_j. However, in beam seas, $\delta_j = \delta_{max}$ and the phases are equal for all WECs, as would be expected. This is unlike the results in table 6.3, since in this case the WECs were optimised for constrained motions. Thus for beam seas, where the wave hits all WECs at the same time, the array is contrived such that the displacement limit is reached for all WECs, thereby maximising power capture. Furthermore, it should be noted that the optimal array layout in beam seas is symmetric about the middle device for both applied constraints.

6.3.2.1 Head Seas $\beta_0 = 0$

Figure 6.1 shows the unconstrained optimal layout ($\mathbf{n}^*$) and the constrained optimal layouts ($\mathbf{n}_{opt}$) for the general layout optimisation in head seas. The constrained optimal layouts for both constraints are very similar, so the diagram corresponding to $\delta \leq 3$ is omitted. The detailed optimisation results for $\beta_0 = 0$ are listed in Appendix D in tables D.1 and D.2 for $\delta \leq 2$ and $\delta \leq 3$ respectively.

As in Section 6.3.1, it is clear that the imposition of constraints has a large impact on the performance of the array, with the best arrays achieving $\overline{I} = 0.49441, 0.58438$ for $\delta \leq 2, 3$ respectively. This is a reduction in performance of between 60.5% and 66.6% relative to the corresponding unconstrained array. Allowing the array layout to be optimised in the constrained regime results in different spacings, where the group of four devices becomes slightly more separated. This is probably due to a similar physical explanation, as given in Chapter 4. Since the devices can no longer oscillate at as large an amplitude, maximum constructive interference cannot be achieved by simply allowing the devices as close as possible. It seems a slightly more separated layout enables the best interaction to be achieved with the amplitude limits enforced. Note that WECs 2 & 3 are still placed very close together, which may still cause some physical difficulties such as shadowing and possible collisions.

The performance of the arrays under consideration is shown in figures 6.2 and 6.3 for variation in kL and β respectively. The performance of all constrained arrays are much poorer compared to the unconstrained case. Overall, the best constrained array is the $\mathbf{n}_{opt}, \delta \leq 3$ array, as expected. In general, the $\delta \leq 3$ arrays perform better than the $\delta \leq 2$ arrays; while within this pattern the $\mathbf{n}_{opt}$ layouts perform better then the $\mathbf{n}^*$ ones. There are some specific values of kL where this pattern is broken, though this pattern holds when performance over

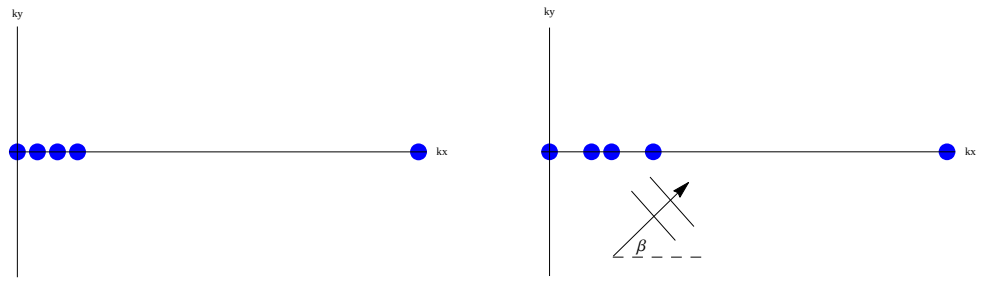

(a) Unconstrained (b) $\delta \leq 2, 3$

Figure 6.1: Constrained and unconstrained optimal linear arrays for $\beta_0 = 0$. The optimal layout for the $\delta \leq 3$ case is very similar to the $\delta \leq 2$ case and is omitted for clarity

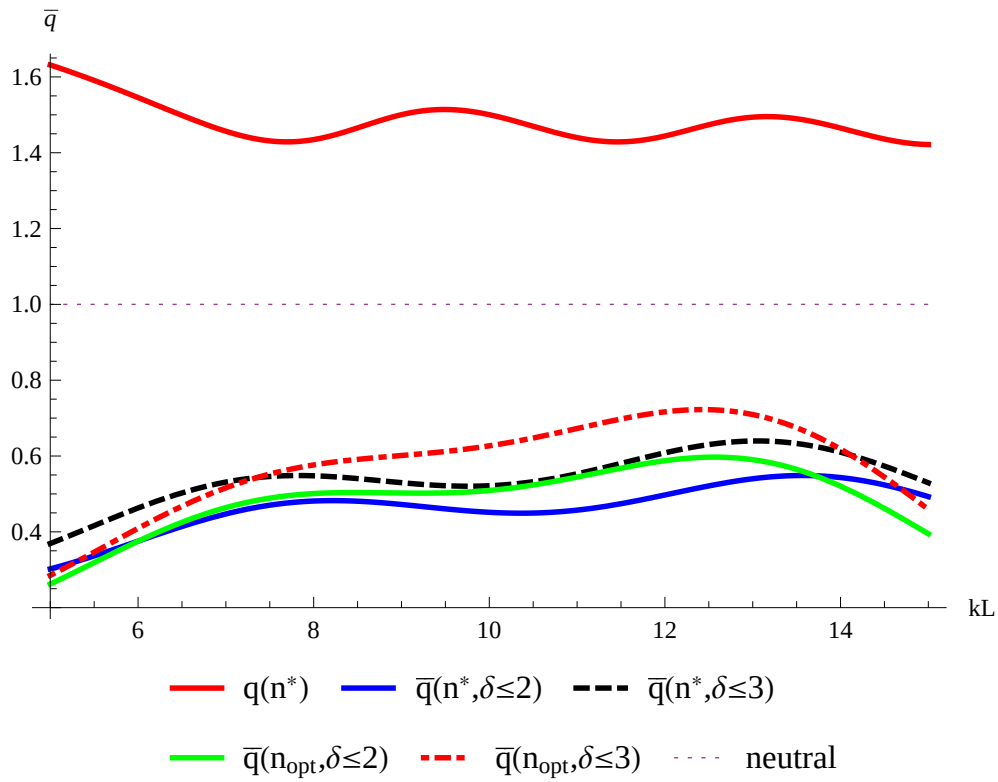

Figure 6.2: Performance of constrained and unconstrained linear arrays for variation in kL with $\beta = \beta_0 = 0$

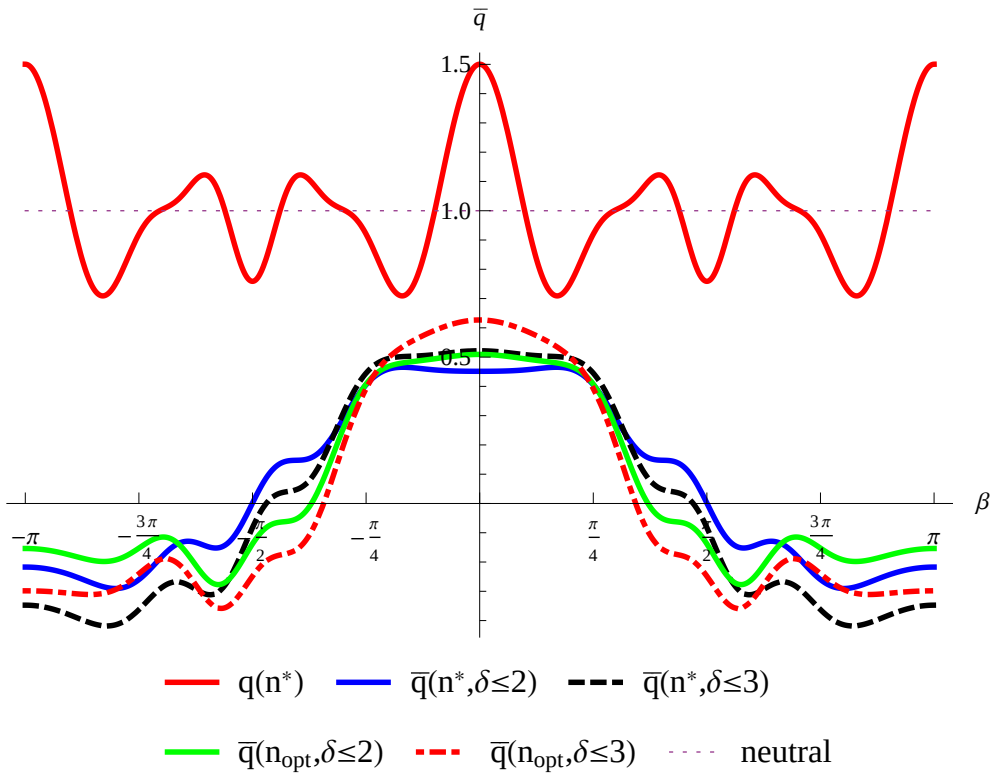

Figure 6.3: Performance of constrained and unconstrained linear arrays for variation in β with $\beta_0 = 0$ and $kL = 10$

the entire range of $kL \in [5, 15]$ is considered.

From figure 6.2, the overall behaviour of the constrained arrays is seen to be similar to the unconstrained array, in that there is small variation throughout $kL \in [5, 15]$. Interestingly, from figure 6.3, it is clear the the constrained arrays have a much broader peak performance in β-variation than the unconstrained array, although the peak is much lower. The unconstrained array has a range of approximately $\pm\frac{\pi}{8}$ where $q > 1$, while the constrained arrays have a large range of $\pm\frac{\pi}{4}$ where $\overline{q} \approx 0.5$. This coupled with the low variation of $\overline{q}$ with kL suggests a large stability of performance for these constrained arrays, although the performance achieved is rather poor in comparison to the optimal performance of the same number of isolated devices. It should also be noted from figure 6.3 that the $\overline{q}$ values become negative outside a certain range, indicating a that the power absorbed by the array is negative in this constrained case and the WECs are injecting power into the waves rather than absorbing power.

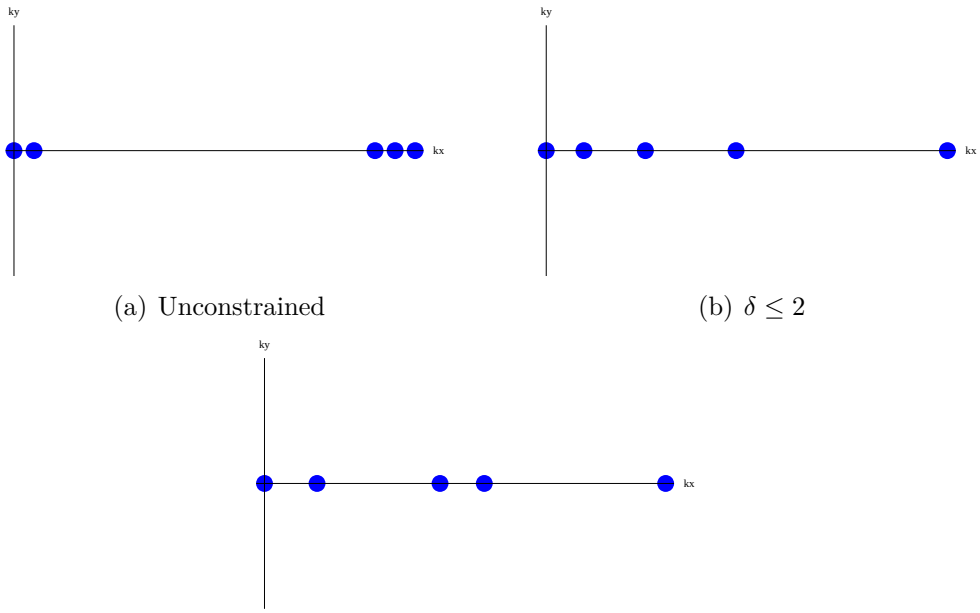

(a) Unconstrained (b) $\delta \leq 2$

(c) $\delta \leq 3$

Figure 6.4: Constrained and unconstrained optimal linear arrays for $\beta_0 = \frac{\pi}{4}$.

6.3.2.2 Intermediate Seas $\beta_0 = \frac{\pi}{4}$

Figure 6.4 illustrates the unconstrained and constrained optimal layouts for the $\beta_0 = \frac{\pi}{4}$ case, while tables D.3 and D.4 in Appendix D give the detailed optimisation results for $\delta \leq 2$ and $\delta \leq 3$ respectively. As for head seas, the optimal constrained arrays are more separated than the unconstrained optimal layout. However, the optimal layouts corresponding to $\delta \leq 2$ and $\delta \leq 3$ differ. In both constrained cases, WEC 5 is relatively isolated at the right of the array. For the $\delta \leq 2$ array, WECs 1 - 4 have an increasing separation between them, with the smallest separation between WECs 1 & 2 being 9.4% of the total length. In contrast, the $\delta \leq 3$ array has two pairs of devices approximately $0.11kL - 0.13kL$ apart, with the distance between the pairs being approximately $0.3kL$.

Figures 6.5 and 6.6 show the performance of all constrained arrays, together with the unconstrained case, with kL and β-variation respectively for $\beta_0 = \frac{\pi}{4}$. As for head seas, the application of amplitude constraints has a considerable detrimental effect on the array performance, with an overall reduction from $q \in [0.9, 1.3]$ to $\overline{q} \in [0.1, 0.6]$. This is probably due to the presence of closely spaced groups of WECs and the associated large motions in the optimal unconstrained case.

The expected trend of $\delta \leq 3$ outperforming $\delta \leq 2$ is not maintained, as it is

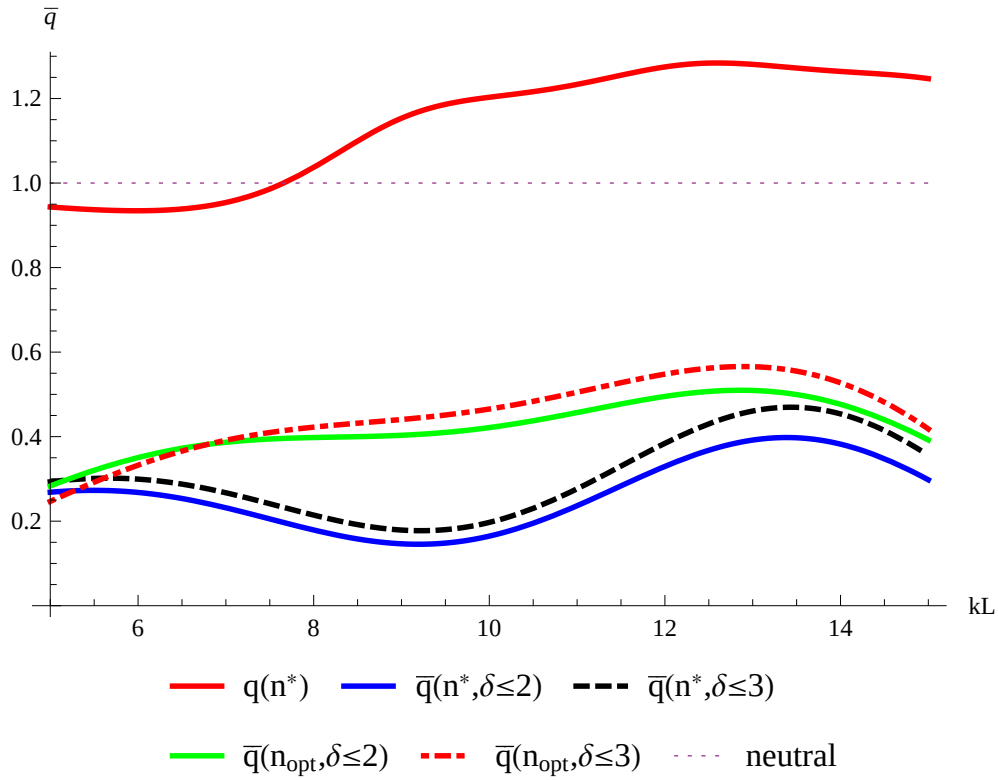

Figure 6.5: Performance of constrained and unconstrained linear arrays for variation in kL with $\beta = \beta_0 = \frac{\pi}{4}$

clear from figure 6.5 that $\overline{q}(\mathbf{n}_{opt}, \delta \leq 2) > \overline{q}(\mathbf{n}^*, \delta \leq 3)$. This is perhaps because the optimal array layout is noticeably different when constraints are applied. Therefore, applying constraints to the unconstrained optimal layout may result in very poor performance. This figure also shows that

$$\overline{I}(\mathbf{n}_{opt}, \delta \leq 3) > \overline{I}(\mathbf{n}_{opt}, \delta \leq 2) > \overline{I}(\mathbf{n}^*, \delta \leq 3) > \overline{I}(\mathbf{n}^*, \delta \leq 2),$$

in contrast with the expectation (6.9) and the results of the head seas case.

As with head seas, figure 6.5 shows that the constrained array performance varies relatively slowly with kL. This indicates that the performance of the array is relatively stable to changes in kL, although a large reduction in interaction factor is again seen when constraints are imposed. Examination of figure 6.6 shows a similar behaviour to head seas, where a broader performance with respect to β is achieved around $\beta = 0$. This is not beneficial, as the target wave angle is $\beta_0 = \frac{\pi}{4}$, around which are significant variations in $\overline{q}$. This is particularly evident for $|\beta| > \frac{\pi}{4}$, where the $\mathbf{n}_{opt}$ arrays give $\overline{q} < 0$ for $|\beta| > \frac{3\pi}{8}$. The $\mathbf{n}^*$ arrays are slightly more stable around the target wave angle, although

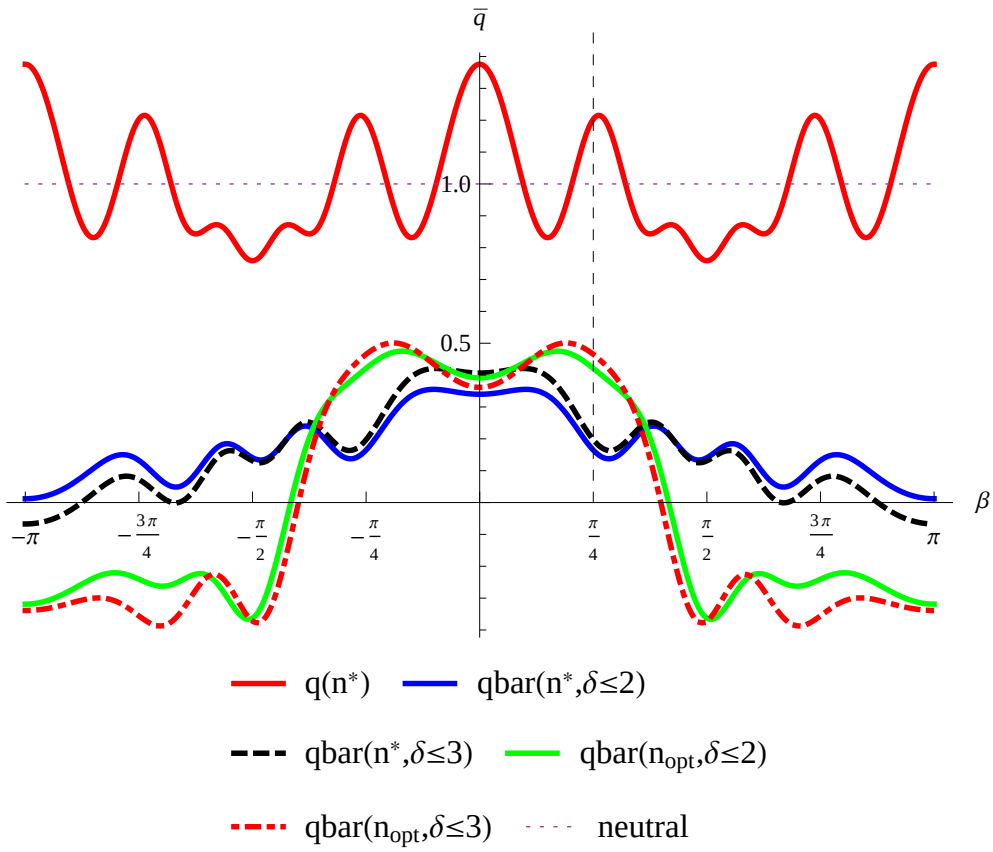

Figure 6.6: Performance of constrained and unconstrained linear arrays for variation in β with $\beta_0 = \frac{\pi}{4}$ and $kL = 10$

the performance of these arrays is not as high as the $\mathbf{n}_{opt}$ arrays.

6.3.2.3 Beam Seas $\beta_0 = \frac{\pi}{2}$

Figure 6.7 shows the optimal constrained and unconstrained array layouts for beam seas. The optimal array layout in both the constrained cases is very close to a uniform array. This reinforces the idea that constrained arrays tend to have their optimal layouts more widely spaced apart, avoiding groups of WECs, with the exception of head seas. It is also consistent with the idea that greater frontage to the waves gives greater power absorption, since an array with greater frontage to the incident wave has a greater amount of wave-power incident upon it. However, as shown in previous studies, this is not always equivalent into increased power absorption or better WEC interference.

The detailed constrained optimisation results are given in Appendix D in tables D.5 and D.6 for $\delta \leq 2$ and $\delta \leq 3$ respectively. Most notably, these tables only

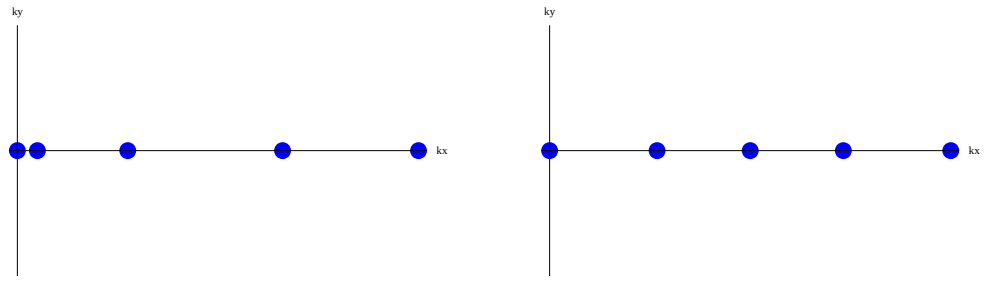

(a) Unconstrained (b) $\delta \leq 2, 3$

Figure 6.7: Constrained and unconstrained optimal linear arrays for $\beta_0 = \frac{\pi}{2}$. The optimal layout for $\delta \leq 3$ is identical to the $\delta \leq 2$ case and is omitted for clarity

contain one entry; this is because each run of the optimisation for different combinations of starting parameters converged to one optimal solution, or an analogous one by symmetry. Similar behaviour of the optimisation was observed in the unconstrained beam seas case, where only two optimal solutions were attained by the routine. This suggests that the optimal solutions, constrained or otherwise, are relatively stable for $\beta_0 = \frac{\pi}{2}$, since there is only one or two optimal layouts found. The condition $\overline{I} > 1$ is achieved for the $\delta \leq 3$ constraint at this wave angle; this is the only case where average constructive interference is maintained after the application of constraints on a linear array.

The performance of the arrays for beam seas are shown in figures 6.8 and 6.9 for variation in kL and β respectively. Both figures show that the application of constraints do not have as severe a negative impact on $\overline{q}$ in comparison to other wave angles. A loss is seen for the $\overline{q}$ values compared to q but constructive interference is still achieved in some cases. As with $\beta_0 = 0$, a constraint of $\delta \leq 2$ has a greater impact on performance than $\delta \leq 3$; within this pattern, the $\mathbf{n}_{opt}$ arrays perform better than the $\mathbf{n}^*$ layouts, so that (6.9) holds true as expected.

As in the previous two configurations, figure 6.8 shows the slow variation of $\overline{q}$ with kL, indicating that a small change in kL produces only a small change in array performance. In general, this figure shows the better performance is achieved for larger values of kL within the domain examined. Constructive interference $\overline{q} > 1$ is achieved for the $\delta \leq 3$ arrays, while the best case for $\delta \leq 2$ is $\overline{q} \approx 1$ at $kL = 15$ for the $\mathbf{n}_{opt}$ layout. Both configurations with $\delta \leq 2$ resulted in $\overline{q} \leq 1$. The fact that $\overline{q}(\mathbf{n}_{opt}, \delta \leq 3) \approx 1.2$ for $kL \in [10, 15]$ is promising, as this indicates that constructive interference is still possible after the imposition of a reasonable constraint. This layout is also almost uniformly-spaced and so avoids the problems associated with closely spaced devices.

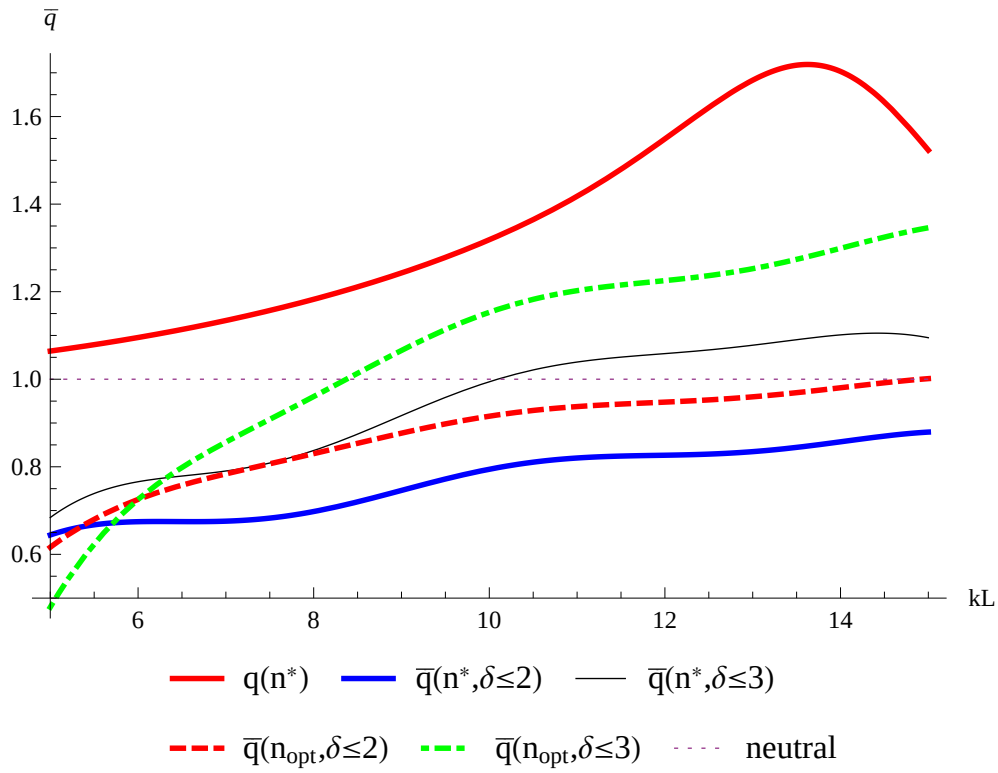

Figure 6.8: Performance of constrained and unconstrained linear arrays for variation in kL with $\beta = \beta_0 = \frac{\pi}{2}$

The β-variation of the array performances are shown in figure 6.9. Contrary to head and intermediate seas, the imposition of constraints results in a narrower peak performance around $\beta = \beta_0 = \frac{\pi}{2}$ compared to the unconstrained case. A high peak value is achieved with $\max[\overline{q}] \in [0.8, 1.2]$ depending on the constraint and layout but the peak is significantly narrower. This results in $\overline{q} < 0$ for a relatively small change of $\beta_0 \pm \frac{\pi}{12}$, which may be undesirable and is highly dependent upon the angular variation within the incident wave-field.

The results of figure 6.8 can be compared with the work on constrained motion performance of the uniform array in Thomas & Evans (1981). In both cases, the constrained array examined is almost identical in geometry, since the constrained array presented here ($\mathbf{n}_{opt}$) for beam seas is almost uniform. Note in Thomas & Evans (1981) that the quantity examined is the absorption length scaled by the total WEC covering in the array $\frac{l_{abs}}{10a}$. Furthermore, this quantity was assessed with respect to variation in the device spacing kd, not the array length kL. Agreement is seen, however, in the overall performance of the array with respect to the application of constraints, i.e. an application of a constraint of three times the wave amplitude still allows for constructive interference, while

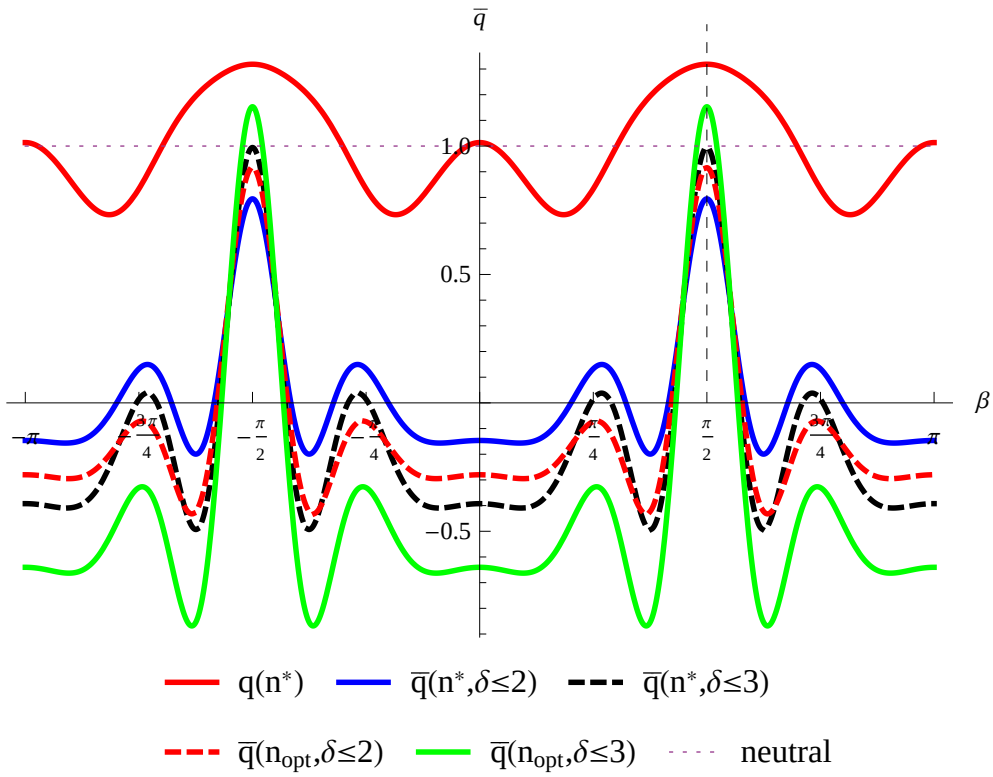

Figure 6.9: Performance of constrained and unconstrained linear arrays for variation in β with $\beta_0 = \frac{\pi}{2}$ and $kL = 10$

a constraint of twice the wave amplitude is severely limiting and results in destructive interference dominating.

6.4 Discussion of Results

This chapter considers the extension of linear arrays to where the WECs are constrained to oscillate at most two or three times the incident wave amplitude. This is necessary as most of the optimal arrays resulted in predicted optimal displacement amplitudes well in excess of the incident wave amplitude. Such large displacements would not only cause significant physical and engineering difficulties but also violate the underlying linear wave theory, which assumes WEC motions are at most the same order of magnitude as the wave motions and are assumed small in some sense.

Initially, two different objective functions $\overline{I}$ and I_{gen} were defined for the constrained arrays and which depended on two quality measures, namely the averaged interaction factor $\overline{q}$ and the generalised interaction factor q_{gen}

respectively. Although the numerical calculations in this chapter were performed using both the averaged and generalised objective functions, the findings related to I_{gen} are omitted. These results follow the same overall patterns of $\overline{I}$ and so their inclusion would not be additionally informative; for $\delta \leq 3$, the averaged and generalised results were almost identical. This was because the optimal performance of an isolated device resulted in an optimal motion amplitude of $\delta_{1,opt} \approx 3.307$, which is only slightly greater than the imposed constraint of $\delta \leq 3$. A noticeable difference was seen for the lower constraint of $\delta \leq 2$ but the behaviour of I_{gen} and q_{gen} were merely slightly increased versions of $\overline{I}$ and $\overline{q}$. Both objective functions produced identical optimal array layouts and the resulting performances, as measured by either $\overline{q}$ or q_{gen}, followed similar patterns.

The imposition of constraints had a significant impact on array performance, particularly when optimal performance was accompanied by very large device motions. In previous chapters, the impression of good performance was given by the large values of q achieved. However, these were accompanied in most cases by unacceptably large motion amplitudes. Therefore, the application of constraints was expected to have a large negative impact on array performance. This was particularly true with groups of closely spaced devices, which were associated with the largest predicted optimal motions.

This effect is most clearly seen by comparing the results of head seas and beam seas in figures 6.1 and 6.7. The $\beta_0 = 0$ unconstrained optimal layout from Chapter 4 contained a close group of four devices and predicted very unrealistic motions of the order of 1000 times the wave amplitude. When constraints are applied, the array performance is reduced by approximately 60% and resulted in the domination of destructive interference ($\overline{q} < 1$). In contrast, the $\beta_0 = \frac{\pi}{2}$ unconstrained optimal array was more spaced, although it still contained a closely spaced pair of WECs. The application of constraints resulted in a smaller performance reduction of approximately 30% (for $\delta \leq 3$) and allowed the possibility of constructive interference ($\overline{q} > 1$).

When the array layout parameters were added as optimisation variables, noticeably different layouts were obtained in comparison to the unconstrained optimisation ($\mathbf{n}^* \neq \mathbf{n}_{opt}$). This resulted in a more separated layout in each case, which reduced the number closely spaced WECs within the array or eliminated these groups of WECs altogether. For $\beta_0 = 0$, the constrained optimal layout separated the group of four devices slightly but still retained a closely spaced

pair. This was very similar for both $\delta \leq 2$ and $\delta \leq 3$. In the intermediate case of $\beta_0 = \frac{\pi}{4}$, no closely spaced devices remained in the constrained optimal layouts. Most notably, the different constraints resulted in significantly different optimal layouts at this wave angle. A symmetric and almost uniform layout was found to be optimal when the constraints were applied in the beam seas case, with the exact same layout found for both $\delta \leq 2$ and $\delta \leq 3$. This optimisation eliminated the pair of closely spaced devices on the left of the unconstrained optimal layout for this wave angle. This was also the best performing constrained array with the largest $\overline{I}$ for both constraints, with mean constructive interference ($\overline{I} > 1$) maintained for the $\delta < 3$ constraint. The finding that the optimal array layout changes with the imposed constraint agrees with the result of Garcia-Rosa, Bacelli, & Ringwood (2015), which shows that the control problem is related to the array layout problem.

Although both constraints considered were within the $\mathcal{O}(1)$ regime, the $\delta \leq 2$ constraint had a more severe detrimental impact on array performance; this was not unexpected. In general, the arrays with the $\delta \leq 3$ constraint performed better than the $\delta \leq 2$ arrays, with varying differences between these depending on the wave angle and layout considered. Previous studies, such as Thomas & Evans (1981) and Fitzgerald (2006), have discussed how the imposition of a constraint of three times the wave amplitude still allows for constructive interference in some cases, while a constraint of two times the wave amplitude is severely restrictive. This idea is echoed here, where $\delta \leq 2$ had a greater negative impact on all arrays considered, while constructive interference was still possible in some cases for $\delta \leq 3$.

It would be reasonable to argue that the best linear array presented in this chapter was the almost uniform layout found for $\beta_0 = \frac{\pi}{2}$. This array had the greatest overall performance with constraints imposed, by a considerable margin. The array was widely spaced and symmetric, which avoided the problems of closely spaced WECs. Most importantly, mean constructive interference was possible for the larger constraint and stable performance with respect to changes in kL was also observed. However, the array was very sensitive to changes in incident wave angle. Moving away from the target wave angle by $\pm\frac{\pi}{12}$ resulted not only in destructive interference, but $\overline{q} < 0$, indicating that the array is adding power to the waves rather than extracting it.

The results obtained in this chapter show that a trade-off is made either in overall performance of the array or in the sensitivity of the optimal array. When

examining the β-plot for the head seas case (figure 6.3), it is clear that the imposition of constraints widens the peak performance of the $\overline{q}$ against β curve compared to the unconstrained case, although the overall performance is severely reduced. However, the opposite is seen for beam seas (figure 6.9), where reasonable performance is maintained under the imposition of constraints, but the peak performance is significantly narrowed, thus severely increasing the sensitivity of the array to changes in the incident wave angle. Within the current analysis, it does not seem to be possible to have an array under motion constraints that both performs well and is stable to parameter changes.

In subsequent chapters, a more detailed investigation of this trade-off will be undertaken. One possible method would be to consider the objective function as the mean performance over the incident wave angle, rather than a non-dimensional length. This is motivated by the greater effect that β has on the optimal array formation compared to changes in kL (or kr). This formation of the objective function would also allow for a generalised 2D array layout optimisation, since no array geometry need be imposed. It would also assess whether this trade-off is present in general WEC arrays or if it is specific to linear arrays. Chapter 7 considers this β-optimisation applied to linear arrays and is compared with the results of this chapter and Chapter 4, while Chapter 8 considers the general 2D variant of the β-optimisation, without any prescribed array geometry.

Chapter 7

Optimisation of Linear Arrays over Incident Wave Angle in Regular Waves

7.1 Introduction

Previous array layout optimisations involved maximising the mean of the interaction factor over a prescribed range of non-dimensional length. This was implemented for both constrained and unconstrained WEC motions. The results have shown that, although variations in non-dimensional length have a considerable influence on the optimal array performance, changes in the incident wave angle appear to have a larger impact on the optimal array layout and performance.

To address this perceived deficiency, a new objective function is proposed and is the mean of the array performance (q or $\overline{q}$) over a small range of the incident wave angle β. It is hoped that this will identify arrays that perform well over a given range of β. It is also anticipated that the variation with respect to non-dimensional lengths, i.e. variation in wavelength, will be stable and that sensitivity of the optimal array performance is avoided. This optimisation is applied herein to linear arrays and enables comparison with the results of Chapters 4 and 6. Both unconstrained and constrained optimisations are considered and the results are compared. Chapter 8 will consider the extension of this method to general 2D arrays without any imposed geometry.

7.2 Optimisation Methodology

Optimal arrays, and indeed arrays in general, seem to be more sensitive to changes in β than non-dimensional length (wavelength). Therefore, if an array site is chosen such that wave angle variation is within a known range, it seems more appropriate to optimise arrays with respect to mean performance over that range of wave angle. In this way, it is hoped that satisfactory array performance would be found that is stable to changes in array parameters (k, β), without an excessively intensive numerical optimisation.

The optimisation method follows the same procedure as before, with some minor changes in implementation. For maximum power absorption and optimal motions, the mean of the interaction factor q is taken to be the objective function. With the same linear array set up as in Section 4.2, and $\beta \in [\beta_l, \beta_u]$ being the range of interest of incident wave angle, the objective function is defined as

$$I_\beta(\mathbf{ks}) = \frac{1}{\beta_u - \beta_l} \int_{\beta_l}^{\beta_u} q(\mathbf{ks}, \beta)\ d\beta, \tag{7.1}$$

where $\mathbf{ks}$ is an $N-1$ component vector containing all the consecutive spacings ks_j between the WECs (figure 4.1). It is not necessary to re-parameterise the ks_j variables, since kL is no longer being integrated in the optimisation.

Analogous to Chapter 6, a constrained version of the above objective function is also employed,

$$\overline{I_\beta}(\mathbf{ks}, \boldsymbol{\delta}, \boldsymbol{\psi}) = \frac{1}{\beta_u - \beta_l} \int_{\beta_l}^{\beta_u} \overline{q}(\mathbf{ks}, \boldsymbol{\delta}, \boldsymbol{\psi}, \beta)\ d\beta, \tag{7.2}$$

where $\boldsymbol{\delta}$ and $\boldsymbol{\psi}$ are N-component vectors containing the displacement amplitudes and phases of each WEC respectively and $\overline{q}$ is the averaged interaction factor. In this constrained optimisation, there are in general $N-1$ WEC position variables and $2N$ displacement variables, giving a total of $3N-1$ optimisation variables.

This optimisation can be performed for a non-specified length kL of the array, in which case the optimisation contains $N-1$ position variables, since the first WEC is always fixed at the origin. The upper and lower limits should then be placed on $kL = \sum_{j=1}^{N-1} ks_j$ to avoid excessively large or small array sizes. Alternatively, a fixed non-dimensional length kL can be prescribed and the optimisation contains $N-2$ variables. This optimisation will give the ideal separation of a line of WECs with the first and last fixed at either end of the

array. An optimisation of this type is less general than the case with a non-specified kL but may be more useful if a WEC array site/area has been identified and is to be utilised. This also has the advantage of reducing the difficulty of the numerical optimisation by removing one of the WEC position variables. In either case, upper and lower limits on the individual WEC separations ks_j must also be enforced, to prevent the WECs being placed too close together or too far apart.

An array of a fixed non-dimensional length is considered in this chapter. In order to allow comparison with previous work, the non-dimensional length of the array is fixed at

$$\sum_{j=1}^{N-1} ks_j = kL = 10, \tag{7.3}$$

which removes one separation variable. The objective function is thus written as in equation (7.1) for an unconstrained optimisation or equation (7.2) for a constrained optimisation, with **ks** being a $(N-2)$-component vector containing the non-dimensional position variables of the unassigned WECs. As before, the individual separations are also limited to remain within $0.5 < ks_j < 8.5$. The lower limit of 0.5 is chosen as this is the closest that the WECs can reasonably be situated and it is also the smallest value which avoids numerical difficulties in calculating the objective function. The upper limit of 8.5 is chosen to allow for the possibility that all other WEC separations are exactly the minimum limit of 0.5. To allow comparison with the results of previous chapters, consideration is limited to linear arrays of five WECs.

Previous constrained optimisation studies have shown that a motion amplitude constraint of three times the incident wave amplitude still allows for constructive interference in some cases, while a constraint of two times the wave amplitude is severely limiting. For the constrained optimisations within this chapter, limits of $\delta_{max} = 2, 3$ are again imposed, so that the ranges of the displacement variables enforced are $-\delta_{max} \leq \widetilde{\delta}_j \leq \delta_{max}$ and $0 \leq \psi_j \leq \pi$. (Note that a negative value of $\widetilde{\delta}_j$ is equivalent to adding a phase of π to ψ_j.) As in previous chapters, it is found that the $\widetilde{\delta}_j$ variables were better behaved than the ψ_j variables in terms of convergence of the optimisation. Thus the displacements are implemented in this manner to improve the numerical optimisation, by increasing the range of $\widetilde{\delta}_j$ and decreasing the range of ψ_j.

Three ranges of optimisation $\beta \in [\beta_l, \beta_u]$ are considered, namely $\beta \in [-\frac{\pi}{8}, \frac{\pi}{8}]$, $[\frac{\pi}{8}, \frac{3\pi}{8}]$, $[\frac{3\pi}{8}, \frac{5\pi}{8}]$. There is no need to consider higher ranges as

Table 7.1: Performance of unconstrained uniform linear array with $ks_1 = ks_2 = ks_3 = ks_4 = 2.5$

$[\beta_l, \beta_u]$	I_β
$[-\frac{\pi}{8}, \frac{\pi}{8}]$	0.9880
$[\frac{\pi}{8}, \frac{3\pi}{8}]$	0.9123
$[\frac{3\pi}{8}, \frac{5\pi}{8}]$	1.1873

symmetry would ensure the same results as those listed. These three cases correspond to head, intermediate and beam seas respectively, where the midpoint of the ranges is considered to be the target wave angle. A variation in the incident wave angle of $\pm\frac{\pi}{8}$ is considered. This range of variation is chosen arbitrarily but intended to represent a typical case. It is assumed that all wave angle variation at a given site will be encompassed by this variation around the target cases of $\beta_0 = 0$, $\beta_0 = \frac{\pi}{4}$ and $\beta_0 = \frac{\pi}{2}$.

7.3 Uniform Array Performance

A uniform array layout is prescribed initially and the performance of this array is assessed using the objective functions described above. This is provided as a benchmark and intended to allow comparison of the optimal results in subsequent sections to assess the performance of the layout optimisations. For constrained motions, the displacement variables were fed into the optimisation routine with the uniform layout fixed.

Table 7.1 shows the objective function values I_β for an unconstrained linear array for each wave angle range considered. Similarly, table 7.2 shows the optimal displacement variables and objective function values $\overline{I_\beta}$ for a constrained uniform array. The variation of the array performance with incident wave angle for both constrained and unconstrained uniform arrays is shown in figures 7.1 - 7.3 for each range of β considered. Figure 7.4 shows the performance of all uniform arrays for variations in wavenumber.

Firstly examining the unconstrained uniform array, the best performance is found for beam seas $\beta \in [\frac{3\pi}{8}, \frac{5\pi}{8}]$ where a value of $I_\beta = 1.1873$ is achieved. Mean performance over β is less than unity for the for the head and intermediate seas cases, even in this unconstrained case. Since this is the best possible performance, this initially suggests that these incident wave angle ranges should

Table 7.2: Performance of constrained uniform linear array with $ks_1 = ks_2 = ks_3 = ks_4 = 2.5$

$[\beta_l, \beta_u]$	δ_{max}	$\widetilde{\delta_1}$	$\widetilde{\delta_2}$	$\widetilde{\delta_3}$	$\widetilde{\delta_4}$	$\widetilde{\delta_5}$	ψ_1	ψ_2	ψ_3	ψ_4	ψ_5	$\overline{I_\beta}$
$[-\frac{\pi}{8}, \frac{\pi}{8}]$	3	-3.0000	3.0000	-3.0000	-3.0000	3.0000	1.1490	0.6799	0.3174	3.0993	2.6404	0.9369
	2	-2.0000	2.0000	-2.0000	-2.0000	2.0000	1.3495	0.7702	0.3165	3.0070	2.4350	0.7910
$[\frac{\pi}{8}, \frac{3\pi}{8}]$	3	-3.0000	3.0000	1.7461	0.7775	-0.8988	1.7658	0.3724	2.1440	3.0866	1.2992	0.4516
	2	-2.0000	2.0000	1.9453	-0.9293	-0.4957	1.7862	0.3519	2.1046	0.2882	1.4741	0.4108
$[\frac{3\pi}{8}, \frac{5\pi}{8}]$	3	-3.0000	-3.0000	-2.2323	-0.0880	0.2571	1.7266	1.7266	1.7266	1.7266	1.7266	0.4544
	2	-2.0000	-2.0000	-2.0000	-0.1647	0.2742	1.7266	1.7266	1.7266	1.7266	1.7266	0.3872

be avoided and the intuitive beam sea array should be utilised. This is enhanced by comparing the red curves in figures 7.1 - 7.3. Performance with respect to β is lower for head and intermediate seas in comparison to beam seas, where $q \approx 1.2$ for the majority of the range $\beta \in [\frac{3\pi}{8}, \frac{5\pi}{8}]$, hence the resulting values of I_β.

Clearly the application of constrained motions has a detrimental effect on the uniform array performance, as expected. In each case, the values of $\overline{I_\beta}$ are less than the corresponding values of I_β, with the lower constraint having a greater detrimental impact. However, in the case of constrained motions, the best performing array is in head seas $\beta \in [-\frac{\pi}{8}, \frac{\pi}{8}]$. This is contrary to the results for unconstrained motions and is rather unexpected. Applying a constraint of three times the wave amplitude results in a performance reduction of only 5% in head seas, while a constraint of twice the wave amplitude results in a drop of approximately 20%. This is a much lower detrimental effect than for other wave angle ranges considered, where performance reductions of more than 50% are observed between the constrained and unconstrained arrays.

This is echoed in figures 7.1 - 7.3 which show the β-variation of the uniform array performance. In figure 7.1, $\overline{q} \approx 1$ for the majority of the range $\beta \in [-\frac{\pi}{8}, \frac{\pi}{8}]$ for the constraint $\delta_{max} = 3$, while $\overline{q} \approx 0.8$ for the lower constraint of $\delta_{max} = 2$. It should also be noted that these values are very stable, such that the performance stays approximately the same over all $\beta \in [-\frac{\pi}{8}, \frac{\pi}{8}]$. In contrast, the $\overline{q}$ values for intermediate and beam seas are not as consistent and vary between $\overline{q} \in [0, 0.6]$. Furthermore, it should be noted that all arrays exhibit symmetry in performance about $\beta = \frac{\pi}{2}$ and $\beta = 0$ as intuitively expected, since the arrays are uniformly spaced.

It is noteworthy that the displacement amplitude variables in table 7.2 did not

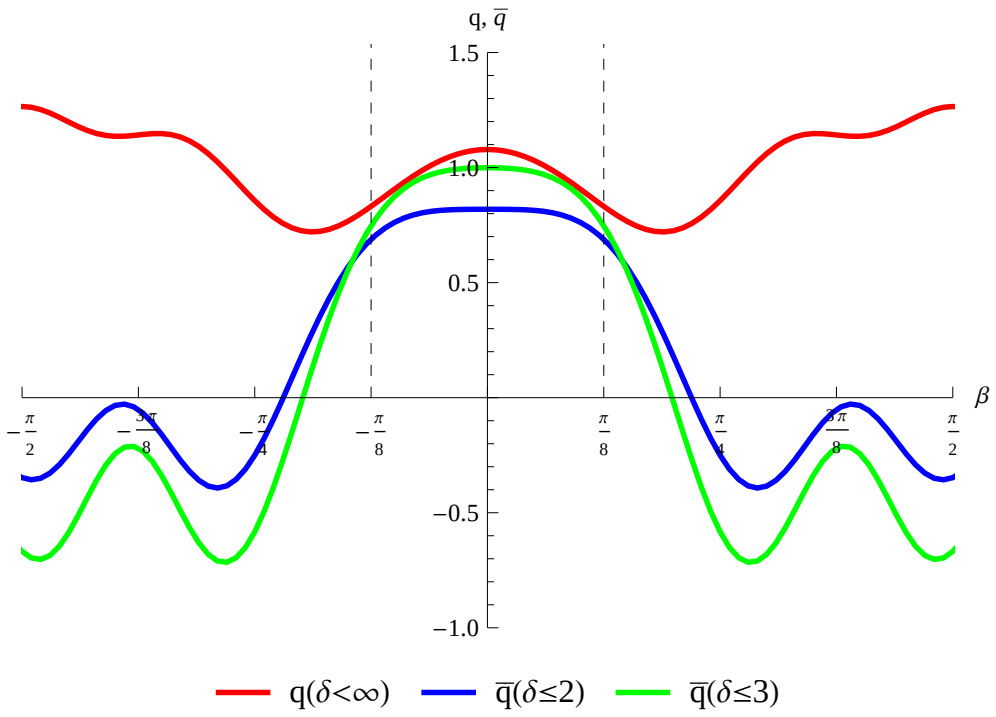

Figure 7.1: Performance of uniform array against incident wave angle for target range $\beta \in [-\frac{\pi}{8}, \frac{\pi}{8}]$ (shown by horizontal dashed lines)

all require the allowed limit of $\delta_{max} = 2$ or $\delta_{max} = 3$, with the exception of the $\beta \in [-\frac{\pi}{8}, \frac{\pi}{8}]$ case. For intermediate and beam seas, this suggests that the best case is not to have all devices working equally as hard. This is particularly unusual for the $\beta \in [\frac{3\pi}{8}, \frac{5\pi}{8}]$ case, as this approximates beam seas where the wave strikes all WECs at the same time. Clearly the variation of $\pm\frac{\pi}{8}$ around this target angle of $\beta = \frac{\pi}{2}$ has a considerable impact when compared to fixed incident wave angle results of previous chapters. However, as expected, the WECs all operate in phase for beam seas. In the head seas case, all WEC displacement amplitudes did reach the maximum allowed values and this may be in part the reason for the better constrained performance within this wave angle range. All five WECs oscillate at different phases to each other in the head seas array. There is also a slight difference in the optimal phases between the two constraints applied.

Figure 7.4 shows the variation of all constrained uniform arrays for variation in wavenumber. This is implemented as a change in the relative wavenumber $\frac{k}{k_{opt}}$, where for a fixed array layout k_{opt} corresponds to the optimal value of k for which the mean array performance was maximised in the optimisation. A variation of ±50% is considered, so that $\frac{k}{k_{opt}} \in [0.5, 1.5]$. This is equivalent to

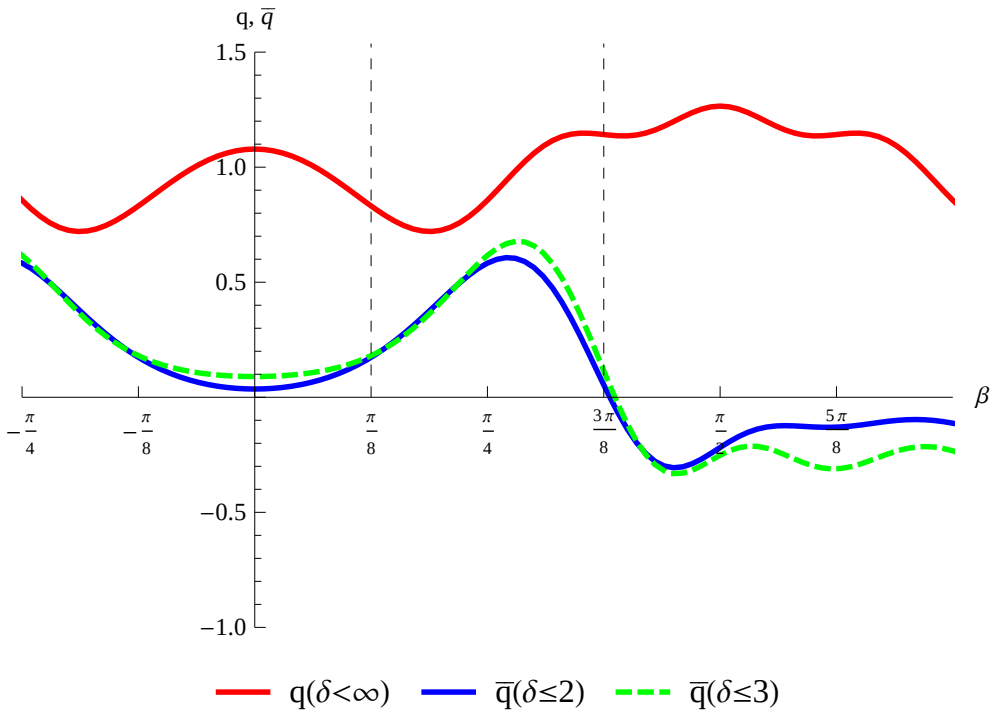

Figure 7.2: Performance of uniform array against incident wave angle for target range $\beta \in [\frac{\pi}{8}, \frac{3\pi}{8}]$ (shown by horizontal dashed lines)

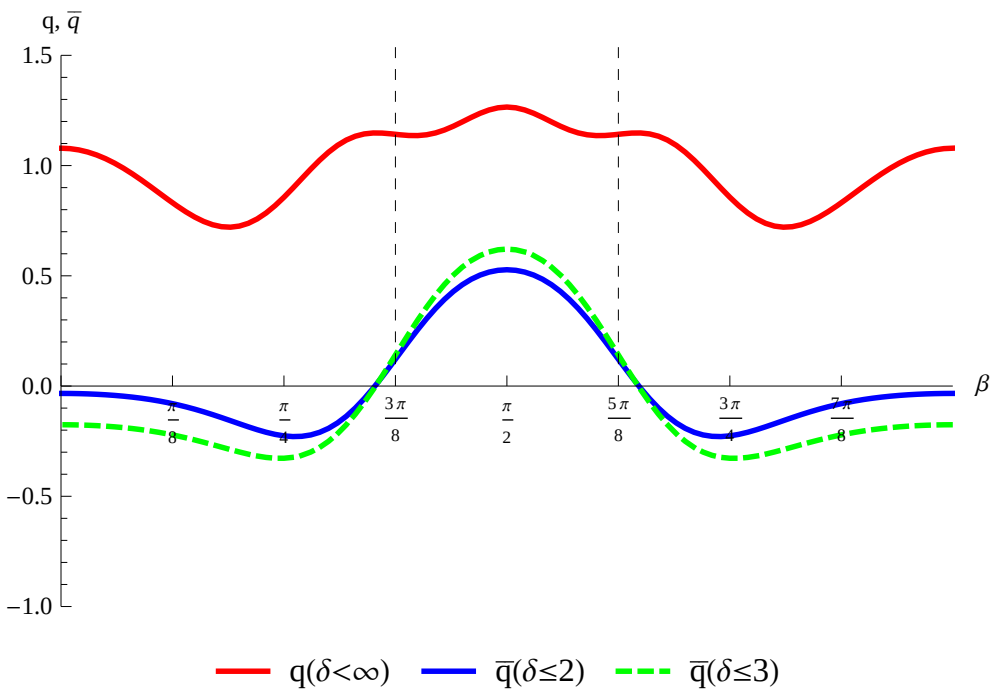

Figure 7.3: Performance of uniform array against incident wave angle for target range $\beta \in [\frac{3\pi}{8}, \frac{5\pi}{8}]$ (shown by horizontal dashed lines)

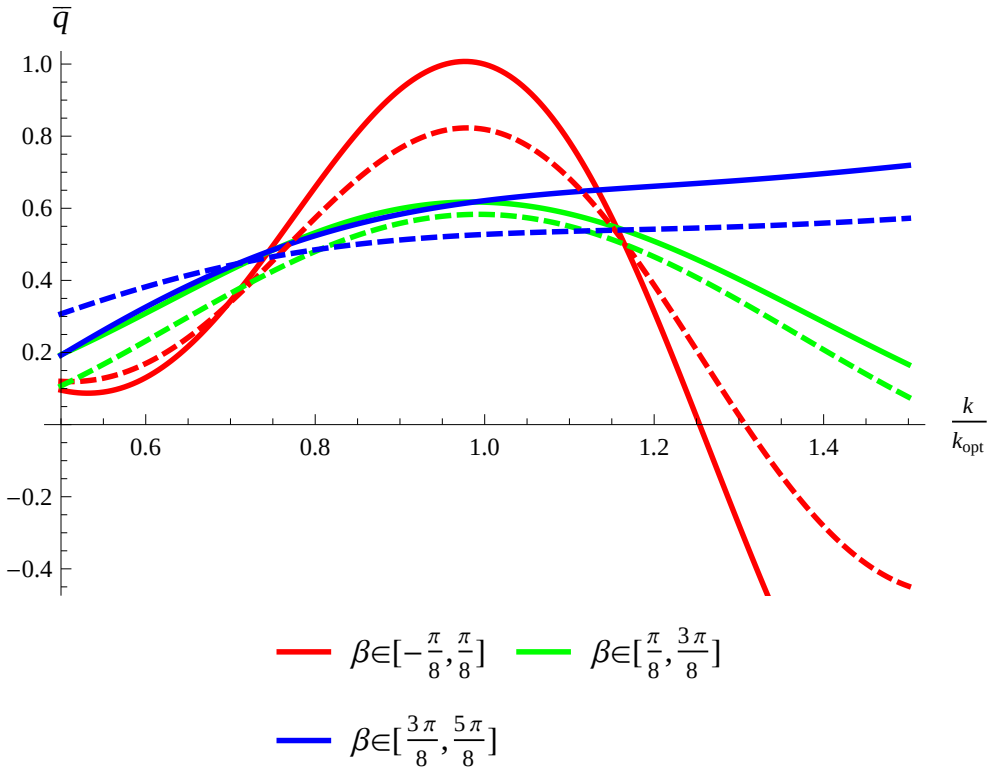

Figure 7.4: Performance of constrained uniform arrays against relative incident wavenumber. The target β ranges are given in the legend. For each curve, β is fixed at the midpoint of the appropriate target range. Solid curves represent a constraint of $\delta_{max} = 3$ while dashed curves correspond to $\delta_{max} = 2$

scaling all the WEC radial positions kd_j. For a fixed physical linear array layout, this corresponds to $kL \in [5, 15]$ since $kL = 10$ is fixed and allows comparison with the optimal results of previous chapters. The unconstrained unform array was previously examined in a similar manner by Thomas & Evans (1981) and discussed in Chapter 3.

The variation in performance with wavenumber is different for each of the optimal uniform arrays considered. The beam seas array appears to be the most stable to changes in $\frac{k}{k_{opt}}$, with a relatively slow and steady change over the range considered. A similar argument can be made for intermediate seas, although the variation is slightly more pronounced. For both beam and intermediate seas, a change of up to ±20% results in only a 0.1 change in $\overline{q}$ (a 20% relative change). The greatest variation is seen for the head seas array, which achieved the highest constrained objective function values and is the best performing in terms of β-variation. A ±20% change results in a reduction of up to 80% for the constraint of $\delta_{max} = 3$ and 55% for $\delta_{max} = 2$. Variation of greater than +25% results in negative $\overline{q}$ values, which is highly undesirable. This again

indicates that there is a trade-off between stability of performance with respect to variation in wavelength and variation in wave angle.

Another point of note is that for the head and intermediate seas arrays, the peak in $\overline{q}$ is achieved at a value of $\frac{k}{k_{opt}}$ slightly less than unity. One would expect the peak to occur at $\frac{k}{k_{opt}} = 1$ so that the wavenumber corresponds to the case at which the optimisation was performed. However, within this work, the non-dimensional length of the array was fixed at $kL = 10$, which results in a slight loss of generality within the optimisation. Since the peak occurs at $\frac{k}{k_{opt}} \approx 0.98$, this indicates that having an array length that is slightly shorter (such as $kL \approx 9.8$) may result in a slight improvement in performance. However, as this improvement is very subtle, the fixed array length of $kL = 10$ is retained for convenience and to allow comparison with previous chapters.

It should also be noted for the beam seas array that the performance increases with $\frac{k}{k_{opt}}$, even above the expected maximum of $\frac{k}{k_{opt}} = 1$. This suggests that a larger array length is desirable, in line with the intuitive idea that a greater frontage allows for greater power absorption. It would perhaps be limited, since at some point the large gaps between the WECs would be detrimental to array performance.

7.4 Layout Optimisation Results

This section considers the constrained optimal performance of a linear array whose layout is not fixed or prescribed. The array length is retained at $kL = 10$, thus reducing the number of position variables to three. The WEC positions (ks_1, ks_2, ks_3) are fed into the optimisation as variables, subject to minimum and maximum values of $ks_j \geq 0.5$ and $ks_j \leq 8.5$ respectively. Section 7.4.1 outlines the unconstrained optimisation of linear arrays of five WECs, where maximum power absorption is assumed, while Section 7.4.2 considers constrained optimisation, where a limit on the WEC displacement amplitudes is enforced. As in previous chapters, two displacement constraints are considered, namely $\delta_{max} = 3$ and $\delta_{max} = 2$.

The optimisation results are presented in this section while a detailed analysis of both constrained and unconstrained optimal arrays is provided in Section 7.5, where diagrams of the optimal arrays are presented and compared. The performance of the arrays is also assessed for variation in incident wave angle

Table 7.3: Optimal array parameters for the unconstrained five-device linear array

$[\beta_l, \beta_u]$	ks_1	ks_2	ks_3	ks_4	I_β
$[-\frac{\pi}{8}, \frac{\pi}{8}]$	0.6107	0.5000	0.5000	8.3893	1.2293
$[\frac{\pi}{8}, \frac{3\pi}{8}]$	0.5000	4.5000	4.5000	0.5000	1.0397
$[\frac{3\pi}{8}, \frac{5\pi}{8}]$	3.9767	5.0233	0.5000	0.5000	1.3520

and wavenumber; this performance is then compared to the benchmark of the uniform linear arrays of Section 7.3.

7.4.1 Unconstrained Optimisation

As with the optimisations in previous chapters, an exhaustive search of the space of starting points for the optimisation is implemented. All permissible combinations of starting points with $ks_j = \{0.5, 1.0, 1.5, \ldots, 8.5\}$ for $j = 1, \ldots, 4$ were investigated, with some combinations omitted due to consistency considerations in line with equation (7.3). The optimal results for each run of the optimisation were then tabulated.

A summary of the unconstrained optimisation results are given in table 7.3. The optimisation was found to be relatively stable, with only two to four unique solutions converged to by the routine for each wave angle considered, the best of which are listed. This indicates that the exhaustive search of the starting space resulted in much repetition of the optimal results. As for the results of previous chapters, this gives confidence in the optimal solution as the optimisation routine repeatedly converged to the same solution for many combination of starting variable values.

It is clear from table 7.3 that the best performing array is for beam seas, where an objective function value of $I_\beta = 1.3520$ is achieved. It is noteworthy that the optimal beam sea array layout is not symmetric, with ks_3 and ks_4 both attaining the lowest allowed value. This may indicate that it is better to have increased interaction between the closer spaced WECs at one side of the array, rather than spreading the devices evenly. It should be further noted that the mirror version of these separations is necessarily optimal, via equation (2.165). The poorest performing optimal array is for intermediate seas where the optimal objective value achieved is only $I_\beta = 1.0397$. This is the only optimal array with symmetry in the spacings about the middle device.

It should be stressed that these results are the best that are theoretically possible, as they assume maximum power absorption of the array. Hence the resulting displacements are expected to exceed the $\mathcal{O}(1)$ requirement for linear wave theory, as shown in Section 7.5.

In each optimal array, at least one of the separation variables converged to the minimum allowed value of $ks_j = 0.5$. This suggests that the resulting optimal array layouts will contain closely spaced groups of WECs. This may be undesirable as it could result in WECs which are almost touching; it may also invalidate the point absorber approximation, as shadowing may have a significant effect at such close ranges, even for relatively small devices.

Further analysis of the optimal array layouts and the optimal displacements, along with their performance with respect to variation of wave parameters, is given in Section 7.5.

7.4.2 Constrained Optimisation

A constrained optimisation, with a maximum WEC displacement amplitude constraint enforced is now undertaken. Retaining the fixed array length of $kL = 10$ for an array of $N = 5$ WECs, the optimisation has the objective function given by equation (7.2). This contains three WEC position variables and ten WEC displacement variables, giving a total of thirteen optimisation variables. Upper limits of $\delta_{max} = 3$ and $\delta_{max} = 2$ are enforced, in line with previous work.

The same ranges of optimisation $\beta \in [\beta_l, \beta_u]$ are considered, namely $\beta \in [-\frac{\pi}{8}, \frac{\pi}{8}]$, $[\frac{\pi}{8}, \frac{3\pi}{8}]$, $[\frac{3\pi}{8}, \frac{5\pi}{8}]$. The optimisation results for these ranges are summarised in tables 7.4 and 7.5, which respectively show the position and displacement variables of the optimal arrays converged to by the optimisation. The same symmetry arguments hold for the constrained optimisation as for the unconstrained case, hence higher ranges of β were not examined.

As with the unconstrained optimisation, an exhaustive search of the starting points of the variables was implemented. The combinations of starting points were $ks_j = \{0.5, 1.0, 1.5, \ldots, 8.5\}$ for $j = 1, \ldots, 4$, $\widetilde{\delta_n} = \{-3, -1, 1, 3\}$ and $\psi_n = \{0, \frac{\pi}{2}, \pi\}$ for $n = 1, \ldots, 5$, with some combinations omitted due to consistency considerations. A similar justification as in previous chapters is given for this choice of starting ranges, i.e. it was found that the optimisation

Table 7.4: Optimal array layout parameters for the constrained five-device linear array

$[\beta_l, \beta_u]$	δ_{max}	ks_1	ks_2	ks_3	ks_4	$\overline{I_\beta}$
$[-\frac{\pi}{8}, \frac{\pi}{8}]$	3	2.4426	2.5624	2.5458	2.4492	0.9376
	2	2.3554	2.6440	2.6347	2.3658	0.7940
$[\frac{\pi}{8}, \frac{3\pi}{8}]$	3	1.7723	3.3716	3.5179	1.3382	0.4749
	2	1.0427	1.9800	3.1850	3.7923	0.4428
$[\frac{3\pi}{8}, \frac{5\pi}{8}]$	3	0.5000	3.0723	0.5000	5.9277	0.4751
	2	0.5000	2.7338	0.9798	5.7864	0.4593

Table 7.5: Optimal displacement parameters for the corresponding optimal constrained five-device linear arrays identified in table 7.4

$[\beta_l, \beta_u]$	δ_{max}	δ_1	δ_2	δ_3	δ_4	δ_5	ψ_1	ψ_2	ψ_3	ψ_4	ψ_1
$[-\frac{\pi}{8}, \frac{\pi}{8}]$	3	-3.0000	3.0000	-3.0000	-3.0000	3.0000	1.1444	0.6776	0.3175	3.0998	2.6449
	2	-2.0000	2.0000	-2.0000	-2.0000	2.0000	1.3355	0.7337	0.3153	3.0365	2.4456
$[\frac{\pi}{8}, \frac{3\pi}{8}]$	3	-3.0000	3.0000	1.7977	-1.6736	-1.0155	1.4724	0.3535	1.9746	0.3025	2.8425
	2	-2.0000	-2.0000	2.0000	1.6228	-0.8107	1.4437	2.7426	0.9473	2.5307	1.2772
$[\frac{3\pi}{8}, \frac{5\pi}{8}]$	3	-3.0000	-1.6952	-3.0000	-1.1724	0.4273	1.7266	1.7266	1.7266	1.7266	1.7266
	2	-2.0000	-2.0000	-2.0000	-2.0000	0.4732	1.7266	1.7266	1.7266	1.7266	1.7266

converged to the optimal values of $\widetilde{\delta_n}$ and ψ_n relatively quickly and reliably, with convergence to the same optimal values achieved for most starting points chosen. Therefore, a relatively small set of starting points for $\widetilde{\delta_n}$ and ψ_n was implemented to reduce the numerical intensity of the optimisation. However, the convergence of the WEC position variables ks_j was not as straightforward, as many local optimal were found. Thus, in order to guarantee the routine converged to a global optimum, a larger set of starting points was required for ks_j.

For constrained motions, table 7.4 shows that the best performing arrays are in head seas, where a mean performance of $\overline{I_\beta} = 0.9376$ is achieved for the larger motion constraint. Similar but reduced performance is seen for the lower constraint in head seas, where $\overline{I_\beta} = 0.7940$, however this still outperforms all constrained arrays at the other wave angles investigated. The poorest performance is seen for the intermediate arrays, where $\overline{I_\beta} = 0.4749$ and $\overline{I_\beta} = 0.4428$ for the higher and lower constraints respectively. However, only a slight improvement on this poorer performance is achieved in beam seas. In general, the arrays with a constraint of $\delta_{max} = 3$ outperformed those with

$\delta_{max} = 2$, as expected.

The beam sea arrays were the only optimal layouts to contain position variables that converged to the minimum allowed value of $ks_j = 0.5$, suggesting that these are the only constrained optimal arrays to contain closely spaced WECs. For head seas, the optimal layout variables are very close to that of a uniform array layout for both constraints considered. This resulted in only a slight improvement of less than 0.5% compared to the uniform layout.

For the head seas optimal array, the displacement amplitude variables all converged to their maximum value of $\widetilde{\delta} = \pm 2$ or $\widetilde{\delta} = \pm 3$, with all array members operating out of phase with each other. Since this optimal array is very similar to the uniform one considered in Section 7.3, the phase values deviate only slightly from the uniform values. For the other ranges of β, not all WECs converged to the maximum allowed displacement amplitudes, which indicates that the optimal case is not when all WECs are required to work equally hard. As expected, all five WECs oscillate in phase in the optimal beam seas array.

Further analysis of these optimal array layouts and their performance with respect to changes in wave parameters is provided in Section 7.5.

7.5 Analysis of Optimal Arrays

This section provides a deeper analysis of the optimal arrays presented in Sections 7.4.1 and 7.4.2. For clarity, the analysis is split into the relevant ranges of β considered within the optimisation, namely $\beta \in [-\frac{\pi}{8}, \frac{\pi}{8}]$, $\beta \in [\frac{\pi}{8}, \frac{3\pi}{8}]$ and $\beta \in [\frac{3\pi}{8}, \frac{5\pi}{8}]$.

The optimal array layouts are presented and analysed for each case. The performance of each array is then assessed with respect to variation in incident wave angle β and in wavenumber $\frac{k}{k_{opt}}$. For the unconstrained arrays, the optimal displacement amplitudes are also presented. The results of this section are compared to the benchmark uniform array results of Section 7.3.

7.5.1 Head Seas $\beta \in [-\frac{\pi}{8}, \frac{\pi}{8}]$

The optimal layout of both the constrained and unconstrained arrays are shown in figure 7.5 for head seas and the constrained array layouts are very similar for

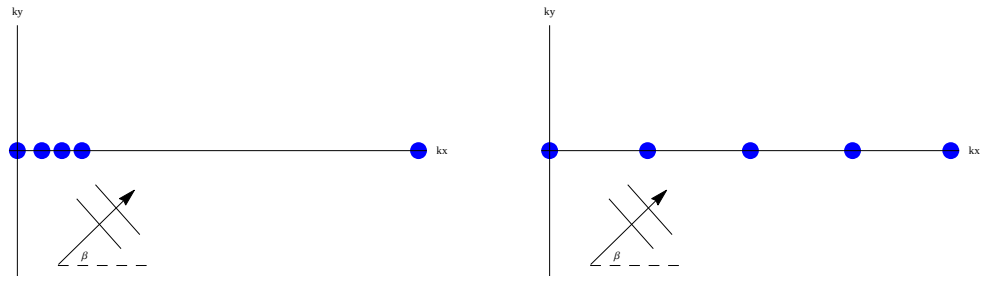

(a) Unconstrained (b) $\delta \leq 2, 3$

Figure 7.5: Constrained and unconstrained optimal linear arrays for head seas ($\beta \in [-\frac{\pi}{8}, \frac{\pi}{8}]$). The optimal layout for the $\delta \leq 3$ case is very similar to the $\delta \leq 2$ case and is omitted for clarity

both constraints. The unconstrained array is similar to that found in Section 4.3.1, with four WECs grouped closely together on the left of the array with an isolated WEC to the right. This close separation between WECs could cause physical difficulties with the operation of the devices and might also invalidate the point absorber approximation, since shadowing effects may became significant at such short ranges. Interestingly, the constrained arrays are almost uniformly spaced, with only slight perturbations in the layout variables from the uniform case.

Figure 7.6 shows the performance of the constrained and unconstrained optimal arrays in head seas with variation in incident wave angle. For all three cases ($\delta < \infty$, $\delta \leq 3$ and $\delta \leq 2$) it is clear that the curve is forced to perform as well as possible within the range of interest $\beta \in [-\frac{\pi}{8}, \frac{\pi}{8}]$. For the unconstrained array, a peak of $q = 1.5$ is seen at $\beta = 0$ and $q > 0.8$ for all of the range of interest. Good performance is also seen for the constrained arrays; for the larger constraint, $\overline{q} \approx 1$ for the majority of $\beta \in [-\frac{\pi}{8}, \frac{\pi}{8}]$, while the lower constraint results in $\overline{q} \approx 0.8$ for the majority of this range. As expected, poor performance is seen outside of the region of interest, where $\overline{q} < 0$ for $\beta \notin [-\frac{\pi}{4}, \frac{\pi}{4}]$.

The variation of optimal array performance for changes in incident wavenumber is shown in figure 7.7. The unconstrained optimal array is very stable to changes in $\frac{k}{k_{opt}}$, with $q \approx 1.5$ for the domain considered. However, the constrained arrays are much more sensitive to wavenumber changes; for both constraints, a change in k of approximately 20% from the optimal case results in negative $\overline{q}$ values. Even a variation of 10% results in a 15% to 50% drop in performance. The peak in the constrained array curves occurs just slightly lower than $\frac{k}{k_{opt}} = 1$; this suggests that having an array length of less than $kL = 10$ may produce slightly better results.

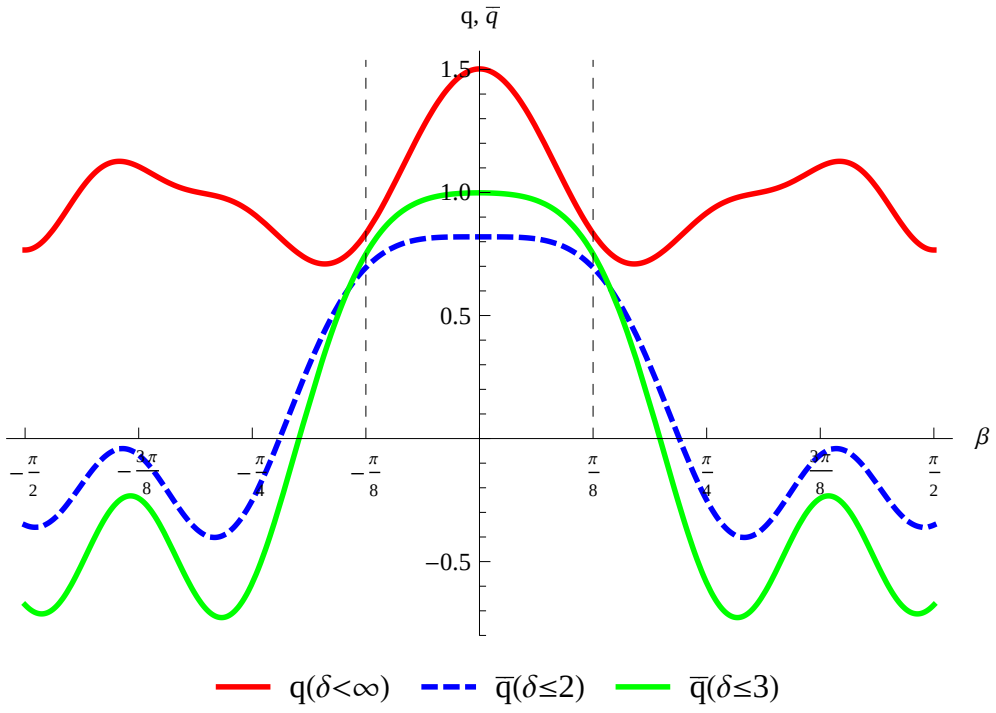

Figure 7.6: Interaction factor against incident wave angle β for optimal constrained and unconstrained linear five-WEC array, optimised for $\beta \in [-\frac{\pi}{8}, \frac{\pi}{8}]$. The target range of wave angles is indicated by the vertical dashed lines.

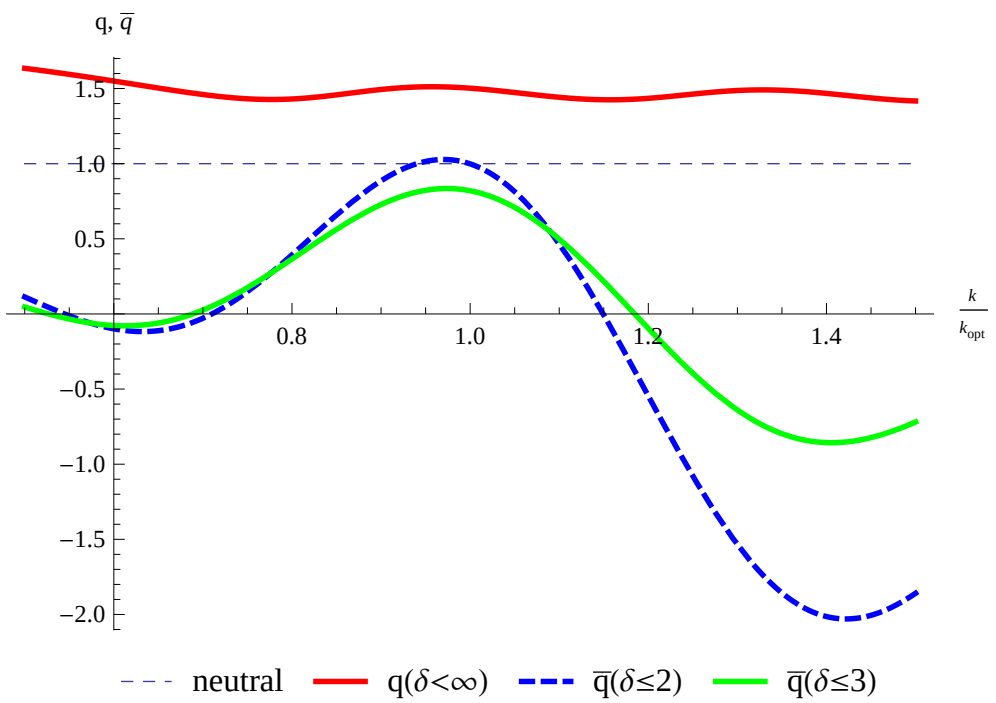

Figure 7.7: Interaction factor against wavenumber k for optimal constrained and unconstrained linear five-WEC array, optimised for $\beta \in [-\frac{\pi}{8}, \frac{\pi}{8}]$.

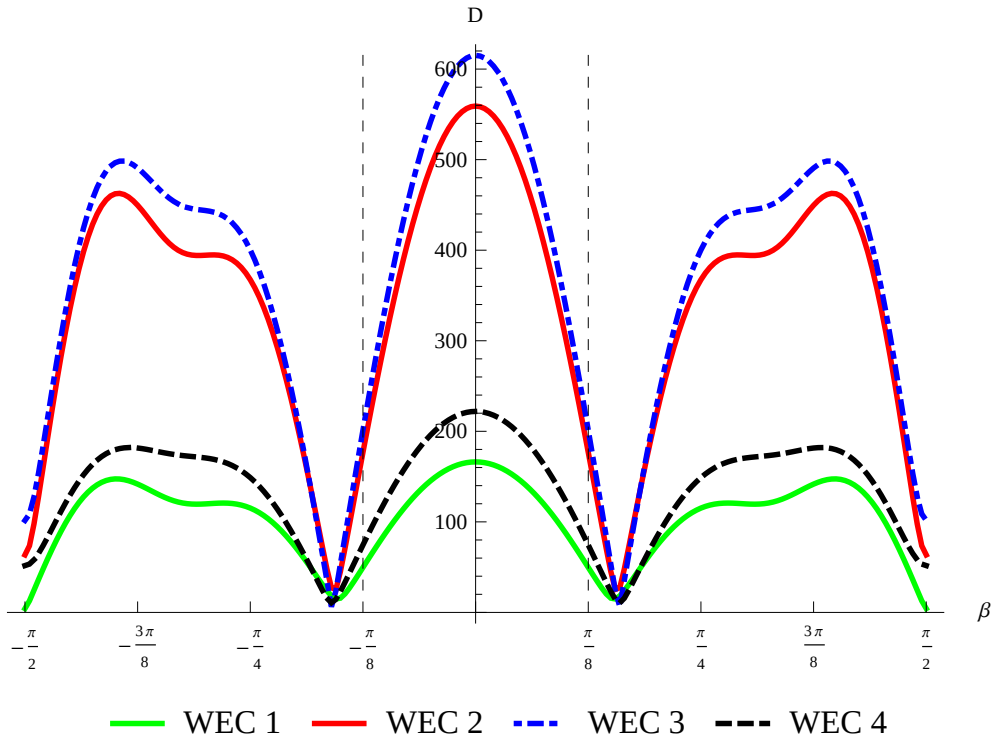

(a) WECs 1-4

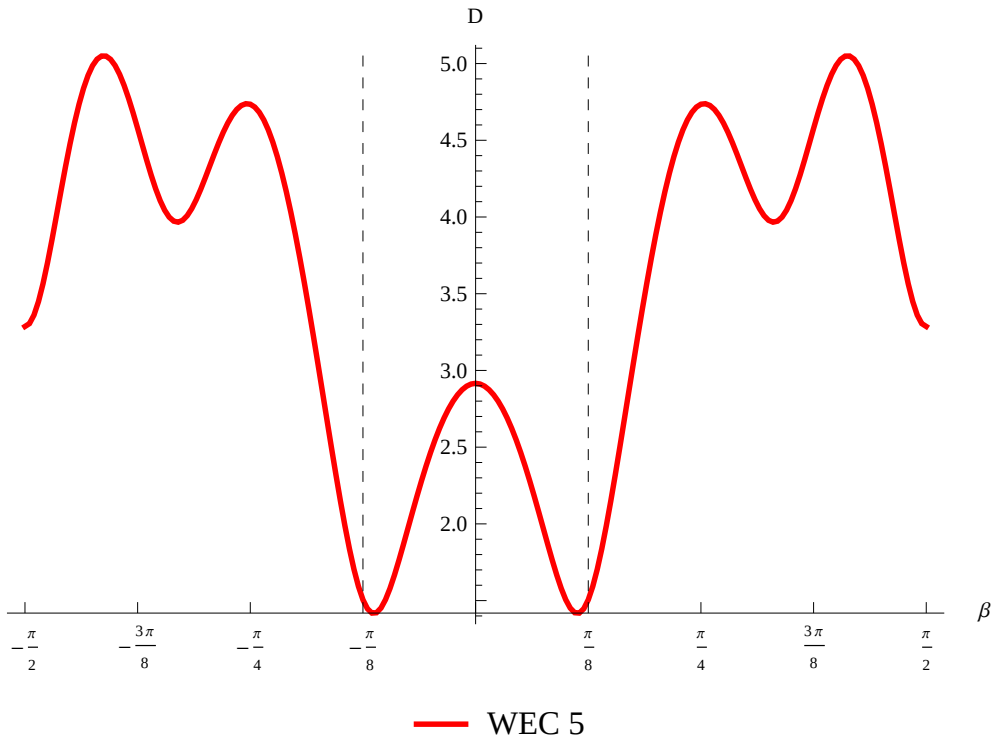

(b) WEC 5

Figure 7.8: Optimal displacement amplitudes against incident wave angle for optimal unconstrained linear five-WEC array, optimised for $\beta \in [-\frac{\pi}{8}, \frac{\pi}{8}]$ (shown by horizontal dashed lines)

The predicted optimal displacements are shown for the optimal unconstrained array in figure 7.8 for variation in incident wave angle. As expected, these displacements are unacceptably large for the grouped devices (WECs 1 - 4) within the range of interest of β. These motions are $\mathcal{O}(100)$ relative to the incident wave amplitude and so would invalidate the model. The motion amplitude of WEC 5 is less than three times the incident wave amplitude for $\beta \in [-\frac{\pi}{8}, \frac{\pi}{8}]$ and so does not violate the $\mathcal{O}(1)$ assumption.

7.5.2 Intermediate Seas $\beta \in [\frac{\pi}{8}, \frac{3\pi}{8}]$

Schematics of the optimal constrained and unconstrained array layouts are shown in figure 7.9 for intermediate seas and different array layouts are found to be optimal for each of the different constraints applied. The optimal unconstrained array possesses a pair of closely spaced WECs on each side of the array, with an isolated WEC in the centre. These closely spaced pairs of WECs are expected to cause physical and theoretical difficulties. The constrained array layouts have all WECs unevenly dispersed across the line with no devices very close together. It is important to note that the different displacement constraints result in significantly different layouts. All these arrays are considerably different to the uniform layouts considered in Section 7.3.

The sensitivity of these optimal arrays to changes in incident wave angle is shown in figure 7.10. For the unconstrained array, relatively variable performance is seen in the area of interest $\beta \in [\frac{\pi}{8}, \frac{3\pi}{8}]$ where $q \in [0.8, 1.25]$. Poor performance is seen in the same region for the constrained arrays, with $\overline{q} \in [0.1, 0.73]$ for $\delta_{max} = 3$ and $\overline{q} \in [0.1, 0.63]$ for $\delta_{max} = 2$. Even poorer performance is seen outside this range, except for the symmetrically analogous region of $\beta \in [-\frac{3\pi}{8}, -\frac{\pi}{8}]$. It is noteworthy that there is very little difference between the performance of the constrained arrays. This indicates that the imposition of the stricter constraint has little effect on the array performance, hence the similar $\overline{I_\beta}$ values in table 7.4.

The performance of the optimal arrays in intermediate seas, with respect to variation in wavenumber, is shown in figure 7.11. The unconstrained array is not very stable to changes in k, with $q \in [0.8, 1.3]$ for $\beta \in [\frac{\pi}{8}, \frac{3\pi}{8}]$. A 20% reduction in $\frac{k}{k_{opt}}$ results in $q < 1$, while an increase in $\frac{k}{k_{opt}}$ gives an increase in q. Unlike the head sea arrays, the constrained intermediate sea arrays are more stable to changes in $\frac{k}{k_{opt}}$. The upper constraint results in $\overline{q} \in [0.45, 0.7]$ for $\frac{k}{k_{opt}} \in [0.8, 1.2]$,

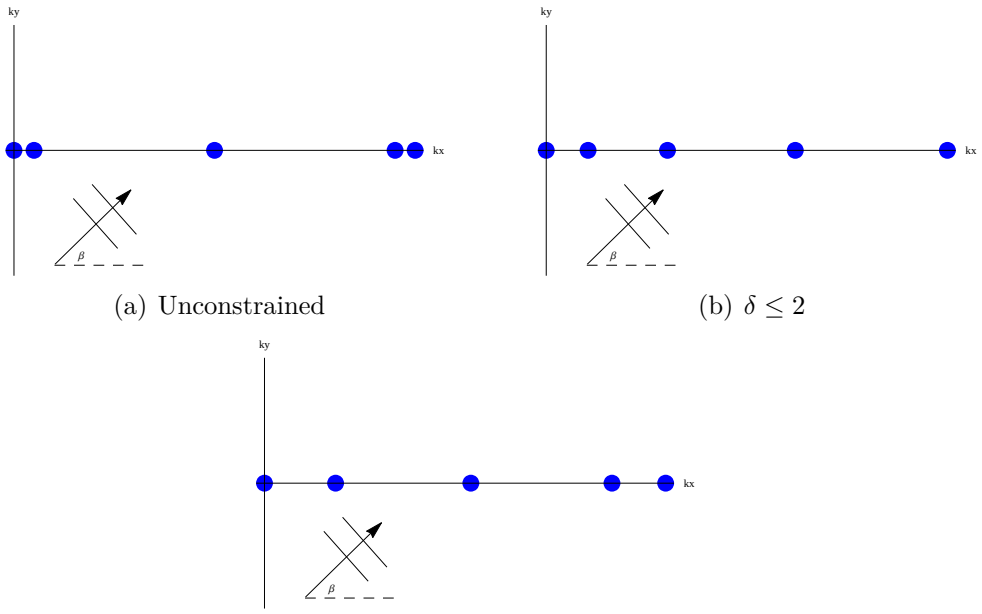

(a) Unconstrained

(b) $\delta \leq 2$

(c) $\delta \leq 3$

Figure 7.9: Constrained and unconstrained optimal linear arrays for intermediate seas ($\beta \in [\frac{\pi}{8}, \frac{3\pi}{8}]$).

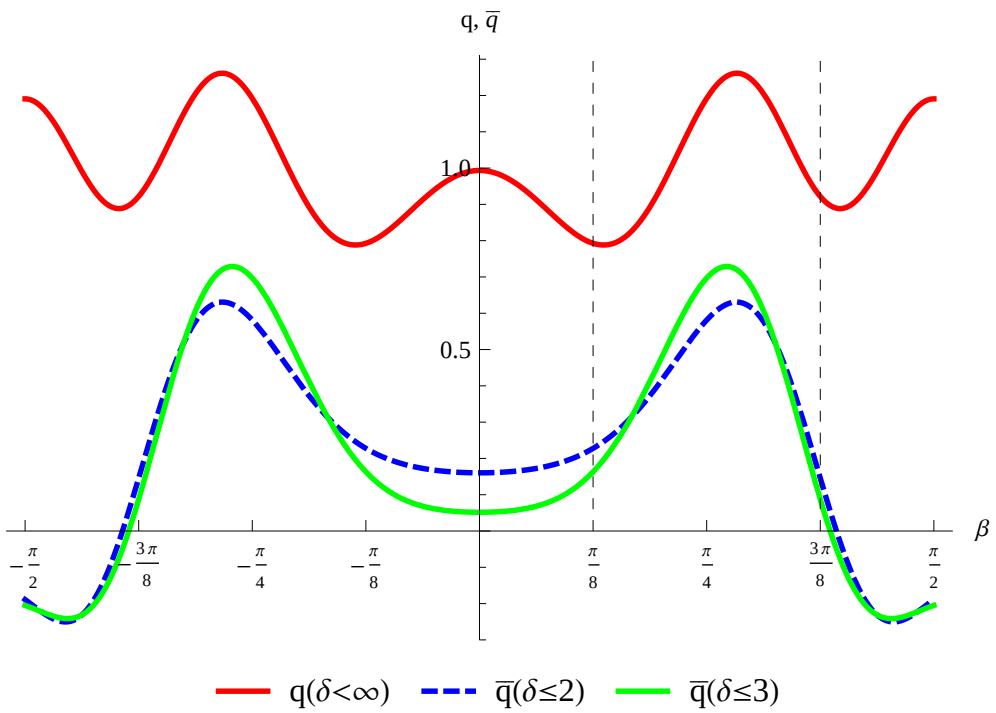

Figure 7.10: Interaction factor against incident wave angle β for optimal constrained and unconstrained linear five-WEC array, optimised for $\beta \in [\frac{\pi}{8}, \frac{3\pi}{8}]$. The target range of wave angles is indicated by the vertical dashed lines.

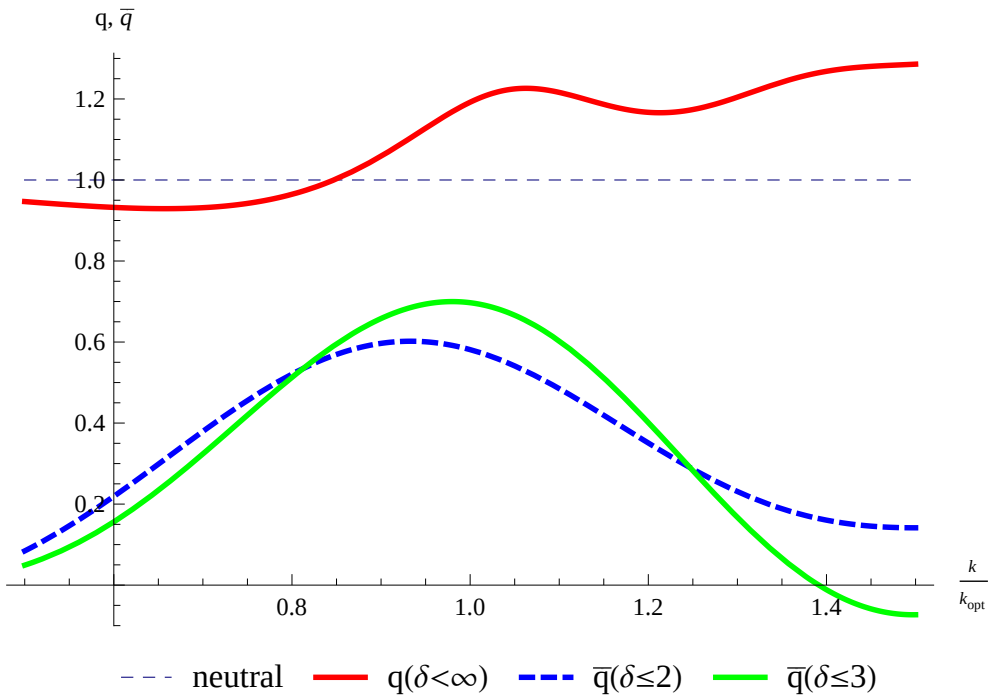

Figure 7.11: Interaction factor against wavenumber k for optimal constrained and unconstrained linear five-WEC array, optimised for $\beta \in [\frac{\pi}{8}, \frac{3\pi}{8}]$.

while the lower constraint gives $\overline{q} \in [0.37, 0.59]$ for $\frac{k}{k_{opt}} \in [0.8, 1.2]$. Critically, these values all remain positive, so that power is being extracted from, rather than input into, the waves. The peak in performance for the constrained arrays occurs at $\frac{k}{k_{opt}} \approx 0.98$ for $\delta_{max} = 3$ and at $\frac{k}{k_{opt}} \approx 0.93$ for $\delta_{max} = 2$. This again suggests that a slight improvement in optimal performance may be achieved by allowing a smaller array length than $kL = 10$.

The predicated optimal displacements for the unconstrained optimal array in intermediate seas are shown in figure 7.12. The unconstrained optimal array is symmetric about the middle WEC, therefore the WEC displacements are also symmetric. The grouped devices (WECs 1,2 and 4,5) have similar motions and these are between eight to seventeen times the wave amplitude in the desired range of β. The grouped WEC motions are unacceptably large and exceed the $\mathcal{O}(1)$ requirement for linear wave theory. The isolated middle WEC exhibits lower motions of $\delta \in [1, 6]$ for $\beta \in [\frac{\pi}{8}, \frac{3\pi}{8}]$. Although the middle WEC has lower a motion amplitude, this can also be considered to violate the $\mathcal{O}(1)$ requirement.

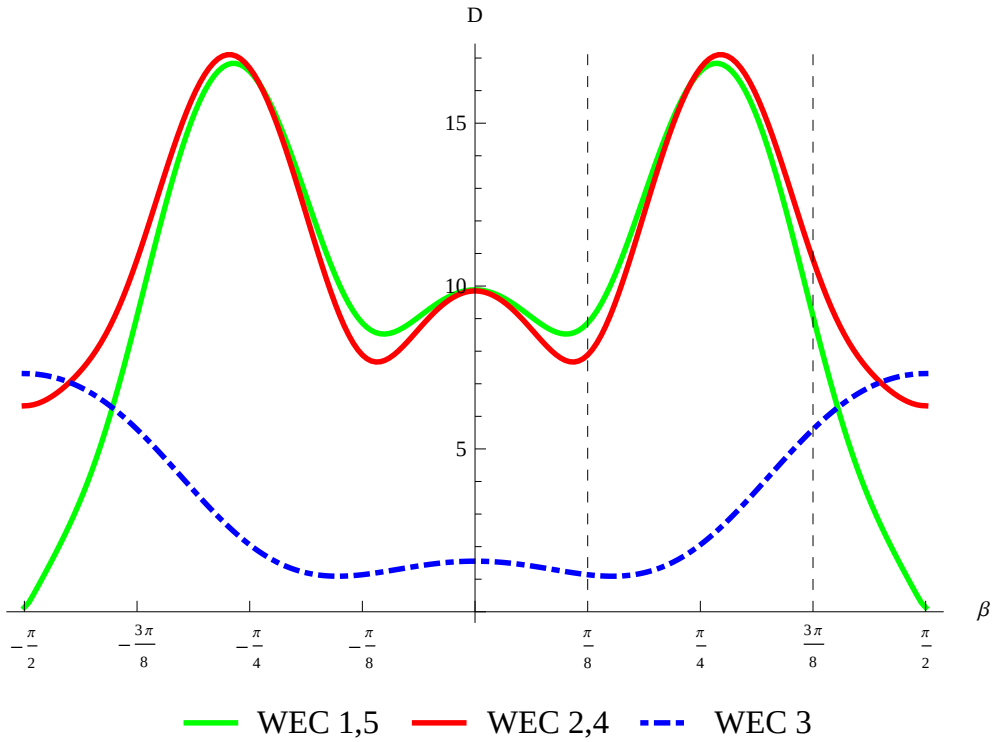

Figure 7.12: Optimal displacement amplitudes against incident wave angle for optimal unconstrained linear five-WEC array, optimised for $\beta \in [\frac{\pi}{8}, \frac{3\pi}{8}]$ (shown by horizontal dashed lines)

7.5.3 Beam Seas $\beta \in [\frac{3\pi}{8}, \frac{5\pi}{8}]$

The constrained and unconstrained optimal layouts for the β-optimised beam seas arrays are shown in figure 7.13. The unconstrained optimal array is comprised of a closely spaced group of three WECs to the right and two isolated devices to the left. This group would cause the same physical and theoretical difficulties as previously outlined. The constrained array layouts are only slightly different for the two constraints considered. Both involve two pairs of closely spaced WECs to the left of the array and an isolated WEC to the right. The larger constraint results in both pairs being as close together as allowed, while the smaller constraint causes the middle pair (WECs 3 and 4) to separate slightly more. All three of these arrays are significantly different from the benchmark uniform layouts considered in Section 7.3.

The performance of these arrays with respect to changes in incident wave angle is shown in figure 7.14. High stable performance is seen for the unconstrained array, where $q \approx 1.35$ within the the majority of the range of interest $\beta \in [\frac{3\pi}{8}, \frac{5\pi}{8}]$. Considerably lower performance is seen for the constrained arrays,

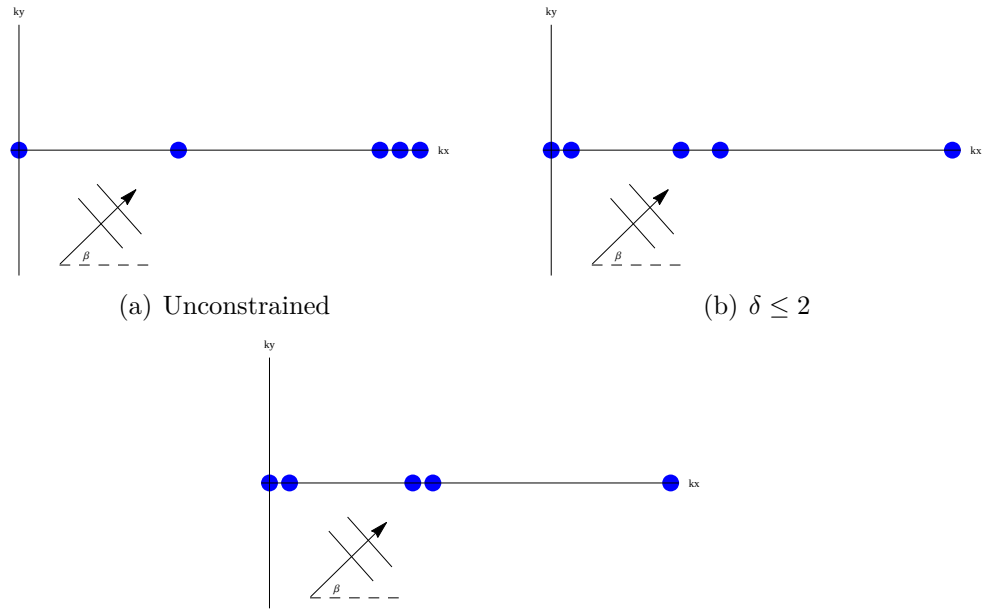

(a) Unconstrained (b) $\delta \leq 2$

(c) $\delta \leq 3$

Figure 7.13: Constrained and unconstrained optimal linear arrays for beam seas ($\beta \in [\frac{3\pi}{8}, \frac{5\pi}{8}]$).

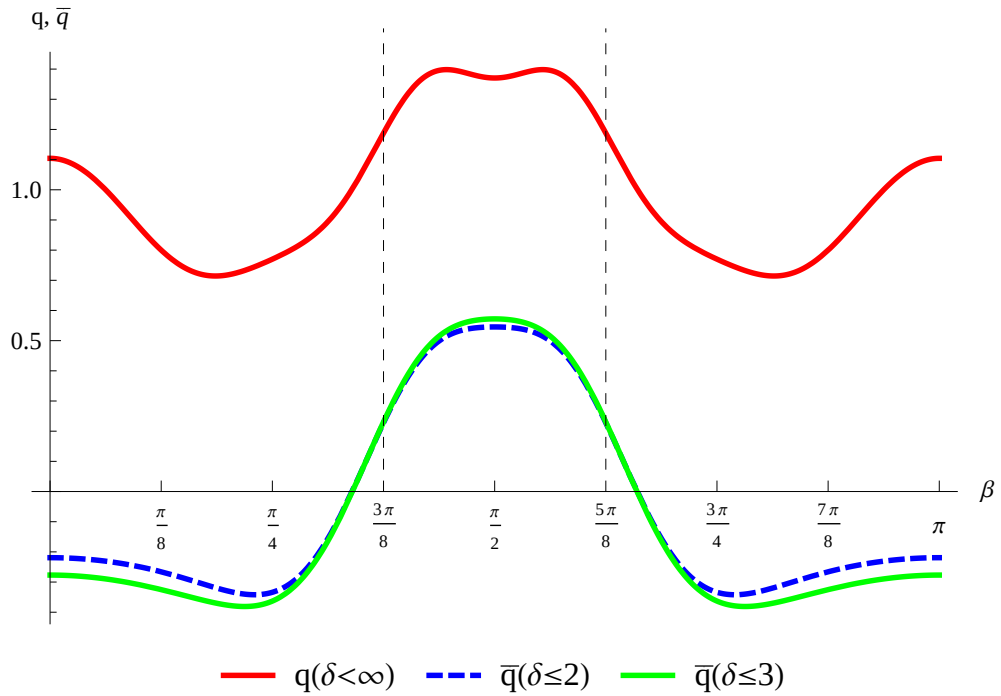

Figure 7.14: Interaction factor against incident wave angle β for optimal constrained and unconstrained linear five-WEC array, optimised for $\beta \in [\frac{3\pi}{8}, \frac{5\pi}{8}]$. The target range of wave angles is indicated by the vertical dashed lines.

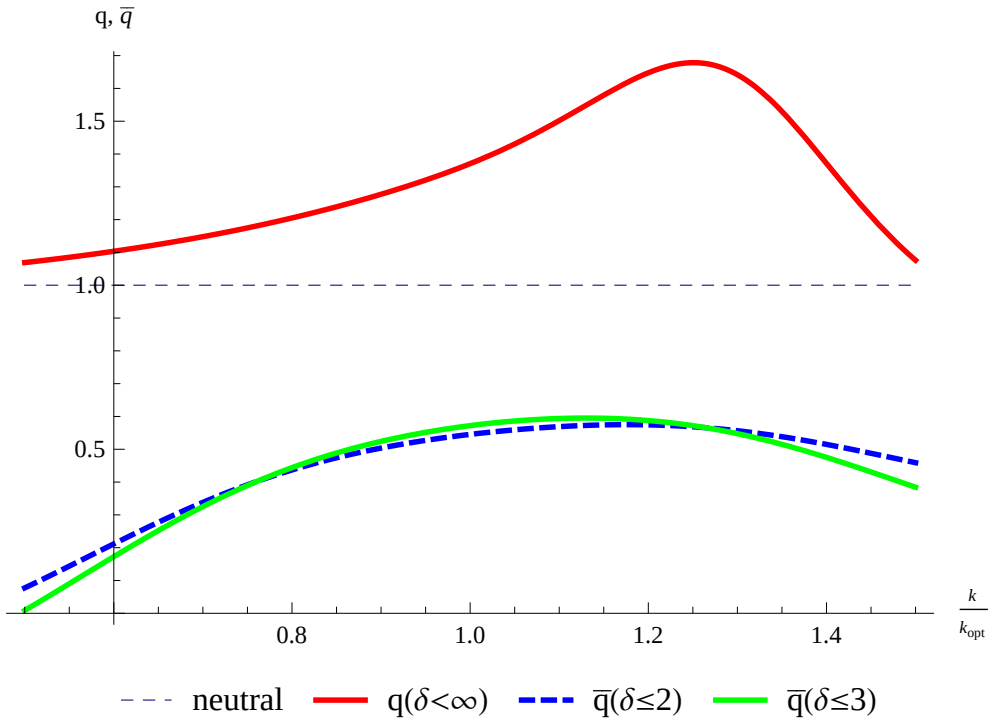

Figure 7.15: Interaction factor against wavenumber k for optimal constrained and unconstrained linear five-WEC array, optimised for $\beta \in [\frac{3\pi}{8}, \frac{5\pi}{8}]$.

where $\overline{q} \in [0.25, 0.55]$ within the range of interest. It should be noted, however, that there is very little difference in performance between $\delta_{max} = 2$ and $\delta_{max} = 3$, indicating that the lower constraint has little further detrimental effect on array performance. This is also supported by the optimal $\overline{I_\beta}$ values in table 7.4, which show very little difference between the two constraints.

The effect on the optimal beam seas arrays of varying the incident wavenumber is shown in figure 7.15. As expected, good overall performance is seen for the unconstrained array, where $q > 1$ for $\frac{k}{k_{opt}} \in [0.5, 1.5]$. Although lower performance is seen for the constrained arrays, they are more stable to k-variation than head and intermediate seas arrays. The $\overline{q}$ against $\frac{k}{k_{opt}}$ curves vary smoothly, indicating that a small change in k results in only a small change in $\overline{q}$. Interestingly, for the constrained arrays, the peak in performance is seen at $\frac{k}{k_{opt}} \approx 1.15$. This suggests that better performance would be achieved if a larger array than $kL = 10$ was allowed and this is in contrast to the head and intermediate seas arrays, where the peak occurred at a value of $\frac{k}{k_{opt}}$ less than unity.

The predicted optimal displacements for the optimal unconstrained beam seas array is shown in figure 7.16. As expected, the largest displacement amplitudes

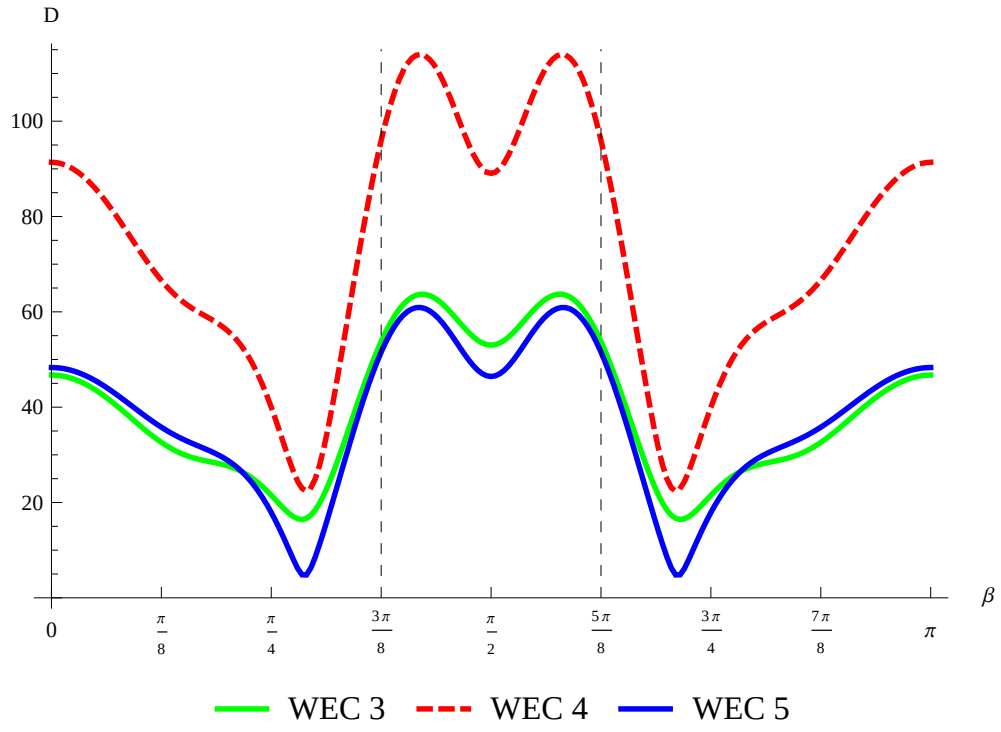

(a) WECs 3-5

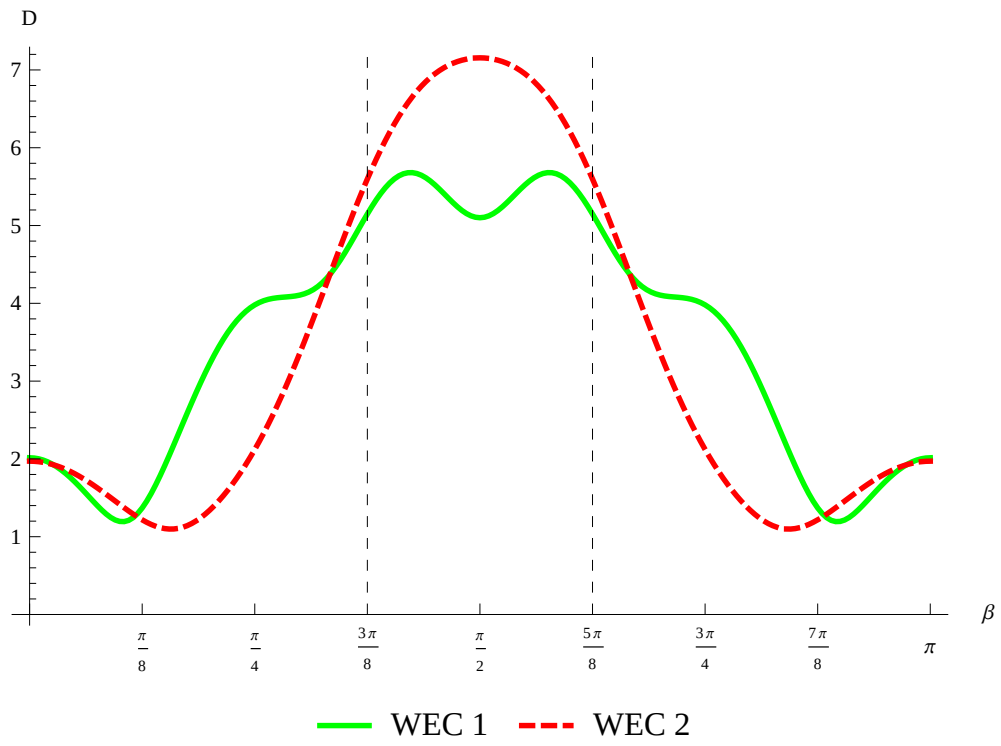

(b) WEC 1 & 2

Figure 7.16: Optimal displacement amplitudes against incident wave angle for optimal unconstrained linear five-WEC array, optimised for $\beta \in [\frac{3\pi}{8}, \frac{5\pi}{8}]$ (shown by horizontal dashed lines)

are seen for the closely spaced group of three devices (WECs 3 - 5). These WECs exhibit motion amplitude of $\mathcal{O}(50)$ to $\mathcal{O}(100)$ times the incident wave amplitude, which are unacceptable. The isolated WECs have smaller motions of between five and seven times the wave amplitude. However, these are still too large to be considered $\mathcal{O}(1)$ and thus also violate the underlying linear wave theory.

7.6 Discussion of results

This chapter considers an alternative optimisation to previous chapters by employing a different objective function. Previously, the mean of the averaged interaction factor was maximised over a prescribed non-dimensional length. Herein, the maximisation was taken over a prescribed range of incident wave angle. This was motivated by the relatively high sensitivity of previously identified optimal arrays to changes in β. This optimisation is applied to both constrained and unconstrained arrays to allow comparison with previous chapters. Initially, consideration is limited here to linear arrays but will be extended to a general geometry in Chapter 8.

Section 7.3 analysed the performance of uniform arrays with respect to this new objective function. This provided an immediate comparison of uniform arrays with the objective function of previous chapters and served as benchmark for the layout optimisation results of this chapter.

In a comparison of the unconstrained uniform and optimal arrays, a significant improvement of between 13% to 25% in performance is achieved by the optimised arrays, relative to the uniform layouts. In all cases, the optimised layouts differed considerably from a uniform layout and contained closely spaced groups of two to four WECs; it is acknowledged that these close spacings may cause physical and theoretical problems. Another concern with all of the unconstrained arrays is that the displacement amplitudes of the WECs were unacceptably large, which would cause physical engineering difficulties; more importantly in the present context this would invalidate the mathematical model, which assumes linear wave theory is applicable.

The optimal constrained arrays achieved an improvement of between 0.4% to 18.6% relative to the analogous uniform arrays. This increase was smallest for the head seas array, where an improvement of less than 1% on the uniform array

was achieved for both constraints and was due to the optimal array layouts being very close to uniform, with only small perturbations from the uniform case giving an increase in objective function value. A moderate improvement is achieved for beam seas by moving some of the WECs as close as possible, creating two closely spaced pairs of WECs. However, there are acknowledged difficulties with these close spacings. Therefore a more uniform array may be more desirable, since only a small reduction in performance would result and there is no significant increase in sensitivity of the array to changes in β or k.

Following previous discussion, one possible solution to the problem of closely spaced WECs is to consider larger devices. It may be possible to recreate the appropriate interaction effects by replacing groups of WECs with a suitably larger WEC. One drawback with this approach is that the WECs in the group may be oscillating out of phase with each other and replacing these with a single device may not be possible, unless the large device can operate in more than one mode of motion. Nonetheless, the optimal constrained array in beam seas had all WECs operating in phase, indicating that replacement of groups with a single larger WEC may be possible. It is unclear though how the replacement of a group with a larger WEC will affect the β-sensitivity of the array. The notion of arrays of differently sized WECs has not been extensively considered in the literature and may provide a novel solution to this difficulty.

The best overall constrained array identified in this chapter is for head seas. For the constraint of $\delta_{max} = 3$, an average performance of $\overline{I_\beta} = 0.9376$ is achieved, such that destructive interference has only a relatively small impact. Reasonable performance of $\overline{I_\beta} = 0.794$ is achieved for the lower constraint of $\delta_{max} = 2$. Most significantly, the stability of this array for changes in β is ideal, as performance remains relatively constant over the range $\beta \in [-\frac{\pi}{8}, \frac{\pi}{8}]$, where $\overline{q} \approx 1$ for the higher constraint and $\overline{q} \approx 0.8$ for the lower constraint. In both cases, this means that a small change in β will result in a negligible change in $\overline{q}$ for this array. However, the one weakness is the relative sensitivity to changes in wavenumber, where a 10% change in k can result in a 50% reduction in performance.

An interesting observation is the lack of symmetry of the optimal beam sea arrays for both constrained and unconstrained motions. Unlike the results of Chapter 3, symmetry is not enforced herein and the WEC spacings are independent of one-another within the optimisation routine. These results suggest that better overall performance is achieved when some devices are placed in close proximity to one another, even for constrained motions. This is

contrary to the intuitive idea of equal spacing for normal wave incidence. It should be stressed that the mirror image of the each of the optimal beam sea layouts are also necessarily optimal via equation (2.165). It is unclear why symmetry is not achieved in the optimal beam sea arrays. It may be that having non-symmetric layouts allows for greater constructive interaction or greater stability of performance over the range of β considered.

In general, comparing all constrained arrays considered in this chapter, there appears to be a trade-off between β-stability and k-stability. The results suggest that if an array is stable to changes in β, then it is more sensitive to changes in k, and visa-versa. This was also encountered in Chapter 6 where a similar phenomenon was noticed. Previously, the arrays were forced to exhibit stability to changes in k since the optimisation maximised the mean performance over some non-dimensional length measure (kL for linear arrays). This then results in high β-sensitivity of the optimal arrays, particularly for the better performing arrays. In the present application, the array is forced to perform well with respect to β, since the mean over β is maximised. In some cases herein, this results in a considerable k-sensitivity of the optimal arrays, especially for arrays with the highest performance.

This suggests a limitation on what can be achieved in terms of the stability of linear array performance, i.e. that a linear array cannot be stable to changes in both k and β. Thus, care must be taken both when an array site is being chosen and in the design of the array. A site that has large variation in both incident wave angle and wavelength is undesirable. It may also be desirable to have a variation in one parameter instead of another. A careful study of the variation of site conditions and resulting performance of the array should be carried out before any given WEC array site is utilised.

It is clear that there is a relationship between the optimal array layout and the applied constraint in each case examined. As the constraint becomes less strict (i.e. as $\delta_{max} \to \infty$), the optimal layout must approach that of the unconstrained case. By examining the two constraints applied for intermediate and beam seas, it can be seen that there is at most only a slight difference between the optimal layouts for $\delta \leq 2$ and $\delta \leq 3$. This suggests that the evolution from the constrained optimal layout to the unconstrained optimal layout occurs continuously and that the optimal layout does not suddenly jump from one formation to another as δ_{max} increases.

Another interesting phenomenon is the contrast in performance at different

wave angles between the constrained and unconstrained optimal arrays. For unconstrained motions, the best performance is seen for beam seas. This is to be expected intuitively, as the greater frontage of a terminator-type layout to the incident wave would allow a greater power absorption in principle. However, when constrained motions are considered, the best performance is seen for the head seas arrays. This suggests a considerable shift in optimal geometry once motion constraints are applied and is due to the inherent β-sensitivity of linear arrays in beam seas. The relative β-stability seen for head seas may be because head sea arrays absorb less power, thus applying constraints would have less of a relative detrimental impact. Beam sea arrays tend to absorb more power and exhibit greater interaction factor values for unconstrained motions, thus the application of constraints would have a greater relative impact in beam seas which adversely affects the overall performance of the array, including the β-stability.

One possible extension to the method described in this chapter is to consider a weighted version of the optimisation. If detailed information about the variation of the incident wave angle at a given site is known, then this can be incorporated into a weighting function within the objective function. For example, a large proportion of the waves will often come from one wave angle, with a smaller fraction incident from other angles. Therefore, optimising equally over all incident wave angles is not appropriate and will give equal weight to the smaller proportion of waves.

A suitable optimisation could easily be implemented by including a weighting function $W(\beta)$ to model the proportion of incident waves over the wave angle range. For unconstrained motions, the objective function would be altered to

$$I_\beta^W(\mathbf{ks}) = \frac{1}{\beta_u - \beta_l} \int_{\beta_l}^{\beta_u} W(\beta) q(\mathbf{ks}, \beta)\ d\beta, \tag{7.4}$$

while for constrained motions the objective function would be written as

$$\overline{I_\beta^W}(\mathbf{ks}, \boldsymbol{\delta}, \boldsymbol{\psi}) = \frac{1}{\beta_u - \beta_l} \int_{\beta_l}^{\beta_u} W(\beta) \overline{q}(\mathbf{ks}, \boldsymbol{\delta}, \boldsymbol{\psi}, \beta)\ d\beta. \tag{7.5}$$

The weighting function would also have to be normalised and a possible candidate is

$$\int_{\beta_l}^{\beta_u} W(\beta)\ d\beta = 1. \tag{7.6}$$

This would ensure that the net effect on the objective function is neutral.

A preliminary exercise employing this weighted optimisation was undertaken using a cosine squared weighting of the form

$$W(\beta) = \frac{2}{\beta_u - \beta_l} \cos^2\left[\frac{\pi}{\beta_u - \beta_l}\left(\beta - \frac{\beta_u + \beta_l}{2}\right)\right], \tag{7.7}$$

for $\beta_u - \beta_l = \frac{\pi}{4}$. However, this caused no significant change in the results presented in this chapter. If a more specific knowledge of a given WEC site is known, and $W(\beta)$ can be constructed to accurately model the incident wave climate, then this weighted optimisation may give better optimal results for that specific site. This method can be considered as halfway between a regular and irregular wave implementation. The advantage of this method is its relative simplicity and reduced computation time compared to an irregular wave implementation. A discussion of an irregular wave optimisation is given in Chapter 9.

Chapter 8

Optimisation of General 2D Arrays over Incident Wave Angle

A principal weakness of the optimisation presented in Chapters 3 - 6 is the requirement to prescribe an array geometry prior to the optimisation. This is necessary in order to define a meaningful non-dimensional length measure, over which the mean of the interaction factor is defined. In a general two-dimensional optimisation of N WECs, there is no obvious length measure over which a mean should be taken. The most reasonable measure may perhaps be the sum of the distances of all the WECs from each other or from the origin. However, maximising the mean performance over either of these length measures will have a net effect of penalising array layouts that are spread apart and result in moving the devices as close to each other, or the origin, as possible.

One benefit of the wave angle optimisation presented in Chapter 7 is that it does not require a prescribed geometry, since the incident wave angle β is well defined irrespective of the array layout. This allows the implementation of a more general two-dimensional optimisation of the array formation. An extension of the wave angle optimisation of Chapter 7 is thus considered here, where the array geometry is not prescribed as linear. This is applied to constrained and unconstrained motions. Both position variables of each WEC (kd_j and α_j) are fed into the optimisation, along with the displacement variables if constrained motions are considered.

Following the increased generality introduced into the optimisation process, it is anticipated that better performing arrays will be found relative to Chapter 7. This will facilitate further analysis of the trade-off between performance and

stability of performance over the array variables. The more general optimisation will also confirm if this trade-off is an artefact of certain array geometries or if it applies to arrays in general. In this sense it addresses a very important topic in array design.

The increased generality clearly adds to the computational demand of the numerical optimisation due to the increased number of variables, as well as the larger search space for each variable. In previous chapters, the WEC position variables required greater computational effort to achieve convergence to optimal solutions; therefore a fine scan over these variables is required. As a consequence, increasing the number of WEC position variables will have a considerable impact on the computational power required for the optimisation.

8.1 Optimisation Methodology

The overall method follows that described in Chapter 7, with the change that the array is not prescribed as linear. In the case of a non-prescribed geometry and a general 2D optimisation, the coordinates of all but the first device (which is fixed at the origin) are fed into the optimisation as variables. The physical coordinates of the jth device are (d_j, α_j), which give its distance and angle from the origin, as described in Section 2.4.3. Therefore, the non-dimensional coordinates utilised are (kd_j, α_j).

Using these variables, the objective function for a 2D unconstrained array is defined as

$$I_\beta(\mathbf{kd}, \boldsymbol{\alpha}) = \frac{1}{\beta_u - \beta_l} \int_{\beta_l}^{\beta_u} q(\mathbf{kd}, \boldsymbol{\alpha}, \beta)\, d\beta, \tag{8.1}$$

where $\mathbf{kd}$ and $\boldsymbol{\alpha}$ are $N-1$ component vectors whose elements contain the kd_j and α_j variables respectively. In an attempt to limit the search space of the optimisation and to restrict the array layout to a reasonable area, an upper limit of $kd_j \leq 20$ is imposed for $j = 2, \ldots, N$. To avoid replication of results, the array is also forced to lie in the upper plane by enforcing constraints on α_j such that $0 \leq \alpha_j \leq \pi$ for $j = 2, \ldots, N$. These constraints limit the area of the array to within a semicircle in the upper half plane of radius 20.

Constrained versions of the above objective function are also considered, where device motion amplitudes are limited to an upper value (usually $\delta \leq 2$ or $\delta \leq 3$). Similar objective functions are utilised with the interaction factor q replaced by the averaged interaction factor $\overline{q}$. Therefore, the constrained version

of the objective function is given by

$$\overline{I_\beta}(\mathbf{kd}, \boldsymbol{\alpha}, \boldsymbol{\delta}, \boldsymbol{\psi}) = \frac{1}{\beta_u - \beta_l} \int_{\beta_l}^{\beta_u} \overline{q}(\mathbf{kd}, \boldsymbol{\alpha}, \boldsymbol{\delta}, \boldsymbol{\psi}, \beta)\ d\beta, \tag{8.2}$$

where $\boldsymbol{\delta}$ and $\boldsymbol{\psi}$ are N-component vectors containing the displacement amplitude and phase variables respectively.

Analogous objective functions can be defined using the generalised interaction factor q_{gen}. However, as was discussed in Chapter 6, q_{gen} appears to behave as a scaled version of $\overline{q}$ with very minor differences. Following the increased computational demand of the optimisations with q_{gen}, objective functions employing the generalised interaction factor will not be implemented in this work.

There should be no need to examine different target values of incident wave angle, since it is clear that if an optimal array is found for one wave angle range, then a different target range should simply produce a rotation of the original optimal layout. Therefore, rather than examining different target wave angles, several range lengths are instead considered with the mid-point of each range remaining the same. For convenience, the target wave angle is assumed to be $\beta = \frac{\pi}{2}$ and the optimisation ranges are taken to have variations of $\pm\frac{\pi}{16}$, $\pm\frac{\pi}{8}$ and $\pm\frac{\pi}{4}$. Thus the corresponding optimisation ranges investigated are $\beta_0 \in [\frac{7\pi}{16}, \frac{9\pi}{16}]$, $[\frac{3\pi}{8}, \frac{5\pi}{8}]$ and $[\frac{\pi}{4}, \frac{3\pi}{4}]$ which will be referred to as narrow, intermediate and broad-banded β-variation ranges respectively.

Within this optimisation, the array was constrained to lie in the upper half plane $y \geq 0$ by enforcing the condition that the angular positions of all devices was $\alpha_j \in [0, \pi]$. An analogous layout that would be discovered in the lower half plane performs identically by symmetry, therefore limiting the optimisation to one half plane reduces the search space without loss of generality. Limits on the minimum and maximum size of the array were enforced by limiting the radial position of all WECs to $1 \leq kd_j \leq 20$. For a typical ocean wavelength of 150m, this corresponds approximately to $d \in [23\text{m}, 480\text{m}]$. To minimise calculation difficulties and to retain physical consistency, a further limit on the non-dimensional separation distance between any two WECs was also enforced such that $1 \leq kd_{nm} \leq 40$; note that this limit is consistent with the constraint on kd_j. A minimum separation of unity between any two WECs was enforced in order to avoid touching WECs and also to avoid numerical difficulties associated with small WEC separations. This prevented WECs being placed too close

together, while maintaining consistency with the search domain.

In principle, all array configurations can be considered in the upper half plane in this manner. As one array member must lie at a lower or equal y-coordinate relative to all other members, the coordinate system can be chosen so that this WEC is at the origin (or on the x-axis) and all other array members then lie in the upper plane. However, this only holds if the maximum non-dimensional separation between any two array members is less than 20, otherwise it may not be possible to perform a coordinate translation such that all WECs are maintained within $kd_j \in [1, 20]$.

For unconstrained optimisations of this type, the optimisation contains $2(N-1)$ variables, corresponding to the radial and angular positions of each WEC when WEC 1 is fixed at the origin. The constrained optimisations contain an additional $2N$ variables, comprising of the displacement amplitudes and phases of each WEC, resulting in a total of $4N-2$ optimisation variables. In order to keep the optimisation feasible from a numerical perspective, and to allow comparison with previous chapters on linear arrays, an array of five WECs is examined in this chapter. This results in eight optimisation variables for unconstrained motions and eighteen variables for the constrained optimisation.

As with previous optimisations of this type, an exhaustive search over the possible starting points of the optimisation is required. As a consequence of the larger number of variables and the increased freedom of each variable, this exhaustive search required considerable computational resources. For the unconstrained optimisation, all possible combinations of starting points with $kd_j = \{4, 8, 12, 16, 20\}$ and $\alpha_j = \{0, \frac{\pi}{5}, \ldots, \pi\}$ for $j = 2, \ldots, 5$ were investigated, with combinations involving coincident devices forbidden. This involved a total of approximately 225,000 iterations in the optimisation, hence the large computation time of typically between five and ten hours for the unconstrained optimisation. The results of this scan of staring points were encouraging, as in each case the optimisation routine repeatedly converged to a single optimal solution, to an analogous one by symmetry or to one obtained by interchanging the WECs. The best optimal solution was converged to repeatedly by the optimisation between 1000 to 5000 times, indicating the stability of the optimisation and confirming the optimality of the solution.

The aspect of computation time is more severe for constrained motions, where there is an extra ten displacement variables which must be scanned over. However, as discussed in previous chapters, these displacement variables

converged to their optimal solution much better than the position variables. This meant that a more sparse scan of the stating point space could be implemented for these variables. Thus, the starting point space for constrained motions was $kd_j = \{5, 10, 15, 20\}$, $\alpha_j = \{0, \frac{\pi}{4}, \ldots, \pi\}$ for $j = 2, \ldots, 5$ and $\widetilde{\delta_n} = \{-3, 0, 3\}$, $\psi_n = \{0, \frac{\pi}{2}\}$ for $n = 1, \ldots, 5$, with combinations involving coincident WECs excluded. This resulted in approximately 185,000 calls of the optimisation routine, which is slightly less than the unconstrained optimisation. However, the optimisation had greater difficultly converging to the optimal set of variables and was required to make more steps within the minimisation process, thus making more calls to the objective function. This increased the computational effort significantly, resulting in run times of approximately 20 hours.

The optimisation results for constrained motions cannot be considered as reliable as those for unconstrained motions, as the optimisation routine did not converge repeatedly to the best set of variables found for an appropriate number of runs. Most cases resulted in the optimisation converging to the same optimal result approximately 100 times but in some cases the optimal solution was converged to only on three occasions. Thus the constrained optimisation is not as stable as the unconstrained version. Therefore, the results for the constrained arrays are not presented as optimal with confidence, but rather the best case found by the optimisation within a reasonable calculation time.

8.2 Optimisation Results

This section presents the results of both the constrained and unconstrained β-optimisation of general two-dimensional five-WEC arrays. The best performing array variables and the resulting objective function values are listed in tables and the results discussed. A detailed analysis of each optimal array is provided in Section 8.3.

8.2.1 Unconstrained Motions

The optimisation results for the unconstrained optimisation are shown in table 8.1 for each of the ranges of incident wave angle considered. There are many analogous layouts found to those presented; these involved an interchanging of WECs or a symmetric layout about the y-axis. In each case, the optimal array

Table 8.1: Optimal position variables for the general 2D unconstrained five-device array

$[\beta_l, \beta_u]$	kd_2	kd_3	kd_4	kd_5	α_2	α_3	α_4	α_5	I_β
$[\frac{7\pi}{16}, \frac{9\pi}{16}]$	8.8663	4.2112	4.7345	9.2854	0.0840	0.0000	0.1911	0.1842	1.9451
$[\frac{3\pi}{8}, \frac{5\pi}{8}]$	8.8717	4.4099	8.4211	3.9625	2.9222	2.9272	3.0256	3.1416	1.7744
$[\frac{\pi}{4}, \frac{3\pi}{4}]$	7.1035	3.4967	7.1750	3.6061	3.1416	3.1416	3.0018	2.8608	1.4466

(or an analogous array) was a convergence by the optimisation at least 1000 times, giving confidence in the optimal solution.

Firstly, it is clear from table 8.1 that better performance is achieved in the case of narrower wave angle ranges. This is to be expected, even when optimal motions are enforced for all wave angles, since the performance of an array with respect to β is limited by

$$\frac{1}{2\pi}\int_0^{2\pi} q \; d\beta = 1, \tag{8.3}$$

as shown by Fitzgerald (2006). Thus, better performance can be achieved by contriving the array to perform well in a small β-range, since poor performance outside this range is of no concern. For broader β-ranges, (8.3) limits overall performance and results in lower objective function values.

As a consequence, the best performing array was for the narrow β-variation ($\beta \in [\frac{7\pi}{16}, \frac{9\pi}{16}]$), where very high mean performance of $I_\beta = 1.9451$ was achieved. The intermediate and broad wave angle ranges resulted in a mean performance drop of approximately 9% and 26% respectively relative to the narrow-banded case. As expected, the poorest performing array is for the broad-banded variation, where a mean performance of $I_\beta = 1.4466$ was achieved.

In each optimal array, neither the upper nor the lower limit of kd_j is reached for any WEC, however the lower limit of $kd_{nm} = 1$ has been encountered for some devices in each array. This is clear in the array diagrams in Section 8.3. The limits of α_j are not as important, other than when they feed into the kd_{nm} constraint. It is also worth noting that a value of $\alpha_j = 0$ or $\alpha_j = \pi \approx 3.1416$ indicates that a WEC is placed on the x-axis, while a value of $\alpha_j = \frac{\pi}{2} \approx 1.5708$ would indicate that the device is placed on the y-axis.

A schematic showing the optimal array layouts for the unconstrained optimisation is presented in figure 8.1. It is clear that the optimal layouts are similar for each range of incident wave angle considered. In each case, the WECs are located close to the x-axis in two closely spaced pairs. The

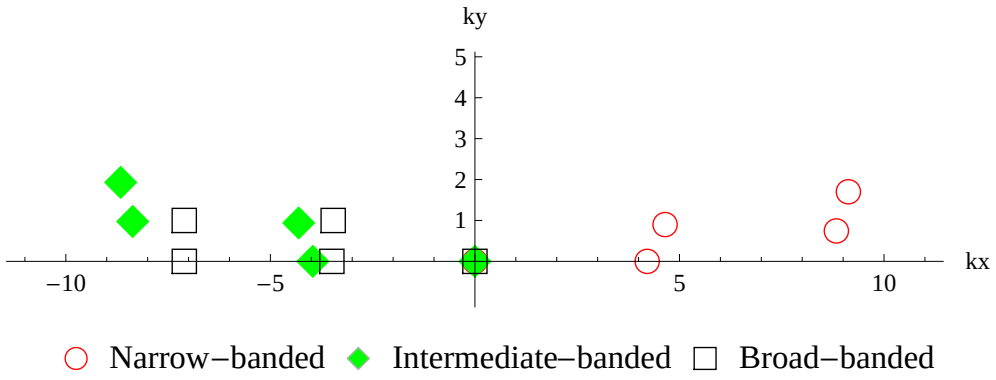

Figure 8.1: Diagram of optimal unconstrained arrays for each range of incident wave angle

narrow-banded optimal array is more spread out from the origin, while the broad-banded layout is closer to the origin. For the narrow-banded case, the WECs are positioned to the right of the origin, while the WECs are located to the left for the intermediates and broad-banded cases. This is probably due to the numerical optimisation arbitrarily converging to one orientation or the other, since the arrays will perform analogously if reflected about the y-axis via equation (2.165).

A slight improvement or a reduction in the optimal performance of the array was seen in some cases for alternate target wave angle ranges of the same size. For example, an intermediate-band range of $\beta \in [-\frac{\pi}{8}, \frac{\pi}{8}]$ resulted in a slightly better optimal array, which achieved $I_\beta = 1.7815$, a 0.4% improvement on the result presented in table 8.1. This is due to the limits of $kd_j < 20$ and $0 \leq \alpha \leq \pi$ forbidding the analogous rotated array from being found and so the optimisation converges to a slightly poorer performing array that is optimal given the optimisation parameters.

This difficulty cannot be avoided without a significant increase in the variable space within the optimisation. This would not only increase the space over which the optimisation must converge but also increase the starting point space for the WEC position variables, which would significantly reduce the performance of the optimisation routine. One possible solution would be to allow the optimisation to scan the whole plane, rather than just the upper half plane. However, this would significantly increase the run-time due to the increased parameter space. It would also result in increased repetition in the converged solutions, as the optimisation would find continuously analogous arrays due to rotation, translation or interchanging of WECs.

Table 8.2: Optimal position variables for the general 2D constrained five-device array

$[\beta_l, \beta_u]$	δ_{max}	kd_2	kd_3	kd_4	kd_5	α_2	α_3	α_4	α_5	$\overline{I_\beta}$
$[\frac{7\pi}{16}, \frac{9\pi}{16}]$	3	3.2631	2.9228	3.4293	1.8838	2.4752	2.9546	0.0000	0.9289	1.2137
	2	3.4037	2.9600	3.3490	1.9423	3.1416	0.2224	0.7160	2.1902	0.9293
$[\frac{3\pi}{8}, \frac{5\pi}{8}]$	3	5.2541	5.2541	2.5260	2.5260	1.2300	1.9116	0.1224	3.0192	1.0574
	2	5.3703	2.4178	5.3703	2.4178	1.8954	2.9652	1.2462	0.1764	0.8363
$[\frac{\pi}{4}, \frac{3\pi}{4}]$	3	2.0031	2.3468	2.3468	2.0031	0.1996	0.9252	2.2164	2.9420	0.7085
	2	1.9465	2.4384	1.9465	5.1714	2.7676	1.5708	0.3740	1.5708	0.6350

Table 8.3: Optimal displacement variables for the corresponding general 2-D constrained five-device arrays in table 8.2

$[\beta_l, \beta_u]$	δ_{max}	$\widetilde{\delta_1}$	$\widetilde{\delta_2}$	$\widetilde{\delta_3}$	$\widetilde{\delta_4}$	$\widetilde{\delta_5}$	ψ_1	ψ_2	ψ_3	ψ_4	ψ_5
$[\frac{7\pi}{16}, \frac{9\pi}{16}]$	3	-3.0000	3.0000	-3.0000	-3.0000	-3.0000	1.7660	0.7140	2.1235	1.6480	3.1416
	2	-2.0000	-2.0000	-2.0000	2.0000	2.0000	1.7927	1.6695	2.2991	0.8278	0.1598
$[\frac{3\pi}{8}, \frac{5\pi}{8}]$	3	-3.0000	-3.0000	-3.0000	-3.0000	-3.0000	1.6092	0.4051	0.4051	1.9592	1.9592
	2	-2.0000	-2.0000	-2.0000	-2.0000	-2.0000	1.6721	0.4837	2.0958	0.4837	2.0958
$[\frac{\pi}{4}, \frac{3\pi}{4}]$	3	-2.2652	-3.0000	3.0000	3.0000	-3.0000	1.3953	2.1598	0.3995	0.3995	2.1598
	2	-2.0000	-2.0000	2.0000	-2.0000	-2.0000	1.4044	2.4292	0.7421	2.4292	0.4403

Further analysis of the optimal array layouts and the optimal displacements, along with their performance with respect to variation of wave parameters, is presented in Section 8.3.

8.2.2 Constrained Motions

Following the practice of previous chapters, two displacement amplitude limits are considered in the constrained optimisation with the displacements limited to two or three times the incident wave amplitude, so that $\delta_{max} = 2$ or $\delta_{max} = 3$ respectively. Tables 8.2 and 8.3 show the optimisation results for both constraints for all incident wave angle ranges considered. As a consequence of the large number of variables to be presented, the optimal WEC position variables are given in table 8.2, while the optimal displacement variables corresponding to the same arrays are displayed in table 8.3.

As with the unconstrained motions, the best performance is seen for the narrower ranges of β. The array with the highest optimal value of $\overline{I_\beta} = 1.2137$ is the one optimised over the narrow-banded range of β with the constraint

$\delta_{max} = 3$. This indicates, that despite the motion constraint applied to the WECs, constructive interaction is maintained. The same is true for the intermediate-banded optimal array with $\delta_{max} = 3$, where $\overline{I_\beta} = 1.0574$ is achieved. Although this performance is lower, constructive interaction still dominates.

Significantly reduced performance is seen for the lower constraint of $\delta_{max} = 2$ in comparison to $\delta_{max} = 3$, as expected. In each case, the $\delta_{max} = 2$ arrays result in a reduction of between 10% and 25% compared with analogous $\delta_{max} = 3$ arrays. No array with this lower constraint achieved $\overline{I_\beta} \geq 1$, indicating that this constraint is more restrictive and destructive interference dominates. However, for the narrow-banded array, $\overline{I_\beta} = 0.9293$ is achieved, which is only slightly lower than unity, indicating that modest performance is maintained.

In general, arrays optimised over larger ranges of β return lower objective function values. This is due to the increased range over which the mean is defined. For a narrow-banded variation of β, it is possible to tune the WECs to perform well within the entirety of a small incident wave angle range. However, for broader ranges, this is not possible as the array cannot perform well over all of this broader range, thus lower overall performance is seen. Although equation (8.3) does not apply to constrained motions, the same argument can be made whereby the array cannot perform well at all angles, hence the lower performance for broader β ranges.

For constrained motions, it does not appear that any of the WEC position variables reached either limit on kd_j or kd_{nm}, indicating that no WEC is within close proximity to another. This is in line with the results of previous chapters, where in general applying constraints on WEC motions resulted in more spread-out arrangements, with no grouped WECs.

It is clear from table 8.3 that all WECs reached the maximum allowed amplitude constraint of $\delta_{max} = 2$ or $\delta_{max} = 3$ for each optimal array, with the exception of the broad-banded $\delta_{max} = 3$ array. This indicates that the WECs are working equally hard in each of these arrays and absorb the same amount of energy. In the narrow-banded optimal arrays, the WECs have different phases to each other. However, in the intermediate and broad-banded optimal arrays, at least one pair of WECs operate at the same phase. This is due to symmetry in the optimal layout, as will be considered in Section 8.3.

In the broad-banded $\delta_{max} = 3$ case, the motion amplitude of WEC 1 does not

reach its maximum allowed value, unlike all other optimal constrained arrays. This indicates that reduced amplitude of this WEC somehow increases the mean performance with respect to β-variation. It may be that this reduces the peak performance slightly but improves the β-sensitivity of this optimal array, thus allowing the array to perform its best over the entire range of $\beta \in [\frac{\pi}{4}, \frac{3\pi}{4}]$.

8.3 Analysis of Optimal Arrays

In this section, the optimal arrays found in Section 8.2 are analysed in more detail. For convenience, the analysis is conducted by the range of incident wave angle considered. Thus all constrained and unconstrained narrow-banded arrays are analysed in Section 8.3.1, similarly for intermediate-banded arrays in Section 8.3.2 and broad-banded arrays in Section 8.3.3. In each case, a diagram of the optimal constrained and unconstrained array layouts is presented. The performance of each array with respect to β-variation and wavenumber variation is also assessed. Finally, the optimal WEC displacement amplitudes for the unconstrained array are presented and analysed.

8.3.1 Narrow-Banded $\beta \in [\frac{7\pi}{16}, \frac{9\pi}{16}]$

A diagram of the optimal constrained and unconstrained narrow-banded optimal arrays is shown in figure 8.2. It is clear that an appreciably different layout is found for each of the different displacement limits. The unconstrained array results in two pairs of closely-spaced WECs separated to the right of the origin. The separation between each of these pairs and the origin is approximately five units, while the paired WECs are placed as close to each other as allowed by the optimisation, with a unitary separation between them. The two constrained arrays are more central and contained within five units of the origin, with two WECs either side of the y-axis. Initially it would appear that the $\delta_{max} = 2$ and $\delta_{max} = 3$ constraints result in considerably different optimal layouts. However, an examination of both arrays shows that they are almost mirror images of each other about the y-axis. Closer inspection reveals that the layouts are not exact mirror images of each other, as the $\delta_{max} = 2$ optimal array is slightly more separated from the origin. This suggests that the mirror arrangement of each array is analogously optimal for the given constraint but that the optimisation routine arbitrarily converged to the different symmetries in each case.

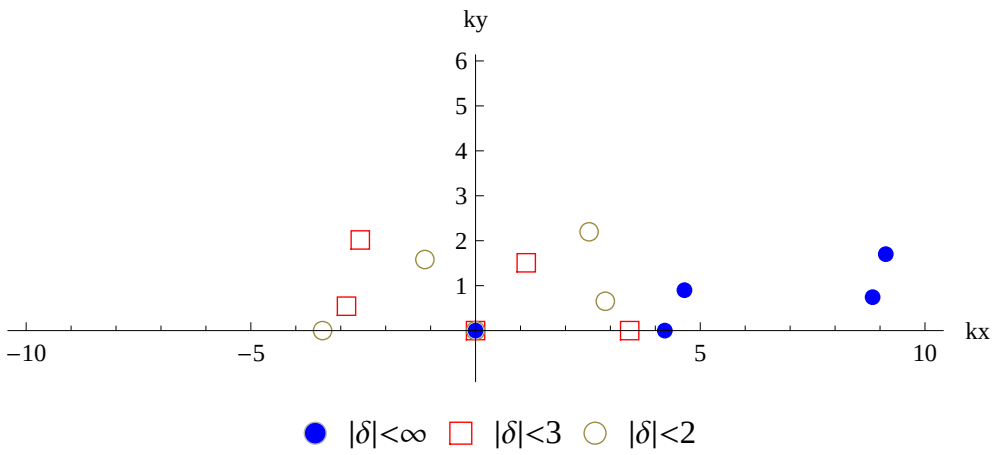

Figure 8.2: Diagram of optimal arrays for narrow-banded range of incident wave angle $\beta \in [\frac{7\pi}{16}, \frac{9\pi}{16}]$

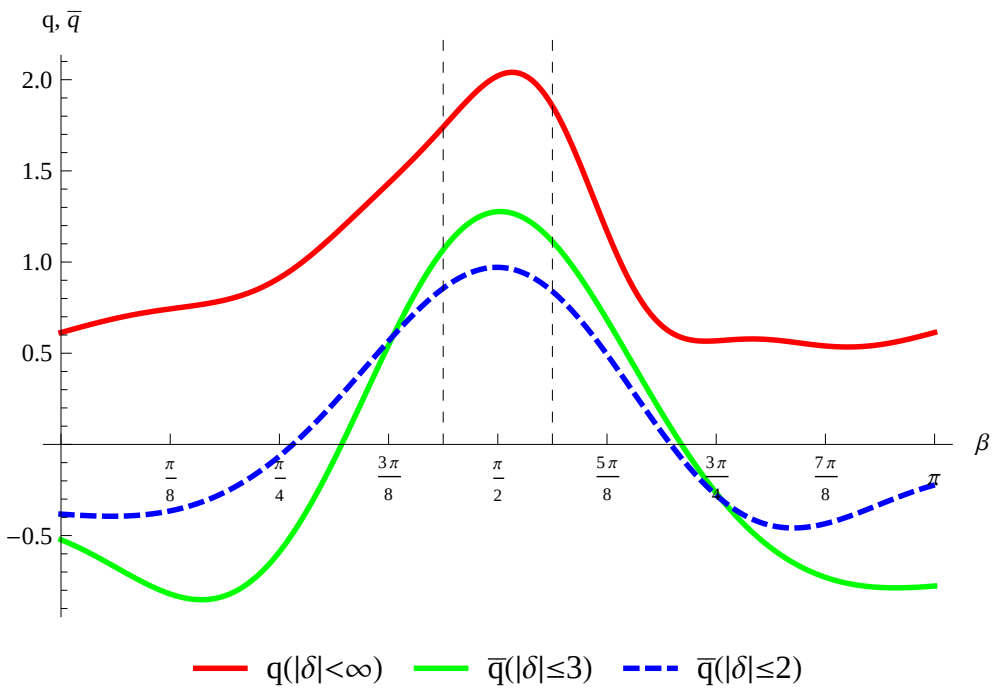

Figure 8.3: Interaction factor against incident wave angle β for optimal constrained and unconstrained five-WEC arrays, optimised for $\beta \in [\frac{7\pi}{16}, \frac{9\pi}{16}]$. The target range of wave angles is indicated by the vertical dashed lines.

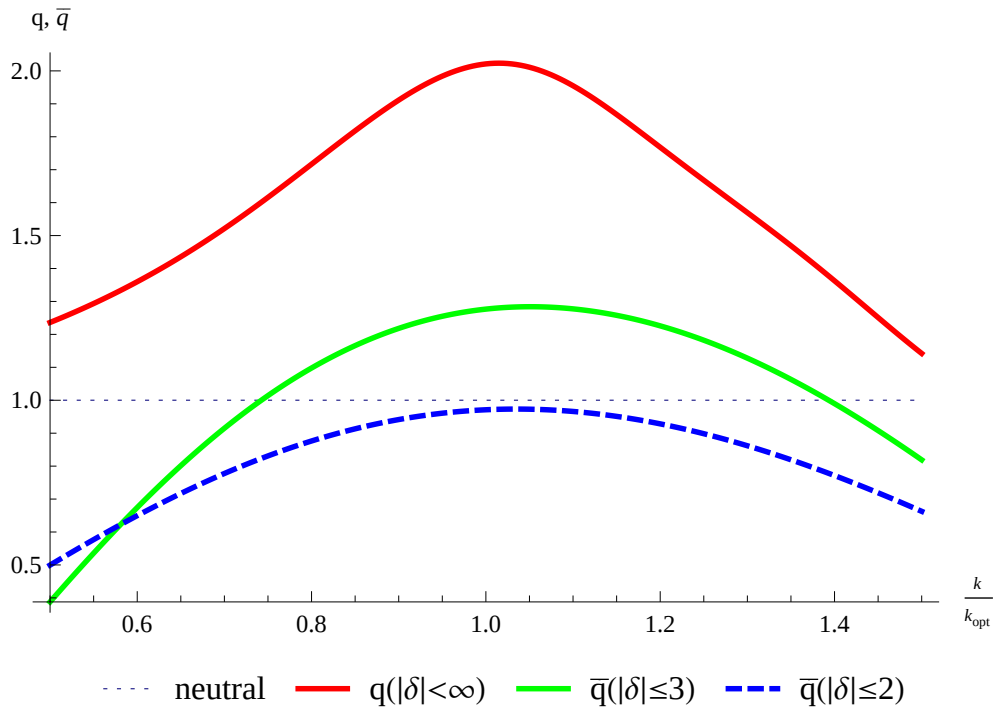

Figure 8.4: Interaction factor against wavenumber $\frac{k}{k_{opt}}$ for optimal narrow-banded constrained and unconstrained five-WEC arrays, with $\beta = \frac{\pi}{2}$.

The performance of the optimal arrays with respect to β-variation is shown in figure 8.3. It is clear that each array is forced to perform best within the range of interest $\beta \in [\frac{7\pi}{16}, \frac{9\pi}{16}]$, since the performance of each array peaks in this range and the unconstrained array maintains a high interaction factor with $q \in [1.7, 2.1]$ within the range of interest. The two constrained arrays show a considerably reduced performance and return averaged interaction factors of the order of half of the unconstrained case. However, constructive interference is maintained in the $\delta_{max} = 3$ case, with $\overline{q} \in [1.1, 1.3]$ for all $\beta \in [\frac{7\pi}{16}, \frac{9\pi}{16}]$. Even though this is not the case for $\delta_{max} = 2$, adequate performance is maintained with $\overline{q} \in [0.85, 1.0]$.

The influence of wavenumber variation on each optimal narrow-banded array is shown in figure 8.4. The unconstrained optimal array maintains $q > 1$ performance for up to a 50% variation about k_{opt}. The application of constraints causes a reduction in performance for the upper constraint, with constructive interference maintained for $\frac{k}{k_{opt}} \in [0.75, 1.4]$, indicating that at least a 25% change in k is required to move from constructive to destructive interference. Due to the lower constraint having a greater effect on performance, $q < 1$ holds for all values of $\frac{k}{k_{opt}}$ considered. Each array is relatively stable

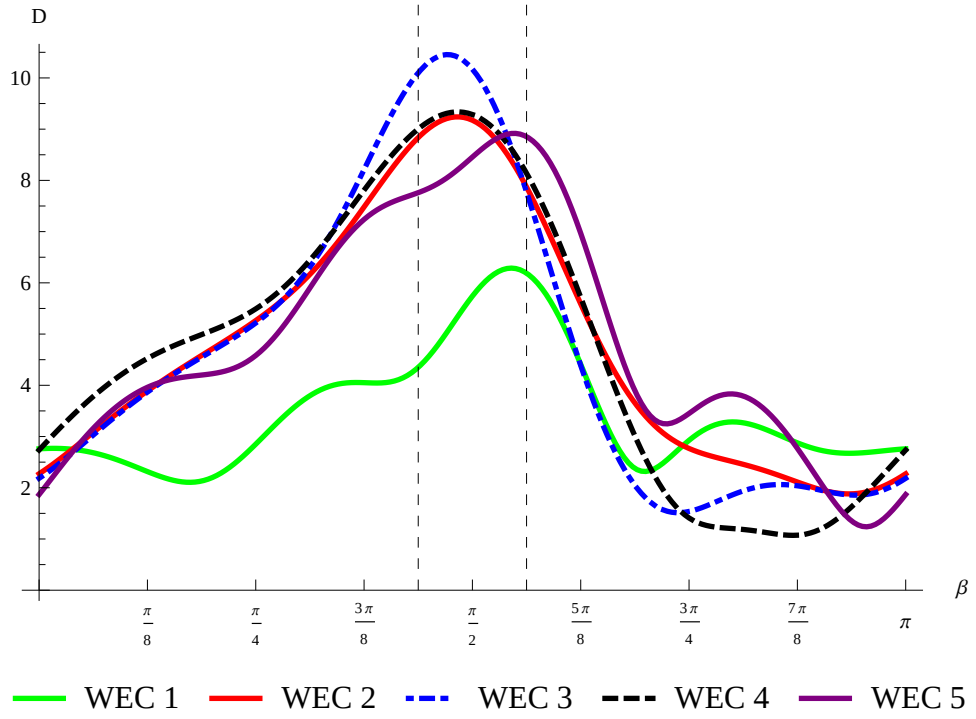

Figure 8.5: Optimal displacement amplitudes against incident wave angle for optimal unconstrained five-WEC array, optimised for $\beta \in [\frac{7\pi}{16}, \frac{9\pi}{16}]$ (shown by horizontal dashed lines)

overall to changes in wavenumber, with a small relative change in k producing only a small change in q or $\overline{q}$. It is noteworthy that the peaks in figure 8.4 occur at values slightly above $\frac{k}{k_{opt}} = 1$.

Finally, the predicted optimal WEC displacement amplitudes for the unconstrained array are shown in figure 8.5. It is clear that there is a correlation between the peak in performance in figure 8.3 and the peaks in WEC displacements in figure 8.5. The paired devices (WECs 2 - 5) exhibit larger motions than the relatively isolated WEC at the origin. However, all WECs have $\delta > 4$ within the range of interest $\beta \in [\frac{7\pi}{16}, \frac{9\pi}{16}]$ and so violate the $\mathcal{O}(1)$ requirement of the model. It is worth noting that although the displacements violate the $\mathcal{O}(1)$ requirement, they are two orders of magnitude smaller than the optimal linear array displacements from Chapters 3, 4 and 7.

8.3.2 Intermediate-Banded $\beta \in [\frac{3\pi}{8}, \frac{5\pi}{8}]$

A schematic of the optimal array layouts for intermediate-banded β-ranges are shown in figure 8.6 for constrained and unconstrained motions. A similar

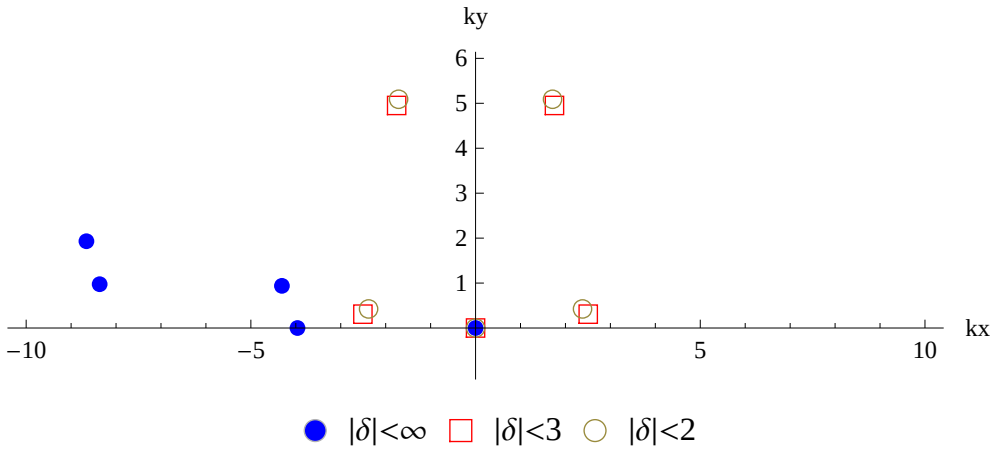

Figure 8.6: Diagram of optimal arrays for intermediate-banded range of incident wave angle $\beta \in [\frac{3\pi}{8}, \frac{5\pi}{8}]$

optimal unconstrained layout to the narrow-banded case is found, with all WECs on the left of the origin rather than the right. Again, this contains two closely spaced pairs of WECs with unitary separation. The pairs have a separation of approximately four units between them and the isolated WEC at the origin. At first glance, it may appear that the optimal array layouts for the narrow- and intermediate-banded spectra are mirror images of each other. However, the WECs in the narrow-banded case are more widely-spaced from the origin. For both constrained arrays, an almost identical layout is found to be optimal. It is interesting to note that each of the constrained arrays are also symmetric about the y-axis, with WECs 2 - 5 surrounding WEC 1.

The behaviour of the constrained and unconstrained optimal arrays to variation in incident wave angle is shown in figure 8.7. As with the narrow-banded case, the unconstrained array maintains constructive interference within the range of interest, with $q \in [1.35, 2.05]$ for $\beta \in [\frac{3\pi}{8}, \frac{5\pi}{8}]$. The constrained arrays have reduced performance compared to the unconstrained case; in each constrained case destructive interference is present within the range of interest. The upper constraint resulted in $\overline{q} \in [0.75, 1.25]$ for $\beta \in [\frac{3\pi}{8}, \frac{5\pi}{8}]$, while the lower constraint resulted in $\overline{q} \in [0.6, 0.95]$.

In contrast to the narrow-banded case, it is clear that a reduced performance occurs within the range of interest. This is due to the larger range over which optimal performance is enforced and results in a reduced peak performance in order to improve the interaction factors over the larger range.

The influence of wavenumber variations on the intermediate-banded optimal

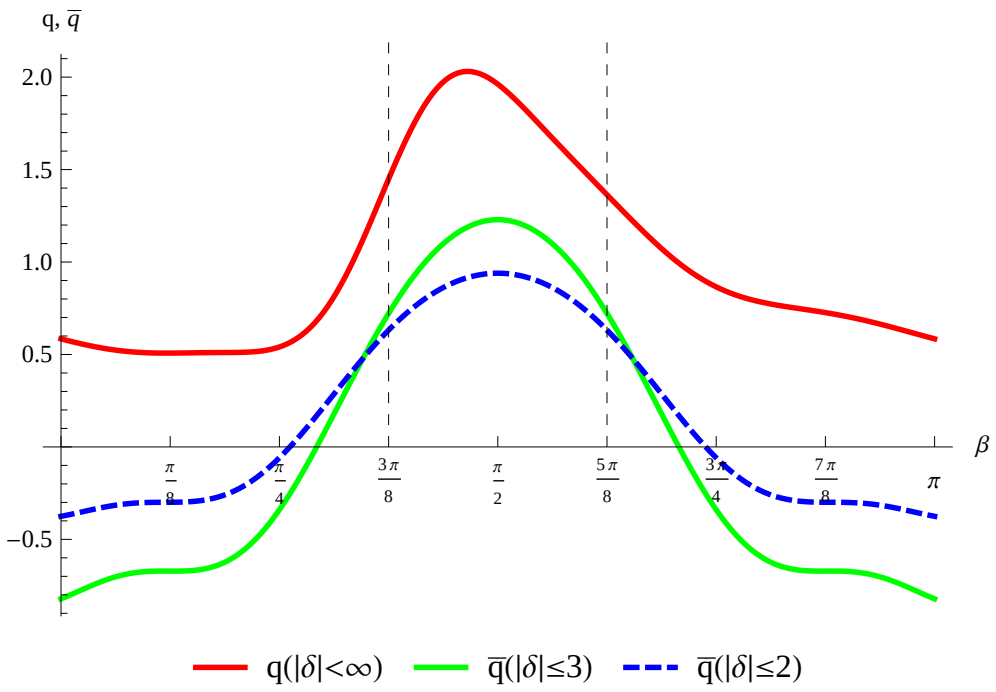

Figure 8.7: Interaction factor against incident wave angle β for optimal constrained and unconstrained five-WEC arrays, optimised for $\beta \in [\frac{3\pi}{8}, \frac{5\pi}{8}]$. The target range of wave angles is indicated by the vertical dashed lines.

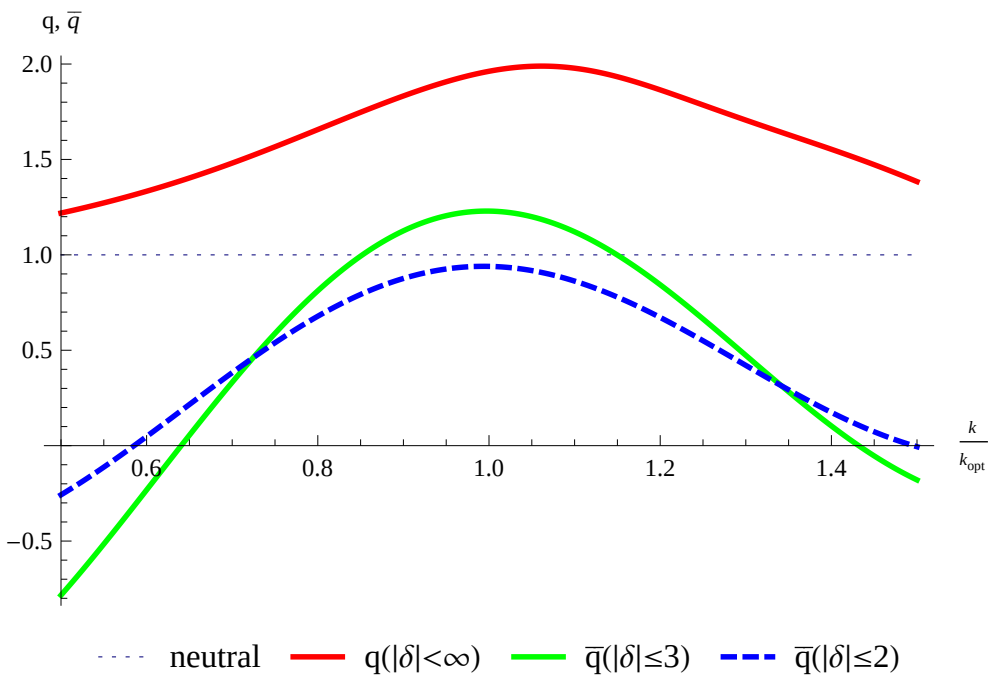

Figure 8.8: Interaction factor against wavenumber $\frac{k}{k_{opt}}$ for optimal constrained and unconstrained five-WEC arrays, optimised for $\beta \in [\frac{3\pi}{8}, \frac{5\pi}{8}]$, with $\beta = \frac{\pi}{2}$.

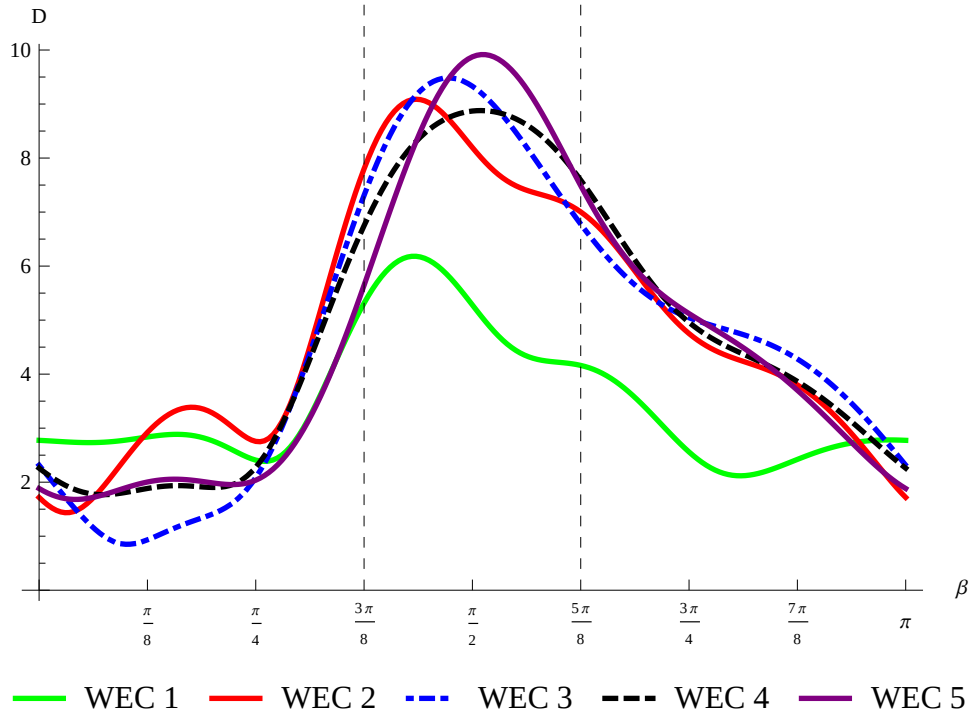

Figure 8.9: Optimal displacement amplitudes against incident wave angle for optimal unconstrained five-WEC array, optimised for $\beta \in [\frac{3\pi}{8}, \frac{5\pi}{8}]$ (shown by horizontal dashed lines)

arrays is shown in figure 8.8. The unconstrained array maintains good performance for up to a 50% change in k, with $q > 1.2$ for all values considered. Note that the peak in performance is achieved at $\frac{k}{k_{opt}} \approx 1.06$, not $\frac{k}{k_{opt}} = 1$ as expected. A reduced performance and an increased sensitivity is seen for the constrained arrays. The lower constraint possesses destructive interference for all wavenumbers considered, with a 30% change in k resulting in a 50% drop in $\overline{q}$. Constructive interference with $\overline{q} > 1$ is seen for the upper constraint for $\frac{k}{k_{opt}} \in [0.85, 1.15]$. This indicates that a 15% change in wavenumber results in a destructive interference. Note also that a 40% change in k for the upper constraint results in negative $\overline{q}$ values, indicating that the array is injecting power into the water rather than absorbing it.

The displacement amplitudes for the optimal unconstrained intermediate-banded array are presented in figure 8.9. This once more shows that the WEC displacements are largest for range of interest and so have a strong correlation with the high q-factor values in figure 8.7. As with the narrow-banded regime, the largest motions are seen for the paired WECs. All five WECs exhibit $\delta > 4$ and so violate the $\mathcal{O}(1)$ requirement of the model.

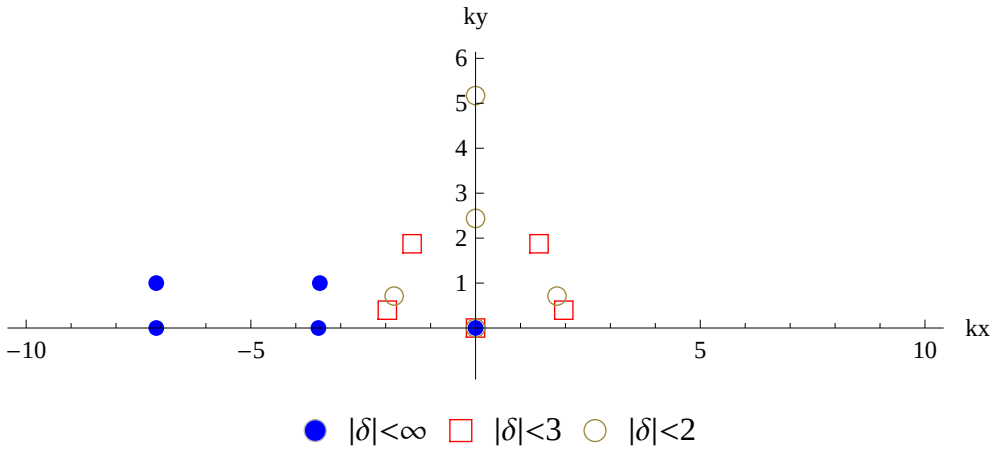

Figure 8.10: Diagram of optimal arrays for broad-banded range of incident wave angle $\beta \in [\frac{\pi}{4}, \frac{3\pi}{4}]$

8.3.3 Broad-Banded $\beta \in [\frac{\pi}{4}, \frac{3\pi}{4}]$

The optimal broad-banded array layouts for constrained and unconstrained motions are shown in figure 8.10. The unconstrained array layout is similar to the intermediate-banded case, with two closely spaced pairs of WECs separated to the right of the origin. Each pair had a separation of approximately 3.5 units between them and from WEC 1. Both the constrained arrays have a symmetric layout about the y-axis. In the $\delta_{max} = 3$ case, this is comprised by two WECs on each side of the y-axis. However, in the $\delta_{max} = 2$ case, there is one WEC on each side of the y-axis, while 2 WECs are placed along the y-axis and separated by approximately 2.5 units.

The behaviour of the optimal broad-banded arrays with β-variation is shown in figure 8.11. As with previous cases, the peak in performance occurs at or near the centre of the range of interest $\beta \in [\frac{\pi}{4}, \frac{3\pi}{4}]$. Even in the unconstrained case, constructive interference is not maintained over the entirety of this range, since $q < 1$ at the edges of $\beta \in [\frac{\pi}{4}, \frac{3\pi}{4}]$. As expected, the constrained cases have a much reduced performance in comparison to the unconstrained case. The upper constraint of $\delta_{max} = 3$ achieves $q > 1$ for a relatively small range of $\beta \in [\frac{7\pi}{16}, \frac{9\pi}{16}]$, with quite poor performance seen outside of this range. The $\delta_{max} = 2$ performance varies slightly slower but destructive interference dominates with $q < 1$ for the entire range of interest.

The effect of variation of the wavenumber $\frac{k}{k_{opt}}$ on the optimal broad-banded array performance is shown in figure 8.12. Once more, the unconstrained array maintains a $q > 1$ performance for a 50% change in wavenumber but

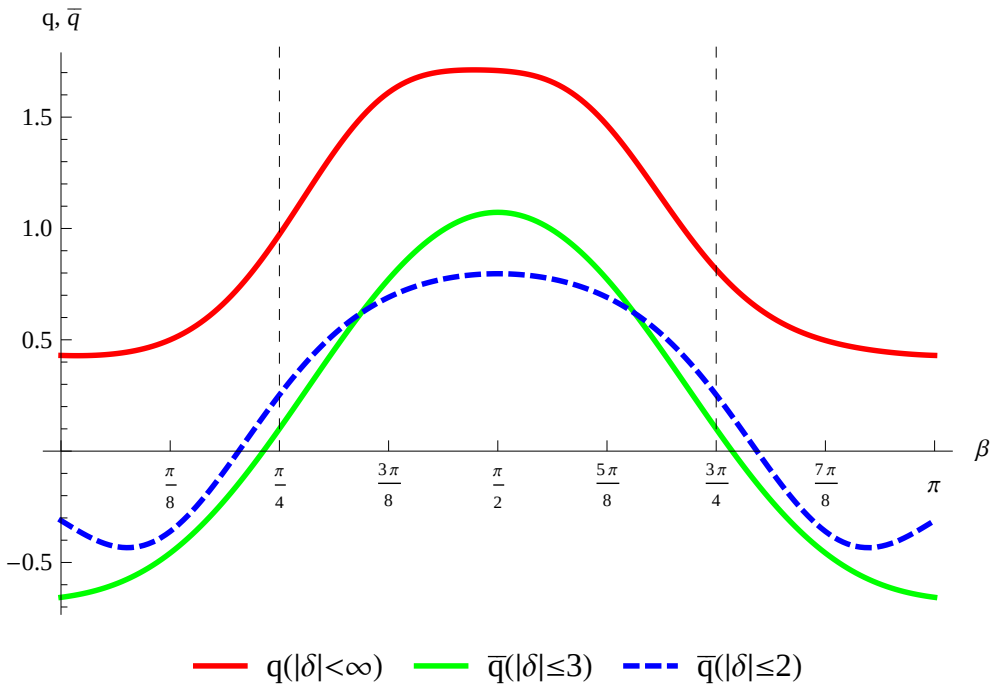

Figure 8.11: Interaction factor against incident wave angle β for optimal constrained and unconstrained five-WEC arrays, optimised for $\beta \in [\frac{\pi}{4}, \frac{3\pi}{4}]$. The target range of wave angles is indicated by the vertical dashed lines.

considerably lower performance is seen for the constrained arrays. The $\delta_{max} = 3$ array achieves $q > 1$ for $\frac{k}{k_{opt}} \in [0.9, 1.26]$, while the $\delta_{max} = 2$ array has $q \leq 0.8$ for all values considered. As in the narrow and intermediate-banded case, the peaks in figure 8.12 occur slightly away from $\frac{k}{k_{opt}} = 1$ for all three arrays. The unconstrained array performance peaks at $\frac{k}{k_{opt}} \approx 1.25$, while the $\delta_{max} = 3$ array performance peaks at $\frac{k}{k_{opt}} \approx 1.08$. Interestingly, the $\delta_{max} = 2$ array peaks at $\frac{k}{k_{opt}} \approx 0.95$; this is the only case where the peak in performance with respect to wavenumber occurs at a value less than unity.

The optimal WEC displacement amplitudes for the unconstrained broad-banded array are presented in figure 8.13. As with narrow and intermediate-banded arrays, the motions of the paired devices (WECs 2 - 5) are larger than those for the isolated device (WEC 1). However, as with previous cases, most WECs maintain $\delta > 4$ for all the range of interest $\beta \in [\frac{\pi}{4}, \frac{3\pi}{4}]$, with the exception of WEC 1 which had $\delta \approx 3$ near the upper end of this range. These WEC motions all violate the $\mathcal{O}(1)$ requirement for the majority of the domain and so would invalidate the underlying linear wave theory.

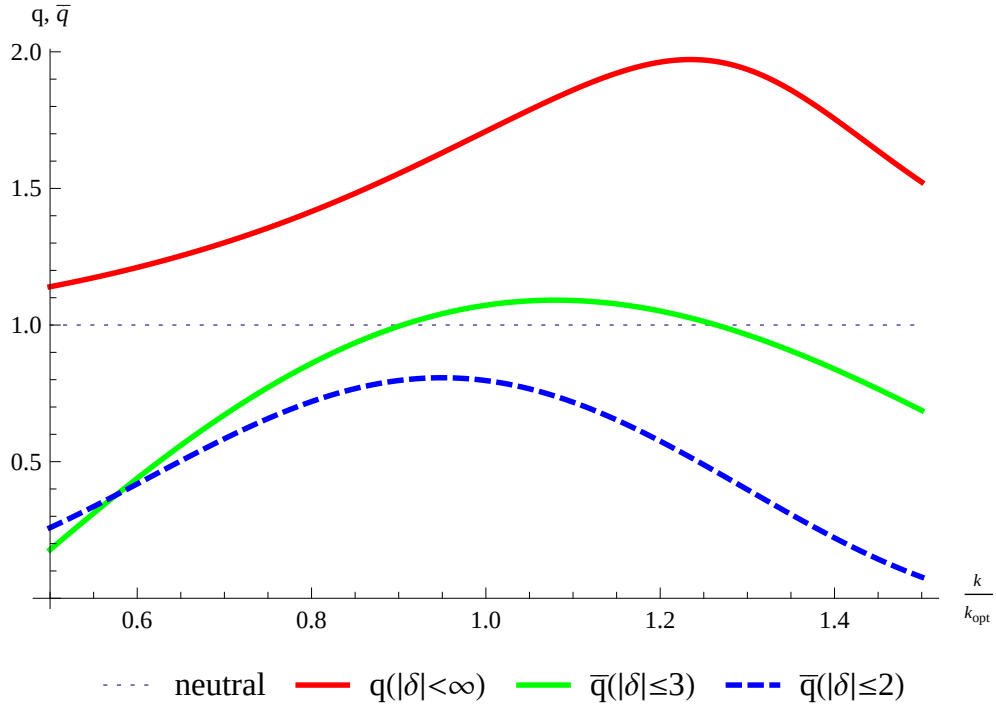

Figure 8.12: Interaction factor against wavenumber $\frac{k}{k_{opt}}$ for optimal constrained and unconstrained five-WEC arrays, optimised for $\beta \in [\frac{\pi}{4}, \frac{3\pi}{4}]$, with $\beta = \frac{\pi}{2}$.

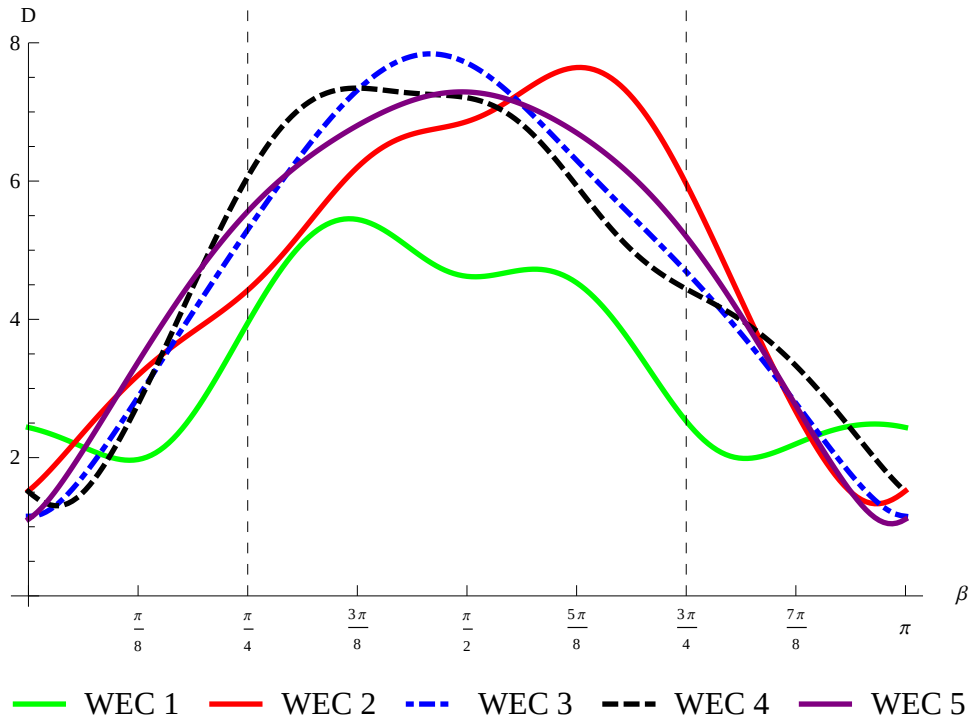

Figure 8.13: Optimal displacement amplitudes against incident wave angle for optimal unconstrained five-WEC array, optimised for $\beta \in [\frac{\pi}{4}, \frac{3\pi}{4}]$ (shown by horizontal dashed lines)

8.4 Discussion of Results

This chapter extends the investigation of the previous chapter by considering the β-optimisation of general five-WEC arrays, without any prescribed geometry. This allows for a general layout optimisation and is the first time non-prescribed geometries are considered in this thesis. One difficulty with this increased generality is the associated increase in computational resources required for the optimisation, which limits the scope of investigations of this type.

The optimal objective function values obtained in this chapter are in general greater than the analogous results from Chapter 7. Better performing arrays are determined due to the increased freedom within the optimisation, as the WECs are not forced to lie on a straight line. Comparing the intermediate-banded optimal constrained arrays from this chapter to the analogous results from Chapter 7 (i.e. $\beta \in [\frac{3\pi}{8}, \frac{5\pi}{8}]$), increases in $\overline{I_\beta}$ of approximately 89% and 139% are seen for $\delta_{max} = 2$ and $\delta_{max} = 3$ respectively, while an increase of approximately 71% is seen in I_β for the unconstrained array.

It is clear that the optimal layouts obtained by the optimisation differ considerably depending on the range of wave angles permitted and the applied motion constraint. The unconstrained array layouts were all similar, with two pairs of closely-spaced WECs placed to one side of the y-axis. The optimal unconstrained narrow-banded array was placed to the right of the y-axis, while the analogous intermediate and broad-banded arrays were placed to the left. From considerations of symmetry, arrays mirrored about the y-axis perform the same and it is just a numerical artefact that the narrow-banded array resulted in WECs to the right instead of the left. It should also be noted that the WEC pairs are situated closer to the origin for broader β-ranges. In either case, the optimal unconstrained array is quite similar to two rows of linear WECs; it would be interesting to see what the optimal layout would be if say ten WECs were considered. However, this is numerically intractable due to the parameter explosion of including more WECs in the array.

The range of incident wave angle had a larger impact on the optimal constrained array layouts, with noticeably different arrangements discovered in the constrained cases. For intermediate and broad-banded β-variation, the optimal constrained arrays for both constraints were symmetric about the y-axis. This may seem unexpected, since the wave angle range considered is centred on $\beta = \frac{\pi}{2}$ and is also symmetric about the y-axis. This is in direct

contrast to the optimal unconstrained layouts, which were placed to one side of the y-axis. In the narrow-banded case, asymmetric layouts were obtained as the best cases and the array found for each constraint were mirror reflections of each other about the y-axis.

The area in which the optimal arrays lay should also be noted. The unconstrained arrays all lie within a non-dimensional area of 18 to 22 square units. This also holds for all constrained arrays, with the exception of the broad-banded constrained array with $\delta_{max} = 3$, which lies within a smaller area of 10 square units. Considering the non-dimensional area as $kd \times kd = k^2d^2 = \left(\frac{4\pi^2}{\lambda^2}\right) d^2$ and assuming a typical ocean wavelength of approximately 200m implies that a scaling of approximately 10^3 applies between dimensional and non-dimensional areas due to the $\left(\frac{4\pi^2}{\lambda^2}\right)$ factor shown above. This means that the optimal arrays of this chapter lie within a physical area of approximately 10000m^2 (100m by 100m) to 22000m^2 (150m by 150m). The optimisation routine limited the array area to a semicircle of radius 20 units but all optimal arrays were formed within a much smaller area closer to the origin. Of course, smaller or larger areas can be enforced within the optimisation if required for economic or engineering reasons.

Lower overall array performance was seen for the broader β-ranges, for both constrained and unconstrained motions. This is to be expected, since there are limitations on how well an array can perform constructively. For example, it is well known for unconstrained motions that the mean interaction factor over all wave angles is unity, as shown by Fitzgerald (2006). A similar limitation would apply to constrained motions whereby the array cannot be forced to perform exceptionally well for a broad range of wave angles. Good performance can be achieved and maintained if a relatively small β-range is considered, as shown for the narrow-banded constrained arrays.

The trade-off identified previously between optimal performance and stability of performance is clearly shown in this chapter for β-variation. If a broad-banded range of incident wave angle is the range of optimisation, this essentially requires that the array perform as well as possible over the entirety of this range of β. It is seen that broader ranges of β produce lower objective function values and hence lower overall performance. However, a trade-off between β-stability and k-stability is not evidently observed, as the $\frac{k}{k_{opt}}$ curves are broadly similar for all ranges of β considered. This suggests that this phenomenon was connected primarily with linear arrays and that optimising in a general two

dimensional regime ameliorates this pitfall.

As discussed in Chapter 7, there clearly exists a relationship between the optimal array formation and the applied motion constraint. As the constraint becomes less strict, at some point the optimal layout must switch or evolve to that of the unconstrained case. The results of Chapter 7 tentatively indicate that the evolution of the optimal array layout relative to the applied constraint is continuous, i.e. the optimal formation does not suddenly jump from one layout to another for a small change in the applied constraint. This is not as evident from the results here, as in most cases the constrained optimal layouts were the same or similar for both $\delta_{max} = 2$ and $\delta_{max} = 3$. However, considering the results and discussion of Chapter 7, the same conclusion may be drawn here, since there is nothing to indicate that allowing a general array geometry, as opposed to a linear one, will alter this relationship between the optimal layout and the applied constraint. It should be stressed that this is a tentative deduction based upon the results of this chapter and the related results of Chapter 7. This relationship between the optimal layout and the applied constraint requires further investigation beyond the scope of this thesis.

The best array performance is seen for the narrow-banded optimisation, where the range of interest is $\beta \in [\frac{7\pi}{16}, \frac{9\pi}{16}]$. Even for the $\delta_{max} = 3$ constraint, constructive interference was maintained throughout this range. Performance was also relatively stable to changes in wavenumber, with $\overline{q} > 1$ being maintained for up to a 25% change in k. Thus, if a site is identified with a relatively low variation in both β and k, which remain within the above limits, then this array may be an ideal choice.

In a preliminary study, the optimisation was tested at other wave angle ranges, before those targeting $\beta = \frac{\pi}{2}$ were chosen. In some cases, it was noted that a slightly better or a poorer optimal result was obtained at other wave angles, such as those centred on $\beta = 0$. This improvement or deterioration was less than 1%. In principle, the optimisation should be able to find the same array in both cases, due to symmetry. The optimal array at one angle should just be the rotation of the optimal array at a different angle. However, the same array may not be able to be found at other rotated angles due to the limits imposed on the variables. A rotation of $\frac{\pi}{2}$ may cause one of the WECs to be placed outside $kd_j \in [1, 20] \cup \alpha_j \in [0, \pi]$. Another possible explanation for this discrepancy is the large number of variables and the large size of the parameter space, particularly for the constrained optimisations. It may be that the optimisation

failed to converge to the same results at different wave angles due the numerical intensity of the calculations, or some numerical difficulty at certain values of β. Thus the optimal arrays in this chapter are not advertised as globally optimal, but are the best cases found within the computational limits present.

In some cases, the peak in q against $\frac{k}{k_{opt}}$ occurred at a value other than $\frac{k}{k_{opt}} = 1$. This suggests that an increased performance could be achieved by having the non-dimensional radial positions of the WECs (kd_j) slightly larger or smaller. However, given that the optimisation routine did not converge to such a case, this suggests that the increased performance at the larger/smaller kd_j values also gives an increased β-sensitivity and poorer performance over the range of interest of β, as this was the main consideration within the objective function. It also points towards the possible trade-off between stability in some array variables and sensitivity to others. However, the effect is very slight, as the peaks in $\frac{k}{k_{opt}}$ occurred very close to unity in all cases.

In many physical array sites, the variation of incident wave angle will not be uniform about a given range. In most cases, there is a spectral behaviour where most of the wave would come from a range of angles, with decreased resource from angles outside this range. To assess the effect of this concentration of the resource, an alteration of the objective function is proposed, where a weighting function $W(\beta)$ is included in the integral, as described in the discussion of Chapter 7. This altered objective function could be written as

$$I_\beta^W(\mathbf{kd}, \boldsymbol{\alpha}) = \frac{1}{\beta_u - \beta_l} \int_{\beta_l}^{\beta_u} W(\beta) q(\mathbf{kd}, \boldsymbol{\alpha}, \beta)\ d\beta, \tag{8.4}$$

for unconstrained motions. For constrained motions, this is altered to

$$\overline{I_\beta^W}(\mathbf{kd}, \boldsymbol{\alpha}, \boldsymbol{\delta}, \boldsymbol{\psi}) = \frac{1}{\beta_u - \beta_l} \int_{\beta_l}^{\beta_u} W(\beta) \overline{q}(\mathbf{kd}, \boldsymbol{\alpha}, \boldsymbol{\delta}, \boldsymbol{\psi}, \beta)\ d\beta. \tag{8.5}$$

The weighting function must be normalised to unity, thus $\int_{\beta_l}^{\beta_u} W(\beta)\ d\beta = 1$ is also enforced.

A cosine squared type weighting function, such as equation (7.7), could be taken as a first approximation. This type of optimisation will give a more detailed idea of the effect of β-variation, as spectrum variability is incorporated in this implementation in some sense. Since regular waves and ideal power absorption are still assumed in the unconstrained optimisation, this objective function essentially assumes that ideal power is absorbed at all wave angles.

Chapter 9

Optimisation of Linear Arrays in Irregular Waves

9.1 Introduction

This chapter extends the work of previous chapters by considering an array of WECs in an irregular wave regime. A summary of the work contained within is provided in McGuinness & Thomas (2017b). This is an important extension, as often results obtained in regular wave regimes cannot be replicated when irregular waves are incident onto the array. The existing literature is rather sparse but suggests that interaction between array members tends to be less influential in irregular waves, as indicated by Babarit (2010).

A major problem with extending the previous work to irregular waves is the increase in numerical intensity of the associated optimisation problem. A wave spectrum that represents the irregular sea state must be incorporated in some way, together with some measure of the array performance. This increases the numerical intensity of the calculations and thus increases the optimisation run-time significantly. As a consequence, only arrays with three devices are examined, as including five or more WECs, as with previous chapters, makes the resulting numerical problem almost intractable.

9.2 Optimisation Method

As an irregular wave regime is under consideration, the wave spectrum must be specified prior to the optimisation. A JONSWAP spectrum is chosen for this purpose, with the energy density S_ω of the waves at a frequency ω given by

$$S_\omega(\omega) = \frac{\alpha_p g^2}{\omega^5} \exp\left[-\frac{5}{4}\left(\frac{\omega_p}{\omega}\right)^4\right] \gamma_p^Y \tag{9.1}$$

$$Y = \exp\left[-\frac{1}{2}\left(\frac{\frac{\omega}{\omega_p}-1}{\sigma_p}\right)^2\right], \tag{9.2}$$

where α_p is the Phillips constant, γ_p is the peak enhancement factor, σ_p is the peak width parameter and ω_p is the value of the frequency ω at the spectrum peak. Typical values of the above constants, such as those used in Child (2011), are

$$\alpha_p = 0.0081, \tag{9.3}$$

$$\sigma_p = \begin{cases} 0.07 & \text{for} \quad \omega \leq \omega_p \\ 0.09 & \text{for} \quad \omega > \omega_p \end{cases}. \tag{9.4}$$

Three values of the peak enhancement factor

$$\gamma_p = 1, 3.3, 10 \tag{9.5}$$

are employed to represent broad, intermediate and narrow-banded spectra respectively. Figure 9.1 shows the normalised spectrum for each value of γ_p, where the spectrum is scaled by the targeted power contained within the spectrum P_T, given by equation (2.186), to ensure that the area under each curve is unity. There is more power contained in the spectra corresponding to higher γ_p values but a normalised version is utilised within the optimisation in order to compare array performance within different spectra. A brief discussion on the comparison of wave energy extraction between two different spectra, namely those found at Pico and South Uist, is given by Thomas (2008).

The power absorbed by the array at a given frequency ω, as in equation (2.136), is

$$P_{abs}^{(N)} = \frac{1}{8}\mathbf{X}^\dagger \mathbb{B}^{-1}\mathbf{X} - \frac{1}{2}\left(\boldsymbol{\mathcal{U}} - \frac{1}{2}\mathbb{B}^{-1}\mathbf{X}\right)^\dagger \mathbb{B}\left(\boldsymbol{\mathcal{U}} - \frac{1}{2}\mathbb{B}^{-1}\mathbf{X}\right), \tag{9.6}$$

where the superscript is included to explicitly show the number of devices in the array.

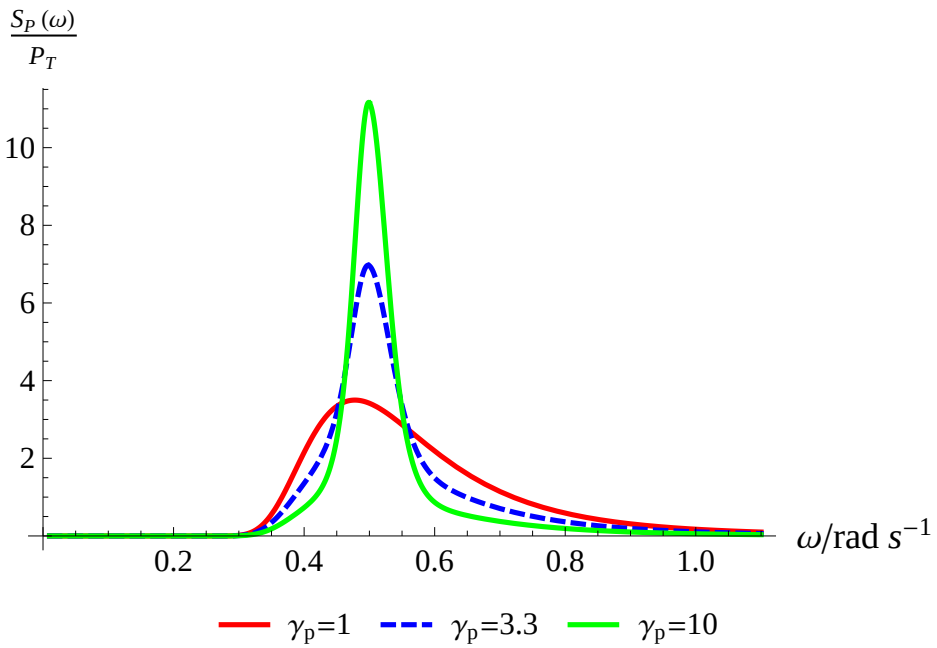

Figure 9.1: Normalised Power spectrum $\frac{S_P(\omega)}{P_T}$ against frequency ω for several values of γ_p.

Previously, the WEC displacements were non-dimensionalised relative to the incident wave amplitude A and displacement limits of two or three times the wave amplitude were enforced. However, as the present work concerns frequency components over a given wave spectrum, the wave amplitude is not fixed universally and depends upon the frequency. It is therefore more sensible to non-dimensionalise with respect to a fixed quantity that remains constant over the entire spectrum. The device radius a is a natural choice, such that the velocity of the devices at a given frequency ω is

$$\boldsymbol{\mathcal{U}}(\omega) = -i\omega a\mathbf{D}. \tag{9.7}$$

This allows a displacement limit to be fixed that would apply for all frequencies in the spectrum. The implementation of a no slamming condition (such that the WECs do not leave the water) simply requires that the amplitude of the non-dimensional displacements are less than unity for a semi-spherical device.

The wave amplitude still appears in the excitation forces, and hence the power absorbed; thus its variation must still be accounted for. By relating the wave spectrum $S_\omega(\omega)$ to the energy contained in a wave train $E = \frac{1}{2}\rho g A^2$, the

amplitude can be written in terms of the spectrum as

$$A(\omega) = \sqrt{\frac{2S_\omega(\omega)}{\rho g}}. \tag{9.8}$$

Using equations (2.143), (2.144), (2.145) and (2.157), the excitation force vector and radiation damping matrix can be written as

$$\mathbf{X} = -2\pi\rho g a^2 A(\mathcal{C} - i\mathcal{D})\, \boldsymbol{\ell}, \tag{9.9}$$

$$\mathbb{B} = \frac{2\pi^2\rho a^4\omega^3}{g}(\mathcal{C}^2 + \mathcal{D}^2)\, \mathbb{J}. \tag{9.10}$$

From (9.6), (9.7), (9.9) and (9.10), the mean power absorbed by the array at each frequency is

$$P_{abs}^{(N)} = \pi\rho a^3\omega \left(-gA \operatorname{Re}\left[(\mathcal{D} + i\mathcal{C})\mathbf{D}^\dagger\boldsymbol{\ell}\right] - \frac{\pi a^3\omega^4}{g}(\mathcal{C}^2 + \mathcal{D}^2)\mathbf{D}^\dagger\mathbb{J}\mathbf{D} \right). \tag{9.11}$$

The aim of the optimisation strategy is to seek an array layout whose performance matches the power distribution within the target spectrum. Thus the objective function must account for both the performance of the array and the effect of the wave spectrum and must be done in a manner that is meaningful and consistent with the frequency variation allowed for within the spectrum. For example, maximum power capture cannot be assumed as adding a P_{opt} term to the integral objective function would implicity assume that the WECs are all optimally tuned for all frequencies, which is not possible. Further care must be taken if the array performance is scaled with respect to single WEC performance in the objective function, as the optimisation may seek to minimise the single WEC performance (to improve the ratio) rather than maximising the array performance as desired.

An appropriate objective function is the frequency integral of the product of the power spectrum and the power absorbed by the array,

$$Q(\mathbf{s}, \mathbf{D}; \beta_0) = \frac{1}{P_T}\int_{\omega_l}^{\omega_u} S_P(\omega) P_{abs}^{(N)}(w, \mathbf{s}, \mathbf{D}; \beta_0)\, d\omega, \tag{9.12}$$

where $\mathbf{s}$ is a $(N-1)$-component vector containing the positions of the WECs in the array (the first WEC is fixed at the origin), $\mathbf{D}$ is a vector containing the complex displacements of the WECs and β_0 is a fixed prescribed incident wave angle. The power spectrum is scaled by P_T, so that it does not contribute to the

magnitude of the objective function values since $\int_{\omega_l}^{\omega_u} \frac{S_P(\omega)}{P_T}\, d\omega = 1$. The objective function can be re-written in terms of real variables using equation (6.3),

$$Q(\mathbf{s}, \boldsymbol{\delta}, \boldsymbol{\psi}; \beta_0) = \frac{1}{P_T} \int_{\omega_l}^{\omega_u} S_P(\omega) P_{abs}^{(N)}(w, \mathbf{s}, \boldsymbol{\delta}, \boldsymbol{\psi}; \beta_0)\, d\omega, \tag{9.13}$$

where $\boldsymbol{\delta}$ and $\boldsymbol{\psi}$ are N-component vectors containing the displacement amplitudes and phases of each WEC respectively.

The objective function values are essentially a weighted sum of all power absorbed by the array within the power spectrum. This is a relative measure which forces the absorption associated with the array layout to match the incident wave spectrum as closely as possible, but the objective function values have no direct physical meaning. However, the objective function values can be compared relative to each other to identify better performing arrays in irregular waves.

Clearly this objective function depends on the Havelock coefficients $\mathcal{C}$ and $\mathcal{D}$ through equation (9.11). These coefficients depend upon the non-dimensional radius of the WECs $ka = \frac{\omega^2 a}{g}$. Thus, the values of these coefficients will be different throughout the range of ω considered in the spectrum and $\mathcal{C}$ and $\mathcal{D}$ must be included as varying functions of $\frac{\omega^2 a}{g}$ within the objective function. Given the calculation method of Havelock (1955), it is not sensible to recalculate these accurately for each frequency within the objective function integral (9.13). To address this, accurate solutions were obtained for $\mathcal{C}$ and $\mathcal{D}$ for an appropriately large number of values within the range of interest ($ka \in [0, 1]$) and these were used to create Chebyshev interpolation functions for both $\mathcal{C}$ and $\mathcal{D}$. These interpolation functions were then included in the objective function and this significantly reduced the intensity of the calculations.

It should be noted that the inclusion of a spectrum, and the interpolating functions within an objective function that contains $3N - 2$ variables, demands a numerical effort considerably more intense than optimisations performed in previous chapters. Another numerical difficulty that limited the scope of this work was the requirement that the optimisation routine needed to read in a starting point from which it converged to an optimal solution. As in previous optimisations in Chapters 4 - 8, this required the implementation of an exhaustive search of the possible space of starting points, resulting in many iterations of the optimisation and many more calls to the objective function.

Although the point absorber approximation requires that $ka \ll 1$, it has been

shown by Mavrakos & McIver (1997) to be accurate for $ka \leq 0.8$. Consequently, care must be exercised when considering a spectrum of performance, as there may be some range of ω such that the above tolerance of the point absorber approximation is exceeded. This would invalidate the underlying theory of the optimisation and perhaps also cause numerical difficulties. Hence, a reasonable value of a must be specified such that the above limit on ka is not exceeded. This was also the reason that the interpolated values of $\mathcal{C}$ and $\mathcal{D}$ were limited to $ka \in [0, 1]$. Care must also be taken to ensure that the interpolation functions for $\mathcal{C}$ and $\mathcal{D}$ are applicable and accurate for all values of ω within the range of interest in the spectrum.

9.3 Optimisation of Three-WEC Linear Arrays with Fixed Length

Despite the efforts outlined in the previous section to reduce the computational demand, the optimisation remains numerically intensive and requires long run-times. To overcome these difficulties, the problem was simplified as much as possible in order to obtain results in a reasonable time. Therefore, linear arrays of only three WECs are considered. The first WEC is fixed at the origin and the array length is also specified and fixed at $L = 300$m. This essentially means that the first and third WECs are fixed in space and the optimisation only considers the position of the middle device (WEC 2), along with the displacement variables for all three WECs, thus giving a total of seven array variables in general. A diagram of the array considered is shown in figure 9.2. This simplified set-up resulted in run-times of the order of twenty to thirty hours.

Since the objective function involves an integral over the frequency ω, the problem cannot be studied in a non-dimensional manner, as was the case with previous studies in regular waves. Thus, the variables of the optimisation become the physical positions of the WECs, along with the non-dimensional displacement variables. This also requires several physical values to be specified prior to the optimisation, such as the device radius a. Within this chapter, the WEC radius was taken to be $a = 2.5$m. This was chosen as it is a reasonable physical value representative of physical devices. This value also avoids the pitfall of violating the point absorber approximation for the wave frequency range of interest. In this calculation, the value of ρ is taken to be the density of

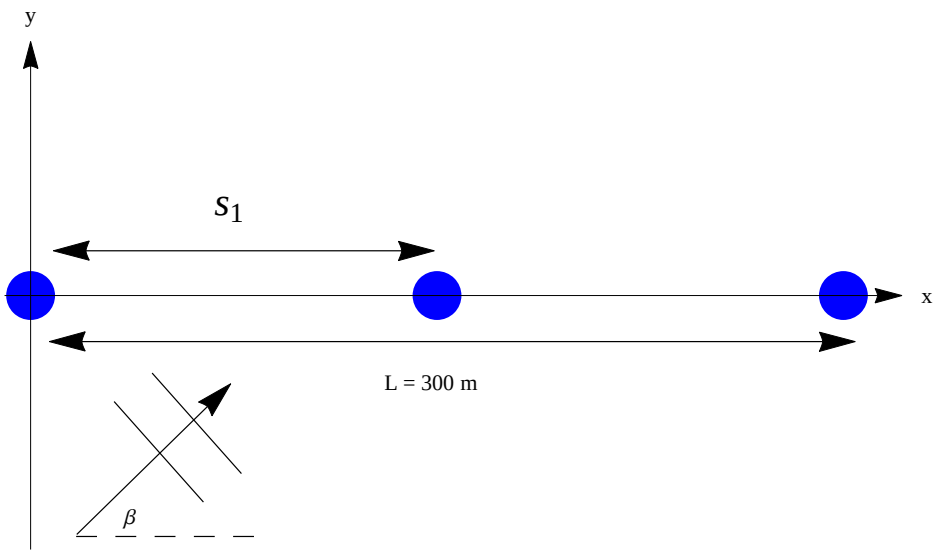

Figure 9.2: Diagram of three-WEC uniform linear array.

fresh water, i.e. $\rho = 1000$ kgm^{-3}kg m^{-3}.

The peak frequency of the JONSWAP spectrum was taken to be $\omega_p = 0.5$rad s^{-1} and the imposed upper and lower bounds of frequency were $[\omega_l, \omega_u] = [0.1, 1.1]$. This value of ω_p is intended to represent typical ocean waves of wavelength of approximately 250m. This also enables the majority of the non-zero JONSWAP spectrum to fall within $\omega \in [0.1, 1.1]$, thus avoiding interpolation difficulties with $\mathcal{C}$ and $\mathcal{D}$. Taking this value of ω_p and $L = 300$m also allows a comparison with previous chapters regarding regular waves, where a similar non-dimensional target value of $kL = 10$ was assumed, although less WECs are considered in this case.

The interpolation points of $\mathcal{C}$ and $\mathcal{D}$ were accurate solutions for the constants for $ka = \{0, 0.1, 0.2, \ldots, 1.0\}$. It was found that including more interpolated values produced a marginal increase in accuracy, at the expense of either significantly longer run times for the optimisation or an ill-conditioned interpolation procedure due to over-specification. The above range of interpolation points resulted in the interpolated values of $\mathcal{C}$ and $\mathcal{D}$ being accurate to three to five significant figures.

The optimisation algorithm is implemented in Fortran with the aid of Numerical Analysis Group (NAG) routines. As in previous chapters, the optimisation routine chosen to find the maximum of equation (9.13) is E04UCF[1], with appropriate algorithms employed for the calculation of Bessel

[1]https://www.nag.co.uk/numeric/fl/manual/pdf/E04/e04ucf.pdf

functions, quadrature and interpolation.

In common with previous optimisations, it was found that the displacement variables δ_j and ψ_j behaved well from a numerical perspective and converged to the optimal case without the need for an overly dense search space. Thus, the search examined all possible starting points for $\delta_j = \{0, 0.25, 0.50, 0.75, 1\}$ and $\psi_j = \left\{0, \frac{\pi}{2}, \pi, \frac{3\pi}{2}, 2\pi\right\}$ for the displacement variables. For cases involving optimisation of the array layout, a finer scan of the search space was required for the layout variable, such that $s_1 = \{20, 40, 60, \ldots, 280\}$.

The minimum separation between devices enforced was 20m, as placing the WECs closer may invalidate the point absorber approximation and cause numerical difficulties. Furthermore, having WECs closer than 20m would result in significant engineering difficulties in practice. Therefore, limits were placed on each variable within the optimisation such that $0 \leq \delta_j \leq 1$, $0 \leq \psi_j \leq 2\pi$ and $20 \leq s_1 \leq 280$.

The performance of uniform arrays are first optimised and examined to assess the effect of the array layout. This will then provide a benchmark for a layout optimisation and allow a comparison between the array layouts and resulting performance.

9.3.1 Uniform Layout

A uniform array of three WECs is initially investigated, where the positions of all three WECs are fixed at 0m, 150m and 300m along the line (i.e. $s_1 = 150$m). Only the displacement variables are fed into the optimisation, giving a total of six variables. This was implemented in order to create a benchmark with which to compare the optimised layouts. The displacement amplitudes and phases would also change when the layout is optimised, so comparison can also be drawn between the behaviour of these displacement variables. The results of the uniform array optimisation are listed in table 9.1. This fixed uniform layout was investigated for head, intermediate and beam seas. The variation of the power absorbed by the optimal uniform arrays with frequency is shown in figures 9.3 – 9.5, while the effect of incident wave angle variation is shown in figures 9.6 – 9.8.

It is clear from the tabular results that the array performance improves as the spectrum becomes more narrow-banded. This is also echoed in figures 9.3 - 9.8,

Table 9.1: Optimisation results for uniform three-WEC linear array

γ_p	β_0	δ_1	δ_2	δ_3	ψ_1	ψ_2	ψ_3	Q
1.0	0	0.3981	0.1269	0.0358	4.7179	2.4679	5.1826	812.42
	$\frac{\pi}{4}$	0.3949	0.1818	0.0782	4.7287	1.4247	3.5621	912.57
	$\frac{\pi}{2}$	0.4133	0.4272	0.4133	4.7259	4.7259	4.7259	2290.07
3.3	0	0.7532	0.4528	0.2785	4.6730	2.4356	6.2688	3158.83
	$\frac{\pi}{4}$	0.7318	0.4935	0.3776	4.7511	1.2606	3.8254	3555.88
	$\frac{\pi}{2}$	0.8469	0.9350	0.8469	4.7227	4.7227	4.7227	7145.26
10	0	1.0000	1.0000	1.0000	4.6148	2.3381	0.0692	14341.05
	$\frac{\pi}{4}$	1.0000	1.0000	1.0000	4.7875	1.2215	3.8358	15312.29
	$\frac{\pi}{2}$	1.0000	1.0000	1.0000	4.7211	4.7211	4.7211	21804.11

where the largest peak in each case corresponds to $\gamma_p = 10$. This is to be expected, since the device displacements can be optimised for a small set of conditions for narrow spectra, allowing for better performance at the spectrum peak. For a broader spectrum, the optimisation requires good performance over a wider set of conditions, which generally results in a reduced overall performance.

Table 9.1 clearly shows that, for each spectra considered, the array performs best in beam seas, i.e. as a terminator type configuration. This was shown to be the case for linear arrays in regular waves in Chapters 3, 4 and 6, in agreement with the preliminary results of Thomas & Evans (1981), though an increased sensitivity often accompanied this optimal performance. It is also evident that the array performs poorest in head seas, indicating that this type of attenuator array layout is to be avoided. It may be associated with the first WEC shadowing WECs 2 and 3, by absorbing some of the incident power and resulting in destructive interference. In the case of beam seas, the waves strike all devices at the same time, which would avoid this shadowing effect. In principle, this also allows the possibility of creating constructive interference between the WECs, given the appropriate control.

This is further supported by the optimal displacement variables δ_j and ψ_j in table 9.1. For beam seas, the WECs are all in phase and the amplitudes are symmetric about the middle device, with the amplitude of WEC 2 slightly larger to ensure constructive interference (for $\gamma_p = 10$, they are all equal at the maximum allowed value). For head and intermediate seas with $\gamma_p = 1, 3.3$, all values of δ_j and ψ_j are different, with δ_1 being the largest of the amplitude

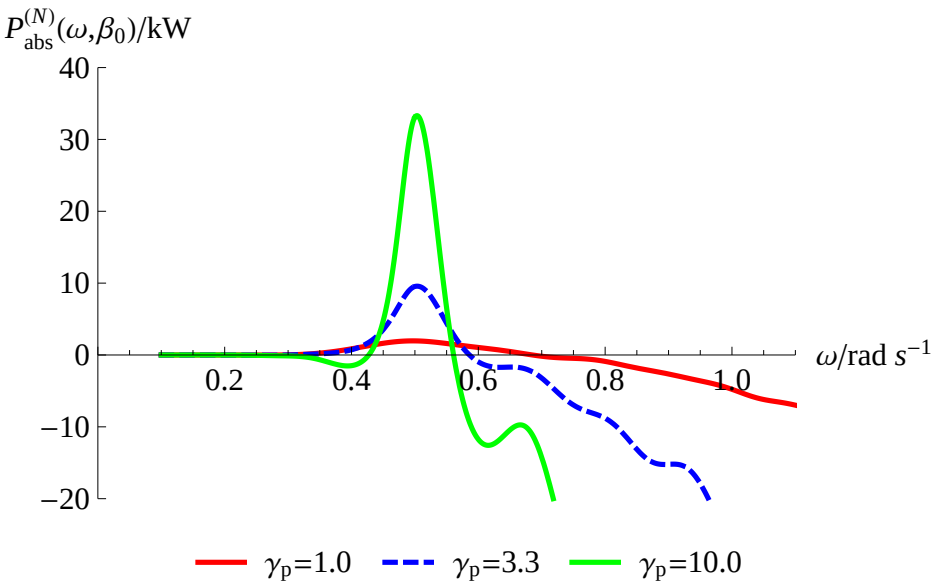

Figure 9.3: Power absorbed $P_{abs}^{(N)}(\omega, \beta_0)$ in kilowatts against frequency ω for optimised uniform arrays with $\beta_0 = 0$ (head seas).

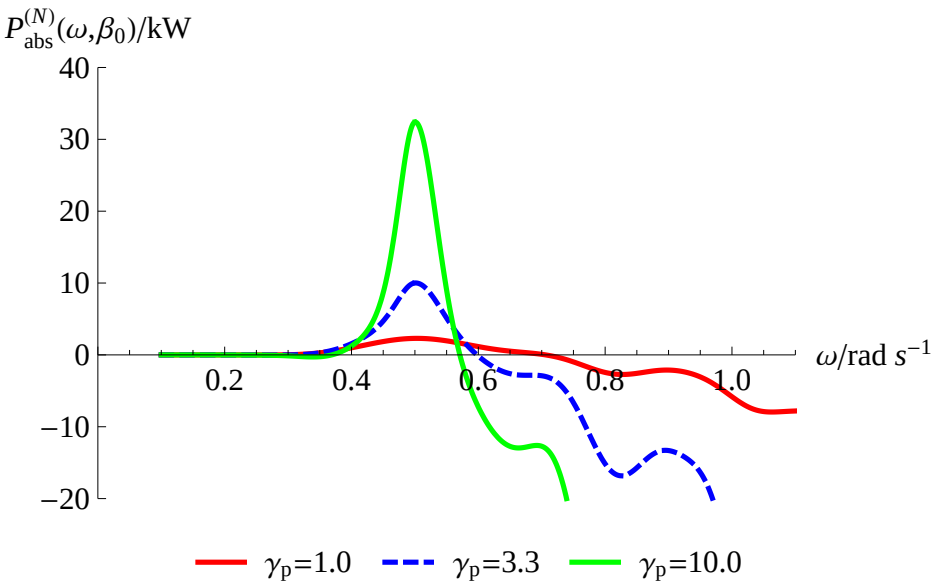

Figure 9.4: Power absorbed $P_{abs}^{(N)}(\omega, \beta_0)$ in kilowatts against frequency ω for optimised uniform arrays with $\beta_0 = \frac{\pi}{4}$ (intermediate seas).

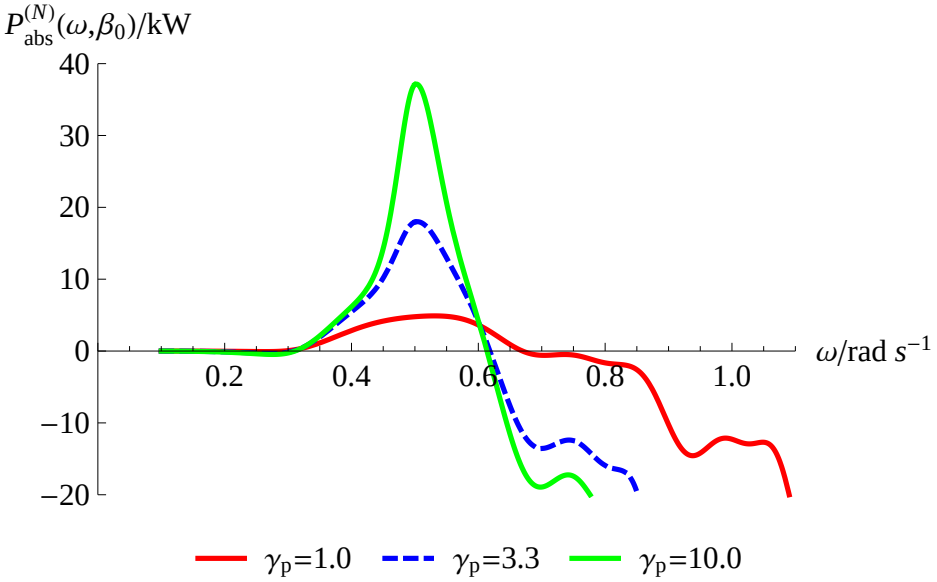

Figure 9.5: Power absorbed $P^{(N)}_{abs}(\omega, \beta_0)$ in kilowatts against frequency ω for optimised uniform arrays with $\beta_0 = \frac{\pi}{2}$ (beam seas).

variables. This shows that WEC 1 is working the hardest and thus absorbing the most energy, while WECs 2 and 3 are shadowed and have smaller optimal displacement amplitudes. For $\gamma_p = 10$, the amplitude variables all converge to the largest allowed value $\delta_j = 1$. Since the spectrum is narrow-banded, this allows the WECs to be highly tuned to the peak performance and thus the displacement limit is reached.

For all cases presented in figures 9.3 - 9.5, the power absorbed by the array becomes negative for values of approximately $\omega > 0.6$rad s^{-1}. This indicates that the array is injecting power into the waves for these wave frequencies rather than extracting power as desired. This is perhaps a consequence of the optimisation maximising the power absorbed in the spectrum peak around $\omega_p = 0.5$rad s^{-1}, which results in poor performance away from this value. This is largely inconsequential as these ranges of ω correspond to low spectrum values, particularly for $\gamma_p = 3.3, 10$. Therefore, this negative performance contributes very little to the objective function and the overall performance of the array in the given sea conditions. For $\gamma_p = 1.0$, the spectrum does have significant non-zero values in this range, and this contributes to the reduced performance of the arrays in the broad-banded spectrum.

Examining the frequency sensitivity of the optimal arrays in figures 9.3 - 9.5, it is clear that arrays optimised for narrow and intermediate spectra are more sensitive to changes in comparison to broad-banded spectra but this is not a

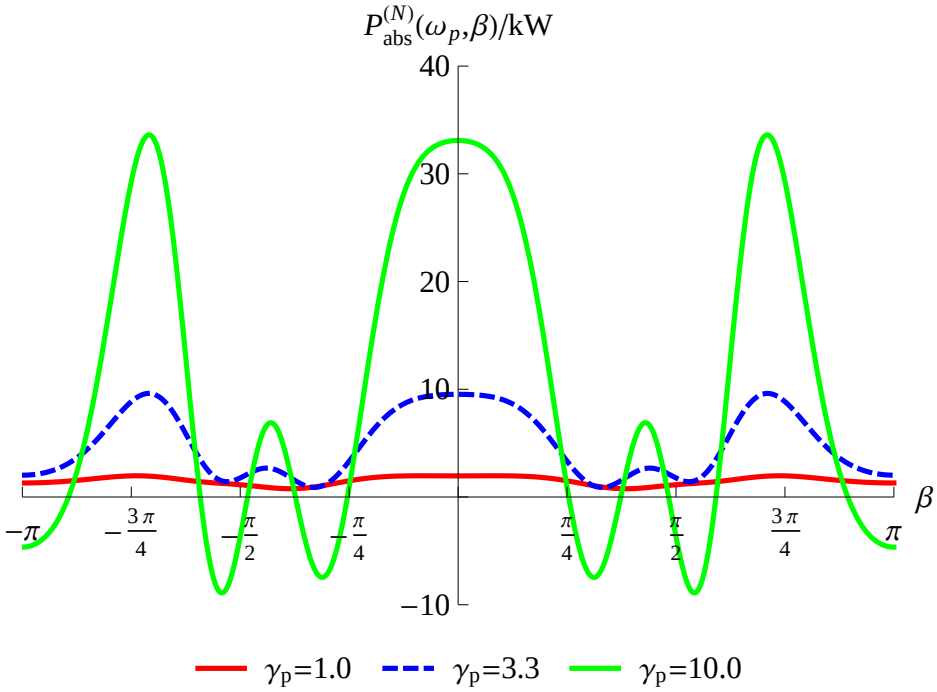

Figure 9.6: Power absorbed $P^{(N)}_{abs}(\omega_p, \beta)$ in kilowatts at peak frequency $\omega = \omega_p = 0.5$ against incident wave angle β for uniform arrays optimised in head seas with $\beta_0 = 0$ (shown by y-axis).

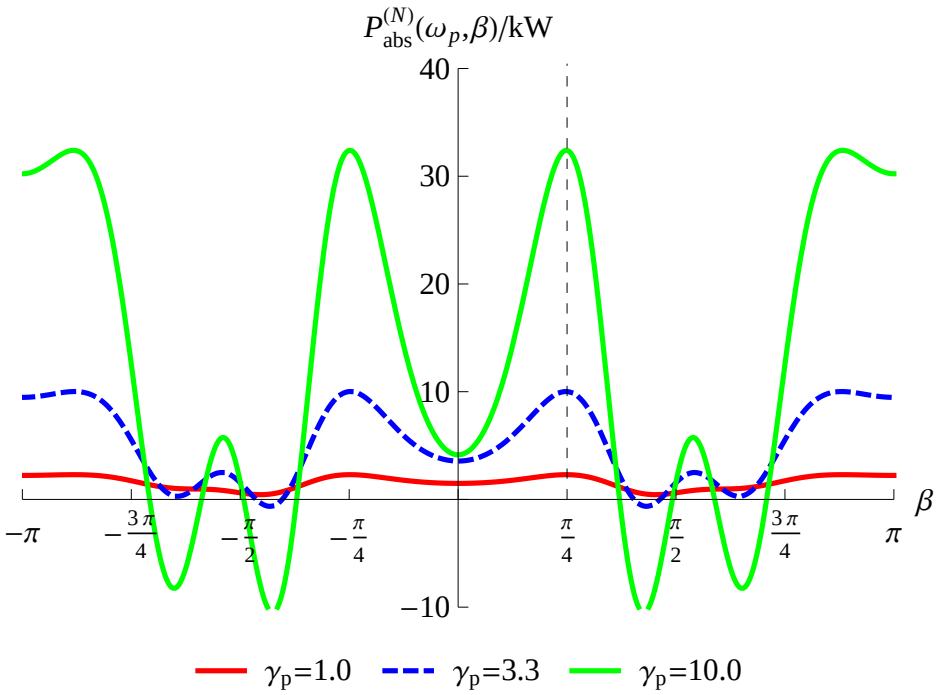

Figure 9.7: Power absorbed $P^{(N)}_{abs}(\omega_p, \beta)$ in kilowatts at peak frequency $\omega = \omega_p = 0.5$ against incident wave angle β for uniform arrays optimised with $\beta_0 = \frac{\pi}{4}$ (shown by the vertical dashed line).

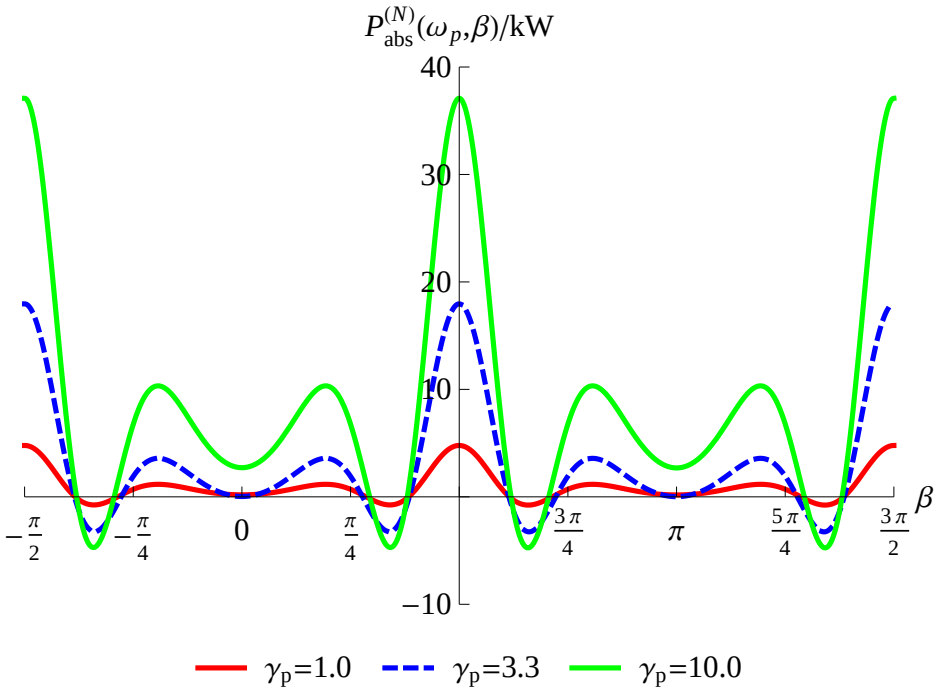

Figure 9.8: Power absorbed $P_{abs}^{(N)}(\omega_p, \beta)$ in kilowatts at peak frequency $\omega = \omega_p = 0.5$ against incident wave angle β for uniform arrays optimised in beam seas with $\beta_0 = \frac{\pi}{2}$ (shown by y-axis).

concern as the $P_{abs}^{(N)}$ peaks correspond to the spectrum peaks. This may be problematical if the wave conditions are more varied than indicated by the spectrum fed into the optimisation. Since the broad-banded spectra arrays attempt to perform well over a broader range, this results in more stable but significantly reduced performance. It is also clear from figure 9.5 that the beam seas arrays are slightly more stable to changes in ω with both higher and wider peaks. This is an important point, since real seas may be composed of widely differing sea states. This is one of the many considerations associated with site selection.

In contrast, figure 9.6 shows that the head seas arrays are more stable to β-variation in comparison to intermediate (figure 9.7) and beam seas (figure 9.8), indicating this may be a better option for sites with large β-variability. This again shows the trade-off between higher performance and stability of performance in different array variables. For the $\gamma_p = 10$ case, the peak reduction between beam and head seas is approximately 10%, while the range over which $P_{abs}^{(N)} > 30$kW is significantly increased from approximately $\beta = \frac{\pi}{2} \pm \frac{\pi}{24}$ to $\beta = 0 \pm \frac{\pi}{8}$, thereby tripling this range. Similarly for $\gamma_p = 3.3$, there is approximately a 45% peak reduction between beam and head seas, but the

range of β for which $P_{abs}^{(N)} > 9$kW is increased from approximately $\beta = \frac{\pi}{2} \pm \frac{\pi}{16}$ to $\beta = 0 \pm \frac{\pi}{8}$, which doubles this stability range. Performance is much lower for $\gamma_p = 1.0$ in general. The beam seas array achieves a peak performance of $P_{abs}^{(N)} \approx 5$kW, which drops to near zero around $\beta = \frac{\pi}{2} \pm \frac{\pi}{8}$. However performance is much smoother with very little variation for head seas, where $P_{abs}^{(N)} \approx 2$kW for all values of $\beta \in [-\pi, \pi]$. This indicates that although power absorption is quite low for this array, it is one of the most stable to changes in incident wave angle.

For $\beta_0 = 0, \frac{\pi}{4}$, secondary peaks of comparable height are observed in the $P_{abs}^{(N)}$ vs β plots away from the target incident wave angle β_0. For head seas, a secondary peak occurs at $\beta \approx \frac{3\pi}{4}$, which corresponds to an array layout more akin to the intermediate seas case. For intermediate seas, a secondary peak occurs near $\beta \approx \frac{7\pi}{8}$, which when extended shows a wide area of good performance at $\beta = \pi \pm \frac{\pi}{5}$, corresponding to a mirrored head seas case. If stability to β-variability is more desirable, then applying the optimal displacement variables for $\beta_0 = \frac{\pi}{4}$ to the head seas case may be ideal. However, it is possible that this would result in an increased ω-sensitivity and thus may not perform well over the frequency spectrum.

9.3.2 Optimised Layout

Consider the case where only the first and third WECs are fixed (at 0m and 300m along the line respectively). The middle WEC is now free to move within the optimisation procedure; this adds an extra variable (s_1) to the previous optimisation, resulting in seven variables in total. The method follows the previous section and the optimisation results for the non-uniform arrays are listed in table 9.2, together with a schematic of the optimal array layout. The variation of the power absorbed by the optimised arrays with respect to frequency ω and incident wave angle β is also shown in figures 9.9 - 9.11 and figures 9.12 - 9.14 respectively.

This configuration behaves in a similar manner to the previous one, as seen by comparing the values in tables 9.1 and 9.2. The array once more performs better for more narrow spectra and performance is also greatest for beam seas. The results in table 9.2 are slightly greater than (or equal to) those in table 9.1, attributable to the increased freedom of the position of WEC 2. As with the uniform array, the displacement limit of $\delta_j = 1$ is reached for all arrays with $\gamma_p = 10$.

Table 9.2: Optimisation results for non-uniform three-WEC linear array

γ_p	β_0	s_2	δ_1	δ_2	δ_3	ψ_1	ψ_2	ψ_3	Q	Array Layout
	0	35.54	0.3947	0.3334	0.0383	4.5516	6.1237	5.1849	1223.85	* * *
1.0	$\frac{\pi}{4}$	46.28	0.3932	0.3420	0.0822	4.6848	5.8524	3.6110	1293.87	* * *
	$\frac{\pi}{2}$	97.71	0.4306	0.4333	0.4014	4.7259	4.7259	4.7259	2311.22	* * *
	0	50.43	0.7840	0.6847	0.2864	4.5997	0.0009	6.1768	4060.11	* * *
3.3	$\frac{\pi}{4}$	63.17	0.7644	0.7024	0.4292	4.6735	6.0691	3.8395	4431.33	* * *
	$\frac{\pi}{2}$	150.00	0.8469	0.9350	0.8469	4.7227	4.7227	4.7227	7145.26	* * *
	0	70.11	1.0000	1.0000	1.0000	4.6306	0.3645	6.2151	16346.12	* * *
10	$\frac{\pi}{4}$	74.07	1.0000	1.0000	1.0000	4.6973	6.1832	3.8742	17635.17	* * *
	$\frac{\pi}{2}$	150.00	1.0000	1.0000	1.0000	4.7211	4.7211	4.7211	21804.11	* * *

In the majority of cases, the optimal layout diverges from the uniform array and tends to place WEC 2 closer to WEC 1. For head and intermediate seas, the separation between WECs 1 and 2 is reduced and the value of δ_2 is comparable to δ_1, indicating that both WECs work similarly hard. The shadowing effect is still observed for WEC 3, with a significantly lower value of δ_3, except for $\gamma_p = 10$, where $\delta_j = 1$ for all WECs. For beam seas, with $\gamma_p = 3.3, 10$, the optimal layout is the uniform array layout and the results of table 9.1 are repeated.

For $\gamma_p = 1$, a slight improvement on the uniform beam sea case is achieved by moving WEC 2 closer to WEC 1, with the same phases and slightly altered amplitudes. This may be because it is more beneficial to maximise the constructive interaction between WECs 1 and 2, rather than to minimise the interaction by having the devices as separated as possible in a uniform layout. However, it should be noted that the improvement in comparison to the corresponding uniform array in table 9.1 is less than 1%. As discussed previously, the Havelock coefficients are accurate to three to five significant figures, implying a similar accuracy for the objective function and the optimisation results. The corresponding error may absorb the difference of 1% between the uniform and non-uniform array performances. Thus the 1% improvement seen in this case may be due to a numerical anomaly caused by the level of accuracy employed.

Figures 9.9 - 9.14 exhibit similar behaviour to figures 9.3 - 9.8, with a slight increase in relative performance. In some cases, the stability of performance is also increased slightly. The major difference is seen in the β-plots, where the secondary peaks seen for the uniform arrays are no longer present for the

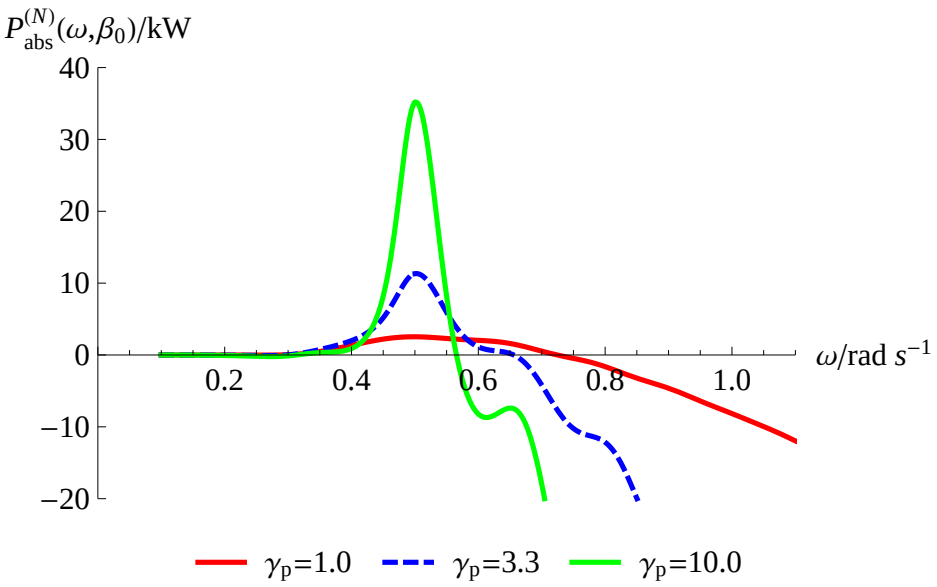

Figure 9.9: Power absorbed $P_{abs}^{(N)}(\omega, \beta_0)$ in kilowatts against frequency ω for optimised non-uniform arrays with $\beta_0 = 0$ (head seas).

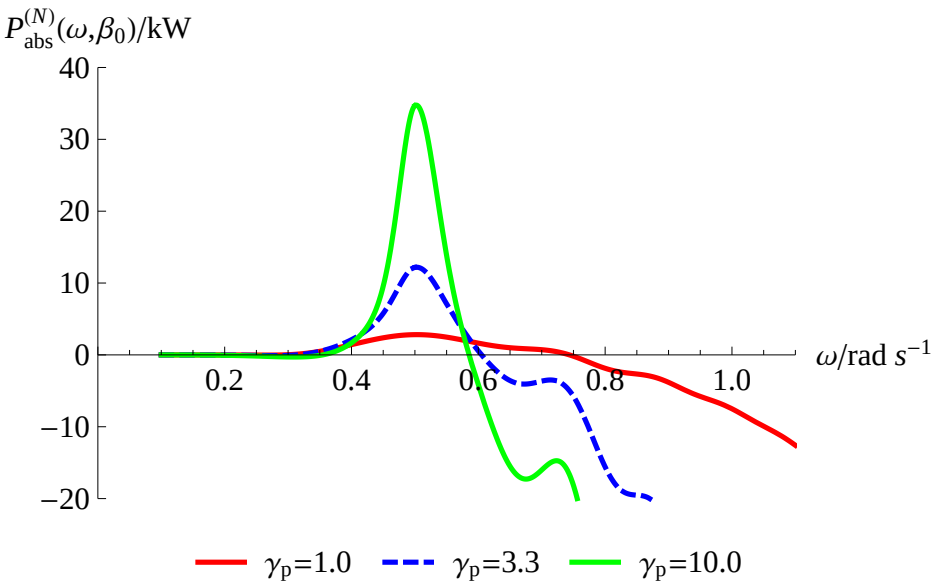

Figure 9.10: Power absorbed $P_{abs}^{(N)}(\omega, \beta_0)$ in kilowatts against frequency ω for optimised non-uniform arrays with $\beta_0 = \frac{\pi}{4}$ (intermediate seas).

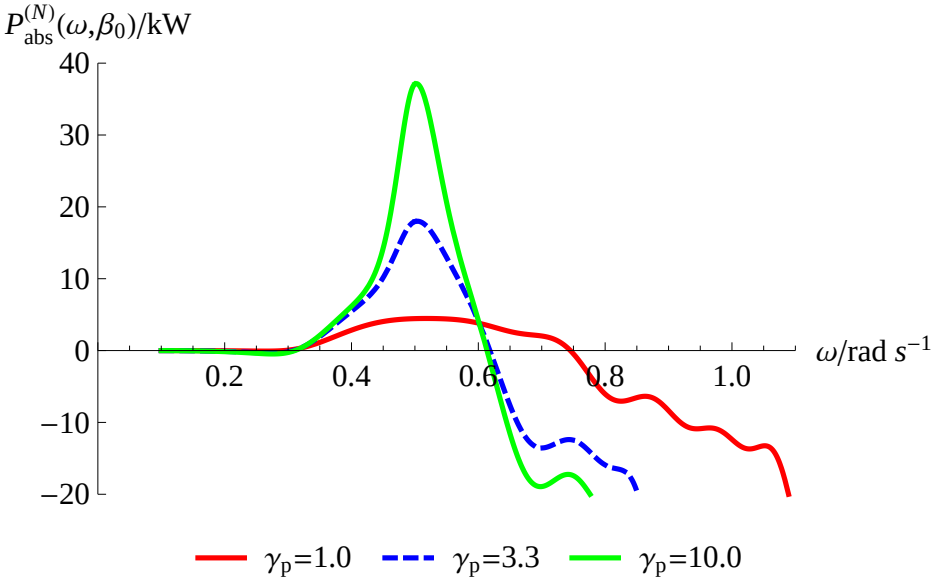

Figure 9.11: Power absorbed $P^{(N)}_{abs}(\omega, \beta_0)$ in kilowatts against frequency ω for optimised non-uniform arrays with $\beta_0 = \frac{\pi}{2}$ (beam seas).

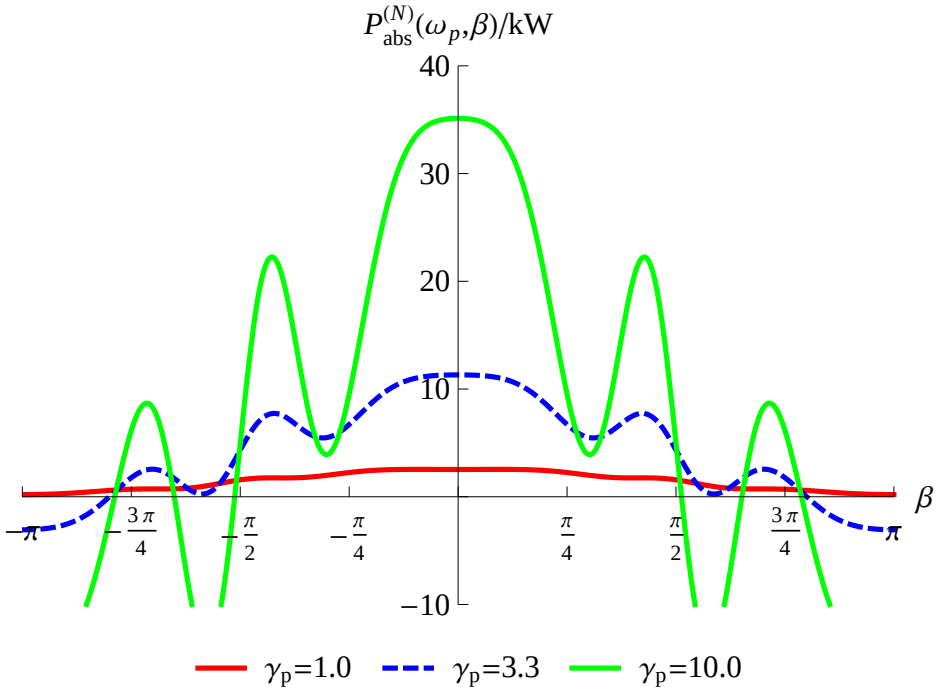

Figure 9.12: Power absorbed $P^{(N)}_{abs}(\omega_p, \beta)$ in kilowatts at peak frequency $\omega = \omega_p = 0.5$ against incident wave angle β for non-uniform arrays optimised in head seas with $\beta_0 = 0$ (shown by y-axis).

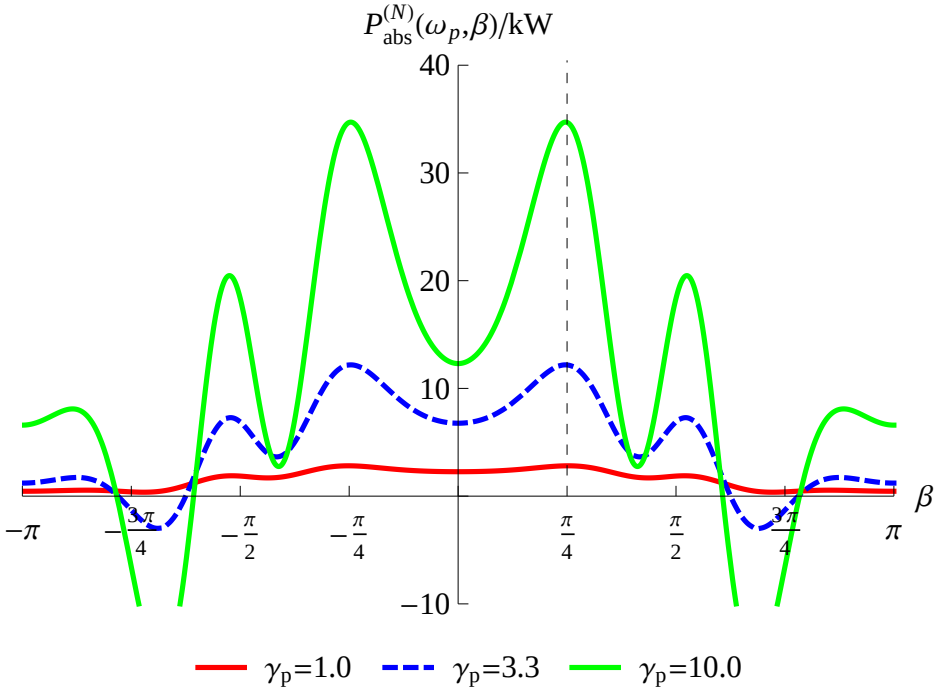

Figure 9.13: Power absorbed $P^{(N)}_{abs}(\omega_p, \beta)$ in kilowatts at peak frequency $\omega = \omega_p = 0.5$ against incident wave angle β for non-uniform arrays optimised with $\beta_0 = \frac{\pi}{4}$ (shown by the vertical dashed line).

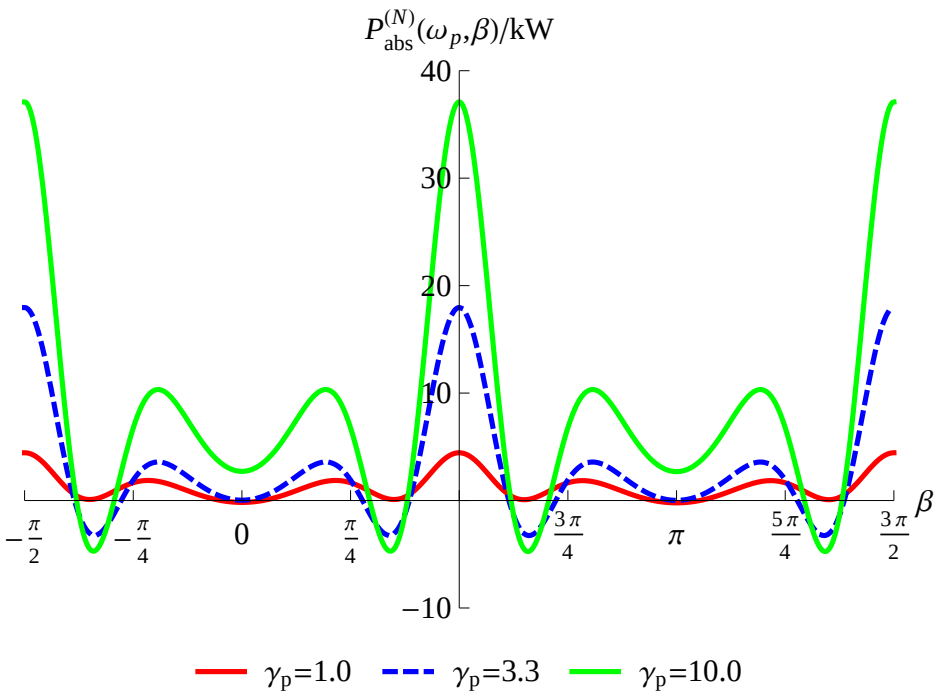

Figure 9.14: Power absorbed $P^{(N)}_{abs}(\omega_p, \beta)$ in kilowatts at peak frequency $\omega = \omega_p = 0.5$ against incident wave angle β for non-uniform arrays optimised in beam seas with $\beta_0 = \frac{\pi}{2}$ (shown by y-axis).

majority of cases with optimised layouts.

9.4 Discussion of Results

This chapter describes a preliminary implementation of a numerical optimisation method for linear arrays of three identical WECs in irregular waves. This is an initial extension of previous work that was targeted at regular wave regimes. A JONSWAP spectrum was employed in this study but the method is applicable for any given spectrum. It is assumed that all wave components are long-crested and approach the array from a single wave angle. In principle, a wave angle spectrum can be incorporated into the method but the objective function would then require a double integral, over both ω and β, which would increase the computational time required.

Early studies on array optimisation targeted the maximisation of array performance, which resulted in highly sensitive optimal arrays. This output was improved in earlier chapters of this thesis by maximising the mean performance of the array over some domain of non-dimensional array variables, which resulted in more stable performance. The extension to irregular waves has been made by maximising the weighted sum of the power absorbed by the array over a range of frequency, where the weighting is the normalised power spectrum. This involves a frequency integral and the problem can no longer be studied in a non-dimensional manner, thus dimensional quantities must be utilised. This requires certain quantities to be specified prior to the optimisation, most significantly the device radius a. A relatively small value of $a = 2.5$m was chosen in order to avoid calculation difficulties with the Havelock coefficients and to ensure the point absorber approximation was not violated.

Within this chapter, the WEC displacements are non-dimensionalised with respect to the device radius a, whereas previously these were non-dimensionalised with respect to the wave amplitude A. For a wave spectrum, the wave amplitude will vary across the spectrum as a function of ω and $A = A(\omega)$. In principle, this can be implemented into the optimisation via equation (9.8) but this increases the numerical demand of the optimisation. From a physical perspective, it is also impractical to implement a controlled displacement amplitude that will depend on the wave frequency. A fixed known displacement is essential from an engineering perspective and by non-dimensionalising with respect to a, this means that the displacement

amplitudes values will remain fixed over the spectrum. This also allows a sensible no-slamming limit to be placed on the motion amplitudes such that the WEC does not leave the water, i.e. $0 \leq \delta_j \leq 1$ for a semi-spherical device.

Two types of linear 3-WEC arrays were considered: a uniform array with the positions of all WECs fixed and a non-uniform array where the middle WEC is free to move in the optimisation. The calculation was simplified in order to reduce the computational requirement by fixing the total length of the array (the position of WEC 3) at $L = 300$m. Three types of JONSWAP spectrum were considered, chosen to represent narrow-banded, intermediate-banded and broad-banded spectra. Optimal values for peak power absorbed in the order of 30kW to 40kW were achieved for narrow-banded spectra, while peak values of between 1kW to 4kW were obtained for broad-banded spectra. This indicates an $\mathcal{O}(10)$ difference between the array performance in narrow- and broad-banded spectra. The optimisation forced the $P_{abs}^{(N)}$ curve to match the shape of the peak of the spectra closely in most cases, thus maximising the utilisation of the resource.

Negative power values were seen for larger frequencies for all three spectra. This is attributed to the devices having forced motions which are tuned to absorb as much of the spectrum as possible. This generally resulted in high $P_{abs}^{(N)}$ values near the peak of $\omega_p = 0.5$rad s^{-1}. However for larger frequencies, the negative $P_{abs}^{(N)}$ are associated with detuning of the forced WEC motions at these frequencies. The WECs would effectively be creating waves rather than absorbing them. However, this generally has little effect as the spectrum possessed small or negligible values at these frequencies.

The optimal arrays performed better when optimised for narrow-banded spectra as expected, as the WECs can be tuned more easily to the peak of the spectrum. Arrays also achieved higher objective function values for beam seas, in agreement with the intuitive idea that a greater frontage to the waves allows a greater power take off. For arrays in head and intermediate seas with narrow- and intermediate-banded spectra, a shadowing effect was seen in the optimal cases, where WEC 1 (which was first to meet the wave) operated at a higher displacement amplitude than WECs 2 and 3, with all WECs having differing phases. This implies that WEC 1 takes off the most power and the other WECs are shadowed by WEC 1, hence their lower motion amplitudes. For beam seas (where the waves strikes each WEC at the same time), the motion amplitudes were symmetric about the middle WEC and all devices moved in phase. This

indicates that constructive interference is possible and further agrees with the shadowing phenomenon for other wave angles. For the narrow-banded spectrum with $\gamma_p = 10$, the displacement amplitude limit was reached for all arrays, due to the WECs being as highly tuned as allowed to the spectrum peak.

An increase in optimal array performance occurred in all but two cases when WEC 2 was free to move within the optimisation. Optimal layouts for head and intermediate seas consisted of WEC 2 being placed closer to WEC 1 with altered displacement variables relative to the uniform layout. In two of the three spectra, the optimal array layout for beam seas was the uniform arrangement, with WEC 2 placed exactly half way between WECs 1 and 3, and with the same displacement values as the uniform optimisation result. This suggests that when narrow-banded spectra are present at a site, a uniform terminator type layout performs best.

It must be noted that the beam seas array is sensitive to incident wave angle variability, with a $\frac{\pi}{24}$ change resulting in significant power loss. Comparing this to the analogous head seas array, which is of attenuator type, the peak performance is lowered by approximately 10% but the array is much more stable to β-variation, with good power absorption maintained for a change of up to $\frac{\pi}{8}$. As with McGuinness & Thomas (2017a), this highlights the trade off that exists between obtaining high performance and maintaining good performance over a range of different array variables.

Overall, the preliminary results in this study suggests that, if WEC arrays are deployed in irregular waves with considerable frequency variation, then the best layout is that of a uniform array in a terminator type layout (beam seas). This can be considered as resorting to an average layout in order to best account for the variation in wave conditions. It should be stressed that this is a tentative deduction based upon preliminary results considering small linear arrays of fixed length containing three WECs. The result that a uniform array is optimal may be an artifact of considering such a small number of array members. It is possible that non-uniform and non-symmetric array may be optimal in irregular waves if more than three WECs and different configurations are considered. Previous work conducted primarily in regular waves often suggested that non-uniform and non-symmetric arrays performed well. Though, in certain cases, uniform layouts were also found to be optimal in regular waves. This suggests that array layout optimisations in regular waves cannot always be transferred to irregular waves, particularly if there is considerable variation

within the spectrum.

The main restriction on this work was the numerical intensity and long run-times of the calculations involved. In principle, this method can be extended to arrays of five or more WECs, however became prohibitive with the resources available due to the "parameter explosion" effect of including extra WECs. For this reason, the formulation was kept as simple as possible by limiting the number of optimisation variables and assuming a fixed incident wave angle. Future research should attempt to extend this to include more WECs, where the interaction between the devices would be more complex, and to include the wave angle variation into the power spectrum. This can be done relatively easily using equations (2.175), (2.176), (2.183) and (2.184). Other array geometries could also be investigated, with the ultimate goal of a general layout optimisation with no prescribed geometry.

Chapter 10

Discussion & Conclusion

10.1 Summary & Discussion

Chapter 1 introduced the concept of wave energy and described a number of types of WECs, including the heaving point absorber considered in this thesis. The chapter summarised the relevant literature and identified those areas where existing knowledge is not sufficient. A primary concern identified from available literature on arrays in wave energy is the relative sensitivity of optimal arrays to changes in array parameters. This was noted particularity in the work of Fitzgerald (2006) and Child (2011), where either the optimal array layouts were very close in configuration to the poorest performing arrays or the optimal arrays resulted in a sharp peak in performance surrounded by large troughs. The principal cause was the deterministic optimisations implemented in these studies, where the performance of the array was maximised directly with respect to the array layout. This identified the primary aim of this thesis: to optimise an array layout such that good performance is maintained for small changes in sea conditions. In this sense, the stability of the optimal array performance is the primary goal.

The mathematical formulation is outlined in Chapter 2. This begins with an outline of water wave theory and the linear wave theory approximation. The hydrodynamic modelling of the interaction between regular waves and a floating body, including the radiation and scattering problems for small body motions, is introduced. This is followed by the modelling of a single WEC and its power absorption, before an array formulation for many such WECs operating in a single mode of motion is presented. The point absorber approximation is then

introduced to simplify the calculations and explicit expressions for the power absorbed by the array are obtained. The interaction factor is introduced as a measure of the interaction effects within the array, for both optimal and sub-optimal motions. Finally, a brief description of irregular wave theory is given.

A preliminary investigation of a robust optimisation was performed in Chapter 3. The simplest form of the problem was first examined, which considered a linear array of five WECs with an enforced symmetry in the array layout. In order to achieve stable constructive interaction, the optimisation should maximise the average array performance in some manner, rather than directly maximising the performance for a very specific set of parameter values. The objective function was defined as the continuous mean of the interaction factor over some range of non-dimensional length of the array kL. With the enforced symmetry and the assumption of optimal motions, this optimisation was a function of one variable only. This represented the simplest possible case of the optimisation and also yielded a visualisation of the performance of the array with respect to this one variable. Many different cases were examined, involving different incident wave angles and considering a number of enforced symmetries. Three basic symmetries were investigated for five different wave angles between head seas and beam seas.

It was found for unconstrained motions that this robust optimisation resulted in stable constructive interference over the majority of the range of interest of $kL \in [5, 15]$ for most incident wave angles. However, incident wave angles near $\beta_0 = \frac{\pi}{8}$ resulted in very poor performance, even in the optimal case with unconstrained motions. In order to confirm the stability of the optimal performance, a sensitivity analysis was performed which showed that small changes in WEC positions resulted in only small changes in the interaction factor. It was shown that the incident wave angle had a considerable impact on the optimal array layout, with significantly different layouts found for different values of β. In general, it was found that arrays performed best in beam seas with the largest mean interaction factors but head sea arrays also achieved comparable constructive interference. Some optimal arrays were shown to be highly sensitive to changes in β, despite being stable to changes in non-dimensional array length kL.

The predicted optimal displacements of all arrays obtained in Chapter 3 were excessively large. The underlying linear theory requires that the WEC motions

are at most the same order of magnitude as the wave amplitude. For each optimal array of Chapter 3, the individual device motions were $\mathcal{O}(100)$ to $\mathcal{O}(1000)$ times the wave amplitude. This would violate the underlying linear wave theory. Furthermore, these displacements would not be implementable using a realistic PTO, which would damp the WEC motions and result in a reduction in the optimal array performance.

This approach was extended in Chapter 4 to examine general linear arrays of five WECs, without any imposed symmetry and the results of Chapter 3 were confirmed in a more general arena. The topic of closely-spaced WECs was identified in both Chapters 3 and 4, where optimal arrays typically contained closely-spaced groups of between two to four WECs. There are several shortcomings associated with these closely-spaced WECs such as possible collisions and associated maintenance and engineering difficulties. As in Chapter 3, these WECs are also accompanied by very large optimal motion amplitudes, which invalidates the underlying linear wave theory. Furthermore, it may be unreasonable to treat these closely-spaced WECs as point absorbers, since there may be considerable scattering or shadowing effects for WECs in such proximity.

Better performing arrays were obtained in Chapter 4 in comparison to Chapter 3, due to the increased freedom of the WEC positions within the optimisation. However, the much simpler optimisation in Chapter 3 yielded results comparable with the more general implementation of Chapter 4, with at most an 11% difference between the resulting objective function values. This illustrates the benefit of considering the simple problem before generalising to more sophisticated cases. The single variable optimisation also enabled visualisation of the array performance in detail, which is not possible for several variables.

Chapter 5 is associated with an array of WECs in a circular arrangement. Arrays of six or seven WECs are considered, with six WECs constrained to lie on the circle circumference and a seventh WEC placed in the circle centre in some cases. This configuration was chosen as it allowed for a more two-dimensional geometry to be investigated in comparison to a linear array, while maintaining a relatively low number of optimisation variables. The objective function for the circular arrays was defined as the mean of the interaction factor over a range of non-dimensional radius of the array kr. Only unconstrained motions are considered for circular arrays due to the relative numerical intensity of the optimisations. As a consequence of the increased number of WECs and increased freedom of the WEC positions, greater values of

the objective function were found relative to the linear array cases.

The optimal circular arrays were found to maintain constructive interference over all the range of $kr \in [5, 15]$ considered. In each case, the performance of the array with respect to incident wave angle was forced to peak at the prescribed value of the angle of incidence β_0. In most cases, the optimal circular array layouts consisted of all WECs being placed in a semi-circle opposite to the incident wave direction. The inclusion of the central seventh WEC resulted in slightly lower objective function values, although these arrays may absorb more power relative to the six-WEC arrays due to the presence of the extra device.

Constrained motions of WECs in linear arrays was considered in Chapter 6. The displacement amplitudes of the WECs are limited to two or three times the incident wave amplitude. Enforcing suboptimal motions requires the inclusion of an extra $2N$ variables in the optimisation, corresponding to the displacement amplitudes and phases for each WEC; this increases the computational effort significantly. It was found that the optimisation was well-behaved in terms of convergence to the optimal solutions for the displacement variables. Thus a more sparse scan of these variables was implemented, while a finer scan of the WEC position variables was performed.

The optimal constrained layouts of Chapter 6 were compared to the analogous unconstrained layouts of Chapter 4 and it was found that the constrained layouts were generally more widely spread. The unconstrained layouts were also assessed within the constrained regime and it was shown that the imposition of constraints severely degraded the performance and prevented constructive interaction from being maintained. Most of the optimised constrained layouts did not achieve constructive interference, with the exception of the $\delta_{max} = 3$ case for beam seas. It was shown that the constraint of three times the wave amplitude allowed for modest performance in some cases, while the lower constraint of twice the wave amplitude was severely limiting, in agreement with preliminary findings in the previous literature.

Although considerably lower performance was seen for the constrained arrays in head and intermediate seas, a much greater β-stability was observed. In contrast, the better performing arrays in beam seas were much more sensitive to changes in the incident wave angle. This suggests that there exists a trade-off between high performance and stability of performance when WEC motion constraints are applied, where lower overall performance is more stable to β-variation and higher performance results in greater β-sensitivity.

An alternative objective function was introduced in Chapter 7, in which the mean is taken over the incident wave angle rather than the non-dimensional array length. This was applied to linear arrays for a number target incident wave angles with a variation of $\pm\frac{\pi}{8}$ in the range considered. Uniform linear arrays were investigated initially, with the objective function for both constrained and unconstrained motions utilised to provide a benchmark for comparison. Optimised layouts were also considered and gave an improvement on the uniform arrays, although this improvement was only slight for constrained motions. As with the previous optimisations, the unconstrained optimal layouts contained closely spaced WECs, while in general the constrained arrays were more widely-spaced, though some still contained closely spaced WECs. The constraint applied also had a considerable effect on the optimal layout, with different optimal layouts found for the different constraints in most cases.

The beam sea arrays performed best for unconstrained motions, while the head sea arrays obtained the highest objective function values for constrained motions. This illustrates a considerable shift in the best array layout when constraints are applied. In all cases, the resulting interaction factors were forced to perform as well as possible in the specified range of β, with broad peaks occurring near the target wave angle. For head seas, a relatively small reduction in performance was obtained following the imposition of constraints but a much greater wavenumber sensitivity was also obtained. In contrast, for beam seas, the imposition of constraints produced a significant reduction in performance but a much better wavenumber stability. Once more, this indicates that there is a trade-off between high performance and performance stability. More specifically, the trade-off is between β-stability and k-stability, since the optimisation forces the array to perform as well as possible with respect to β within the range of interest.

One advantage of this β-optimisation is that it does not require a prescribed geometry and is well defined for a general 2D array layout, which is considered in Chapter 8. Both constrained and unconstrained motions were investigated. It was found that the constraint applied had a considerable effect on the optimal layout, with noticeably different arrangements obtained in some cases. Better performance was obtained for the narrower β-ranges, as this allowed the WECs in the arrays to be more tuned to the peak performance. The trade-off between β-stability and k-stability is not as evident for these general array layouts, indicating that this phenomenon is limited primarily to linear arrays. However,

there does exist a trade-off between higher performance and β-stability, with lower overall performance of the broader β-ranges.

A preliminary investigation of a robust optimisation in irregular waves was presented in Chapter 9. An irregular wave implementation involves a frequency integral over a wave energy spectrum and this requires that physical (dimensional) separations of the WECs be considered; certain physical quantities (such as WEC radius) must also be specified. This reduces the generality of the formulation, as it can no longer be considered in a non-dimensional manner. It is not consistent to implement optimal motions across a spectrum and so constrained motions are also enforced. An objective function, which was the frequency integral of the product of the wave energy spectrum and the power absorbed by the array, was employed. This is a relative measure which forces the absorption associated with the array layout to match the incident wave spectrum as closely as possible, but the objective function values have no direct physical meaning. Implementing a scaled version of this objective function, such as a measurement relative to isolated WECs, is difficult due to the intensity of the numerical optimisation.

A further limit on this implementation is the computational demand of the optimisation, as detailed in Chapter 9. As a consequence, an elementary linear array of three WECs is examined. To further simplify the formulation, one WEC position variable is removed by fixing the total length of the array. Three JONSWAP wave spectra are considered, ranging from broad to narrow-banded. Uniform layouts are investigated initially as a benchmark case, before considering a layout optimisation. As expected, better performance is seen for the narrow-banded spectrum since the WECs are able to be tuned to the relatively small frequency range of importance. Within this pattern, the best performance is also seen for beam seas arrays, which for most cases of consideration was a uniform layout. The trade-off between high performance and both k-stability and β-stability is observed, as with previous linear arrays.

Throughout this thesis, optimal linear array layouts were obtained in beam seas which did not exhibit symmetry about the middle WEC, as would be anticipated. It is not fully understood why this is the case, as symmetry was initially expected for beam seas since the wave is normally incident onto the linear array. It may be that having some of the WECs in close proximity at one side of the array gives greater constructive interaction, or that this layout gives a greater stability in performance to kL or β variation. Another possible

explination is that the q-factor may be an imperfect measure of the array performance, as it assumes optimal motions and considers array interaction only.

It should be noted that all models of the type implemented within this work inherently overestimate the the physical power absorption of a WEC. This model considers the hydrodynamic power absorbed by the device, so the PTO is essentially assumed to be 100% efficient. If a PTO term were included in the equation of motion and the power absorbed calculated from this term alone, then this term would absorb some fraction of the total available hydrodynamic power. However, this would result in more intensive calculations and increase the difficulty of a numerical optimisation of the type performed in this preliminary work.

This work is intended to extend previous studies of this nature; it should not be placed on a plinth but rather utilised as part of the existing literature. This thesis highlights the importance of considering the stability of optimal array performance. It is intended to inform prospective WEC array developers of the importance of considering the stability of the performance, particularly in terms of the interaction between array members, as opposed to simply maximising the array performance for a very specific set of conditions or parameter values.

10.2 Conclusion & Recommendations

This thesis highlights the need to consider the stability of optimal array performance, not just the optimal performance itself. This is an important element of WEC array design, as often the incident wave conditions will contain some variability or uncertainty. In order to make WECs economically viable, the reliability of the array performance is a necessary hurdle that must be overcome. It is clearly undesirable that a small change in incident wave conditions results in a large detrimental impact on optimal array performance. Thus, the array should be arranged such that its overall performance, within the variability of the incident waves, is as high as possible. It may also be desirable that this performance be as smooth as possible, without large drops in performance for small changes in wave conditions.

This thesis utilises several approximate methods to achieve this goal. The approach is developed from the simplest case in Chapter 3 to the general 2D layout optimisation of Chapter 8 and the irregular wave implementation of

Chapter 9. The importance of examining approximate methods, particularly with unconstrained optimal motions, should not be underestimated; this provides an insight into the best possible theoretical performance. Without the requirement of a sophisticated numerical optimisation, it was deduced at a preliminary stage that an incident wave angle of $\beta = \frac{\pi}{8}$ should be avoided for linear arrays, as this gave very poor performance even in the optimal unconstrained case. Similarly, limited performance was seen for intermediate seas, with $\beta = \frac{\pi}{4}$, and this is confirmed by the more accurate calculations of later chapters.

The preliminary results of Chapter 3 were confirmed in a more general arena in Chapters 4 and 6, where it was again shown that linear arrays perform very poorly near $\beta = \frac{\pi}{8}$, even when optimised for this wave angle. Most notably, the results of these chapters also showed that considerably different array layouts are found for different incident wave angles, indicating the importance of including the influence of this array parameter.

A general finding was that the optimal unconstrained layouts for head seas consisted of closely spaced groups of WECs, which would cause physical and theoretical difficulties, as previously identified. This also indicates that these layouts are accompanied with excessively large motions and the imposition of constraints would have a severe detrimental impact on array performance. In contrast, the optimal beam sea arrays were often more widely-spaced, in order to maximise the frontage to the incoming wave in some sense. As a consequence, these beam sea linear arrays were often accompanied by less extreme motion amplitudes and thus may be more desirable.

One aspect of linear WEC array behaviour, particularly when WEC motion amplitude constraints are enforced, is the trade-off between high mean performance and the stability of the performance to change in incident wavenumber or wave angle. Throughout Chapters 6 - 9, it was shown that higher objective function values were associated with a greater sensitivity to β-variation, while lower objective values had a greater stability to β-variation. Depending upon the WEC array site, it may be more beneficial or desirable to sacrifice the greater performance for a greater stability. Clearly, a site with as little incident wave variation as possible is more desirable as better performance can be achieved, but this is often not the case in practice.

This trade-off does not seem to be as pronounced for the general 2D arrays which not placed in a line, as seen in Chapter 8. This suggests that it is possible

to maintain stable performance for variation of wave conditions in certain cases. Although a linear array may seem to be desirable for a WEC array developer due to its simple geometry and sea area requirements, the findings of Chapter 8 suggest that other array layouts are more beneficial, not only for the greater constructive interference achieved but also for the increased stability to both incident wavenumber and wave angle. However, the ability to achieve both high and stable performance is greatly dependent upon the incident wave conditions at the given site.

10.3 Future Work

One of the most interesting avenues of future research was identified during the relatively simple optimisations undertaken in Chapters 3 and 4. The presence of groups of closely spaced WECs in most unconstrained optimal array layouts suggested that it may be possible to replace the group of closely-spaced WECs by an appropriately-sized larger single WEC. Hopefully, this would recreate the constructive interaction pattern created by the group, without the difficulties of the close proximity of WECs or the associated large WEC motions. From the present perspective, this would only be valid if all of the WECs in an interacting group operated in phase with each other; preliminary calculations have shown this is not the case for the arrays of Chapters 3 and 4, where the grouped WECs were π out of phase. However, it may still be possible to recreate the desired interaction with a larger WEC that operates in two or more modes.

Arrays of differently sized WECs have not been considered within the literature to date. An investigation into this possibility would require a more accurate mathematical model than that implemented in this thesis, as clearly the WECs are no longer identical and the point absorber approximation would possibly not be valid for the larger WECs. Previous work has considered the optimisation of single WEC sizes, for example Weber & Thomas (2000, 2003, 2005) considered the design optimisation of a OWC device and Thomas & Gallachóir (1993) considered the design optimisation of a Bristol Cylinder WEC. One possibility for future work would be to include the WEC sizes (ka) along with the WEC positions and displacements as variables within an optimisation similar to that implemented in this thesis. It is acknowledged that this would add an additional N variables to the optimisation (or more depending on the size/shape implementation) and thus increase the

computational demand significantly. The requirement of a more accurate model would also add to the numerical intensity, which together with the increased number of variables may render it untractable.

The concept of maximising the mean performance of WEC arrays has been utilised throughout this thesis, where "mean" is defined over a range of non-dimensional array length in Chapters 3 - 6, while it is defined over a range of incident wave angle in Chapters 7 and 8. A further extension of this work would be to consider a combination in which the mean is defined over both non-dimensional length and incident wave angle. This would include both the incident wave number and wave angle and thus would ideally produce array configurations that are stable to variations in all incident wave parameters.

This concept was briefly investigated in Chapter 3 but was not pursued as the optimisation over both kL and β required a double integral, resulting in a considerably increased computational demand. The results were not significantly different than those obtained for a kL-optimisation for the single variable linear arrays. It may be possible though, to obtain improved behaviour for more general array configurations. One potential difficulty is that a general 2D optimisation cannot be performed in this manner, as there does not seem to be a suitable procedure to define a non-dimensional length measure for a non-prescribed geometry. Unless a reasonable way to define this measure of mean performance of a general 2D layout is identified, the double integral optimisation cannot be performed.

An extension of the circular array geometry of Chapter 5 would be to consider a semi-circular layout. The optimal unconstrained circular array configurations seemed to position all WECs in a semicircle opposite the incident wave direction. This suggests that the semicircle may be a more natural choice for a prescribed geometry than a circular one and would reduce the intensity of the numerical calculations due to the reduced variable domain. The extension to constrained motions could also be examined; this was omitted in this thesis in favour of moving to the β-optimisation of Chapters 7 and 8 and the irregular wave optimisation of Chapter 9. An important obstacle with examining a constrained optimisation of the circular arrays is the large number of associated variables. For a circular array of seven WECs, with one WEC fixed in the centre and the angular position of another fixed, the optimisation contains five WEC position variables and fourteen WEC displacement variables. This gives a total of nineteen optimisation variables, which exceeds the number considered in

the general 2D optimisation of Chapter 8 and would require substantial computational resources.

The methods presented in this thesis could be readily extended to other array geometries, such as square, rectangular, elliptical, triangular, double row or triple row layouts. Some preliminary work on triangular and elliptical layouts with unconstrained WEC motions was undertaken by Fennell (2015) and Lawton (2017) respectively. These alternate geometries may be of interest if a certain area must be utilised and the array geometry has been decided *a priori*. Although arrays of more than five to seven WECs could also be considered and may provide interesting results, the implementation would be limited by the computational resources available.

One possible extension of the β-optimisation of Chapters 7 and 8 is a weighted version of the objective function, such as in equations (8.4) and (8.5). This approach is particularly useful if there is an incident wave angle variation that is not uniform. In most wave climates, the majority of waves come from a small range of angles, while a reduced resource occurs away from the dominant direction. If an accurate description of the angle of the incident waves is known, then an appropriate weighting function can be added to the objective function to model this functionality. It is essential to ensure that this weighting function be normalised, so that it has no net effect or contribution to the integral in the objective function. This may be regarded as a move towards an irregular wave regime that accounts for the complete wave angle spectrum. However, this weighted regular wave implementation allows the non-dimensionality of the problem to be maintained and also requires considerably less computational resources in comparison to a full irregular wave regime.

Several avenues of extension exist for the irregular wave implementation of Chapter 9. The most obvious is to consider arrays of more than three WECs, to enable a direct comparison with the findings of earlier chapters. Another extension would be to consider alternative array geometries in irregular waves or even a general 2D unprescribed geometry. These advancements, however desirable, would require a considerably increased computational effort and may not be tractable in some cases. Alternate spectra could also be examined, including the possibility of using a real measured spectrum from a given ocean site. Finally, the variation of the incident wave angle could also be included into the spectrum and accounted for within the optimisation, as described in Section 9.4. The objective function would then involve a double integral over both ω

and β, which would once more require additional computational resources.

Future studies should consider the importance of the WEC geometry, particularly for irregular waves. In Chapter 9, hemispherical devices were assumed and a displacement constraint relative to the hemispherical radius was imposed to prevent the device from leaving the water. However, it is acknowledged that a hemispherical WEC is an ideal modelling assumption and a more practical shape would be a vertical circular cylinder with a hemispherical base. With this WEC geometry, the importance of the device draught on both the applied constraint and the hydrodynamic forces should be considered. It may be more appropriate the apply a motion constraint relative to the draught to allow reasonable motions while preventing any slamming forces. Furthermore, the majority of the hydrodynamic forces will occur over the base of the WEC, which may be at a lower depth in comparison to a hemispherical WEC. Therefore the draught may also have a significant influence on resulting forces and hence the power absorbed.

The influence of finite depth on WEC arrays is not considered by a large majority of the available literature. This adds an additional variable to the formulation, namely the water depth. Optimisation of arrays in finite depth is an interesting yet considerable task; it is unclear currently how finite depth affects array performance and consequently, how it affects the optimal array configuration. The inclusion of finite depth effects often arises when a wave spectrum is employed to describe an irregular sea state, as the spectrum may contain non-zero components corresponding to frequencies that belong in a finite depth regime. In this case, it would be necessary to apply finite depth calculations over the entire spectrum.

Other interesting questions related to the influence of finite depth can also be identified. For example: Does the optimal array configuration change if the water depth is changed, and if so, how does it change? This could be investigated by extending the work of Linton (1991) to address the above tasks, although it is acknowledged that Linton's work is only valid for spherical devices. A different formulation would be needed for different device shapes, which is another topic of considerable interest.

The principal limitation encountered in the latter parts of this thesis is the associated computational demand of the optimisations performed. As more general cases are considered with more accurate approximations, the computation time of the calculations becomes a limiting factor in what can be

reasonably achieved. The number of WECs included is also limited by this effect, as increasing the number of WECs causes a "parameter explosion" effect, where the number of optimisation variables quickly becomes intractable. For example, in the general 2D optimisation of Chapter 8, an array of five WECs (with one fixed at the origin) results in eighteen optimisation variables. Even this number of variables is too many for numerical confidence and hence the reason why the results of Chapter 8 are not advertised as globally optimal. Increasing the array to ten WECs requires 38 variables, identifying the "parameter explosion" effect. The extension to irregular waves also resulted in significantly increased computation times, which further limited the scope of this thesis. If greater computational resources were available, further extensions such as those listed here could be examined.

Appendix A

Supplementary Results to Chapter 3

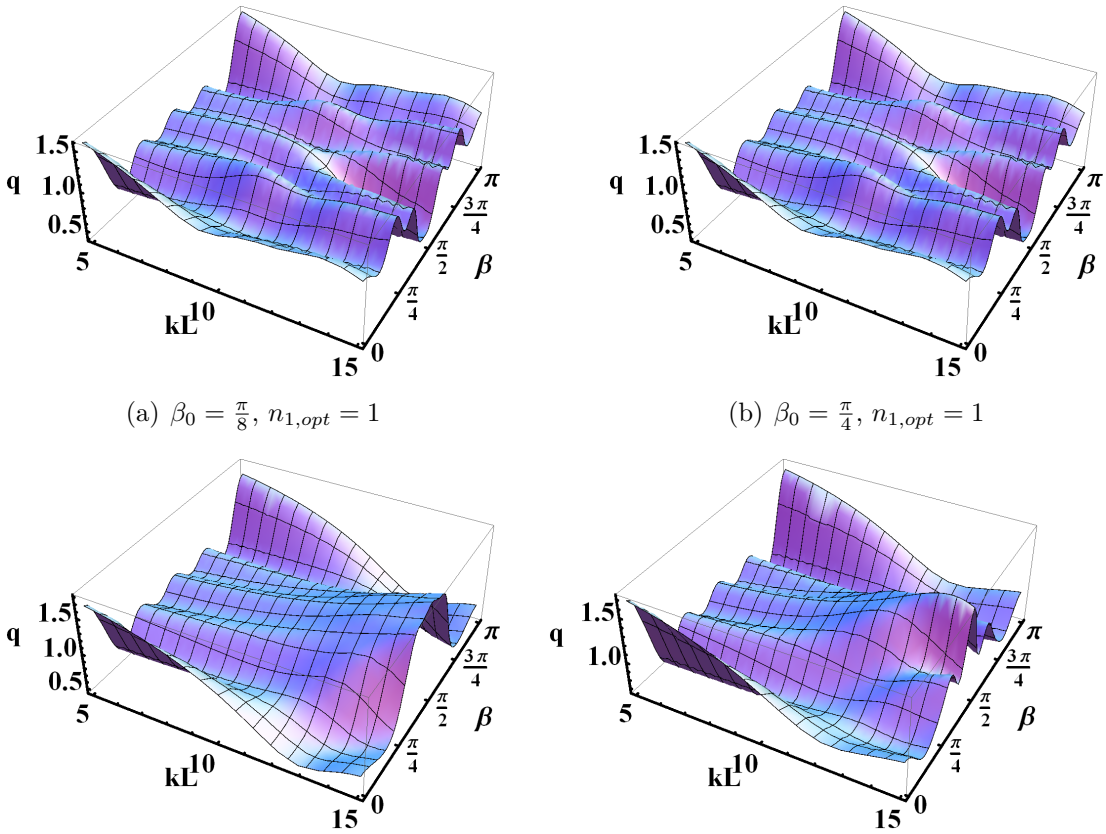

(a) $\beta_0 = \frac{\pi}{8}$, $n_{1,opt} = 1$

(b) $\beta_0 = \frac{\pi}{4}$, $n_{1,opt} = 1$

(c) $\beta_0 = \frac{3\pi}{8}$, $n_{1,opt} = 25$

(d) $\beta_0 = \frac{\pi}{2}$, $n_{1,opt} = 34$

Figure A.1: Interaction factor q vs kL vs β for array LS1 optimised for several values of β_0.

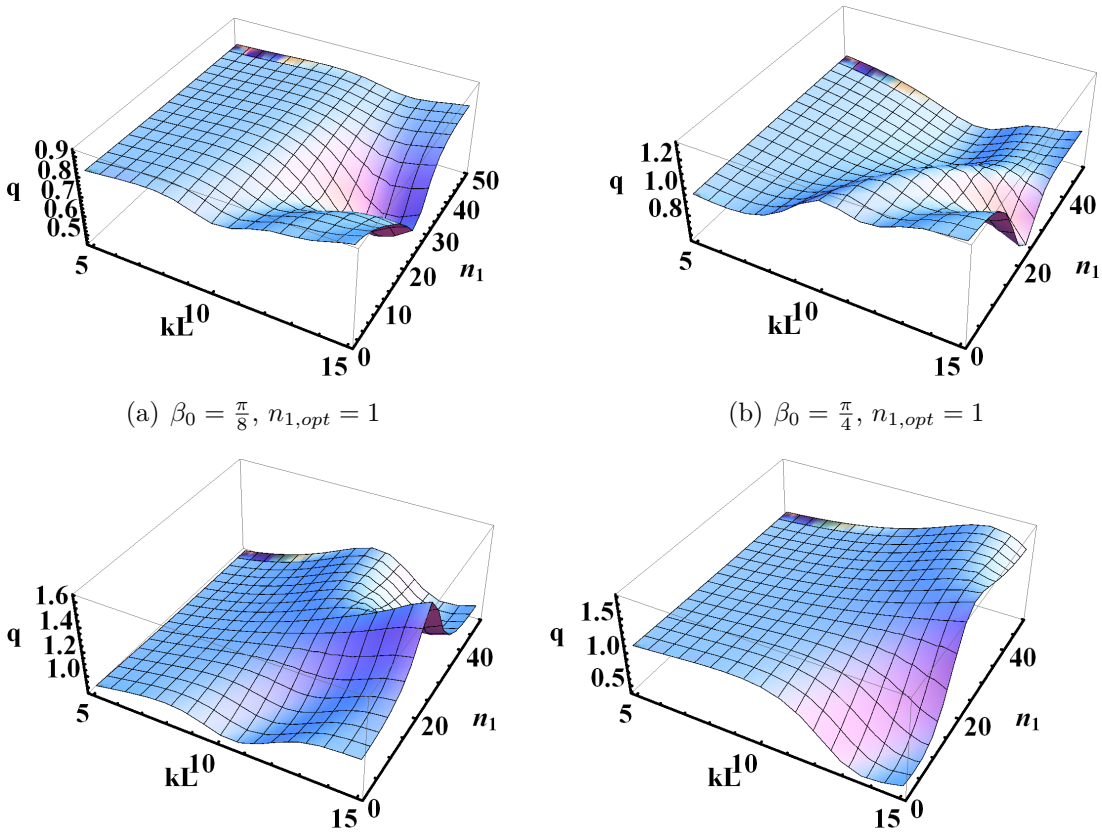

(a) $\beta_0 = \frac{\pi}{8}$, $n_{1,opt} = 1$

(b) $\beta_0 = \frac{\pi}{4}$, $n_{1,opt} = 1$

(c) $\beta_0 = \frac{3\pi}{8}$, $n_{1,opt} = 25$

(d) $\beta_0 = \frac{\pi}{2}$, $n_{1,opt} = 34$

Figure A.2: Interaction factor q vs kL vs n_1 for array LS1 for several values of β_0.

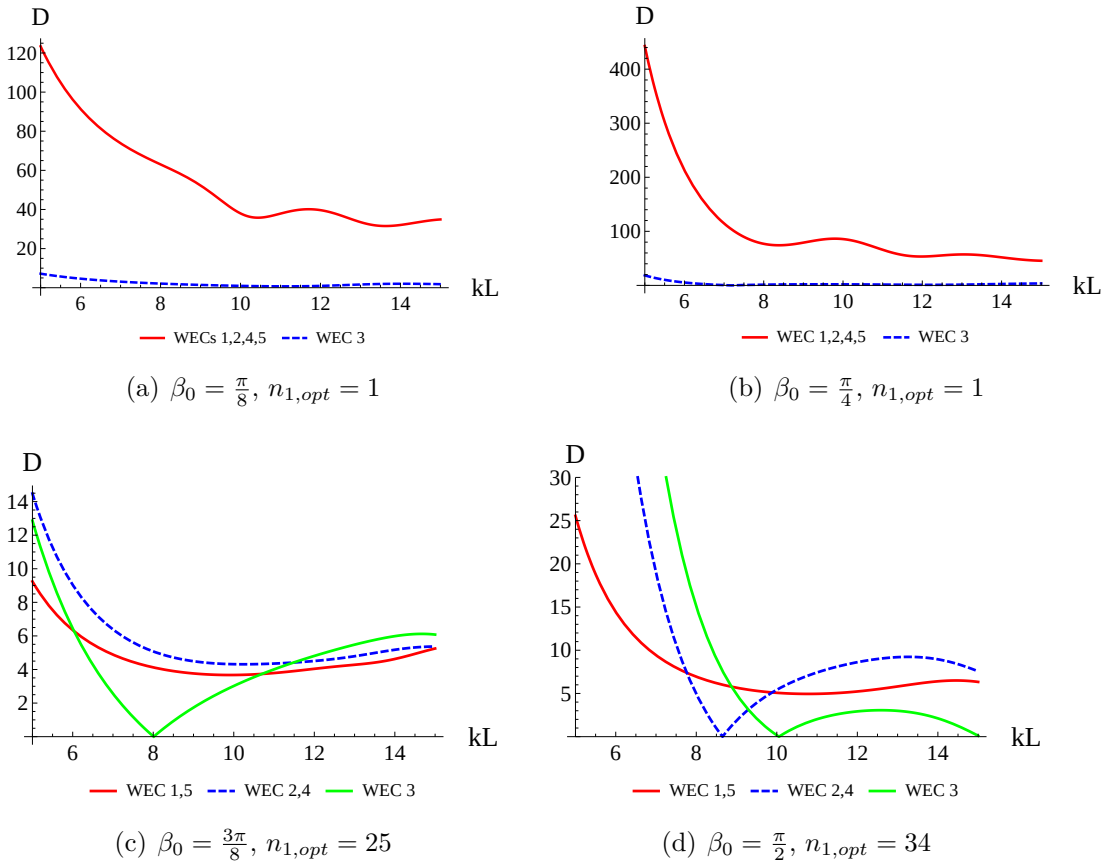

(a) $\beta_0 = \frac{\pi}{8}$, $n_{1,opt} = 1$

(b) $\beta_0 = \frac{\pi}{4}$, $n_{1,opt} = 1$

(c) $\beta_0 = \frac{3\pi}{8}$, $n_{1,opt} = 25$

(d) $\beta_0 = \frac{\pi}{2}$, $n_{1,opt} = 34$

Figure A.3: Predicted optimal displacement amplitudes for array LS1 for several values of β_0.

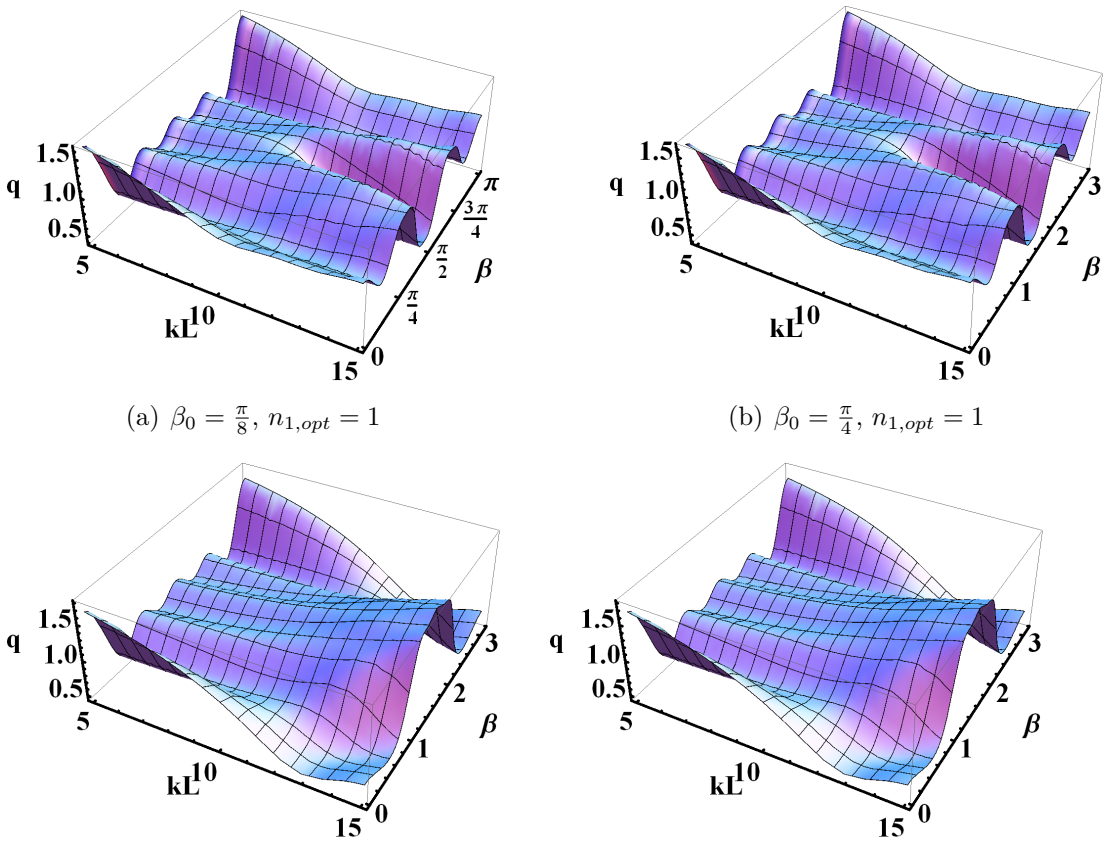

(a) $\beta_0 = \frac{\pi}{8}$, $n_{1,opt} = 1$

(b) $\beta_0 = \frac{\pi}{4}$, $n_{1,opt} = 1$

(c) $\beta_0 = \frac{3\pi}{8}$, $n_{1,opt} = 25$

(d) $\beta_0 = \frac{\pi}{2}$, $n_{1,opt} = 25$

Figure A.4: Interaction factor q vs kL vs β for array LS2 optimised for several values of β_0.

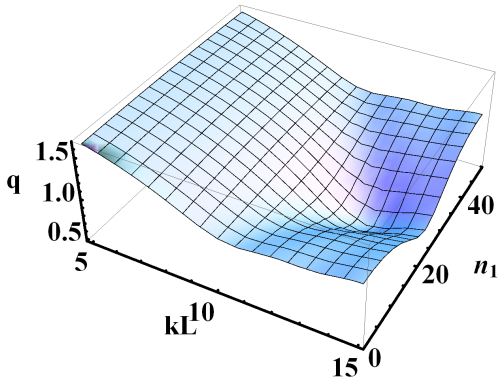

(a) $\beta_0 = 0$, $n_{1,opt} = 49$

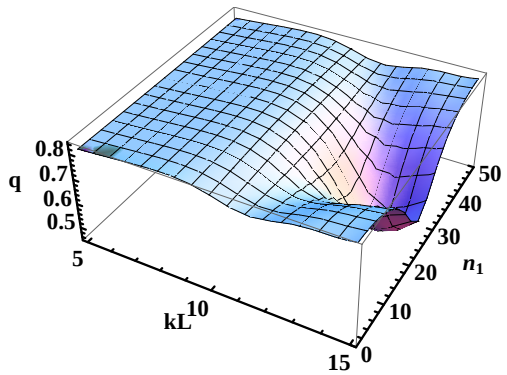

(b) $\beta_0 = \frac{\pi}{8}$, $n_{1,opt} = 1$

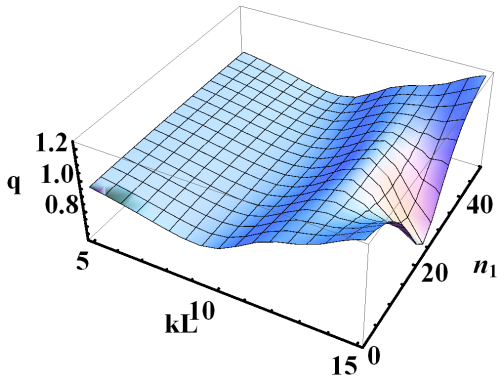

(c) $\beta_0 = \frac{\pi}{4}$, $n_{1,opt} = 1$

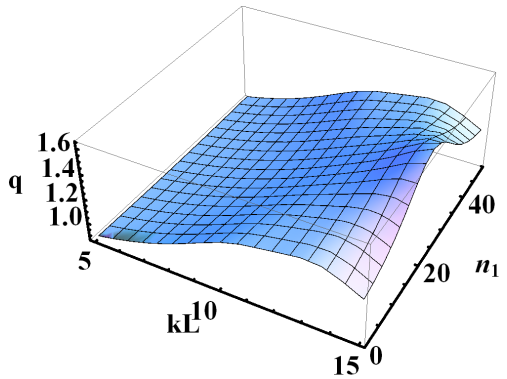

(d) $\beta_0 = \frac{3\pi}{8}$, $n_{1,opt} = 25$

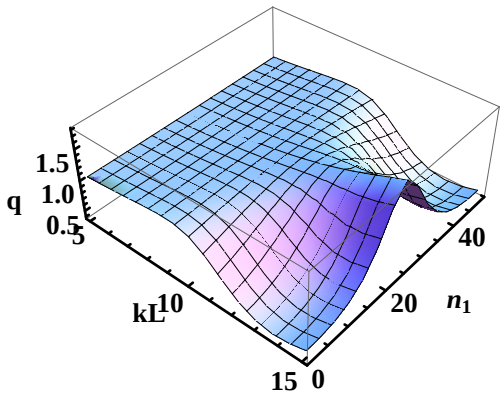

(e) $\beta_0 = \frac{\pi}{2}$, $n_{1,opt} = 34$

Figure A.5: Interaction factor q vs kL vs n_1 for array LS2 for several values of β_0.

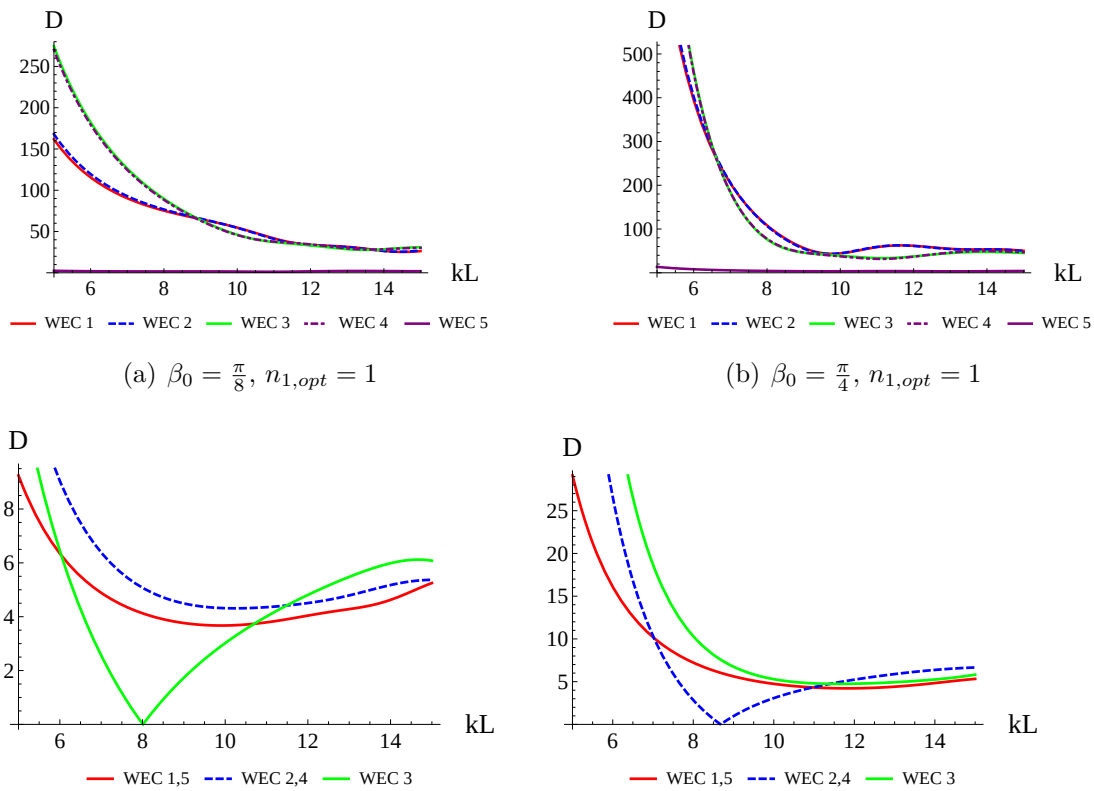

(a) $\beta_0 = \frac{\pi}{8}$, $n_{1,opt} = 1$

(b) $\beta_0 = \frac{\pi}{4}$, $n_{1,opt} = 1$

(c) $\beta_0 = \frac{3\pi}{8}$, $n_{1,opt} = 25$

(d) $\beta_0 = \frac{\pi}{2}$, $n_{1,opt} = 25$

Figure A.6: Predicted optimal displacement amplitudes for array LS2 for several values of β_0.

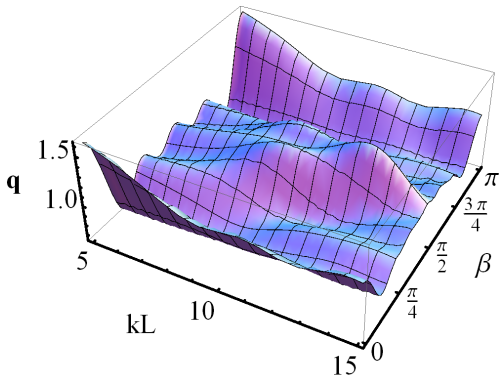

(a) $\beta_0 = 0$, $n_{1,opt} = 3$

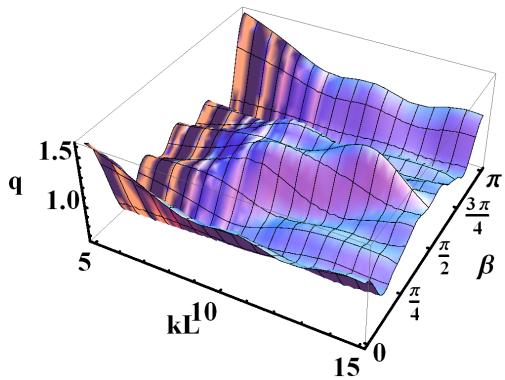

(b) $\beta_0 = \frac{\pi}{8}$, $n_{1,opt} = 1$

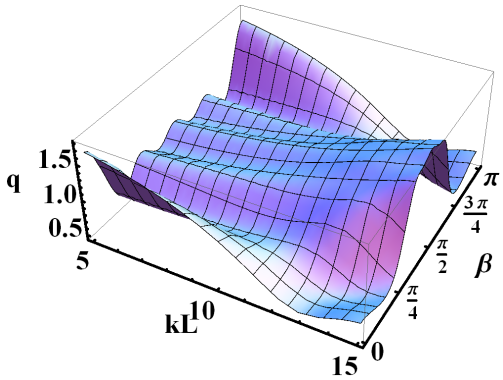

(c) $\beta_0 = \frac{\pi}{4}$, $n_{1,opt} = 25$

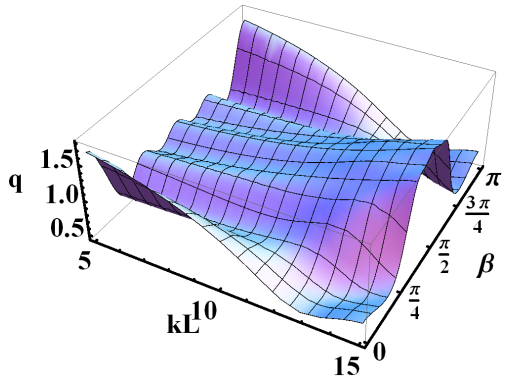

(d) $\beta_0 = \frac{3\pi}{8}$, $n_{1,opt} = 25$

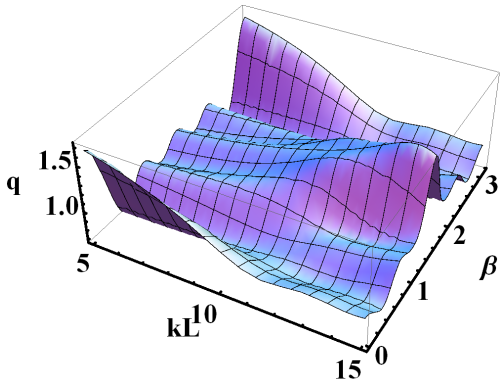

(e) $\beta_0 = \frac{\pi}{2}$, $n_{1,opt} = 16$

Figure A.7: Interaction factor q vs kL vs β for array LS3 optimised for several values of β_0.

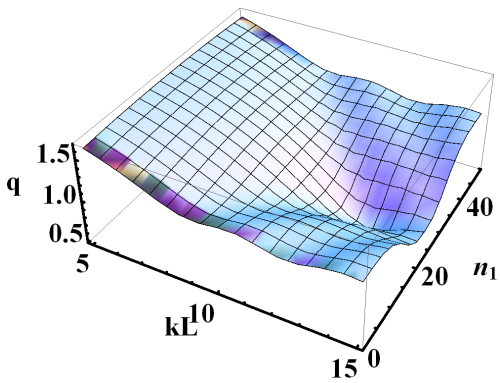

(a) $\beta_0 = 0$, $n_{1,opt} = 3$

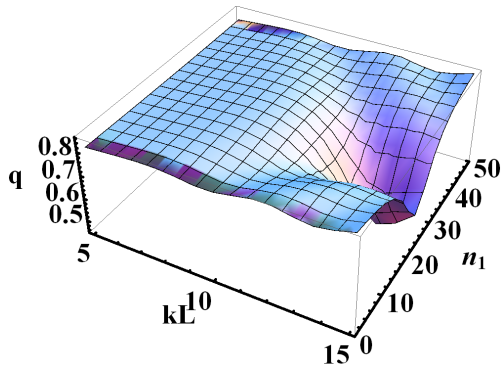

(b) $\beta_0 = \frac{\pi}{8}$, $n_{1,opt} = 1$

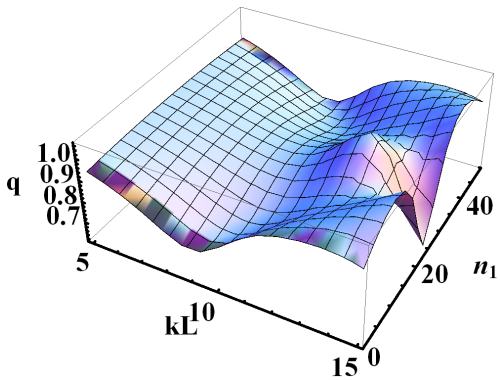

(c) $\beta_0 = \frac{\pi}{4}$, $n_{1,opt} = 25$

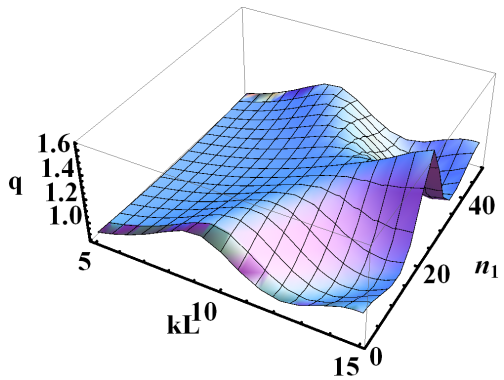

(d) $\beta_0 = \frac{3\pi}{8}$, $n_{1,opt} = 25$

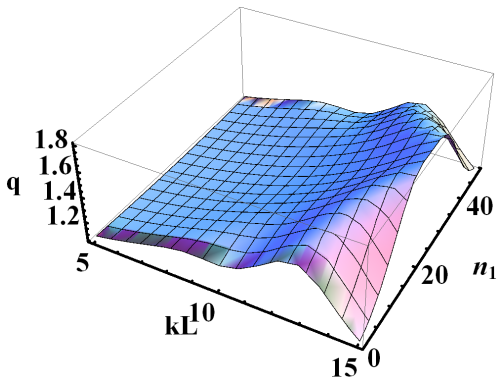

(e) $\beta_0 = \frac{\pi}{2}$, $n_{1,opt} = 16$

Figure A.8: Interaction factor q vs kL vs n_1 for array LS3 for several values of β_0.

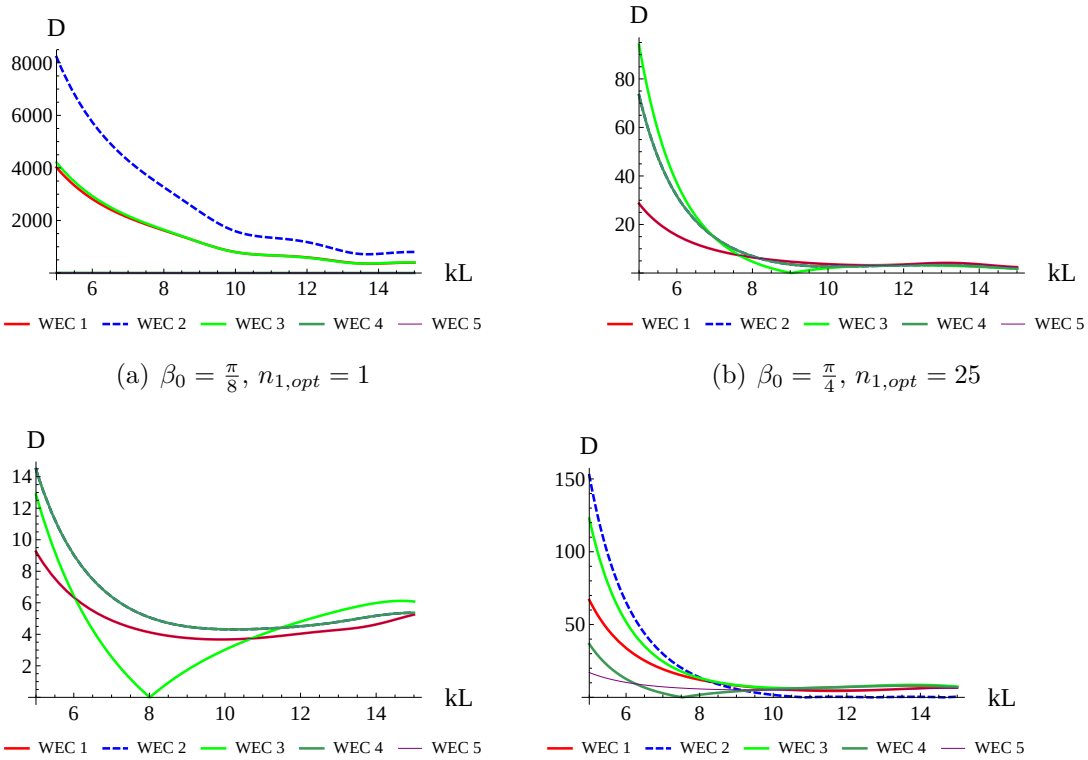

(a) $\beta_0 = \frac{\pi}{8}$, $n_{1,opt} = 1$

(b) $\beta_0 = \frac{\pi}{4}$, $n_{1,opt} = 25$

(c) $\beta_0 = \frac{3\pi}{8}$, $n_{1,opt} = 25$

(d) $\beta_0 = \frac{\pi}{2}$, $n_{1,opt} = 16$

Figure A.9: Predicted optimal displacement amplitudes for array LS3 for several values of β_0.

Appendix B

Supplementary Results to Chapter 4

Table B.1: Optimal linear array parameters for $\beta_0 = 0$

n_1	n_2	n_3	n_4	I_{opt}
0.0500	0.0500	0.0500	0.8500	1.4802
0.0500	0.8500	0.0500	0.0500	1.3501
0.0500	0.4500	0.4500	0.0500	1.2058

Table B.2: Optimal linear array parameters for $\beta_0 = \frac{\pi}{8}$

n_1	n_2	n_3	n_4	I_{opt}
0.0500	0.8500	0.0500	0.0500	0.8794
0.0500	0.0500	0.0500	0.8500	0.8364
0.0500	0.0500	0.1606	0.7394	0.8363
0.0500	0.4500	0.4500	0.0500	0.8326
0.0500	0.0500	0.4816	0.4184	0.8267

Table B.3: Optimal linear array parameters for $\beta_0 = \frac{\pi}{4}$

n_1	n_2	n_3	n_4	I_{opt}
0.0500	0.8500	0.0500	0.0500	1.1431
0.0500	0.4500	0.4500	0.0500	1.1049
0.0500	0.0500	0.0500	0.8500	0.8662

Table B.4: Optimal linear array parameters for $\beta_0 = \frac{3\pi}{8}$

n_1	n_2	n_3	n_4	I_{opt}
0.2512	0.2488	0.2488	0.2512	1.1822
0.0500	0.3998	0.1752	0.3750	1.1637
0.0500	0.0950	0.2296	0.6254	1.1266
0.3000	0.6000	0.0500	0.0500	1.0199

Table B.5: Optimal linear array parameters for $\beta_0 = \frac{\pi}{2}$

n_1	n_2	n_3	n_4	I_{opt}
0.0500	0.2252	0.3859	0.3359	1.3643
0.3419	0.1581	0.1581	0.3419	1.3437

Appendix C

Supplementary Results to Chapter 5

Table C.1: Optimal array parameters for the six-device circular array (without middle device) with $\beta_0 = 0$. The best result found by McGuinness & Thomas (2016) is marked "M"

θ_1	θ_2	θ_3	θ_4	θ_5	I_{opt}
0.1000	1.4868	1.4171	0.1000	0.1000	1.5910
0.1000	3.0972	0.1000	1.4153	1.4707	1.5907 M
0.1000	3.0044	0.1000	0.1000	1.3617	1.5895
0.1000	0.1000	1.3148	1.6284	0.1000	1.5878
0.1000	0.1000	1.0850	0.3233	0.3529	1.5877
0.1000	0.1000	1.3424	1.4756	0.1000	1.5870
1.5755	1.5424	0.1000	1.4984	1.4669	1.5809
0.1000	1.1992	0.3233	0.3531	4.2076	1.5791

Table C.2: Optimal array parameters for the six-device circular array (without middle device) with $\beta_0 = \frac{\pi}{8}$

θ_1	θ_2	θ_3	θ_4	θ_5	I_{opt}
1.1547	1.4619	0.1000	0.1000	3.3666	1.5802
1.0544	0.3376	1.1613	0.1000	3.5298	1.5738
1.0403	0.3367	1.2632	0.1000	3.4430	1.5733
0.1000	0.9337	0.3367	1.3169	0.1000	1.5707
0.1000	1.0407	1.4760	0.1000	0.1000	1.5699
0.1000	0.9705	0.3406	1.1077	0.1000	1.5673
2.7081	0.1000	0.1000	1.2923	1.9829	1.5569
1.1145	0.3390	0.8566	0.1000	3.7737	1.5561

Table C.3: Optimal array parameters for the six-device circular array (without middle device) with $\beta_0 = \frac{\pi}{4}$. The best result found by McGuinness & Thomas (2016) is marked "M"

θ_1	θ_2	θ_3	θ_4	θ_5	I_{opt}
0.6388	0.3423	1.2086	0.1000	0.1000	1.5563
0.7380	1.5292	0.1000	0.1000	3.7028	1.5306
0.6787	0.3334	1.3131	0.1000	3.7463	1.5280
0.1000	0.6512	1.5252	0.1000	0.1000	1.5101 M
0.6214	0.3844	0.8682	0.1000	4.1959	1.5036
0.1000	0.6055	0.3320	1.2812	0.1000	1.4940
2.3500	0.1000	0.1000	1.1174	0.3102	1.4882
0.4810	0.3283	0.3106	1.0354	0.1000	1.4814

Table C.4: Optimal array parameters for the six-device circular array (without middle device) with $\beta_0 = \frac{3\pi}{8}$

θ_1	θ_2	θ_3	θ_4	θ_5	I_{opt}
0.3539	0.3235	1.1056	0.1000	0.1000	1.5883
0.3238	0.3741	4.4075	0.1000	0.1000	1.5540
0.4303	1.4350	0.1000	0.1000	3.9840	1.5056
0.4270	1.4475	0.1000	3.1593	0.1000	1.5026
0.4000	1.3221	0.1000	3.5833	0.1000	1.4997
0.4451	1.3823	0.1000	0.1000	3.5184	1.4961
0.4468	1.3921	0.1000	0.1000	3.3160	1.4934
0.4802	1.3115	0.1000	0.1000	0.1000	1.4924

Table C.5: Optimal array parameters for the six-device circular array (without middle device) with $\beta_0 = \frac{\pi}{2}$. The best result found by McGuinness & Thomas (2016) is marked "M"

θ_1	θ_2	θ_3	θ_4	θ_5	I_{opt}
1.4417	0.1000	0.1000	3.1329	0.1000	1.5921
0.3152	1.0723	0.1000	0.1000	4.3317	1.5855
1.5208	0.1000	1.5208	1.5208	0.1000	1.5824 M
0.3097	0.8228	0.1000	3.6801	0.1000	1.5472
0.2983	1.0820	0.1000	0.1000	4.0926	1.5387
0.3043	1.0285	0.1000	3.3942	0.1000	1.5369
0.2863	1.0837	0.1000	0.1000	2.6281	1.5309
0.2929	1.0833	0.1000	0.1000	3.4943	1.5247

Table C.6: Optimal array parameters for the six-device circular array (without middle device) with $\beta_0 = \frac{5\pi}{8}$

θ_1	θ_2	θ_3	θ_4	θ_5	I_{opt}
4.3001	0.1000	0.1000	1.1056	0.3235	1.5883
0.9778	0.1000	0.1000	4.4075	0.3741	1.5540
0.2338	3.9840	0.1000	0.1000	1.4350	1.5056
1.0493	0.1000	3.1593	0.1000	1.4475	1.5026
0.7778	0.1000	3.5833	0.1000	1.3221	1.4997
0.7374	3.5184	0.1000	0.1000	1.3823	1.4961
0.9283	3.3160	0.1000	0.1000	1.3921	1.4934
4.1915	0.1000	0.1000	0.1000	1.3115	1.4924

Table C.7: Optimal array parameters for the six-device circular array (without middle device) with $\beta_0 = \frac{3\pi}{4}$

θ_1	θ_2	θ_3	θ_4	θ_5	I_{opt}
3.8935	0.1000	0.1000	1.2086	0.3423	1.5563
0.1131	3.7028	0.1000	0.1000	1.5292	1.5306
0.1117	3.7463	0.1000	1.3131	0.3334	1.5280
3.8068	0.1000	0.1000	1.5252	0.6512	1.5101
0.1132	4.1959	0.1000	0.8682	0.3844	1.5036
3.8645	0.1000	1.2812	0.3320	0.6055	1.4940
2.3057	0.3102	1.1174	0.1000	0.1000	1.4882
4.0279	0.1000	1.0354	0.3106	0.3283	1.4814

Table C.8: Optimal array parameters for the six-device circular array (without middle device) with $\beta_0 = \frac{7\pi}{8}$

θ_1	θ_2	θ_3	θ_4	θ_5	I_{opt}
0.1000	3.3666	0.1000	0.1000	1.4619	1.5802
0.1000	3.5298	0.1000	1.1613	0.3376	1.5738
0.1000	3.4430	0.1000	1.2632	0.3367	1.5733
3.4958	0.1000	1.3169	0.3367	0.9337	1.5707
3.4665	0.1000	0.1000	1.4760	1.0407	1.5699
3.6644	0.1000	1.1077	0.3406	0.9705	1.5673
0.1000	1.9829	1.2923	0.1000	0.1000	1.5569
0.1000	3.7737	0.1000	0.8566	0.3384	1.5561

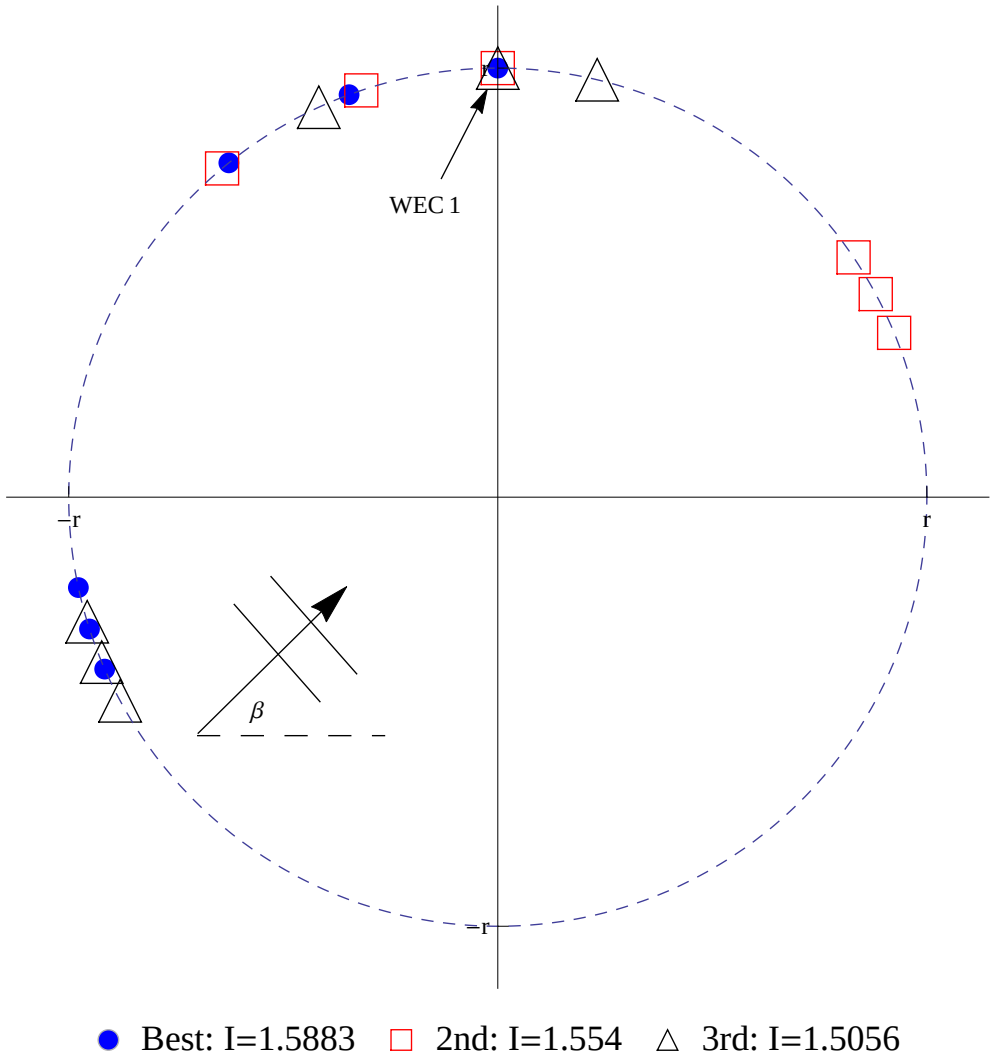

Figure C.1: Optimal six-device circular arrays for $\beta_0 = \frac{5\pi}{8}$

Table C.9: Optimal array parameters for the seven-device circular array (including a middle device) with $\beta_0 = 0$. The best result found by McGuinness & Thomas (2016) is marked "M"

θ_1	θ_2	θ_3	θ_4	θ_5	I_{opt}
0.1000	2.9420	0.1000	0.1000	2.9420	1.5680
0.1000	0.1000	2.8270	0.1000	0.1000	1.5408 M
0.1000	1.4838	1.2789	0.1000	3.2204	1.5366
0.1000	1.4738	1.4706	0.1000	0.1000	1.5146
0.1000	1.4118	1.7719	0.1000	2.7994	1.5139
0.1000	0.1000	1.3797	1.2066	0.1000	1.5136
0.1000	0.1000	3.0606	0.1000	1.3241	1.5132
0.1000	0.1000	1.2963	1.7589	0.1000	1.5103

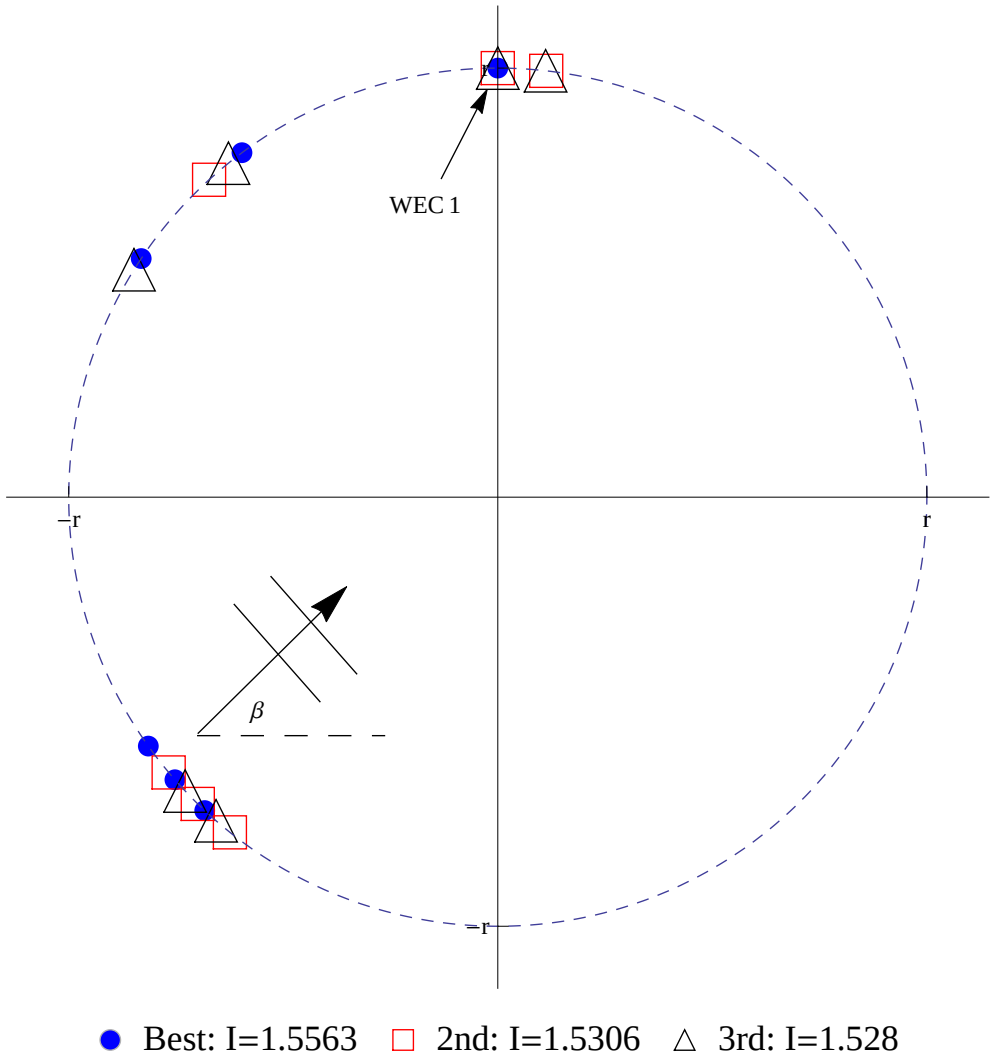

Figure C.2: Optimal six-device circular arrays for $\beta_0 = \frac{3\pi}{4}$

Table C.10: Optimal array parameters for the seven-device circular array (including a middle device) with $\beta_0 = \frac{\pi}{8}$

θ_1	θ_2	θ_3	θ_4	θ_5	I_{opt}
1.1503	1.4850	0.1000	0.1000	3.3479	1.5320
0.1000	1.0448	1.4793	0.1000	0.1000	1.5197
2.6702	0.1000	0.1000	1.3456	1.9674	1.4915
1.0536	0.3389	1.0827	0.1000	3.6080	1.4899
1.0178	0.3331	1.2799	0.1000	0.1000	1.4825
1.1092	0.3362	0.8741	0.1000	3.7637	1.4814
0.1000	0.8160	0.3310	1.0241	0.1000	1.4788
0.1000	1.0096	0.3309	0.8214	0.1000	1.4788

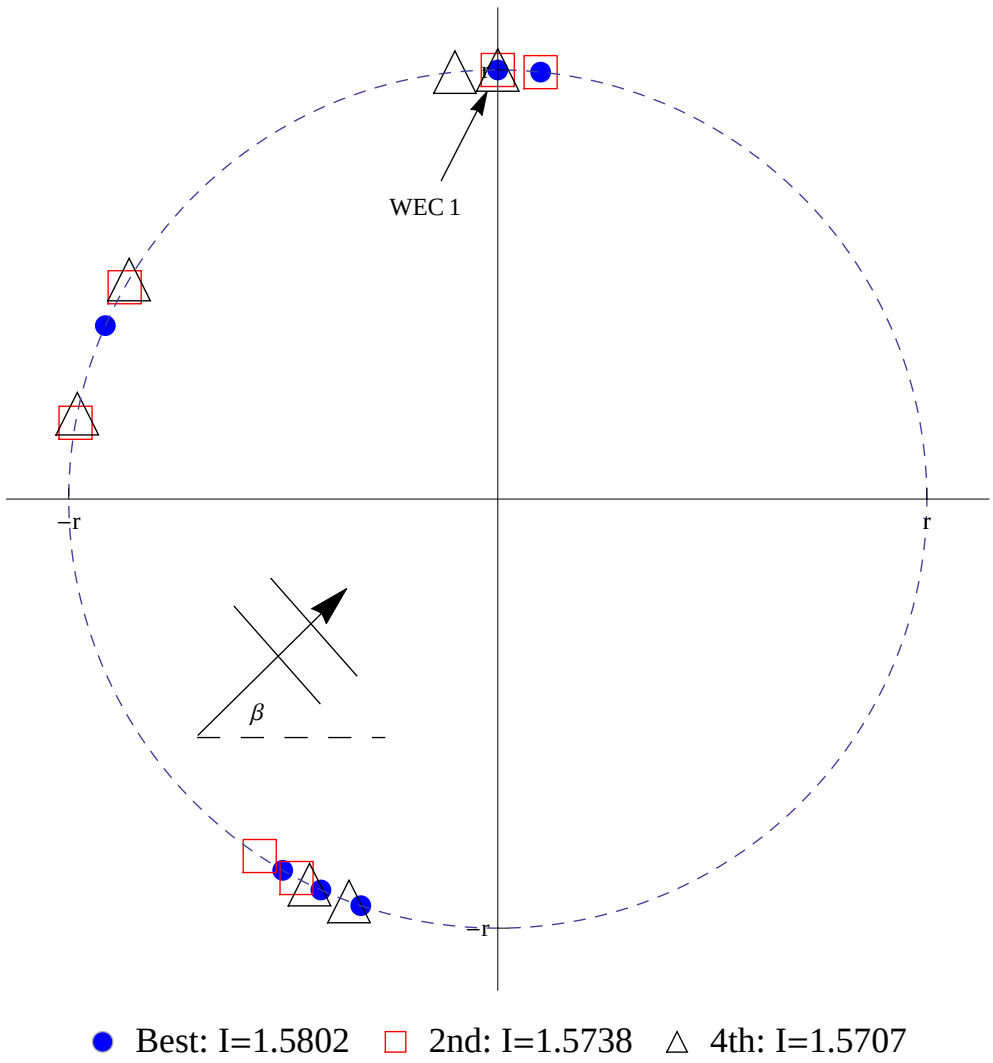

Figure C.3: Optimal six-device circular arrays for $\beta_0 = \frac{7\pi}{8}$. The third array is very similar to the second and is omitted for clarity

Table C.11: Optimal array parameters for the seven-device circular array (including a middle device) with $\beta_0 = \frac{\pi}{4}$. The best result found by McGuinness & Thomas (2016) is marked "M"

θ_1	θ_2	θ_3	θ_4	θ_5	I_{opt}
0.7534	1.4852	0.1000	0.1000	3.7020	1.4957 M
0.6333	0.3336	1.2604	0.1000	0.1000	1.4759
0.1852	0.5914	1.4754	0.1000	0.1000	1.4645
0.1000	0.6599	1.4931	0.1000	0.1000	1.4641
0.6812	0.3227	1.3021	0.1000	3.7448	1.4365
0.7031	0.3357	1.1011	0.1000	3.9150	1.4340
0.6486	0.3175	1.5301	0.1000	3.5552	1.4330
0.7891	1.4185	0.1000	0.1000	0.1000	1.4264

Table C.12: Optimal array parameters for the seven-device circular array (including a middle device) with $\beta_0 = \frac{3\pi}{8}$

θ_1	θ_2	θ_3	θ_4	θ_5	I_{opt}
0.3465	0.3231	1.1262	0.1000	0.1000	1.4785
0.3263	0.3662	4.3849	0.1000	0.1000	1.4450
0.4368	1.4314	0.1000	0.1000	3.2881	1.4317
0.4364	1.2737	0.1000	3.4408	0.1000	1.4310
0.3272	0.3394	0.8322	0.1000	3.9719	1.4240
0.4354	1.4234	0.1000	0.1000	3.9749	1.4171
0.3197	0.3509	0.7762	3.9619	0.1000	1.4152
0.4288	1.4179	0.1000	0.1000	3.5061	1.4113

Table C.13: Optimal array parameters for the seven-device circular array (including a middle device) with $\beta_0 = \frac{\pi}{2}$. The best result found by McGuinness & Thomas (2016) is marked "M"

θ_1	θ_2	θ_3	θ_4	θ_5	I_{opt}
1.3060	0.1000	3.2065	0.1000	0.1000	1.5361 M
1.4453	0.1000	0.1000	2.8821	0.1000	1.5055
1.3774	0.1000	1.6642	1.6642	0.1000	1.4965
0.3134	1.0854	0.1000	0.1000	4.3294	1.4753
0.3020	0.8243	0.1000	3.8186	0.1000	1.4677
1.2937	0.1000	3.5037	0.1000	0.9844	1.4616
1.3198	1.9006	1.3732	0.1000	0.1000	1.4528
0.2888	1.1404	0.1000	0.1000	3.3680	1.4513

Table C.14: Optimal array parameters for the seven-device circular array (including a middle device) with $\beta_0 = \frac{5\pi}{8}$

θ_1	θ_2	θ_3	θ_4	θ_5	I_{opt}
4.2874	0.1000	0.1000	1.1262	0.3231	1.4785
1.0058	0.1000	0.1000	4.3849	0.3662	1.4450
0.9269	3.2881	0.1000	0.1000	1.4314	1.4317
0.9323	0.1000	3.4408	0.1000	1.2737	1.4310
0.7125	3.9719	0.1000	0.8322	0.3394	1.4240
0.2495	3.9749	0.1000	0.1000	1.4234	1.4171
0.7745	0.1000	3.9619	0.7762	0.3509	1.4152
0.7304	3.5061	0.1000	0.1000	1.4179	1.4113

Table C.15: Optimal array parameters for the seven-device circular array (including a middle device) with $\beta_0 = \frac{3\pi}{4}$

θ_1	θ_2	θ_3	θ_4	θ_5	I_{opt}
0.1426	3.7020	0.1000	0.1000	1.4852	1.4957
3.8558	0.1000	0.1000	1.2604	0.3336	1.4759
3.8313	0.1000	0.1000	1.4754	0.5914	1.4645
3.8301	0.1000	0.1000	1.4931	0.6599	1.4641
0.1324	3.7448	0.1000	1.3021	0.3227	1.4365
0.1282	3.9150	0.1000	1.1011	0.3357	1.4340
0.1317	3.5552	0.1000	1.5301	0.3175	1.4330
3.7756	0.1000	0.1000	0.1000	1.4185	1.4264

Table C.16: Optimal array parameters for the seven-device circular array (including a middle device) with $\beta_0 = \frac{7\pi}{8}$

θ_1	θ_2	θ_3	θ_4	θ_5	I_{opt}
0.1000	3.3479	0.1000	0.1000	1.4850	1.5320
3.4590	0.1000	0.1000	1.4793	1.0448	1.5197
0.1000	1.9674	1.3456	0.1000	0.1000	1.4915
0.1000	3.6080	0.1000	1.0827	0.3389	1.4899
3.4524	0.1000	0.1000	1.2799	0.3331	1.4825
0.1000	3.7637	0.1000	0.8741	0.3362	1.4814
3.9121	0.1000	1.0241	0.3310	0.8160	1.4788
3.9214	0.1000	0.8214	0.3309	1.0096	1.4788

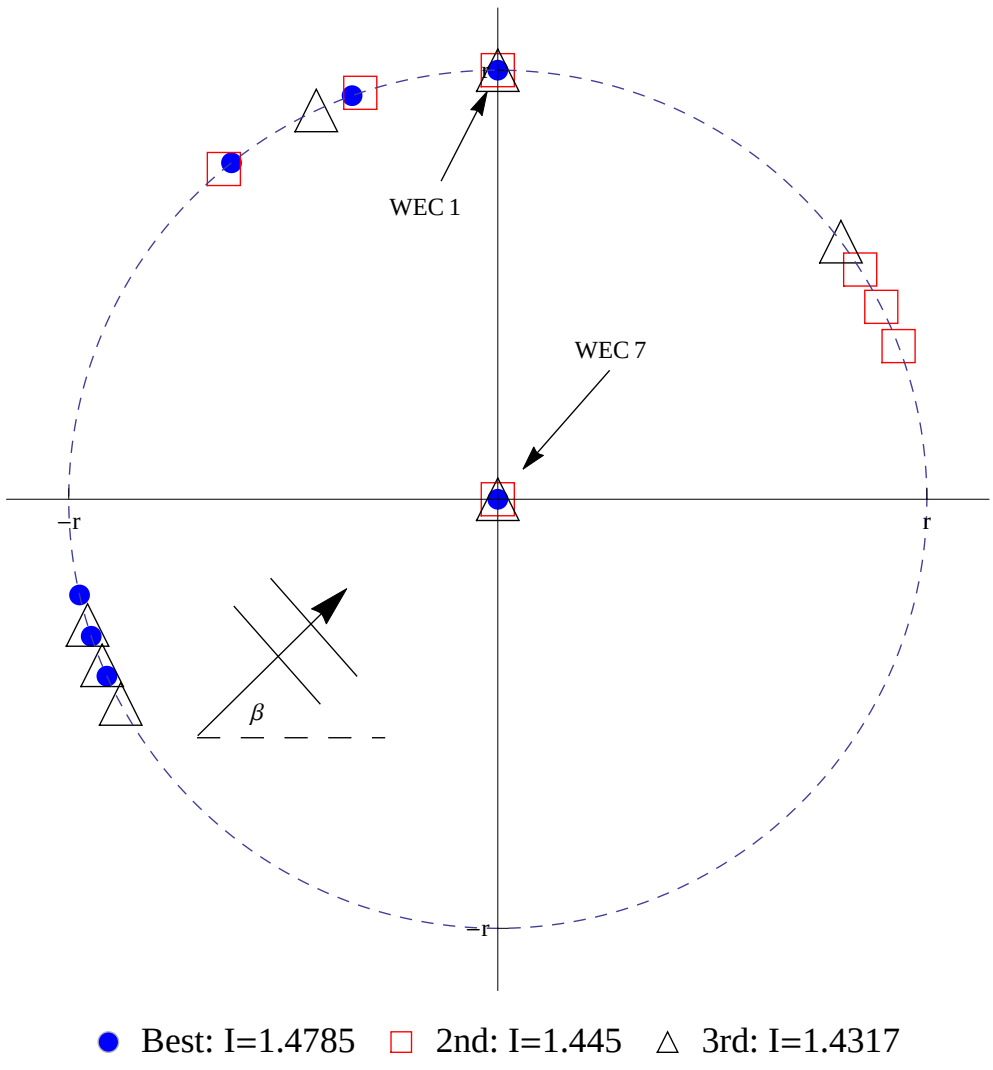

Figure C.4: Optimal seven-device circular arrays for $\beta_0 = \frac{5\pi}{8}$

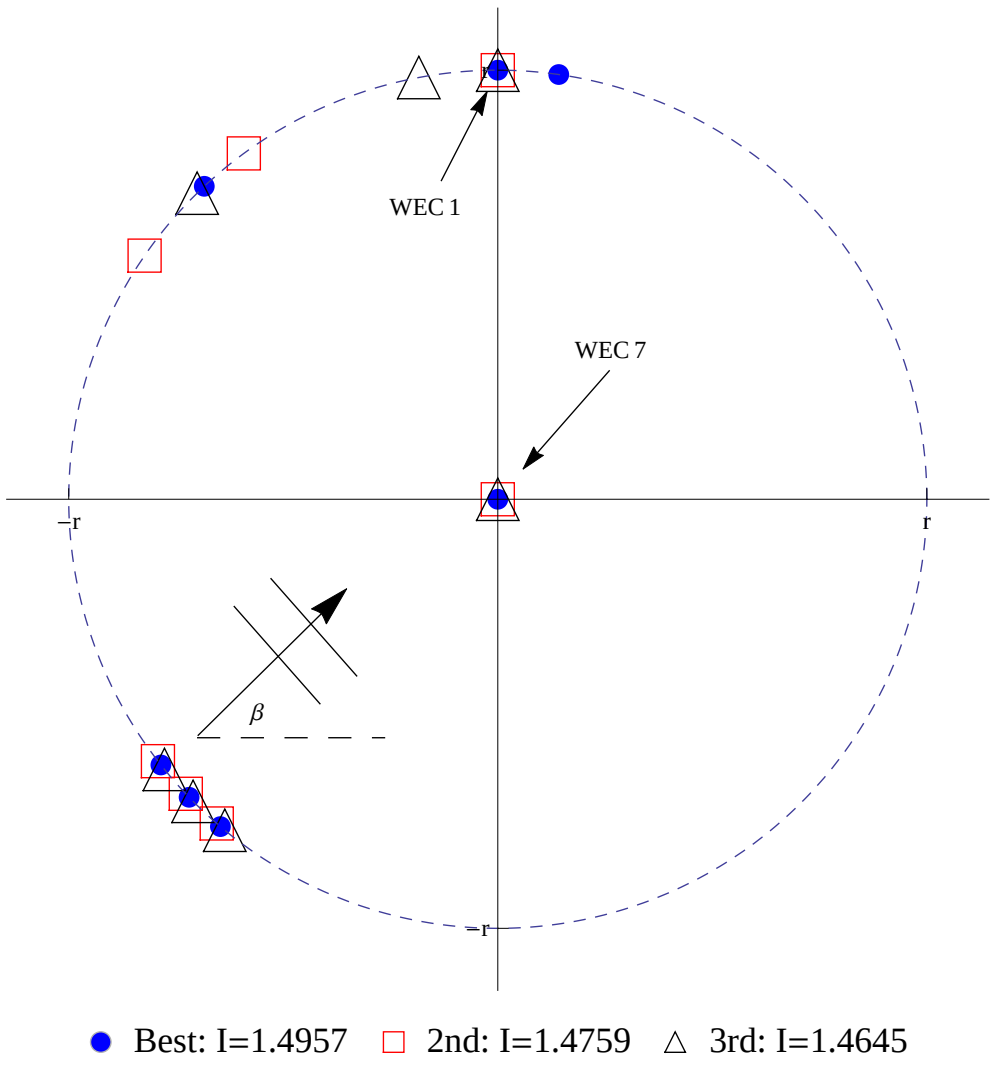

Figure C.5: Optimal seven-device circular arrays for $\beta_0 = \frac{3\pi}{4}$

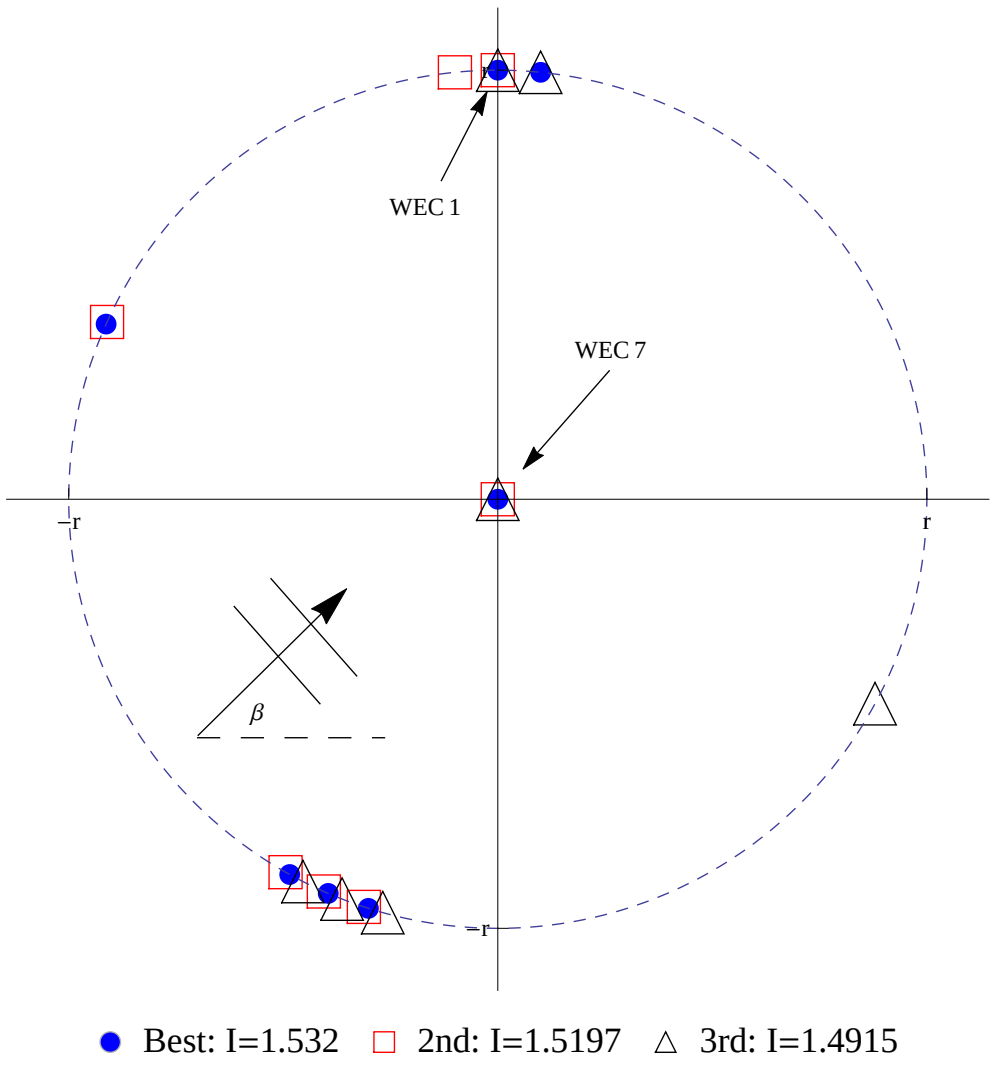

Figure C.6: Optimal seven-device circular arrays for $\beta_0 = \frac{7\pi}{8}$

Appendix D

Supplementary Results to Chapter 6

Table D.1: Optimal linear array layout parameters subject to $\delta \leq 2$ for $\beta_0 = 0$

n_1	n_2	n_3	n_4	$\overline{I}_{opt}$
0.0978	0.0532	0.1139	0.7351	0.49441
0.0839	0.0500	0.1076	0.7585	0.49113
0.1229	0.0500	0.1185	0.7086	0.48502
0.1230	0.0500	0.1182	0.7088	0.48315
0.1197	0.0967	0.1261	0.6575	0.47595

Table D.2: Optimal linear array layout parameters subject to $\delta \leq 3$ for $\beta_0 = 0$

n_1	n_2	n_3	n_4	$\overline{I}_{opt}$
0.1057	0.0504	0.1048	0.7391	0.58438
0.0869	0.0500	0.0988	0.7643	0.57784
0.1236	0.0500	0.0990	0.7274	0.57028
0.1237	0.0500	0.0989	0.7274	0.56885
0.1309	0.0819	0.0872	0.7000	0.56573

Table D.3: Optimal linear array layout parameters subject to $\delta \leq 2$ for $\beta_0 = \frac{\pi}{4}$

n_1	n_2	n_3	n_4	$\overline{I}_{opt}$
0.0940	0.1532	0.2259	0.5269	0.42508
0.0832	0.1473	0.1538	0.6157	0.41728
0.1243	0.1979	0.1605	0.5173	0.41682
0.1398	0.2328	0.1741	0.4533	0.41388
0.1234	0.1959	0.1504	0.5303	0.41383

Table D.4: Optimal linear array layout parameters subject to $\delta \leq 3$ for $\beta_0 = \frac{\pi}{4}$

n_1	n_2	n_3	n_4	$\overline{I}_{opt}$
0.1310	0.3066	0.1103	0.4521	0.45507
0.1267	0.2848	0.1424	0.4461	0.45480
0.1193	0.2732	0.1600	0.4475	0.45350
0.1333	0.3235	0.0862	0.4570	0.45303
0.1620	0.6131	0.1240	0.1009	0.40869

Table D.5: Optimal linear array layout parameters subject to $\delta \leq 2$ for $\beta_0 = \frac{\pi}{2}$

n_1	n_2	n_3	n_4	$\overline{I}_{opt}$
0.2679	0.2321	0.2321	0.2679	0.87771

Table D.6: Optimal linear array layout parameters subject to $\delta \leq 3$ for $\beta_0 = \frac{\pi}{2}$

n_1	n_2	n_3	n_4	$\overline{I}_{opt}$
0.2679	0.2321	0.2321	0.2679	1.06779

D. Supplementary Results to Chapter 6

References

Alves, M., Traylor, H., & Sarmento, A., 2007. Hydrodynamic optimization of a wave energy converter using a heave motion buoy. In *Proceedings of the 7th European Wave and Tidal Energy Conference*, Porto, Portugal. 8 pages.

Babarit, A., 2010. Impact of long separating distances on the energy production of two interacting wave energy converters. *Ocean Engineering*, 37(8-9): 718–729.

Babarit, A., 2013. On the park effect in arrays of oscillating wave energy converters. *Renewable Energy*, 58(0):68–78.

Beels, C., 2009. *Optimization of the Lay-Out of a Farm of Wave Energy Converters in the North Sea Analysis of Wave Power Resources, Wake Effects, Production and Cost*. PhD thesis, Ghent University.

Bellew, S., Stallard, T., & Stansby, P. K., 2009. Optimisation of a heterogeneous array of heaving bodies. In *Proceedings of the 8th European Wave and Tidal Energy Conference*, pages 519–527, Uppsala, Sweden.

Borgarino, B., Babarit, A., & Ferrant, P., 2012. Impact of wave interactions effects on energy absorption in large arrays of wave energy converters. *Ocean Engineering*, 41(0):79–88.

Budal, K., 1977. Theory for absorption of wave power by a system of interacting bodies. *Journal of Ship Research*, 21(4):248–253.

Child, B. F. M., 2011. *On the configuration of arrays of floating wave energy converters*. Phd thesis, The University of Edinburgh.

Child, B. F. M. & Venugopal, V., 2007. Interaction of waves with an array of foating wave energy devices. In *Proceedings of the 7th European Wave and Tidal Energy Conference*, Porto, Portugal. 11 pages.

Child, B. F. M. & Venugopal, V., 2008. Non-optimal tuning of wave energy

device arrays. In *Proceedings of the 2nd International Conference on Ocean Energy*, pages 15–17, Brest, France.

Child, B. F. M. & Venugopal, V., 2009. Modification of power characteristics in an array of floating wave energy devices. In *Proceedings of the 8th European Wave and Tidal Energy Conference*, pages 309–318, Uppsala, Sweden.

Child, B. F. M. & Venugopal, V., 2010. Optimal configurations of wave energy device arrays. *Ocean Engineering*, 37(16):1402–1417.

Costigan, C., 2014. Modelling circular arrays of wave-power devices. Technical report, AM4090 Module, University College Cork.

Cruz, J., Sykes, R., Siddorn, P., & Eatock Taylor, R., 2009. Wave farm design: Preliminary studies on the influences of wave climate, array layout and farm control. In *Proceedings of the 8th European Wave and Tidal Energy Conference*, pages 736–745, Uppsala, Sweden.

De Backer, G., Vantorre, M., Beels, C., De Rouck, J., & Frigaard, P., 2009. Performance of closely spaced point absorbers with constrained floater motion. In *Proceedings of the 8th European Wave and Tidal Energy Conference*, pages 806–817, Uppsala, Sweden.

Evans, D. V., 1979. Some theoretical aspects of three-dimensional wave-energy absorbers. In *Symposium on Ocean Wave Energy Utilization*, Gothenburg, Sweden. 37 pages.

Falnes, J., 1984. Wave-power absorption by an array of attenuators oscillating with unconstrained amplitudes. *Applied Ocean Research*, 6(1):16–22.

Falnes, J., 2002. *Ocean waves and oscillating systems : linear interactions including wave-energy extraction.* Cambridge University Press, Cambridge.

Falnes, J. & Budal, K., 1982. Wave-power absorption by parallel rows of interacting oscillating bodies. *Applied Ocean Research*, 4(4):194–207.

Fennell, S., 2015. Modelling triangular arrays of wavepower devices. Technical report, AM4090 Module, University College Cork.

Fitzgerald, C., 2006. Optimal configurations of arrays of wave power devices. Master's thesis, University College Cork.

Fitzgerald, C. & Thomas, G. P., 2007. A preliminary study on the optimal

formation of an array of wave power devices. In *Proceedings of the 7th European Wave and Tidal Energy Conference*, Porto, Portugal. 9 pages.

Folley, M. & Whittaker, T. J. T., 2009. The effect of sub-optimal control and the spectral wave climate on the performance of wave energy converter arrays. *Applied Ocean Research*, 31(4):260–266.

Garcia-Rosa, P. B., Bacelli, G., & Ringwood, J. V., 2015. Control-informed optimal array layout for wave farms. *IEEE Transactions on Sustainable Energy*, 6(2):575–582.

Garnaud, X. & Mei, C. C., 2009a. Wave-power extraction by a compact array of buoys. *Journal of Fluid Mechanics*, 635:389–413.

Garnaud, X. & Mei, C. C., 2009b. Comparison of wave power extraction by a compact array of small buoys and by a large buoy. In *Proceedings of the 8th European Wave and Tidal Energy Conference*, pages 934–942, Uppsala, Sweden.

Gill, P. E., Murray, W., Saunders, M. A., & Wright, M. H., 1986. User's guide for npsol (version 4.0): A fortran package for nonlinear programming. Technical report, DTIC Document.

Goggins, J. & Finnegan, W., 2014. Shape optimisation of floating wave energy converters for a specified wave energy spectrum. *Renewable Energy*, 71(0):208 – 220.

Havelock, T. H., 1955. Waves due to a floating sphere making periodic heaving oscillations. *Proceedings of the Royal Society of London. Series A. Mathematical and Physical Sciences*, 231(1184):1–7.

Hughes, S. A., 1993. *Physical models and laboratory techniques in coastal engineering*, volume 7. World Scientific.

Hulme, A., 1982. The wave forces acting on a floating hemisphere undergoing forced periodic oscillations. *Journal of Fluid Mechanics*, 121:443–463.

Justino, P. A. P. & Clement, A. H., 2003. Hydrodynamic performance for small arrays of submerged spheres. In *Proceedings of the 5th European Wave and Tidal Energy Conference*, pages 266–273, Cork, Ireland.

Lamont-Kane, P., Folley, M., & Whittaker, T., 2013. Investigating uncertainties in physical testing of wave energy converter arrays. In *Proceedings of the 10th European Wave and Tidal Energy Conference*, Aalborg, Denmark. 10 pages.

Lawton, B., 2017. Modelling elliptical arrays of wavepower devices. Technical report, AM4090 Module, University College Cork.

Lewis, A. W., 2014. Ce6005: Ocean energy. Lecture Series, University College Cork.

Linton, C. M., 1991. Radiation and diffraction of water waves by a submerged sphere in finite depth. *Ocean Engineering*, 18(1-2):61–74.

Linton, C. M. & McIver, P., 2001. *Handbook of mathematical techniques for wave/structure interactions*. Chapman & Hall/CRC, Boca Raton, FL.

Mavrakos, S. A., 1991. Hydrodynamic coefficients for groups of interacting vertical axisymmetric bodies. *Ocean Engineering*, 18(5):485–515.

Mavrakos, S. A. & Koumoutsakos, P., 1987. Hydrodynamic interaction among vertical axisymmetric bodies restrained in waves. *Applied Ocean Research*, 9 (3):128–140.

Mavrakos, S. A. & McIver, P., 1997. Comparison of methods for computing hydrodynamic characteristics of arrays of wave power devices. *Applied Ocean Research*, 19(5-6):283–291.

McCabe, A. P., 2013. Constrained optimization of the shape of a wave energy collector by genetic algorithm. *Renewable Energy*, 51(0):274–284.

McCabe, A. P., Aggidis, G. A., & Widden, M. B., 2009. A pilot study into the optimisation of the shape of a wave energy collector by genetic algorithm. In *Proceedings of the 8th European Wave and Tidal Energy Conference*, pages 330–337, Uppsala, Sweden.

McCabe, A. P., Aggidis, G. A., & Widden, M. B., 2010. Optimizing the shape of a surge-and-pitch wave energy collector using a genetic algorithm. *Renewable Energy*, 35(12):2767–2775.

McGuinness, J. P. L., 2013. Modelling arrays of wave-power devices. Technical report, AM4090 Module, University College Cork.

McGuinness, J. P. L. & Thomas, G., 2015. Optimal arrangements of elementary arrays of wave-power devices. In *Proceedings of the 11th European Wave and Tidal Energy Conference*, Nantes, France. 10 pages.

McGuinness, J. P. L. & Thomas, G., 2016. Hydrodynamic optimisation of small

arrays of heaving point absorbers. *Journal of Ocean Engineering and Marine Energy*, 2(4):439–457.

McGuinness, J. P. L. & Thomas, G., 2017a. The constrained optimisation of small linear arrays of heaving point absorbers. part i: The inuence of spacing. *International Journal of Marine Energy.* Accepted Manuscript, In press.

McGuinness, J. P. L. & Thomas, G., 2017b. Optimisation of elementary arrays of wave-power devices in irregular waves. In *12th European Wave and Tidal Energy Conference*, Cork, Ireland. 10 pages.

McIver, P., 1993. The hydrodynamics of arrays of wave-energy devices. In "wave energy converters - generic technical evaluation study", report prepared for the commission of the european communities by danish wave power aps. 20 pages.

McIver, P., 1994. Some hydrodynamic aspects of arrays of wave-energy devices. *Applied Ocean Research*, 16(2):61–69.

McIver, P., Mavrakos, S., & Singh, G., 1996. Wave-power absorption by arrays of devices. In *Proceedings of the Second European Wave Power Conference*, pages 126–133, Lisbon, Portugal.

Mitchell, M., 1998. *An introduction to genetic algorithms (complex adaptive systems).* MIT press.

Newman, J. N., 1977. *Marine hydrodynamics.* MIT, Cambridge, Mass.

O'Boyle, L., Elsaesser, B., Folley, M., & Whittaker, T., 2011. Assessment of wave basin honogeneity for wave energy converter array studies. In *Proceedings of the 9th European Wave and Tidal Energy Conference*, Southampton, United Kingdom. 8 pages.

Sarmento, A. & Thomas, G., 2008. *Guidelines for laboratory testing of WECs.* Springer Berlin Heidelberg, in ocean wave energy: current status and future prespectives edition.

Snyder, L. V., 2013. q-factor optimisation for 2-wec arrays. Technical report, Lehigh University.

Snyder, L. V. & Moarefdoost, M. M., 2014. Layouts for ocean wave energy farms: Models, properties, and heuristic. In *Proceedings of the 2nd Marine Energy Technology Symposium*, Seattle, WA, USA. 8 pages.

Snyder, L. V. & Moarefdoost, M. M., 2015. Optimizing wave farm layouts under uncertainty. In *Proceedings of the 3rd Marine Energy Technology Symposium*, Washington, D.C., USA. 6 pages.

Srokosz, M. A., 1979. *Some Theoretical Aspects of Wave Power Absorption.* PhD thesis, University of Bristol.

Stratigaki, V., 2014. *Experimental Study and Numerical Modelling of Intra-Array Interactions and Extra-Array Effects of Wave Energy Converter Arrays.* Phd thesis, Ghent University.

Stratigaki, V., Troch, P., Stallard, T., Forehand, D., Kofoed, J. P., Folley, M., Benoit, M., Babarit, A., & Kirkegaard, J., 2014. Wave basin experiments with large wave energy converter arrays to study interactions between the converters and effects on other users in the sea and the coastal area. *Energies*, 7(2):701–734.

Thomas, G. P. & Evans, D. V., 1981. Arrays of three-dimensional wave-energy absorbers. *Journal of Fluid Mechanics*, 108:67–88.

Thomas, G., 2008. *The Theory Behind the Conversion of Ocean Wave Energy: a Review.* Springer Berlin Heidelberg, in ocean wave energy: current status and future prespectives edition.

Thomas, G. & Gallachóir, B., 1993. An assessment of design parameters for the bristol cylinder. In *Proceedings of the First European Wave Energy Symposium*, pages 139–144, Edinburgh, Scotland.

Weber, J. & Thomas, G., 2000. Optimisation of the hydrodynamic-aerodynamic coupling for an oscillating water column wave energy device. In *Proceeding of the Fourth European Wave Energy Conference*, pages 251–259, Aalborg, Denmark.

Weber, J. & Thomas, G., 2003. Some aspects of the design optimisation of an owc with regard to multiple sea-states and combined object functions. In *Proceedings of the Fifth European Wave and Tidal Energy Conference*, pages 141–148, Cork, Ireland.

Weber, J. & Thomas, G., 2005. An efficient flexible engineering tools for multi-parametric hydrodynamic analysis in the design & optimisation of wecs. In *Proceedings of the 6th European Wave and Tidal Enegy Conference*, pages 543–548, Glasgow, Scotland.

Wolgamot, H. A., Taylor, P. H., & Eatock Taylor, R., 2012. The interaction factor and directionality in wave energy arrays. *Ocean Engineering*, 47(0): 65–73.

Wu, G. X., 1995. The interaction of water waves with a group of submerged spheres. *Applied Ocean Research*, 17(3):165–184.